CRANFIELD UNIVERSITY

SCHOOL OF MECHANICAL ENGINEERING

PhD

Academic Year 2001-2

M.S.HOWARD

Pedestrian accident simulation and protection technology evaluation

Supervisors : Professor R.S.Sharp
Dr. M.M.Sadeghi

December 2002

©Cranfield University, 2002 . All rights reserved . No part of this publication may be reproduced without the written permission of the copyright holder

ProQuest Number: 10832374

All rights reserved

INFORMATION TO ALL USERS
The quality of this reproduction is dependent upon the quality of the copy submitted.

In the unlikely event that the author did not send a complete manuscript
and there are missing pages, these will be noted. Also, if material had to be removed,
a note will indicate the deletion.

ProQuest 10832374

Published by ProQuest LLC (2018). Copyright of the Dissertation is held by Cranfield University.

All rights reserved.
This work is protected against unauthorized copying under Title 17, United States Code
Microform Edition © ProQuest LLC.

ProQuest LLC.
789 East Eisenhower Parkway
P.O. Box 1346
Ann Arbor, MI 48106 – 1346

Abstract

Pedestrian safety is an important societal issue and as one of the stakeholders, vehicle manufacturers are attempting to improve pedestrian protection by enhancing vehicle design. In order to enhance vehicle design, first it is necessary to gain an improved understanding of the interactions between a pedestrian and a vehicle during an accident. Secondly, this knowledge needs to be transformed into vehicle design and technology changes. This thesis focuses on the construction of new models and methodologies to provide an improved understanding and the application of this understanding to design, develop and evaluate a number of pedestrian protection technologies.

A review of the pedestrian safety issue and different approaches to pedestrian protection research provide the background to the chosen approach. This is described in terms of an overall methodology for any pedestrian protection technology that also provides a framework for this research.

The construction and evaluation of pedestrian accident simulations with a reference C class vehicle are described in detail. The influence of accident conditions and the expected ranges of various quantitative pedestrian injury and motion measures are identified. Vehicle impact velocity, pedestrian size and stance have significant influences on these measures. Therefore it is not possible to state, for instance, that under all accident conditions, one vehicle impact location is likely to cause lower injury measures than another is. There is a clear increase in pedestrian measures (e.g. head velocity, HIC, tibia acceleration, knee bending) with a large increase in impact velocity (i.e. 25 to 40 km/h). However, some measures (e.g. HIC) do not necessarily increase with a small increase in impact velocity (e.g. 25 to 30 km/h) because of the new pedestrian motion (e.g. a new head impact location). Large differences exist between the 6 year old pedestrian and adult pedestrian model measures (e.g. larger post head impact motion but smaller HIC and tibia acceleration) and pedestrian stance has a complex influence on all measures with few overall trends.

Pedestrian protection headlamp, bumper system and hood system concepts are developed in biomechanical, analytical and numerical component models. These concepts are used to construct and subsequently benchmark, with pedestrian accident simulations, two modified vehicle models that incorporate different combinations of the technologies. Both the absolute measures and ranges of the measures from the reference vehicle simulations are compared. There are large differences between the pedestrian measures from the reference and modified vehicles but much smaller differences between the modified vehicles. Impacts with the modified vehicles cause the largest differences in pedestrian motion at 40 km/h, for the 6 year old pedestrian, in stance 'A', in the early (up to 20 ms) and late (after 140 ms) stages of the accident simulations. Although the modified vehicles reduce pedestrian injury measures for some of the accident conditions, neither of them reduce all measures for all of the conditions. However, significant improvements in experimental sub system measures [EEVC 1998] are achieved with a prototype modified vehicle that incorporates some of the technologies.

Benchmarking is hindered by complex injury measure trends and by pedestrian and vehicle model limitations. Recommendations are made with respect to all of these factors. Further recommendations include the need for optimisation of the modified vehicle technologies in accident simulations, a more complete investigation of other technology functional requirements (e.g. low speed damageability) and accident reconstruction as a means to achieve improved model validation.

Acknowledgements

I would like to thank Professor Sharp for his invaluable academic guidance and advice during the development of this research and thesis. I am also grateful to Dr. Majid Sadeghi, in particular for his encouragement and help in initiating the PhD process and Dr. Frode Maaseidvaag who entrusted me with the creation and development of the FFA pedestrian protection research program. Similarly I would like to thank Dr. Pim Van der Jagt who continued to actively support this research and my colleagues Dr. Yiqin Mao, Dr. Karl Siebertz, Dr. Harold Schreiber and Dr. Werner Koch. Finally I would like to thank all the university committee members whose questions and comments helped me to keep heading in the right direction.

List of Contents

List of Figures IV

List of Tables XI

Notation XIV

Common Abbreviations XV

1. Introduction 1

1.1. **The nature of pedestrian safety** 1

1.2. **Social responsibility** 1

1.2.1. National statistical trends 1

1.2.2. Detailed small case study statistics 4

1.3. **Directive pressure** 6

1.4. **The PhD research** 8

2. Literature Review 11

2.1. **Literature sources** 11

2.2. **Approaches to pedestrian safety research** 11

2.2.1. Pedestrian accident analysis 12

2.2.2. Human body characterisation 15

2.2.3. Vehicle characterisation 16

2.2.4. Sub-system testing 17

2.2.5. Pedestrian accident simulation 19

2.2.6. Vehicle design improvements 24

3. Research strategy 30

3.1. **Pedestrian protection technology methodology** 30

3.2. **Reference vehicle pedestrian accident simulations** 32

3.3. **Modified vehicle pedestrian accident simulations** 34

4. Reference vehicle pedestrian accident simulations 37

4.1. **Context in overall methodology** 37

4.2. **Software tools** 37

4.3. **Reference vehicle model 'p'** 41

4.3.1. Background 41

4.3.2. The construction of the vehicle model 42

4.3.3. Refinements to the vehicle model 67
4.4. **Pedestrian humanoid models** 69
4.4.1. Background 69
4.4.2. The construction of the humanoid models 71
4.4.3. Refinements to the humanoid model 72
4.5. **Pedestrian accident simulations with reference vehicle** 77
4.5.1. Methodology for pedestrian accident simulations 77
4.5.2. Results from pedestrian accident simulations 80
4.5.3. Discussion of results 101
4.5.4 Reference vehicle accident simulation conclusions 109
5. Pedestrian protection technology models 113
5.1. **Context in overall methodology** 113
5.2. **A review of pedestrian protection requirements** 113
5.3. **Design of Experiments (DoE)** 116
5.4. **Pedestrian protection headlamp (PAH)** 121
5.4.1. Biomechanical models of PAH 121
5.4.2. Description of PAH 128
5.4.3. Analytical models of PAH 129
5.4.4. Numerical headlamp evaluation model 130
5.5. **Pedestrian protection bumper system (POBSY)** 151
5.5.1. Biomechanical models of POBSY 151
5.5.2. Description of POBSY 156
5.5.3. Analytical models of POBSY 157
5.5.4. Numerical bumper evaluation model 161
5.6. **Pedestrian protection hood kinematic system (PEHKS)** 186
5.6.1. Biomechanical models of PEHKS 186
5.6.2. Description of mechanically deployed hood systems 188
5.6.3. Analytical models of mechanically deployed hood systems 192
5.6.4. Numerical hood evaluation model 198
6. Modified vehicle pedestrian accident simulations 199
6.1. **Context in overall methodology** 199
6.2. **Vehicle models 'd1' and 'd2'** 200
6.2.1. The construction of the vehicle models 200

6.2.2. The bumper undertray model..... 205
6.2.3. The bumper foam model..... 208
6.2.4. The headlamp model..... 212
6.2.5. The hood system model..... 213
6.3. **Pedestrian accident simulations with modified vehicles.** 214
6.3.1. Background..... 214
6.3.2. Methodology for comparing pedestrian accident simulations..... 214
6.3.3. Comparison of results from pedestrian accident simulations..... 215
6.3.4. Discussion of comparative results..... 232
6.3.5 Modified vehicle accident simulation conclusions..... 237
7. Experimental Testing of Pedestrian Safety Vehicle (PSV) **241**
7.1. **Context in overall methodology**..... 241
7.2. **The PSV's**..... 241
7.3. **Experimental testing of the PSV**..... 242
8. Summary and Conclusions 244
8.1. **A new systematic methodology**..... 244
8.2. **New pedestrian protection technologies and models**..... 245
8.3. **Improved understanding of pedestrian & vehicle interaction** 245
9. Recommendations..... **248**
9.1. **Technology and model improvements**..... 248
9.2. **Accident case study validation**..... 250
References..... **252**
Appendix A - Pedestrian accident forms for accident reconstruction..... 268
Appendix B - The software and hardware tools used..... 271
Appendix C - Master Series to LS-DYNA translation in N/CODE..... 272
Appendix D - Pre and post processing model quality guidelines..... 273
Appendix E - CAD & FE data sources for the reference vehicle model..... 274
Appendix F - Vehicle model moment of inertia calculations..... 277
Appendix G – Brief element theory and its role in hourglassing..... 278
Appendix H - Pedestrian accident simulation procedure..... 280
Appendix I - Calculating physical properties for hood analytical model..... 287
Appendix J - Original data vehicle 'p' pedestrian accident simulations..... 289

List of Figures

Figure 1.1 Pedestrian fatality trends 2
Figure 1.2 Pedestrian fatality and injury trends 2
Figure 1.3 Breakdown of road user fatalities by user group 3
Figure 1.4 Breakdown of road users injured by user group 4
Figure 1.5 Breakdown of injuries by age categories 5
Figure 1.6 Percentage of body regions attributed to injury levels 5
Figure 1.7 The context of the PhD research 9
Figure 2.1 A categorisation of pedestrian safety research approaches 12
Figure 2.2 One of the proposed pedestrian protection test procedures 18
Figure 2.3 A comparison of two simulation approaches 19
Figure 2.4 MADYMO and LS-DYNA approaches contrasted 21
Figure 2.5 A detailed MADYMO vehicle approach 22
Figure 2.6 A detailed MADYMO pedestrian approach 23
Figure 2.7 Headlamp patent DE 3728752 27
Figure 2.8 Bumper patent FR 2759655 28
Figure 2.9 Ford mechanically deployed hood systems 29
Figure 3.1 Pedestrian protection technology methodology (all tasks) 31
Figure 3.2 Four phase one enabling projects 33
Figure 3.3 Four phase two enabling projects 34
Figure 3.4 Overview of all project tasks and interrelationships 35
Figure 4.1 Pedestrian protection technology methodology (ref. vehicle) 37
Figure 4.2 The pre-processing, solving and post-processing methodology 38
Figure 4.3 An overview of the reference vehicle model 42
Figure 4.4 The vehicle rear end structure model 44
Figure 4.5 The main vehicle structure model 46
Figure 4.6 Parts connected to the rear end structure model 47
Figure 4.7 The elastic plastic behaviour of material 3 47
Figure 4.8 The actual radiator cooling pack and a simplified model 51
Figure 4.9 The high strength Steel parts 52
Figure 4.10 Component validation methodology 55
Figure 4.11 The validated vehicle component models 56
Figure 4.12 Elastic plastic behaviour of the GOR bake hardening steel 56

Figure 4.13 The hood hinge model 63
Figure 4.14 The hood latch model 64
Figure 4.15 Vehicle parts removed from the vehicle to vehicle contact 65
Figure 4.16 The pedestrian accident simulation boundary conditions 66
Figure 4.17 The refined radiator grille mesh 68
Figure 4.18 The first pedestrian humanoid model concept 69
Figure 4.19 The pedestrian humanoid model research vision 70
Figure 4.20 Simplified and detailed pedestrian accident simulation models 71
Figure 4.21 The reference pedestrian humanoid model 71
Figure 4.22 Observed problems with the pedestrian model 73
Figure 4.23 Excessive leg to leg contact penetration 74
Figure 4.24 The original and modified pelvis mesh geometry 75
Figure 4.25 The original and modified arm mesh geometry 75
Figure 4.26 Unrealistic pedestrian model motion 76
Figure 4.27 The pedestrian model stances 78
Figure 4.28 Some example pedestrian impact motions 81
Figure 4.29 All impact timing ranges at 25 km/h 83
Figure 4.30 All impact timing ranges at 40 km/h 84
Figure 4.31 50th percentile pedestrian CMD at 25, 30, 35, 40 km/h 85
Figure 4.32 All CMD ranges at 25 km/h 85
Figure 4.33 All CMD ranges at 40 km/h 86
Figure 4.34 50th percentile head trajectories at 25, 30, 35, 40 km/h 87
Figure 4.35 All head motion ranges at 25 km/h 87
Figure 4.36 All head motion ranges at 40 km/h 88
Figure 4.37 50th percentile relative head velocity at 25,30,35,40 km/h 89
Figure 4.38 All relative head velocity ranges at 25 km/h 89
Figure 4.39 All relative head velocity ranges at 40 km/h 90
Figure 4.40 50th percentile pedestrian HIC at 25, 30, 35, 40 km/h 91
Figure 4.41 All HIC ranges at 25 km/h 91
Figure 4.42 All HIC ranges at 40 km/h 92
Figure 4.43 50th percentile pelvis acceleration at 25,30,35,40 km/h 93
Figure 4.44 All pelvis acceleration ranges at 25 km/h 93
Figure 4.45 All pelvis acceleration ranges at 40 km/h 94

Figure 4.46 50th percentile pedestrian knee shear at 25, 30, 35, 40 km/h 95
Figure 4.47 All knee shear ranges at 25 km/h 95
Figure 4.48 All knee shear ranges at 40 km/h 96
Figure 4.49 50th percentile knee bending at 25, 30, 35, 40 km/h 97
Figure 4.50 All knee bending ranges at 25 km/h 97
Figure 4.51 All knee bending ranges at 40 km/h 98
Figure 4.52 50th percentile tibia acceleration at 25,30,35,40 km/h 99
Figure 4.53 All tibia acceleration ranges at 25 km/h 99
Figure 4.54 All tibia acceleration ranges at 40 km/h 100
Figure 4.55 All first tibia and femur fracture locations 101
Figure 4.56 All relative head velocity and impact timing ranges at 25 km/h 105
Figure 4.57 All relative head velocity and impact timing ranges at 40 km/h 105
Figure 5.1 Pedestrian protection technology methodology (technologies) 113
Figure 5.2 An example of an orthogonal two level design array 117
Figure 5.3 Classes of experimental design 118
Figure 5.4 A response surface for three factors 119
Figure 5.5 Types of response surface designs 119
Figure 5.6 A central composite design for three factors 120
Figure 5.7 Adult and child headlamp impact 122
Figure 5.8 The adult femur and surrounding muscles 123
Figure 5.9 Conceptual view of the adult femur loading condition 123
Figure 5.10 Non-comminuted femur fractures 124
Figure 5.11 The adult male pelvis 125
Figure 5.12 Conceptual view of child pelvis and abdomen loading 126
Figure 5.13 Envisaged deformation of PAH 128
Figure 5.14 Various headlamp designs to achieve desired deformation 129
Figure 5.15 Analytical models for strut and plate buckling 130
Figure 5.16 One of the headlamp evaluation models 131
Figure 5.17 The headlamp models 134
Figure 5.18 Headlamp evaluation model contacts 135
Figure 5.19 Headlamp evaluation model problems 136
Figure 5.20 Headlamp evaluation model problem & solution 137
Figure 5.21 Excessive buckling of the headlamp model body 137

Figure 5.22 Interpretation of EEVC 1998 upper leg impactor energy limits 139
Figure 5.23 Interpretation of EEVC 1998 upper leg impactor velocity 139
Figure 5.24 Interpretation of EEVC 1998 upper leg impactor impact angle 140
Figure 5.25 Headlamp evaluation model DoE factors and factor levels 141
Figure 5.26 Headlamp evaluation model force responses 144
Figure 5.27 Headlamp evaluation model moment responses 144
Figure 5.28 Headlamp evaluation model force and moment rankings 144
Figure 5.29 Pareto chart for the sum of the forces 146
Figure 5.30 Main effects graph for the sum of the forces 147
Figure 5.31 Interaction effects graph for the sum of the forces 148
Figure 5.32 Standardised effect for the maximum bending moment 148
Figure 5.33 Main effects graph for the maximum bending moment 149
Figure 5.34 Interaction effects graph for the maximum bending moment 150
Figure 5.35 Adult and child bumper impact 152
Figure 5.36 The adult tibia and fibula and surrounding muscles 153
Figure 5.37 The adult knee joint 153
Figure 5.38 Conceptual view of the adult knee and lower leg loading 154
Figure 5.39 Various pedestrian knee injury mechanisms 155
Figure 5.40 The adult knee shear injury mechanism 155
Figure 5.41 The main objective of the bumper technology 156
Figure 5.42 Some bumper designs to achieve the desired loading 156
Figure 5.43 An overview of POBSY 157
Figure 5.44 First level of model construction 158
Figure 5.45 Second level of model construction 159
Figure 5.46 The boundary conditions for the upper leg motion 160
Figure 5.47 The boundary conditions for the lower leg motion 160
Figure 5.48 Leg impactor knee bending moment characteristics 161
Figure 5.49 Numerical bumper evaluation model 163
Figure 5.50 Bumper foam material properties 164
Figure 5.51 Bumper evaluation model contacts 165
Figure 5.52 Different bumper mesh geometries used in screening study 167
Figure 5.53 Bumper evaluation model factors and factor levels 168
Figure 5.54 The bumper mesh geometry's used in the DoE study 169

Figure 5.55 Bumper evaluation model tibia acceleration 170
Figure 5.56 Bumper evaluation model knee bending angle 171
Figure 5.57 Bumper evaluation model knee shear displacement 171
Figure 5.58 Bumper evaluation model response rankings 171
Figure 5.59 Bumper evaluation model tibia acceleration 173
Figure 5.60 Bumper evaluation model knee bending angle 173
Figure 5.61 Bumper evaluation model knee shear displacement 173
Figure 5.62 Numerical bumper model total rank responses 174
Figure 5.63 Numerical bumper model partial rank responses 174
Figure 5.64 Pareto chart for tibia acceleration 179
Figure 5.65 Main effects graph for tibia acceleration 180
Figure 5.66 Interaction effects graph for tibia acceleration 180
Figure 5.67 Pareto chart for the bending angle 181
Figure 5.68 Main effects graph for bending angle 182
Figure 5.69 Pareto chart for the shear displacement 182
Figure 5.70 Main effects graph for shear displacement 183
Figure 5.71 Interaction effects graph for shear displacement 183
Figure 5.72 Adult and child hood impacts 186
Figure 5.73 Conceptual view of the adult head loading condition 187
Figure 5.74 Conventional and mechanically deployed hood 189
Figure 5.75 CAD model of the PP hood module device 190
Figure 5.76 GOR motion in an upper leg impactor simulation 191
Figure 5.77 An overview of PEHKS 191
Figure 5.78 Undeployed and deployed positions of the front module 192
Figure 5.79 Undeployed and deployed positions of the hinge 193
Figure 5.80 First level of model construction 193
Figure 5.81 Second level of model construction 194
Figure 5.82 Determining the value of 'r' 196
Figure 5.83 The location of the hood at time t=0 and t=t1 197
Figure 5.84 Absolute hood displacement in global coordinates 198
Figure 6.1 Pedestrian protection technology methodology (mod. vehicle) 199
Figure 6.2 Matched component stiffness to support the pedestrian legs 200
Figure 6.3 The modified parts in vehicle model 'd1' 201

Figure 6.4 The modified parts in vehicle model 'd2' 201
Figure 6.5 Parts removed from the automatic single surface contact 202
Figure 6.6 Parts and nodes in the second vehicle to vehicle contact 202
Figure 6.7 Parts removed from the automatic single surface contact 204
Figure 6.8 Parts included in the second vehicle to vehicle contact 204
Figure 6.9 The main development stages of the undertray model 206
Figure 6.10 The deformation behaviour of second stage undertray model 207
Figure 6.11 The deformation behaviour of the final undertray model 207
Figure 6.12 The final undertray model 208
Figure 6.13 The pedestrian protection bumper foam model 209
Figure 6.14 The modified beam and longitudinals parts 209
Figure 6.15 The material model used for polyurethane foam 209
Figure 6.16 Standard and modified headlamp models 212
Figure 6.17 The hood technology joint models 213
Figure 6.18 50th percentile accident simulations with vehicles 'p', 'd1', 'd2' 216
Figure 6.19 6 year old accident simulations with vehicles 'p', 'd1', 'd2' 217
Figure 6.20 Detailed 50th percentile simulations with vehicles 'p' and 'd1' 219
Figure 6.21 Comparison of impact timing ranges and values at 25 km/h 220
Figure 6.22 Comparison of impact timing ranges and values at 40 km/h 221
Figure 6.23 Comparison of CMD ranges and values at 25 km/h 222
Figure 6.24 Comparison of CMD ranges and values at 40 km/h 222
Figure 6.25 Comparison of head motion ranges & trajectories at 25 km/h 223
Figure 6.26 Comparison of head motion ranges & trajectories at 40 km/h 223
Figure 6.27 Comparison of head velocity ranges and values at 25 km/h 224
Figure 6.28 Comparison of head velocity ranges and values at 40 km/h 225
Figure 6.29 Comparison of HIC ranges and values at 25 km/h 225
Figure 6.30 Comparison of HIC ranges and values at 40 km/h 226
Figure 6.31 Comparison of pelvis acceleration ranges and values 25 km/h 227
Figure 6.32 Comparison of pelvis acceleration ranges and values 40 km/h 227
Figure 6.33 Comparison of knee shear ranges and values at 25 km/h 228
Figure 6.34 Comparison of knee shear ranges and values at 40 km/h 229
Figure 6.35 Comparison of knee bending ranges and values at 25 km/h 229
Figure 6.36 Comparison of knee bending ranges and values at 40 km/h 230

Figure 6.37 Comparison of tibia acceleration ranges and values 25 km/h 231
Figure 6.38 Comparison of tibia acceleration ranges and values 40 km/h 231
Figure 7.1 Pedestrian protection technology methodology (PSV) 241
Figure 7.2 The pedestrian protection technology demonstration vehicle 242
Figure A.1 All vehicle impact event timing at 25 km/h 289
Figure A.2 All vehicle impact event timing at 40 km/h 289
Figure A.3 All CMD values for vehicle at 25 km/h 290
Figure A.4 All CMD values for vehicle at 40 km/h 290
Figure A.5 All vehicle relative head trajectories at 25 km/h 291
Figure A.6 All vehicle relative head trajectories at 40 km/h 291
Figure A.7 All head velocities relative to hood leading edge at 25km/h 292
Figure A.8 All head velocities relative to hood leading edge at 40km/h 292
Figure A.9 50th percentile head acceleration at 25, 30, 35, 40 km/h 293
Figure A.10 All HIC values for vehicle at 25 km/h 293
Figure A.11 All HIC values for vehicle at 40 km/h 294
Figure A.12 All pelvis acceleration values for vehicle at 25 km/h 294
Figure A.13 All pelvis acceleration values for vehicle at 40 km/h 295
Figure A.14 50th percentile knee shear time histories 295
Figure A.15 All knee shear values for vehicle at 25 km/h 296
Figure A.16 All knee shear values for vehicle at 40 km/h 296
Figure A.17 50th percentile knee bending time histories 297
Figure A.18 All knee bending values for vehicle at 25 km/h 297
Figure A.19 All knee bending values for vehicle at 40 km/h 298
Figure A.20 All tibia acceleration values for vehicle at 25 km/h 298
Figure A.21 All tibia acceleration values for vehicle at 40 km/h 299

List of Tables

Table 2.1 General design and technology improvements 24
Table 2.2 Pedestrian protection bumper, headlamp and hood patents 26
Table 3.1 The PhD research timing plan 36
Table 4.1 Rigid material card for the vehicle rear end structure 45
Table 4.2 Part inertia card for the vehicle rigid rear end structure 45
Table 4.3 RADIOSS & LS-DYNA material cards for mild steel (SAE 1010) 48
Table 4.4 RADIOSS & LS-DYNA material cards for ABS 48
Table 4.5 RADIOSS & LS-DYNA material cards for the windscreen 49
Table 4.6 RADIOSS & LS-DYNA material cards for polypropylene 50
Table 4.7 RADIOSS & LS-DYNA material cards for the plenum chamber 50
Table 4.8 RADIOSS & LS-DYNA material cards for the cooling pack 51
Table 4.9 Material card for the cooling pack rubber mounts 51
Table 4.10 Material card for dummy high strength parts 52
Table 4.11 RADIOSS and LS-DYNA material cards for high strength steel 53
Table 4.12 RADIOSS and LS-DYNA material cards for the ABS undertray 53
Table 4.13 Material card for the ground 54
Table 4.14 Material card for general rigid parts 54
Table 4.15 Material card for the GOR bake hardening steel 57
Table 4.16 Material card for the GOR BAYER PA6 polymer 57
Table 4.17 Material card for the headlamp polycarbonate 58
Table 4.18 Material card for the headlamp polypropylene 58
Table 4.19 Material card for the bumper polypropylene 59
Table 4.20 Material card for air filter box polypropylene 59
Table 4.21 Material card for the intercooler pipe steel 60
Table 4.22 Section card for all solids 60
Table 4.23 An example of a section card for shells 60
Table 4.24 RADIOSS and LS_DYNA material cards windscreen adhesive 61
Table 4.25 Material card for hood adhesive 61
Table 4.26 Discrete element card for all springs 61
Table 4.27 Section discrete card for all springs 62
Table 4.28 Spot weld cards 62
Table 4.29 Revolute joint card for the hood hinges 63

Table 4.30 Contact and part set cards for all vehicle to vehicle contacts 65
Table 4.31 Global load and define curve cards for gravity 66
Table 4.32 Prescribed motion and curve cards for the vehicle rear end 67
Table 4.33 Initial velocity card for the vehicle front end 67
Table 4.34 Pedestrian accident simulation parameters 77
Table 4.35 Pedestrian accident simulation matrix for reference vehicle 79
Table 4.36 All impact timing ranges 84
Table 5.1 A prioritisation of pedestrian and vehicle impact regions 114
Table 5.2 LS-DYNA material card for the vehicle simulator base 132
Table 5.3 LS-DYNA joint card for the hood and bumper mounting 132
Table 5.4 LS-DYNA spring card for the hood and bumper mounting 132
Table 5.5 LS-DYNA define curve cards for the bumper & hood springs 133
Table 5.6 LS-DYNA material card for the bumper and hood 133
Table 5.7 LS-DYNA global load card and define curve card for gravity 138
Table 5.8 Vehicle geometry and impactor configurations 140
Table 5.9 DoE responses and objective criteria 142
Table 5.10 Headlamp evaluation model DoE study results 143
Table 5.11 Headlamp evaluation model overall rankings 145
Table 5.12 Headlamp evaluation model optimum levels 150
Table 5.13 LS-DYNA material card for reference bumper foam 164
Table 5.14 LS-DYNA material card for reference undertray 165
Table 5.15 Automatic nodes to surface contact upper leg to foam nodes 166
Table 5.16 DoE responses and objective criteria 169
Table 5.17 Screening study results 170
Table 5.18 Numerical bumper model detailed study DoE array 172
Table 5.29 Bumper evaluation model optimum levels 184
Table 6.1 Automatic single surface contact and part set cards 203
Table 6.2 Automatic nodes to surface contact, node and part set cards 203
Table 6.3 Automatic single surface contact and part set cards 205
Table 6.4 Automatic nodes to surface contact, node and part set cards 205
Table 6.5 Material card for the ABS pedestrian protection undertray 208
Table 6.6 Material card for lower density polyurethane foam 210
Table 6.7 Material card for higher density polyurethane foam 211

Table 6.8 Material card for the modified bumper beam 212
Table 6.9 Joint cards for the hood technology 214
Table 6.10 Pedestrian accident simulation matrix vehicle models 'd1', 'd2' 215
Table 6.11 Impact timing differences of reference and modified vehicle 220
Table 7.1 The reference vehicle and PSV lower leg impactor test results 243
Table 7.2 The reference vehicle and PSV upper leg impactor test results 243
Table 9.1 The recommended accident conditions and measures 250
Table 9.2 Questions and search criteria to be addressed by case studies 251

Notation

g	Gravitational acceleration constant	9.81 m/s^2
a, b, l	Length	m
A	Area	m^2
d	Thickness	m
I	Second moment of area	m^4
m	Mass	Kg
ν	Poissons ratio	-
σ	True stress	N/m^2
ε	True strain	-
E	Youngs Modulus	N/m^2
u	Initial translational velocity	m/s
v	Final translational velocity	m/s
F	Force	N
θ, α	Angle	Radians
w	Initial angular velocity	Radians/s
ω	Final angular velocity	Radians/s
J	Polar mass moment of inertia	Kgm^2
c	Damping coefficient	Ns/m
k	Linear spring stiffness	N/m
T	Torque	Nm
S	Energy	J
t	Time	s

Common Abbreviations

FFA	Ford Forschungszentrum Aachen
CIC	Cranfield Impact Centre
fka	forschungsgesellschaft kraftfahrwesen aachen
EU	European Union
EEC	European Economic Community
NHTSA	National Highway Traffic Safety Administration
JARI	Japan Automobile Research Institute
ISO	International Standards Organisation
EEVC	European Enhanced Vehicle Safety Committee
TRL	Transport Research Laboratory
ACEA	Association des Constructeurs Europeans d'Automobiles
TNO	Toegepast Natuurwentenscapppelijk Ondersek
INRETS	Institut National de Recherche sur les Transports et Leur Sécurité
BAST	Bundesanstalt für Straßenwesen
NCAP	New Car Assessment Program
EurNCAP	European New Car Assessment Program
EUCAR	European Car Program
MADYMO	Mathematical Dynamic Models
CAE	Computer Aided Engineering
CAD	Computer Aided Design
CAM	Computer Aided Manufacturing
DoE	Design of Experiments
CMD	Composite Maximum Displacement
HIC	Head injury criteria
AIS	Abbreviated Injury Scale
PAH	Pedestrian Protection Headlamp
POBSY	Pedestrian Protection Bumper System
PEHKS	Pedestrian Protection Hood Kinematic System

1. Introduction

1.1. The nature of pedestrian safety

Pedestrian safety is an important societal issue. As a societal issue the largest improvements in pedestrian protection can only be achieved by the contribution of many stakeholders to reduce the number of pedestrian fatalities and injuries. Many factors affect pedestrian safety and each stakeholder in society has a limited area of influence in which he/she can provide pedestrian protection solutions. For example, vehicle manufacturers can directly influence vehicle design but have limited and indirect influence on the development of safer public transport infrastructures. The research described in this thesis was initiated as part of the Ford Motor Company's contribution to improve the understanding of the pedestrian safety issue and hence improve the opportunity to improve pedestrian protection. There are two main pressures on vehicle manufacturers to undertake pedestrian protection research: social responsibility and directive pressure.

1.2. Social responsibility

1.2.1. National statistical trends

The most obvious measure of pedestrian safety as a social issue is the number of pedestrian fatalities per year in various countries and regions as shown in Figure 1.1 [OECD 1999]. The countries and regions are chosen according to their economic importance and the availability of reliable, consistent data.

It is interesting to note that 20 years ago there were almost twice as many fatalities in Europe as compared to USA but now the figures are comparable. The downward fatality trend in the EU has been dramatic and this is clearly reflected in the UK and German figures. However, Japan does not have a clear downward trend except possibly in recent years. There are many influencing factors and stakeholder actions behind these figures such as the pedestrian exposure level (e.g. in the USA the proportion of pedestrians is smaller). In general, these figures indicate that the number of pedestrian fatalities is decreasing but is still unacceptably high.

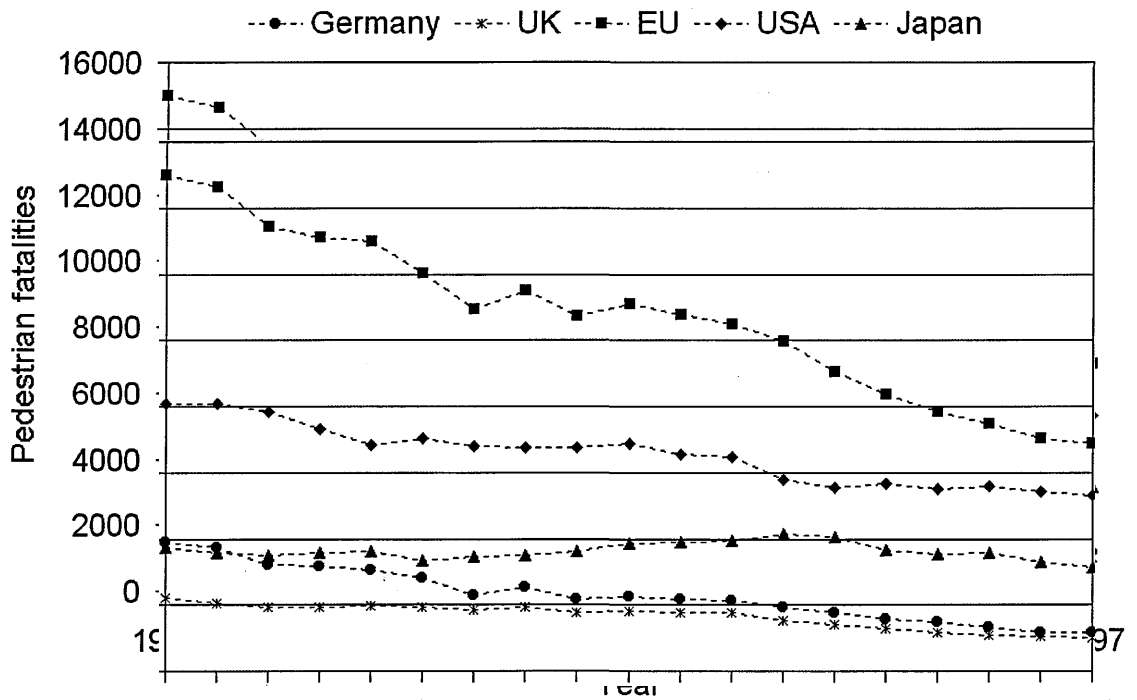

Figure 1.1 Pedestrian fatality trends

Figure 1.2 [OECD 1997, NHTSA 1997] shows the downward trend in fatalities and injuries. Although the trends are similar, these data gives a more complete picture of the problem and the large number of pedestrians involved in accidents.

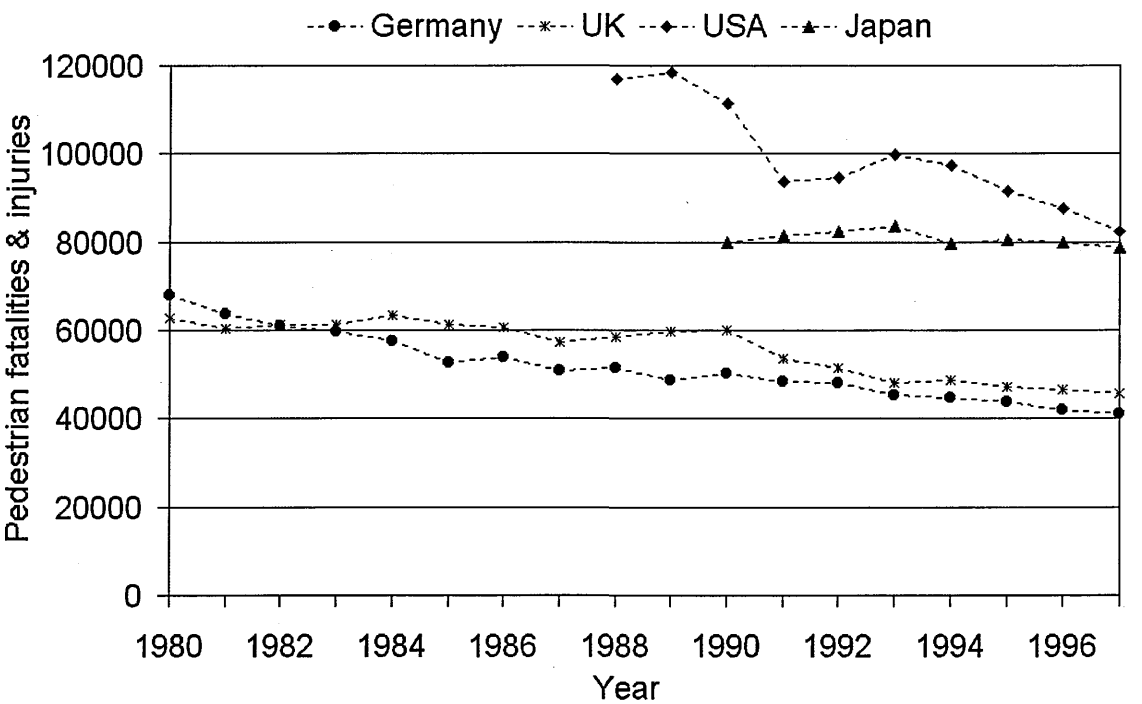

Figure 1.2 Pedestrian fatality and injury trends

Pedestrians form one of the road user groups and it is useful to identify what proportion of all road user group fatalities and injuries pedestrians represent. Figure 1.3 shows a breakdown of the road user fatalities by road user group [OECD 1997].

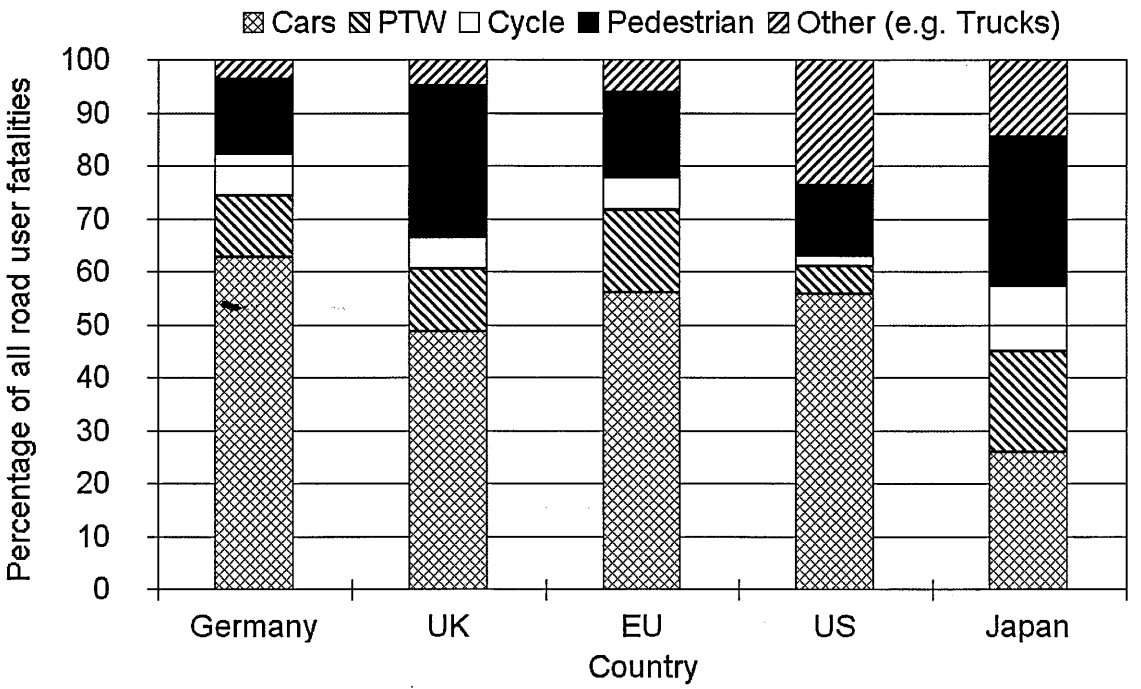

Figure 1.3 Breakdown of road user fatalities by user group

With the exception of Japan, there are more fatalities in the car occupant group than in any other road user group. In the EU as a whole, the pedestrians form the second largest road user fatality group and this is also reflected in the UK and Germany but not in the USA. In Japan, the pedestrian group is the largest fatality group by a large margin. It can be concluded that pedestrians are a major road user fatality group, particularly in Japan but also in Europe.

If one considers road user group injuries, as shown in Figure 1.4, another perspective on the pedestrian safety issue emerges [OECD 1997]. As with the road user group fatalities, car occupants dominate the road user group injuries. However, the pedestrian group is less significant. The most important conclusion from this is that pedestrians are a vulnerable road user group because the relative proportion of pedestrian fatalities is higher and this is particularly clear in the Japanese data.

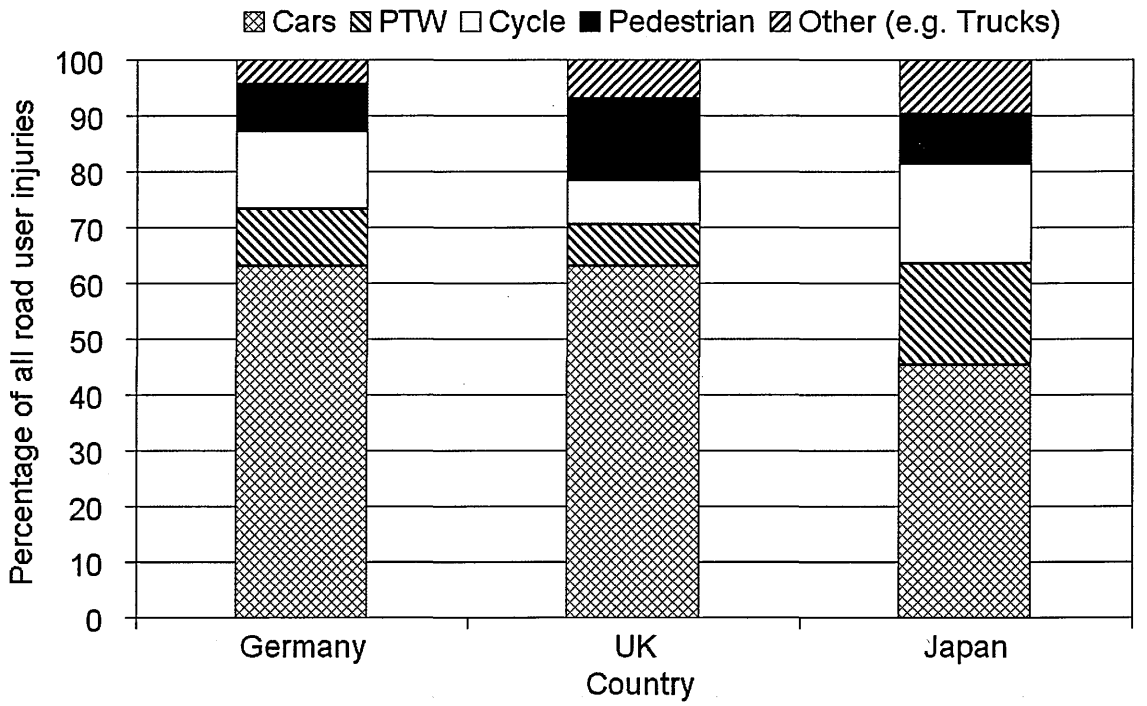

Figure 1.4 Breakdown of road users injured by user group

1.2.2. Detailed small case study statistics

Having considered population data, it is useful to analyse small sample studies. These studies describe specific accident cases and provide a more detailed analysis of pedestrian accidents. Only recent samples should be used because car population designs are changing over time and this has a significant influence on the distribution of pedestrian injuries [Foret Bruno 1998]. Small sample data may be presented in many ways and the next two figures show just two examples from a small (262 cases), recent (1996/7) German sample.

Figure 1.5 shows the fatalities and injury levels in various age groups [Metzler-Poeschel 1998]. The most interesting feature of the data is the trend towards a higher proportion of fatalities in older pedestrian groups and a higher proportion of serious injuries in younger groups. This indicates the importance of targeting specific pedestrian groups with pedestrian safety solutions. It also provides a complex dilemma for vehicle manufacturers who must meet the needs of all pedestrians despite the wide differences with respect to, for instance, age (e.g. injury susceptibility), size and weight.

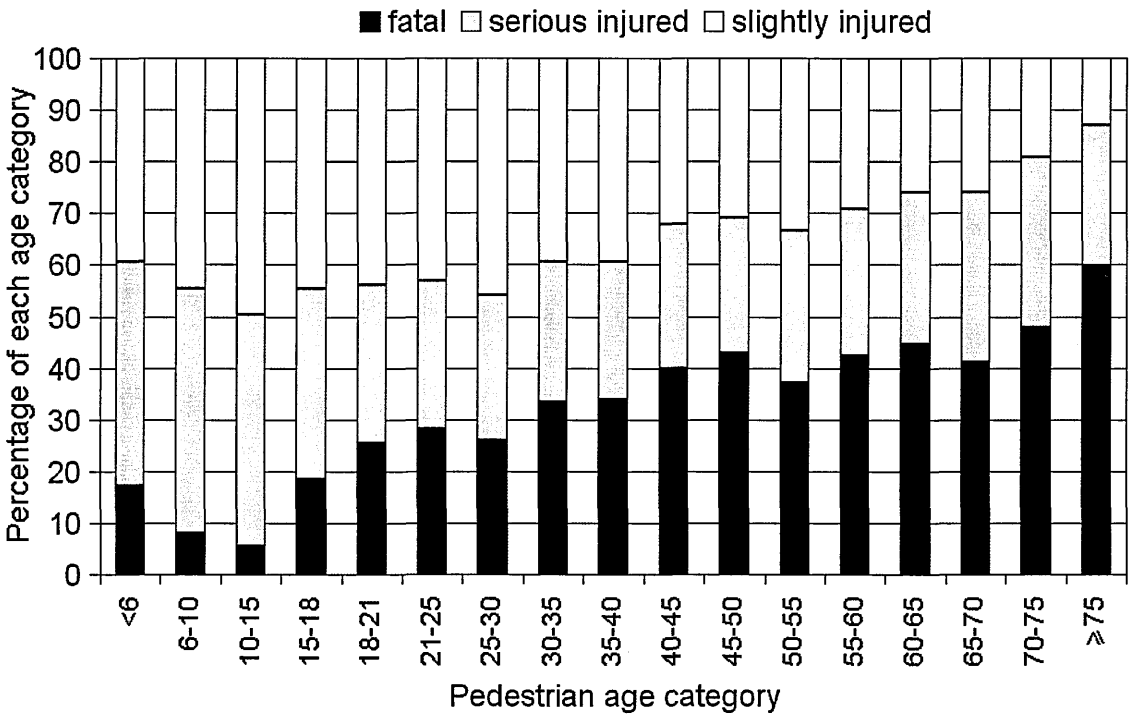

Figure 1.5 Breakdown of injuries by age categories

If the same sample data are broken down by injury severity, as measured by the Abbreviated Injury Scale (AIS), for each body region, Figure 1.6 is obtained [Ford 1998]. Although not shown, ISS (Injury severity score based on the square root of the AIS values squared) may be used to indicate overall severity [Trauma 2002].

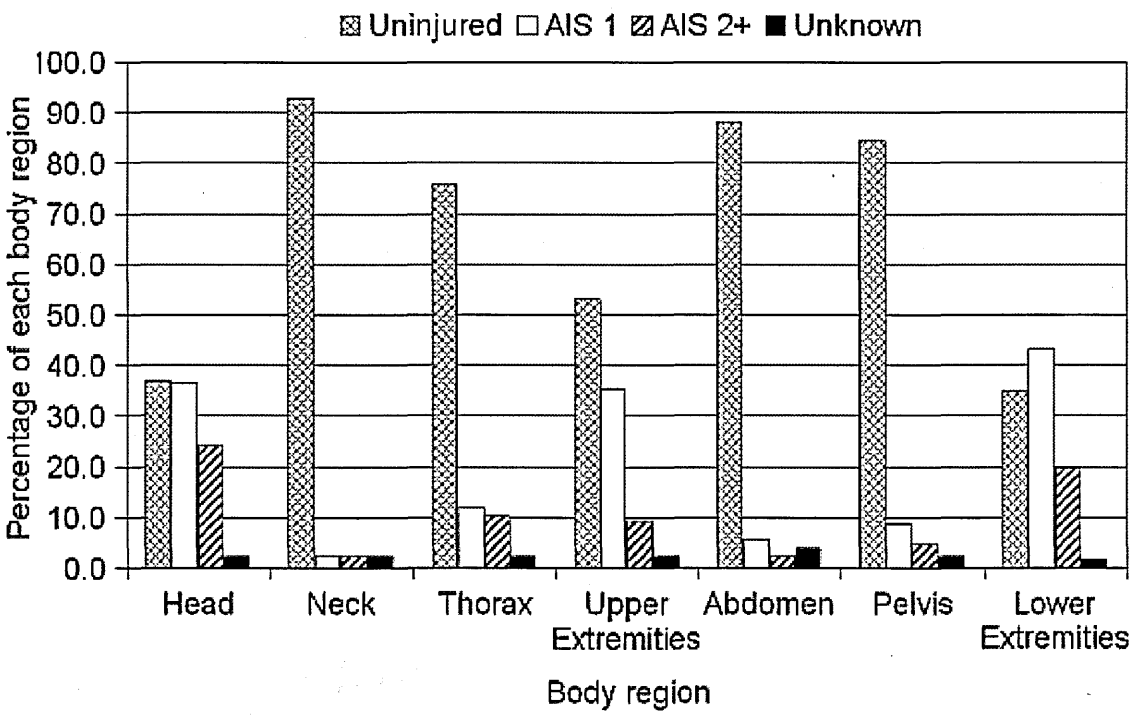

Figure 1.6 Percentage of body regions attributed to injury levels

In general, the data appear to indicate that the neck, thorax, abdomen and pelvis receive relatively minor injuries whereas the head, upper extremities and lower extremities represent more significant injury groups. This information is important to vehicle manufacturers because in conjunction with an understanding of pedestrian impact kinematics and dynamics, it provides a clue as to which parts of a vehicle may be redesigned to improve pedestrian protection. Further studies are described in a number of additional references that were undertaken in Germany [Otte 1991, 1999, Koch 2001] and the USA [Isenburg 1998, Jarrett 1998].

1.3. Directive pressure

In the past, potential directive test procedures were being developed in the USA, Europe and Japan. During recent years little has been published in the USA by the National Highway Transportation Safety Administration (NHTSA) [Laughlin 1990] but an increasing amount is being published by the Japan Automobile Research Institute (JARI) [Sakurai 1994] on the development of an International Standards Organisation (ISO) test procedure. However, the vast majority of research has been undertaken with the European Enhanced Vehicle Safety Committee (EEVC) test proposal, and historically, this was of the most interest to vehicle manufacturers because it existed as a draft directive proposal [EEVC 1998].

During the early 1980's the EEVC identified that there was a large proportion of pedestrians and cyclists being injured or killed by impacts involving the front of passenger cars. Having recognised a societal issue, the EEVC initiated several working group studies in the field of pedestrian safety. Based on these studies various recommendations for the front structure of passenger cars were developed and test methods to assess pedestrian protection [EEVC 1982, 1985]. In 1987 a European Economic Community (EEC) ad-hoc working group 'ERGA Safety' studied the original test proposal and it was concluded that the basis of the proposal was promising but additional research was needed [CEC 1984]. The EEVC was asked to co-ordinate this research and at the end of 1987, Working Group 10 'Pedestrian Protection' was set up to co-ordinate the development of a sub systems vehicle test procedure. The studies necessary to develop the test methods were summarised in the first EEVC working group 10 report [EEVC 1989].

Since the first research was undertaken the original test procedure has been developed with inputs from various stakeholders, including vehicle manufacturers and research institutes [Harris 1991, Matsui 1998, Cesari 1991, Zellmer 1994, Otubushin 1998]. In more recent years there has been a larger amount of discussion with vehicle manufacturers over the effectiveness and validity of the test procedure. In this respect the Transport Research Laboratory (TRL) which is based in the UK produced an extensive costs and benefits analysis report [Lawrence 1993] to support the introduction of a test procedure. On the other side the Association des Constructeurs Europeans d'Automobiles (ACEA), who represent the European vehicle manufacturers produced a counter costs and benefits analysis presentation [ACEA 1992] with different costs and benefits conclusions.

TRL argued that pedestrian fatalities and injuries were a major societal issue and passenger cars were the main cause of this [Lawrence 1993]. In 1992 there were approximately 10,000 pedestrian fatalities and 90,000 seriously injured pedestrians in the European community. 60% of these casualties were struck by the front of passenger cars. An independent contractor was consulted to estimate the extra cost per vehicle of the design changes that they considered necessary to meet the proposed test requirements. The changes included a lighter, taller and lower mounted foam bumper, a weaker hood leading edge, more under hood clearance and weaker fender edges, hinge area and scuttle (the region between and below the rear hood edge and the windscreen). It was estimated that the cost per car would be less than £10 (at 1991 prices) and by multiplying this by a prediction of the number of new vehicles the total cost of the changes was derived. Concerning the benefits, these were estimated from the reduction in the societal costs of fatalities and serious injuries (e.g. hospital costs). The calculations made allowance for the fact that the proposal only addressed passenger car fronts, impact speeds below 40 km/h, and areas of the car that were covered by the proposal. The 40 km/h limit was based on studies such as [Ashton 1979] and [Harris 1985] that indicate this is an impact speed at which effective car design improvements are both feasible, from a vehicle manufacturer's perspective, and can lead to a significant reduction in pedestrian fatalities and injuries.

Car manufacturers, through ACEA, argued that the proposed draft directive was not acceptable for a number of reasons [ACEA 1992]. They argued that there was a long term reducing trend in pedestrian fatalities due to the efforts of the industry and that the contribution of passenger cars to pedestrian accidents was overestimated. The percentage of pedestrians in all road user group fatalities had decreased and there was a dramatic decline in the percentage of pedestrians killed in all passenger car accidents. This was despite the fact that the exposure of pedestrians to passenger cars had increased by all measures (e.g. miles travelled or the percentage of passenger cars in the road user fleet). In addition, there were some parameters such as vehicle speed or secondary impacts of the pedestrian with the ground that could not be easily controlled with vehicle design changes. The directive would have only addressed a small percentage of real world accidents, for example, within the test speed range and with a new vehicle that meets the requirements (i.e. a relatively small percentage of the car population). In addition, the procedure was not finalised when the costs and benefits study was undertaken.

Due to all these factors ACEA argued that the directive was not cost effective because the cost of car modifications would exceed any societal benefit and the design modifications would compromise other requirements (e.g. fuel economy due to a raised hood design). They concluded by stating that it would be more cost effective for governments to address other major causes of death like tobacco smoking and traffic management (e.g. crossings, education and speed limits).

At the end of 1998, Working Group 17 (a new pedestrian safety group) submitted a draft directive proposal [EEVC 1998] to the European parliament. In the first half of 2000 the parliament decided to delay their decision concerning the acceptance, partial acceptance or rejection of the proposal until the car industry provided its own set of recommendations. Discussions are ongoing and one of the proposed test procedures is described in a later chapter.

1.4. The PhD research

The context of the research can be considered at three levels as shown in Figure 1.7: the macro environment, the micro environment and the organisation.

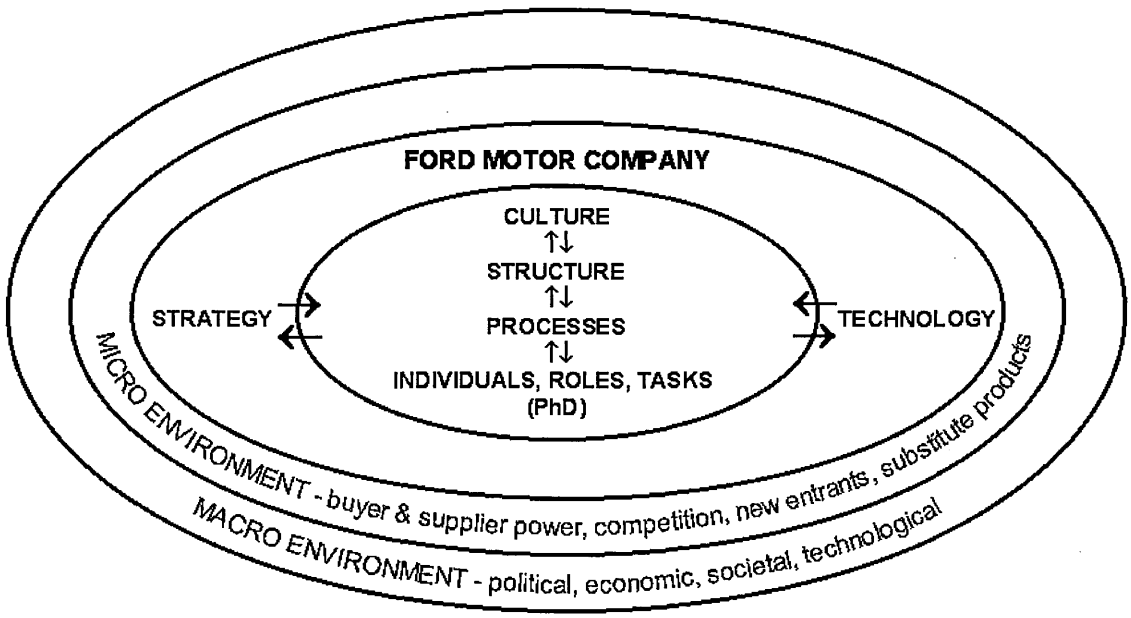

Figure 1.7 The context of the PhD research

At the *macro environment* level Ford is one of the largest companies in the world. It employs a large number of people and has a significant impact on the economy of every country in which it operates. As such, it is a significant stakeholder in society and the many issues it faces. The European parliament may be viewed as another stakeholder that has been empowered by society to address these issues by various means, including European legislation. Of particular interest in the context of pedestrian safety is their stated aim to reduce traffic injuries and deaths in Europe by for instance, introducing a pedestrian protection directive. Meanwhile Ford has publicly stated that it is committed to corporate citizenship, preserving the environment for future generations, and improving the society in which we live [Camp 1999]. At the same time rapid changes in the technological environment are opening up new opportunities to use computer simulations to develop vehicle design solutions.

At the *micro environment* level and over the past thirty years, the vehicle industry has been transformed with take-overs, mergers, and the appearance of a few dominant manufacturers. The bargaining power of car buyers has greatly increased because of industry over capacity and margins have become smaller. These pressures have been passed on to suppliers who have transformed in a manner similar to manufacturers with the emergence of a few dominant suppliers. The

remaining manufacturers and suppliers are now building their future on the development of networks of relationships whilst trying to differentiate their products and their companies in order to prosper in a much more competitive industry.

The *Ford Motor Company* is a large multinational vehicle manufacturer, with a bureaucratic structure (i.e. hierarchical and administrative) and a matrix overlay (i.e. multiple reporting responsibility) that ties many of the departments and divisions together by vehicle type. Ford's public position on the pedestrian safety issue has often been presented [Camp 1999] and the importance of pedestrian safety is acknowledged. It is working with many industry groups (e.g. ACEA) to gain a better understanding of the pedestrian safety issue and how it might be best addressed.

The research being undertaken by the Ford Forschungszentrum Aachen (FFA) exists in the context of these environments. It is based in a building remote from the main Ford site in Germany, has a flatter organisation structure and closer ties to a network of universities and related institutes than many other Ford sites. There are three main FFA strategies. These are to provide new technologies and processes, participate in beneficial European R&D projects with universities and institutes and provide outstanding personnel. Until 2001 the FFA was addressing pedestrian safety and the PhD research covered a large number of these activities.

The PhD *objectives* were to:

- Create non-linear finite element models and methodologies to study the interaction between pedestrians and vehicles during pedestrian accidents
- Apply the models and understanding to design, develop and evaluate a number of pedestrian protection technologies.

In choosing such objectives several challenges became apparent. The scope of the research was very large. As a consequence of this it was necessary to sub contract some of the tasks in order to complete the research within a realistic timescale. After a review of different approaches to pedestrian safety research in the next chapter, the chosen strategy is described in more detail.

2. Literature Review

2.1. Literature sources

The chosen approach to pedestrian safety research was identified with a review of the literature. This revealed the scope of pedestrian safety as a research topic and helped to position the research in this context. There was access to many literature sources and references:

1. Two technical paper libraries focusing on all aspects of pedestrian safety research, one of which had been collected over a period of 12 years
2. Annual report reference lists created in each research project
3. Pedestrian protection technical papers, internal reports and joint research reports regularly circulated within Ford
4. The Ford RLIS general research library
5. Various internet sites, including patent offices and national safety institutes [Patent offices 2002]
6. A general Ford pedestrian safety research database created in Microsoft Access that summarised all pedestrian safety research information available in Ford (including all of the above)

2.2. Approaches to pedestrian safety research

For more than thirty years there have been various approaches to pedestrian safety research. These approaches have included experimental accident simulation, computer accident simulation, on the scene pedestrian accident analysis and the experimental testing of cadavers to determine the mechanical properties of various parts of the body. A new conceptual framework was presented in a lecture entitled "Pedestrian Safety Research – Past, Present, Future" [Howard 1998-1] to categorise different approaches to pedestrian safety research. This framework was later developed into the one shown in Figure 2.1 [Howard 2000-3] and this provides a convenient means by which to examine the different types of research approaches. Each of these approaches will be examined in turn.

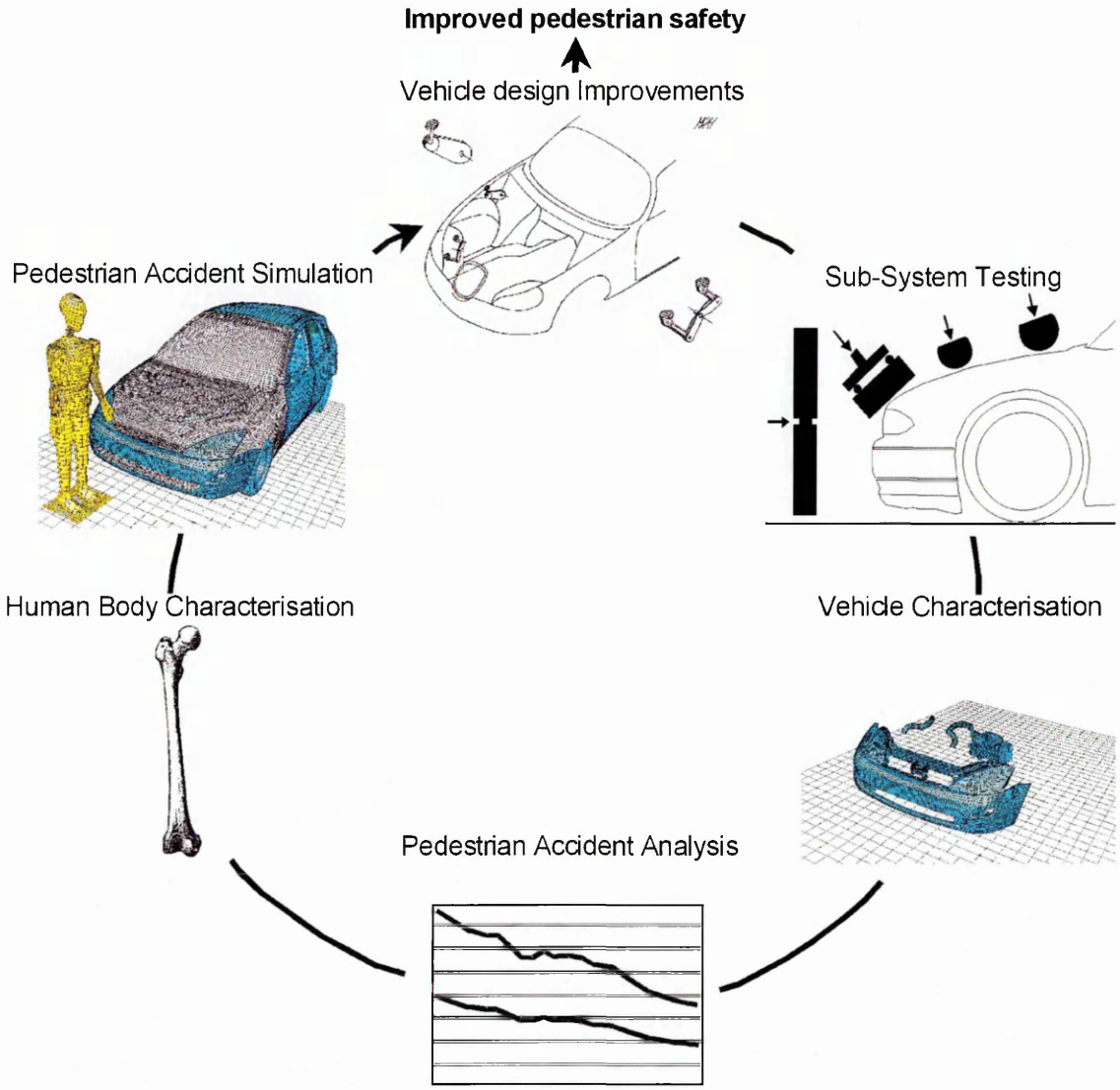

Figure 2.1 A categorisation of pedestrian safety research approaches

2.2.1. Pedestrian accident analysis

In essence, accident analysis is the force behind, and is a measure of, the effectiveness of pedestrian safety research in improving pedestrian safety. Stakeholders in pedestrian safety research (e.g. governments) are often called upon to quote accident statistics to support a particular point of view and therefore there is an extremely large quantity of literature in this field. Pedestrian accident analysis can be essentially broken down into two fields: large population studies (e.g. national statistics) and smaller (but more detailed) regional or sample studies.

Most European community countries (e.g. UK and Germany), the USA and Japan

maintain national accident databases that include pedestrians as one of the road user groups. Some reports published from these databases were used in the introduction and many others are available through government agencies such as the Department of the Environment (DoE) in the UK [DoE 1998]. The figures do not usually record more than the size of the injury severity groups (including fatalities) in the total population and the trends over time. However, some reports, notably by the National Highway Traffic Safety Agency (NHTSA) in the USA include other measures such as the pedestrian age distribution, the accident location (intersection/non-intersection), the vehicle type, initial point of contact and even the factors that led to the accident [NHTSA 1997].

Large population studies are updated annually, at least one year in arrears and are not sufficiently detailed to reconstruct individual pedestrian accident cases. However, they provide important measures of the scale and nature of the pedestrian safety issue in different countries (although the data in some countries is very unreliable) and provide a means to compare data with other road user groups.

Some of the key institutes in small sample studies have included the Japan Automobile Research Institute (JARI), for example [Ishikawa 1991], NHTSA [Jarrett 1998, Isenberg 1998], the Medical University of Hannover (MHH) [Otte 1991], Birmingham Accident Research Unit [Ashton 1981] and Peugeot-Citroën/Renault [Foret Bruno 1998]. Small sample studies often concentrate on a wide range of issues in order to answer such questions as:

- What is the pedestrian pre impact motion?
- Which regions of the pedestrian body are most commonly injured and what is the injury severity in each of these regions?
- In detail, what are the common types of injury mechanisms?
- What is the relationship between the pedestrian age/size distribution, vehicle impact speed and the injuries sustained?
- Which regions of the vehicle are damaged, how does this relate to the injuries, and how have changes in vehicle design influenced these?

If one were to attempt some brief answers to these questions, they would be as

follows. One of the largest and most recent detailed case study programs was undertaken by NHTSA and is known as the Pedestrian Crash Data Study or PCDS [Isenberg 1998, Jarrett 1998]. This indicated that in more than 90% of the 292 accident cases analysed the pedestrian was either walking (56%) or running/jogging (38%). In 86% of the cases the pedestrian was trying to cross the road and in 78% of the cases the chest orientation was not towards the vehicle (i.e. at some other angle). During the impact most pedestrians were either wrapped around the car or carried (41%) or directly knocked to the ground (25%). In only 2% of the cases the pedestrian completely passed over the vehicle. Ground impact usually leads to less severe head injuries [Mizuno 2000] and is more difficult to control than the primary vehicle impact. Therefore vehicle manufacturer's usually concentrate on solving the problems associated with the primary vehicle impact.

The most significant serious injuries are to the legs and knees because of the likelihood of long-term disability, and to the head because of the high fatality risk. JARI [Matsui 1998] and others have argued that pelvis or upper leg injuries are no longer such significant injuries because of vehicle design trends (e.g. more aerodynamic) although TRL historically defended the inclusion of an upper leg impactor in the sub system impactor test procedure.

Typical leg injuries include less serious mid span fractures of the tibia, fibula or femur. More serious leg injuries include fractures near to either end of these bones (condyles) or especially with knee ligament and/or patella disruption [Manoli 1986]. Head injuries are more complex but in brief there are two types: direct head contact causing a skull fracture and brain impingement or indirect inertial loading causing damage to the brain structure [CIC 1998].

Child pedestrians are usually shorter than adult pedestrians are and therefore different parts of the pedestrian body come into contact with different vehicle body regions during a pedestrian accident. Adult and child bodies also have different mechanical properties (e.g. bone strength). In addition to these factors, the vehicle impact speed is clearly a critical factor in the injury severity because it provides the

energy input to cause injuries. [EEVC 1998] was based on the assumption that it is only practical to address impact speeds up to 40 km/h.

There are three main pedestrian accident contacts for both adults and children: the leg to bumper contact, upper leg to vehicle face (adults) or abdomen to vehicle face (children) contact and finally the head to vehicle hood or fender contact. However, in line with the argument from JARI [Matsui 1998] the vehicle face contact is becoming less significant because of less stiff (e.g. integrated polymeric front end modules) and rearward sloping vehicle faces (i.e. more aerodynamic). Deeper and lower stiffness polymeric bumpers (e.g. Polypropylene) with foam energy absorbing elements may also have reduced leg injuries.

Small sample studies are usually undertaken when and where required by the funding organisation or organisations. They are also highly customised to the requirements of the study and this may or may not include detailed pedestrian accident case studies. These two factors have meant that much of the small sample literature is confidential to the funding organisations or contains information in a form that is not necessarily useful. For instance, nearly all the public domain studies examined have insufficient data to reconstruct individual pedestrian accidents. Therefore the FFA have initiated a new accident study [Ford 2001-1, Koch 2001].

2.2.2. Human body characterisation

Human body characterisation is another field of research that has been initiated from the findings of real world accident research. Two main research topics are the human neck and the human knee. Chalmers University of Technology [Yang 1992] frequently appear in the knee research literature, and Toegepast Natuurwentenscapppelijk Ondersek (TNO) in the Netherlands in the neck research literature [de Jager 1994]. Other literature sources include those from the field of medicine [Fakhry 1975] and various Doctoral theses [Lawson 1998]. Data concerning the properties of other biological materials, such as bones [Yamada 1970] are also available but are often from sources not necessarily directly related to pedestrian injuries [Guillemot 1998] and from a limited sample size. This is particularly true with data that refers to children because of ethical concerns.

A typical approach to human characterisation is to experimentally create and analyse different injury mechanisms in cadavers and then attempt to create and correlate a computer model against these measurements. Volunteer data has not been frequently used because of the injury risk in many tests. However, some non-injurious data is available, notably for the neck response when subjected to low decelerations [Thunnissen 1995]. Human limb and joint data have been used in the development of pedestrian accident simulation and sub system impactor models.

It is difficult to obtain high quality and extensive human biomechanical data in general and even more difficult to obtain dynamic properties and particularly injury data. The properties of much human tissue are highly non-linear and strain rate dependent and the ethical considerations in obtaining injury measures are always likely to remain with us. The alternatives to living subjects, such as cadavers, are limited in both the quality of the data and the range of subjects. In certain age groups there is virtually no data, for example, children. These facts severely limit any attempts to create computer models of humans and this situation is unlikely to change in the foreseeable future. One possible way forward, in addition to using the available biological data, is to use actual accident case studies to validate general injury trends against complete human models. This was one of the reasons for initiating the FFA pedestrian accident study [Koch 2001].

2.2.3. Vehicle characterisation

In [Howard 1998-2] it was proposed that vehicle characterisation was a fresh field of research. The reason for this was that very little literature was available that concerned the creation of appropriate test methodologies and component computer models to simulate the behaviour of vehicle components under the impact energy levels experienced in pedestrian impacts. Many researchers had focused on the pedestrian surrogate [Yang 1992] but few on the vehicle characteristics [Yoshida 1999]. This was due to a number of factors including the difficulty involved in obtaining the dynamic properties of many different proprietary materials and the historical limitations of not being able to model the vehicle structure in detail.

Some components (in particular polymeric components) are not defined in other

types of vehicle computer models or they are highly simplified (e.g. headlamps in frontal crash models) because they have little influence on the vehicle response in these impact conditions. However, they are critical to the pedestrian impact and therefore better component models need to be constructed. Most of the literature focuses on material properties in general [Sherwood 1991] or on technology and design improvements, for example [Grösch 1989], but not on the development of new component models. One of the exceptions was a research paper related to the thesis research of [Philipps 1999] that described a systematic modelling and testing methodology to characterise vehicle components under pedestrian impact conditions. Simulation models of both sub system testing and pedestrian accidents should incorporate such component models to ensure their usefulness and validity.

Every vehicle manufacturer needs to generate data for their own specific vehicle components and by using a systematic testing and modelling methodology it is possible to obtain high quality and extensive dynamic material properties for a whole range of vehicle components. This is increasingly important as manufacturers use more polymeric and hence non-linear and strain rate dependent materials in vehicle components that are more complex to model. Such an approach was used in the construction of the vehicle model described in this thesis. However, it should be noted that in some of the component material models, strain rate dependency was not included because it did not significantly influence the component validation.

2.2.4. Sub-system testing

More literature has been created about sub-system testing than any other field of pedestrian safety research [Schuster 1998, Konosu 1998, Otubushin 1998, Matsui 1998, Lawrence 1998, Konosu 1998, Sakurai 1994, Lawrence 1989, Harris 1985-1, Harris 1985-2] and this indicates the importance that researchers attached to it, for instance [EEVC 1998]. As described in the introduction there are now two main test procedures being developed from this: one of these, as already described, is being developed in Europe and the other as an International Standards Organisation (ISO) standard. Although there are some technical differences the ISO standard is based upon the first test procedure. Harris and Lawrence from TRL undertook much of the initial research in developing the original test procedure and [Lawrence

1989] provides a useful (although dated) insight into the assumptions behind the sub system approach. This approach involves breaking down the pedestrian accident into three main impacts between the vehicle and the pedestrian. In each impact, a different impactor is used to simulate the relevant part of the pedestrian body (with a given mass and velocity) and estimating injuries using measures such as Head Injury Criteria (HIC), bending moment and force. Figure 2.2 [updated Howard 1998-2] shows one version of the test procedure being evaluated.

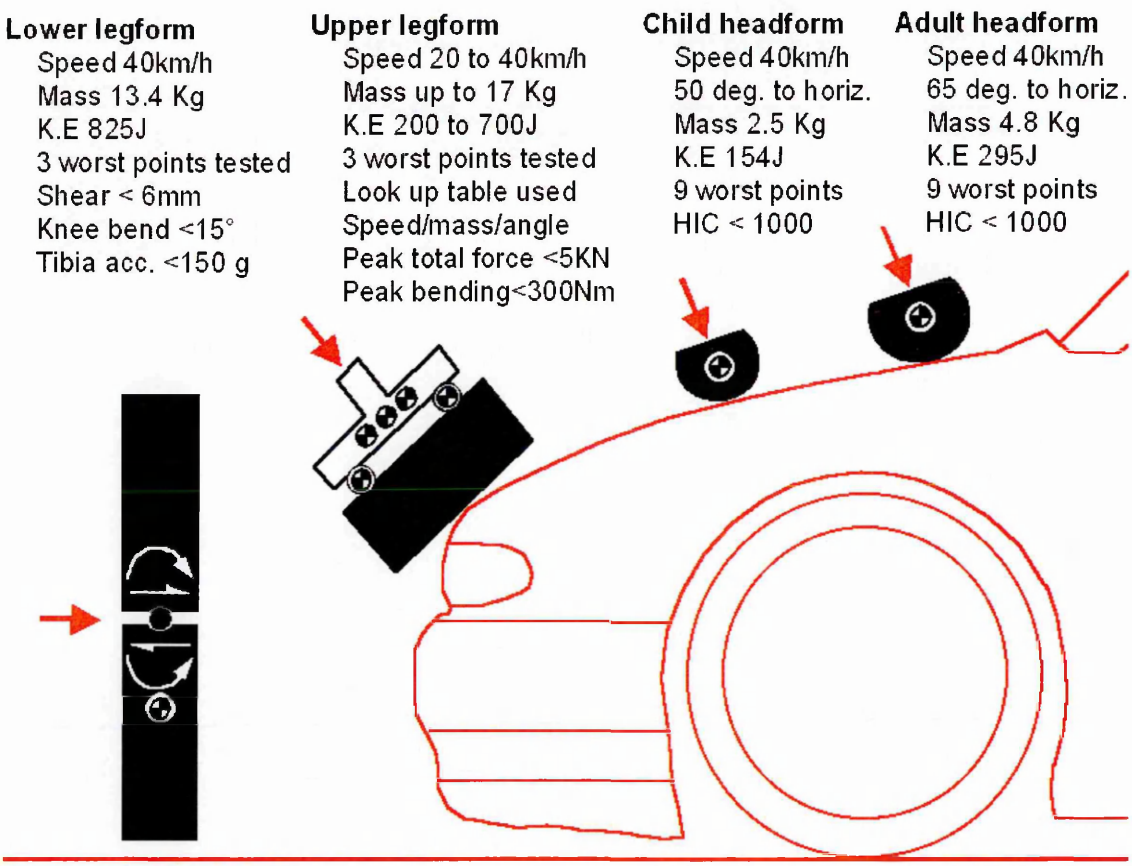

Figure 2.2 One of the proposed pedestrian protection test procedures

In addition to undertaking experimental tests, finite element models of the impactors have also been developed by Jaguar [Howard 1991, 1995-2], in collaboration projects [EUCAR 2000, Howard 2000-2] and by others [Otubushin 1998, Konosu 2000]. In [Lawrence 1998] an overview is provided of how the impactors were developed. Others involved in the development of the impactors included the Institut National de Recherche sur les Transports et Leur Sécurité (INRETS) in France for the leg impactor [Cesari 1991] and the Bundesanstalt für Straßenwesen (BASt) in Germany for the head impactors [Zellmer 1994].

Based on the test procedure described in [EEVC 1998] independent tests are now being used by the New Car Assessment Program (NCAP) to create new vehicle pedestrian protection ratings. Periodically, a new range of cars is evaluated and the results published on the Internet [EuroNCAP 2002] and in magazines.

2.2.5. Pedestrian accident simulation

Another approach involves the simulation of pedestrian accidents with a pedestrian surrogate that is used to recreate the pedestrian motion and accident conditions. A comparison of this approach to the previous one is shown in Figure 2.3.

Pedestrian surrogate		Injury regions	Sub system	
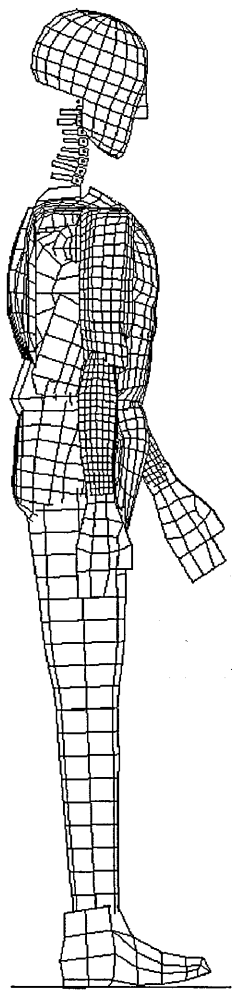	✓	Head	✓	
	✓	Neck	×	
	✓	Arms	×	
	✓	Thorax	×	
	✓	Abdomen	×	(child abdomen injury partially covered)
	✓	Pelvis	✓	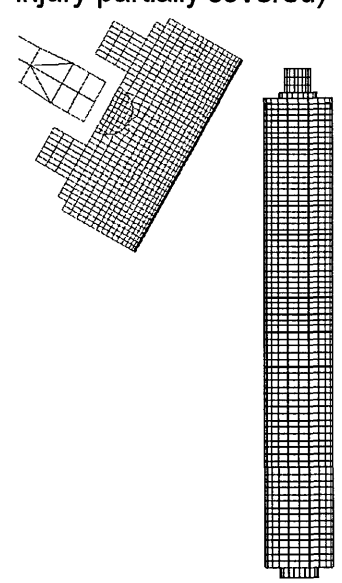
	✓	Femur	✓	
	✓	Knee	✓	
	✓	Tibia and Fibula	×	
	✓	Ankle	×	

Figure 2.3 A comparison of two simulation approaches

In this example a 50th percentile pedestrian humanoid model [Howard 2000-3] is compared against models of sub system impactors [EUCAR 2000]. Pedestrian

surrogates are used to simulate the behaviour of the complete pedestrian and incorporate, to a lesser or greater degree, different biomechanical data. At the simplest level this may simply mean some limited joint motion and appropriate body part inertia values or, as is the case here, a whole range of additional human data and injury measures such as leg fractures. In the sub system approach each pedestrian impact is simplified into a single pedestrian body region to vehicle impact as already described and the injury measures are limited. Only the former approach can be used to fully understand the motion of a pedestrian during a pedestrian accident and the influence of vehicle design changes or pedestrian protection technologies.

Some of the main experts in the pedestrian accident simulation approach include Peugeot S.A/Renault [Brun-Cassan 1983-1, 1983-2, 1984], JARI [Akiyama 1999], The University of Heidelburg [Kallieris 1988], Chalmers University of Technology [Aldman 1987] and TNO [Wijk 1983]. Most of this research concentrates on reconstructing actual pedestrian accidents with cadavers or dummies in order to have a better understanding of the injury mechanisms and motion involved or to assist in the development of new pedestrian dummies. As with sub-system testing, experimental testing and computer modelling is often used. There are two main types of computer modelling approach used to simulate pedestrian accidents: a multibody approach such as MADYMO and a finite element approach as described in this thesis. MADYMO has been used for many years as the main means to simulate pedestrian accidents. It has represented the state of the art and therefore will be directly compared to the finite element approach.

In principle only finite element models can be used to describe the complex geometry and material behaviour of human tissue, muscle and bone. MADYMO models are based upon a gross representation of the pedestrian body segments. For example a single experimentally determined stiffness value is used for the upper thorax ellipsoid characteristics. On the other hand a finite element model may include a complex geometric representation of the human thorax rather than just an ellipsoidal representation. There may be many material properties, the sum of which

should also represent the gross properties of the body segment but may be examined in detail for stress, strain, contact interactions and injury mechanisms. These ideas are illustrated in Figure 2.4 where a traditional MADYMO and a finite element approach are compared [Yang 1992, Howard 2000-3].

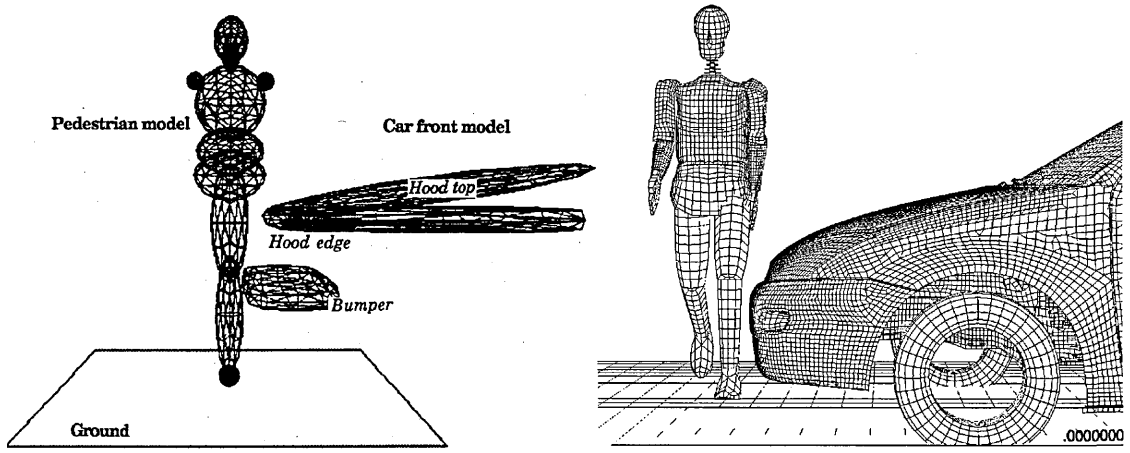

Figure 2.4 Traditional MADYMO and LS-DYNA approaches contrasted

It can be clearly seen that in the MADYMO model the vehicle is only represented by a small number of parts. For instance the bumper is often constructed as one part which approximates the bumper geometry with an ellipsoid that has a single stiffness characteristic experimentally determined under given impact conditions. Due to the nature of the contact force relationship to the body deformation and ellipsoid geometry, great care is required to ensure that both the force direction and magnitude represent the correct resultant influence of the bumper. When the bumper is combined with other bodies representing, for instance the hood edge and top, the problem is further complicated and it becomes clear why, historically, most MADYMO models used highly simplified representations of the vehicle. In comparison, the finite element approach allows one to closely model both the geometry and material of the bumper, foam and all the surrounding structure. In more recent research using MADYMO the limitations of such a simple vehicle model have been acknowledged by, for instance, Yoshida in attempting to develop more detailed but relatively simple vehicle models within the MADYMO environment as shown in Figure 2.5 [Yoshida 1998]. In this case there are more possibilities to simulate variations in vehicle stiffness (e.g. the hood).

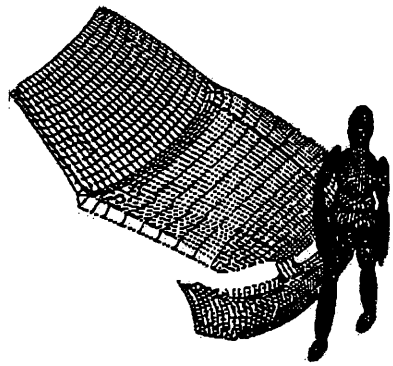

Figure 2.5 A detailed MADYMO vehicle approach

In a manner similar to the vehicle model the MADYMO pedestrian is also highly simplified. The pedestrian model is created with a number of rigid bodies assigned inertia and mass and connected by joints. Ellipsoids are defined on top of these rigid bodies to give them penetration stiffness when interacting with other bodies. These must be large enough to avoid unrealistic discontinuities when the ellipsoids contact the edges of vehicle parts. For instance the thorax ellipsoid must be large enough to correctly contact the hood leading edge and does not necessarily represent real human geometry. Multiple ellipsoids also need to be avoided because this may lead to unrealistic vehicle stiffness due to overlapping contacts.

Historically, one of the major limitations of a rigid body approach has been that there is no bending of the upper and lower legs during contact with the vehicle and this affects the local knee and tibia motion, with the results that knee shear displacement and bending are significantly overestimated. The majority of MADYMO pedestrian models also lack bone fracture mechanisms and again this significantly influences knee injury measures. Whilst in some cases this has been necessary because the objective of the MADYMO simulations was to examine global trends and correlate the results to a pedestrian dummy, for example [Okamoto 2000], in other cases, and more recently, this limitation has been acknowledged [Yang 2000]. Yang included a leg fracture mechanism in the MADYMO pedestrian model as shown in Figure 2.6 [Yang 2000] although this was still only at a single location on the lower leg. The most recent releases of the MADYMO models now incorporate both upper and lower leg bending mechanisms.

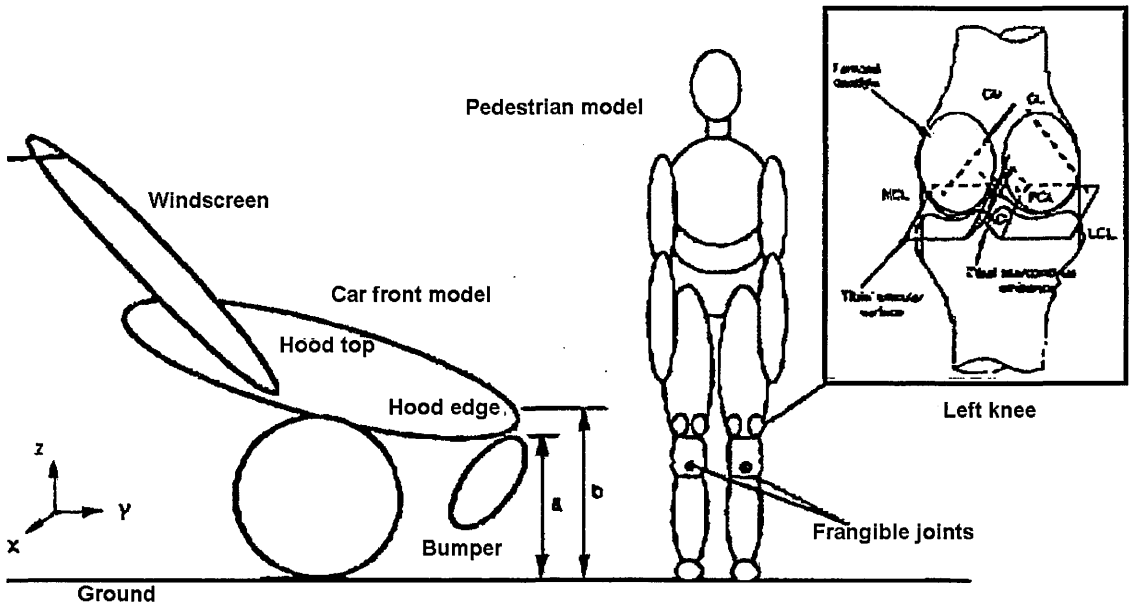

Figure 2.6 A detailed MADYMO pedestrian approach

In the finite element approach described in [Howard 2000-3] there are a number of beams representing the tibia/fibula and the femur and these are surrounded by solids that simulate the skin and muscle properties. The beams are connected to one another such that when a critical bending moment is reached at the ends of the beams they can rotate with limited resistance and hence represent a leg fracture condition (or plastic hinge) at more than one position on both the lower and upper legs. Up until this critical moment the beams carry bending and deform in an appropriate manner based on averaged human bone data from [Nyquist 1986].

In terms of its advantages over a finite element approach, MADYMO provides a very rapid means to evaluate a large number of general vehicle and pedestrian model parameters. It also requires much less data concerning the vehicle and subsequently may be used when such information is not available (e.g. very early prototypes) or there are insufficient resources to gather and model the information.

Detailed human finite element models are also being developed for other applications such as occupant modelling [Watanabe 2001] and these provide additional sources of information relevant to pedestrian modelling. In the future it would be useful to use a single human model for many applications and convergence of these models may eventually occur.

2.2.6. Vehicle design improvements

The final field of research is vehicle design improvements, which leads on from the preceding research. In principle, this should have a direct impact on real world fatalities and injuries although it should also be remembered that vehicle design changes are only one of the potential means to achieve this. These changes are usually proprietary and usually only published when technologies have been incorporated into a production vehicle or show car. As a result of this the best sources of information and particularly technology trends are patent applications. The Technical University Berlin [Appel 1978-1, Wollert 1983], Daimler Benz AG [Grosch 1989] and more recently Honda [Yoshida 1999] have published a number of significant papers in this field. Ford [Cady 1994, Howard 1995-1] and others, [Daimler Benz 1990, 1988, VW 1978, Mercedes Benz 1990, Appel 1978-2, Nissan 1983, Toyota 1996-1, 1996-2, 1996-3] have pursued various patents. A summary of general design improvements proposed in these references is shown in Table 2.1.

Impact event	Vehicle design improvements
Leg to bumper	Lower stiffness bumper with lower density, deeper energy absorbing foam. Integrated soft front end module with materials as above but integrates component. Lower and deeper conventional bumper with increased package space for foam. Unconventional bumper construction e.g. air bladder or eggcrate. A deployable or fixed secondary bumper below the conventional bumper. Similar to the above except the bumper undertray is stiffened Bumper mounted air bag and sensor. Relocate components above bumper forward to support upper leg e.g. headlamp
Upper leg or thorax to vehicle face	Mechanically deployed hood for increasing a controlled rearward deflection of hood. A low long and gently inclined vehicle face. Collapsible vehicle face e.g. stroking grille, collapsible hood hinge platform. Increase package surface below vehicle face surfaces by relocating components. Rearward moving, collapsible or lower mass headlamps. Vehicle face mounted air bag.
Head to hood, fenders or windscreen	Mechanically or pyrotechnically deployed hood for increasing package clearance. Sandwich construction hood with polymeric or thin metallic outer and foam interlayer. Similar construction to above on fenders, A posts or plenum chamber wall. Sharply rearward sloping windscreen. Covered windscreen wiper spindles. Low vertical stiffness at fender/hood joint, plenum chamber wall & hood inner panel. Increasing the package space below outer surfaces e.g. relocate suspension towers Reduce the vertical stiffness of the engine ancillaries above. Windscreen, scuttle or hood air bags (below/above hood).
Body to ground	Pedestrian retaining bar integrated into hood Hood mounted air bag covered in adhesive Optimised vehicle structure to absorb the impact energy and catch pedestrian.

Table 2.1 General design and technology improvements

Many of the potential solutions have probably been optimised to meet for instance, [EEVC 1998] requirements rather than actual pedestrian accident requirements because it is difficult to determine these. One of the purposes of the PhD research is to create the tools necessary to evaluate pedestrian protection technologies under more realistic pedestrian accident conditions and hence simulate these requirements. This thesis focuses on four pedestrian protection technologies and these concern the bumper, headlamp and hood.

In order to gain background information there were two databases used to search for patents related to these areas of the vehicle. One of these was a proprietary Ford pedestrian safety database in Microsoft Access and the other a Micropatent internet web site in which any Ford employee can simultaneously search across US, Japanese and European patent databases. The patents discovered are listed in Table 2.2.

A patent and publication list had previously been contributed to the Ford pedestrian safety database and from a total of 136 records, the 42 patents shown were identified as directly relevant to bumpers, headlamps or hood systems. In order to reduce the number of patents requiring examination any technologies that involved stored energy devices (e.g. air bags) as the prime energy absorber were excluded because they were not purely structural or mechanical solutions that controlled or used the impact energy (e.g. for hood deployment).

With regard to the Micropatent internet web site a search was undertaken using the single keyword 'pedestrian' and all patents since January 1999. This provided a second check on all the patents recorded in the Ford database and yielded 413 records, 9 relevant patents and subsequently only 6 additional patents that were not already recorded in the Ford database.

FORD pedestrian database			
1976	US 3992047	Daimler-Benz AG	Bumper(moveable bumper)
1978	DE 2645823	Daimler-Benz AG	Bumper (pneumatic lower)
1978	DE 2641887	Hoper, G	Bumper
1978	DE 2711339 A1	University Berlin	Mechanically deployed hood
1980	FR 2445783	Auto Citroen and Peugeot	Hood (car front)
1980	DE 3051041	Daimler-Benz AG	Bumper (lower bumper)
1980	DE 3003568	Daimler-Benz AG	Bumper (lower spoiler)
1981	BE 889844	Van Handenhoven E	Hood
1981	GB 2076344	Daimler-Benz AG	Hood
1981	US 4249632	Volkswagen AG	Hood
1982	DE 2804400	Daimler-Benz AG	Hood
1982	US 4359120	Daimler-Benz AG	Hood to fender interface
1983	JP 58030874	Nissan	Hood (front structure)
1983	JP 57104848	Nissan	Mechanically deployed hood
1983	JP 58211975	Nissan	Hood
1984	US 4475148	Daimler-Benz AG	Headlamp pivoted mount
1984	GB 2069940	Mitsuboshi Belting Kk	Bumper
1985	DE 3434844	Volkswagenwerk AG	Bumper
1985	JP 60060051	Nissan	Mechanically deployed hood
1986	JP 61057504	Juttemann F	Bumper
1987	US 4644447	Daimler-Benz AG	Headlamp mounting
1988	DE 3728752	Daimler-Benz AG	Headlamp cover interface
1989	DE 3802104	Bayerische Motoren Werke	Headlamp spring mounting
1989	DE 3047969	Daimler-Benz AG	Hood
1993	US 5263546	Jaguar Cars Ltd	Mechanically deployed hood
1994	JP 6144154	Mitsubishi Electric Corp	Hood
1994	EP 0509690B1	Jaguar Cars Ltd	Mechanically deployed hood
1995	EP 0630801B1	Jaguar Cars Ltd	Mechanically deployed hood
1995	GB 2265117	Daimler-Benz AG	Bumper
1995	DE 19519110	Raufoss Automotive AS	Bumper
1995	DE 4401023 C1	Daimler-Benz AG	Hood to fender interface
1995	US 5706908	Nissan	Hood (inner panel design+others)
1997	US 5697467	Jaguar Cars Ltd	Mechanically deployed hood
1997	DE 19721565	Volkswagen AG	Hood latch mechanism
1997	JP 9315266	Mitsubishi	Hood
1997	JP 9315243	Mitsubishi	Hood (grille)
1998	JP 10218022	Mitsubishi	Hood (front structure)
1998	JP 10119823	Nissan	Hood
1998	JP 10230798	Mitsubishi	Hood
1998	FR 2759655	Lin Pac Mouldings Ltd	Bumper
1999	JP 11078734	Mitsubishi	Bumper
1999	JP 11078732	Nissan	Bumper
Micropatent			
1998	JP 11208389A	Nissan	Bumper
1998	EP 0926018	Peugeot	Bumper (foam inserts)
1998	JP 10217983A	Honda	Hood
1999	EP 0894664A2	Honda	Headlamp small size
1999	EP 0 983 909 A1	Ford	Bumper
2000	EP 0989354A2	Ichikoh Industries Ltd.	Headlamp small size

Table 2.2 Pedestrian protection bumper, headlamp and hood patents

There are 6 headlamp patents listed. US 4475148 described a design in which the complete headlamp assembly was pivoted from the lens cover base and restrained by a rubber or plastic energy absorbing spacer on the top of the lens cover. Under impact the complete headlamp rotated into the car by deforming the energy absorbing spacer. DE 3802104 described a design that utilised horizontal springs as headlamp mounts so that under impact the headlamp moved rearward. Other designs, such as those described in EP 0894664A2 focused on alternative lamp technologies to allow smaller headlamps. The closest design to the one described in this thesis [Howard 2001-5, 2001-7] was DE 3728752. As shown in Figure 2.7 this was a headlamp with a deformable connection between the lens cover and headlamp body. It was assumed that the lens cover could move independently of the headlamp body under impact and that the connecting material was able to absorb the impact energy of a pedestrian.

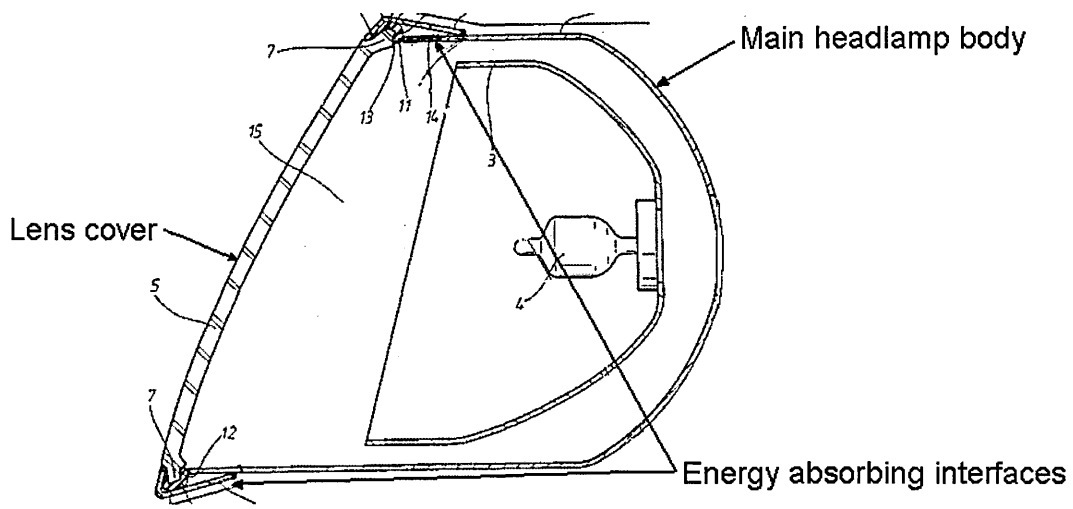

Figure 2.7 Headlamp patent DE 3728752

Table 2.2 lists 16 patents related to pedestrian protection bumper designs. From the earliest patents examined in 1976, such as US 3992047 the benefits of a low, protruding and soft bumper were clearly recognised as a possible way to reduce leg injuries. The means by which this was implemented varied considerably. In one of the designs described in DE 2645823 a soft secondary bumper was deployed in front of and below the primary bumper. Another design adopted the alternative approach of splitting the primary bumper into two parts and mounting the lower part on pneumatic struts to allow it to be deployed like a secondary bumper.

In addition to these relatively complex designs a number of patents exist where structural rather than mechanism type solutions were proposed. In one design described in EP 0926018 softer foam is added to the bumper top and in front of the hood leading edge. Another patent FR 2759655 by Lin Pac Mouldings Ltd. described a range of solutions from using the deformation of structural plastic bumper inserts behind the bumper face to the use of different combinations of foam inserts behind a rearward sloping bumper face. One of the claims within this patent is shown in Figure 2.8 and this was the closest to the bumper technology described in this thesis [Howard 1999-2, 2001-8].

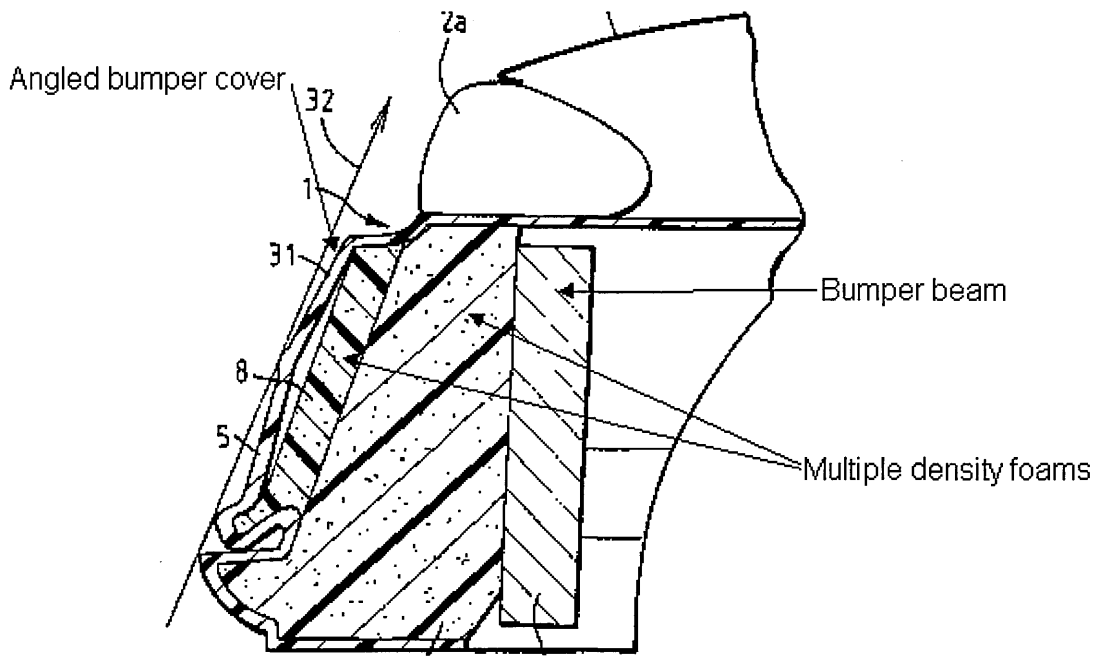

Figure 2.8 Bumper patent FR 2759655

There are more patents associated with hood systems than any other pedestrian protection technology category. This is probably because the hood covers a large part of the vehicle front and is important in many types of pedestrian injuries. The most relevant hood patents date back to 1978 when Professor Appel from the University of Berlin patented a number of hood technologies and the underlying principles have been used in many car manufacturers' (e.g. Jaguar, Nissan and Daimler Benz AG) patents. These principles included designing the hood hinge and latch mechanisms to raise the hood and allow it to move rearward under a pedestrian impact, and deformable hinges and fenders. Initially Nissan and Jaguar

concentrated on the hinge and latch mechanisms whilst Daimler Benz concentrated on detailed energy absorbing latch designs and body panel profiles (e.g. fender to hood interface). However, in a more recent Nissan patent they have also focused on very detailed descriptions of 'ideal' hood inner panel sections and materials, and the hood to fender interface sections. Ford has a long history of developing mechanically deployed hood system concepts from as early as 1991 when the author first described some basic design concepts as shown in Figure 2.9.

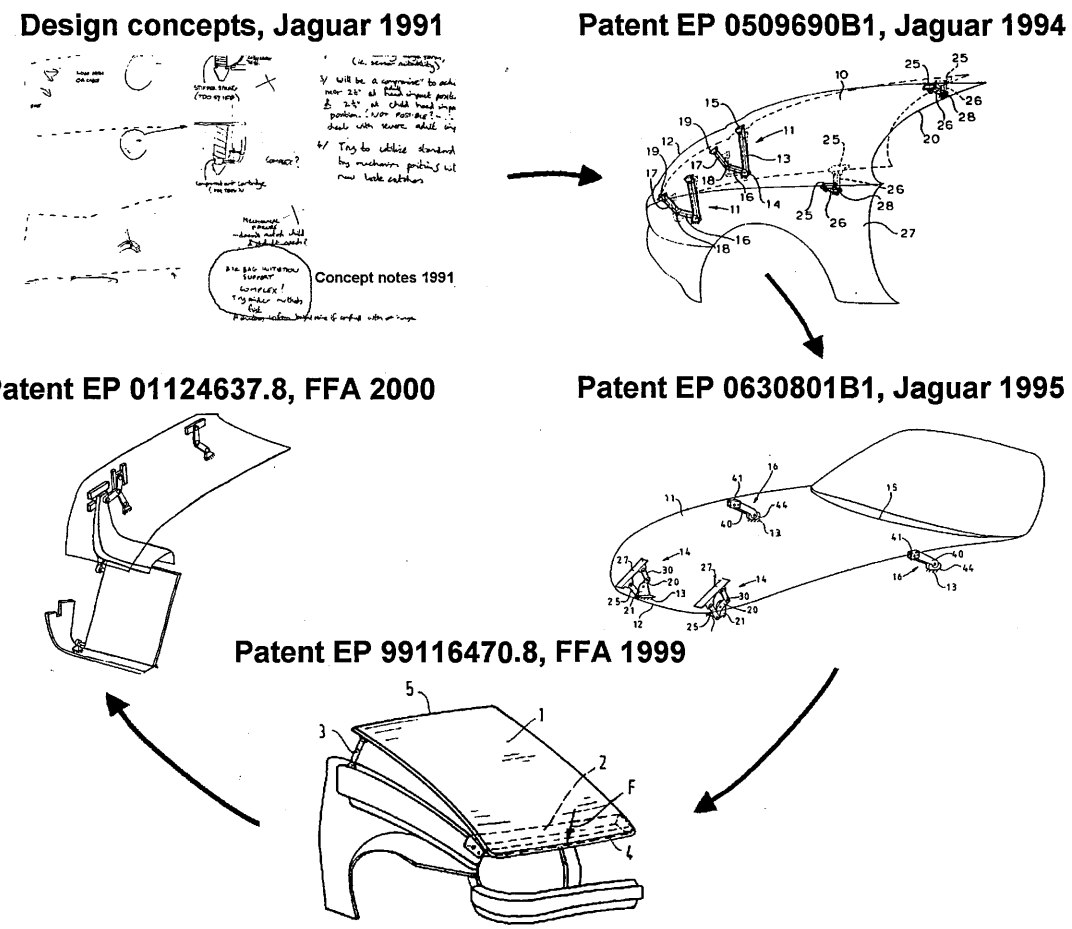

Figure 2.9 Ford mechanically deployed hood systems

The patent described in [Howard 1995-1] and shown in Figure 2.9 as Jaguar 1995 is the predecessor to the patents described in [Howard 2001, 2001-6] and shown as FFA 1999 and FFA 2000. In a manner similar to all these patents it utilised a mechanical means to transfer the pedestrian impact energy into the rearward and upward motion of the complete hood system.

3. Research strategy

At the beginning of the research the literature review provided a more extensive view of all the possible approaches to pedestrian safety research and this was used to develop a research vision [Howard 1999-3]. In the early stages this was to create non linear finite element models capable of reconstructing any real world pedestrian accident. It was envisioned that by identifying accident conditions (e.g. the sequence of events), vehicle details (e.g. type, impact velocity, damage details) and pedestrian details (e.g. size, age) in the pedestrian accident simulation forms shown in the appendices, any specific pedestrian accident could be simulated. Based on this vision, projects were initiated to create a new family of scaleable pedestrian models and improved non linear finite element vehicle models.

As the research progressed the potential of the models and methodologies to develop and evaluate pedestrian protection technologies became more apparent and this led to a change in the original vision. Instead of focusing on accident reconstruction the research vision became more focused on creating a methodology for developing and evaluating pedestrian protection technologies under a larger range of conditions than [EEVC 1998]. This vision was broken down further into the research objectives described in the introduction.

3.1. Pedestrian protection technology methodology

The methodology that was developed during the research is shown in Figure 3.1 [Howard 2001-1]. Due to the large number of tasks involved only the highlighted tasks are described.

The two left hand columns were concerned with the development and evaluation of a reference vehicle whilst the central column concerned the creation and maintenance of CAE (computer aided engineering) models and methodologies and the two right hand columns the development and evaluation of a modified vehicle. A modified vehicle was one that featured pedestrian protection technologies.

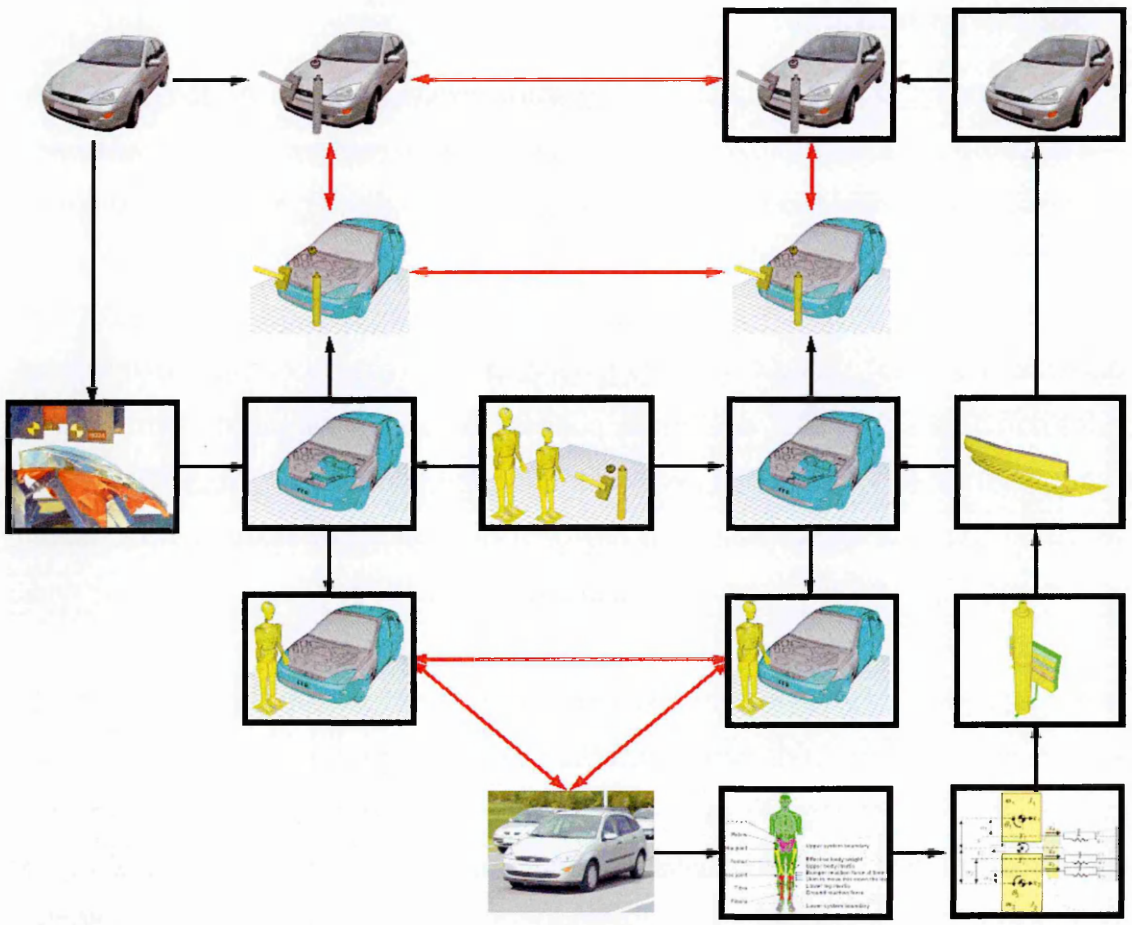

Figure 3.1 Pedestrian protection technology methodology (all tasks)

In the left hand columns it was important to construct and evaluate a validated and reference vehicle model that was suitable for pedestrian accident simulations. This was achieved by creating a database of validated component models [Howard 2000-1] that were subsequently incorporated into a vehicle model that was used in sub system impactor simulations [Howard 2000-2] and pedestrian accidents simulations [Howard 1998-2, 2000-3]. Although not described in this thesis, sub system impactor simulations were correlated against experimental tests as one of the means to validate the complete vehicle model. A large matrix of different pedestrian accident simulations was undertaken in order to study general trends in the manner in which the injury measures and impact motion of four pedestrian humanoid models were influenced by the pre-impact stance, vehicle impact location and velocity. The accident simulations showed how the vehicle design could be improved and subsequently provided a benchmark against which the performance of modified vehicle models was compared.

In the right hand columns a similar procedure was undertaken with a modified vehicle model except that the technologies were developed with some additional stages. The prime sources of ideas for the new technologies were the pedestrian accident simulations using the reference vehicle model, some initial findings from pedestrian accident case studies and patent searches. Biomechanical and analytical models were used to describe and refine these ideas into patent applications [Howard 1999-2, 2001, 2001-5, 2001-6, 2001-7, 2001-8]. The underlying technology principles were better understood by creating and evaluating simplified numerical models using design of experiment (DoE) techniques to undertake parametric studies [Howard 2001-2, 2001-3, 2001-4]. These provided some initial optimisation for the technology models used in the modified vehicle. The performance of the modified vehicle with different technologies was evaluated by using a reduced set of pedestrian accident simulations from the reference vehicle simulation matrix.

Finally, the central column concerned benchmarking of the reference and modified vehicles, the creation and maintenance of the CAE models and methodologies [CIC 1997, 1998, 1999, 2000, 2001, EUCAR 2000], and the collection of detailed pedestrian accident case studies [Koch 2001]. In the long term it was envisaged that actual pedestrian accident case studies could be used to assess the real world performance of the pedestrian protection technologies and provide enhanced validation.

3.2. Reference vehicle pedestrian accident simulations

The first phase of the strategy was to create and apply the models and methodologies to a reference vehicle. In order to do this four enabling projects were identified as shown in Figure 3.2 [Howard 1998-1]. The first two projects were initiated because the existing vehicle models in Ford were not suitable for pedestrian accident simulations. In a similar manner there were no existing non-linear dynamic finite element pedestrian models and hence there was a requirement for the third project. The final project entailed the combination and application of all the models created with the knowledge gained from, for instance, pedestrian accident studies.

Create CAE models and methodologies for reference vehicle			
⇓	⇓	⇓	⇓
Project 1 (Author)	Project 2 (Author/fka)	Project 3 (Author/CIC)	Project 4 (Author/FFA)
Reference finite element vehicle models suitable for pedestrian accident simulations	A systematic testing & modelling methodology to create validated finite element models of the most important vehicle front end components	A new family of scaleable pedestrian humanoid finite element models that feature the most important pedestrian injury mechanisms & more realistic human like properties than conventional models	Pedestrian accident simulation models with realistic boundary conditions & an evaluation of different accident conditions using a matrix of simulations

Figure 3.2 Four phase one enabling projects

The author undertook projects 1 and 4. Due to the large amount of research and facilities (e.g. test laboratory) required, external contracts with the forschungsgesellschaft kraftfahrwesen aachen (fka) in Germany and Cranfield Impact Centre (CIC) in England, were initiated to assist with projects 2 and 3.

Partial German government (Ministerium für Wissenschaft und Forschung des Landes Nordrhein-Westfalen) funding was obtained for project 2 over a three year period. During this period the fka undertook a literature search, jointly developed a component test and finite element modelling methodology and applied this to create validated vehicle component models for the vehicle model. The main task undertaken by CIC in project 3 was to create pedestrian humanoid models by combining the best features of available dummy models and developing new more human like model features. Other tasks included a literature search, the creation of a scaling methodology, development of the pedestrian models to incorporate FFA user requirements and feedback, and pedestrian model validation based on the available literature. Projects 1 and 4 focused on the complete construction of a vehicle model suitable for pedestrian accident simulations and the development of modelling methodologies for pedestrian accident simulations. An essential part of this was also providing feedback to CIC on how the humanoid models could be developed further.

3.3. Modified vehicle pedestrian accident simulations

The second phase of the strategy was to create and apply the models and methodologies to modified vehicle models that incorporated pedestrian protection technologies. In order to do this four enabling projects were identified as shown in Figure 3.3 [Howard 2000-4].

Create and apply CAE models and methodologies to modified vehicle			
⇓	⇓	⇓	⇓
Project 1 (Author/FFA)	Project 2 (Author)	Project 3 (Author)	Project 4 (Author/Imperia)
Pedestrian protection technology patents and biomechanical and analytical models of these with optimised finite element component models	Finite element vehicle models that incorporate different combinations of optimised finite element technology component models	An evaluation of different accident conditions using the modified vehicle models and a matrix of simulations	Demonstration and test vehicles constructed & subsequently evaluated using [EEVC 1998]

Figure 3.3 Four phase two enabling projects

In project 1 that was mainly undertaken by the author, the first steps were to identify real world and sub system impactor requirements for pedestrian protection. With these requirements established the next step was to undertake a patent search. This provided an indication of what other researchers believed to be significant pedestrian injury problems. It also identified different types of possible solutions and more importantly approaches to the problem. Finally a patent search was also a necessary part of the process in filing an invention disclosure within Ford and an external patent application. A number of pedestrian protection technologies were created as part of this research and each of these was filed at the European patent office [Howard 1999-2, 2001, 2001-5, 2001-6, 2001-7, 2001-8]. Analytical models of the various technologies were created in order to have a better understanding of the manner in which they operated, so that this knowledge could be used in the construction and optimisation of finite element models.

In project 2, two modified vehicle models were created with the pedestrian protection technologies. These were subsequently evaluated in project 3 with a subset of the pedestrian accident simulation matrix used for the reference vehicle model.

Finally test and demonstration cars were built in project 4 and the test car tested with sub system impactors to determine whether the technologies provided an experimentally tested benefit. No experimental dummies existed to evaluate the test car using pedestrian accident tests and only the experimental test results using [EEVC 1998] are listed.

A summary of how all the projects were undertaken and interrelated is shown in Figure 3.4.

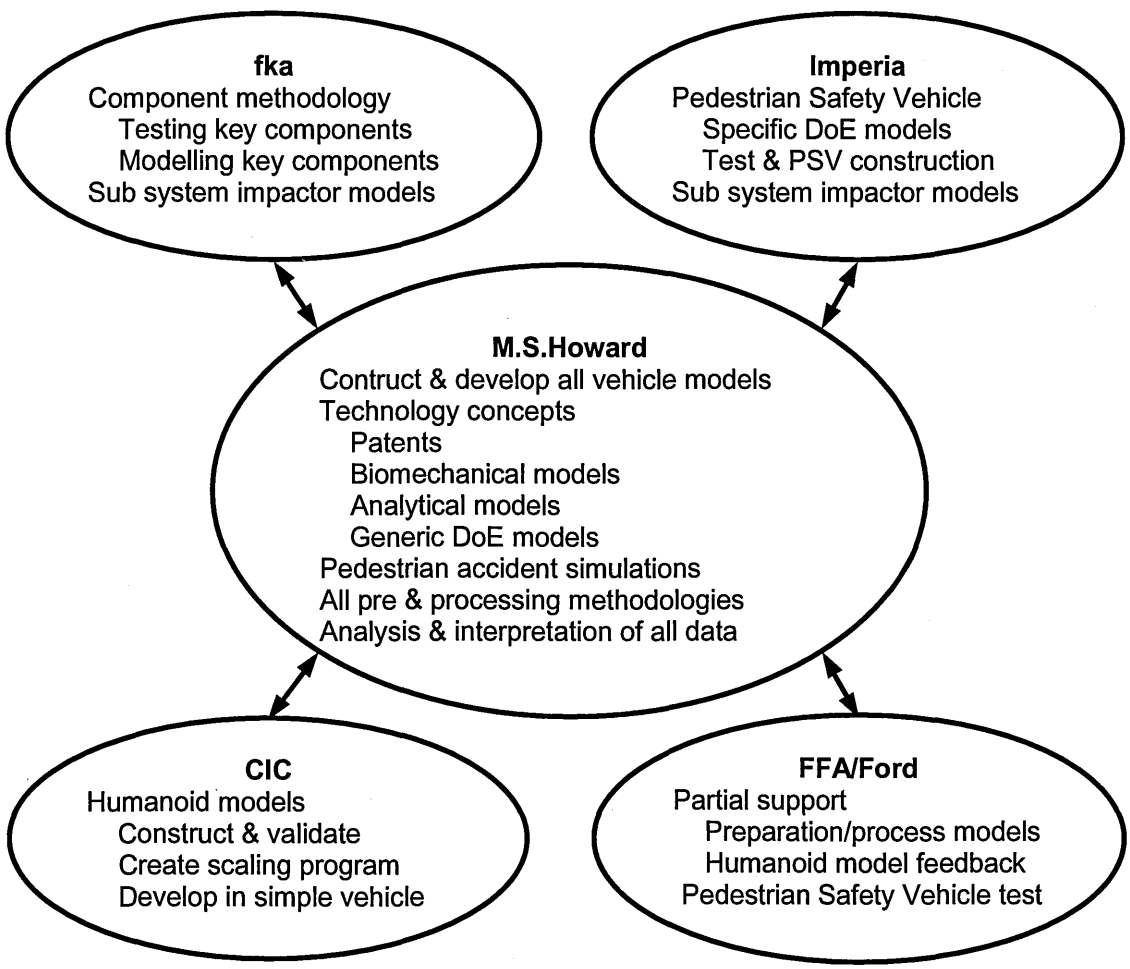

Figure 3.4 Overview of all project tasks and interrelationships

The complete timing plan for the PhD research is shown in Figure 3.1.

Research tasks	1998		1999				2000				2001				2002			
	3	4	1	2	3	4	1	2	3	4	1	2	3	4	1	2	3	4
Initial registration	◆																	
Create CAE tools and methodologies for unmodified vehicle	▒	▒	▒	▒	▒	▒	▒	▒	▒	▒	▒	▒	▒	▒				
Create non linear dynamic finite element vehicle model	■	■	■															
Create pedestrian accident simulation forms			■	■														
Create test pilot simulation models, give feedback to CIC/ika			■	■	■													
Support ika to validate draft directive impactors using vehicle model					■	■												
Based on above further develop vehicle model as appropriate						■	■											
Integrate humanoid updates and component models as available							■	■	■									
Parametric simulation studies with 9 yr old, 5th, 50th and 95th humanoids							■	■	■	■	■	■	■	■				
Create CAE tools and methodologies for modified vehicle		▒	▒	▒	▒	▒	▒	▒	▒	▒	▒	▒	▒	▒	▒			
Create technology concepts		■	■	■														
Create fully surfaced Master Series CAD model of technologies				■														
Undertake patent search for pedestrian protection technologies.					■													
Develop categorised technology matrix					■	■												
Pursue invention disclosure and patent process					■	■	■	■	■	■	■	■	■	■				
Create analytical models of each technology concept									■	■	■							
Create and evaluate DoE technology models									■	■	■	■						
Create technology models for modified vehicle model												■	■					
Integrate technology models into simulation models													■	■				
Evaluate effectiveness of the technologies in simulation models													■	■	■			
Build & test technology test and demonstration vehicles												■	■					
Publications	▒	▒	▒	▒	▒	▒	▒	▒	▒	▒	▒	▒	▒	▒				
"The Simulation of Real World Car to Pedestrian Accidents.....", IJC	◆																	
"Pedestrian Safety Research - Past, Present, Future", Euromotor		◆																
"The FFA Pedestrian Safety Research Program Update", G3P		◆																
"Real World Pedestrian Research", ETSC			◆															
"FE-Simulation von Fahrzeug-Fußgänger-Kollisionen", ATZ				◆														
"FEA Simulation of Vehicle-Pedestrian Collisions", ATZ				◆														
"FFA Pedestrian Safety Research Program", Ford global conference					◆													
"An Integrated Approach to Real World ..", Aachen Colloquium 1999						◆												
"Developments in the Simulation of Real World Car to .....", IJC							◆											
"A Systematic Modelling and Testing Methodology ...", NRW report							◆											
"Validation and Application of a Finite Element ...", IRCOBI									◆									
"The construction, certification, validation & correlation..", Ford report									◆									
"Models make an impact ", Automotive Engineer										◆								
"Ganzhetlicher Ansatz zur ", Ernst-Moritz-Arndt-Univesität											◆							
"FFA pedestrian safety research program", Volvo												◆						
"The design and development of a PP headlamp .." Ford report												◆						
"The design and development of a PP bumper .." Ford report												◆						
"The design and development of a PP hood .." Ford report													◆					
Thesis				▒	▒	▒	▒	▒	▒	▒	▒	▒	▒	▒	▒	▒	▒	▒
Create draft				■	■	■	■	■	■	■	■	■	■	■	■	■		
Submit draft for comments																◆		
Make suggested changes																■		
Submit final thesis																		◆

Table 3.1 The PhD research timing plan

4. Reference vehicle pedestrian accident simulations

4.1. Context in overall methodology

This chapter concerns the highlighted tasks shown in Figure 4.1 [Howard 2001-1], namely the creation of a reference or unmodified vehicle model 'p' suitable for pedestrian accident simulations and the evaluation of these simulations to determine a set of reference data and trends.

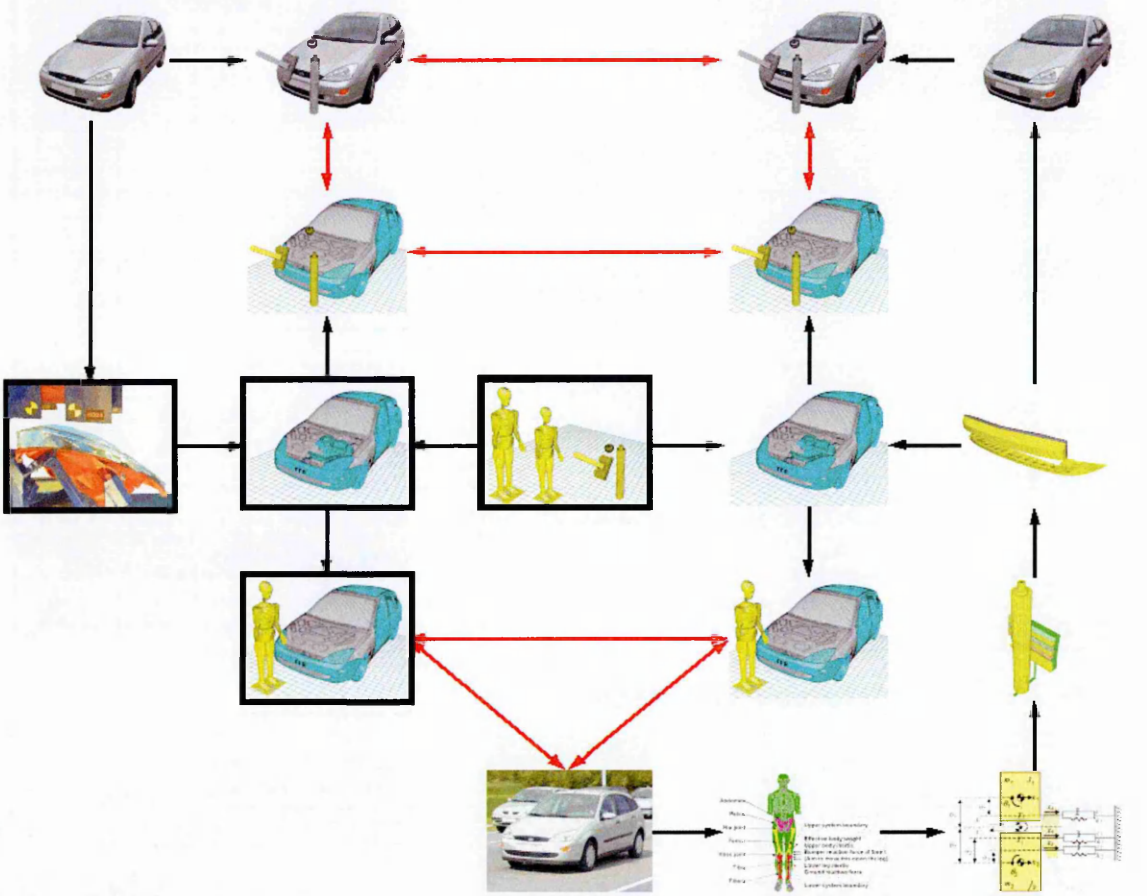

Figure 4.1 Pedestrian protection technology methodology (reference vehicle)

4.2. Software tools

The software tools were chosen on the basis of prior experience and various Ford Motor Company standards (e.g. C3P - computer aided engineering, manufacturing and design with product information manager). An overview of the complete pre-processing, solving and post-processing steps using these tools is shown in Figure 4.2 (a detailed software and hardware list is shown in the appendices).

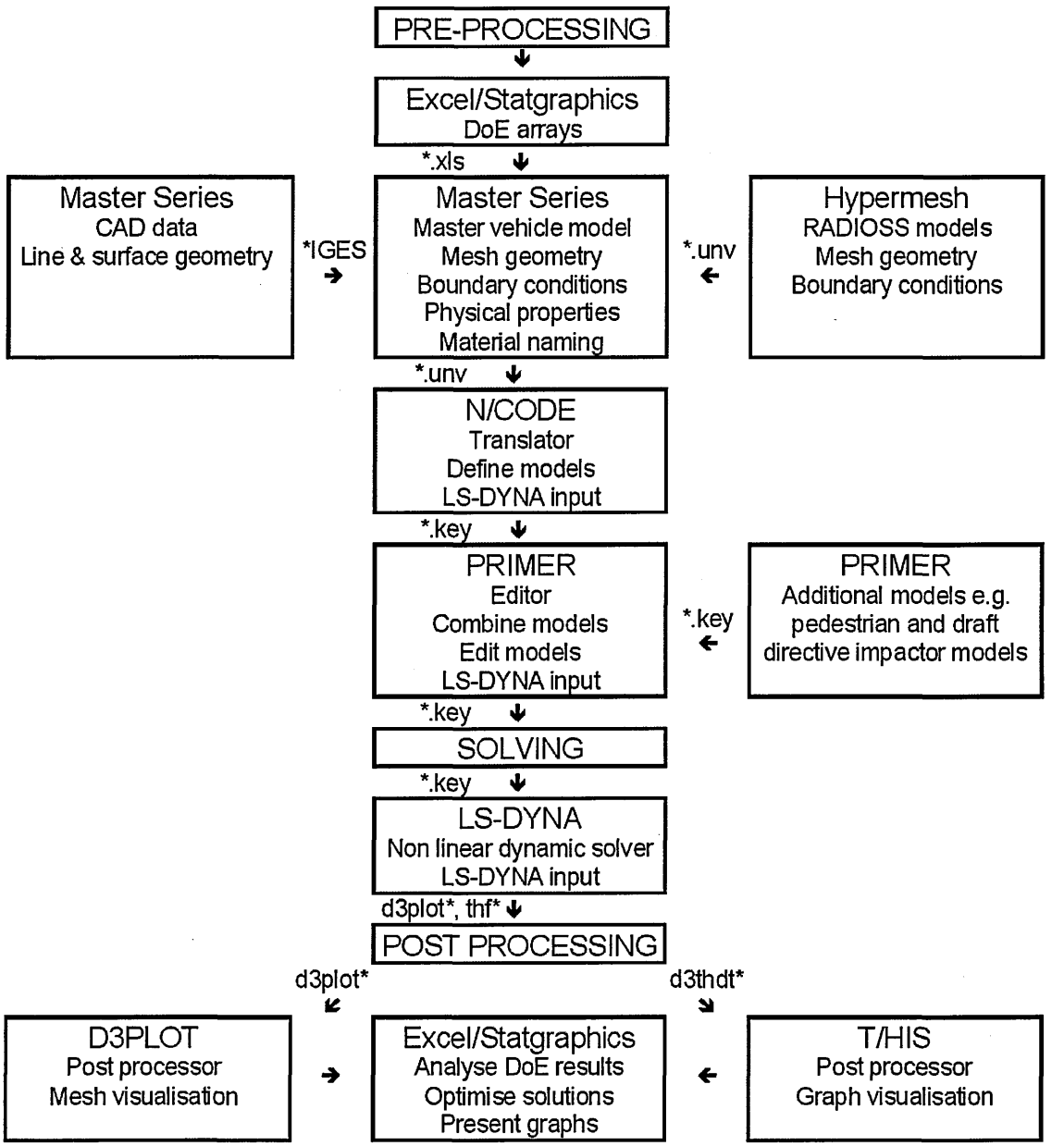

Figure 4.2 The pre-processing, solving and post-processing methodology

Where DoE studies were undertaken two software packages were used in the construction of the design arrays: Excel is spreadsheet software developed by Microsoft and Statgraphics is general statistics software developed by Manugistics that includes DoE pre and post processing capability.

The reference CAD data and finite element model data were stored in Master Series. Master Series is an integrated computer aided design, manufacturing and engineering (CAD/CAM/CAE) software developed by EDS. In the context of this

research it was only used to read, translate, construct and store CAD data and finite element models as part of the pre processing tasks (e.g. creating mesh geometry and boundary conditions). All modifications to the vehicle models were undertaken in Master Series so that any LS-DYNA input file could be traced back to a master model. Where additional finite element models were originally constructed in the explicit non linear dynamic finite element program RADIOSS (developed by Mecalog) an additional pre processing software Hypermesh (developed by Altair Engineering) was used to translate these files into a universal file format that could be read into Master Series.

LS-DYNA is an explicit 3D non linear dynamic finite element solver code developed by LSTC. It ".... is a general purpose finite element code for analysing the large deformation response of structures including structures coupled to fluids". "The main solution methodology is based on explicit time integration". "A contact-impact algorithm allows difficult contact problems to be easily treated with heat transfer included across the contact interfaces" [LS-DYNA 1999-2]. Such a finite element approach allowed the input of material data based on experimental tests and exact part geometry, rather than for instance, a black box approach with springs and dampers. Local stresses and strains could be calculated and part failure closely reproduced with geometric (e.g. element deletion) and material property changes (e.g. very low joint stiffness). The capability of LS-DYNA to deal with large and dynamic deformations of structures, complex part geometry, part contacts, and numerous material models, enabled the interaction of the vehicle and pedestrian to be more closely simulated. In addition to this, it was chosen because of the background experience of everyone involved and the perceived advantages over alternative codes such as RADIOSS (e.g. more advanced foam models).

In LS-DYNA "Spatial discretization is achieved by use of four node tetrahedron and eight node solid elements, two node beam elements, three and four node shell elements, eight node solid shell elements, truss elements, membrane elements, discrete elements, and rigid bodies" [LS-DYNA 1999-2]. In the PhD research the

default element types were used in the construction of the vehicle models and the DoE studies. To assist in minimising any potential disadvantages of these elements, the model quality guidelines listed in the appendices were applied. For instance, out of a choice of more than ten types of shell element the default Belytschko-Lin-Tsay shell element was used in the majority of the models. According to [LS-DYNA 1999-2] "Because of its computational efficiency, the Belytschko-Lin-Tsay shell element is usually the shell element formulation of choice. For this reason, it has become the default shell element formulation" and "An additional advantage of this element for crashworthiness analysis is the numerical robustness of the formulation where warp angles of 180 degrees usually do not cause coredumps" [DuBois 2001]. The inability of this type of shell element to account for warping (the nodes are assumed to be planar in the calculation of nodal positions) is also a disadvantage. Therefore, in line with the model quality guidelines, a 15 degrees warping limit with no concentration of warped elements in any one region [Du Bois 2001] was applied. Where necessary, mesh refinement was used to eliminate hourglassing, (described in the appendices) and more closely match part geometry (e.g. curved surfaces).

It was necessary to obtain a means to translate files from Master Series into an LS-DYNA input file, to combine different LS-DYNA input files and post process the results. The software suite OASYS N/CODE, PRIMER, D3PLOT & T/HIS distributed by Ove Arup, provided a means to achieve this. N/CODE was used to translate a Master Series universal file (*.unv) into an LS-DYNA input file (*.key). The manner in which the model was defined in Master Series for the correct translation into LS-DYNA is shown in the appendices. All the models were constructed with the units of Newtons, tonnes, mm, seconds, Kg and MPa. PRIMER enabled several LS_DYNA input files (e.g. the vehicle and a pedestrian) to be combined and manipulated to create a single input file (e.g. a pedestrian accident simulation). D3PLOT provided a means to visualise the model behaviour (e.g. deformations and kinematics) and T/HIS to create for instance time history graphs of specific parameters. For ease of presentation the ASCII data for these graphs were cut and pasted into Excel files.

4.3. Reference vehicle model 'p'

4.3.1. Background

It was necessary to construct a new vehicle model in LS-DYNA because the existing models were not appropriate for simulating pedestrian accidents. In general they did not utilise appropriate mesh densities, incorporate suitable vehicle component models and were only available in RADIOSS.

The unsuitability of other crash and NVH (noise, vibration, harshness) models has been highlighted in other reports [Ford 1997]. For example, models of the vehicle structure forward of the header rail, that equates to zones 1 and 2 as defined by [Ford 1997] had a recommended element size for vehicle to vehicle crash models between 10 mm and 50 mm. However, the new vehicle model needed to be more detailed in both zones 1 and 2 in order to correctly represent the stiffness of smaller vehicle features that are unimportant in vehicle to vehicle accidents but are critical for pedestrian to vehicle accidents. In the new vehicle model an average element size of 12 mm was used for non-critical parts (e.g. away from impact region) and no less than 5 mm for critical parts. In contrast, NVH models mainly consisted of elements, as small as 4 mm [Ford 1995] and many of the important components for pedestrians were not modelled (e.g. headlamps). The element size of 5 mm was specified because this equated to a timestep of about 1×10^{-6} s for a steel shell element according to the following equation.

$$\text{Stable timestep} = \frac{\text{Characteristic element length}}{\text{Acoustic wave speed in element material}}$$

$$\text{where dilatational wave speed} = \sqrt{\frac{203000}{0.780\times10^{-8}\left(1\text{-}0.3^2\right)}} = 5240000 \text{ mm/s for steel}$$

$$\text{and element length} = \frac{A}{\max(L_1, L_2, L_3, L_4)} = \frac{25}{5} = 5 \text{ for a 4 noded shell element}$$

$$\text{hence stable timestep} = \frac{5}{5240000} \approx 1\times10^{-6}\text{s}$$

This timestep value was often used in crashworthiness simulations [Du Bois 2001] to give acceptable solution run times.

4.3.2. The construction of the vehicle model

Using [Du Bois 2001] and [FORD 1997] a number of pre and post processing model quality guidelines (as shown in the appendices) were used in the construction of the new vehicle model shown in Figure 4.3.

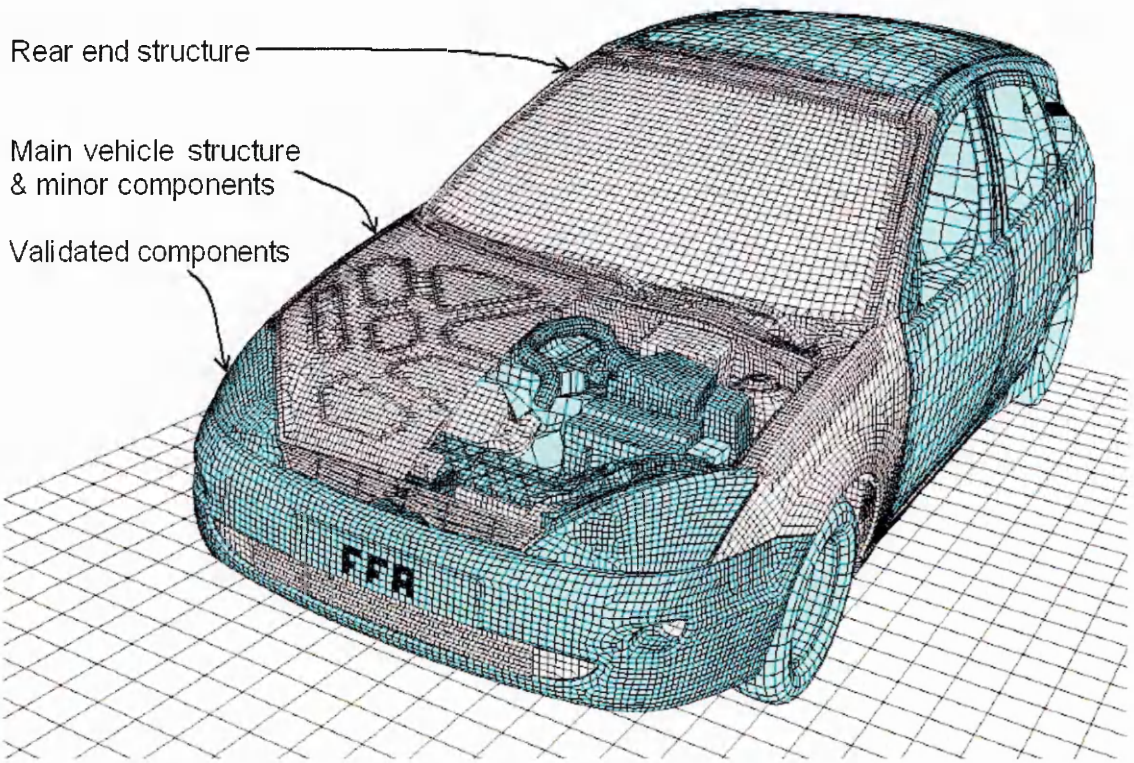

Figure 4.3 An overview of the reference vehicle model

There were three distinct regions: the rigid rear end structure, the main vehicle structure and non critical components and finally the validated components. The rear end structure was transplanted from a frontal crash model and modified for this application by removing unnecessary mesh geometry. This corresponded to zone 3 as defined in [Ford 1997] and was modelled in a rigid material with coarse mesh geometry and an average element size greater than 50 mm. It was assumed that this region of the model would not significantly influence the results. The validity of this assumption was confirmed in sub system impactor [Howard 2000-2] and accident simulations [Howard 2000-3] where no impacts occurred near this region.

The second vehicle region was the main vehicle structure and vehicle components that were defined with standard material properties [Ford 1997] and generally not

directly involved in pedestrian accidents [Howard 2000-2, 2000-3]. Finally, the validated component models that were more critical to pedestrian accidents were developed with a systematic testing and modelling methodology [Howard 2000-1]. The details of the CAD and FE model sources of every vehicle model part are summarised in the appendices.

To assist in the transfer of data between CAD models and the finite element master model, the latter model needed to be oriented and positioned in the same global body co-ordinate system as the former. At the same time, for pedestrian accident simulations the vehicle model needed to be oriented and positioned relative to the ground in an appropriate manner to simulate the influence of braking and actual vehicle suspension height variations. In addition it was easier to simulate gravity in the finite element model if the ground plane was in line with the body co-ordinate system (i.e. gravity was then globally applied in the Z direction). All these factors led to the assumption of no vehicle pitch under maximum braking conditions and hence the ground plane was positioned in the XY plane of the global body co-ordinate system.

Further investigations [Howard 2000-3] revealed the need to at least simulate uniform vehicle dive under braking and the remaining questions concerned where to set the initial ground position before and subsequently after braking. There were significant ride height variations in production vehicles and furthermore it was not known what the ride height of a vehicle would be in an actual pedestrian accident because of the variation in dynamic ride height depending on the vehicle loading and degree of braking. In an attempt to reduce the uncertainty the static bumper heights of ten similar vehicles were measured to determine the possible range of values. A mean value of 53 cm was determined and after moving the ground part in the finite element model to this position it was moved upward by a further 7 cm to simulate brake dive. The latter figure was from internal Ford Motor Company data.

The vehicle rear end structure

It was assumed that the rear half of the vehicle played a minor role in all the simulations and therefore to reduce the amount of modelling required the geometry

from the rear half of a RADIOSS frontal crash model was used [Ford 1999]. This was translated in Hypermesh to a Master Series universal file format and partly remeshed in Master Series to provide the structure shown in Figure 4.4. The structure was subsequently attached to the rest of the vehicle by merging nodes.

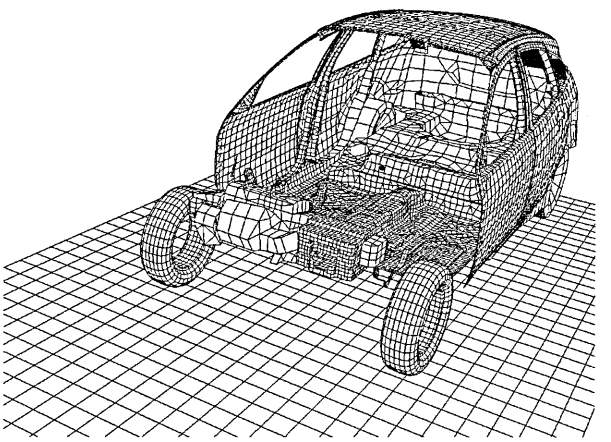

Figure 4.4 The vehicle rear end structure model

In addition to the rear end geometry, some of the other crash model components were also added to form one part (e.g. engine assembly, battery box, tyres). These components were assumed to be less significant in the accident simulations but assisted visualisation and allowed the model to be quickly updated. For instance, the geometry of the battery box was fully defined and it referenced a rigid material card. If pedestrian accident simulations showed that a rigid material description was inadequate, for example because component deformation was expected, then only the material card needed to be changed.

Material law 20 (MAT_RIGID) was used for the rigid rear end with the LS-DYNA keyword parameters based on the mild steel properties described in [Ford 1997]. All global displacements and rotations except the displacement in X were constrained for this part so that it behaved like a guided impact sled in the pedestrian accident simulations. The details of the material card are shown in Table 4.1.

RIGID ENGINE ASSEMBLY & VEHICLE INERTIA Material law 20
$\rho = 0.780E-08\ \text{ton/mm}^3$ $E = 203000\ \text{N/mm}^2$ $\nu = 0.3$ Coupling flag for MADYMO = 0.0 (use normal DYNA updates not MADYMO) Coupling option for MADYMO = 0.0 (not used) Coupling option flag for MADYMO = 0.0 (not used) VDA surface alias name (not used) Centre of mass constraint option = 1.0 (constraints applied in global directions) First constraint parameter = 5.0 (constrained in y and z displacements) Second constraint parameter = 7.0 (constrained in x, y, z rotations) Various local coordinate system options not used
*MAT_RIGID $ Material 15 : RIGID_ENGINE_ASSEMBLY_&_CAR_INERTIA 15 0.780E-8 203000.0 0.3 0.0 0.0 0.0 1.0 5.0 7.0 0 0.0 0.0 0.0 0.0 0.0

Table 4.1 Rigid material card for the vehicle rear end structure

Due to the global nodal constraints in all freedoms except X and the imposition of a rigid body velocity curve in the pedestrian accident simulations, the exact moments of inertia of this part were not critical. However the code still required some values and so initial calculations were undertaken by using [MacInnis 1997] and these are listed in the appendices. The mass and moments of inertia of the rear end vehicle structure were defined with the part inertia card shown in Table 4.2.

RIGID ENGINE ASSEMBLY & VEHICLE INERTIA Part inertia card
Part 16 consisting of section 16 and material 15 X co-ordinate of centre of mass = 2840 mm in global vehicle co-ordinate system Y co-ordinate of centre of mass = 0 mm in global vehicle co-ordinate system Z co-ordinate of centre of mass = (551-70) = 481 mm in global vehicle co-ordinate system when vehicle in diving position Translational part mass = 0.9 tonne (for the rear end of the vehicle) Global inertia tensor I_{xx} = 511406 tonne mm^2 I_{yy} = 6082755 tonne mm^2 I_{zz} = 2115367 tonne mm^2
*PART_INERTIA $ PART ID SECT ID MAT ID RIGID_ENGINE_ASSEMBLY_&_CAR_INERTIA @ RIGID_ENGINE_ASSEMBLY_&_CAR_INERTIA 16 16 15 0.284E+04 0.000E+00 0.481E+03 0.900E+00 0.511E+06 0.000E+00 0.000E+00 0.608E+07 0.000E+00 0.212E+07 0.000E+00 0.000E+00 0.000E+00 0.000E+00 0.000E+00 0.000E+00

Table 4.2 Part inertia card for the vehicle rigid rear end structure

The main vehicle structure

During the creation of the main vehicle structure model, CAD data was imported into Master Series in order to prepare it (e.g. to remove unnecessary data) for pre processing (e.g. mesh generation and boundary conditions) and subsequent translation into an LS-DYNA keyword file. Figure 4.5 shows the mesh geometry.

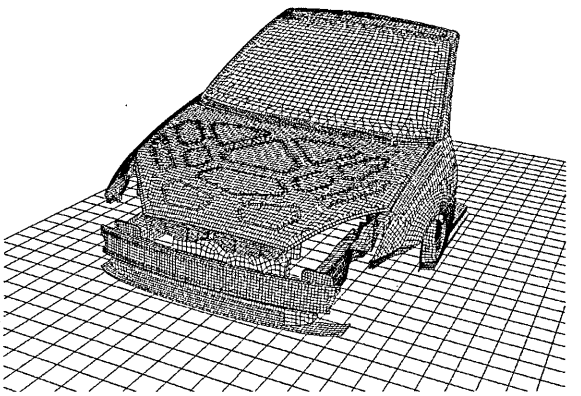

Figure 4.5 The main vehicle structure model

The model was meshed with a target element size between 12 mm and where necessary 5 mm in order to maintain a good representation of certain components. For example, the hood inner panels required smaller elements in order to correctly represent stiffeners and hence panel stiffness. In other parts, such as the fenders, the mesh density was varied from 10 mm to 20 mm according to whether a region of the part played an important role in the simulation (i.e. was likely to be struck or influence the stiffness of the impact locations). In general, regions of the model that were larger and flatter (i.e. the mesh geometry could more easily match the actual geometry) and away from the likely impact locations were meshed with larger elements. This approach was in line with [Ford 1997].

Figure 4.6 shows the parts of the main vehicle structure that were connected to the rigid rear end structure. Some of the validated component models such as the intercooler pipes and air filter box were also rigidly mounted to the rigid rear end structure. It was assumed that they had relatively low inertia and stiffness compared to the mounting structure. The same assumption was also used with the experimental validation of some component models [Howard 2000-1].

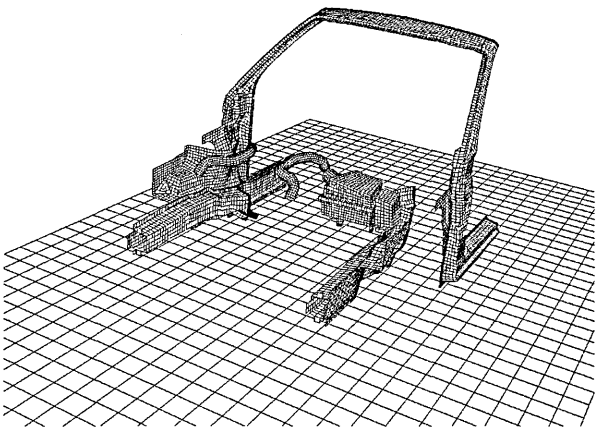

Figure 4.6 Parts connected to the rear end structure model

Most of the main vehicle structure (e.g. fenders) and non critical parts were defined with type 3 (MAT_PLASTIC_KINEMATIC) material properties from [Ford 1997]. This material law provides a cost effective means to represent elastic plastic behaviour in mild steel [LS-DYNA 1999-1] with the model shown in Figure 4.7.

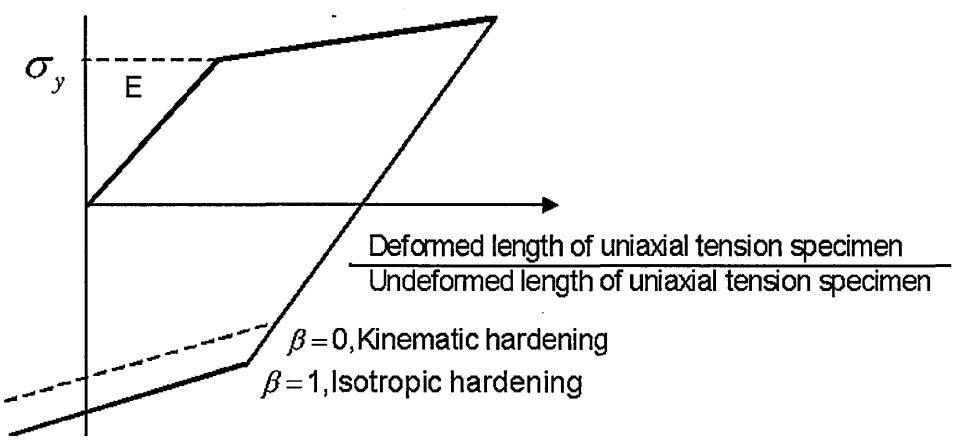

Figure 4.7 The elastic plastic behaviour of material 3

The influence of strain rate on the yield stress can be simulated using Cowper and Symonds equation to scale the yield stress [LS-DYNA 1999-1]:

$$1+\left(\frac{\dot{\varepsilon}}{\mathrm{SRC}}\right)^{\left(\frac{1}{\mathrm{SRP}}\right)}$$

SRC and SRP are two strain rate coefficients for the particular material. An element strain level can also be specified for element failure and subsequent erosion. However these features were not used because mild steel has relatively low strain rate sensitivity under pedestrian impact energy levels and material failure in steel vehicle body parts has not been observed in experimental tests [Howard 2000-2].

The material card was derived from a RADIOSS material model of mild steel specified in [Ford 1997] and shown in Table 4.3.

GENERIC ISOTROPIC STEEL		
RADIOSS material law 2		LS-DYNA material law 3
$\rho = 7.80E-06\,kg/mm^3$	$\varepsilon_{t1} = 0.48$	$\rho = 0.78E-08\,ton/mm^3$
$E = 203.00\,GPa$	$\varepsilon_{m1} = 0.50$	$E = 203000 N/mm^2$
$\nu = 0.30$	$d_{max1} = 0.999$	$\nu = 0.30$
$a = 0.192\,GPa$	$\varepsilon_{f1} =$ default	$\sigma_y = 192\,N/mm^2$
$b = 0.111\,GPa$	$\varepsilon_{t2} = 0.48$	$E_T = 1110\,N/mm^2$
n = 0.22	$\varepsilon_{m2} = 0.50$	$\beta = 0.0$ (kinematic hardening)
$\varepsilon_{max} =$ default	$d_{max2} = 0.999$	SRC = 0.0 (no strain rate effect)
$\sigma_{max} = 0.303\,GPa$	$\varepsilon_{f2} =$ default	SRP = 0. 0 (no strain rate effect)
$c = 0.0$		FS = 0.0 (no element erosion due to failure)
$\dot{\varepsilon}_0 = 1.0$		VP = 0.0 (n.a. scale yield stress for rate)

```
*MAT_PLASTIC_KINEMATIC
$ Material 1 : GENERIC_ISOTROPIC_STEEL
         1  0.780E-8  203000.0       0.3     192.0     1110.0       0.0
       0.0       0.0       0.0       0.0
```

Table 4.3 RADIOSS & LS-DYNA material cards for mild steel (SAE 1010)

The same material card variables were used for an additional material card for the intercooler. Like many of the additional material cards that duplicated material variables, this allowed the properties to be independently changed, if the pedestrian accident simulations revealed that under some conditions a non critical part became critical. Material law 3 was also used for the radiator grille and ABS reservoir but ABS material variables were used from [Ford 1997] as shown in Table 4.4.

RADIATOR GRILLE PLASTIC		
RADIOSS material law 27		LS-DYNA material law 3
$\rho = 2.0E-06\,kg/mm^3$	$\dot{\varepsilon}_0 =$ default	$\rho = 0.20E-08\,ton/mm^3$
$E = 3.0\,GPa$	$\varepsilon_{t1} = 0.06$	$E = 3000\,N/mm^2$
$\nu = 0.25$	$\varepsilon_{m1} = 0.61$	$\nu = 0.25$
$a = 0.062\,GPa$	$d_{max1} =$ default	$\sigma_y = 62\,N/mm^2$
$b = 0.0$	$\varepsilon_{f1} =$ default	$E_T = 50\,N/mm^2$
n = 0.0	$\varepsilon_{t2} = 0.06$	$\beta = 0.0$ (kinematic hardening)
$\varepsilon_{max} =$ default	$\varepsilon_{m2} = 0.61$	SRC = 0.0 (no strain rate effect)
$\sigma_{max} =$ default	$d_{max2} =$ default	SRP = 0. 0 (no strain rate effect)
$c = 0.0$	$\varepsilon_{f2} =$ default	FS = 0.0 (no element failure & erosion)
		VP = 0.0 (n.a. scale yield stress for rate)

```
*MAT_PLASTIC_KINEMATIC
$ Material 6 : RADIATOR_GRILLE_PLASTIC
         6   0.20E-8    3000.0       0.25       62.0       50.0        0.0
       0.0       0.0       0.0       0.0
```

Table 4.4 RADIOSS & LS-DYNA material cards for ABS

The influence of strain rate was not modelled and no element erosion was specified

because the purpose of this part was only to represent vehicle stiffness in the grille area and not component failure. This part also ensured that the pedestrian model legs did not pass behind the vehicle surfaces and cause possible contact problems.

The combined mechanical properties of the windscreen glass and polymer interlayer materials were also modelled with material 3 with the material card variables based on a crash model [Ford 1999] as shown in Table 4.5.

WINDSCREEN GLASS	
RADIOSS material law 2	LS-DYNA material law 3
$\rho = 2.7E-06\ kg/mm^3$ $E = 30\ GPa$ $\nu = 0.20$ $\sigma_y = 0.028 GPa$ $b = 0.008$ (hardening parameter) $n = 1.0$ (hardening exponent) $\varepsilon_{max} = 10000$ (failure plastic strain) $\sigma_{max} = 0.032 GPa$ (maximum stress)	$\rho = 2.70E-09\ ton/mm^3$ $E = 30000\ N/mm^2$ $\nu = 0.20$ $\sigma_y = 28\ N/mm^2$ $E_T = 80\ N/mm^2$ $\beta = 0.0$ (kinematic hardening) SRC = 0.0 (no strain rate effect) SRP = 0. 0 (no strain rate effect) FS = 0.0 (no element failure & erosion) VP = 0.0 (n.a. scale yield stress for rate)
*MAT_PLASTIC_KINEMATIC $ Material 7 : WINDSCREEN_GLASS 7 0.27E-8 30000.0 0.2 28.0 80.0 0.0 0.0 0.0 0.0	

Table 4.5 RADIOSS & LS-DYNA material cards for the windscreen

Further research is needed to confirm that such a model is suitable for pedestrian impact conditions because the material properties of the windscreen are more critical (they greatly influence the pedestrian head acceleration and kinematics) in pedestrian accident simulations.

The bumper grille was also defined with material law 3 but the properties were based on a RADIOSS generic polypropylene material card specified in [Ford 1997] and shown in Table 4.6. The influence of strain rate was not modelled and no element erosion was allowed for the same reasons as for the radiator grille material model.

BUMPER GRILLE PLASTIC		
RADIOSS material law 27		LS-DYNA material law 3
ρ =1.0E-06kg/mm^3	ε_{t1}= 0.2	ρ =0.10E-08 ton/mm^3
E =2.2483GPa	ε_{m1}= 0.21	E =2248 N/mm^2
ν =0.35	d_{max1}= default	ν =0.35
a=0.0410GPa	ε_{f1}= default	σ_y = 41 N/mm^2
b=0.0	ε_{t2}= 0.2	E_T =50 N/mm^2
n=0.0	ε_{m2}= 0.21	β =0.0 (kinematic hardening)
ε_{max} =default	d_{max2}=default	SRC = 0.0 (no strain rate effect)
σ_{max} = default	ε_{f2}= default	SRP = 0.0 (no strain rate effect)
c= 0.1591		FS = 0.0 (no element failure & erosion)
$\dot{\varepsilon}_0$=0.01333ms^{-1}		VP = 0.0 (n.a. scale yield stress for rate)

```
*MAT_PLASTIC_KINEMATIC
$ Material 11 : BUMPER_GRILL_PLASTIC
        11   0.10E-8    2250.0      0.35      41.0      50.0       0.0
       0.0       0.0       0.0
```

Table 4.6 RADIOSS & LS-DYNA material cards for polypropylene

The plastic plenum chamber partition wall used a different set of material card variables from [Ford 1999] as shown in Table 4.7. The same properties but with an additional material card were also used for the electronics box.

PARTWALL PLASTIC	
RADIOSS material law 27	LS-DYNA material law 3
ρ =1.0E-06kg/mm^3	ρ =0.10E-08 ton/mm^3
E =1.707 GPa	E =1707 N/mm^2
ν =0.35	ν =0.35
a=0.0134GPa	σ_y = 13.4 N/mm^2
b=0.025	E_T =25 N/mm^2
n=0.3	β =0.0 (kinematic hardening)
ε_{max} =default	SRC = 0.0 (no strain rate effect)
σ_{max} = default	SRP = 0. 0 (no strain rate effect)
c= 0.0	FS = 0.0 (no element failure & erosion)
	VP = 0.0 (n.a. scale yield stress for rate)

```
*MAT_PLASTIC_KINEMATIC
$ Material 12 : PARTWALL_PLASTIC
        12    1.0E-9    1710.0      0.35      13.4      25.0       0.0
       0.0       0.0       0.0       0.0
```

Table 4.7 RADIOSS & LS-DYNA material cards for the plenum chamber

The primary function of the cooling pack was to limit the body structure deformation. Most of the mild steel variables described earlier for material law 3 were used in this additional material card as shown in Table 4.8. However, the cooling pipes were not modelled and therefore it was necessary to allow for this by increasing the density and hence the part mass to 20 Kg (i.e. the actual component mass). A comparison of the actual component and the simplified model is shown in Figure 4.8.

COOLING PACK			
RADIOSS material law 2			LS-DYNA material law 3
ρ =7.80E-06 kg/mm^3	ε_{t1}= 0.48		ρ =0.53E-07 ton/mm^3 (to give correct 20Kg mass)
E =203.00 GPa	ε_{m1}= 0.50		E =203000N/mm^2
ν =0.30	d_{max1}= 0.999		ν =0.30
a=0.192 GPa	ε_{f1}= default		σ_y = 192 N/mm^2
b=0.111GPa	ε_{t2}= 0.48		E_T =1110 N/mm^2
n=0.22	ε_{m2}= 0.50		β =0.0 (kinematic hardening)
ε_{max} =default	d_{max2}= 0.999		SRC = 0.0 (no strain rate effect)
σ_{max} = 0.303GPa	ε_{f2}= default		SRP = 0. 0 (no strain rate effect)
c= 0.0			FS = 0.0 (no element erosion due to failure)
$\dot{\varepsilon}_0$= 1.0			VP = 0.0 (n.a. scale yield stress for rate)

```
*MAT_PLASTIC_KINEMATIC
$ Material 10 : COOLING_PACK
        10 0.530E-07  203000.0 0.300E+00 0.192E+03 0.111E+04
       0.0       0.0       0.0       0.0
```

Table 4.8 RADIOSS & LS-DYNA material cards for the cooling pack

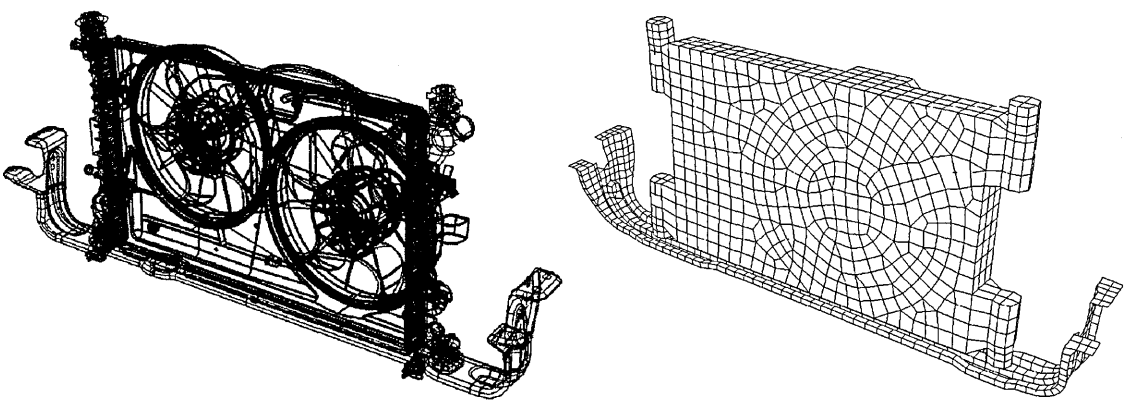

Figure 4.8 The actual radiator cooling pack and a simplified model

In addition to correcting for the mass it was also necessary to correct the boundary conditions because the coolant pipes would normally stiffen the cooling pack mounting. To allow for this the cooling pack support as shown in Figure 4.8 was defined with a dummy high strength material to prevent excessive deformation of this supporting part. Also the cooling pack was mounted on stiff rubber mounts with the solid properties shown in Table 4.9.

COOLING SUSP RUBBER Material law 1
ρ =0.1E-08 ton/mm^3 E =10 N/mm^2 ν =0.40

```
*MAT_ELASTIC
$ Material 14 : COOLING_SUSP_RUBBER
        14 0.100E-08 0.100E+02 0.400E+00
```

Table 4.9 Material card for the cooling pack rubber mounts

It was also not possible to create a fine enough mesh to correctly represent some of the smaller but highly stressed vehicle parts. For instance some of the hinge components had stiffening flanges which were smaller than the minimum target element size. If the correct material properties had been used then these components would have exhibited unrealistic deformation and ultimately premature failure. Therefore a simple mesh was created with a material law 3 model based on the mild steel properties described earlier but with much higher strength and stiffness to avoid these problems as shown in Table 4.10.

DUMMY HIGH STRENGTH Material law 3
ρ =0.789E-08 ton/mm^3 E =1000000 N/mm^2 ν =0.30 σ_y = 1000 N/mm^2 E_T =1500 N/mm^2 β =0.0 (kinematic hardening) SRC = 0.0 (no strain rate effect) SRP = 0.0 (no strain rate effect) FS = 0.0 (no element failure & erosion) VP = 0.0 (n.a. scale yield stress for rate)
*MAT_PLASTIC_KINEMATIC $ Material 16 : DUMMY HIGH STRENGTH 16 0.789E-8 1000000.0 0.3 1000.0 1500.0 0.0 0.0 0.0 0.0

Table 4.10 Material card for dummy high strength parts

The same material properties used for the polycarbonate parts of the validated headlamp described later were also used for the foglamps. Some parts of the vehicle body structure utilised high strength steel and these are shown in Figure 4.9.

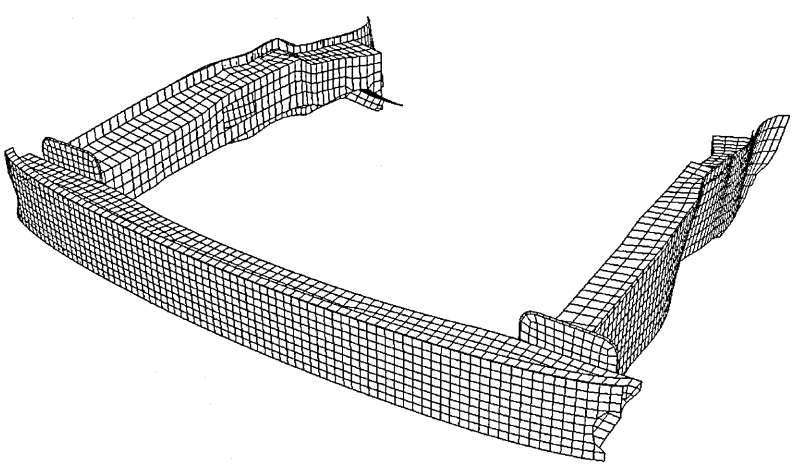

Figure 4.9 The high strength Steel parts

The material variables were determined from a RADIOSS material model specified in [Ford 1997] for generic high strength steel and shown in Table 4.11.

HIGH STRENGTH STEEL		
RADIOSS material law 27		LS-DYNA material law 3
ρ =7.80E-06kg/mm^3	$\dot{\varepsilon}_0$= 1.0	ρ =0.78E-08 ton/mm^3
E =203.00GPa	ε_{t1}= 0.17	E =203000N/mm^2
ν =0.30	ε_{m1}= 0.19	ν =0.30
a=0.345GPa	d_{max1}= 0.999	σ_y = 345 N/mm^2
b=0.095 GPa	ε_{f1}= default	E_T =1110N/mm^2
n=0.160	ε_{t2}= 0.17	β =0.0 (kinematic hardening)
ε_{max} =default	ε_{m2}= 0.19	SRC & SRP = 0.0 (no strain rate effect)
σ_{max} = 0.440GPa	d_{max2}= 0.999	FS = 0.0 (no element erosion due to failure)
c= 0.0	ε_{f2}= default	VP = 0.0 (n.a. scale yield stress for rate)

```
*MAT_PLASTIC_KINEMATIC
$ Material 23 : HIGH STRENGTH STEEL
        23  0.780E-8  203000.0        0.3     345.0    1110.0        0.0
       0.0       0.0       0.0
```

Table 4.11 RADIOSS and LS-DYNA material cards for high strength steel

A modified version of the ABS material card described earlier was also used for the undertray material as shown in Table 4.12. The Youngs Modulus of the undertray was increased to compensate for the lack of panel swages (i.e. they were too small to model within the element guidelines) and this was based on the results of correlated sub system impactor simulations undertaken with the leg impactor model [Howard 2000-2].

UNDERTRAY		
RADIOSS material law 27		LS-DYNA material law 3
ρ =2.0E-06kg/mm^3	$\dot{\varepsilon}_0$= default	ρ =0.20E-08 ton/mm^3
E =3.0GPa	ε_{t1}= 0.06	E =550 N/mm^2 (adjusted in draft directive simulations)
ν =0.25	ε_{m1}= 0.61	ν =0.25
a=0.062GPa	d_{max1}= default	σ_y = 8N/mm^2
b=0.0	ε_{f1}= default	E_T =25N/mm^2
n=0.0	ε_{t2}= 0.06	β =0.0 (kinematic hardening)
ε_{max} =default	ε_{m2}= 0.61	SRC & SRP = 0.0 (no strain rate effect)
σ_{max} = default	d_{max2} =default	FS = 0.0 (no element failure & erosion)
c= 0.0	ε_{f2}= default	VP = 0.0 (n.a. scale yield stress for rate)

```
*MAT_PLASTIC_KINEMATIC
$ Material 24 : UNDERTRAY
        18    2.0E-9      550.0       0.25        8.0       25.0        0.0
       0.0       0.0       0.0
```

Table 4.12 RADIOSS and LS-DYNA material cards for the ABS undertray

Material law 20 (MAT_RIGID) was used for the ground part. The material variables were based on the mild steel properties described earlier but all freedoms were fixed in global displacements and rotations as shown in Table 4.13.

RIGID GROUND FIXED Material law 20
$\rho = 0.780E\text{-}08\ \text{ton/mm}^3$ $E = 203000\ \text{N/mm}^2$ $\nu = 0.3$ Coupling flag for MADYMO = 0.0 (use normal DYNA updates not MADYMO) Coupling option for MADYMO = 0.0 (not used) Coupling option flag for MADYMO = 0.0 (not used) VDA surface alias name (not used) Centre of mass constraint option = 1.0 (constraints applied in global directions) First constraint parameter = 7.0 (constrained in x, y, z displacements) Second constraint parameter = 7.0 (constrained in x, y, z rotations) Various local coordinate system options not used
*MAT_RIGID $ Material 13 : RIGID_GROUND_FIXED 13 0.780E-8 203000.0 0.3 0.0 0.0 0.0 1.0 7.0 7.0 0 0.0 0.0 0.0 0.0 0.0

Table 4.13 Material card for the ground

Material law 20 was also used to represent components that needed to be rigid (e.g. to define joints) or could be modelled with a rigid material without influencing the model response. Such a material law also reduced the model solving time because rigid materials require shorter solution times than other material models [Du Bois 2001]. The variables in the LS-DYNA input deck card were based on mild steel properties as described in [Ford 1997] and shown in Table 4.14.

RIGID GENERAL Material law 20
$\rho = 0.780E\text{-}08\ \text{ton/mm}^3$ $E = 203000\ \text{N/mm}^2$ $\nu = 0.3$ Coupling flag for MADYMO = 0.0 (use normal DYNA updates not MADYMO) Coupling option for MADYMO = 0.0 (not used) Coupling option flag for MADYMO = 0.0 (not used) VDA surface alias name (not used) Centre of mass constraint option = 0.0 (constraints applied in global directions) First constraint parameter = 0.0 (no constraints in x, y, z displacements) Second constraint parameter = 0.0 (no constraints in x, y, z rotations) Various local coordinate system options not used
*MAT_RIGID $ Material 17 : RIGID_GENERAL 17 0.780E-8 203000.0 0.3 0.0 0.0 0.0 0.0 0.0 0.0 0 0.0 0.0 0.0 0.0 0.0

Table 4.14 Material card for general rigid parts

The validated components

Appropriate models of some of the critical vehicle components were not available and therefore a systematic vehicle component testing and modelling methodology was developed to create validated models of these components. This research is only briefly described here but a full description is available [Howard 2000-1].

The tasks concerned with testing included the removal of individual components from a vehicle, the isolated mounting of these components under appropriate boundary conditions on a test rig, and finally the reproduction of component failures observed in experimental tests using [EEVC 1998]. Every component needed to be mounted on the test rig in a manner similar to the way in which it was mounted in the vehicle. In most cases simplified impactors were used with reduced impactor mass (but identical impact velocity) to allow for the effects of mounting a component in isolation from any surrounding structure.

The surrounding structure usually absorbs some of the impact energy when a component is mounted in the vehicle and the supporting structure is not rigid so that some energy is transferred through the component and into the vehicle. If the mass was not reduced (and hence the impact energy) it was not possible to reproduce appropriate component failures and reducing the velocity would have been inappropriate for strain rate dependent materials. After collecting appropriate measures for each component a finite element model of the test rig and component was created to allow model correlation and hence component validation. An outline of the basic methodology is shown in Figure 4.10 [Howard 2000-1].

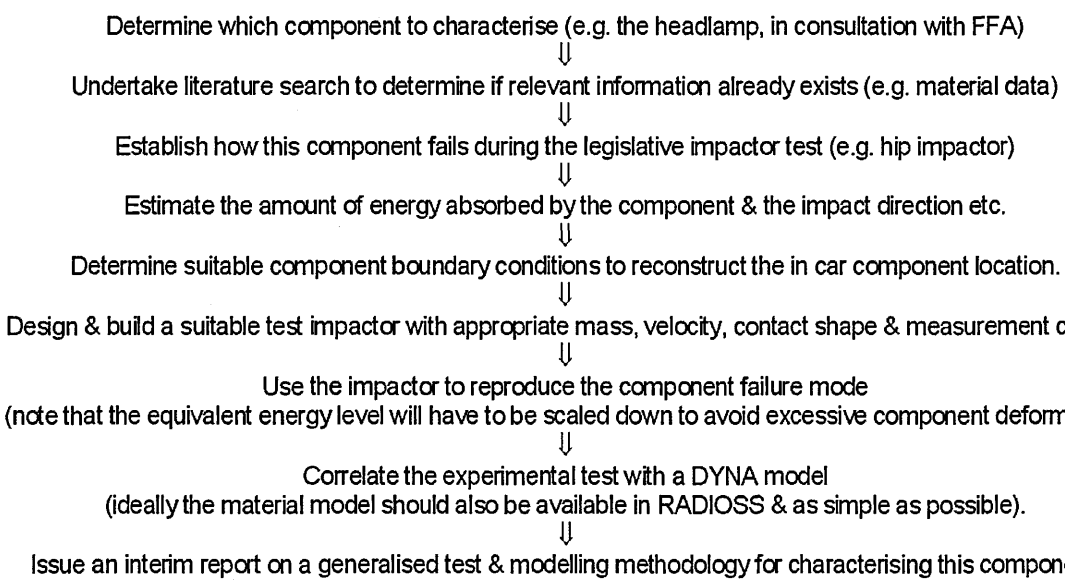

Figure 4.10 Component validation methodology

The validated component models that were used in the new vehicle are shown in Figure 4.11.

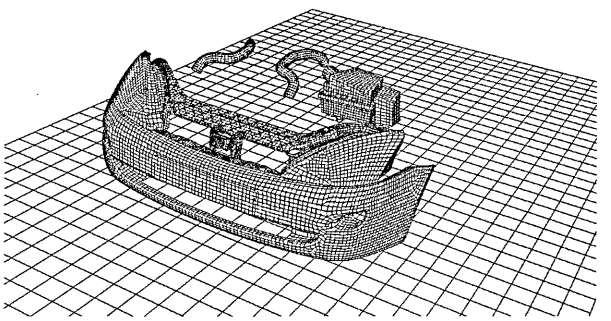

Figure 4.11 The validated vehicle component models

The validated component material properties will now be described. Material law 24 (MAT_PIECEWISE_LINEAR_PLASTICITY) was used to model the material behaviour of the bake hardening steel ZSTE220BH parts in the grille opening reinforcement (GOR). Material law 24 allows the input of an arbitrary stress versus strain curve (e.g. experimentally measured data points) as shown in Figure 4.12 and the input of different stress versus strain curves at different strain rates. It is also possible to input a maximum element plastic strain or minimum time step size for element erosion.

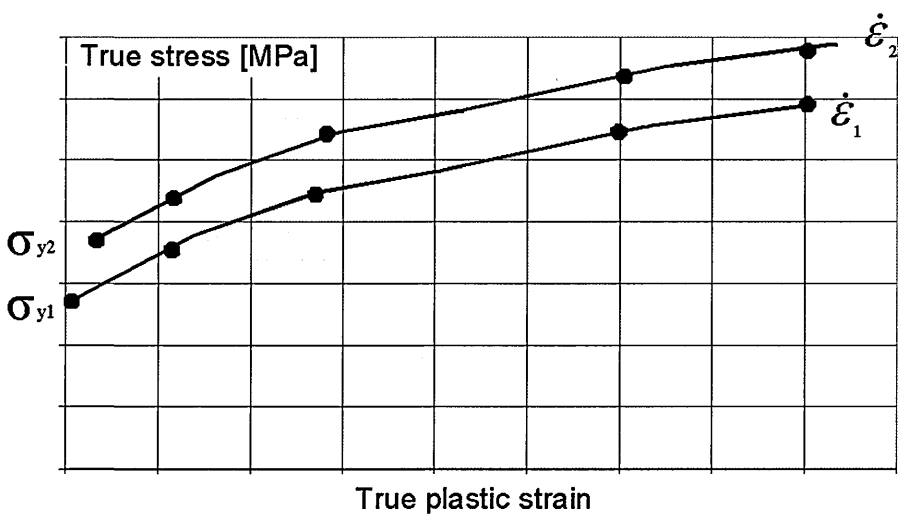

Figure 4.12 Elastic plastic behaviour of the GOR bake hardening steel

The data points for the GOR steel were determined from [fka 1998-1]. Although several stress versus strain curves at different strain rates were measured, only one pseudo static stress versus strain curve was used because the strain rate effect was insignificant. However, element erosion at a plastic strain of 1 was included

because GOR material failures have been observed in experimental tests [EEVC 1998]. The material card is shown in Table 4.15.

GOR ST Material law 24
$\rho = 0.785\text{E-}08\ \text{ton/mm}^3$ $E = 210000\text{N/mm}^2$ $\nu = 0.30$ $\sigma_y =$ 0.0 (not specified so a stress strain curve is expected) $E_T =$ 0.0 (not specified) FAIL=1 (the plastic strain to failure value for element erosion) TDEL = 0.0 (no minimum timestep for element erosion) Strain rate parameters C and P = 0 (no strain rate effects specified) LCSS = 0.0 (load curve not specified) LCSR = 0.0 (load curve for strain rate scaling effects on yield stress not specified) VP =0.0 (scale yield stress for rate effects) EPS1-EPS8 = specified effective plastic strain values with first point corresponding to yield ES1-ES8 = corresponding stress values
*MAT_PIECEWISE_LINEAR_PLASTICITY $ Material 2 : GOR_ST 2 0.785E-8 210000.0 0.3 0.0 0.0 1.0 0.0 0.29E-1 0.58E-1 0.113 0.19 1.0 250.0 332.0 383.0 458.0 558.0 1000.0

Table 4.15 Material card for the GOR bake hardening steel

Material law 24 was also used for modelling the material behaviour of the BAYER PA6 polymer parts in the grille opening reinforcement. In the same manner as for the bake hardening steel the polymer material properties were simulated with a series of experimentally measured data points that were obtained with the methodology described in [fka 1998-1]. The variables used in the material card are shown in Table 4.16.

GOR PA Material law 24
$\rho = 0.136\text{E-}08\ \text{ton/mm}^3$ $E = 6000\text{N/mm}^2$ $\nu = 0.30$ $\sigma_y =$ 0.0 (not specified so a stress strain curve is expected) $E_T =$ 0.0 (not specified) FAIL=0.067 (plastic strain to failure for element erosion) TDEL = 0.0 (no minimum timestep for element erosion) Strain rate parameters C & P = 0 (no strain rate effects specified) LCSS & LCSR = 0.0 (load curve not specified & load curve for strain rate effects on yield stress not specified) VP =0.0 (scale yield stress for rate effects) EPS1-EPS8 = specified effective plastic strain values with first corresponding to yield ES1-ES8 = corresponding yield stress values
*MAT_PIECEWISE_LINEAR_PLASTICITY $ Material 3 : GOR_PA 3 0.136E-8 6000.0 0.3 0.0 0.0 0.666E-1 0.0 0.8E-2 0.19E-1 0.42E-1 0.67E-1 0.0 0.0 36.0 82.0 100.0 112.0 109.0 0.0 0.0

Table 4.16 Material card for the GOR BAYER PA6 polymer

Although the original implementation of this material model included the input of several stress strain curves for different strain rates the input data was eventually reduced to one input curve for the same reasons as with the GOR steel.

Material law 3 was used for the GE Plastics LEXAN LS2 headlamp polycarbonate. The material variables as shown in Table 4.17 were determined from [fka 1998-2] with additional variables to allow for strain rate influences and failure strain erosion. These were necessary because the component tests revealed a high strain rate dependency and failure was observed during testing using [EEVC 1998].

HL PC Material law 3
$\rho = 0.12E-08$ ton/mm^3 $E = 2600$ N/mm^2 $\nu = 0.40$ $\sigma_y = 70$ N/mm^2 $E_T = 10$ N/mm^2 $\beta = 0.0$ (kinematic hardening) SRC = 1.0 (strain rate parameter c) & SRP = 17.0 FS = 1.0 (failure strain for element erosion) VP = 0.0 (scale yield stress)
*MAT_PLASTIC_KINEMATIC $ Material 4 : HL_PC 4 0.12E-8 2600.0 0.4 70.0 10.0 0.0 1.0 17.0 1.0 0.0

Table 4.17 Material card for the headlamp polycarbonate

The same material law was used for the Hostacom T20H563 polypropylene parts in the headlamp with the variables shown in Table 4.18 taken from [fka 1998-2].

HL PP Material law 3
$\rho = 0.104E-08$ ton/mm^3 $E = 3200$ N/mm^2 $\nu = 0.4$ $\sigma_y = 35$ N/mm^2 $E_T = 40$ N/mm^2 $\beta = 0.0$ (kinematic hardening) SRC = 0.0 (no strain rate effect) SRP = 0.0 (no strain rate effect) FS = 0.1 (element strain for failure & erosion) VP = 0.0 (n.a. scale yield stress for rate)
*MAT_PLASTIC_KINEMATIC $ Material 5 : HL_PP 5 0.104E-8 3200.0 0.4 35.0 40.0 0.0 0.0 0.0 0.1 0.0

Table 4.18 Material card for the headlamp polypropylene

Again material law 3 was used for the polypropylene Targor Hostacom XM1 U14

bumper cover. The variables for the material are shown in Table 4.19 and are based on [fka 1999-1]. Strain rate effects were not considered to be significant but element failure was included to allow for the possibility of bumper cover damage because this had been occasionally observed in tests [EEVC 1998].

BUMPERSHELL PLASTIC Material law 3
ρ =0.97E-09 ton/mm^3 E =1110 N/mm^2 ν =0.4 σ_y = 16 N/mm^2 E_T =0.0 N/mm^2 β = 0.0 (kinematic hardening) SRC = 0.0 (no strain rate effect) SRP = 0.0 (no strain rate effect) FS = 0.9 (element strain for failure & erosion) VP = 0.0 (n.a. scale yield stress for rate)
*MAT_PLASTIC_KINEMATIC $ Material 9 : BUMPERSHELL_PLASTIC 9 0.97E-9 1110.0 0.4 16.0 0.0 0.0 0.0 0.0 0.9 0.0

Table 4.19 Material card for the bumper polypropylene

The results of [fka 1999-2] also led to material law 3 being used for the polypropylene GF+P 30 air filter box with the variables used shown in Table 4.20. Strain rate effects were not observed but element failure was included to allow for the air filter box damage that had been observed in the component tests.

AIR FILTER BOX Material law 3
ρ =0.117E-08 ton/mm^3 E =5000 N/mm^2 ν =0.4 σ_y = 40 N/mm^2 E_T =3.5 N/mm^2 β = 0.0 (kinematic hardening) SRC = 0.0 (no strain rate effect) SRP = 0.0 (no strain rate effect) FS = 0.03 (element strain for failure & erosion) VP = 0.0 (n.a. scale yield stress for rate)
*MAT_PLASTIC_KINEMATIC $ Material 21 : AIR FILTER BOX 21 0.117E-8 5000.0 0.4 40.0 3.5 0.0 0.0 0.0 0.3E-1 0.0

Table 4.20 Material card for air filter box polypropylene

The material properties of the intercooler ducting pipe are shown in Table 4.21 and taken from [fka 1999-3]. Again strain rate effects were not significant but element failure was included.

INTERCOOLER PIPE Material law 3
$\rho = 0.785\text{E-}08\ \text{ton/mm}^3$ $E = 210000\text{N/mm}^2$ $\nu = 0.3$ $\sigma_y = 365\ \text{N/mm}^2$ $E_T = 1400\text{N/mm}^2$ $\beta = 0.0$ (kinematic hardening) SRC = 0.0 (no strain rate effect) SRP = 0.0 (no strain rate effect) FS = 0.25 (element strain for failure & erosion) VP = 0.0 (n.a. scale yield stress for rate)
*MAT_PLASTIC_KINEMATIC $ Material 22 : INTERCOOLER PIPE 22 0.785E-8 210000.0 0.3 365.0 1400.0 0.0 0.0 0.0 0.25 0.0

Table 4.21 Material card for the intercooler pipe steel

A SECTION SOLID card as shown in Table 4.22 referenced the solid elements and an example of a SECTION SHELL card is shown in Table 4.23 for the shell elements (the shell thickness and hence shell cards varied between the parts).

SECTION_SOLID
Section property id Constant stress solid element (default) - use a value of 2 for fully integrated selectively reduced element if hourglassing No other factors specified (default)
*SECTION_SOLID 15 1 0 . . .

Table 4.22 Section card for all solids

SECTION_SHELL
Section property id Belytschko-Tsay element (default) No shear factor to scale the transverse shear stress (default) Three through shell thickness integration points (default) Print out average fiber lengths and resultants (default) Absolute value specified is integration rule ID (default) No material angle specified for each layer (i.e. not orthotropic/anisotrpic) 2D solid element formulation type not relevant All shells constant thickness as defined by CAD data – in this case 0.7mm No other factors specified (default)
*SECTION_SHELL 1 2 1.0 3 1.0 0.0 0 0 0.7 0.7 0.7 0.7 0.0 . . . .

Table 4.23 An example of a section card for shells

Part connections and joints

The windscreen was connected to the vehicle structure with non linear springs and the hood inner to the hood outer with elastic springs. The spring values were based on [Ford 1996, 1999]. However, adhesive failures were not expected and therefore

spring failure variables were not set. Material law 134 (MAT_SPRING_NONLINEAR_ELASTIC) was used for the windscreen springs as shown in Table 4.24.

IDEAS MATERIAL 49 (WINDSCREEN ADHESIVE SPRINGS)	
RADIOSS property set type 49	LS-DYNA material law 134
m = 0.002 Kg I = 0.1000000 Iskew = 0.0 Isensor = 0.0 Isflag = 0.0 Ifail (rupture) = 0.0 K (tension stiffness), (tension damping)=0.0 A,B,D coefficients = 0.0 Function number = 1002 Elastoplastic with hardening = 1 -ve & +ve rupture displacement = -1.25mm 1002 – displacement/force curve	Youngs modulus $E = \frac{72}{0.125} = 576\text{N/mm}^2$ Tangent modulus $E_T = \frac{(73-72)}{(1.25-0.125)} = 0.889\text{N/mm}^2$ Yield force $F_y = 72\text{N}$ (from displacement/force curve) No rupture displacement as seen in section discrete card
*MAT_SPRING_ELASTOPLASTIC $ Material 49 : WINDSCREEN ADHESIVE SPRINGS 49 0.576E+03 0.889E+00 0.720E+02	

Table 4.24 RADIOSS and LS_DYNA material cards for windscreen adhesive

The hood adhesive springs were modelled with material law 131 (MAT_SPRING_ELASTIC) as shown in Table 4.25.

IDEAS MATERIAL 119 (HOOD ADHESIVE SPRINGS) Material law 131
$k = 48\text{N/mm}$
*MAT_SPRING_ELASTIC $ Material 119 : HOOD ADHESIVE SPRINGS 119 0.480E+02

Table 4.25 Material card for hood adhesive

An ELEMENT DISCRETE and a SECTION DISCRETE card as shown in Table 4.26 were also referenced by all the windscreen and hood springs.

ELEMENT DISCRETE (WINDSCREEN AND ADHESIVE SPRINGS)								
Spring id, section id, the spring force acts from the first node to the second node with a scale force of 1, is printed out and there is no initial spring offset.								
*ELEMENT_DISCRETE 33456	119	36598	14716	0	1.0	0	0.0	

Table 4.26 Discrete element card for all springs

SECTION DISCRETE (WINDSCREEN AND ADHESIVE SPRINGS)					
Section id and a translational spring No dynamic magnification factor K_d and no dynamic test velocity V_0 for $F_{dynamic} = \left[1 + k_d \frac{V}{V_0}\right] F_{static}$ and hence all the spring forces calculated are only based on the elastic stiffness specified and not scaled for different velocities. No compressive spring displacement before starting material force/displacement curve & hence a compressive spring. No failure deflection, no deflection limits in compression or tension (based on draft directive test observations).					
*SECTION_DISCRETE					
49	0	0.0	0.0	0.0	0.0
0.0	0.0				
119	0	0.0	0.0	0.0	0.0
0.0	0.0				

Table 4.27 Section discrete card for all springs

Vehicle parts were connected with blue coupled degrees of freedom in Master Series so that these would be translated by N/CODE into spot welds in LS-DYNA at the locations specified in the master CAD files listed in the appendices. Some of the small brackets connecting component parts with the main vehicle structure were also modelled with coupled degrees of freedom. There were two reasons for doing this: firstly it was not possible to model small brackets without using elements that were smaller than the model guidelines and secondly no deformation had been observed in these brackets during experimental tests [EEVC 1998]. In both cases setting high spot weld failure loads in the spot weld cards prevented failure. The CONSTRAINED GENERALIZED WELD SPOT and CONSTRAINED SPOTWELD cards used are shown in Table 4.28; the main difference between these is that the latter can only be defined to connect two nodes.

CONSTRAINED GENERALISED WELD SPOT and CONSTRAINED SPOTWELD CARDS					
Node set id. and in the second card the two node numbers Coordinate system id. for data output is the global system Simple averaging of force vector components and no time window Number of nodal pairs Print option for RBDOUT based on control card Failure time at which constraint becomes inactive (default) Effective plastic strain at failure Normal and shear forces at failure are set to very high values in order to avoid any failure. Brittle failure occurs when the sum of the normal and shear forces $\left(\frac{\max(f_n,0)}{S_n}\right)^n + \left(\frac{\lvert f_s \rvert}{S_s}\right)^m \geq 1$ and f_n and f_s are the normal and shear interface forces and n and m the exponents for the normal and shear forces respectively.					
*CONSTRAINED_GENERALIZED_WELD_SPOT					
2	0	0	0.0	0	0
1.0E20	1.0E20	1.0E20	1.0E20	2.0	2.0
*CONSTRAINED_SPOTWELD					
192	5394	1.0E20	1.0E20	2.0	2.0

Table 4.28 Spot weld cards

There were only two joints in the original vehicle model and these were used to represent the hood hinges with revolute joints. The CONSTRAINED JOINT

REVOLUTE variables are shown in Table 4.29.

CONSTRAINED JOINT REVOLUTE CARD						
Four nodes are used to define the revolute joint; nodes 1 and 3 are in rigid body A and nodes 2 and 4 in rigid body B Relative penalty stiffness =1 (default) Damping scale factor = 1 (default)						
*CONSTRAINED_JOINT_REVOLUTE						
8805	54249	54248	8799		1.0	0.0
.	.	.	.		.	.

Table 4.29 Revolute joint card for the hood hinges

The hinge mesh geometry was modelled with a combination of rigid and dummy high strength material properties. Rigid material elements were necessary for the definition of the revolute joints and dummy high strength material properties were used to prevent unrealistic plastic deformation of the mesh geometry and avoid hourglassing (see appendices for definition). The latter problems were caused by the highly simplified geometry of the hinges in which the detailed stiffening features (e.g. ribs and complex curvature) of the hinges were difficult to model within the element size guidelines. Figure 4.13 shows the hood hinge model.

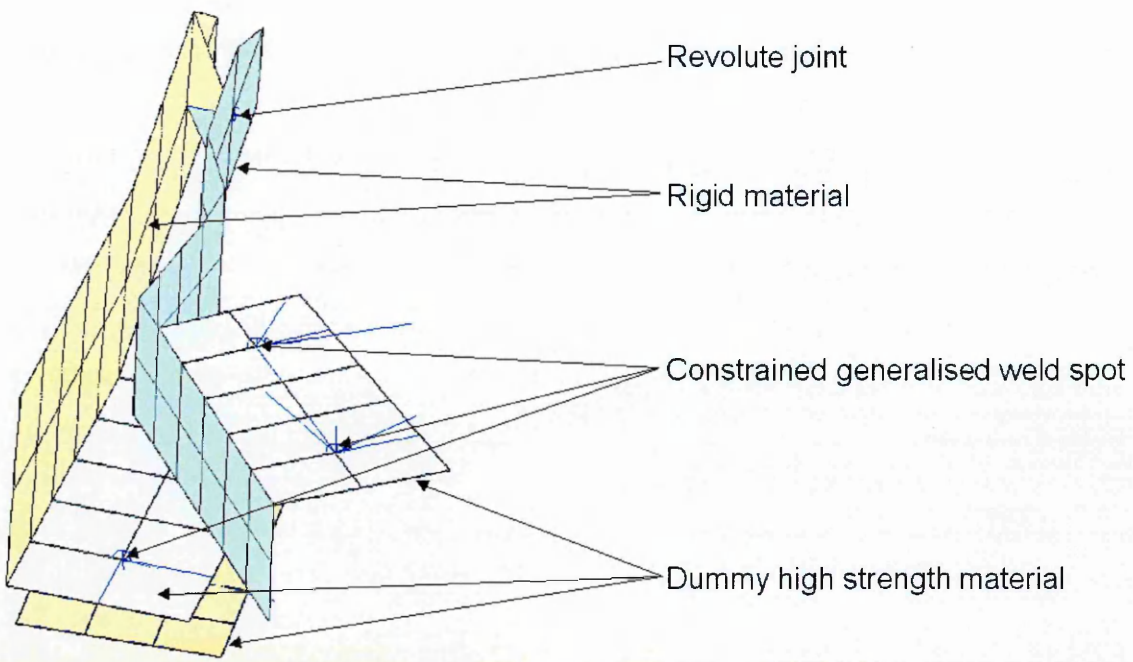

Figure 4.13 The hood hinge model

However, the latch was modelled with standard mild steel properties because deformation of this had been observed in sub system impactor tests (it was directly in line with a possible impact location) and the mesh geometry was sufficiently dense to avoid hourglassing. Figure 4.14 shows the hood latch model.

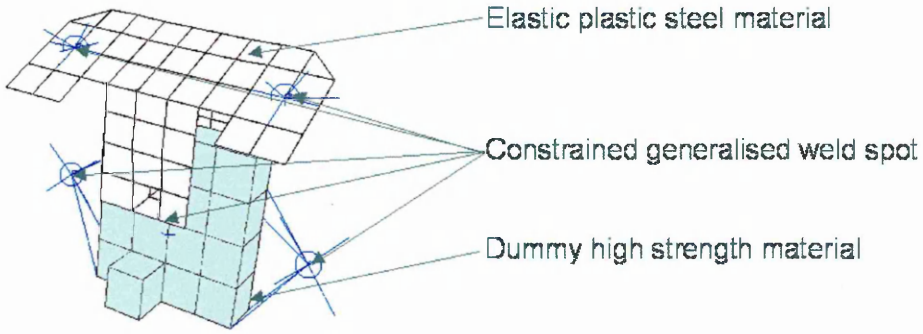

Figure 4.14 The hood latch model

Vehicle model contacts

One vehicle contact was defined with a type 13 or automatic single surface contact as shown in Table 4.30. Additional contacts were added to the vehicle model when it was combined with a pedestrian model in pedestrian accident simulations. This type of contact is two sided and utilises a segment search routine to reduce the computing power required.

The advantages of such a contact type was convenience (e.g. it is only defined by adding part numbers to a contact set) and stability under most modelling conditions. For these two reasons there was one contact surface for the vehicle. However, one of the disadvantages of this type of contact was that the thickness of elements and the initial separation distance of model parts were important. Some component CAD data had not been supplied with surfaces (it was not available at the time the car model was originally constructed), the target element size was relatively large and the validated component models were created separately from the vehicle model. As a result of this there were small errors in the model geometry and initial part penetrations when the whole vehicle model was integrated in Master Series. It was not acceptable to solve the model with these penetrations because they could have caused stresses that exceeded the yield stress and initiated unrealistic model behaviour from time zero (e.g. buckling). The penetration problem was solved by editing the mesh geometry of the problem parts (the largest initial penetrations were listed in the solved model output file) and removing some of the not critical parts from the vehicle to vehicle contact as shown in Figure 4.15.

AUTOMATIC SINGLE SURFACE CONTACT CARD
Contact number 1 named vehicle to vehicle Slave node set id. Master node set id not defined for single surface contact. Part set id definition used. Master segment box id. Slave and master side forces can not be output for this type of surface so the default values are ignored. Static coefficient of friction = 0.2 (default). Dynamic coefficient of friction = 0.2 (default). No normal tensile or shear force failure specified (default). No decay coefficient (default) No exponents for viscous friction or damping (default). Small penetration check is switched off (default). Birth time is zero and death time very large (default). No scale factors on slave or master penalty stiffnesses (default). No override or scale factors on slave or master element thicknesses (default). No coulomb or viscous friction scale factors (default). Penalty rather than soft constraint formulations used (default). Scale factor of 0.1 on soft constraint option (default). Maximum parametric coordinate in segment search set to 1.02 (default). Alternate edge to edge penetration check not used because default penalty method used (default). Search depth set to 2 (default), a value of 1 is quicker but less accurate. No cycles between bucket sorts (default). 1 cycle between contact force updates for penalty contact formulations (default)

```
*CONTACT_AUTOMATIC_SINGLE_SURFACE_TITLE
         1  VEHICLE_TO_VEHICLE
         1         0         2         0         1         0         1         1
       0.2       0.2       0.0       0.0       0.0         0       0.0   1.0E10
       0.0       0.0       0.0       0.0       0.0       0.0       0.0       0.0
         0       0.1         0      1.02       0.0         2         0         1
*SET_PART
         1
         1         2         3         4         5         6         8         9
        10        11        12        13        14        15        16        18
        19        20        21        22        25        28        30        31
        32        33        36        37        38        39        40        41
        42        43        44        45        46        47        48        50
        51        52        54        55        56        57        61        62
        63        68        69        70        71        74        76        77
        78        79        80        81        82        83        84        85
        86        87        88        89        90        91        92        93
        94        95        96        97       103       105       106       107
       108       109       110       111       112       113       114       115
       118
*DEFINE_BOX
         1 0.819E+03 0.508E+04-0.929E+03 0.929E+03 0.980E+02 0.172E+04
```

Table 4.30 Contact and part set cards for all vehicle to vehicle contacts

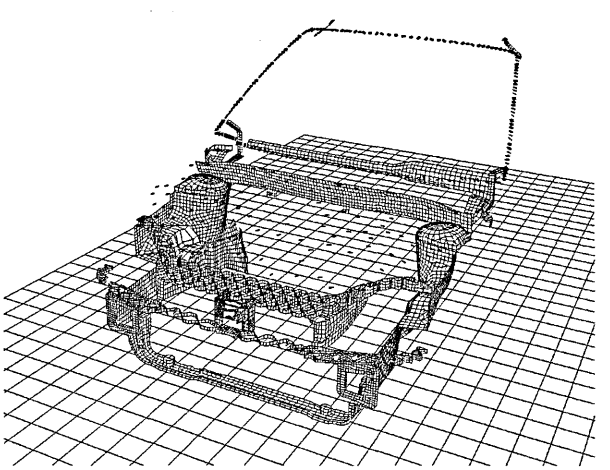

Figure 4.15 Vehicle parts removed from the vehicle to vehicle contact

Vehicle model boundary conditions

The vehicle model incorporated the boundary conditions shown in Figure 4.16 to enable it to be used in pedestrian accident simulations.

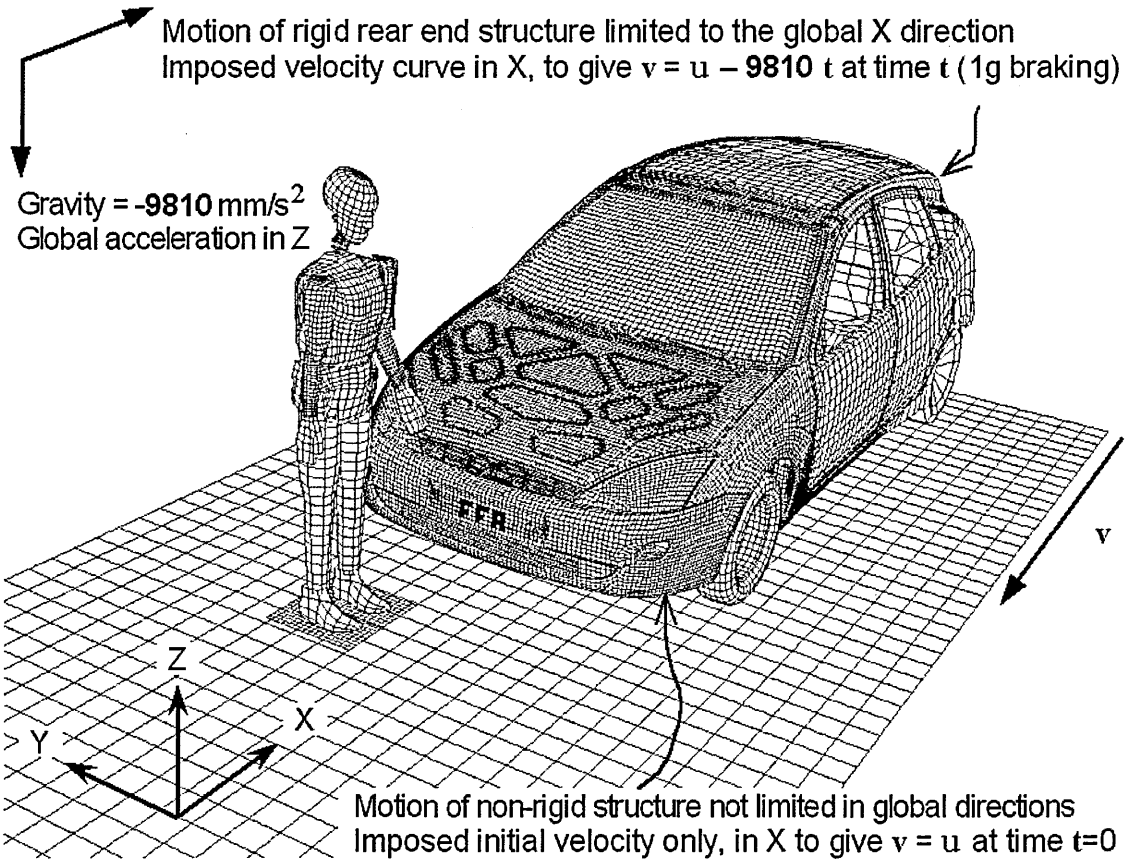

Figure 4.16 The pedestrian accident simulation boundary conditions

Gravity was applied by using the global cards shown in Table 4.31.

LOAD BODY Z and DEFINE CURVE
Load curve id. 1
Load curve scale factor 1.0
No load curve for dynamic relaxation
No X, Y or Z centre of rotations required because no angular rotations are requested
Load curve id.
Load curve used in transient analysis only
Scale factor of 1.0 for X and Y axes
No offset for X and Y values
General XY data with X and Y values in pairs and a value of 9810 mm/s^2
*LOAD_BODY_Z 1 1.000E+00 *DEFINE_CURVE 1 0 0.100E+01 0.100E+01 0.000E+00 0.000E+00 0.00000000E+00 0.98100000E+04 0.10000000E+01 0.98100000E+04

Table 4.31 Global load and define curve cards for gravity

As previously explained the rigid rear end was constrained to motion in X only by setting a variable in the material card. The velocity of this part was controlled by the BOUNDARY PRESCRIBED MOTION CARD and DEFINE CURVE cards shown in Table 4.32.

BOUNDARY PRESCRIBED MOTION RIGID and DEFINE CURVE CARD
Part id. 16
X translational degree of freedom
Velocity motion
Load curve id. 2 controlling velocity
Load curve scale factor 1.0 (default)
No vector id. for DOF values (default)
Death time of prescribed motion is very long (default)
Birth time is zero (default)
Zero offset (default)
Load curve id.
Load curve used in transient analysis only
Scale factor of 1.0 for X and Y axes
No offset for X and Y values
General XY data with X and Y values in pairs
*BOUNDARY_PRESCRIBED_MOTION_RIGID 16 1 0 2 0.100E+01 0 *DEFINE_CURVE 2 0 0.100E+01 0.100E+01 0.000E+00 0.000E+00 0.00000000E+00 -0.11100000E+05 0.11300000E+01 0.00000000E+00

Table 4.32 Prescribed motion and curve cards for the vehicle rear end

The define curve card for the prescribed motion was edited for different initial vehicle velocities so that there was always 1g braking according to the formula shown in Figure 4.16. The initial velocity of the non rigid front end nodes was set to the same value as that of the initial prescribed velocity of the rear end with the INITIAL VELOCITY card shown in Table 4.33.

INITIAL VELOCITY CARD
Node set id. 1 No nodes exempt from imposed velocity No box defined for above Initial velocity in negative X direction 11100 m/s No other initial linear or rotational velocities
*INITIAL_VELOCITY 1 0 0 -11100.0 0.0 0.0 0.0 0.0 0.0

Table 4.33 Initial velocity card for the vehicle front end

4.3.3. Refinements to the vehicle model

When the vehicle model was evaluated in pedestrian accident simulations it was

further developed to accommodate unforeseen requirements. These included the removal of problem component models and element mesh refinement.

Several component models exhibited hourglassing (see appendices for description) because they had a low mesh density (in comparison to the size of the part), low stiffness and low yield strength. They had originally been incorporated into the model in the belief that they might contribute to pedestrian injuries despite their (relatively) low stiffness and strength. For instance, in the original vehicle model a number plate had been incorporated because of its stiffening influence on the bumper cover. However, due to severe hourglassing this component was removed (this could not be eliminated by mesh refinement or shell property changes). It became apparent that the pedestrian impact involved such high energy levels that the influence of the number plate was not significant. In the case of another small, flexible component, the radiator grille, mesh refinement did solve a hourglassing problem. The average element size was reduced to 8 mm and the elements remeshed in a uniform manner as shown in Figure 4.17 and in line with the mesh quality guidelines shown in the appendices.

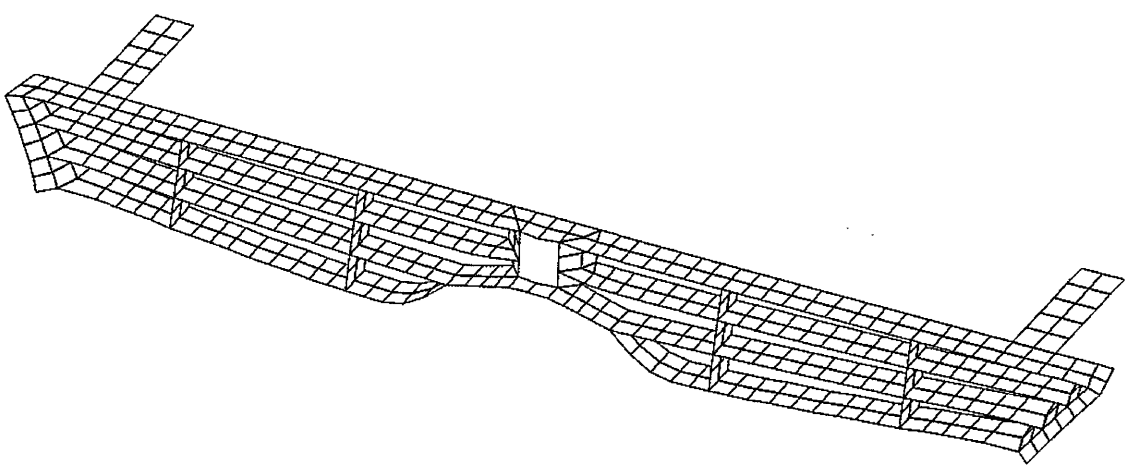

Figure 4.17 The refined radiator grille mesh

This component was important for the accident simulation models because it prevented the pedestrian leg nodes from partially penetrating the vehicle face and causing a variety of node penetration problems with the main vehicle contact surfaces (e.g. nodes the wrong side of the contact).

4.4. Pedestrian humanoid models

4.4.1. Background

The development of a vehicle model was only one of the tools required for pedestrian accident simulations; another was a family of pedestrian models. Before initiating the development of these models it was necessary to create a research vision of what needed to be achieved so that all the necessary research tasks could be identified. Whilst a comprehensive biomechanics literature search was being undertaken [CIC 1997], the author developed some pedestrian model concepts such as the one shown in Figure 4.18 [Howard 1999-1].

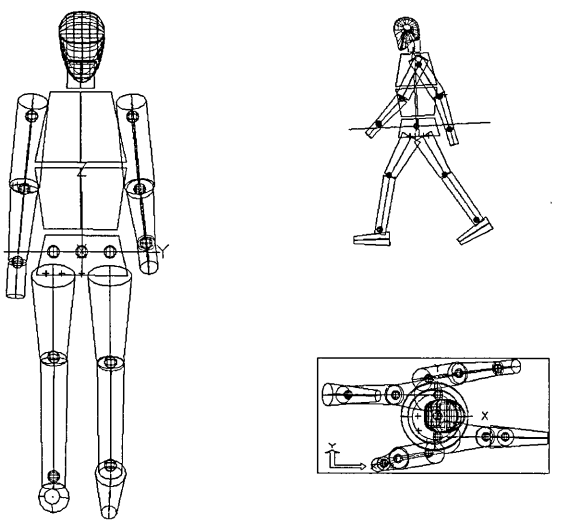

Figure 4.18 The first pedestrian humanoid model concept

This concept had a simple cylindrical geometric description of every body part except the head using just three dimensions – the length of the body part and the diameter at each end. The body was divided into the most important regions (e.g. lower leg, upper leg, pelvis) and a spherical joint with a limited freedom of motion, according to averaged human properties, connected each of these. The legs and arms of the pedestrian were placed in a walking stance with the struck arm forward. Some of the features of this concept were eventually incorporated into the pedestrian models that were subsequently developed.

As more information became available from the literature search the author developed this basic concept into the research vision shown in Figure 4.19.

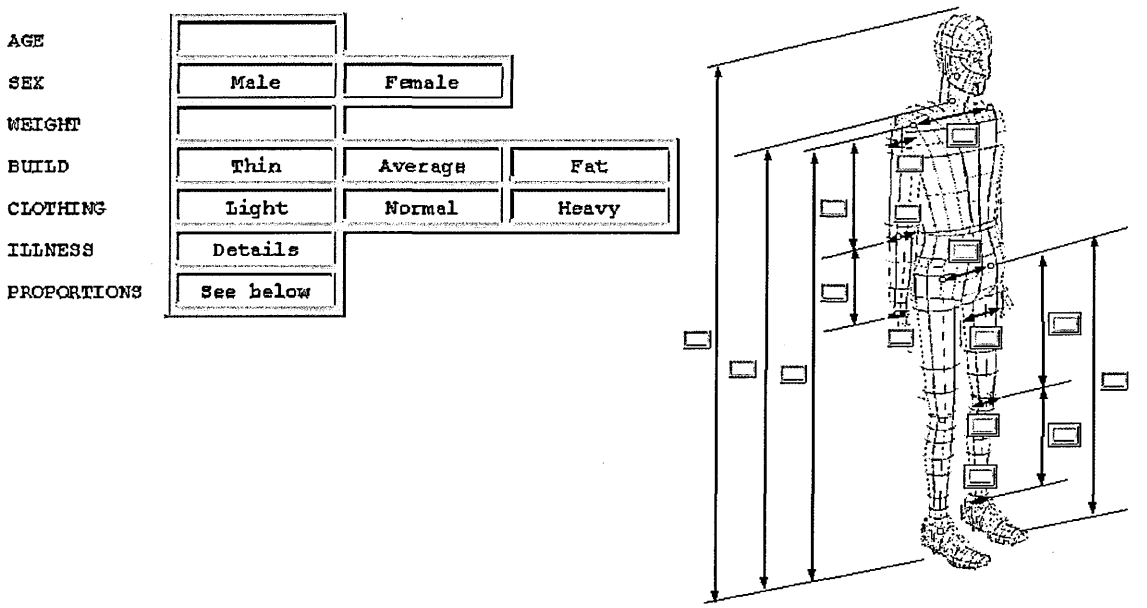

Figure 4.19 The pedestrian humanoid model research vision

The key aspects of this vision included the:

- Ability to create any pedestrian model (e.g. the exact size, weight, body proportions and age of an actual person) by using an interactive graphical user interface and the solver code LS-DYNA
- Incorporation of enough injury mechanisms and model detail to effectively simulate actual pedestrian accidents with the goal of improving vehicles

With this vision in mind there were three main tasks that became apparent. Firstly it was necessary to develop a single pedestrian model that provided the template for further models. Secondly to create a scaling process that could generate the full family of pedestrians from this and thirdly to ensure that the models could be used in detailed pedestrian accident simulations to improve vehicle design.

The development of a family of pedestrian models was undertaken in two parallel projects. In the first project the pedestrians were created, developed and validated by using sub-system models (e.g. for the neck validation) and simplified pedestrian accident simulations in which the vehicle was represented by a small number of rigid parts [CIC 1997, 1998, 1999, 2000, 2001). This approach allowed quick solution times and enabled a focused effort on the creation of the pedestrian models. At the same time the pedestrian models were assessed in detailed

pedestrian accident simulations in which the ability of the models to improve vehicle design could be assessed [Howard 1998-2, 2000-3, Hardy 2000]. The two approaches are shown in Figure 4.20 but only the second one will be described.

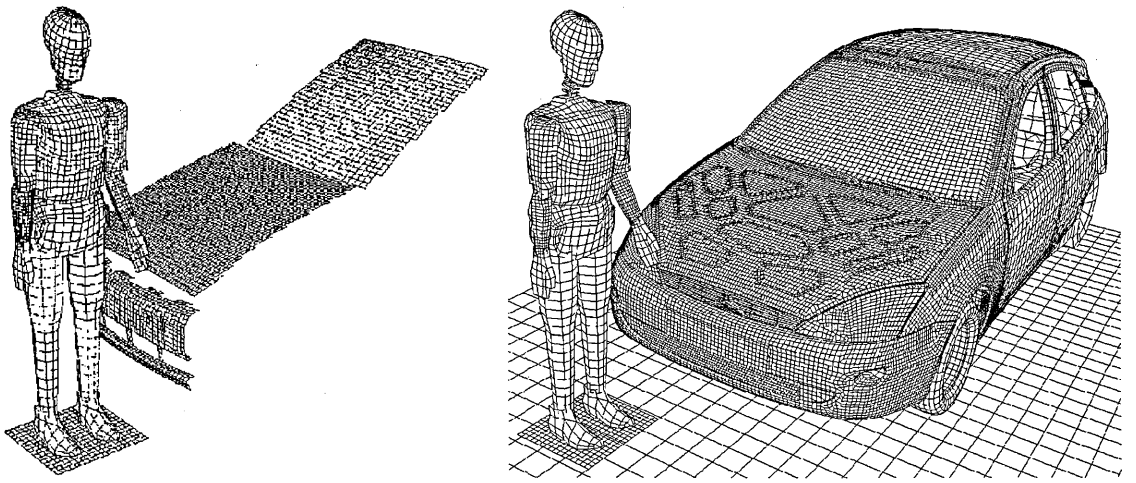

Figure 4.20 Simplified and detailed pedestrian accident simulation models

4.4.2. The construction of the humanoid models

A detailed description of the pedestrian models is available in [Howard 1998-2, 2000-3, Hardy 2000] and the 50th percentile model is shown in Figure 4.21.

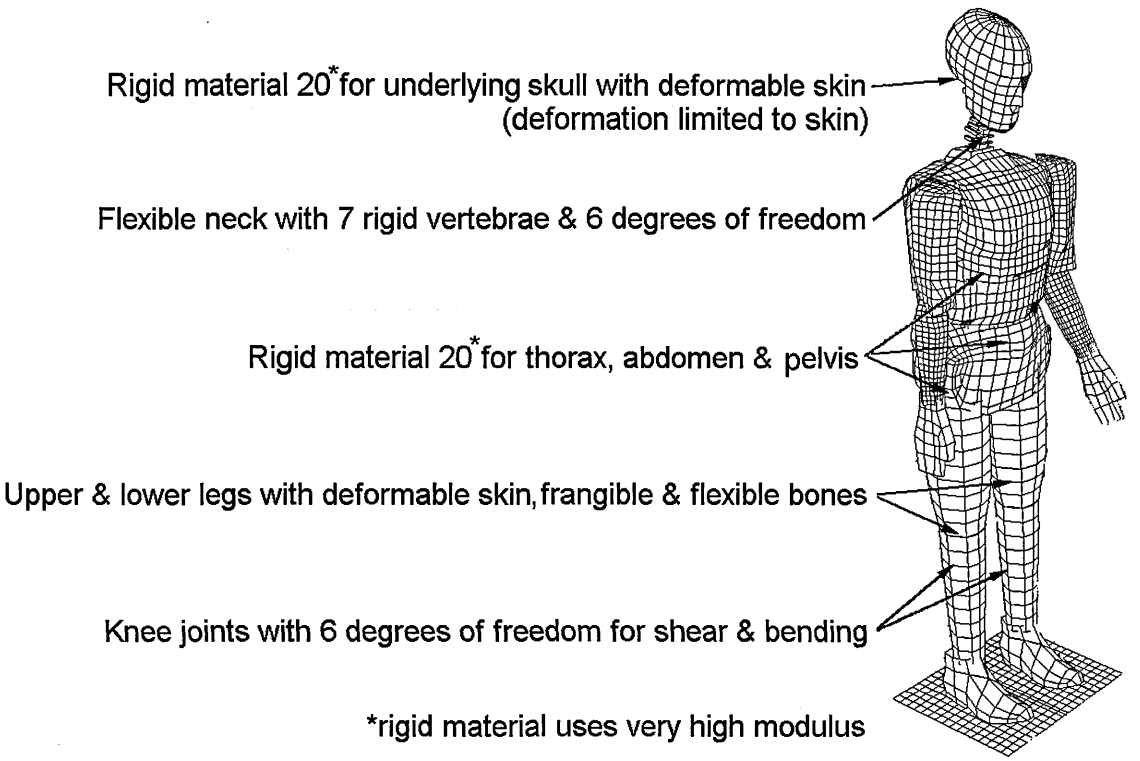

Figure 4.21 The reference pedestrian humanoid model

This model was created in LS-DYNA specifically for pedestrian accident simulations. It contained approximately 7,000 elements and was created with more human like properties than conventional dummies. For example, the legs had deformable solid elements to represent soft tissue and flexible beam elements to represent the femur and tibia. Connections between the beam elements provided bone fracture capability via plastic hinge end moments. A scaling program was also developed to create any sized pedestrian model although with the exception of a validation study most of the simulations were only undertaken with a 6 year old child, 5th percentile female, 50th percentile male and 95th percentile male models.

4.4.3. Refinements to the humanoid models

As each new pedestrian model was developed and evaluated in simplified pedestrian accident simulations it was issued with a version number so that the influence of model changes could be tracked in subsequent detailed simulations. The detailed simulations provided a wide range of simulation conditions (e.g. higher velocities, a deformable vehicle structure, and longer accident simulation times) with which to evaluate how the pedestrian models performed and contributed to the development of the pedestrian models in a number of areas:

- Contact definitions
- Geometry (mesh and joints)
- Pedestrian humanoid model research and development methodology

The first models only incorporated *contact definitions* for the pedestrian self contacts (e.g. foot to foot). New pedestrian to vehicle contact definitions had to be created for the detailed pedestrian accident simulations and these were based upon the observed pedestrian model kinematics. In addition, a naming convention was created so that when a pedestrian model was combined with any new vehicle model it would be clear which parts of the vehicle to add to which pedestrian model contact. For example there was a contact named "lower right leg to bumper/grill/foglamps". This ensured that it was clear that the bumper, grille and foglamp parts should be added to the contact containing the lower right leg.

Other observations concerning the kinematics of each new pedestrian model led to

further model improvements. Figure 4.22 shows a set of 6 animations and some observations on the problems with version 2 of the 50th percentile pedestrian model.

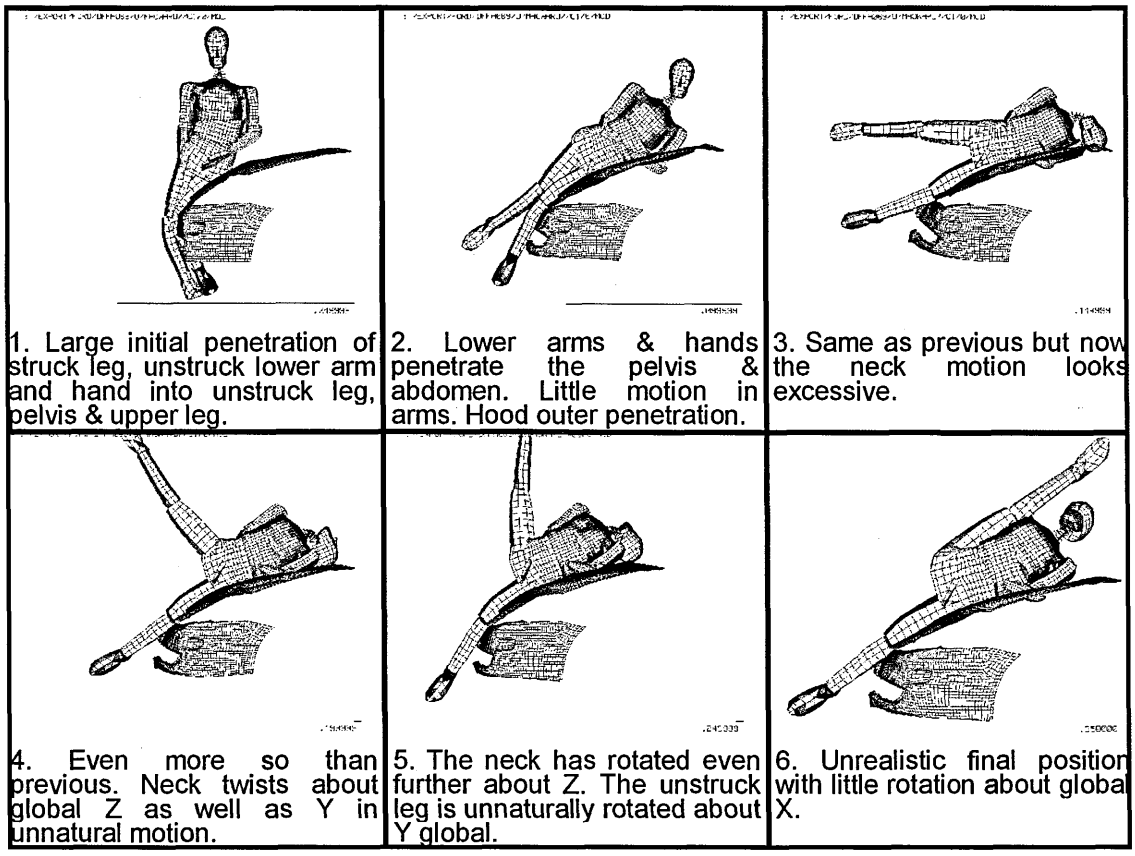

Figure 4.22 Observed problems with the pedestrian model

As more was revealed about the dynamic interaction between the pedestrian model and vehicle, further contacts were defined. For example, in this case new contacts were added to avoid lower left arm to pelvis penetration. Some of the other improvements that were suggested included; more realistic joint motion limits, increased contact stiffness, arm and leg mesh geometry refinement to more closely match the vehicle structure, an improved pelvis mesh geometry and the application of part instead of contact segment definitions.

New contacts were defined to prevent some of the unwanted or excessive contact penetrations such as the upper leg to upper leg penetration shown in Figure 4.23. In this case the contact stiffness scaling factors were increased from 0.1 to 0.5 to prevent such large penetrations.

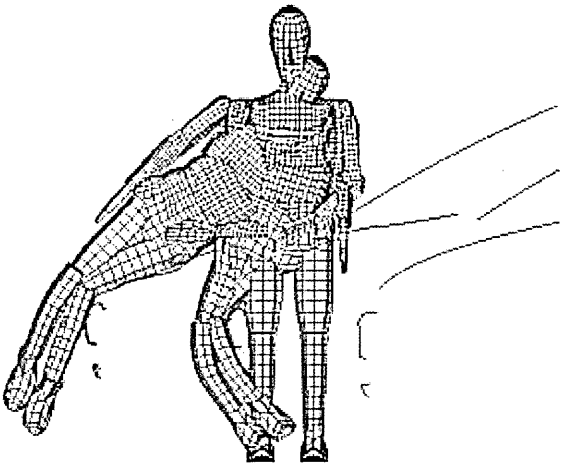

Figure 4.23 Excessive leg to leg contact penetration

The original contact segment definitions for the legs were changed to part based definitions to make the pedestrian models more robust to different loading directions. Originally the lower leg segment definitions only defined half the leg in the contact in an attempt to reduce the model solution time. However this led to the contact being totally missed in some pedestrian stances in which the pedestrian model was not directly hit where the segment was defined and in fact there was no significant increase in the model solution time after the changes.

Other feedback from the detailed simulations related to the *pedestrian model geometry*. One of the initial concerns related to the pelvis and upper leg construction. As the left hand picture in Figure 4.24 shows, the upper legs passed into and partly through the pelvis casing when the pedestrian was in a standing position. The initial penetration of the upper leg and pelvis geometry meant that no contact could be defined between these parts. Depending on the position of the legs it was possible for the vehicle structure to come into contact with two contact surfaces simultaneously, one defined by the pelvis and the other by the upper leg. Under these conditions there was double the contact force and hence unrealistic pedestrian impact motion. A possible solution as shown in the right hand side was proposed and later incorporated. This involved remeshing the upper legs so that they formed semi spheres that represented the pelvis geometry whilst eliminating the pelvis casing and hence two contact forces. This also provided the opportunity to refine the leg mesh density to match the vehicle mesh (improved contact).

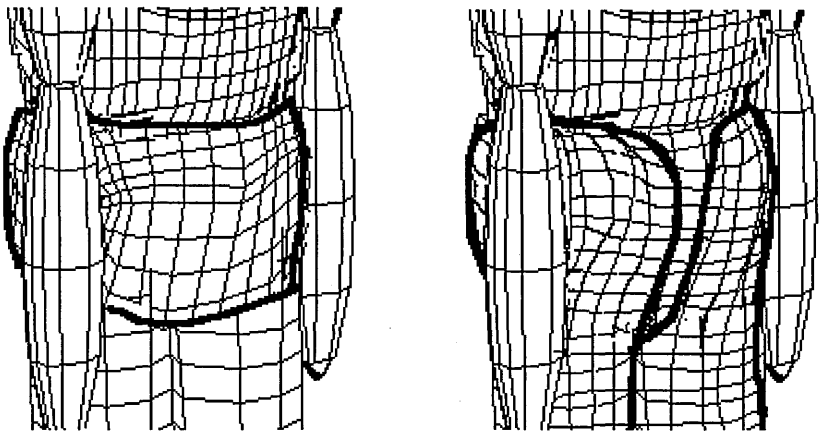

Figure 4.24 The original and modified pelvis mesh geometry

It was also noted in the early simulations that the pedestrian model arms might pass through the hood when the arm impacted the hood vertically. A possible reason for this was also a poor contact condition [Du Bois 2001] as shown on the left hand side of Figure 4.25.

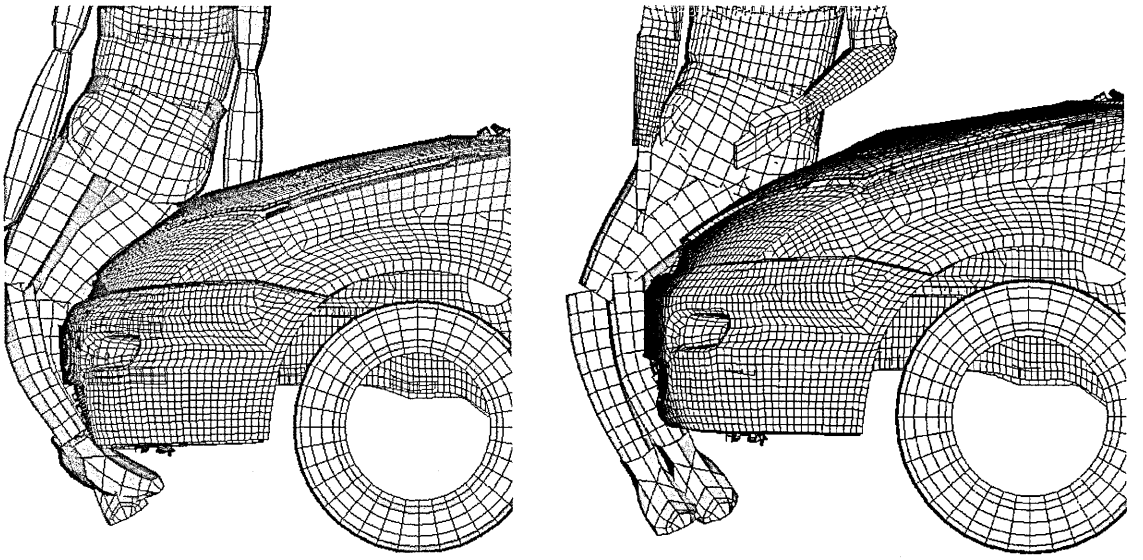

Figure 4.25 The original and modified arm mesh geometry

The arms were subsequently remeshed with a higher density mesh to represent more human like geometry and the lower arm initially bent to provide an improved arm to hood contact as shown on the right hand side of Figure 4.25. In the improved geometry the contacts were planar and parallel to one another.

The first pedestrian models exhibited large leg and arm joint rotations, particularly at higher velocities and after longer run times (e.g. 200 ms) as shown in Figure 4.26.

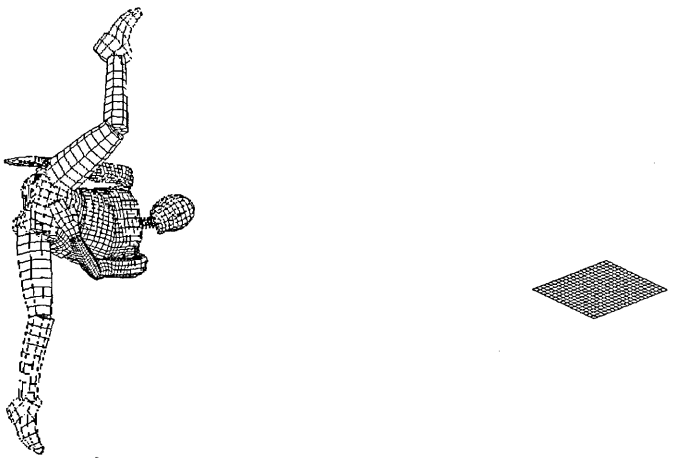

Figure 4.26 Unrealistic pedestrian model motion

In this example the unstruck leg of the pedestrian model rotated so far that during a 40 km/h impact it passed over the pedestrian's head by the completion of the simulation at 0.5 second. As a result of these observations the simplified models were solved with longer run times and at a higher impact velocity, and the properties of the joints were changed. The stiffness of the joints at their maximum limit was scaled until more realistic (i.e. without excessive joint motion) kinematics was observed under a range of accident conditions. Such an iterative approach was necessary because it was not clear how much limb joint rotation could be observed in pedestrians before amputation occurred and if the limit stiffness was too high then there was the possibility of joints unnaturally rebounding.

The feedback of detailed accident simulations also contributed to the *pedestrian research and development methodology* through the prioritisation and identification of tasks. For instance, the research focus was changed at a key point in the pedestrian model development program because it was necessary to establish a baseline total model validation upon which the models could be developed further. The focus was changed from introducing new pedestrian model features (e.g. a more detailed thorax) to complete (i.e. whole body) validation of the pedestrian models. Throughout the research it was necessary to ensure that the pedestrian models were developed as vehicle design tools rather than pure research tools. They needed to be capable of distinguishing which parts of the vehicle might cause an injury, how the severity of these injuries varied throughout the impact sequence

and how the pedestrian impact motion was influenced by the vehicle shape and structure throughout the impact sequence. The pedestrian model validation is fully described in [Howard 2000-3] and was undertaken using a set of cadaver test results that were available in the public domain [Ishikawa 1993].

4.5. Pedestrian accident simulations with reference vehicle

In order to have a better understanding of the interactions between a pedestrian and a vehicle during a pedestrian accident, a matrix of accident simulations was undertaken with the reference vehicle model 'p' and version 7.2 of four pedestrian models. This matrix was designed to identify the influence of various parameters (e.g. impact velocity and location, pedestrian size and stance) on pedestrian motion and injuries, and provide a reference set of data that could be compared to a similar set of simulations with modified vehicle models (that featured different pedestrian protection technologies).

4.5.1. Methodology for pedestrian accident simulations

The construction of the vehicle model and the pedestrian accident simulations has already been described and the general modelling procedure for constructing each pedestrian accident simulation model is shown in the appendices. There was a large number of possible parameters to examine and therefore certain key parameters were identified as shown in Table 4.34.

Vehicle				Pedestrian	
Type	**Velocity**	**Location**	**Braking**	**Type**	**Stance**
C class	25 km/h 30 km/h 35 km/h 40 km/h	Y0 Y500	1g 70mm ride height drop	6 year old child 95th adult male 50th adult male 5th adult female	A - lateral, legs together. B - lateral, unstruck leg forward, struck leg rearward. C - lateral, unstruck leg rearward, struck leg forward. D - facing away, legs together

Table 4.34 Pedestrian accident simulation parameters

As described, there was only one validated vehicle model that was suitable for pedestrian accident simulations but this represented a large proportion of the vehicle fleet because it was a C class or mid sized family saloon. The upper bound on the vehicle impact velocity was set to the same level as [EEVC 1998] and the lower bound at a value that was just below the lowest common speed limit in

Europe (30 km/h). To minimise the number of simulations required, only two impact locations were specified. The first was at the most flexible part of most bumper systems; the vehicle centreline, and the second at the centreline of the vehicle headlamp, in the approximate location of the crash longitudinal where the bumper is rigidly mounted. Based on the results of [Howard 2000-3] 1g deceleration and a ride height drop of 70 mm (with no pitch) were applied to simulate braking.

Four types of pedestrian and stances were used to represent different pedestrian sizes, biomechanical properties and pre-impact positions. The different stances used are shown in Figure 4.27.

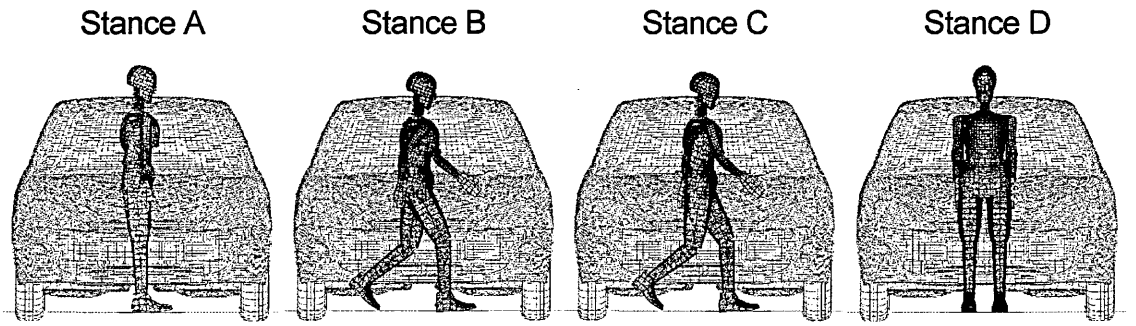

Figure 4.27 The pedestrian model stances

Stances 'A' and 'D' were unlikely to be typical stances for actual pedestrian accidents because pedestrians are usually walking, jogging or running prior to the accident [Isenberg 1998]. However, they provided extreme cases with stance 'A' focusing the initial impact of both legs into a small area of the car structure and stance 'D' different loading, to the back of the knees and the head. Stances 'B' and 'C' were reminiscent of the stances in the original pedestrian humanoid vision and represented a walking or running gait, with either the struck leg forward or backward [CIC 2000]. Due to humanoid model limitations (e.g. the knee joint definitions) none of the stances were facing the vehicle.

The complete simulation matrix is shown in Table 4.35 [Howard 2000-3]. The full matrix would have required 128 simulations. However, with the computer resources available (as listed in the appendices) each simulation took approximately three days (HP 700 with 4*360MHZ CPU's) and therefore it was necessary to reduce the

number of simulations. The 50th percentile pedestrian model had been used and validated [Howard 2000-3] more extensively than the other models and therefore a complete set of simulations was undertaken for this model. There was less confidence in the quality of the data used in the other models (e.g. child properties were scaled because there was no experimental data available) and therefore only the lowest and highest impact velocities were simulated. This reduced the size of the matrix to 80 simulations.

Humanoid	FFA LSDYNA3D humanoid v7.2																											
Vehicle	Unmodified vehicle model (c170_p.key)																											
Velocity (km/h)	25								30								35								40			
Location (mm)	Y0				Y500				Y0				Y500				Y0				Y500				Y0			
Stance	A	B	C	D	A	B	C	D	A	B	C	D	A	B	C	D	A	B	C	D	A	B	C	D	A	B	C	D
50th percentile	1	9	17	25	2	10	18	26	3	11	19	27	4	12	20	28	5	13	21	29	6	14	22	30	7	15	23	31	8	16	24	32
6 year old	33	37	41	45	34	38	42	46																	35	39	43	47	36	40	44	48
95th percentile	49	53	57	61	50	54	58	62																	51	55	59	63	52	56	60	64
5th percentile	65	69	73	77	66	70	74	78																	67	71	75	79	68	72	76	80

Table 4.35 Pedestrian accident simulation matrix for reference vehicle

Two categories of measurements were recorded; the first concerned the pedestrian motion and the second the pedestrian injury measures. In general the 50th percentile pedestrian was used as the reference case to study detailed trends and the response of the other pedestrians used for general trends. Pedestrian motion was analysed in detail by using the displacement of the head in the XZ plane relative to the hood leading edge, resultant head velocity relative to the vehicle and resultant global head acceleration. Overall motion was determined by analysing movie sequences of each simulation, identifying the main impact event timing and calculating a displacement measure, composite maximum displacement (CMD), created by the author, for each global direction X, Y and Z. CMD for the X coordinate for instance was defined as CMDX = HX+UTX+LTX+(KLX+KRX)/2 where the absolute maximum global displacements of the head, upper torso, lower torso, left knee and right knee were HX, UTX, LTX, KLX and KRX respectively.

The purpose of creating CMD was to determine whether it was possible to use a single variable for each global X, Y, Z direction to compare overall pedestrian motion between accident simulations. It was assumed that it would be easier to compare a single variable rather than for instance, head displacement time history, and that the maximum displacement of the main body regions was indicative of overall pedestrian motion. The maximum displacement of the knees was averaged in order to obtain a general indicator of leg motion. To obtain a single value, the absolute maximum displacements of all the bodies were summed. In this manner the amount by which a pedestrian was deflected to either side of the car (i.e. in the Y direction) could be compared for different vehicles.

Pedestrian injury measures included HIC (head injury criteria derived from head acceleration), maximum pelvis acceleration, maximum knee shear and bending angle, maximum tibia acceleration and first fracture locations in the tibia and femur. With the exception of pelvis acceleration and fracture locations, all of these were defined in [EEVC 1998] for pedestrian impactors. Due to the differences between the pedestrians, that represented different pedestrian sizes, and the impactors that only represented parts of a 50^{th} percentile pedestrian, only relative measures were compared rather than absolute injury levels.

4.5.2. Results from pedestrian accident simulations

Figure 4.28 shows four pedestrian accident simulation examples. There are two with a low impact velocity; a 6 year old and a 5^{th} percentile pedestrian, and two with a high impact velocity; a 50^{th} percentile and a 95^{th} percentile pedestrian. The first frames at 0 ms show all four initial stances with the first contact between the closest pedestrian leg and bumper cover. In the next set of frames at 10 ms, with the exception of stance 'D', large knee bending angles and shear displacement were already observed. Some knee shear displacement was observed in stance 'D' but there was mainly a rotation of the upper and lower leg in their natural motion. At 10 ms the initial pedestrian stance remained unchanged in all cases with the feet remaining in contact with the ground because of the initial flexibility of the legs and knee joints and the inertial lag of the connected body parts. Between 10 to 30 ms the pedestrian stances began to change with the timing dependent on the

pedestrian type and impact velocity. The smaller the pedestrian and the higher the impact velocity, the quicker the feet were swept away and the legs visibly buckled, with the upper body beginning to rotate towards the vehicle.

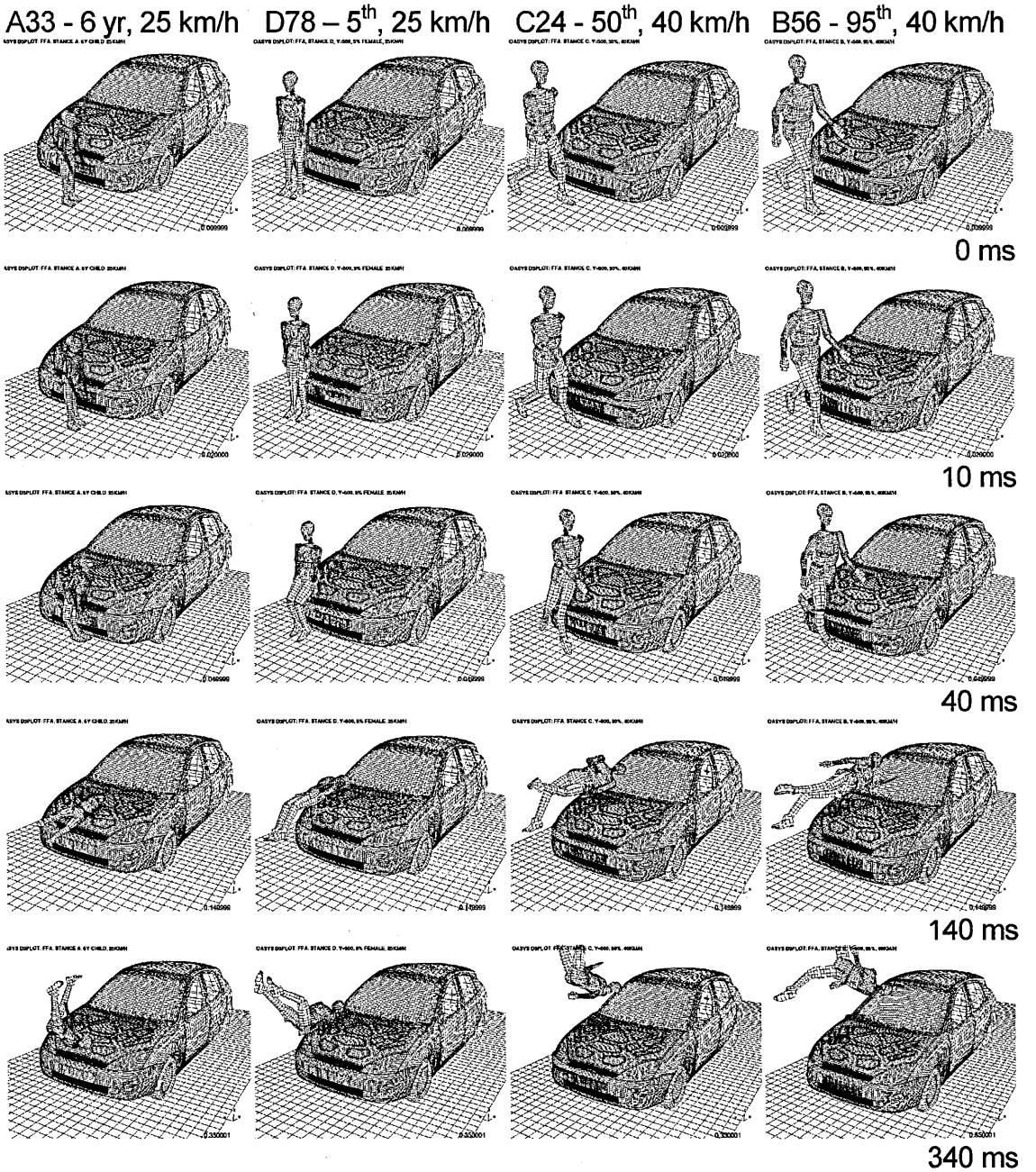

Figure 4.28 Some example pedestrian impact motions

At 40 ms the 6 year old pedestrian in stance 'A' had begun to wrap around the vehicle face and the 5th percentile pedestrian in stance 'D' began to take up a sitting position with increasing knee shear displacement. The forward positioned struck leg of the 50th percentile pedestrian in stance 'C' wrapped around the vehicle face and

the other leg was also struck. This usually led to the beginning of a rotation of the pedestrian on to its back, facing away from the vehicle. A similar leg motion occurred in stance 'B' but there was a larger and more complex distortion of the legs, especially with the rearward positioned struck leg. This indicated a possible limitation of the pedestrian model to cope with the stance 'B' loading where the precise natural motion of the joints, especially the hip joints, was critical. Pelvis contact for the 6 year old and 5th percentile pedestrians had already occurred.

Between 40 ms and 140 ms the pedestrians remained in contact with the hood and to varying degrees the thorax, arms and shoulders deformed it. Pelvis contact occurred for the 50th and 95th percentile pedestrians and head contact with the hood for the 6 year old and 5th percentile pedestrians. With the exception of the 95th percentile pedestrian, the pedestrians continued to rotate away from the vehicle.

From 140 ms until the end of the simulations at 340 ms all of the pedestrians were initially thrown and rotated away from, and above the hood. At the lower impact velocities the 6 year old pedestrian was thrown in front of the vehicle and the 5th percentile pedestrian towards the front of the hood. With the higher velocities the 50th and 95th percentile pedestrians were rotated above the hood and windscreen respectively, after the heads had contacted the windscreen. Although the simulation was not continued beyond 340 ms, it did not appear that any of the pedestrians would be thrown over the vehicle roof. The likelihood of this occurring was reduced due to the application of braking deceleration.

It was difficult to identify specific contact events between the pedestrian and vehicle from the motion because in some cases the arms and shoulders delayed the head contact in an unpredictable manner depending on the position that they fell in to. In principle this should have been more realistic in terms of actual accidents where the pedestrians might also position their arms in an unpredictable manner to protect themselves. However, there were some limitations to the manner in which the shoulders and arms were modelled. For example, the shoulder joints were modelled as rotational joints about a rigidly fixed centre and therefore the shoulders

were too stiff when they struck the hood and hence delayed head contact.

Three common impact events were identified: the pelvis to vehicle face, shoulder to hood and head to hood or windscreen. Observations from the pedestrian motion had clearly indicated that the impact timing was mainly dependent on the impact velocity and the pedestrian type and therefore the timing behaviour was categorised for the complete set of matrix simulations as shown in Figure 4.29 and Figure 4.30. It should be noted that time zero on these graphs was set to the first leg to bumper contact and not time zero for the simulation (that was 10 ms earlier). The original data are shown in the appendices.

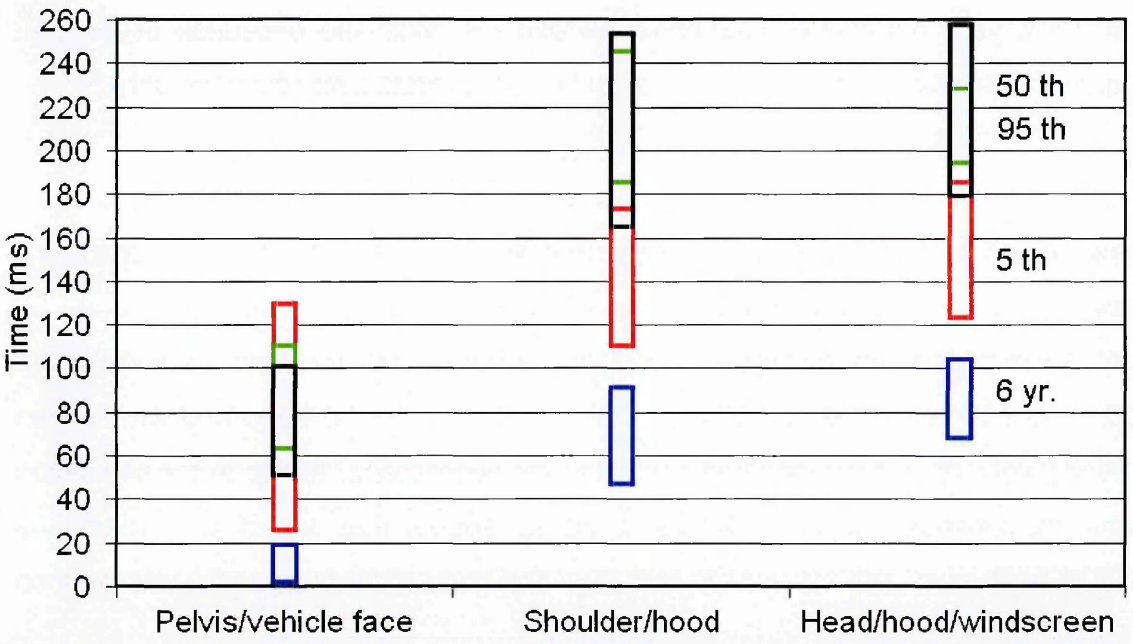

Figure 4.29 All impact timing ranges at 25 km/h

In general, the smaller the pedestrian was, the quicker each impact occurred. Hence the 6 year old pedestrian had the fastest impact timing and the 95th percentile pedestrian the slowest. However, the different pedestrian stances caused a significant amount of overlap between the timing ranges. This was particularly noticeable at the lower impact velocity and for the first impact between the pelvis and vehicle face, where, in some cases with the 5th percentile pedestrian, an arm delayed each impact event.

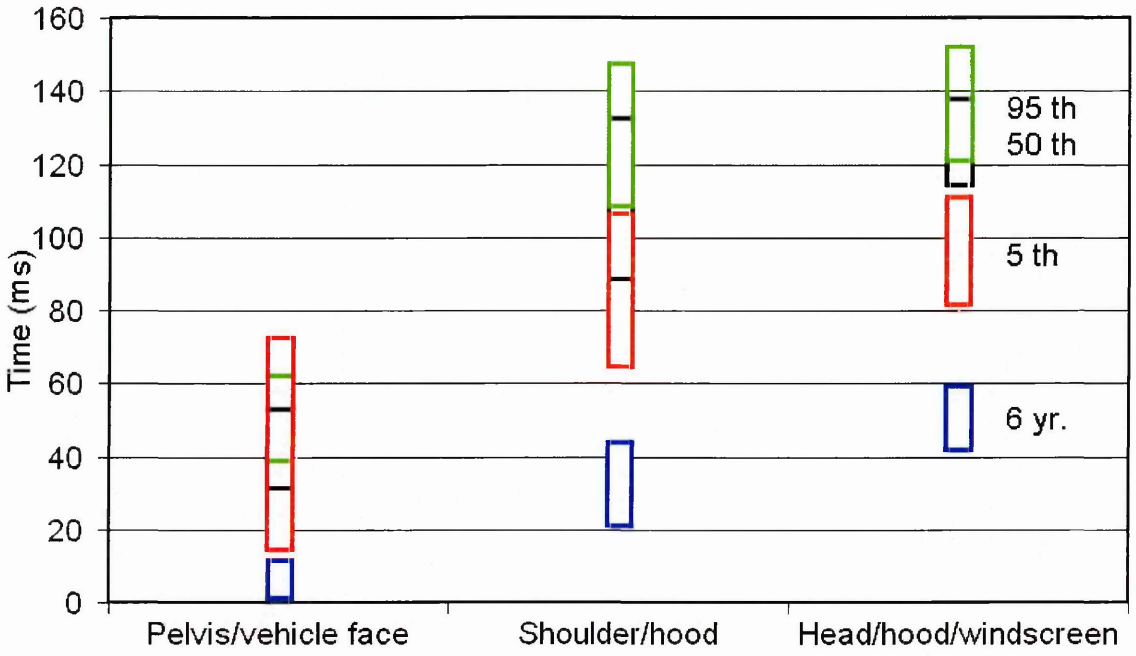

Figure 4.30 All impact timing ranges at 40 km/h

The actual values for each of the timing ranges are summarised in Table 4.36.

Impact velocity (km/h)	Timing range (ms) from first leg to bumper contact to											
	Pelvis impact				Shoulder impact				Head impact			
	6 yr	5 th	50 th	95 th	6 yr	5 th	50 th	95 th	6 yr	5 th	50 th	95 th
25	5 -13	30-125	54-95	68-105	50-86	116-168	173-250	190-242	72-100	128-180	185-255	199-225
40	3-8	17-70	33-50	43-60	29-42	66-104	91-130	110-145	44-58	84-108	117-136	124-150

Table 4.36 All impact timing ranges

Figure 4.31 shows the CMD values for the accident simulations involving the 50th percentile pedestrian. With the exception of a few cases the CMD values increased in all three directions with impact velocity, although the increase was much smaller in the Y and Z directions where the absolute values and range of values were much smaller. The smallest CMD values were in the Y direction and at the higher velocity (and unlike the other directions) the values at Y500 were significantly larger than at Y0.

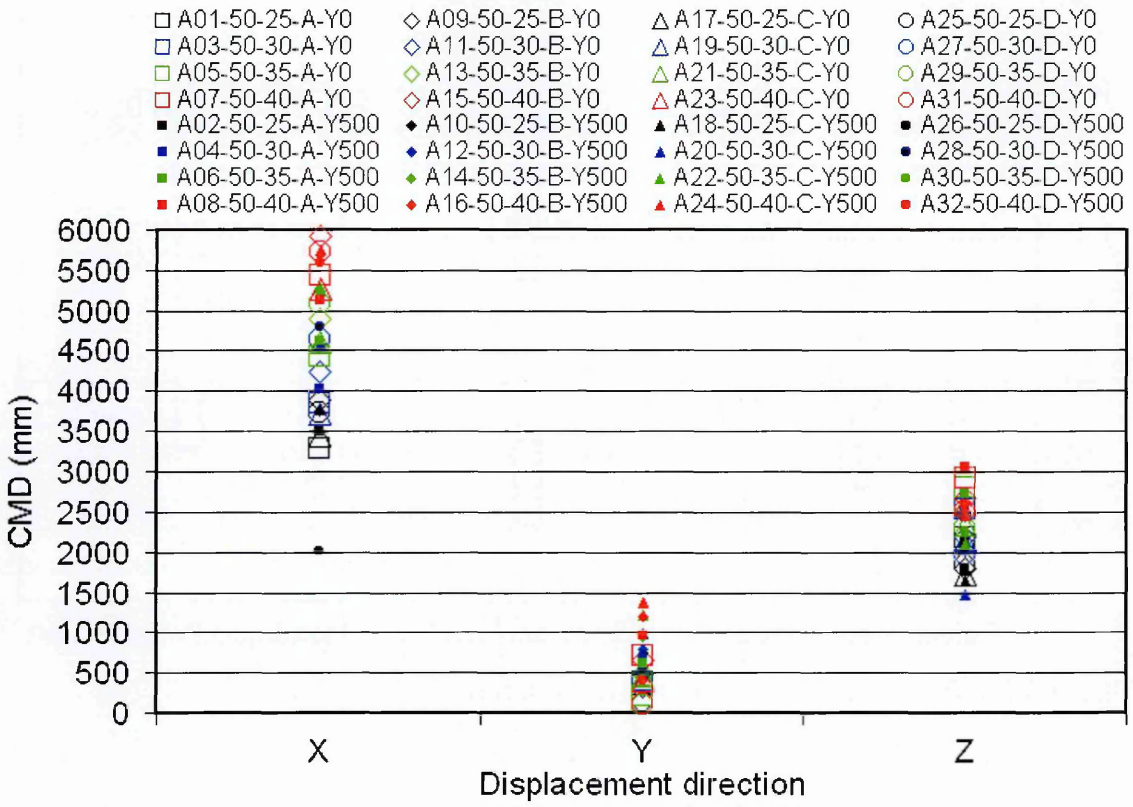

Figure 4.31 50th percentile pedestrian CMD at 25, 30, 35, 40 km/h

Figure 4.32 and Figure 4.33 show the range of CMD values for all four pedestrians at 25 km/h and 40 km/h (the original data are shown in the appendices).

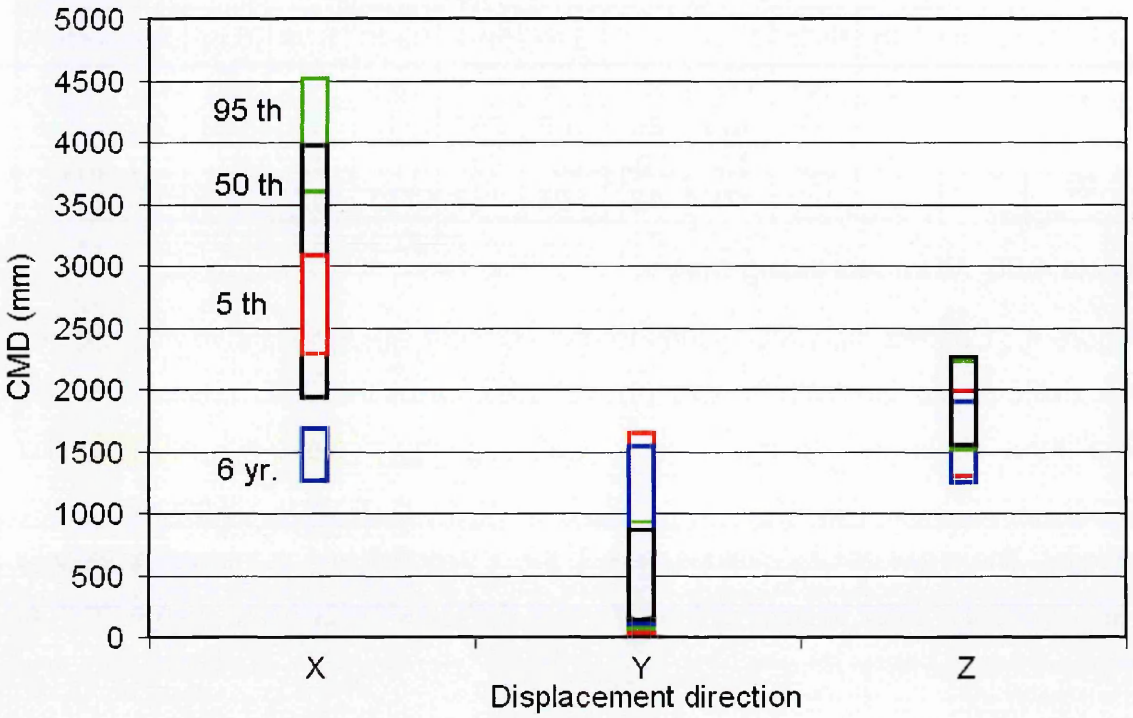

Figure 4.32 All CMD ranges at 25 km/h

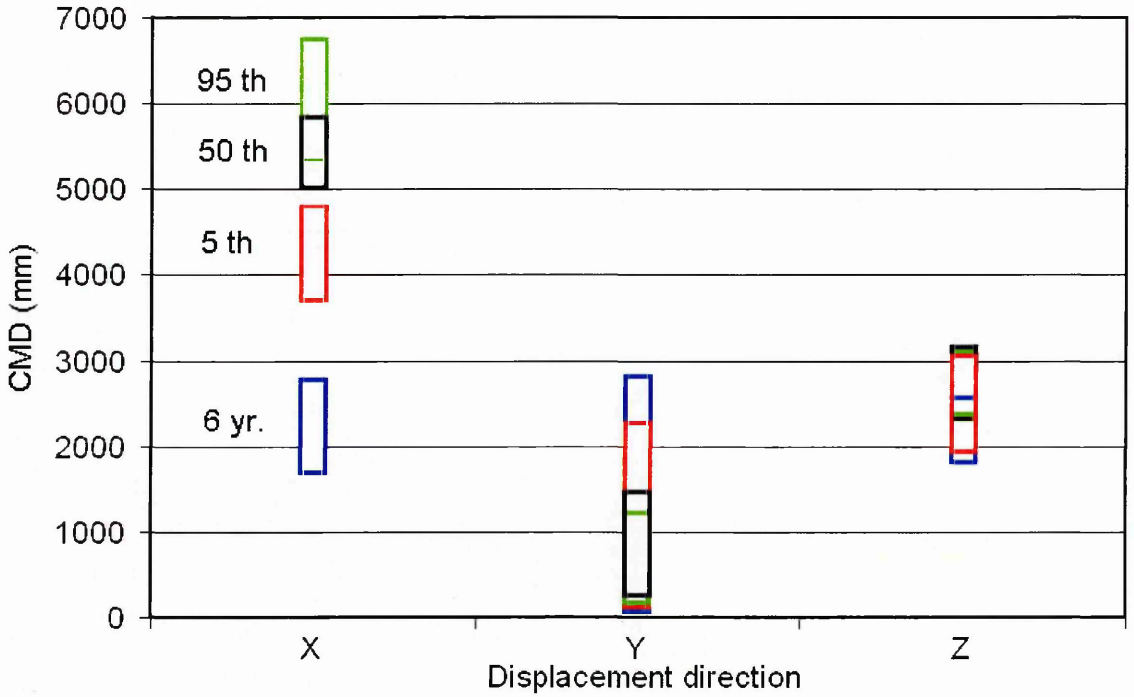

Figure 4.33 All CMD ranges at 40 km/h

At both impact velocities, CMD in the X direction increased with an increase in pedestrian size although there was some overlap due to the large range of values recorded for the 50th percentile pedestrian. In a similar manner to impact timing, the overlap for the Y and Z directions was also larger at the lower impact velocity. However, at 40 km/h there was a clearer distinction between the CMD values in the Y direction with the smaller pedestrian giving a larger value. The 6 year old pedestrian had the smallest differences between CMD values in X, Y and Z.

In addition to studying overall motion, Figure 4.34 shows the 50th percentile pedestrian head trajectories in the region of the head impact locations. The head motion in X increased with impact velocity and was generally larger for stance 'D' but it was not possible to identify consistent trends in the influence of the impact location. Stances 'A' and 'C' consistently led to the shortest head motion in X and Z and the variation in head impact location in X, due to the different stances, was more than 200 mm at the lowest velocity. X varied by about 200 mm for stance 'D' at the lower impact velocity and almost 300 mm for stance 'A' at the higher impact velocity.

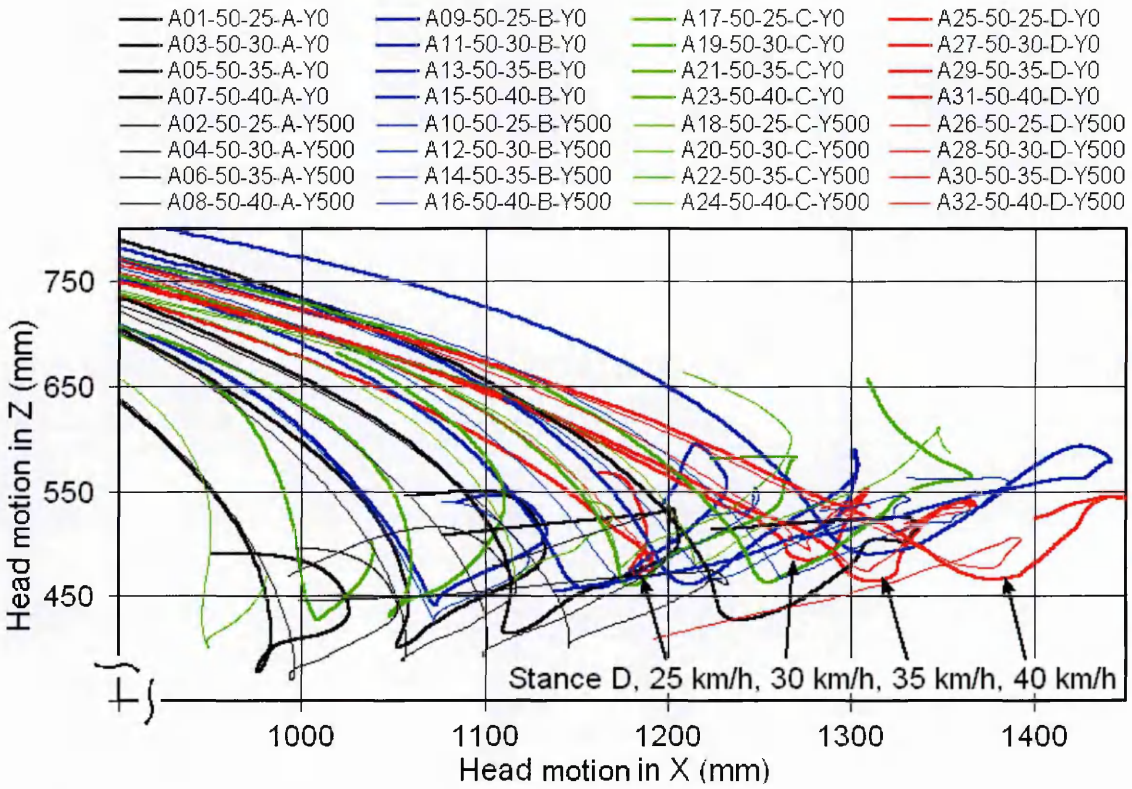

Figure 4.34 50th percentile head trajectories at 25, 30, 35, 40 km/h

The range of all head motions is shown in Figure 4.35 and Figure 4.36.

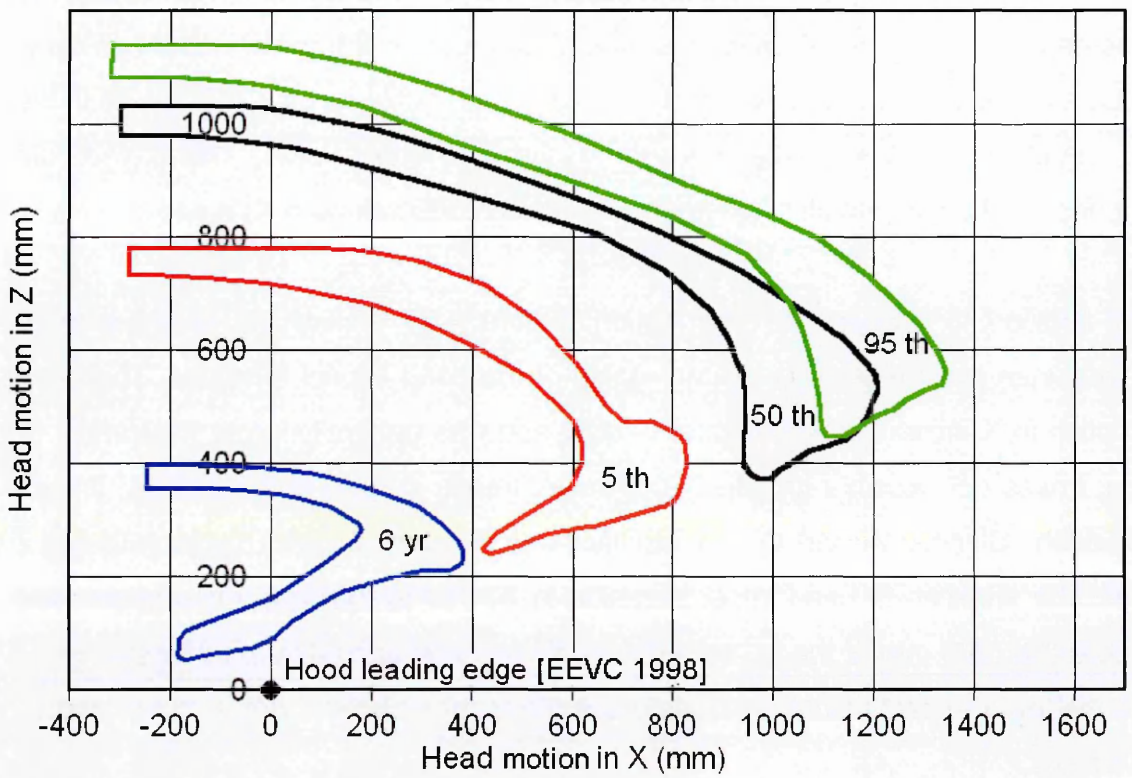

Figure 4.35 All head motion ranges at 25 km/h

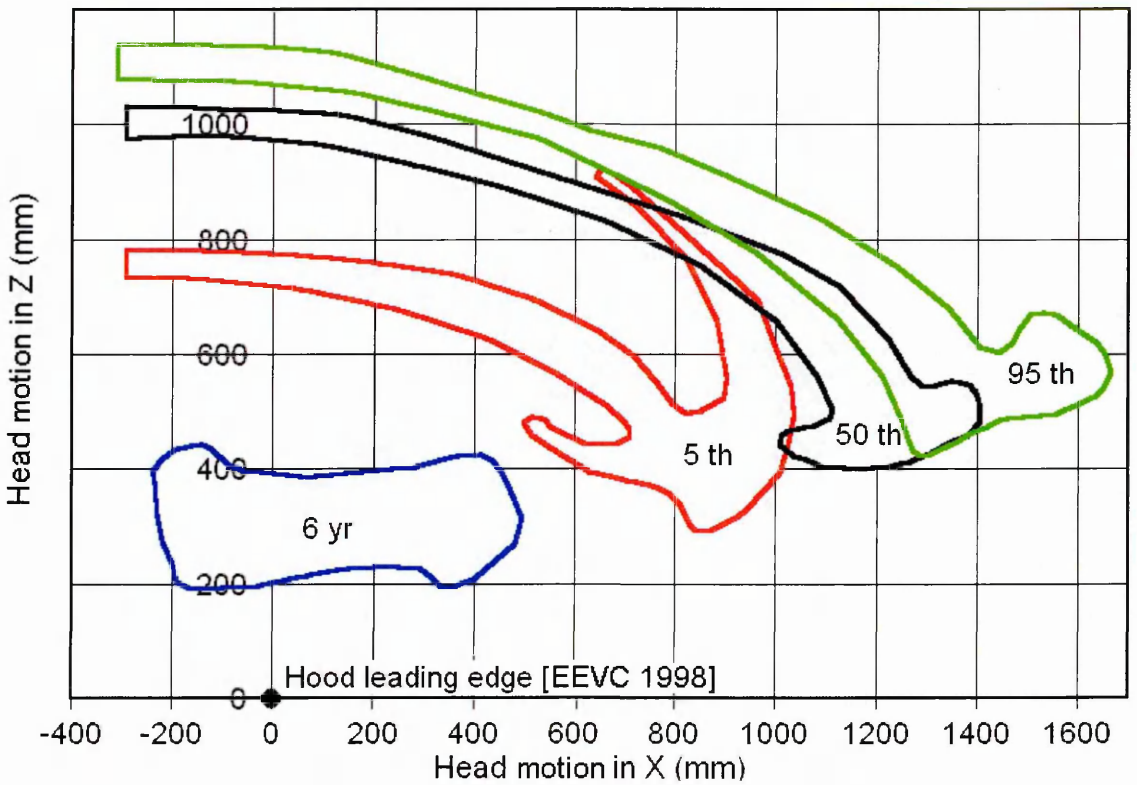

Figure 4.36 All head motion ranges at 40 km/h

The original data are shown in the appendices. These confirmed the CMD findings that the larger pedestrians had a larger motion in X and Z and that the maximum motions in X and Z of the smallest pedestrian were similar. Also, there was some overlap between the pre-impact head trajectories of the 50th and 95th percentile pedestrians. At both impact velocities and in particular at the higher velocity, the head motion range was greatly enlarged by the post impact head motion of the 6 year old and 5th percentile pedestrians.

Figure 4.37 shows all the head velocity time histories, relative to the vehicle, for the 50th percentile pedestrian. To aid clarity the time history is limited to 250 ms. In all cases the head remained almost stationary up to 40 ms after the bumper impact. Then the head velocity increased at a similar rate for each stance and velocity. The increase in maximum head velocity over the impact velocity was larger at higher impact velocities and this pulse started and finished more quickly, especially for the 'D' stance. Stances 'A' and 'D' led to the highest head velocities but at the lowest impact velocity the differences caused by stance were much smaller. There was only a small difference between the Y0 and Y500 results.

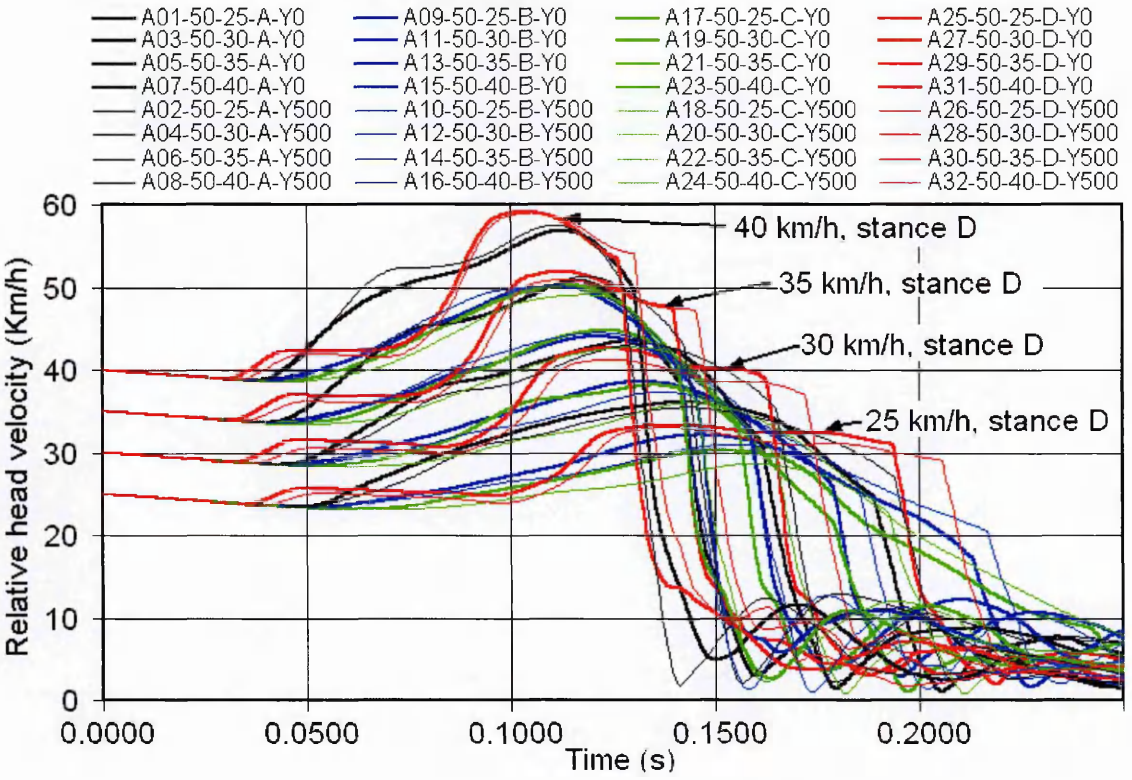

Figure 4.37 50th percentile relative head velocity at 25,30,35,40 km/h

The full results for each pedestrian type and stance at the lowest and highest velocities are shown in Figure 4.38 and Figure 4.39 (original data in appendices).

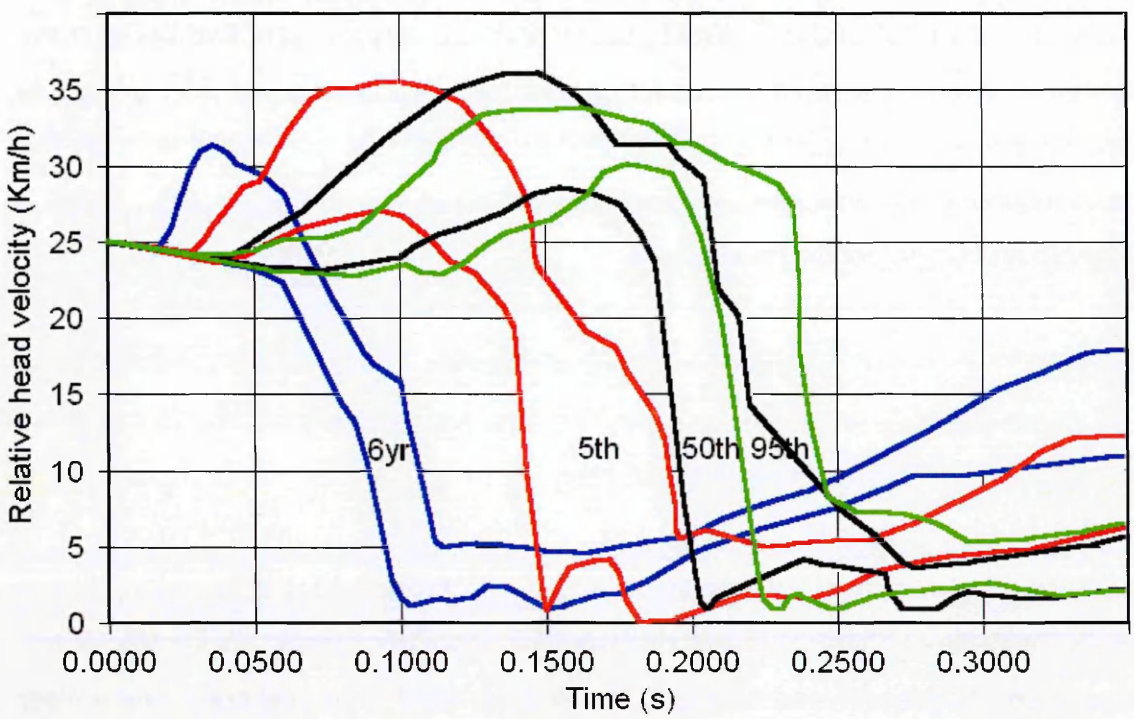

Figure 4.38 All relative head velocity ranges at 25 km/h

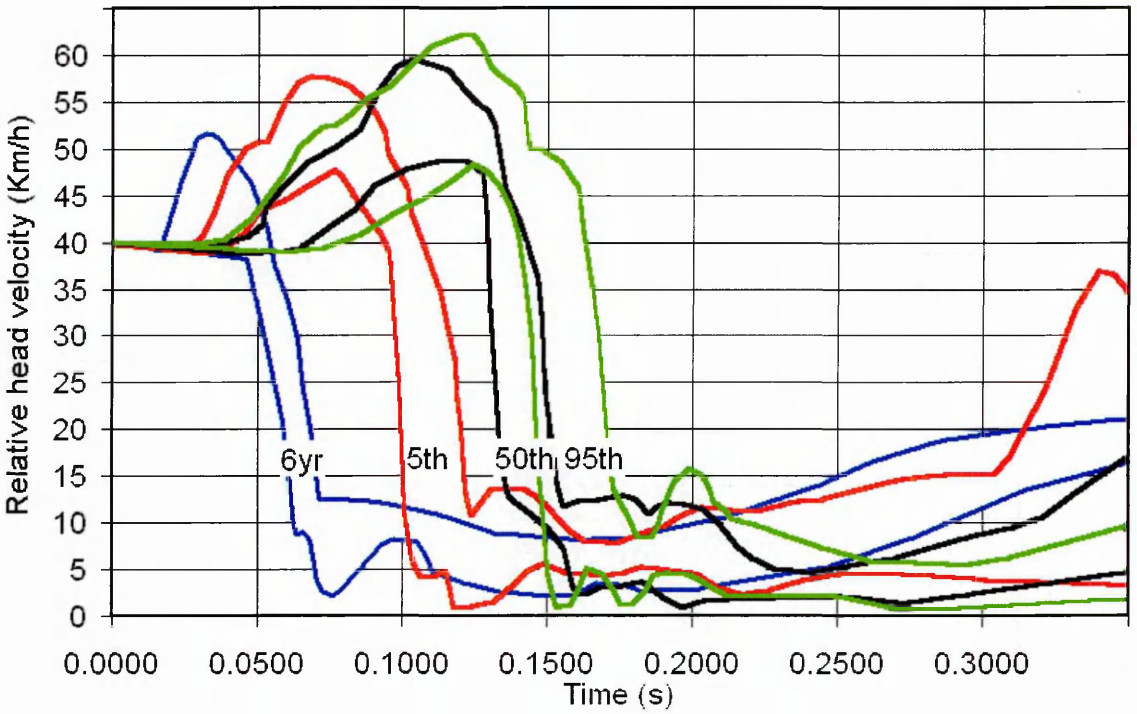

Figure 4.39 All relative head velocity ranges at 40 km/h

At the lowest impact velocity, the maximum head velocities for each pedestrian type were similar but the larger the pedestrian the longer it took for the head velocity to peak. At the higher impact velocity, the differences between the maximum head velocities and the impact velocity and between the pedestrian types were much larger. For example, the maximum velocity for the 95th percentile pedestrian was more than 10 km/h larger than the 6 year old pedestrian peak at 52 km/h. Towards the end of all the simulations the 6 year old and 5th percentile pedestrians measured much higher post impact velocities than the larger pedestrians.

Figure 4.40 shows the 50th percentile pedestrian HIC results (the original head acceleration data are shown in the appendices). For all stances there was a large increase in HIC with increasing vehicle impact velocity. Any differences due to the impact location at Y0 or Y500 were relatively small and did not reveal a clear trend. However, stances 'A' and 'D' led to the highest HIC results and stances 'B' and 'C' led to much lower HIC results.

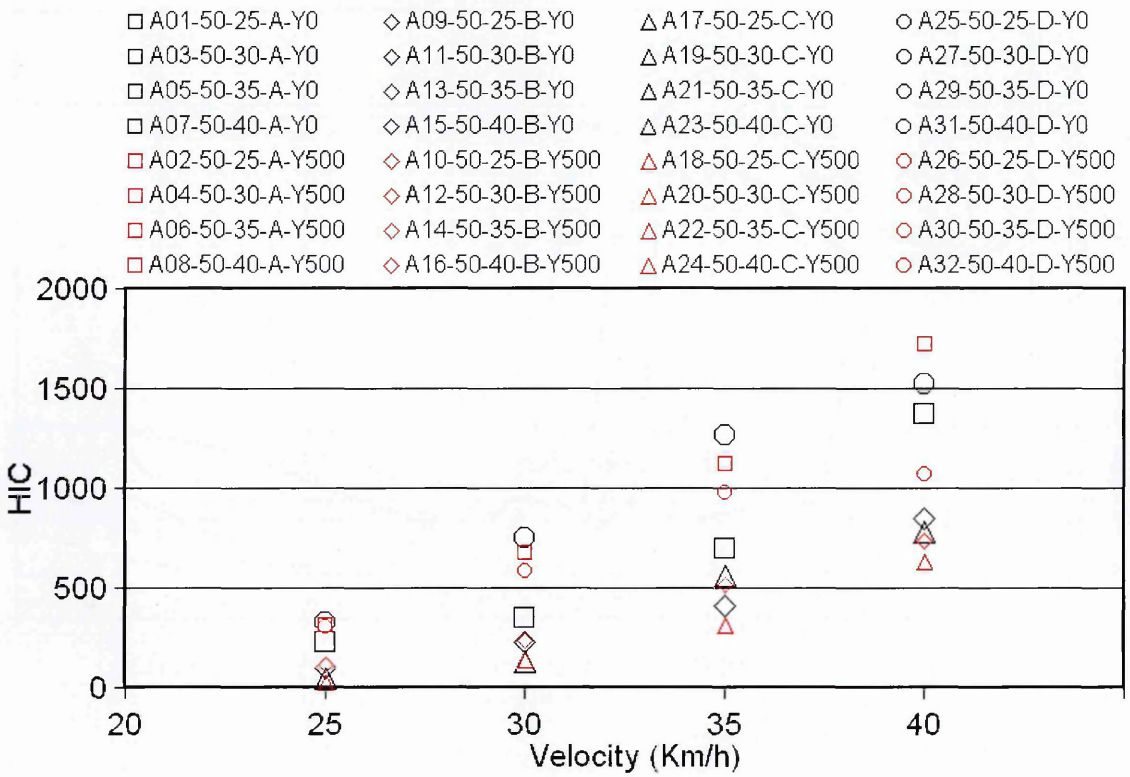

Figure 4.40 50th percentile pedestrian HIC at 25, 30, 35, 40 km/h

The analysis was extended to all pedestrian types as shown in Figure 4.41 and Figure 4.42 (the original data are shown in the appendices).

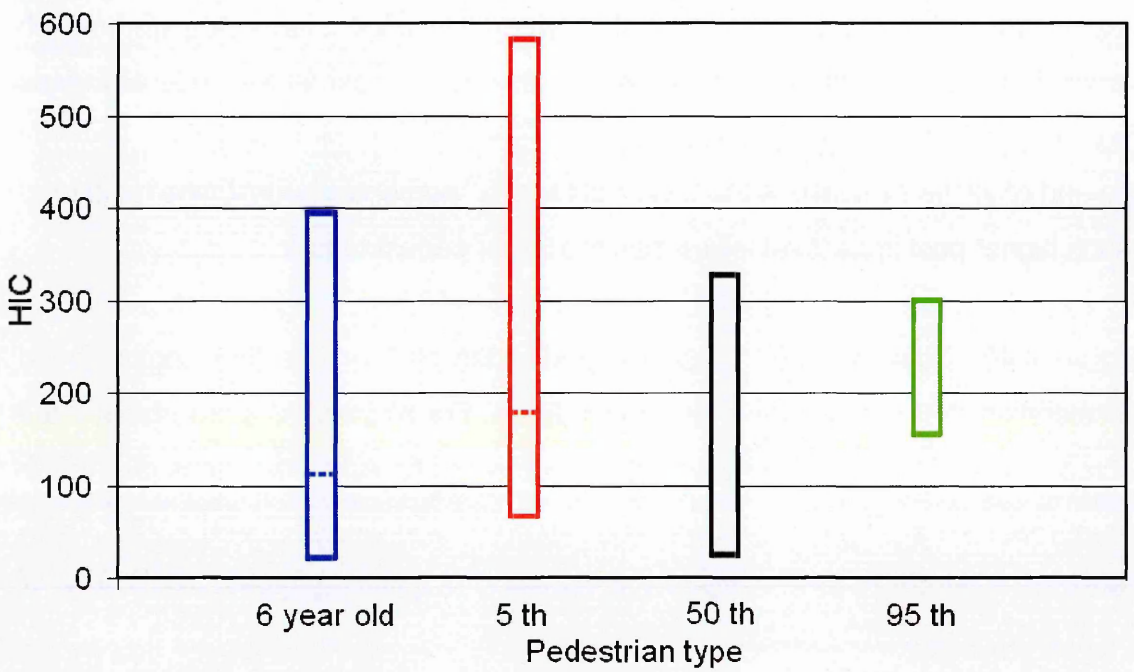

Figure 4.41 All HIC ranges at 25 km/h

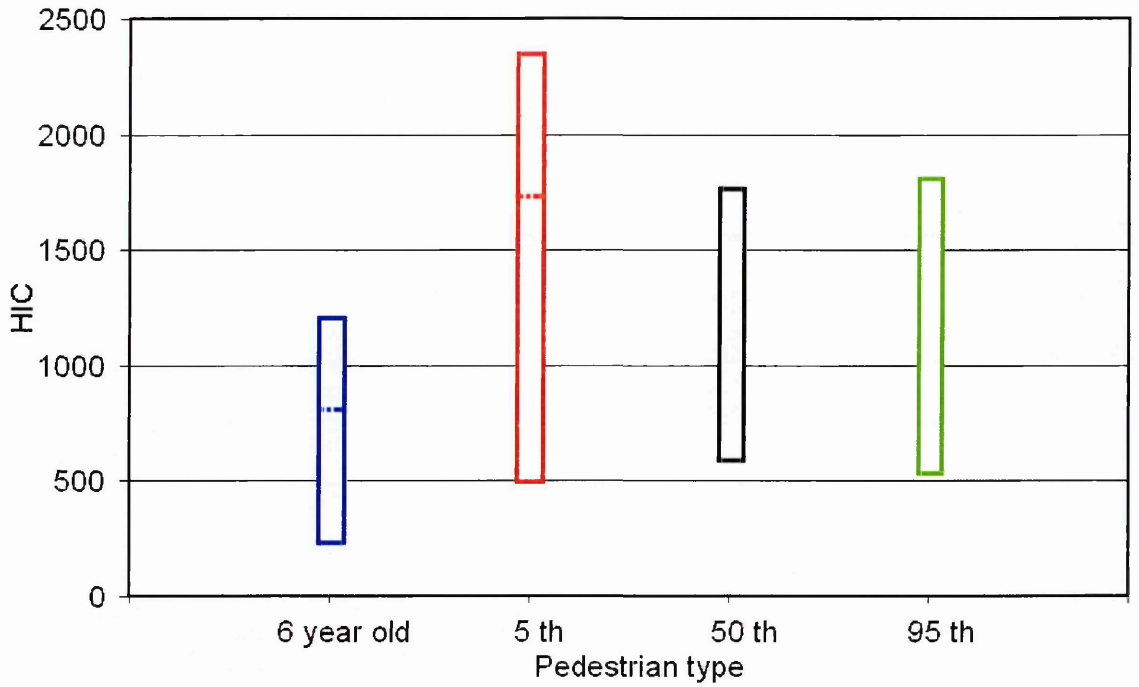

Figure 4.42 All HIC ranges at 40 km/h

At both velocities the largest range of results was measured for the 5th percentile pedestrian although there were only a few very high HIC results for stance 'D' that caused this large variation. A similar situation occurred for the 6 year old pedestrian and in both cases a dashed line is shown to indicate that the majority of the results for each pedestrian were lower than the dashed line value. Taking this into account the trend for the majority of the results was that the 5th, 50th and 95th percentile pedestrians generated the highest HIC results.

Figure 4.43 shows the maximum pelvic accelerations for all the accident simulations involving the 50th percentile pedestrian. In general the maximum pelvic acceleration increased with impact velocity but this was not true for some results, for example, stance 'D', where the results showed no particular trend with increasing impact velocity. For stance 'C' cases at the Y500 impact location, the maximum acceleration was significantly lower than at Y0. Stance 'A' cases at the Y0 impact location exhibited the most consistent increase of maximum acceleration with velocity.

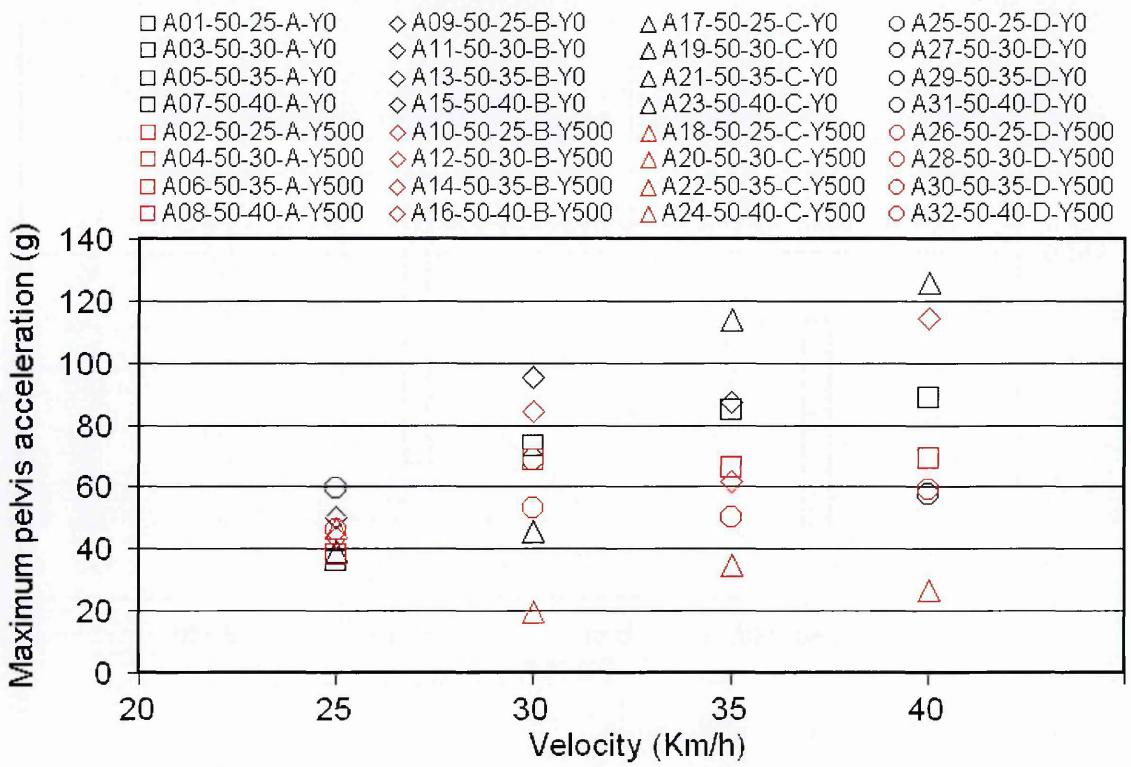

Figure 4.43 50th percentile pelvis acceleration at 25,30,35,40 km/h

The full results for all four pedestrians at impact velocities of 25 km/h and 40 km/h are shown in Figure 4.44 and Figure 4.45 (see appendices for original data).

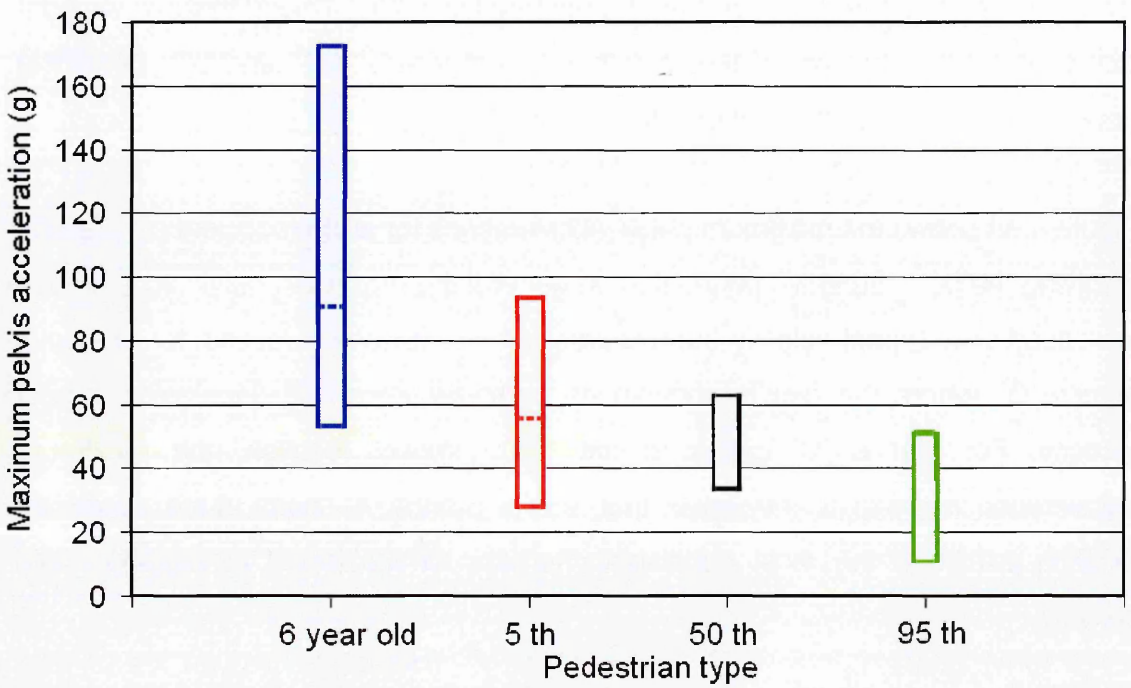

Figure 4.44 All pelvis acceleration ranges at 25 km/h

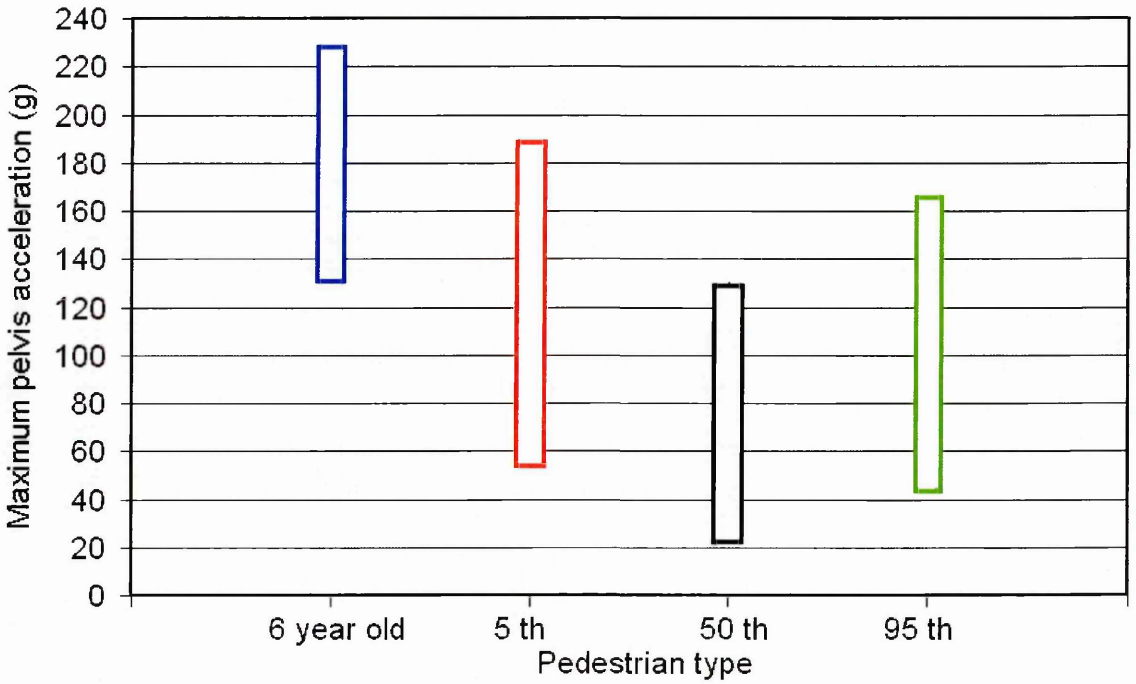

Figure 4.45 All pelvis acceleration ranges at 40 km/h

At the lower impact velocity, the range of pelvis accelerations was higher for the 6 year old and 5th percentile pedestrians than for the larger pedestrians, although this difference was only caused by a few extreme stance 'D' results for the smaller pedestrians. The majority of the low impact velocity results were recorded below the value indicated by the dashed line. Even taking this into account, the 6 year old pedestrian still measured larger pelvic accelerations than the other pedestrians at both impact velocities. Additionally, at the lower impact velocity, pedestrian stance caused a smaller range of pelvis accelerations than at the higher impact velocity.

Figure 4.46 shows the struck knee maximum shear displacements for the 50th percentile pedestrian (the time histories are in the appendices). There was a small increase in maximum shear with impact velocity but the largest influence on this was the pedestrian stance. Stance 'B' and stance 'D' generated very small maximum shear in comparison to the other stances and stance 'A' led to the largest maximum shear. The influence of the impact location varied according to the stance. Stances 'A' and 'D' led to larger maximum shear at Y500, and stance 'B' larger maximum shear at Y0, whereas stance 'C' led to very small differences. The time histories showed that maximum shear was reached within 5 to 10 ms.

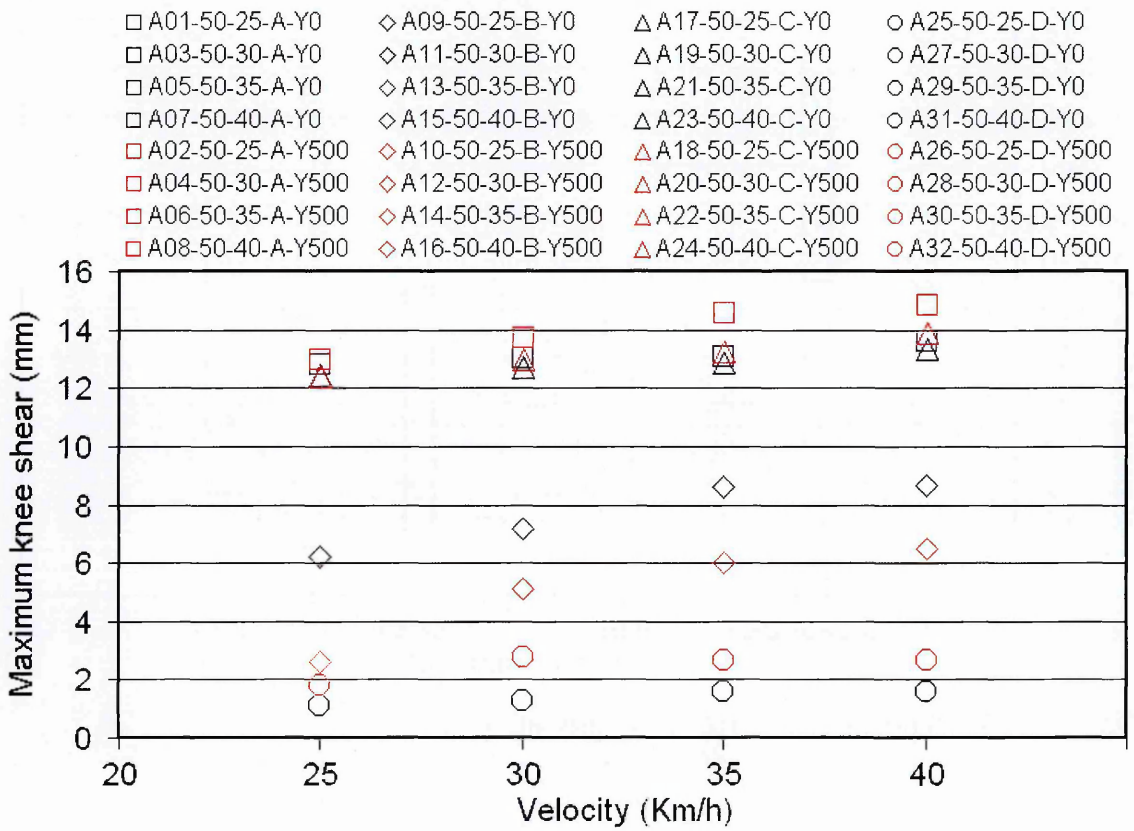

Figure 4.46 50th percentile pedestrian knee shear at 25, 30, 35, 40 km/h

The ranges of struck knee maximum shear displacement for all pedestrians are shown in Figure 4.47 and Figure 4.48 (the original data are in the appendices).

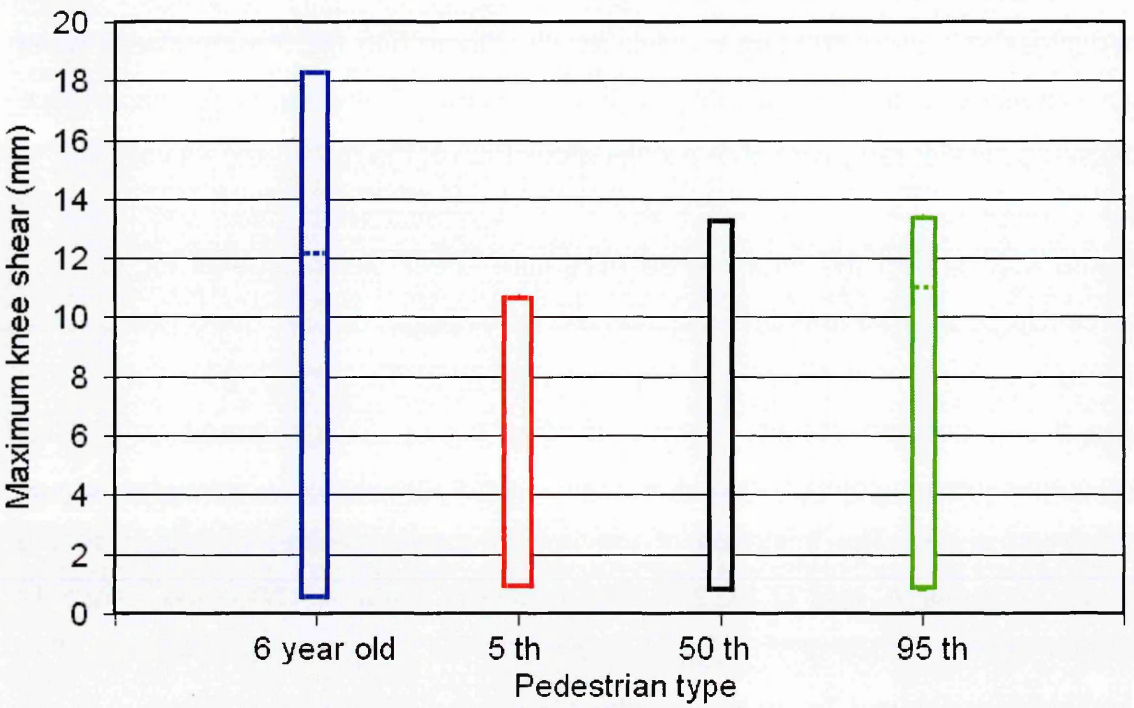

Figure 4.47 All knee shear ranges at 25 km/h

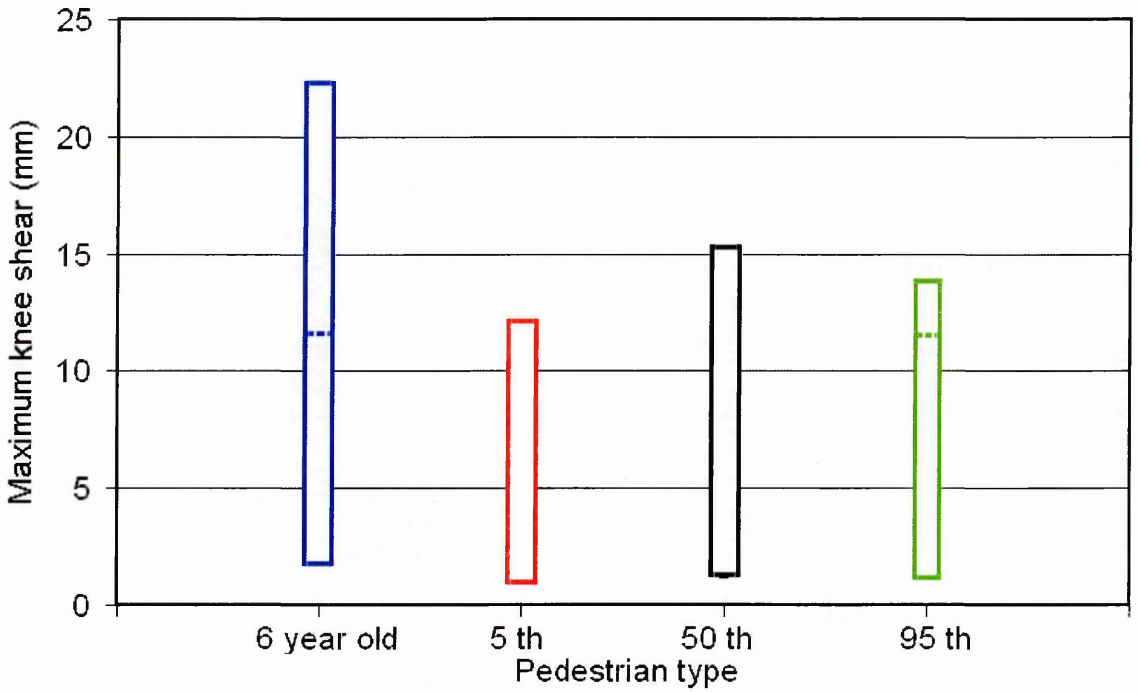

Figure 4.48 All knee shear ranges at 40 km/h

As with HIC and pelvis acceleration, stance 'D' led to extreme maximum shear values and in particular for the 6 year old and 95th percentile pedestrians, where the majority of maximum shear values were above the dashed lines shown. The range of maximum shear values for the 5th and 50th percentile pedestrians was caused by more than just a few stance 'D' results. If the stance 'D' results were included the 6 year old pedestrian measured the largest maximum shear values at both impact velocities.

The struck knee maximum bending angles for the 50th percentile pedestrian are shown in Figure 4.49 and the time histories are shown in the appendices. There was no clear trend between maximum bending angle and impact velocity but for stances 'A' and 'B' and to a lesser extent the other stances the maximum bending angle was smaller at Y500 than Y0. Stance 'D' consistently led to the smallest maximum bending angles and at most impact velocities (except 40 km/h) stance 'A' and the Y0 impact location led to the largest maximum bending angles. Maximum bending angle was reached at many different times depending on the stance and impact velocity and therefore it was not possible to make general observations about this.

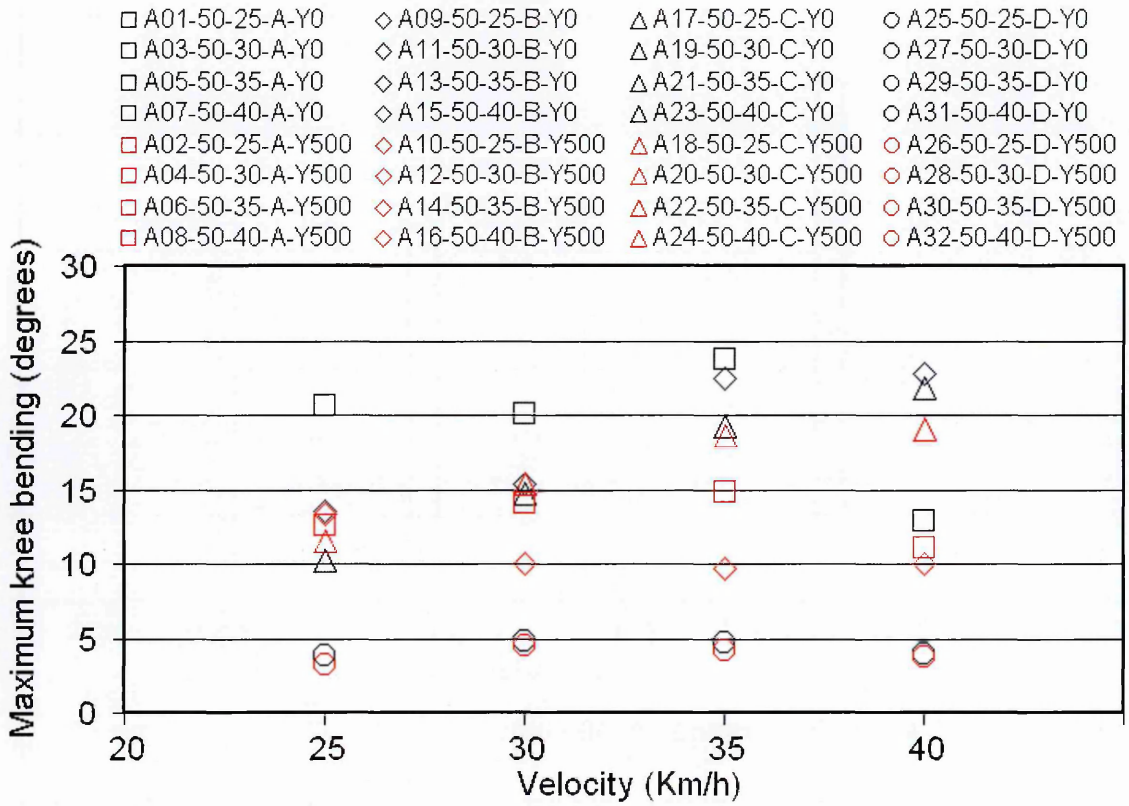

Figure 4.49 50th percentile knee bending at 25, 30, 35, 40 km/h

The ranges of struck knee maximum knee bending angles for all pedestrians are shown in Figure 4.50 and Figure 4.51 (the original data are in the appendices).

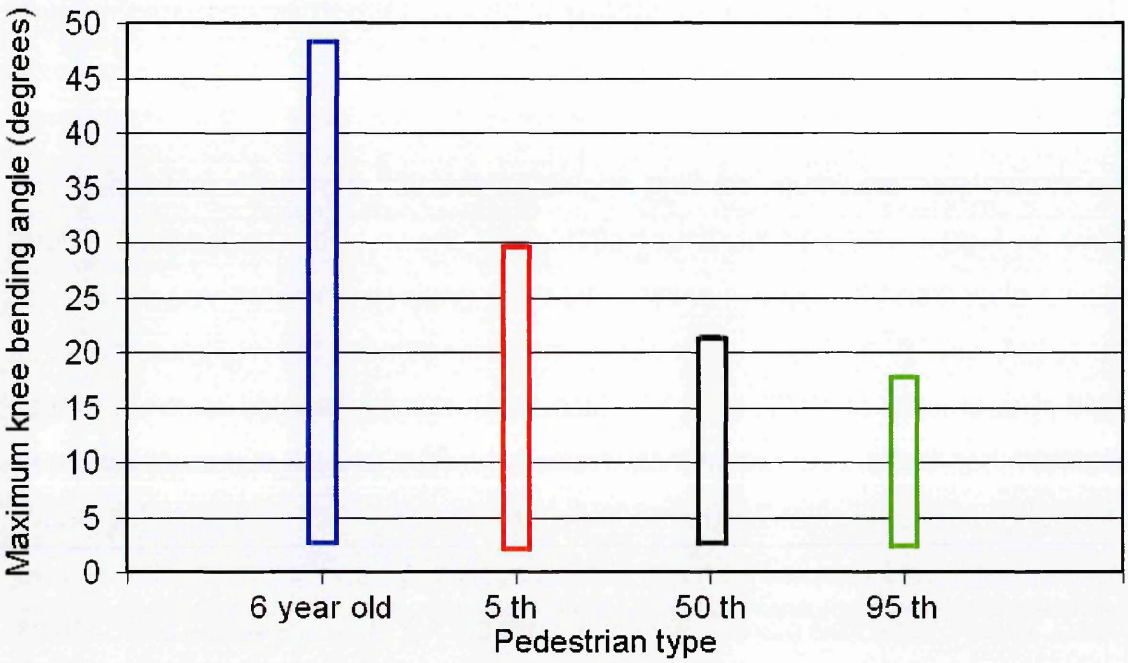

Figure 4.50 All knee bending ranges at 25 km/h

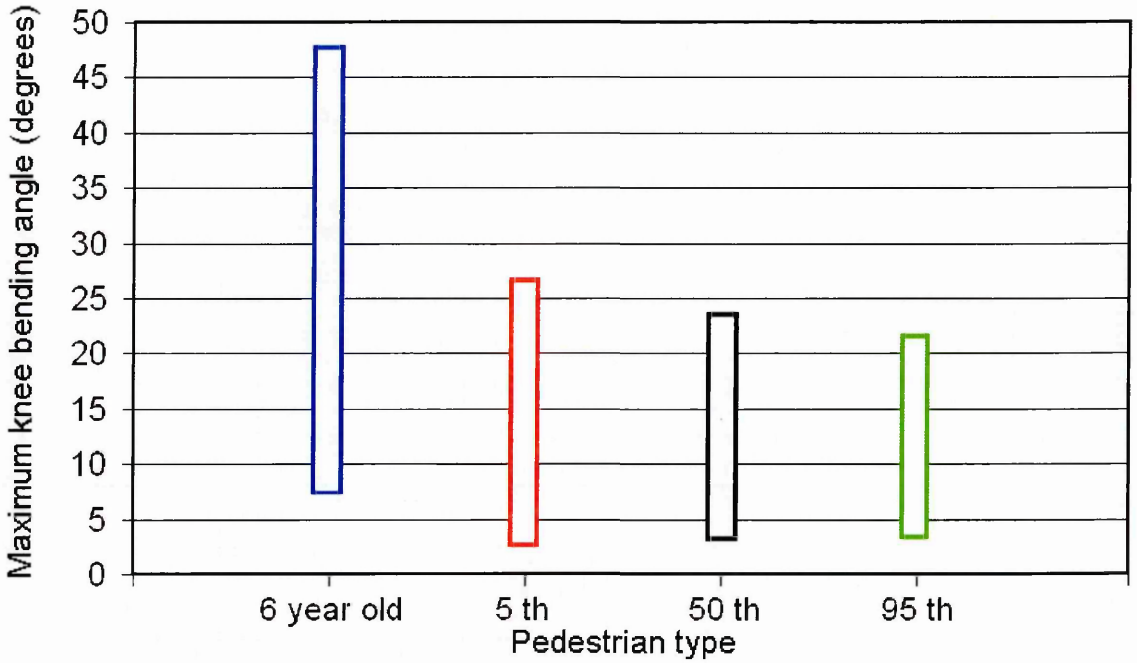

Figure 4.51 All knee bending ranges at 40 km/h

Cases involving the larger pedestrians measured smaller maximum bending angles than those with the smaller pedestrians. The range of bending angles was also smaller for the larger pedestrians. The 6 year old pedestrian measured very high bending angles at both 25 km/h and 40 km/h. As with knee shear, pedestrian stance rather than the impact velocity had the largest influence on the maximum bending angle.

Figure 4.52 shows how the maximum tibia acceleration increased with velocity for all of the 50th percentile pedestrian results. Stance 'D' led to very low accelerations in comparison to the other stances and the increase in maximum acceleration with impact velocity was also smaller. In contrast to this, stances 'A' and 'C' generated the highest accelerations, especially at Y500. Any difference in the results measured at Y0 and Y500 were more noticeable at higher velocities and for stances 'A' and 'B'. However, in stance 'A' the Y500 accelerations were lower than at Y0 and in stance 'B' the opposite occurred. Stances 'C' and 'D' generated a much smaller difference between the maximum accelerations at the two vehicle impact locations.

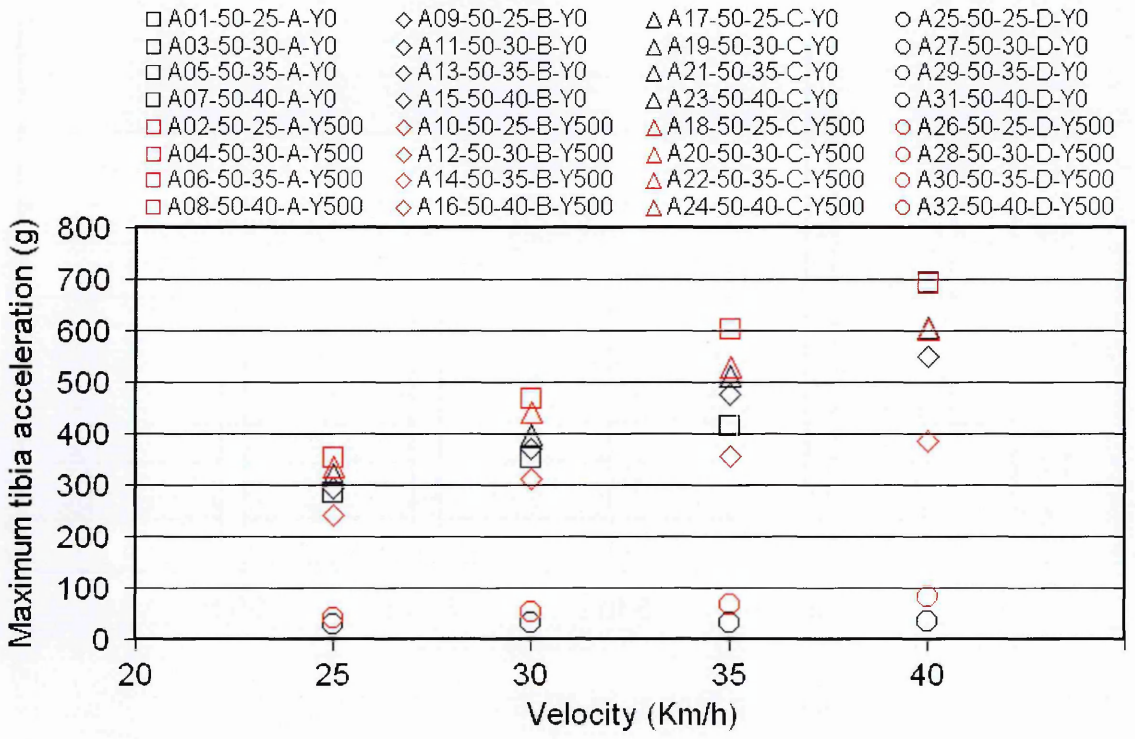

Figure 4.52 50th percentile tibia acceleration at 25,30,35,40 km/h

Figure 4.53 and Figure 4.54 show the range of maximum tibia acceleration results for all the pedestrians, at low and high impact velocities (the original data are shown in the appendices).

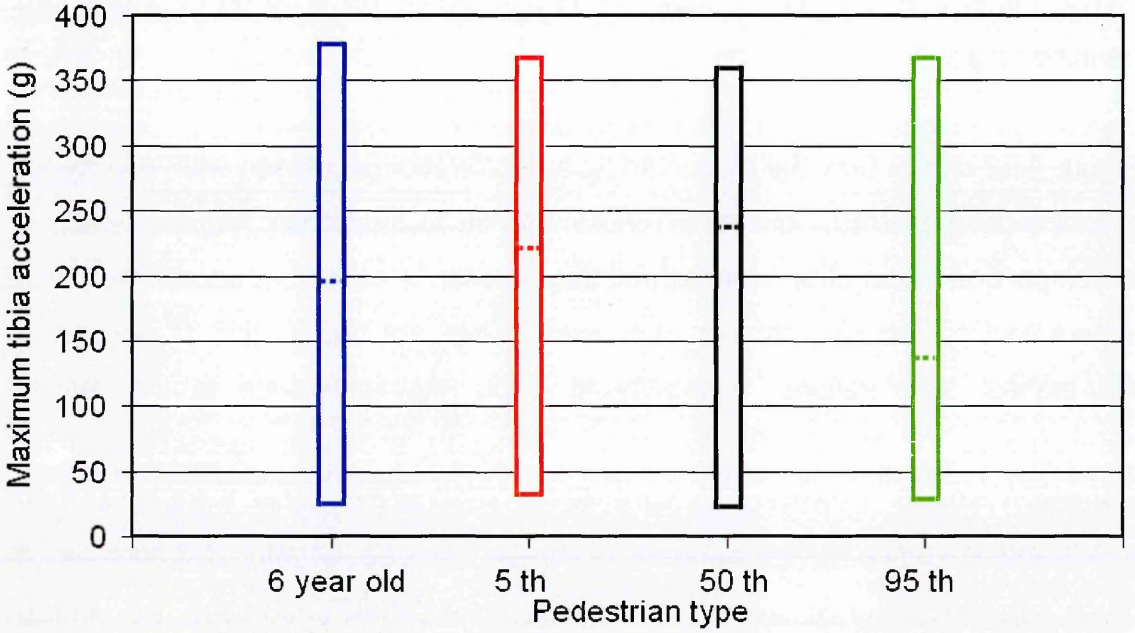

Figure 4.53 All tibia acceleration ranges at 25 km/h

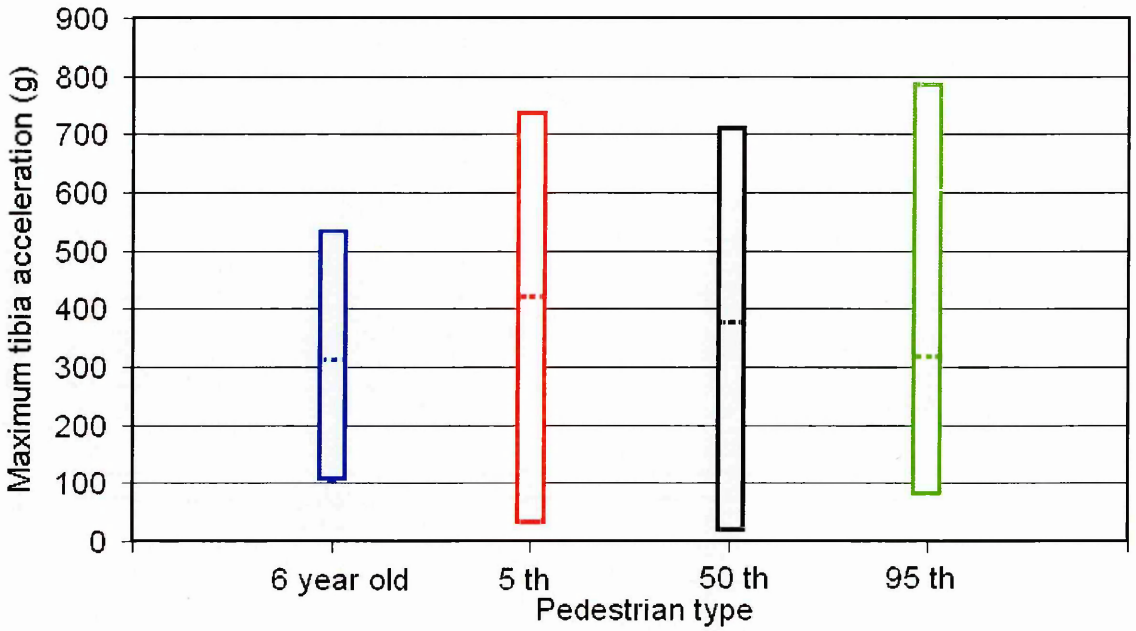

Figure 4.54 All tibia acceleration ranges at 40 km/h

Once again stance 'D' led to lower maximum tibia accelerations than the other stances and most of the results were measured above the dashed line. At the lower impact velocity the difference between the acceleration ranges measured by each pedestrian was small. However, in general, at the higher impact velocity, the highest accelerations were measured with the 95th percentile pedestrian and the lowest with the 6 year old pedestrian.

Figure 4.55 shows the first tibia and fracture locations for all cases. In most of the simulations the first fractures occurred in the central regions of the tibia and femur with the only exceptions occurring with cases involving the 6 year old and 5th percentile pedestrians. There was no clear relationship between impact velocity and fracture locations and leg fracture occurred in both struck and unstruck legs in stance A. Leg fracture also occurred very rapidly in adjacent leg beams (e.g. within 1 ms) when one beam had failed and so it was difficult to determine exactly which beam had failed first. A few cases involving the 6 year old and 5th percentile pedestrians measured no fracture in the tibia and/or femur.

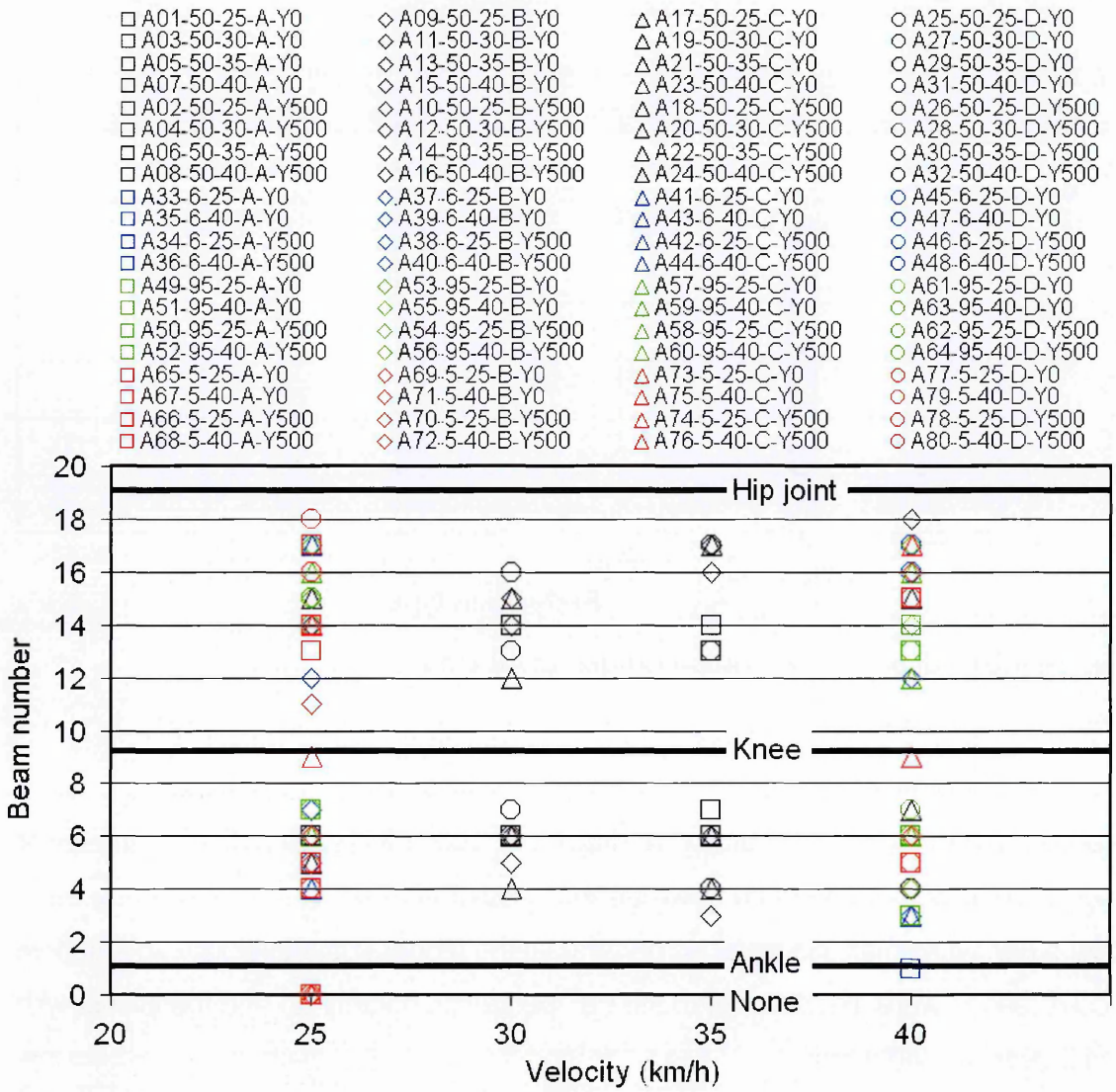

Figure 4.55 All first tibia and femur fracture locations

4.5.3. Discussion of results

Animation files of every accident simulation helped to identify common events in order to generalise about a typical impact sequence. In the first few milliseconds after the first leg to bumper contact the majority of the pedestrian body remained stationary. This was particularly noticeable for larger pedestrians. The lower leg was increasingly loaded and initially translated horizontally in the global X axis direction with the bumper and away from the upper leg. This caused a rapid peak in knee shear and during this time the upper leg began to follow the knee and rotate towards the vehicle face. Within the first 10 ms of each simulation it was possible to visualise both knee shear and bending in the struck leg or legs. Depending on the

stance, the upper leg rotated about the Z axis (e.g. in stances B and C) in addition to the Y axis. In the next 20 ms the lower leg began to rotate under the bumper and the upper leg continued to rotate towards the vehicle face whilst the upper body largely remained upright. As the pelvis began to approach the vehicle face the upper body had already begun to rotate about the Y axis and the lower legs started to rotate away from the bumper. Depending on many factors the knee bending moment peaked at some point during this period. It was useful to observe how the legs were swept away from the vehicle face or, in the case of the 6 year old, how the pedestrian began to wrap around the vehicle face.

By 40 ms and until the end of the simulations at 340 ms the motion of each pedestrian became quite complex. The pedestrian continued to rotate towards the hood and depending on the stance (e.g. for stance 'C') the pelvis and legs began to rotate away from the vehicle about the Z axis. During the approach to the hood the exact positioning of the arms was critical because the subsequent motion was changed by their position. As contact occurred between the hood and arms the arms acted as a pivot point for the whole body about the Y axis and the legs continued to rotate away from the hood. Soon after the shoulder contact, head contact occurred with the windscreen or for the 5^{th} percentile and 6 year old pedestrians with the hood. In some cases, due to the car geometry, head and shoulder contact was simultaneous, the smaller pedestrians tended to rotate about the Z axis (especially at Y500) and often the 6 year old pedestrian was thrown to the front of the vehicle.

In order to make sense of the impact events, they were categorised as the pelvis to vehicle face, shoulder to hood and head to hood or windscreen impacts. Although pedestrian stance significantly changed the impact timing, it did so in an inconsistent manner and it was only possible to clearly identify the difference between the impact timing at low and high velocities and between pedestrian types. In general, the higher impact velocity and smallest pedestrian generated the fastest impacts but there were exceptions to this general trend, largely caused by pelvis and shoulder limitations. The construction of the rigid pelvis meant that in some

cases there might have been two contact forces generated in the region of the pelvis due to overlapping leg and pelvis mesh geometry. In addition the pedestrian shoulders were too stiff because the shoulder pivot centre was fixed (unlike human shoulders) and in some of the animations it was possible to see how the head contact was delayed because of this and/or arm interactions.

CMD was created in anticipation of the difficulty in quantitatively comparing the different pedestrian motion in accident cases. An analysis of the results showed that it correctly revealed general trends. For instance, there was an increase in all the CMD values at higher velocities, the CMD values in the X direction were larger for larger pedestrians and the CMD values in the Y direction were larger for the smaller pedestrians. It also confirmed how the motion in the Y direction was greater with impacts at Y500, at the higher velocity and in the 6 year old pedestrian cases the motion in X, Y and Z was much more similar than in cases involving the other pedestrian types. This was a quantitative way of describing how the 6 year old pedestrian tended to move equally in all directions rather than primarily in the X direction like the larger pedestrian models. The manner in which smaller pedestrians tended to move further in the Y direction than the larger pedestrians had not been obvious in the animations until it was noted in the CMD results.

Due to the manner in which CMD was calculated its main limitation was a lack of sensitivity to the influence of some accident conditions such as pedestrian stance and impact location. CMD was only calculated with the addition of peak displacements in each global direction, of the major body regions. This meant that, for instance, the subtleties of how each body region moved due to different stances were lost. It was difficult to identify consistent trends between the various pedestrian stances (assuming that these existed) and few trends in Y and Z where the CMD values were usually much smaller than the CMD value in X. As a direct result of these limitations CMD was not used to compare the modified vehicle results described later.

In comparison to CMD, the head displacement was a clearly defined measure of

one part of the pedestrian model. As such it was possible to trace the motion of the head with time in X and Z and distinguish the influence of stance more easily. On the other hand, it was also more difficult to quantitatively compare the time histories in a simple manner (especially if the Y motion had also been measured). As with CMD, it showed that head motion increased in X with impact velocity. Stance 'D' led to the largest head motion and stances 'A' and 'C' consistently led to the shortest head motion. The variation in head impact location in X, due to the pedestrian stance was surprisingly large at around 200 mm for the 50th percentile pedestrian whilst the variation due to impact velocity for stance 'A' was almost 300 mm. A particular observation in the head trajectories that could not be observed in the CMD analysis was the much larger post impact head motion of the 6 year old and 5th percentile pedestrians than for the larger pedestrians.

The head velocity results provided another means to understand the impact sequence on a time basis. In all cases there was a delay between the leg to bumper contact and the subsequent head motion. This lasted for more than 40 ms in for example cases involving the 95th percentile pedestrian and stance 'C'. Based on the animation files it was clear that this was due to the initial flexibility of the legs to deform without dragging the upper body with them and due to the inertia of the upper body delaying the upper body motion. The delay shortened and was more quickly followed by a quicker and larger magnitude velocity pulse as the impact velocity increased.

One of the questions that was raised from the results was whether the head impact velocity was also greater than the vehicle impact velocity. Figure 4.56 and Figure 4.57 show the shaded regions in which the head impact occurred, according to the velocity and head impact timing ranges. The shaded regions above the vehicle impact velocity line indicated that it was possible to have relative head impact velocities above the vehicle impact velocity, for all pedestrians except the 6 year old. This was in contrast to the author's previous results described in [Howard 2000-3] where all head velocities were lower at the time of head impact. However, this analysis was originally undertaken with a different vehicle model and only the 50th

percentile pedestrian in stance 'A'.

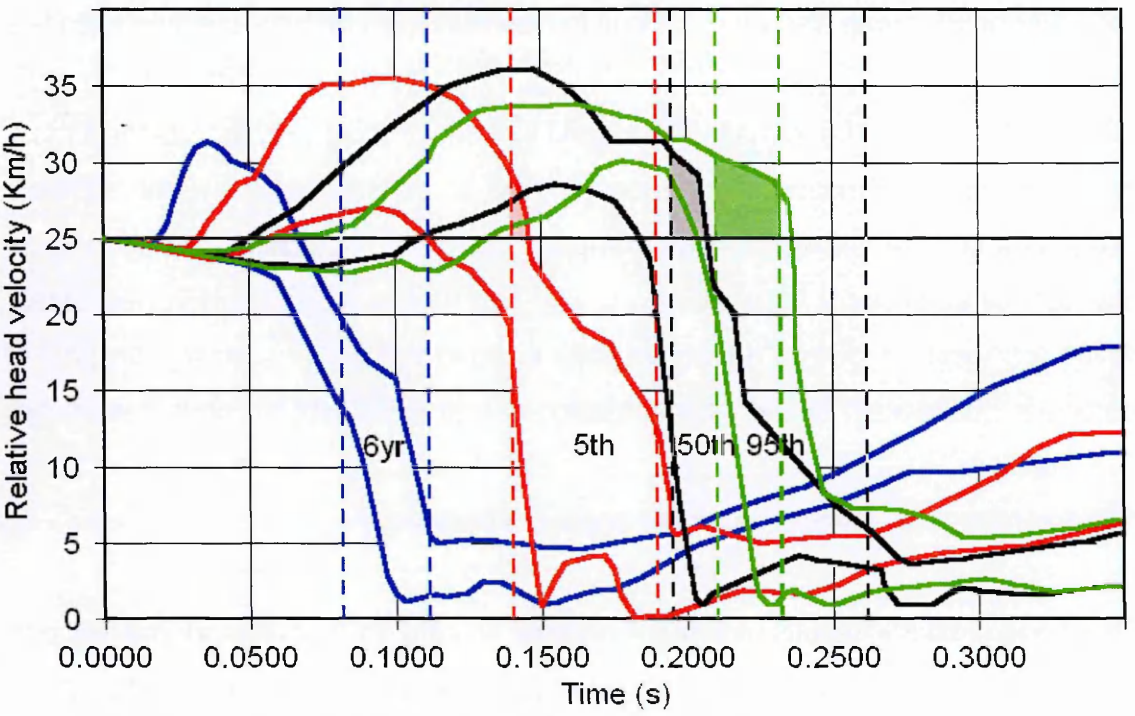

Figure 4.56 All relative head velocity and impact timing ranges at 25 km/h

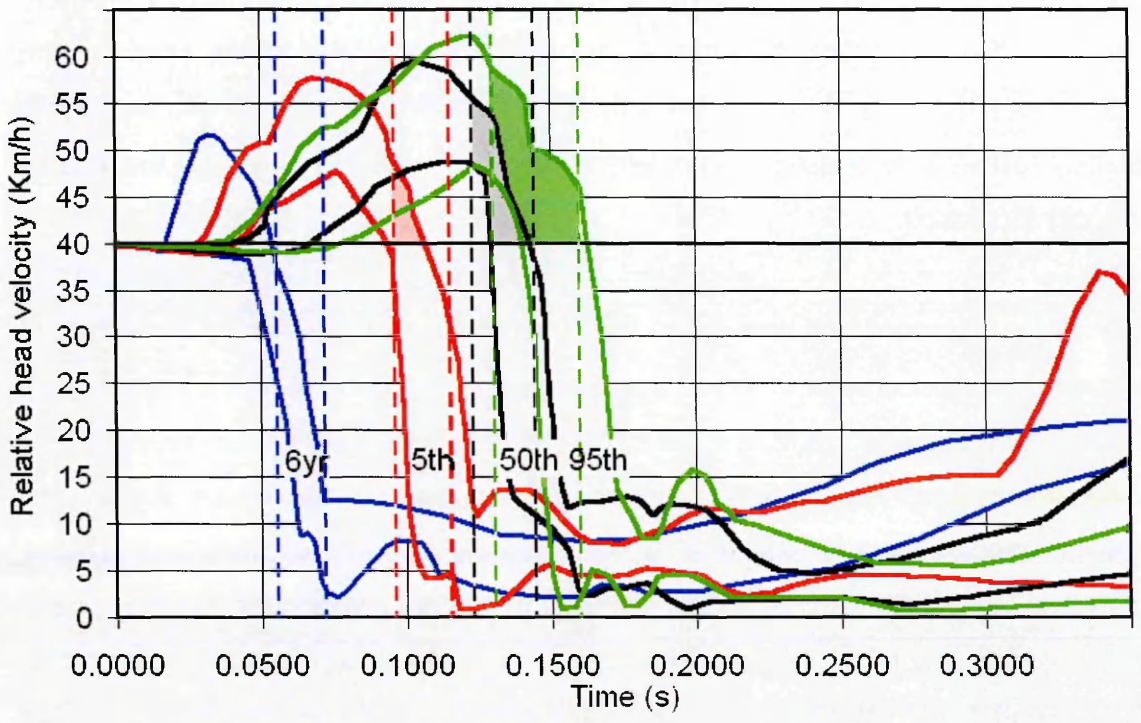

Figure 4.57 All relative head velocity and impact timing ranges at 40 km/h

A more detailed analysis of the results showed that at both vehicle impact velocities stance 'A' and in particular stance 'D' led to the highest head velocities. In stance 'D' this occurred because there was little interaction between the pedestrians (for example the arms) and the vehicle until the head impact. In stance 'A' all of the impact energy was transferred into both pedestrian legs rather than a single leg as in stances 'B' and 'C'. This would have led to a more direct transfer of the impact energy into the pedestrian upper body because both hip joints undertook this transfer into the upper body. The consequence of this, as also indicated by the short head trajectory, was a motion that was more like a skittle being struck than stances 'B' or 'C' where the pedestrians behaved more flexibly as the legs were swept away and the pedestrians rotated about Z. A more direct rotation of the whole pedestrian about Y also contributed to higher head velocities.

The time lag in the upper half of the body following the legs, was most clearly seen in the head velocity profiles, where the head remained almost stationary for longer than 40 ms after the leg impact, in some 95th percentile pedestrian cases. Another interesting feature of the velocity profiles was the much higher post impact velocities of the smaller pedestrians. The large post impact motion of the 6 year old and 5th percentile pedestrians had also been previously observed. If the simulations had been continued until ground contact it was highly probable that such large post impact motion would have led to the smaller pedestrians having higher energy impacts with the ground after they were bounced off the vehicle. Since the ground is relatively rigid this would have led to further serious injury measures, particularly with respect to the head, which appeared to be leading the downward motion in many of the animations.

The HIC results confirmed many of the trends already observed. For instance, as vehicle impact velocity increased, there was a very large increase in HIC and as with head velocity, stances 'A' and 'D' also generated the highest HIC values. This was to be expected because, for a fixed set of impact conditions (e.g. impact surface stiffness), higher pre-impact velocities would generate higher head accelerations and hence HIC's. However, it was important not to overlook that the

impact conditions were not fixed, for instance each stance led to different head impact locations and each of these probably had a different stiffness due to the vehicle design. Although it did not occur in this case it was possible to miss this trend in the stances if there was an unfortunate set of parameters for a particular vehicle. However, this hindered the identification of any trend between HIC and pedestrian type or impact location at Y0 or Y500. Due to the reasons already described it was difficult to compare the HIC results with the injury limits specified in [EEVC 1998]. However it was noted that all of the lower impact velocity results and some of the higher impact velocity results (especially for the 6 year old pedestrian) were less than the injury limit specified in [EEVC 1998] as 1000.

It was very difficult to determine any trends from the pelvis acceleration results. There were two possible causes for this; the construction of the pelvis model as already described and/or the manner in which the pelvis was loaded. The pelvis loading was highly dependent on the pre-impact motion of the pedestrian and this meant that in some cases the pelvis struck a weaker region of the vehicle. Even though the impact velocity was higher, the pelvis acceleration was lower because of the weaker region. A glancing blow to the pelvis also resulted in lower pelvis acceleration because some of the impact energy was transferred into rotational rather than translational acceleration.

The time histories for knee shear displacement had revealed that maximum shear was very quickly reached within 5 to 10 ms after the initial bumper contact. Despite the large amount of energy that was transferred into the legs even at 25 km/h there was still a small but measurable increase of maximum knee shear with increased velocity. The models were also able to distinguish stance 'D' with very low levels of shear because the legs were rotated in their natural motion. However, it was not possible to distinguish consistent relationships between knee shear and stance for all pedestrian types. For example, the 6 year old and 50^{th} percentile pedestrians measured the highest shear values for stance 'A' whilst the 5^{th} and 95^{th} percentile pedestrians measured the highest values for stance 'B'. It was also noted that for instance one stance measured higher shear at Y500 than Y0 but in another stance

it was consistently lower at Y500. This had implications for the optimisation of the vehicle design to minimise shear. In addition, a certain stance for one pedestrian type often generated the largest shear but for another pedestrian type it generated the smallest shear (although stance 'D' always generated the smallest shear values). Another observation from the perspective of distinguishing between impact locations (and hence vehicle bumper designs) was that certain stance and pedestrian type combinations measured larger differences between the two locations. However, the data set was relatively small to draw any decisive conclusions in this respect except to conclude that many parameters were clearly influencing the results and this warrants further research.

In many ways the knee bending angle was a more complex injury measure, particularly from a time history perspective where the maximum bending value was often reached much later than the maximum shear value. It was also difficult to identify a consistent relationship between an increase in vehicle impact velocity and maximum bending angle unless comparing the lowest and highest vehicle impact velocities. Like shear, it also showed that the smallest bending angles were generated by stance 'D' and unlike shear, stance 'A' often generated the largest bending angles for nearly all pedestrian types and vehicle impact velocities. As with knee shear it was not possible to consistently distinguish between the Y500 and Y0 vehicle impact locations for all pedestrian types and stances. The smaller pedestrians also suffered larger bending angles than the larger pedestrians did.

Unlike the knee shear and bending measurements that relied upon a relatively complex joint model, the tibia acceleration was a simple measure. There was a clear relationship between increasing impact velocity and acceleration and as with the previous measure, stance 'D' generated very low accelerations in comparison to the other stances. In contrast to this, stance 'A' always generated very large accelerations. A possible reason for this was that the resistance to leg motion was caused by larger inertia and double the hip joint resistance leading to higher impact forces and hence acceleration on the struck leg. The opposite situation led to the low tibia accelerations for the 6 year old pedestrian cases at the higher impact

velocity.

For each pedestrian type stance 'A' clearly distinguished between the two impact locations at nearly all impact velocities. However, it was noted that there were conflicting trends from the perspective of designing the vehicle. For instance at the lower impact velocity the smaller pedestrians suffered larger accelerations at Y0 whilst the largest pedestrians did the opposite. Also, this trend became less clear at a higher impact velocity where for instance, the acceleration differences measured at the two locations were very small for the smaller pedestrians.

The leg fracture results did not reveal any clear relationship with impact velocity, or pedestrian type and stance but did show that fracture usually occurred (except for a few exceptions) in the central regions of the long bones and almost simultaneously in adjacent regions. Even at the lower impact velocity very few cases involved no leg fracture, and fractures occurred in both struck and unstruck legs in stance 'A'. Due to the lack of clear trends in these data, these results were not measured for the modified vehicle described later.

4.5.4. Reference vehicle accident simulation conclusions

Visual examination of pedestrian accident simulation animations provides a useful and essential means to observe the whole pedestrian impact sequence. It enables the identification of how general changes to the accident conditions lead to different pedestrian impact motions and allows the analysis of other aspects of the motion that are difficult to characterise in quantitative measures (e.g. rotation about the Z axis). The pedestrian impact events can be usefully categorised into pelvis to vehicle face (e.g. headlamps, radiator grill, hood leading edge), shoulder to hood and head to hood or windscreen.

Quantitative measures allow the influence of different parameters to be quantified and generalised into expected ranges but do not replace the need for visual examination of every animation file. It is still necessary to confirm for example that a peak contact force in the pedestrian pelvis really coincides with the first pelvis to hood impact. Defining each impact event for the impact timing is difficult because of

the biofidelic limitations in the shoulder and pelvis regions of version 7.2 of the pedestrian humanoid models. These limitations need to be addressed in future research and perhaps due to these limitations it is not possible to clearly identify how pedestrian stance influences the impact timing. However, the quicker impact with higher vehicle impact velocities and smaller pedestrians is clear, although there is overlap between some of the timing ranges.

CMD measures can be used to compare the influence of pedestrian type and in some cases vehicle impact location, on the overall pedestrian motion in X, Y and Z. However, it is not possible to use CMD measures to compare the influence of different pedestrian stances. The higher the vehicle impact velocity and the larger the pedestrian the greater is the X axis motion. Smaller pedestrians tend to rotate in a small volume of space near the vehicle front and are more sensitive to the vehicle design, for instance being thrown to the side of the vehicle during an impact at Y500 because of the vehicle geometry.

Head trajectory is a more sensitive measure than CMD to different accident conditions although a time history is more difficult to compare than a single value. It can distinguish the influences of pedestrian type, stance and vehicle impact velocity. In addition to confirming CMD observations, it shows that stances 'A' and 'C' lead to the shortest head trajectories along the X axis and 'D' the longest. Post head impact motion of smaller pedestrians is larger than that of other pedestrians.

With increasing vehicle impact velocity the maximum head velocity pulse reaches a peak more quickly, is continued for a shorter period of time and is of a higher magnitude. At 40 km/h the larger the pedestrian, the greater is the head impact velocity but at 25 km/h the differences are minimal for adult pedestrians. Stances 'A' and 'D' lead to the largest head velocities. Although maximum head velocity is always greater than the vehicle impact velocity, the head impact velocity may or may not be, depending on the head impact timing, location, pedestrian size and stance. Post head impact velocity is larger for the smaller pedestrians.

There is a large increase in HIC with increasing vehicle impact velocity. Stances 'A' and 'D' lead to higher HIC values although in both cases the stiffness and mass of the part of the vehicle impacted can distort this trend. For example, if stance 'C' causes the head to impact a stiffer part of the vehicle it can generate higher HIC levels than a stance 'D' result. Possibly for the same reason it is not possible to identify a clear relationship with pedestrian type or vehicle impact location (i.e. at initial leg impact) but the HIC values are frequently lower for a 6 year old pedestrian.

Any trends in pelvis acceleration are difficult to clearly identify, possibly because of limitations of this version of the pedestrian models. However, pelvis acceleration increases with vehicle impact velocity and is higher for a 6 year old pedestrian.

There is a relatively small increase in knee shear with vehicle impact velocity, at least between 25 km/h and 40 km/h. Maximum knee shear varies with pedestrian type and stance. With the exception of stance 'D', that always leads to the smallest shear results, it is not possible to generalise that a particular stance leads to higher shear values unless the pedestrian type is also specified. Hence, the 6 year old child and 50^{th} percentile pedestrian measure the highest values for stance 'A' and for the 5^{th} and 95^{th} percentile pedestrians, stance 'B' leads to the largest shear values. It is also not possible to distinguish between vehicle impact locations in a consistent manner and this has implications for optimising the bumper for all cases.

The knee bending angle generally increases with a large increase in vehicle impact velocity (e.g. 25 to 40 km/h) but does not consistently do so for smaller increases (e.g. 25 to 30 km/h). Smaller pedestrians and stance 'A' lead to the largest bending angles. As with knee shear it is not possible to consistently distinguish the difference between the Y0 and Y500 vehicle impact locations. Smaller pedestrians generally suffer larger knee bending angles.

There is a clear increase in tibia acceleration with vehicle impact velocity and the relative increase in acceleration with velocity depends on the stance. Stance 'A' leads to the highest accelerations and has the largest increase in this acceleration

with velocity. Stance 'D' leads to the lowest accelerations and increases in acceleration. The 6 year old pedestrian yields the smallest tibia accelerations at the highest vehicle impact velocity for most stances but at the lowest velocity there is no difference between the pedestrian types. As with many of the other measures it is not possible to identify a vehicle impact location that consistently led to lower tibia accelerations for all pedestrian types and stances.

Leg fracture is highly likely, even at 25 km/h, with typical fractures in the central regions of the femur and tibia/fibula. Fracture occurs very rapidly in adjacent bone regions and is equally likely in either the struck or unstruck leg. It is not possible to identify any trends for pedestrian type, stance or vehicle impact location but only a few no fracture conditions occurred at the lowest vehicle impact velocity.

A general conclusion is that it is essential to carefully choose an identical set of accident conditions (pedestrian type and stance, impact velocity and location, vehicle brake dive and deceleration) and measures, when comparing different vehicle designs. The conclusions from one set of accident conditions often conflict with those of another set and so vehicle designs need to be compromised, for instance to minimise knee shear for both a 6 year old and a 95^{th} percentile pedestrian.

5. Pedestrian protection technology models

5.1. Context in overall methodology

This chapter describes the design and development of pedestrian protection technologies at a component level as highlighted in Figure 5.1 [Howard 2001-1].

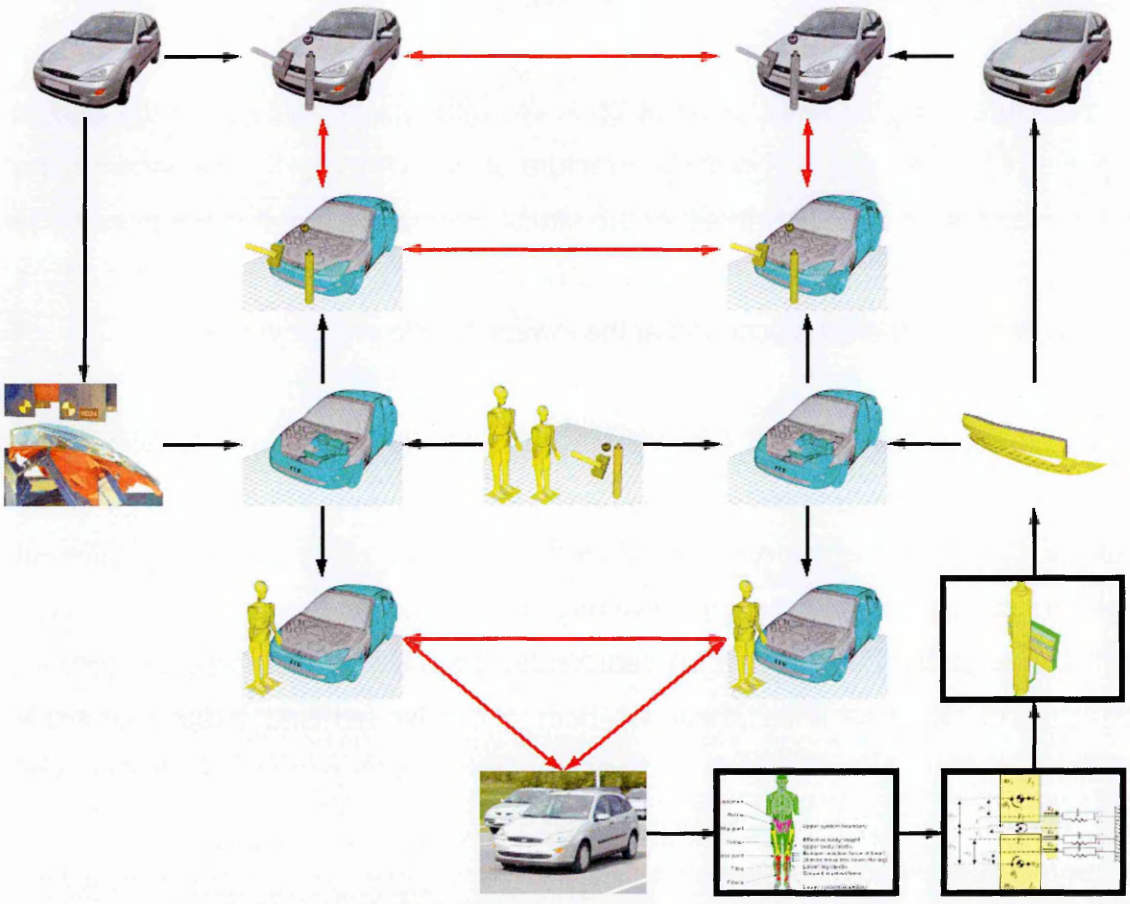

Figure 5.1 Pedestrian protection technology methodology (technologies)

5.2. A review of pedestrian protection requirements

Table 5.1 shows the relationship between pedestrian and vehicle impact regions, some potential protection solutions and a prioritisation for all regions. Reading from left to right, the pedestrian body regions start from the ankle and move up to the head. Similarly the vehicle regions start from the bumper, and move rearward until the windscreen surround. The number of real world pedestrian injuries caused by vehicle regions beyond the windscreen is assumed insignificant [Foret-Bruno 1998]. There is a clear diagonal relationship between pedestrian and vehicle regions.

Possible solutions and subjective priority	Head 1	Neck 9	Arms 11	Spine 10	Thorax 4	Abdomen 6	Pelvis 5	Femur 8	Knee 2	Tibia/fibula 3	Ankle 7
Multiple density foams Lower foam density (and increased depth) **Lower stiffening ribs/bumper geometry** Stiff lower air dam moved forward New bumper material e.g. honeycomb Deployable air bag									✓	✓	✓
Deformable headlamp cover/mount GOR deformable Mechanical deployable hood/module Hood Leading edge below 660mm Increase longitudinal package space Lower latch & latch platform crossmember Energy absorbing grille Deployable air bag					✓	✓	✓	✓	✓		
Distributed, uniform hood stiffness Leading edge deformable Rear edge deformable Design hood to prevent wiper spindles test **Mechanical deployable hood/module** Pyrotechnic deployable hood Clam shell hood Compliance in shotgun & rain channel Side reference within hood area Deployable air bag Vertical compliance in latch/hinge/stops Move hood shutline inboard	✓	✓	✓	✓	✓	✓	✓	✓			
Clearance 65mm in child impact area Clearance 80mm in adult impact area Deformable mounting brackets e.g radiator Minimise contact area and stiffness Low reservoirs/filters/pipes/engine/mounts	✓	✓									
Hide wiper spindles & cowl grille with hood Larger A post section & deformable outer New windscreen material Deployable air bag	✓	✓									
	Windscreen/surround 5		Engine bay 3		Hood and fenders 2			Vehicle face 4		Bumper 1	

Table 5.1 A prioritisation of pedestrian and vehicle impact regions

With respect to the influence of the different vehicle regions it can be seen that the vehicle face, hood and fenders influence the most pedestrian body regions because

they account for the majority of the vehicle area likely to come into contact with a pedestrian. Alternatively, if one first considers pedestrian body regions, then the largest number of vehicle regions influence the neck and head because head contact might occur anywhere on the hood, fenders, windscreen or windscreen surround depending on the vehicle and pedestrian geometry.

From another perspective, (based on the patent search described later) there are more pedestrian protection patents concerning the hood and fenders than any other vehicle regions and the least for the windscreen and windscreen surround. The pedestrian body region injuries may also be prioritised with respect to the long term societal costs and the likelihood of an injury occurring. Various references [Levine 1986, MacLaughlin 1987, Isenburg 1998, Otte 1998] show that the knee and head are the most commonly damaged and this causes the highest societal costs. Knees are difficult to repair. Head injuries are often serious and may lead to death. Arm injuries often occur but are usually less serious. Spinal and neck injuries can lead to long term disablement but rarely occur. In recent years femur, pelvis and thorax injuries have occurred less frequently [Matsui 1999]. Tibia/fibula injuries are rarely serious but they occur frequently. Abdomen injuries are rarely serious and ankle injuries are rarely recorded.

In terms of the vehicle regions, the bumper is always impacted and has the potential to cause very high societal costs. It is therefore given the highest priority. The hood and fenders follow this because they cover such a large region of the vehicle and therefore provide the opportunity to address many potential injuries. Next comes the engine bay, which is a region related to the hood but is more difficult to change due to the constraints of engine and suspension design. The vehicle face, windscreen and windscreen surround have been given the lowest priority because the vehicle face is relatively pedestrian friendly in aerodynamic vehicles. The windscreen is extremely difficult to change, certainly within the short term, because of the complex requirements on it (e.g. optical clarity, toughness).
If one considers the highest priority combinations, then these include knee injuries caused by the bumper, head injuries caused by the hood and, to a lesser extent,

lower body injuries caused by the vehicle face. These are the main injuries to be addressed with the pedestrian protection technologies described in this research.

5.3. Design of Experiments (DoE)

Each of the pedestrian protection technologies was first modelled and evaluated at a component level and then at a vehicle level, as described in the next chapter. The objective of the first approach was to gain a deeper understanding of the technologies, in highly simplified models, so they could be optimised at a component level. The objective of the second approach was to predict the influence of these optimised components in relatively complex accident simulations. A DoE methodology was applied to the first approach with the assistance of statistical software, Statgraphics. This methodology was appropriate because the:

- Component model solution time was low enough to solve many models in an acceptable length of time
- Component models were simple enough to be described by an acceptable number of design parameters
- Objective was to understand how certain design parameters influenced certain responses and then to optimise them in a systematic manner

DoE is a set of systematic statistical methods for determining what intentional changes to the inputs or factors of a system should be made, and subsequently analysing the responses, so that the reasons for the changes in the responses may be better understood. Each of these aspects is briefly described.

All DoE methods involve factors (i.e. a process variable that is changed in the experiment), levels (factor settings used) and responses (measurements used to characterise the process). A two level design is an experiment where all the factors are set at one of two levels: low or high using the notation -1 and 1 or – and + respectively. Similarly, a three level design is an experiment where all the factors are set of one of three levels: low, medium or high, using the notation –1, 0, +1. If all the possible combinations of factors and levels are used to determine all the responses then this is known as a full factorial design. In this case the number of experiments required is given by the following equation:

$$\text{The number of experiments} = \text{Number of levels}^{\text{Number of factors}}$$

The complete set of experiments for 3 factors and 2 levels is shown in Figure 5.2.

	A	B	A×B	C	A×C	B×C	A×B×C	RESPONSE
1	-	-	+	-	+	+	-	3
2	+	-	-	-	-	+	+	5
3	-	+	-	-	+	-	+	7
4	+	+	+	-	-	-	-	8
5	-	-	+	+	-	-	+	4
6	+	-	-	+	+	-	-	3
7	-	+	-	+	-	+	-	1
8	+	+	+	+	+	+	+	9

Av. + (5+8+3+9)/4 = 6.25
Av. - (3+7+4+1)/4 = 3.75
Effect 6.25-3.75 = 2.50

Figure 5.2 An example of an orthogonal two level design array

This shows an orthogonal two level design array with three factors. Orthogonality means that the effects of the factors A, B and C on the responses can be independently determined and do not correlate. In this example the sum of the levels in every product column is zero and this is a check for orthogonality. As shown, the effect of factor A is calculated in two stages. First of all, the response values for all positive, and then all negative factor level experiments, are averaged. This reveals the average response, due to either a positive or negative level in each factor column. By definition, the effect of the factor on the response, is the difference between these two averages [Ford 2001-2]. Every factor and interaction effect (e.g. AB) is calculated in a similar manner.

The main effects are the factors that have the largest influence on the measured responses, when the factor is changed between different levels. An interaction effect exists when the effect of one factor depends on the level of another and usually these are smaller than the main effects. Higher order interactions (e.g. quadratic) are usually assumed to be small [Ford 2001-2]. A fractional factorial experiment is one in which a subset of all the possible combinations is used on the assumption that a similar predictive set of conclusions may be derived from fewer experiments. This may lead to confounding whereby the effects of some factors on the response cannot be measured separately (complete confounding) or the effect is caused by a sum of main and/or interaction effects. Three level designs provide

measures of non linear effects but the interactions are more difficult to see than two level designs. Usually a standard design array is chosen to identify the reduced set of experiments and the nature of this array will depend on which class of experimental design is used [Ford 2001-2]. Some of the different classes are summarised from [Statgraphics 2000] in Figure 5.3.

Screening
A Screening design determines the amount of change that occurs in the response variable (defects per unit) when each factor is changed, and if changing the factors together produces results different from changing the factors individually.

Response Surface
Response surface methodology is a process for locating an optimal value in a higher-order model. It utilizes regression, contour plots, and/or a method of steepest ascent/descent.

Mixture
Mixture designs involve experiments where a product is comprised of two or more ingredients or components.

Multilevel Factorial
Multilevel Factorial designs consist of combinations of specific levels of two or more factors, where the number of levels is set by the user. This design class is intended for quantitative factors only and is analyzed as a R.S.D

Inner/Outer Arrays Designs
Inner/Outer Arrays designs are a variation on an implementation of Taguchi (Robust) designs. The designs in STATGRAPHICS *Plus* consist of both controllable and uncontrollable noise factors. This design class is intended to determine the combination of factors that reduce the sensitivity to uncontrollable sources of variability.

Single Factor Categorical
Single Factor Categorical designs compare levels of a single nonquantitative variable, with or without blocking factors.

Multi-Factor Categorical
Multi-Factor Categorical designs consist of all combinations of specified levels of two or more factors, where the number is set by the user. The design is intended for nonquantitative factors and is analyzed using ANOVA.

Variance Components (Hierarchical)
Variance Components designs quantify the effects of various factors on the variability of a response. The design consists of nested factors.

Figure 5.3 Classes of experimental design

A response surface methodology was used in analysing, all the technology models, because of its capability in handling and optimising multiple factors with different response objectives. According to [Box 1978] this methodology consists "..... of a group of techniques used in the empirical study of relationships between one or more measured responses such as yield, colour index, and viscosity, on the one hand, and a number of input variables such as time, temperature, pressure, and concentration, on the other ". An example response surface is shown in Figure 5.5. The response is maximised in the shaded region with a combination of factor levels.

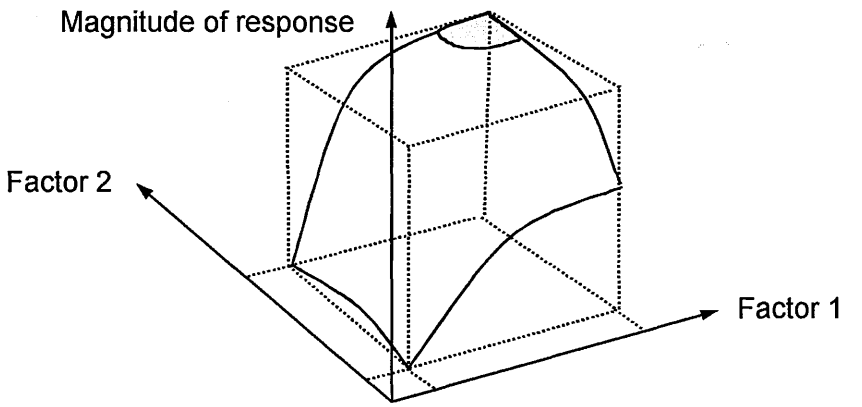

Figure 5.4 A response surface for three factors

The types of standard response surface arrays offered by Statgraphics are shown in Figure 5.5 [Statgraphics 2000] and some of the terminology in Figure 5.6. One term that is not explained is a blocked design. In this type of design the experiments are split by category and the results analysed separately. It is assumed that greater precision can be achieved, if for instance, the experiments undertaken on different days are analysed in separate blocks, to ensure common experimental conditions.

Three-Level Factorial
A design that consists of all combinations of all factor levels. The design is capable of estimating all factors and their interactions. For example, a complete factorial design of three factors, each at three levels, would consist of 3 x 3 x 3 = 27 runs.
Central Composite Designs
Designs that span a set of quantitative factors with fewer points than a standard factorial multilevel design, without a large loss in efficiency. This major class of designs has two parts: a cube and a star. The cube portion corresponds to a factorial screening design. For example, in a three-factor study, eight points in a central composite design form a cube that corresponds to a 2^3 factorial. The star portion of the design consists of an additional set of points arranged at equal distances from the center of the cube on radii that pass through the centerpoint on each face of the cube. The distance from the center of the cube to one of these points is called the *axial distance* of the star.
Central composite designs are desirable because of two attributes: orthogonality and rotatability. Orthogonality allows you to measure the desired effects independently of each other. Nonorthogonal designs result in a dependency of effects that is particularly undesirable; that is, some of the factors are correlated. Rotatability implies that you can estimate the response with equal variance regardless of the direction from the design center.
Box-Behnken Design
Uses a selection of corner, face, and central points to span an experimental space with fewer points than a Complete Factorial Design. It is similar in intent to a Central Composite Design, but differs in that no corner or extreme points are used. It has no extended axial points, so it uses only three-level factors. It can be a blocked or unblocked design.
Draper-Lin
A small central composite design. Rather than a full factorial, the design uses a fractional factorial.
User-Specified Design
Designs created by the user that can be blocked or unblocked.

Figure 5.5 Types of response surface designs

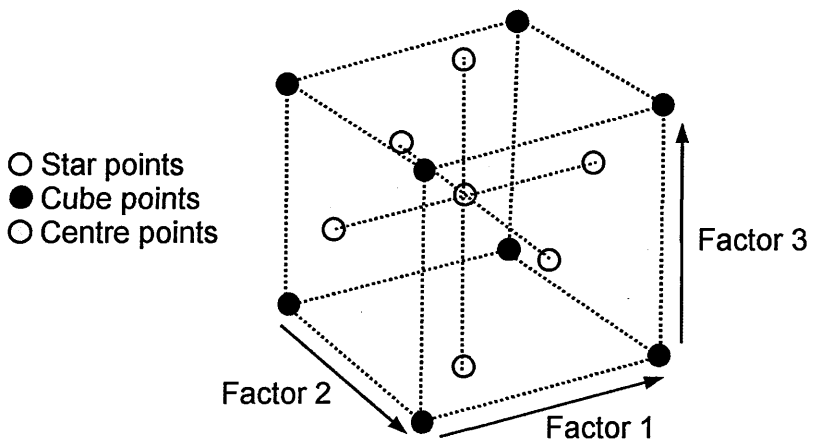

Figure 5.6 A central composite design for three factors

The author's choices of Box Behnken (Behnken 1960), face centred Draper Lin Small Composite (Draper 1990) and user defined arrays, are justified later, in the headlamp and bumper modelling sections.

The second aspect of DoE is the analysis of the results. This was developed from [Ford 2001-2] and [Montgomery 1991] within an overall approach as follows:

- Recognise the problem and write a problem statement
- Choose the main factors and levels
- Select the response variables
- Choose the experimental design
- Perform the experiments
- Plot the response data against each experiment. This allows the raw data to be checked for unexpected results that are particularly high or low compared to the total data set. It also provides an indication of whether the response data is within an expected range of values, compared to comparable experiments (e.g. experimental tests, if available).
- Rank each experiment according to the magnitude of the response/s. Relative comparisons can be made where, for instance, numerical models are not validated against experimental data.
- Evaluate which factors and/or interactions have a statistically significant effect on the response/s at the 95% confidence level. Significance may be evaluated by plotting the standardised effect (the effect divided by the

standard error) of each factor and interaction, with reference to a 95% confidence level line.

- Plot the significant main effects and interaction effects. This provides a graphical visualisation of how the levels are related to the response/s and how much interaction occurs between factors.
- Use the Statgraphics optimisation to find the best factor level combination.
- Draw conclusions and make recommendations

5.4. Pedestrian protection headlamp (PAH)

5.4.1. Biomechanical models of PAH

An essential aspect of developing any pedestrian protection technology is to clearly identify potential injury mechanisms and in order to do this it is useful to begin by listing some anatomical terms for different parts of the body. Anterior and posterior are used to describe the relative fore and aft positions respectively. Medial and lateral describe the side to side positions relative to the body centre with medial closer to this. Proximal and distal are used to describe the vertical position relative to the body centre with proximal closer to the centre. Finally superior and inferior may also be used to describe the vertical position with superior closer to the head.

There is a large variation in pedestrian stature and vehicle design and this means that there are many possible pedestrian injury mechanisms. In addition there are very large differences within the pedestrian population with regards to resistance to injury (e.g. bone strength variation with age) and hence a large variation in the severity of these injuries. However, [EEVC 1998] provides some guidance in this respect because it was founded upon the notion that the child abdomen and adult femur are two important pedestrian injury regions [Lawrence 1989]. Although these two cases are used to demonstrate the manner in which this technology operates, it should be noted that subsequent to the original research studies, car styling has significantly changed and as a result of this, so has the likelihood of such injuries [Matsui 1999]. However, vehicle headlamps are often positioned at the same height as the centre of an adult femur or a child pelvis and/or abdomen and therefore they may cause certain types of pedestrian injury.

During a pedestrian impact with some vehicles the headlamp will impose a distributed force on the pedestrian that changes direction and magnitude. At any single point in time it may be viewed as shown in Figure 5.7.

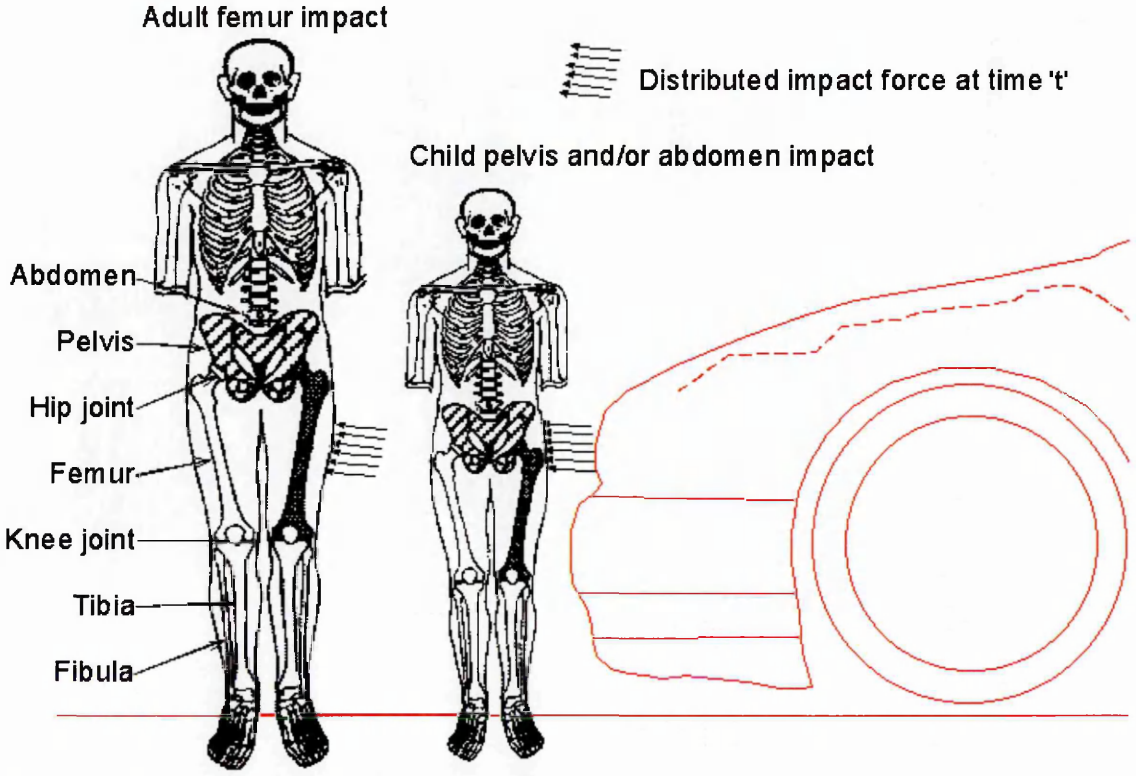

Figure 5.7 Adult and child headlamp impact

In each case there will be a considerable amount of energy dissipated within the impacted body regions. An improved understanding of this may be obtained by firstly examining the femur and secondly the pelvis and abdomen in more detail.

Huelke [Huelke 1986] described the femur as "... the longest and strongest bone in the body and is roughly cylindrical in shape along its shaft. The femur is a very rigid bone, having an upper rounded head, a somewhat narrowed neck, which is at an approximate angle of 125 degrees to the shaft - the longest portion of the femur". Huelke also stated "The lower end of the femur flares out into a large area, the condyles - the articular surfaces that mate with the tibia to form the knee joint". The adult femur and some of the muscles surrounding it are shown in Figure 5.8 [Huelke 1986], and Figure 5.9 shows a conceptual view of the adult loading condition.

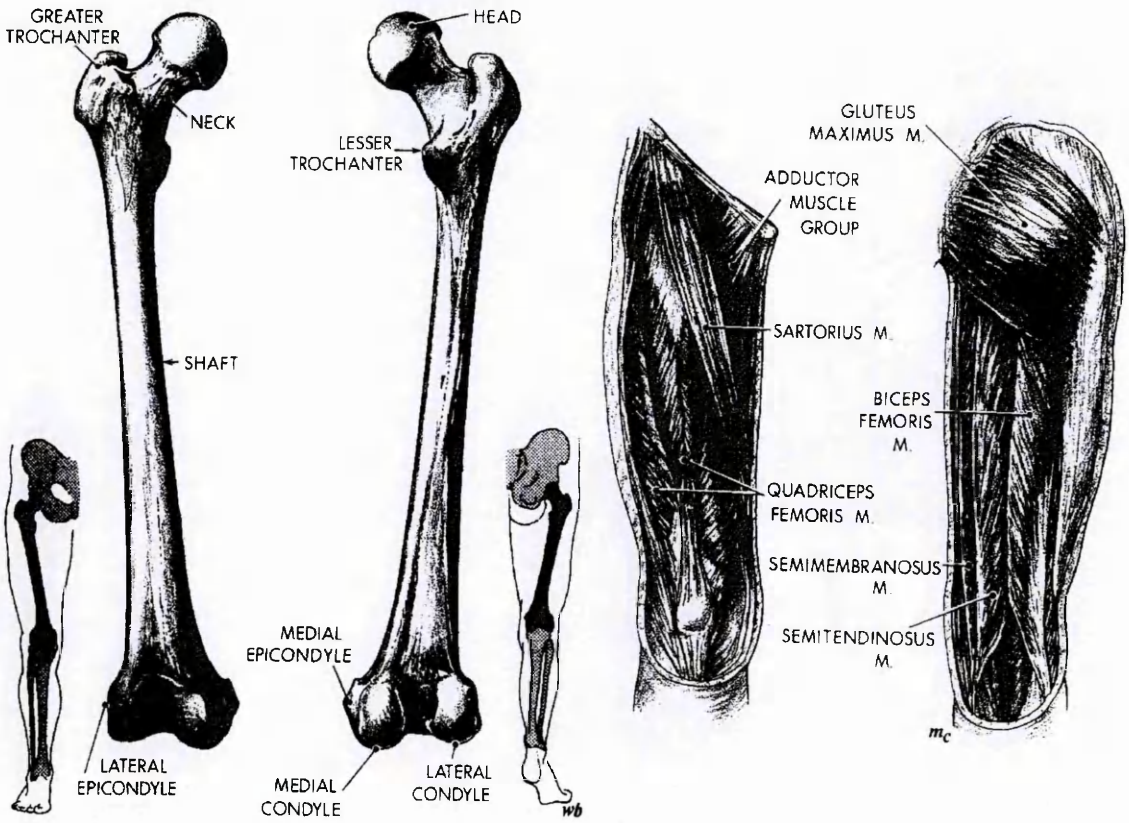

Figure 5.8 The adult femur and surrounding muscles

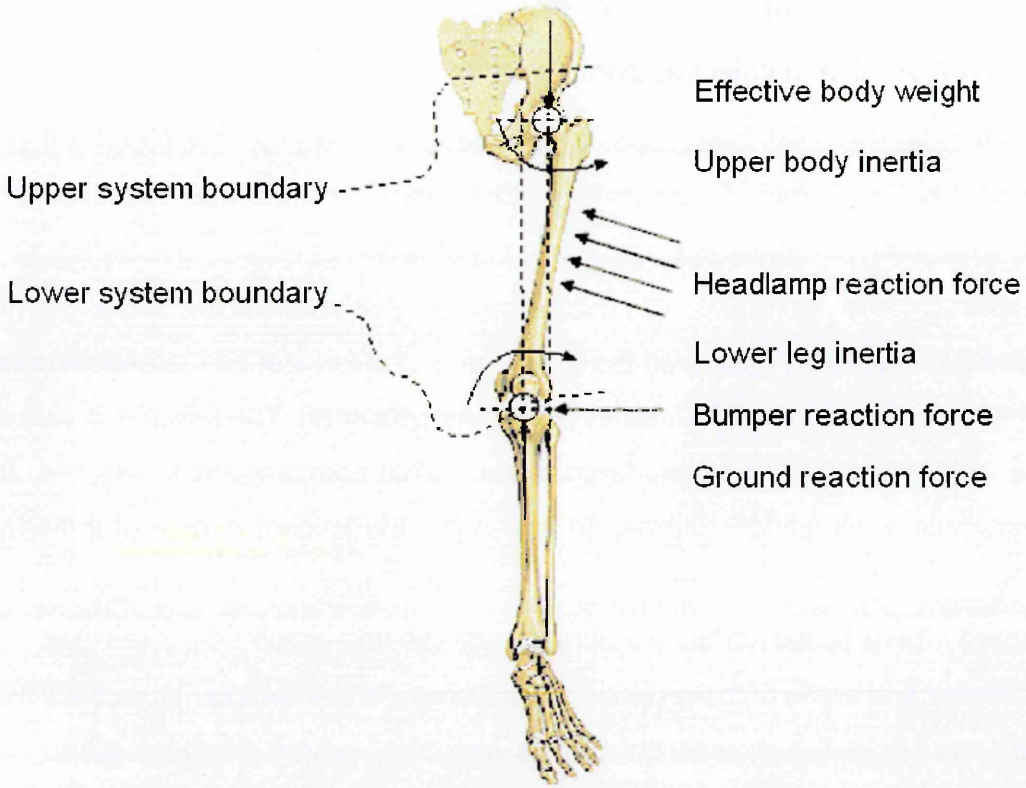

Figure 5.9 Conceptual view of the adult femur loading condition

The boundaries of this loading condition were chosen as the hip and knee joints because to a certain degree, due to the very nature of joints, they are able to uncouple the headlamp reaction force from other body masses connected to the femur. For instance it might be possible that a highly impulsive load at the femur centre might lead to a fracture before significant bending is transmitted into the two end joints. The precise direction of the resultant forces and moments is not known because of the complexity of the loading condition and leg geometry. However, the [EEVC 1998] provides some guidance in regards to the direction of the headlamp reaction force (based on vehicle geometry) and the bumper reaction force (assumed horizontal). Based on these assumptions the femur is primarily loaded under compression and bending. Under such conditions a femur fracture may occur in various locations depending on the bone stress distribution. Some possible non comminuted (non compression) fractures are shown in Figure 5.10 [Kress 1995].

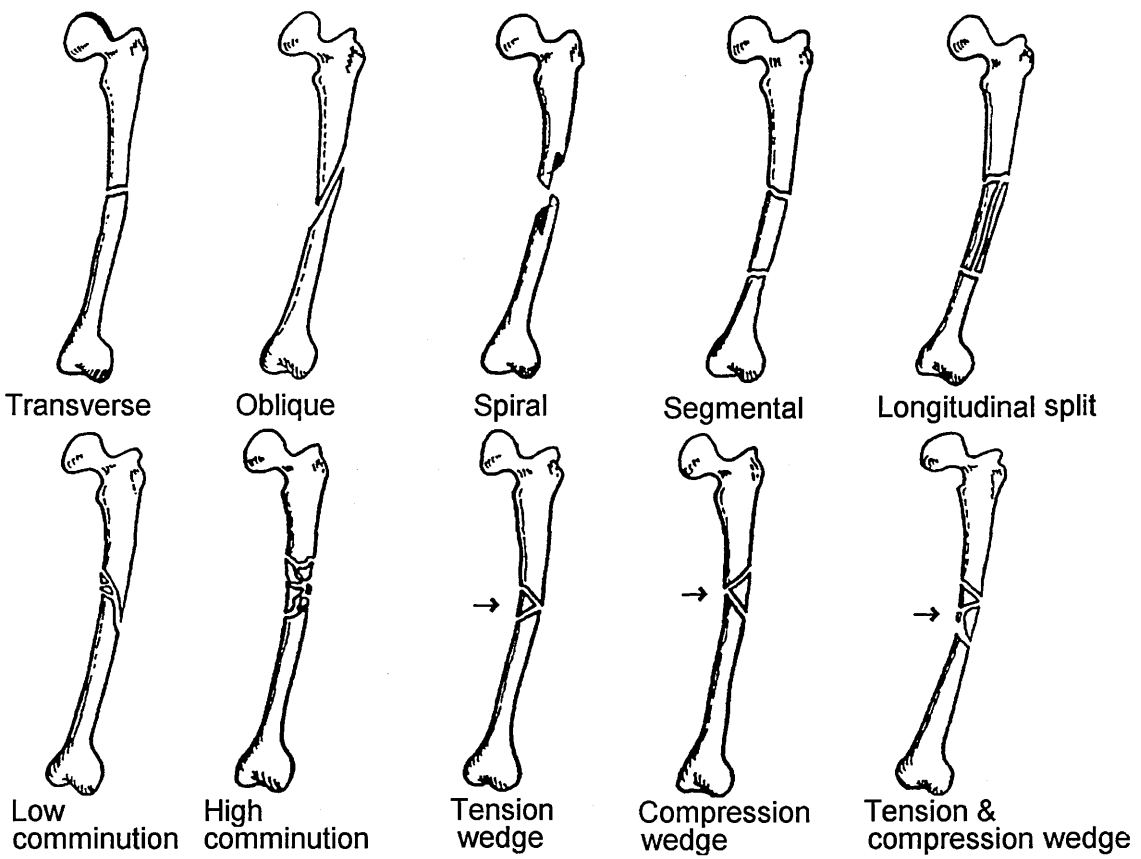

Figure 5.10 Non-comminuted femur fractures

Huelke [Huelke 1986] described the pelvis as "...a ring of bone interposed between the flexible vertebral column and the movable lower limbs. It transmits the weight of

the torso to the lower extremities during walking, and supports the torso when in the seated position. The bony pelvis consists of three bones, and the right and left ox coxae (hip bones) on each side, and posteriorly, the centrally located inverted wedged shaped sacrum. The hip bone is a relatively large, flat, irregularly shaped bone formed by the union of three bones - the ilium, ischium, and the pubis that fuse together at the hip socket - the acetabulum. Along with the sacrum they form a solid ring of bone which is very rigid, relatively immobile and strong". Huelke continues "The acetabulum is that cup shaped depression which is a receptacle for the head of the femur; together they form the hip joint". The exact geometry of the pelvis is even more complicated as shown in Figure 5.11 [Huelke 1986].

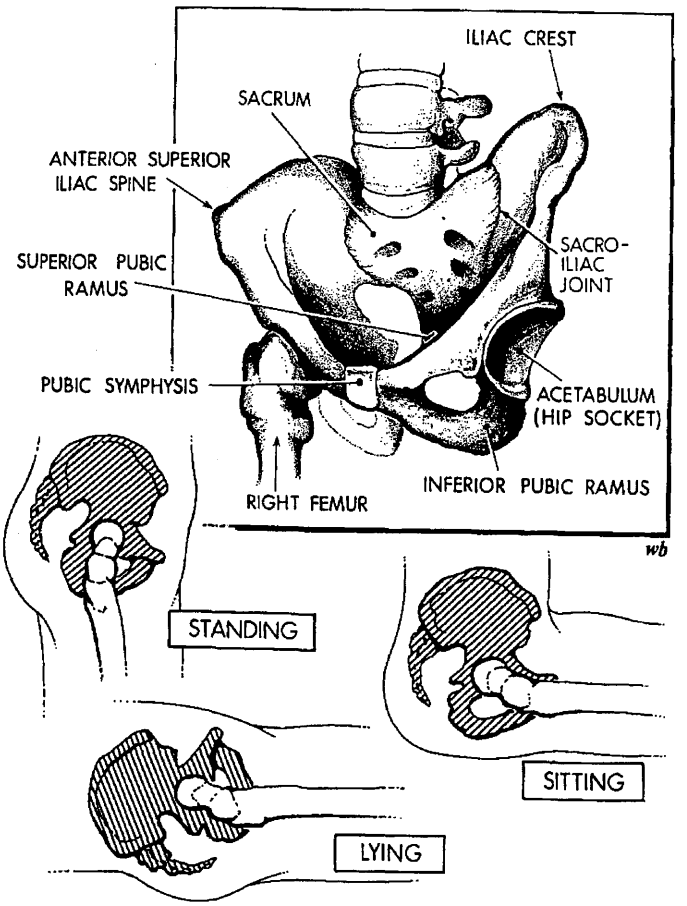

Figure 5.11 The adult male pelvis

The pelvis cannot be considered in isolation from the abdomen and Nusholtz [Nusholtz 1985] described the pelvis and abdomen as follows "The abdomen and the pelvic cavities, although frequently described separately, are continuous from one to another, with bony landmarks used as reference points to separate the two".

They are therefore described together here and Nusholtz continues "Both the liver and spleen are anatomically considered abdominal organs". "The liver is a solid blood filled organ which represents approximately 1/40th of the total body weight" and "Anteriorly, laterally, and posteriorly, the lower ribs cover a major portion of the liver". Then concerning the spleen, Nusholtz says "The spleen is a very small blood filled organ about the size of a fist, which lies against the posterior body wall on the diaphragm at the 9th, 10th and 11th rib level". The abdomen includes the urinary (e.g. bladder, urethra) and bowel (e.g. lower, upper, rectum) systems and a number of major arteries (e.g. iliac, iliolumbar) and nerves (e.g. sciatic).

In a similar manner to the adult femur case, Figure 5.12 shows a conceptual view of the child pelvis and/or abdomen loading condition at a point in time when the peak headlamp reaction force occurs. In this case the boundaries were chosen as the mid position of the femur and upper side of the abdomen because the impact load affects both the pelvis and the abdomen contents.

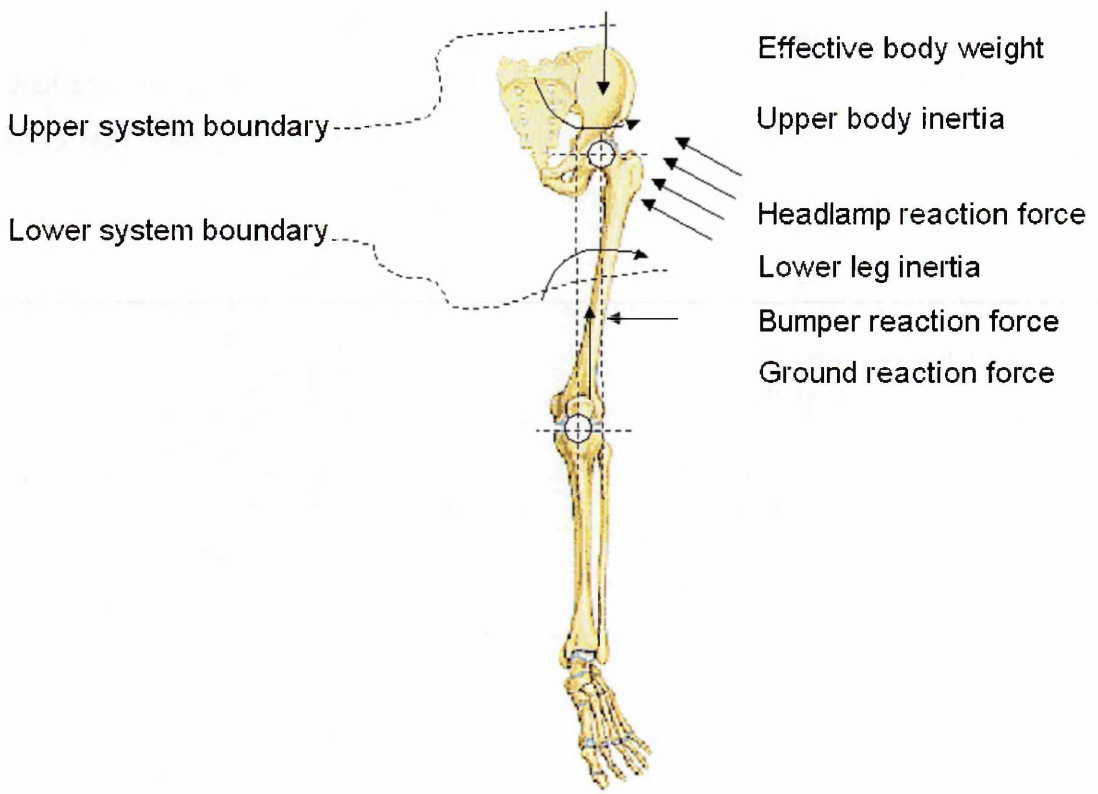

Figure 5.12 Conceptual view of child pelvis and abdomen loading

Conolly [Conolly 1969] analysed two categories of pelvis fracture that were

observed in 200 hospital cases. No reference was given to the cause of these fractures but a useful categorisation distinguishes between and describes major and minor pelvis fractures. A major fracture leads to very high mortality rates and "...is defined as one which involves the line of weight transmission, from the spine to the acetabulum, or one that involves the rami on both sides of the symphasis pubis". Major fractures included fractures of the acetabulum (associated with severe haemorrhage, urinary damage and central hip dislocation) and bilateral fractures of the pubic rami (associated with a ruptured urethra and bladder). Fractures of the hemipelvis, in which separation of the symphosis pubis is combined with fractures of the pubic rami, ilium or sacrum, or dislocations of the sacroilic joint led to the highest mortality rates. The final two major fracture types were symphysis pubis separation and isolated fractures of the sacrum. Minor fractures included unilateral fractures of the pubic rami, isolated fractures of the ilium and avulsion fractures (muscle violence can avulse the anterior, superior and inferior iliac spines and the ischium). Associated abdominal injuries included ruptures of the liver, spleen, bowel, bladder and lacerations of the kidney. Finally Conolly summarised the paper and stated that ".... the three chief factors responsible for morbidity and mortality: haemorrhage ("...usually the plexus of veins and arteries lining the side wall of the pelvis"), urological injuries and acetabular fractures and dislocations".

Ryan [Ryan 1971] examined 387 traffic accident patients in which there were pelvic fractures. Where the type of traffic accident was known, the majority of these were pedestrians but as with Conolly's paper, care is required in interpreting the data because car design has dramatically changed over the last thirty years. There was also no indication of the patient's age. In general the types of injuries described were similar to the last paper but additional detail was provided. The vast majority of the patients suffered pubic rami (305) fractures ("... the most fragile of the bones in the pelvis") followed by acetabulum (89) fractures ("... must be due to the frequency of transmission of accident forces through the femur ...") and ilium (79) fractures ("... the most exposed pelvis bone"). Ryan also stated that " ... the associated injuries more closely influenced the death rate than did the pelvic injury pattern".

The pedestrian protection headlamp concept was founded upon the assumption that by controlling the magnitude and shape of the impact force pulse due to the headlamp impact the severity of all the injuries described would be reduced.

5.4.2. Description of PAH

By increasing the deformation of the headlamp and hence absorbing the impact energy over a greater distance (and time) the magnitude and shape of the impact pulse is controlled. It is assumed that the surrounding headlamp structure such as the hood leading edge is also designed to deform with the headlamp so that the collapse of the headlamp does not expose stiffer surrounding components and lead to the possibility of new injury mechanisms. Figure 5.13 shows the envisaged deformation of PAH due to plastic hinges forming in the S shaped sidewalls [Howard 2001-5, 2001-7].

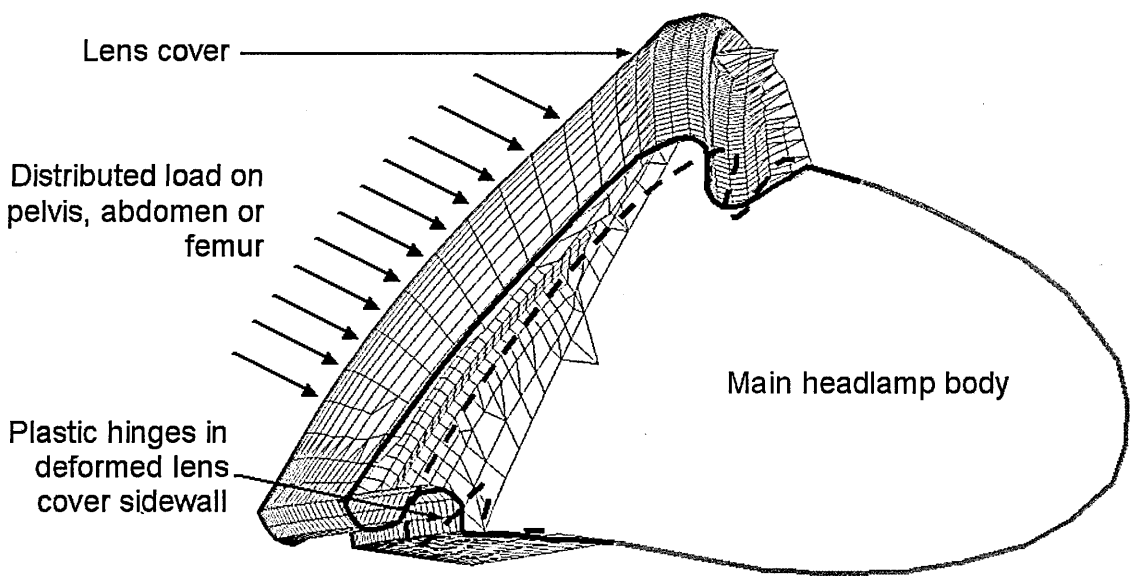

Figure 5.13 Envisaged deformation of PAH

Unlike other headlamp patents for pedestrian protection, controlled deformation of the headlamp volume rather than the rearward movement of the complete headlamp is used to absorb the pedestrian impact energy. The headlamp volume provides a region in which energy can be structurally absorbed in a controlled fashion without the requirement for additional package space behind the headlamp. Both of these aspects provided important advantages over prior patents. For example, DE 3728752 which appears to have less energy absorbing capacity and

US 4475148 which requires package space behind the headlamp. The formation of plastic hinges in the lens cover is achieved by introducing different types of slots or convolutes in critical lens cover side wall regions as shown in Figure 5.14.

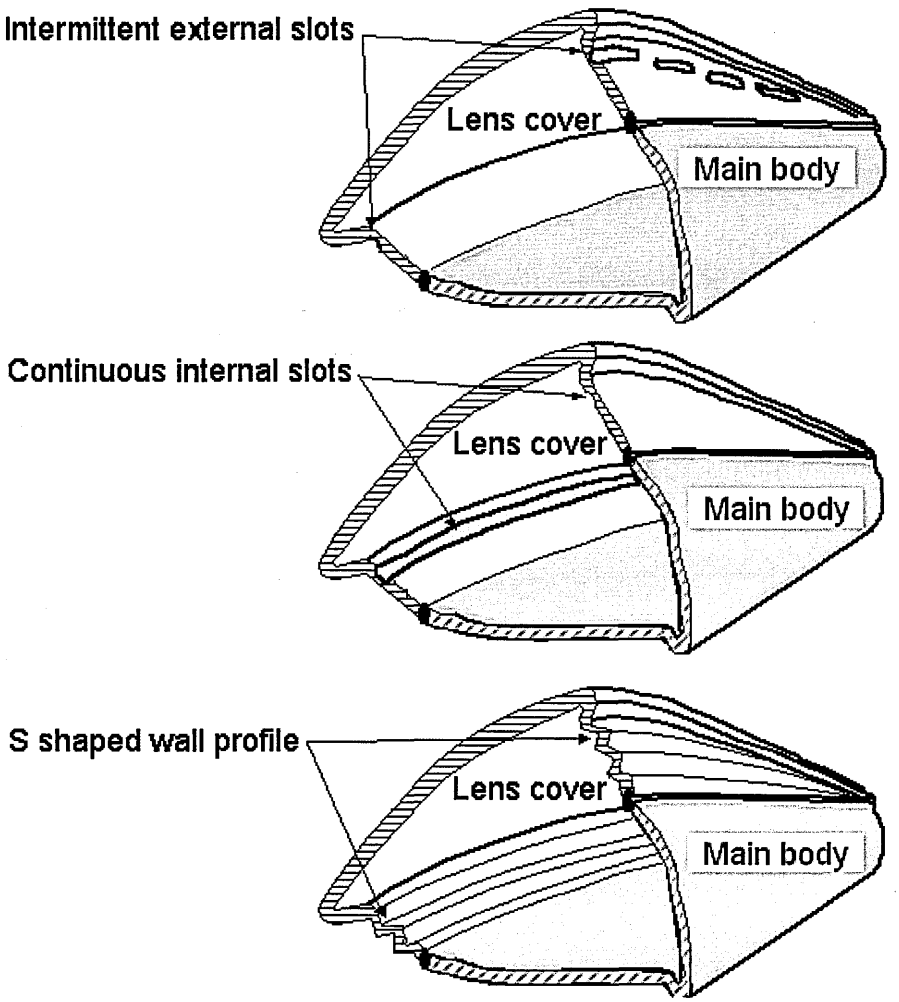

Figure 5.14 Various headlamp designs to achieve desired deformation

5.4.3. Analytical models of PAH

To help identify underlying mechanisms and assist in predicting how certain parameters influenced performance it was helpful to construct analytical models. The collapse behaviour of a thin walled box under dynamic loading is difficult to describe analytically. However, one of the assumptions underlying the headlamp design was that buckling of the main headlamp body should not occur. By considering simpler structures as shown in Figure 5.15 [Fenton 1996] some of the important parameters involved in this buckling were identified.

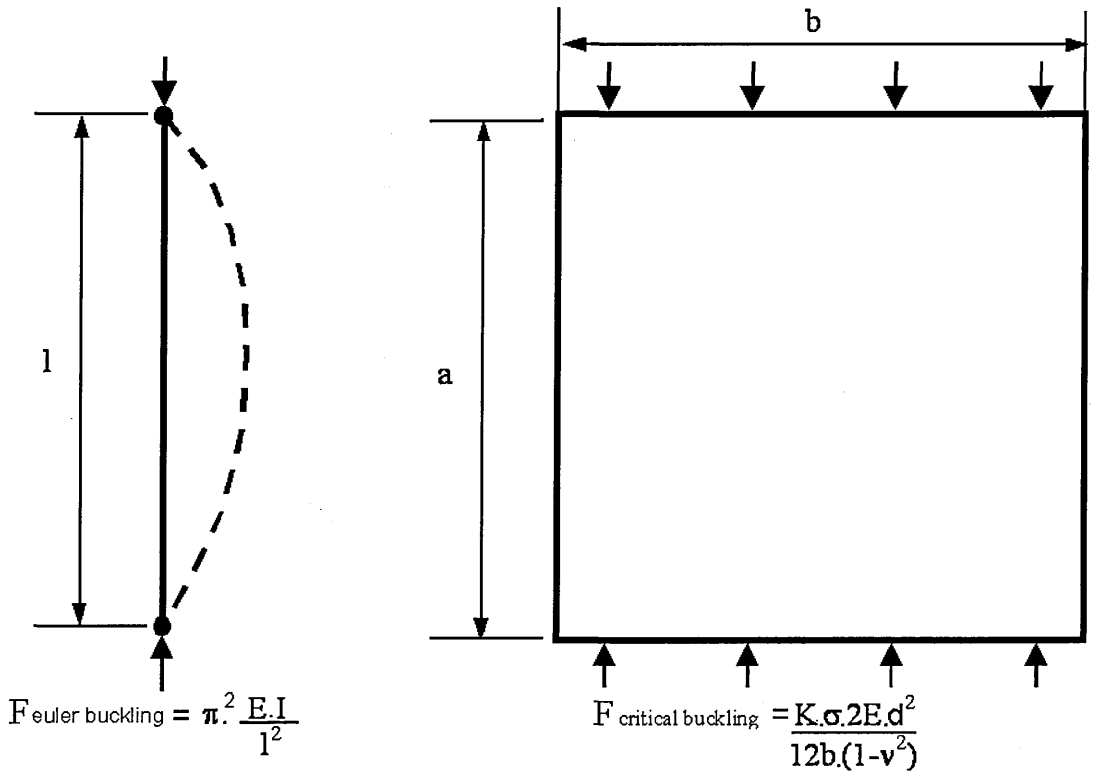

Figure 5.15 Analytical models for strut and plate buckling

In a simple strut with pin jointed ends the load at which buckling initiates depends on the strut length 'l', the material Youngs Modulus 'E' and the second moment of area 'I' of the strut section. Buckling occurs because of the bending moment developed in the deflected section. This model may be extended to different end conditions by using an effective length for 'l'. It should be noted that this only applies to struts and according to [Fenton 1996] is inaccurate below a slenderness ratio l/K=120 where K=√(I/A). When a more complicated plate is considered, then the same parameters are still important but some additional ones also need to be considered. For example, it is necessary to consider, Poissons ratio 'ν' (to account for buckling in the plane at right angles to the one of concern), the length to width ratio and the end conditions (empirically assumed in the determination of 'K' from a standard graph). Based on an understanding of the importance of these parameters, they were subsequently varied in the numerical finite element model described next.

5.4.4. Numerical headlamp evaluation model

To assist in the development of PAH a number of numerical models were designed

for a generic parametric study that examined the benefits of the three headlamp designs with three different types of vehicle geometry. In the base cases the overall size, wall thickness and material properties of the headlamps were based on a highly simplified C class vehicle headlamp. Identical software and modelling guidelines were used as for the reference vehicle model (see appendices).

Model construction and development

The numerical evaluation model shown in Figure 5.16 consisted of a vehicle simulator and a validated upper leg impactor [EUCAR 2000, Howard 2000-2].

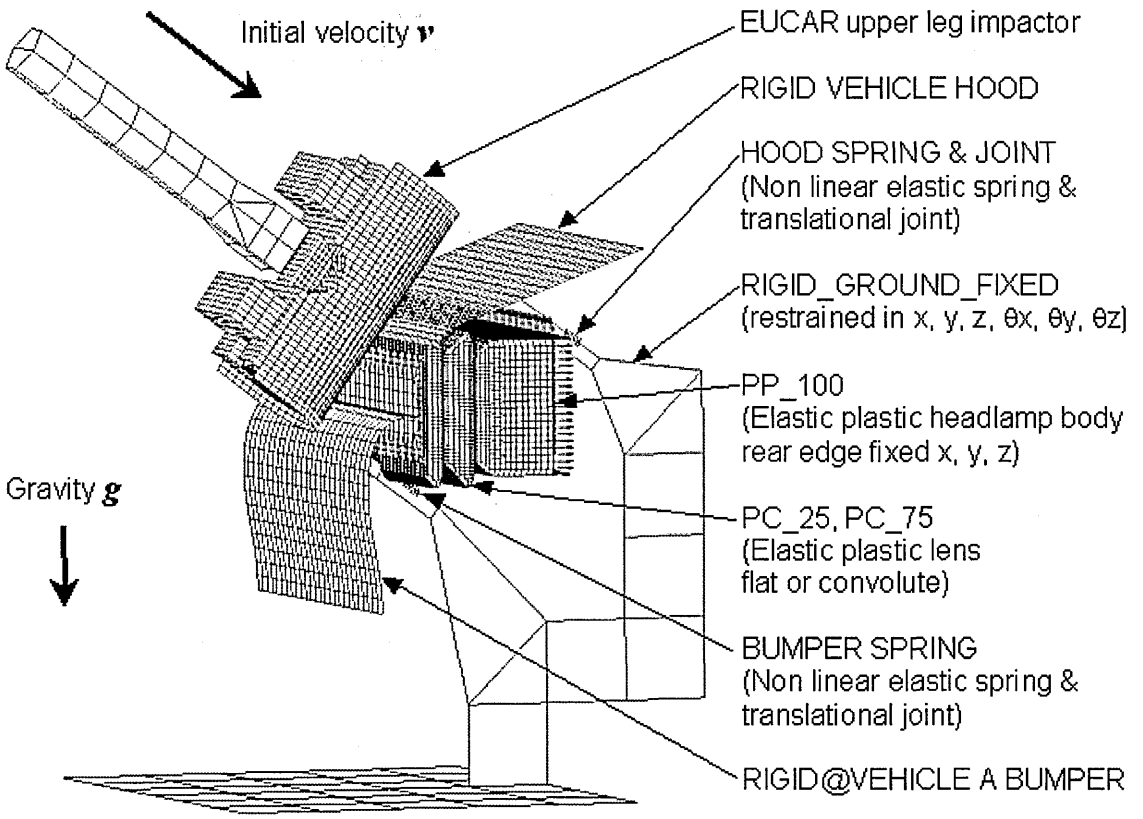

Figure 5.16 One of the headlamp evaluation models

The vehicle simulator represented the geometry of three types of vehicle at Y500 : a C class car, a sports car and an off road car. Each simulator consisted of a rigid and fully restrained base upon which a rigid bumper and hood were attached via non-linear springs and translational joints. An elastic plastic headlamp model was positioned behind the hood and bumper and restrained only along its rear edges. The purpose of the hood and bumper parts was to simulate the influence of the surrounding vehicle structure by absorbing some of the upper leg impact energy.

The material card for the vehicle simulator base was based upon the mild steel properties described in [Ford 1997] and is shown in Table 5.2

RIGID Material law 20
ρ = 0.78E-08 ton/mm^3 (Steel) E = 203000 N/mm^2 (Steel) ν = 0.30 (Steel) Coupling flag for MADYMO = 0.0 (use normal DYNA updates not MADYMO) Coupling option & option flag for MADYMO = 0.0 (not used) VDA surface alias name (not used) Centre of mass constraint option = 1.0 (constraints applied in global directions) First constraint parameter specified (constrained in x, y, z displacements) Second constraint parameter specified (constrained in x, y, z rotations) Various local coordinate system options not used
*MAT_RIGID 1 0.78E-8 203000.0 0.3 0.0 0.0 0.0 1.0 7.0 7.0 0 0.0 0.0 0.0 0.0 0.0

Table 5.2 LS-DYNA material card for the vehicle simulator base

Two translational joints and two springs were attached to the base and positioned at the same angle in the XZ plane as the upper leg impactor to ensure that the impact direction was always in line with the spring motion. This assumed that the main vehicle deformation would occur in the impact load direction. The CONSTRAINED JOINT TRANSLATIONAL variables are shown in Table 5.3.

CONSTRAINED JOINT TRANSLATIONAL
Six nodes are used to define the translation joint; nodes 1, 3 & 5 are in rigid body A & nodes 2, 4 & 6 in rigid body B Relative penalty stiffness =1 (default) Damping scale factor = 1 (default)
*CONSTRAINED_JOINT_TRANSLATIONAL 760 758 762 756 761 755 1.0 0.0 773 771 775 769 774 768 1.0 0.0

Table 5.3 LS-DYNA joint card for the hood and bumper mounting

The hood and bumper stiffness were simulated with two non-linear elastic springs using the material cards shown in Table 5.4.

NON LINEAR ELASTIC SPRING
Material numbers 4 & 5 Load curves 1 & 2 describing force displacement behaviour No curve scale factor (default)
*MAT_SPRING_NONLINEAR_ELASTIC 4 8 0 $ *MAT_SPRING_NONLINEAR_ELASTIC 5 9 0

Table 5.4 LS-DYNA spring card for the hood and bumper mounting

In both cases the spring stiffness characteristics shown in Table 5.5 were determined from experimental impact tests [Howard 2000-3].

DEFINE CURVE
Load curve id.'s 8 & 2 Load curve used in transient analysis only Scale factor of 1.0 for X & Y axes No offset for X and Y values General XY data X and Y values for the hood and bumper stiffness characteristics

```
*DEFINE_CURVE
         8          0        1.0        1.0        0.0        0.0          0
                -69.0   -10000.0
                -56.0    -3500.0
           -6.1999998    -1000.0
                  0.0        0.0
                  5.0     5000.0
                 10.0    10000.0
*DEFINE_CURVE
         9          0        1.0        1.0        0.0        0.0          0
                  0.0        0.0
                 30.0     1000.0
                 60.0    10000.0
                120.0    13000.0
```

Table 5.5 LS-DYNA define curve cards for the bumper & hood springs

The hood and bumper parts were mounted to the impacted side of the springs and therefore made an inertial contribution to the spring force. To reduce this, lightweight ABS properties as specified in [Ford 1997] and shown in Table 5.6 were used.

RIGID Material law 20
$\rho = 0.20\text{E-}08\ \text{ton/mm}^3$ (ABS) $E = 3000\ \text{N/mm}^2$ (ABS) $\nu = 0.25$ (ABS) Coupling flag for MADYMO = 0.0 (use normal DYNA updates not MADYMO) Coupling option for MADYMO = 0.0 (not used) Coupling option flag for MADYMO = 0.0 (not used) VDA surface alias name (not used) Centre of mass constraint option = 1.0 (constraints applied in global directions) First constraint parameter not specified (no constraints in x, y, z displacements) Second constraint parameter not specified (no constraints in x, y, z rotations) Various local coordinate system options not used

```
*MAT_RIGID
         2    0.2E-8      3000.0       0.25        0.0        0.0        0.0
       1.0       0.0         0.0
         0       0.0         0.0        0.0        0.0        0.0
```

Table 5.6 LS-DYNA material card for the bumper and hood

The mesh geometry and physical property naming convention of the three different headlamp models are shown in Figure 5.17. Headlamp 1 was a simple box design measuring 200 mm high by 200 mm deep and 400 mm wide. The other two designs were similar except that they had one or two 15 mm deep convolutes in the lens cover sides. Overall dimensions were similar to those of the C class car headlamp.

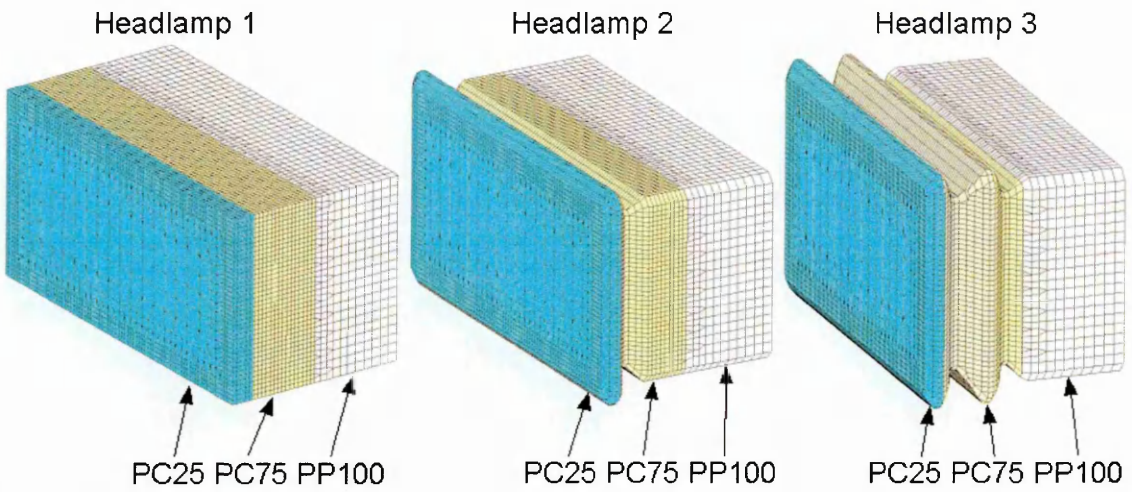

Figure 5.17 The headlamp models

The rear half of the headlamp (PP100) had simple geometry and was not in the impacted region. Therefore it was modelled with uniform mesh geometry and relatively large elements with side lengths of no less than 10 mm. However, the front half (PC25 and PC75) had more complex geometry and was in the impacted region. Therefore it required a higher mesh density to more closely match the component curvature and element side lengths as small as 4 mm to more closely match deformations. On the lens cover front the mesh density was reduced towards the centre where the stress distribution was more uniform with planar geometry.

The headlamp was split into several connected parts to allow the representation of different materials and a different thickness. In the base cases the validated headlamp material properties HL_PC_1, HL_PC_2 and HL_PP as described in [fka 1998-2] were used for the front parts and the rear part of the headlamp respectively. The interface between the front and rear halves was assumed to be continuous (i.e. a very effective adhesive) so that the interface position could easily be moved by changing the element material card properties rather than the mesh geometry.

Nodes on the rear edges of the headlamp were restrained in all translational degrees of freedom to avoid the additional complexity of modelling the influence of different headlamp mounting conditions (e.g brackets). Only translational freedoms were restrained because it was assumed that the part of the headlamp that was not modelled would only prevent translations across this section boundary. Such a

boundary condition led to more energy being absorbed by the headlamp than would have occurred in a complete vehicle. This was because there was no path through which internal energy could be dissipated into the surrounding structure and less headlamp motion to dissipate kinetic energy. There were various potential solutions to this problem including a reduction in the impactor energy or the simulation of surrounding structure to dissipate some of this energy. In the first approach it was possible to reduce the mass of the impactor but not its velocity because various materials in the impactor were strain rate sensitive. The second approach was chosen with additional parts to represent the bumper and hood because it did not involve any modifications to the validated impactor model.

The contacts used between the headlamp, upper leg impactor and vehicle simulator and within one of the headlamp models are shown in Figure 5.18.

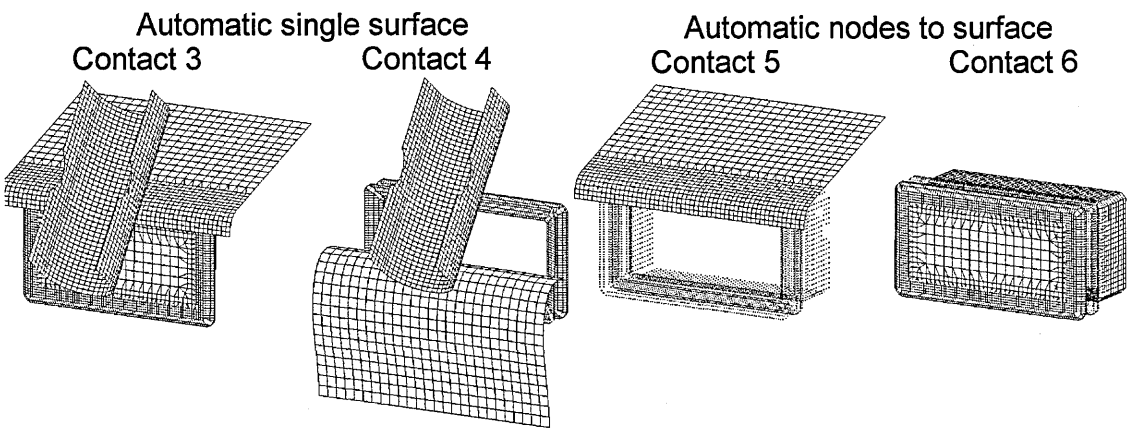

Figure 5.18 Headlamp evaluation model contacts

Contacts 1 and 2 are not described because they only concerned the internal contacts of the upper leg impactor model. Contact 3 was an AUTOMATIC_ SINGLE_SURFACE predefined in the upper leg impactor model and intended for creating a contact between the impactor and any other vehicle structure. Initially this only included the impactor rubber skin and so the headlamp lens cover (PC25) and the hood were added to this contact. Contact 4 was also defined as an AUTOMATIC_SINGLE_SURFACE to handle the contact between the impactor and the hood and convolute self contacts. The bumper and headlamp parts defined in this contact were not included in contact 3 for two reasons. Firstly the headlamp parts had common nodes and this would have caused undesirable initial

penetrations at time zero. Secondly the headlamp geometry was simplified and in some vehicle configurations the hood and bumper unrealistically penetrated the headlamp. Therefore it was necessary to define the bumper in a different contact to the headlamp lens cover. Contacts 5 and 6 were defined as AUTOMATIC_NODES _TO_SURFACE contacts and all the default values as defined by Primer v8.0a were used. Contact 5 ensured that the remaining parts in the headlamp, not specified in contact 3, did not penetrate the hood when the hood moved rearward. Contact 6 was defined to account for contacts between the headlamp parts.

During the initial development of the vehicle simulator models, the headlamp model with the most complex mesh geometry was used to identify any problems. One of the first changes concerned the vehicle simulator rigid hood geometry. As shown on the left hand side of Figure 5.19, the original hood geometry featured a sharply defined hood edge. This came into contact with the impactor foam and rubber skin elements that were defined with a material that had a much lower Youngs Modulus. This led to a poor contact condition with severely distorted foam elements and a negative volume error that caused the simulation to stop.

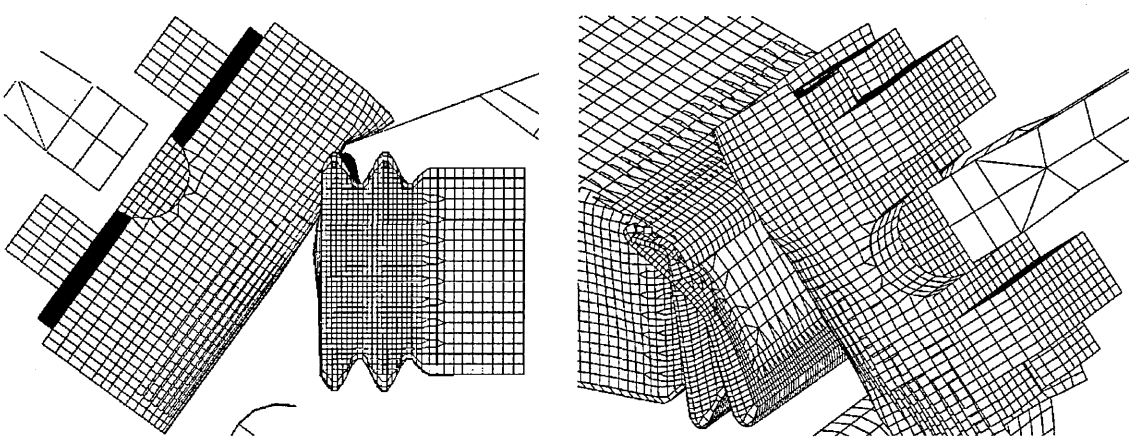

Figure 5.19 Headlamp evaluation model problems

The right hand side shows how the mesh density of the hood leading edge was increased and the elements gently curved downwards and extended beyond the headlamp cover. In this manner the contact area was increased and the impact energy dissipated within a larger volume of the foam. In addition, due to the large stiffness difference the soft constraint option was set in contact 3 with a scaling

factor of 0.1. These modifications eliminated the contact problems but when the headlamp began to collapse further, it became wider than the hood. This led to a distorted mesh as the headlamp elements passed behind the hood contact elements. Extending the hood outwards beyond the headlamp edges solved this.

The left hand side of Figure 5.20 shows how the convolutes passed through each other in this headlamp model because there was no self contact defined. Adding the convolute part to contact 4 eliminated this problem as shown on the right hand side.

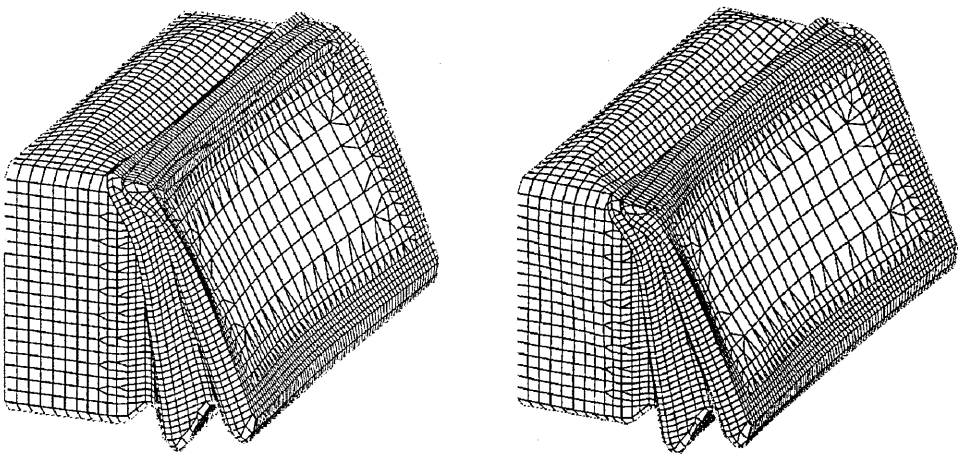

Figure 5.20 Headlamp evaluation model problem & solution

When one of the initial models was solved for a longer period of time, it exhibited a large amount of buckling in the main headlamp body as shown in Figure 5.21 and only a small amount of convolute deformation.

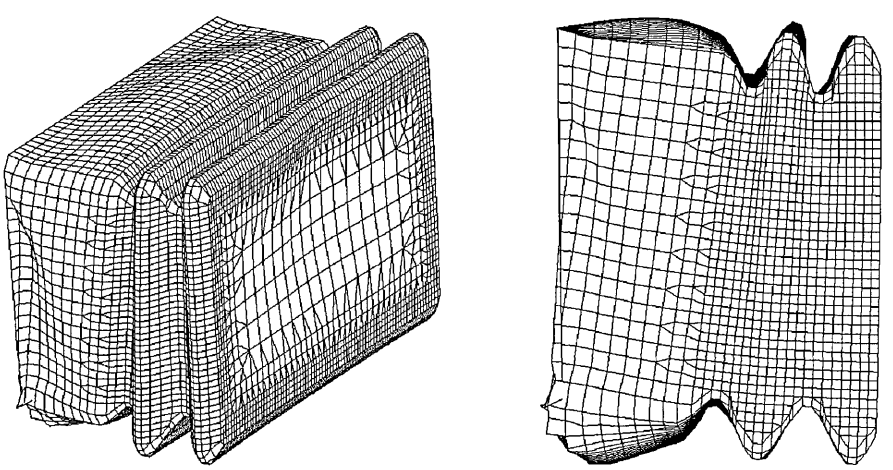

Figure 5.21 Excessive buckling of the headlamp model body

In this test case the convolute thickness was 3 mm and the main body thickness 2 mm. The restraints on the rear edges of the main body imposed an over stiff boundary condition and this led to the excessive buckling of the main body. This represented a worse case scenario in which no rearward motion of the headlamp was possible and the main headlamp body had no geometric form, for example, stiffening ribs. However, the minimum main body thickness was increased to 3 mm to ensure that deformation would always occur in the convolutes.

Gravity was applied to all the headlamp evaluation models by using the global LOAD BODY Z card and the DEFINE CURVE card shown in Table 5.7.

LOAD BODY Z and DEFINE CURVE
Load curve id. 1
Load curve scale factor 1.0
No load curve for dynamic relaxation
No X, Y or Z centre of rotations required because no angular rotations are requested
Load curve id.
Load curve used in transient analysis only
Scale factor of 1.0 for X and Y axes
No offset for X and Y values
General XY data with X and Y values in pairs and a value of 9810 mm/s^2
*LOAD_BODY_Z 1 1.000E+00 *DEFINE_CURVE 1 0 0.100E+01 0.100E+01 0.000E+00 0.000E+00 0.00000000E+00 0.98100000E+04 0.10000000E+01 0.98100000E+04

Table 5.7 LS-DYNA global load card and define curve card for gravity

The simulation models were solved for 15 ms which is the time it took for the hip impactor bending moment and load values to peak in sub system impactor simulations [Howard 2000-2]. The effectiveness of the headlamp designs was evaluated by using different vehicle simulator and headlamp configurations.

Vehicle simulator configurations

The geometry of the vehicle simulator was varied in order to gain an understanding of the influence of a range of different vehicle shapes and impactor configurations on the headlamp response. These configurations were derived from the highest and lowest energy limits specified in [EEVC 1998]. A range of impactor impact angles and velocities were determined from a number of graphs defined in this test procedure. The first of these graphs is shown in Figure 5.22.

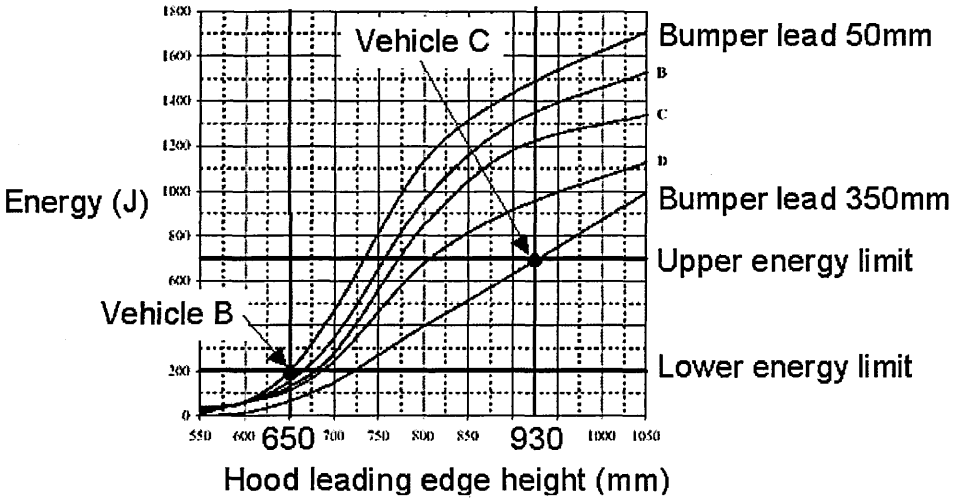

Figure 5.22 Interpretation of EEVC 1998 upper leg impactor energy limits

The smallest and largest bumper leads specified in [EEVC 1998] were 50 mm and 350 mm and the impactor energy 'S' limits were 200 J and 700 J. These values were associated with two hood leading edge heights of 650 mm and 930 mm respectively to represent two extreme vehicle shapes B and C. Using the values from this graph the velocity 'v' was 22 km/h (6.1 m/s) in the lowest energy case and 38 km/h (10.6 m/s) in the highest energy case as shown in Figure 5.23.

The impactor mass was determined by using $m = \frac{2S}{v^2}$

$$m_{lower} = \frac{2 \times 200}{6.1^2} = 10.8\,Kg \text{ and } m_{higher} = \frac{2 \times 700}{10.6^2} = 12.5\,Kg$$

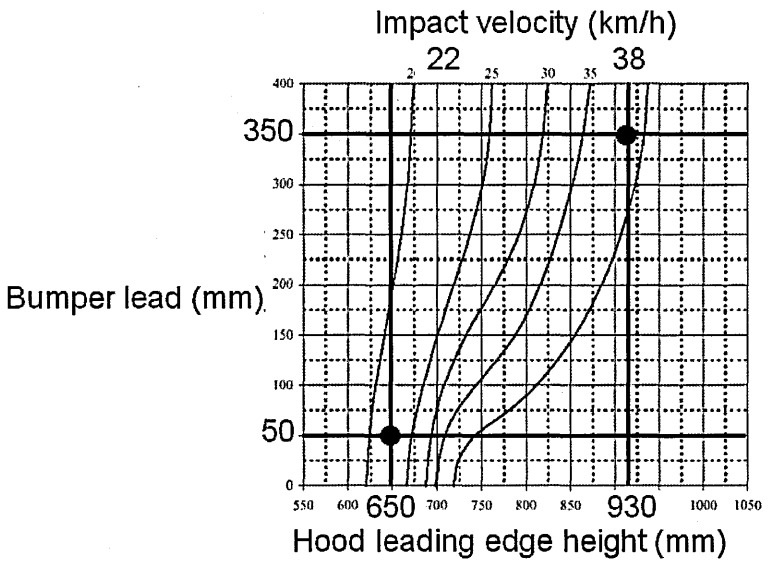

Figure 5.23 Interpretation of EEVC 1998 upper leg impactor velocity

In Figure 5.24 the bumper leads and hood leading edge heights were used to

derive two impact angles of 27 degrees and 31 degrees. In the case of the 350 mm bumper lead the impact angle was limited by [EEVC 1998] to a maximum angle.

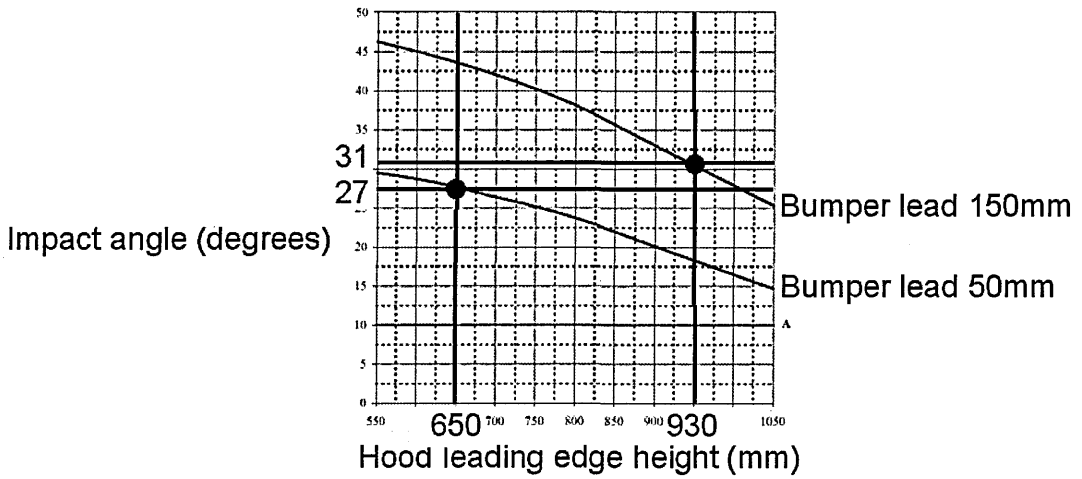

Figure 5.24 Interpretation of EEVC 1998 upper leg impactor impact angle

The impactor and vehicle configurations are summarised in Table 5.8.

Parameters for Y500 position	Vehicle		
	A C class vehicle Ref. [MIRA 1997]	B Sports car Lowest energy	C Off road car Highest energy
Bumper lead (mm)	110	50	350
Hood leading edge height (mm)	683	650	930
Impactor velocity (m/s)	7.98	6.1	10.6
Impactor mass (Kg)	14.12	10.8	12.5
Impactor angle (degrees)	36.3	27	31

Table 5.8 Vehicle geometry and impactor configurations

Using the geometry of the C class car as a reference, the hood angle was set at 20 degrees to the horizontal and the bumper height to 530 mm for all the vehicle models. The bumper geometry was also based on the C class car bumper cross section at Y500 and this was extruded for a short distance in the Y axis to create a bumper with no plan view rearward sweep. The top of the bumper was horizontally extended rearward until it was in line with the hood leading edge and finally the front top of each headlamp was positioned just below the hood leading edge.

Headlamp configurations

The first headlamp part PC25 as shown in Figure 5.17 was modelled as either a flat walled part or a section of a convolute. In all cases the thickness was unchanged at 3 mm because this was the average lens cover thickness of the C class car and this

is necessary for other requirements (e.g. stone chip damage resistance). The next part PC75 was modelled in a similar manner but the thickness was varied between 2 mm, 3 mm or 4 mm with the reference material Youngs Modulus or +/-50% of this value. Finally the part PP100 was left unchanged in thickness or geometry.

Headlamp evaluation model parameter study

The objective of the headlamp evaluation model was to understand how convolutes would influence the upper leg impactor responses with different vehicle designs. Basic analytical models had indicated the importance of the headlamp material Youngs Modulus and thickness in buckling behaviour. In addition, three vehicle designs and headlamp designs had been identified. Therefore, four factors and three levels (to account for non-linearity) were chosen, as shown in Figure 5.25.

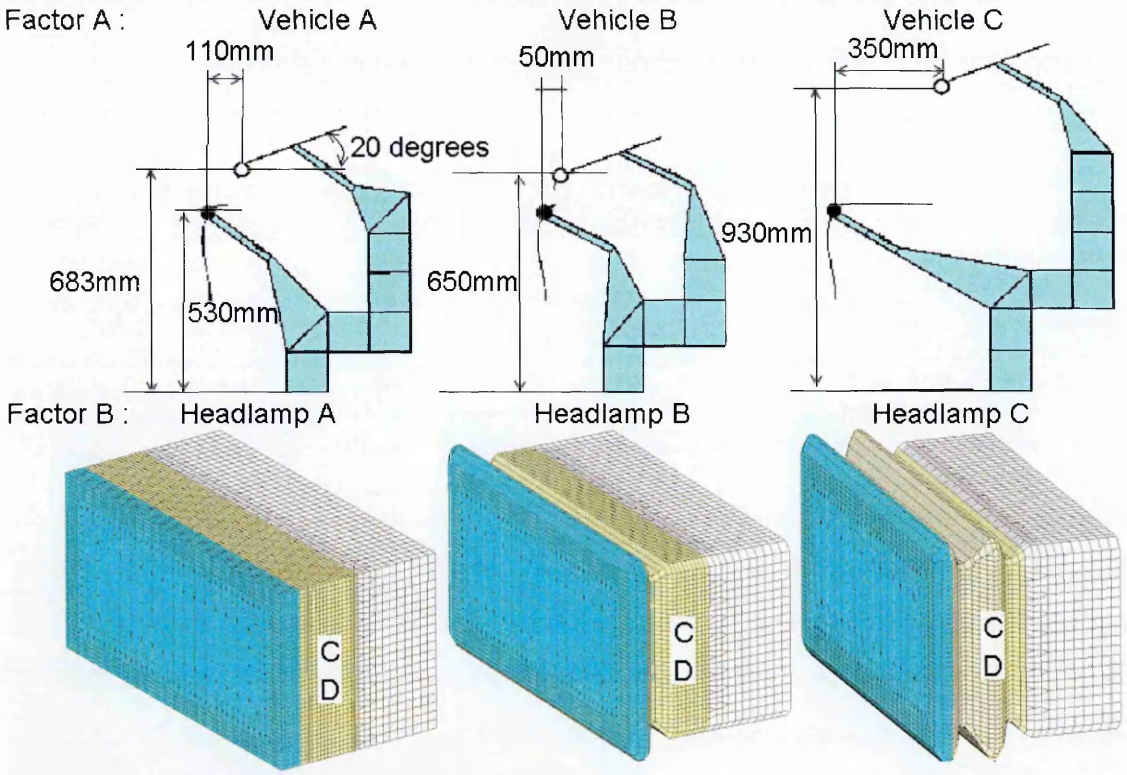

Figure 5.25 Headlamp evaluation model DoE factors and factor levels

When all the vehicle and headlamp models were combined it would have been necessary to conduct 3^3=27 experiments for a full factorial experiment incorporating each headlamp design. In addition this would have needed to be repeated for each of three vehicle designs. Due to the unacceptable solution time required to do this, a

fractional factorial DoE approach was used to reduce the number of experiments and systematically analyse the parameters.

The upper leg impactor model measured five responses and [EEVC 1998] specified limits for these responses. However, the model was not validated and so the objective criterion was only to minimise these as summarised in Table 5.9.

Response	Description	Draft directive criteria (EEVC 1998)	DoE criteria
1	Lower load cell (N)	Sum of 1 & 2 $\leq$ 4000 N	Minimise the sum of the two values.
2	Upper load cell (N)		
3	Lower bending moment N)	Each value $\leq$ 220 Nm	Minimise the maximum of the three values.
4	Middle bending moment (N)		
5	Upper bending moment (N)		

Table 5.9 DoE responses and objective criteria

Using Statgraphics, a response surface methodology was chosen because of its ability to locate optimal values for the factors in a higher level model. Five response variables were selected although only two were strictly required. This approach left open the opportunity to later combine or analyse in more detail each of the responses. Three factors were selected for the headlamp configurations and three levels for each of these.

From the arrays offered a Box Behnken array was chosen. A Box Behnken array offered the least number of experiments with no confounding of the quantitative factors. It is also orthogonal, uses no corner or extreme points (i.e. that may have forced the model to be solved with unrealistic values) and can be used to estimate the entire main, quadratic and two way interaction effects [Statgraphics 2000]. The Box Behnken array contained three identical centrepoint settings that are normally used in experimental testing but were not required for CAE. Therefore 13 rather than 15 experiments were used for each vehicle design. A user defined array as shown in the next section was then created in Statgraphics by using three copies of the Box Behnken array. It was necessary to assume that the factor headlamp design could be treated as a variable and this was justified on the basis that it was possible to interpret changes between designs (e.g. using section stiffness).

Doe study results

The completed array is shown in Table 5.10 [Howard 2001-2].

Case	FACTORS				RESPONSES	
	A : Vehicle design (A, B, C)	B : Headlamp design (1, 2, 3)	C : Thickness (mm)	D : E (% ref.)	Sum of forces (N)	Maximum bending moment (Nm)
1	A	2	3	100	11960	868
2	A	1	2	100	14874	1099
3	A	3	2	100	7175	468
4	A	1	4	100	18051	1425
5	A	3	4	100	14518	987
6	A	1	3	50	15347	1153
7	A	3	3	50	8632	575
8	A	2	3	100	11960	868
9	A	1	3	150	19034	1335
10	A	3	3	150	12834	947
11	A	2	2	50	7200	390
12	A	2	4	50	13231	906
13	A	2	2	150	11087	774
14	A	2	4	150	14232	1097
15	A	2	3	100	11960	868
16	B	2	3	100	12808	883
17	B	1	2	100	13817	910
18	B	3	2	100	8370	514
19	B	1	4	100	20482	1428
20	B	3	4	100	14921	1037
21	B	1	3	50	14796	982
22	B	3	3	50	9868	640
23	B	2	3	100	12808	883
24	B	1	3	150	20487	1404
25	B	3	3	150	14114	989
26	B	2	2	50	6329	402
27	B	2	4	50	15760	1113
28	B	2	2	150	11043	752
29	B	2	4	150	12627	855
30	B	2	3	100	12808	883
31	C	2	3	100	12765	984
32	C	1	2	100	15039	1149
33	C	3	2	100	6436	486
34	C	1	4	100	2213	1738
35	C	3	4	100	14985	1134
36	C	1	3	50	16993	1307
37	C	3	3	50	9315	702
38	C	2	3	100	12765	984
39	C	1	3	150	21457	1689
40	C	3	3	150	13084	985
41	C	2	2	50	6048	453
42	C	2	4	50	12607	960
43	C	2	2	150	9478	719
44	C	2	4	150	15641	1227
45	C	2	3	100	12765	984

Table 5.10 Headlamp evaluation model DoE study results

In line with the objective criterion the results were ranked rather than directly compared to [EEVC1998] and the force responses, bending moment responses and overall ranking are shown in Figure 5.26, Figure 5.27 and Figure 5.28.

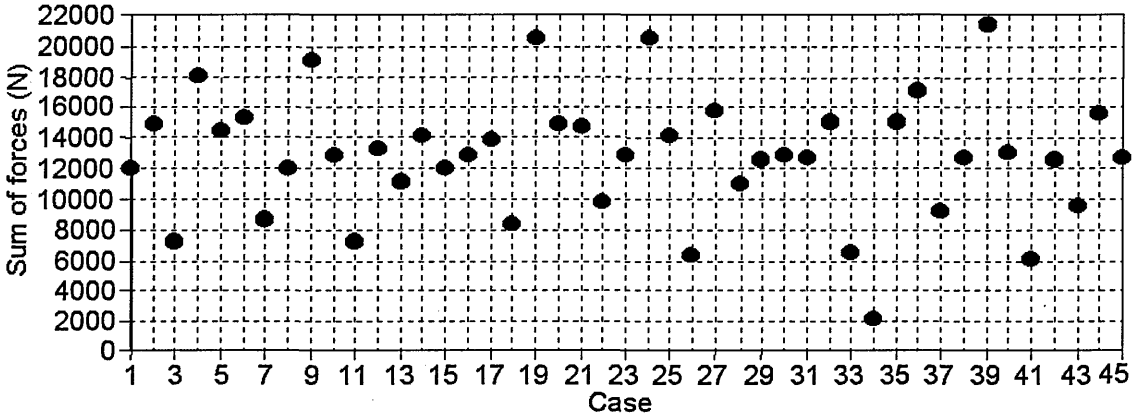

Figure 5.26 Headlamp evaluation model force responses

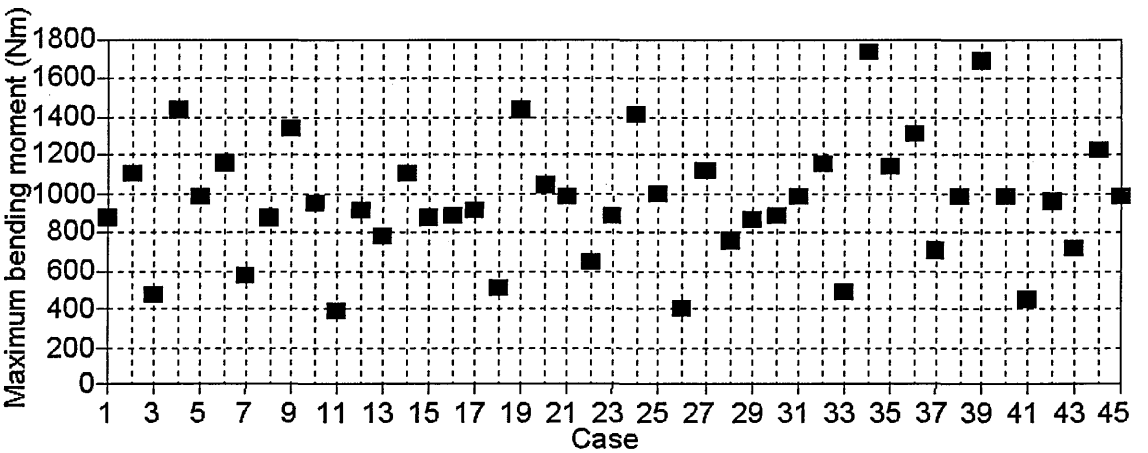

Figure 5.27 Headlamp evaluation model moment responses

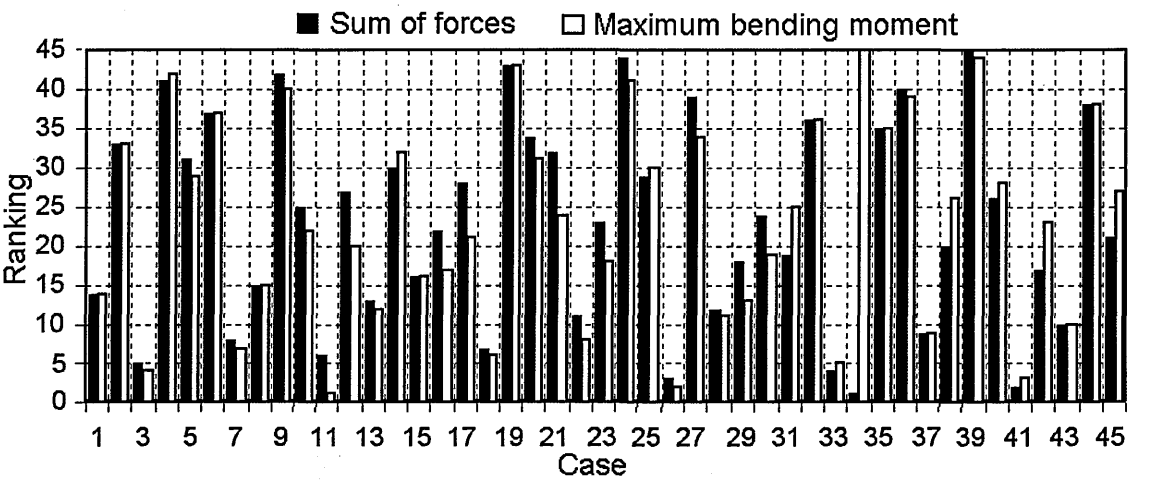

Figure 5.28 Headlamp evaluation model force and moment rankings

Since the inner part of the DoE array contained 13 headlamp configurations that were repeated for 3 vehicle designs an overall rank was determined for each headlamp configuration in 3 different vehicle designs as shown in Table 5.11.

Headlamp config.	Headlamp design (1, 2, 3)	Thickness (mm)	Youngs Modulus (% ref.)	Sum of combined force ranking	Sum of maximum bending moment ranking	Sum of combined force and bending moment ranking	Overall ranking
1	2	3	100	55	56	117 (av.)	5
2	1	2	100	97	90	187	9
3	3	2	100	16	15	31	2
4	1	4	100	85	130	215	12
5	3	4	100	100	95	195	10
6	1	3	50	109	100	209	11
7	3	3	50	28	24	52	3
8	2	3	100	58	59	See 1	-
9	1	3	150	131	125	256	13
10	3	3	150	80	80	160	7
11	2	2	50	11	6	17	1
12	2	4	50	83	77	160	6
13	2	2	150	35	33	68	4
14	2	4	150	86	83	169	8
15	2	3	100	61	62	See 1	-

Table 5.11 Headlamp evaluation model overall rankings

Discussion of DoE study results

Figure 5.26 showed the combined force responses. Particularly high forces were observed in cases 4, 9, 19, 24 and 39. These utilised standard headlamps with either thicker convolutes and/or a higher value of Youngs Modulus. Lower combined force values were observed in cases 3, 7, 11, 18, 26, 33, 34, and 41. With the exception of case 34, these cases utilised one of the headlamp designs with either the thinnest convolutes and/or the lowest or reference convolutes Youngs Modulus.

The maximum bending moment responses were shown in Figure 5.27. The largest responses were observed in cases 4, 9, 19, 24, 34, and 39 and these were also the ones with higher force values with the exception of case 34. Lower values were observed in cases 3, 7, 11, 18, 26, 33 and 41.

Figure 5.28 showed the rank of every case with respect to the sum of the forces

and the maximum bending moment. In most cases the ranking for the force and moment responses was similar and there was clear correlation between these.

Table 5.11 showed the overall combined ranking for each headlamp configuration. The best overall ranking was obtained in configuration 11 that was a single convolute design with the thinnest convolutes and lowest Youngs Modulus. In contrast to this, the worst overall ranking was for a standard headlamp with thick convolutes and the highest Youngs Modulus. There was also an interaction of these with different headlamp designs that was difficult to identify with the ranking method.

Figure 5.29 shows the standardised effect of every factor and interaction on the sum of the load cell forces.

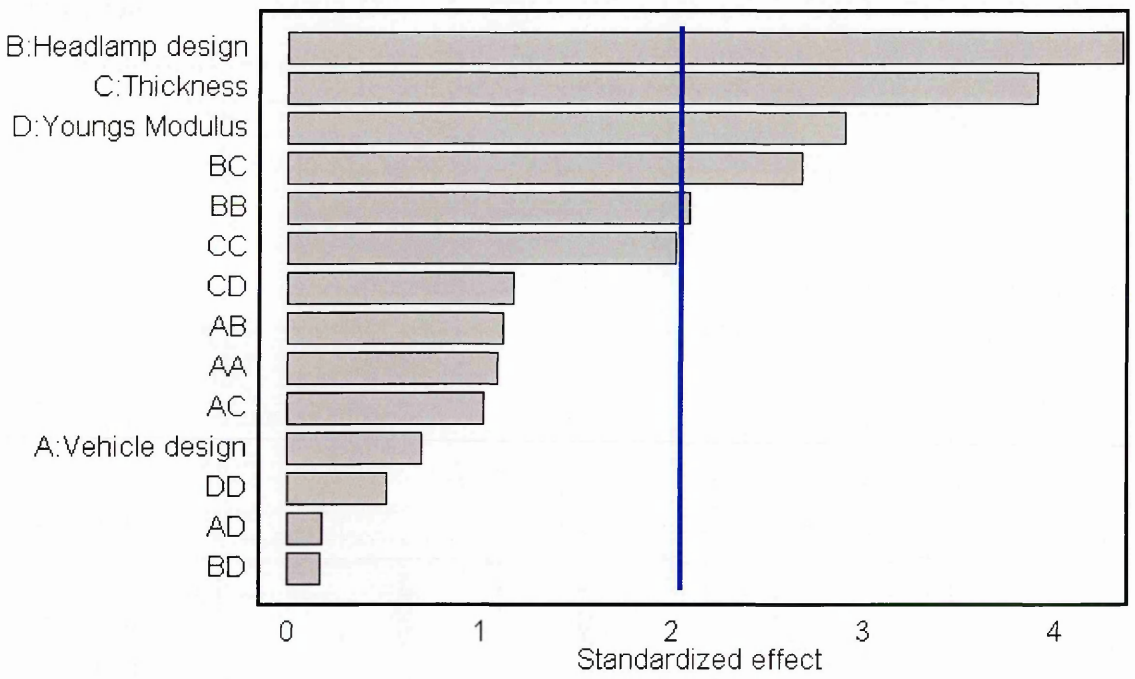

Figure 5.29 Pareto chart for the sum of the forces

This confirmed that the factors, headlamp design, thickness and Youngs Modulus were the main effects at the 95% level of confidence because the standardised effect of these lay to the right hand side of the line dividing insignificant and significant effects. However, the interaction BC and quadratic components 'BB' and 'CC' were also significant. This indicated that there was a strong interaction between headlamp design and convolute thickness (i.e. 'BC') and the effects of

factors 'B' and 'C' were highly non linear (i.e. 'BB' and 'CC'). The non linearity of the thickness was expected because the stiffness of the headlamp wall section was dependent upon the section second moment of area and this is calculated as a non linear function of thickness). Vehicle design was not significant at the 95% confidence level shown.

The influence of changes in the main effects on the sum of the forces is shown in Figure 5.30. A quadratic curve was fitted through each of the three level responses (-1, 0, 1) of every factor. This graph confirmed that a change in the vehicle design levels (A, B or C) produced a smaller response change than the other factors. It was also observed that headlamp 1 (the first curve point) produced much higher forces. However, there was a minimal change in the force response between headlamp designs 2 and 3. Similarly, lower values of the convolute thickness and Youngs Modulus (the first points on the curves) also produced lower force values.

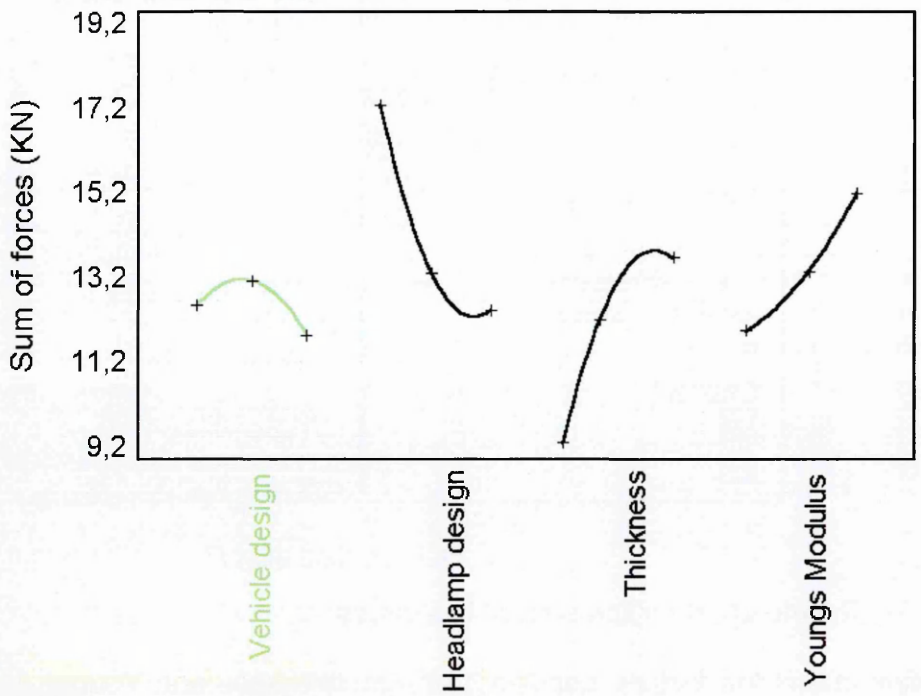

Figure 5.30 Main effects graph for the sum of the forces

Figure 5.31 shows the interaction effects graph for the sum of the load cell forces. The Pareto chart had previously shown that only interaction 'BC' was significant and so only this interaction was examined. This showed that when there was a small convolute thickness 'C' (negative) the force response was more sensitive to the

headlamp design 'B'. One interpretation was that if the sidewalls were too thick then the convolutes would not have buckled in the desired manner. This would have led to uncontrolled global rather than local buckling and the headlamp technology would have been less beneficial in reducing the force response.

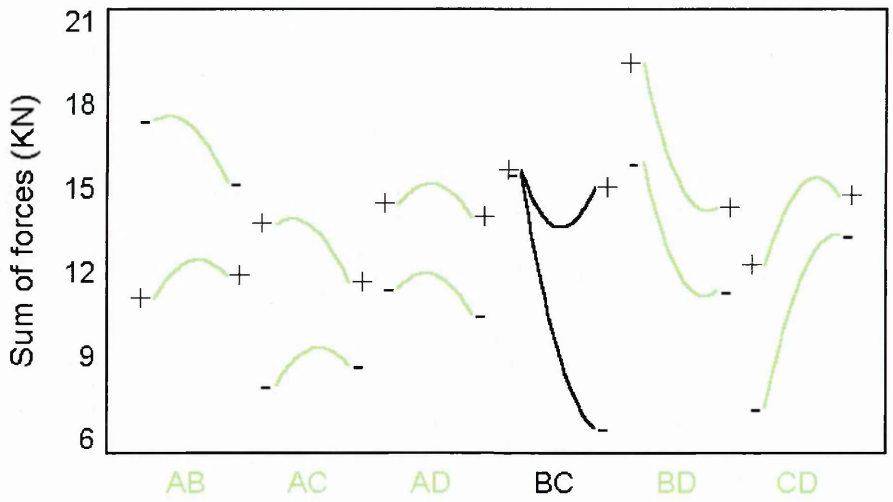

Figure 5.31 Interaction effects graph for the sum of the forces

The Pareto chart for the maximum bending moment is shown in Figure 5.32.

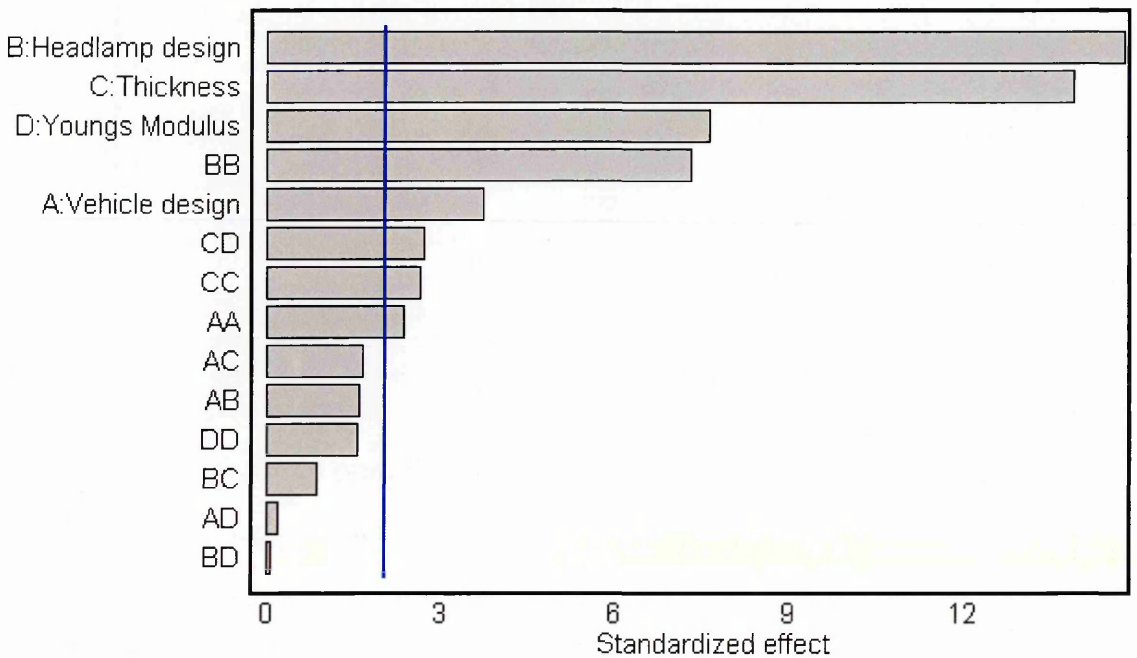

Figure 5.32 Standardised effect for the maximum bending moment

All the factors, including vehicle design, were significant and therefore they were also main effects. The quadratic component 'BB', the interaction 'CD', and the

quadratic components 'CC' and 'AA' followed these. This indicated that vehicle design was more significant to the bending moment than to the force response. As before, the headlamp design, convolute thickness and the interaction between thickness and Youngs Modulus were highly non linear as indicated by the significance of 'BB', 'CC' and 'AA'.

Figure 5.33 shows the influence of changes to the main effects on the maximum bending moment response. In this case vehicle design was significant and designs 'A' and 'B' led to lower bending moment responses. As with the sum of forces the lowest bending moment responses were obtained with headlamp designs 2 and 3, thinner convolutes and a lower value of Youngs Modulus.

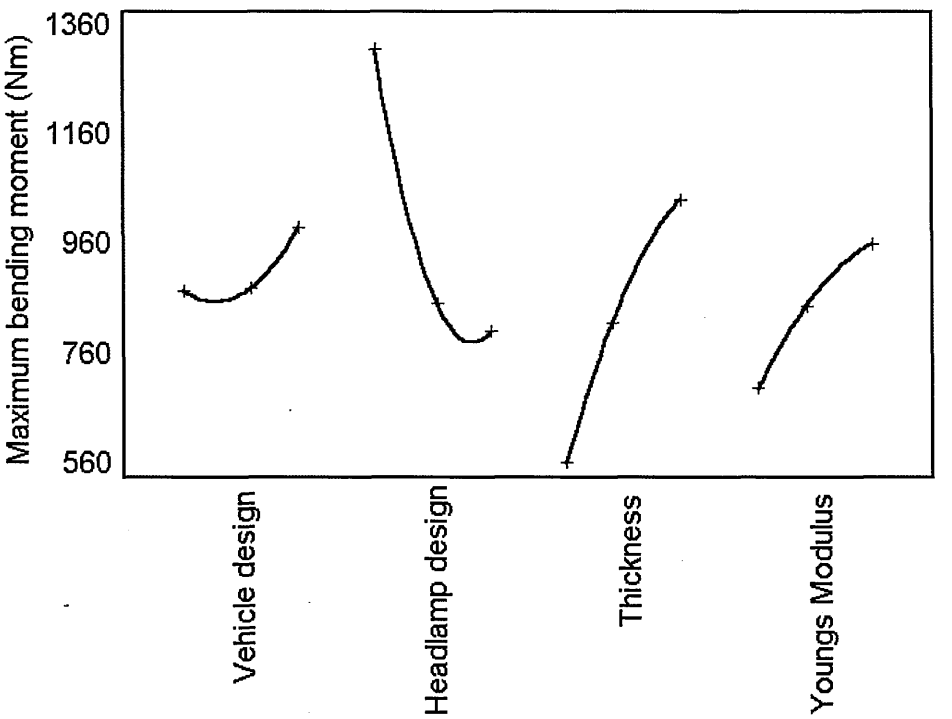

Figure 5.33 Main effects graph for the maximum bending moment

Figure 5.34 shows the change effects of maximum bending moment interactions. Only interaction 'CD' was significant and this showed that when there were thin convolutes, the moment response was more sensitive to changes in Youngs Modulus. This was to be expected because the convolute stiffness was derived from both of these factors and therefore, when one of them had a low value, the contribution of the other would be greater.

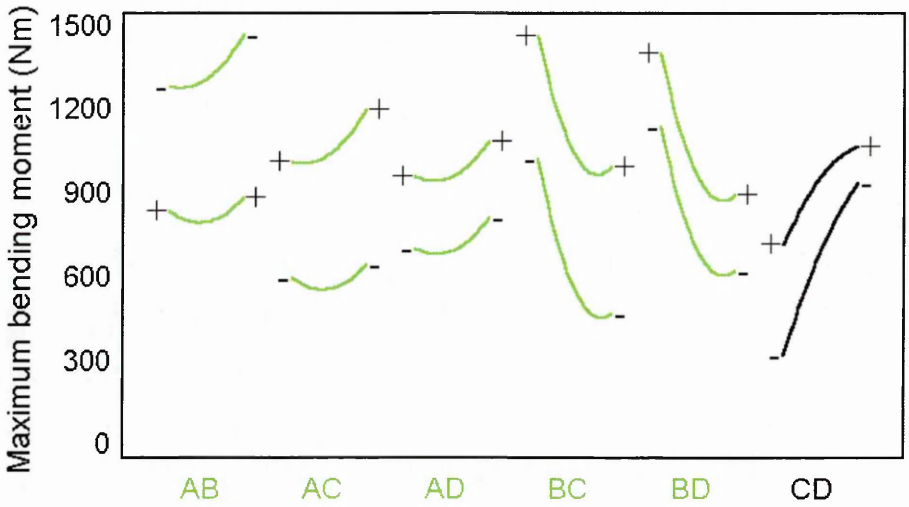

Figure 5.34 Interaction effects graph for the maximum bending moment

Statgraphics provided a multiple response optimisation facility and by seeking to minimise the sum of the forces and maximum bending moment responses an optimal solution was determined for each factor as shown in Table 5.12.

Factor	Low	High	Optimum
A: vehicle design	-1.0	1.0	-1.0
B: headlamp design	-1.0	1.0	0.999098
C: Thickness	-1.0	1.0	-0.999464
D: Young's Modulus	-1.0	1.0	-0.948049

Table 5.12 Headlamp evaluation model optimum levels

This indicated that vehicle design A in combination with headlamp design 3 (two convolutes) using the minimum headlamp convolute thickness and stiffness would give the lowest force and moment responses. The ranking method had identified headlamp design 2 (one convolute) as the optimal solution.

The study provided useful information and from a DoE perspective the array was reliable and simple. All of the design factors were also main effects except vehicle design. However, each vehicle design was only distinguished by different positions of the bumper, hood and headlamp and different loading conditions. The hood and bumper stiffness for each vehicle design were identical and this assumption is unlikely to be correct for actual vehicles (e.g. an off road vehicle will have a stiffer bumper). This was not a major limitation provided that vehicle design was interpreted as a type of loading condition to evaluate the robustness of the

headlamp design. However, the major limitation to this study was that it only provided general trends that were applicable to limiting the upper leg impactor responses and not actual pedestrian injuries or other requirements.

Conclusions

The most important factors for both responses of PAH are the headlamp design, convolute thickness and Youngs Modulus in this order. Vehicle type as defined in a simplified vehicle model is unimportant for the force response but important for the bending moment response. A double convoluted design with thin and low stiffness convolutes provides marginal improvements over a single convolute design. However, there are large improvements compared to a standard headlamp, irrespective of vehicle type (PAH is robust).

5.5. Pedestrian protection bumper system (POBSY)

5.5.1. Biomechanical models of POBSY

It is easier to generalise about the possible injuries that may be caused by a pedestrian impact with the bumper than with the headlamp. Not only does [EEVC 1998] provide some guidance in this respect, but also such injuries are widely reported and researched [Kajzer 1997]. [EEVC 1998] was founded upon the notion that the adult lower leg and the knee were the most important injury regions [Lawrence 1989]. With consideration given to the vehicle and pedestrian geometry, it was assumed that the child femur was another important injury region.

For the purpose of explaining the manner in which the bumper technologies operate, the two types of loading condition are shown in Figure 5.35. One of these concerns the child femur and the other the adult lower leg, including the knee, tibia and fibula. In this analysis the child femur is considered to be similar to the adult femur as previously described. Huelke [Huelke 1986] described the tibia as " ...the second largest bone of the body. It is enlarged above to form the tibial plateau. The shaft is relatively pointed in the front; its medial surface is only covered by skin and subcutaneous tissue, easily palpated (felt) from the knee to the ankle. Huelke continued concerning the fibula "On the lateral side is the fibula, a long narrow bone with a rounded head above that can be palpated just beneath the knee joint". Finally

Huelke commented on the peroneal nerves which " ... turns off at a 30 degree angle (from the sciatic nerve above) to pass around to the front of the leg immediately beneath the head of the fibula. Direct impact at this location can contuse or crush the nerve, deinnervating the muscles causing the symptom of foot drop. In the adult the head of the fibula is approximately 18-22 inches off the ground and is the frequent site of a bumper impact in pedestrians".

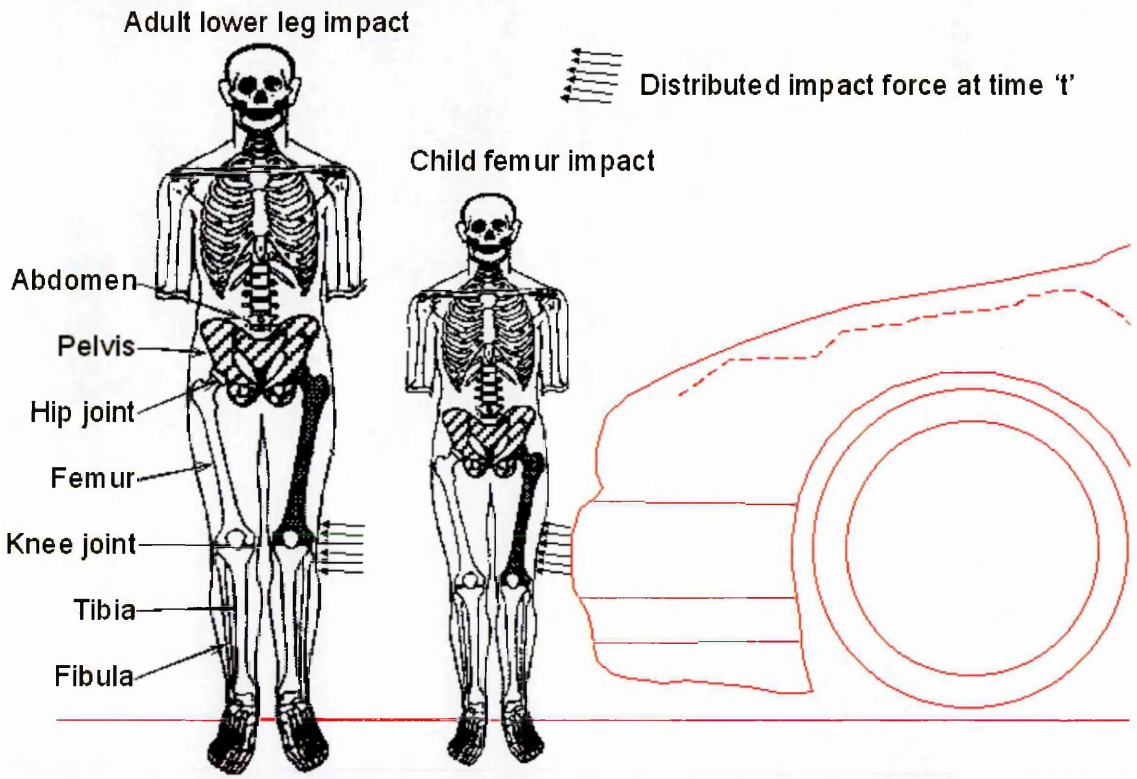

Figure 5.35 Adult and child bumper impact

An overview of the adult fibula and tibia and some of the surrounding muscles is shown in Figure 5.36 [Huelke 1986]. Huelke [Huelke 1986] described the knee joint as "... the most unstable joint of the body for it is composed of the rounded femoral condyles above and a flat tibial plateau below. It, like all other joints, is surrounded by a capsule with synovial membrane inside that provides a lubricating fluid. On each side are ligaments referred to as the medial and lateral collateral ligaments". Huelke continued "Within the knee joint are two ligamentous bands that extend from the centre of the tibial plateau to the area between the two femoral condyles. These ligaments cross each other so that the anterior one attaches most forward on the tibia but more rearward between the condyles. These anterior and posterior cruciate

ligaments help to keep the two bones in contact with each other and limit the range of flexion and extension motion".

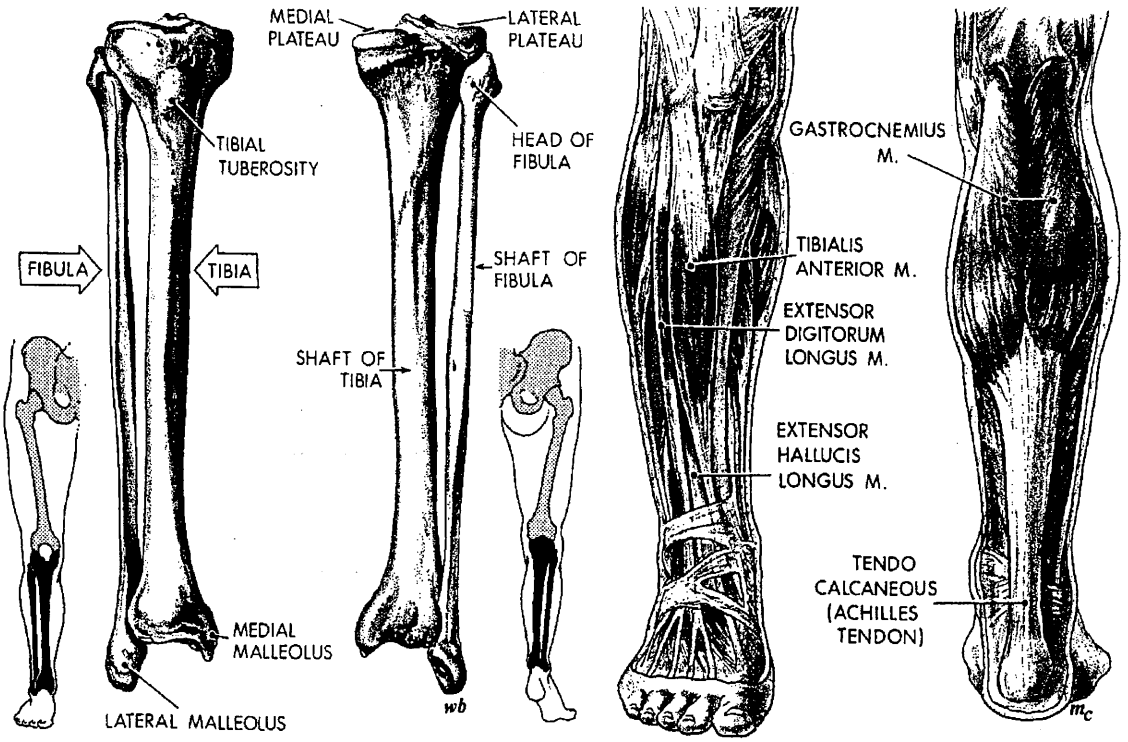

Figure 5.36 The adult tibia and fibula and surrounding muscles

Figure 5.37 shows an overview of the adult knee joint [Huelke 1986].

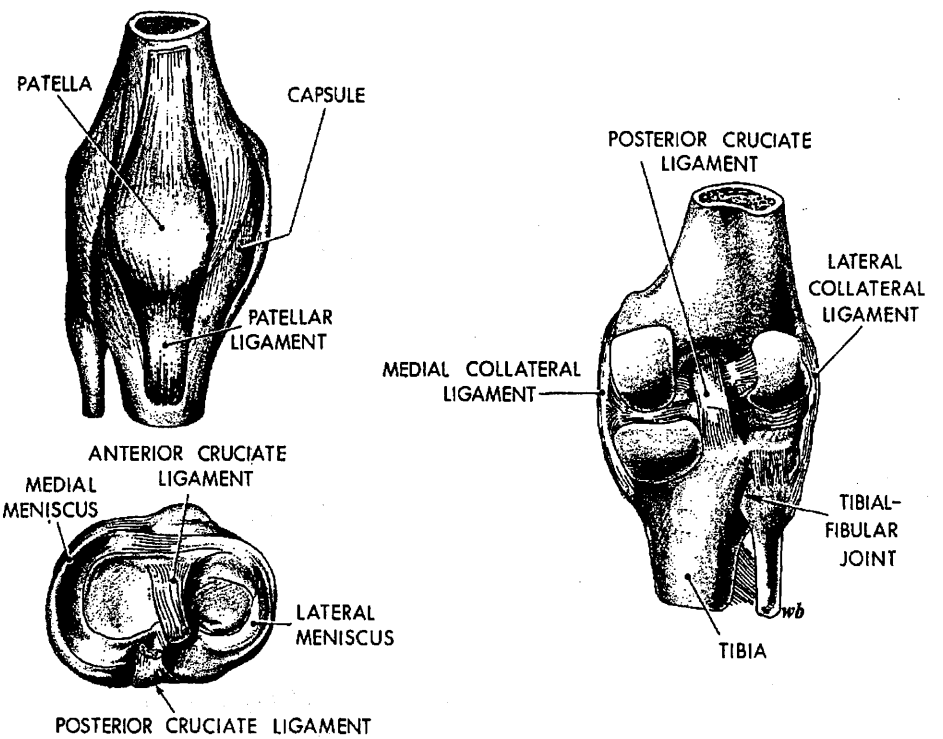

Figure 5.37 The adult knee joint

A conceptual view of the direct contact between the bumper and knee and/or the lower leg when the peak bumper reaction force occurs is shown in Figure 5.38.

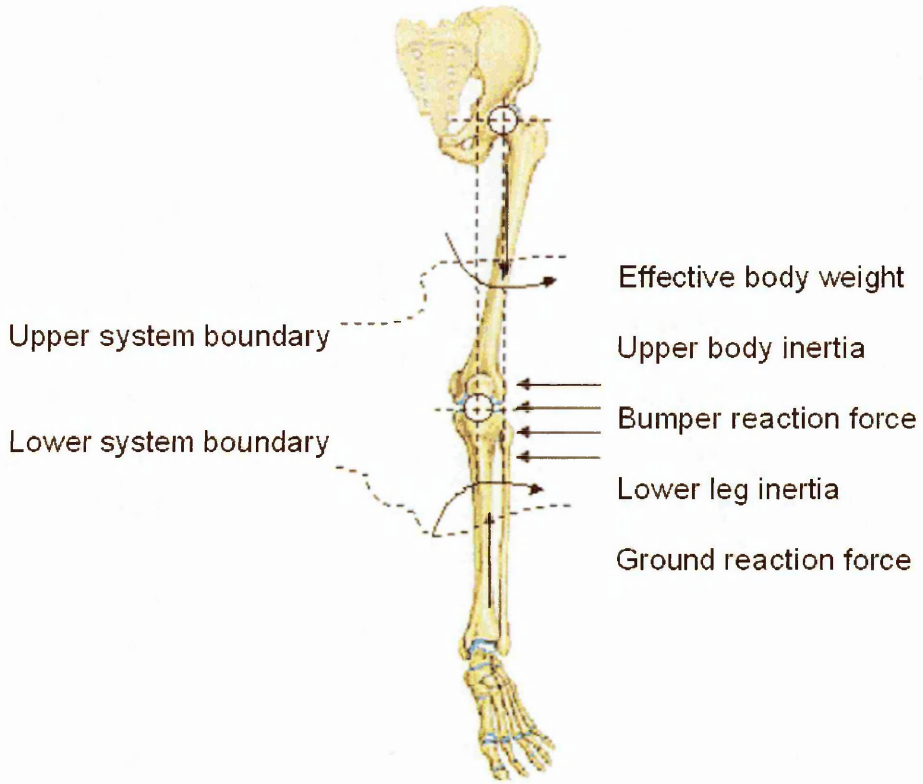

Figure 5.38 Conceptual view of the adult knee and lower leg loading

The boundaries of this loading condition were chosen above and below the knee joint. The condyles (i.e. long bone ends) were included within the system because condyle injuries are more serious than fractures of the centre span of the tibia, fibula or femur. The knee consists of many parts, is relatively unstable and highly loaded even during normal activities. There are also many ligaments in the knee and these take a long time to heal and are difficult to repair. The menisci that assist in reducing the friction between the relative rotations of the condyles raise similar problems. Finally, many knee injuries involve extensive damage to the whole region because it is a highly localised contact that absorbs the initial impact energy.

Some knee injury mechanisms are shown in Figure 5.39 [Kajzer 1997]. The tests on the top row were constructed to represent a shearing condition and those on the bottom row a bending condition. These show how the femur, tibia and ligaments may fail under this particular type of impact loading condition.

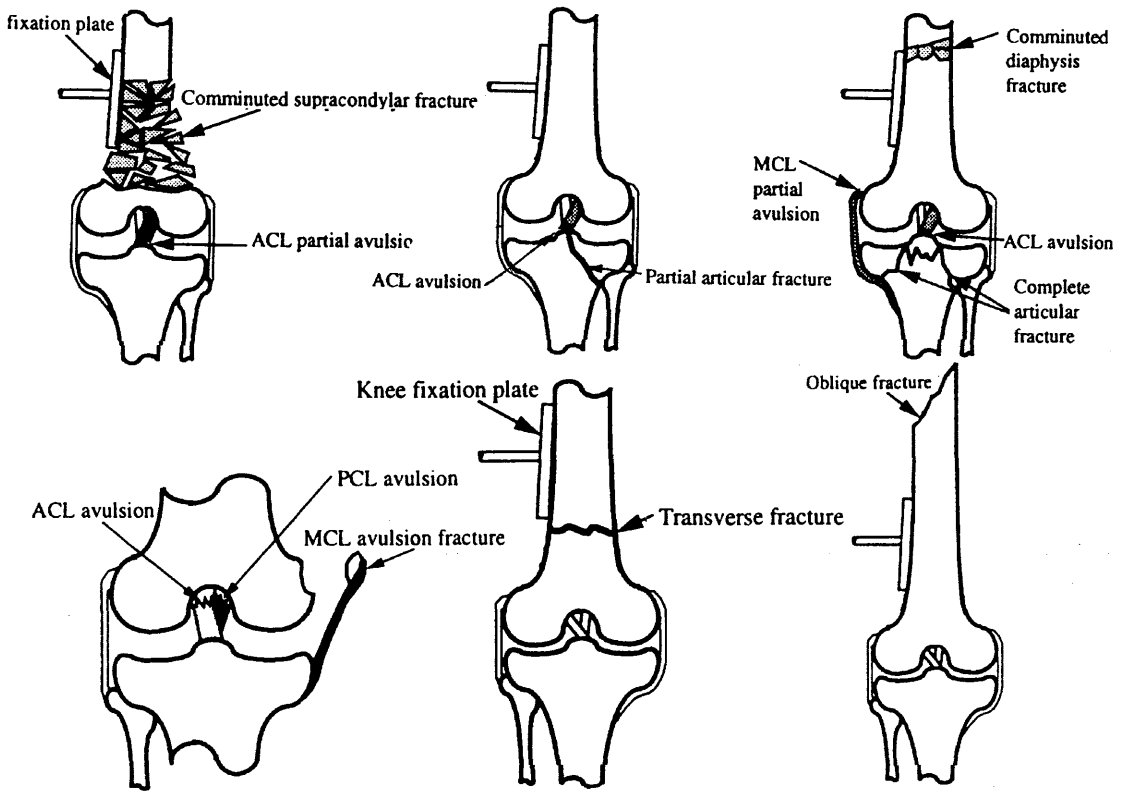

Figure 5.39 Various pedestrian knee injury mechanisms

The complexity of the knee joint injury mechanism is more clearly seen in Figure 5.40 [Kajzer 1997] with a more detailed view of the knee shear mechanism.

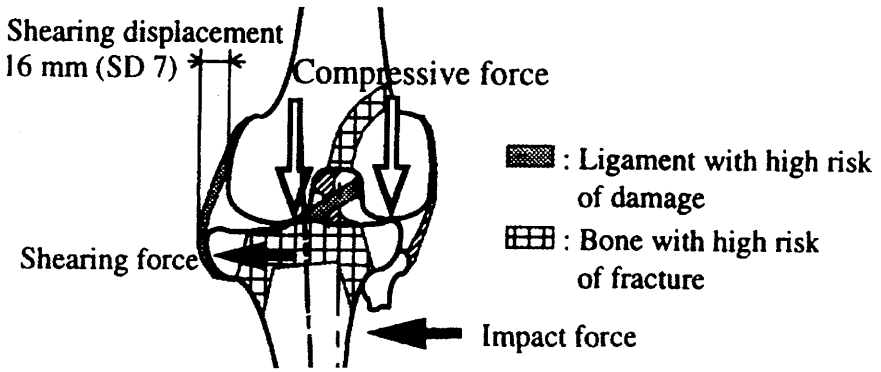

Figure 5.40 The adult knee shear injury mechanism

In all the injury cases described, it was assumed that reducing the magnitude of the force pulse would reduce the severity of these injuries. In the case of the adult knee it was also assumed that moving the impact location towards the central span of the tibia would assist in either lifting the lower leg during an accident, or isolating the contact region from the knee by fracturing the tibia and fibula [Kajzer 1997]. These were the basic assumptions upon which the bumper technologies were founded.

5.5.2. Description of POBSY

The objective of the bumper technology was therefore to reduce the load on a pedestrian knee and lower the effective height of the bumper stiffness centre so that the impact force was moved downwards and away from the knee as shown in Figure 5.41.

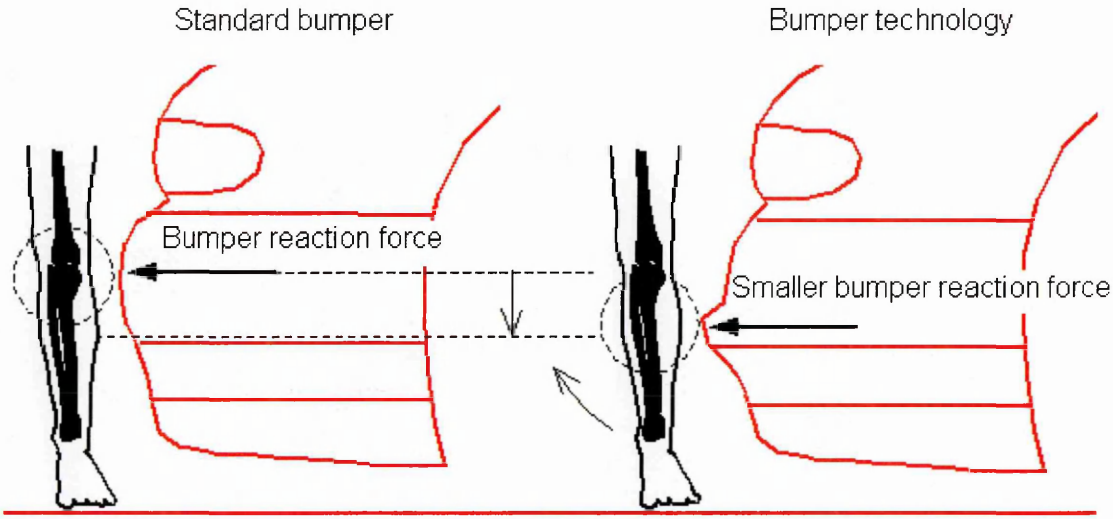

Figure 5.41 The main objective of the bumper technology

There were many ways in which this could be achieved and some of the bumper designs from [Howard 1999-2] are shown in Figure 5.42.

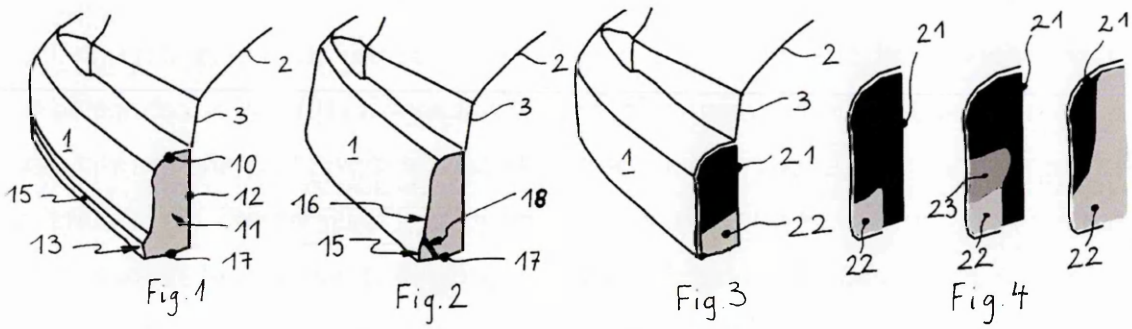

Figure 5.42 Some bumper designs to achieve the desired loading

From left to right it is possible to incorporate a lower bumper face extension for example by using a chrome strip or bumper cover styling feature. Alternatively or in addition to this the bumper face can be sloped rearward or a stiffening rib added behind the lower edge of the bumper cover. Multiple density foams may also be used to achieve a similar stiffness distribution by varying the foam density from low density at the top to higher density at the bottom or similarly from front to rear.

The bumper spoiler may also be reinforced with a variety of methods to further lower the effective bumper stiffness height and support the lower leg. One of these methods is to use a structural undertray (9) as shown in Figure 5.43 [Howard 2001-8] in combination with the multiple density foams (4).

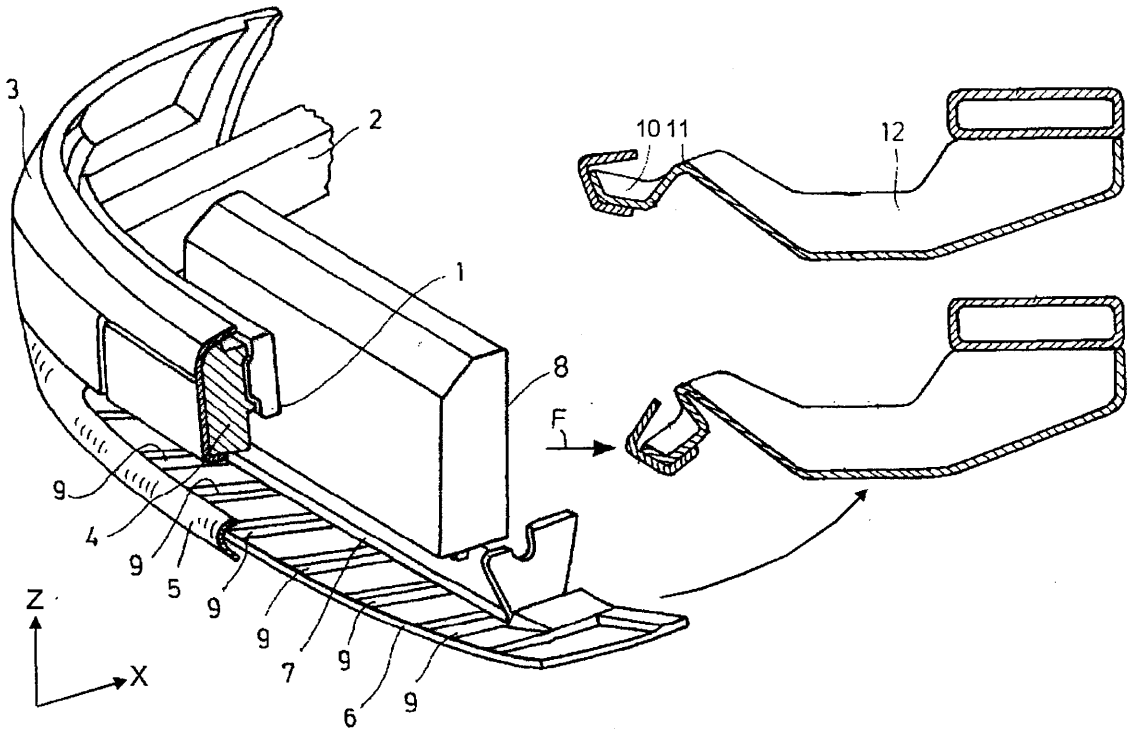

Figure 5.43 An overview of POBSY

On the right hand side there is a cross section in the XZ plane through the undertray. There are three main regions: the front region (10) that is connected to the lower edge of the bumper shell, the flexible central region (11) and the stiff rear region (12) that is connected to the cooling pack crossmember (7). During a pedestrian leg impact the central region deforms in a predefined manner (i.e. without large scale buckling) due to the formation of a plastic hinge at the apex of the V shape. The deformation has a predefined limit (due to the geometry) so that it supports the lower leg without being a rigid contact and causing further leg injuries.

5.5.3. Analytical models of POBSY

Along with the headlamp technology, a number of analytical models were constructed to gain an improved understanding of how POBSY should function. The first level of model construction is shown in Figure 5.44, with the struck side pedestrian leg in isolation from the rest of the pedestrian.

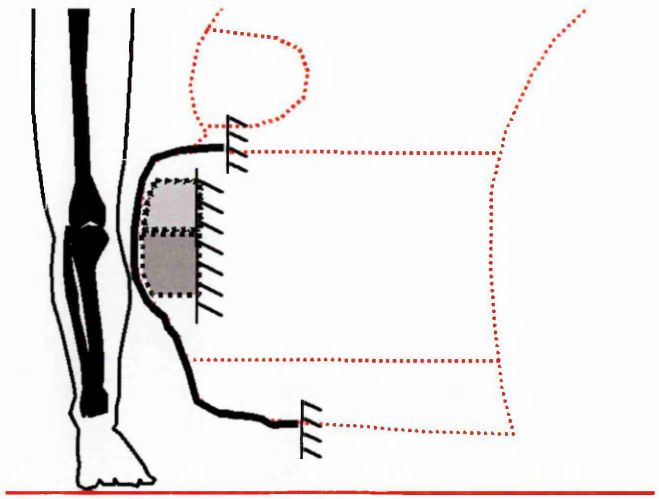

Figure 5.44 First level of model construction

During the first stage of the pedestrian impact the leg is subjected to bending about the knee joint and shear, as it is accelerated away from the bumper, due to direct bumper contact and inertial loading. There is no initial leg to leg contact and minimal resistance to rotation at the hip joint. Hence the struck leg can be isolated in this manner. These assumptions underlie the leg impactor test procedure [EEVC 1998].

The vehicle has a large mass and stiffness compared to the pedestrian leg and therefore it is assumed that the bumper system may be isolated from the rest of the vehicle and restrained by rigid boundary conditions. This is valid provided that there is minimal deformation of the supporting structure behind the bumper and limited support for the leg from the structure around the bumper. However care needs to be taken with such an assumption because there is usually significant energy transfer between the bumper and supporting structure. A rigid boundary will overestimate the energy the bumper absorbs.

At the second level of model construction shown in Figure 5.45 the human leg is represented by two rigid body masses 'm_1' and 'm_2'. 'J_1' and 'J_2' are the moments of inertia of the same masses about the centre of gravity. Forces 'F_1' and 'F_2', and moments 'T_1' and 'T_2' represent shear, and bending across the joint. For the purpose of simplifying the model, it is assumed that there is no shear across the joint. Therefore, the forces are equal in magnitude i.e. $F_1 = F_2 = F_j$. The motions of the centres of gravity of the upper and lower leg masses are defined by the linear

horizontal motions 'x_1' and 'x_2' and angular rotations 'θ_1' and 'θ_2' in radians. The leg model is similar to the leg impactor described in [EEVC 1998] except there are only two degrees of freedom for each mass and no shear across the joint.

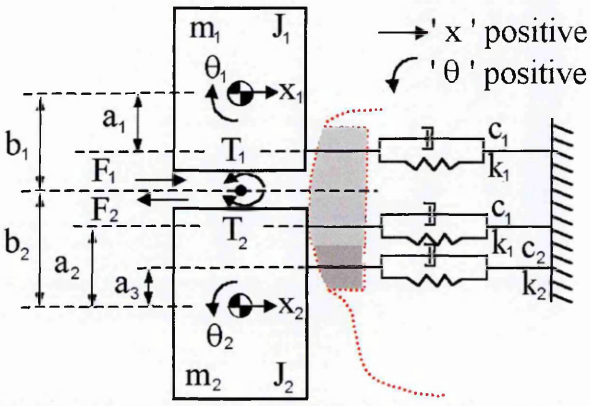

Figure 5.45 Second level of model construction

Three parallel spring and damper models represent the vehicle bumper foam with two spring stiffnesses 'k_1' and 'k_2' and damping coefficients 'c_1' and 'c_2'. The non linear stiffness distribution of the bumper foam can be varied in the lower part of the bumper contacting the lower leg.

There are many assumptions in this model. In a similar manner to [EEVC 1998], such a rigid body approach does not consider the influence of femur, tibia or fibula bending or fracture. For short periods of time (e.g. 10 ms), in which the horizontal velocity is much greater than the vertical velocity, there is insignificant motion in the Y axis. However, to assume no shear, eliminates the possibility of determining whether an improvement in the knee bending angle compromises shear displacement. From the perspective of the bumper model, the resultant force of each part of the foam acts at the centre of the relevant volumes and there is no bumper cover. Although the cover has a significant influence on the bumper stiffness, it does not have a large influence on changes to the foam distribution. These are more acceptable assumptions, because they still allow an understanding of the influence of the bumper to be obtained with some equations of motions.

Figure 5.46 shows the conditions for the upper leg motion about its centre of gravity. All the forces, angles and moments are shown in the positive global directions.

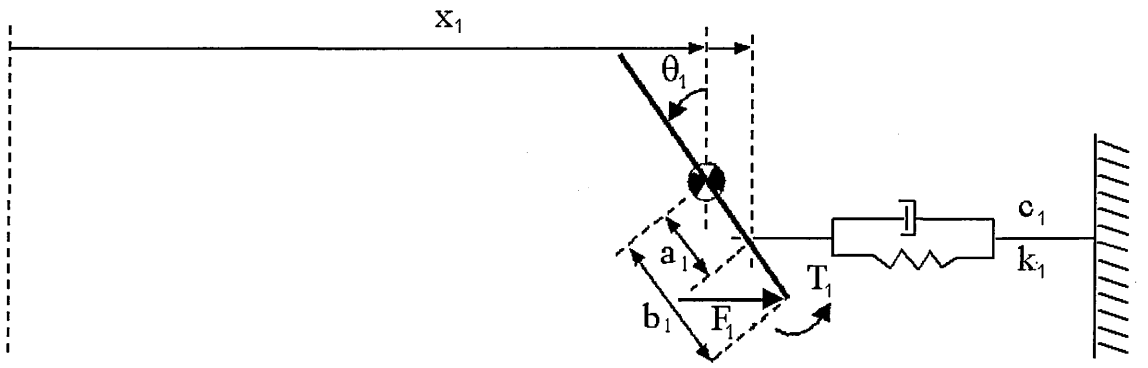

Figure 5.46 The boundary conditions for the upper leg motion

The displacement of the damper and spring for small values of θ_1 is given by $x_1 + a_1\theta_1$. Hence, for the equilibrium of forces on 'm_1':

$$m_1\ddot{x}_1 = -c_1\frac{d}{dt}(x_1 + a_1\theta_1) - k_1(x_1 + a_1\theta_1) + F_1$$

$$m_1\ddot{x}_1 = -c_1(\dot{x}_1 + a_1\dot{\theta}_1) - k_1(x_1 + a_1\theta_1) + F_1 \quad .....(1)$$

Similarly for the equilibrium of moments on 'm_1':

$$J_1\ddot{\theta}_1 = -c_1\frac{d}{dt}(x_1 + a_1\theta_1)a_1 - k_1(x_1 + a_1\theta_1)a_1 + F_1 b_1 + T_1$$

$$J_1\ddot{\theta}_1 = -c_1(\dot{x}_1 + a_1\dot{\theta}_1)a_1 - k_1(x_1 + a_1\theta_1)a_1 + F_1 b_1 + T_1 \quad .....(2)$$

Figure 5.47 shows the conditions for the lower leg motion about its centre of gravity.

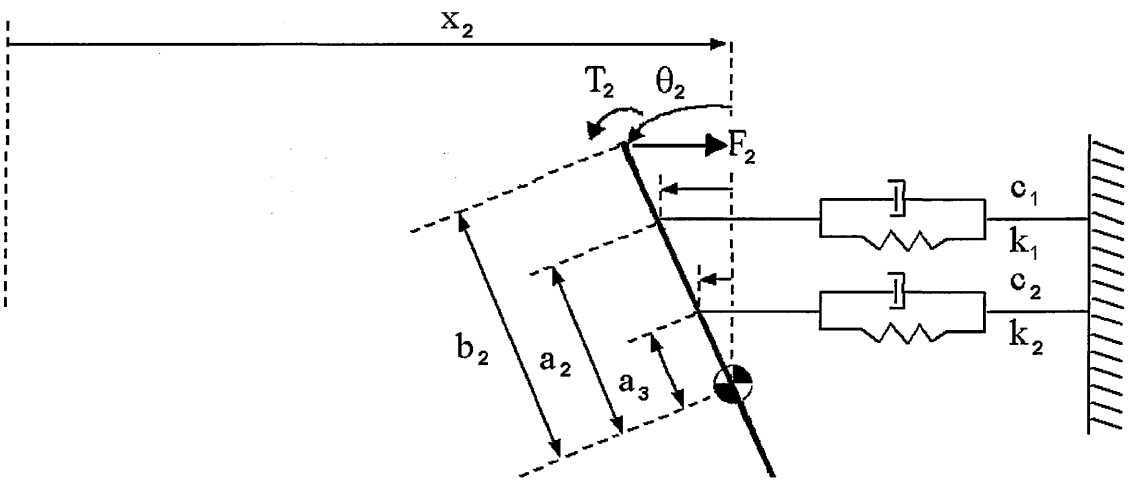

Figure 5.47 The boundary conditions for the lower leg motion

For the lower leg the displacement of the damper and spring for small angles is given by given by $x_2 - a_2\theta_2$ and $x_2 - a_3\theta_2$. Hence, for the equilibrium of forces on 'm_2':

$$m_2\ddot{x}_2 = -c_1(\dot{x}_2 - a_2\dot{\theta}_2) - k_1(x_2 - a_2\theta_2) - c_2(\dot{x}_2 - a_3\dot{\theta}_2) - k_2(x_2 - a_3\theta_2) + F_2 \quad \text{.....(3)}$$

Similarly for the equilibrium of moments:

$$J_2\ddot{\theta}_2 = -c_1(\dot{x}_2 - a_2\dot{\theta}_2)a_2 - k_1(x_2 - a_2\theta_2)a_2 - c_2(\dot{x}_2 - a_3\dot{\theta}_2)a_3 - k_2(x_2 - a_3\theta_2)a_3 + F_2b_2 + T_2 \ldots (4)$$

Equations (1) and (2) may be rearranged in terms of F_j ($F_1 = F_2 = F_j$) and then substituted in equations (3) and (4) to eliminate F_j. [EEVC 1998] indirectly specifies the joint torque T_j ($T_1 = T_2 = T_j$) in terms of $\theta = \theta_1 - \theta_2$ as shown in Figure 5.48.

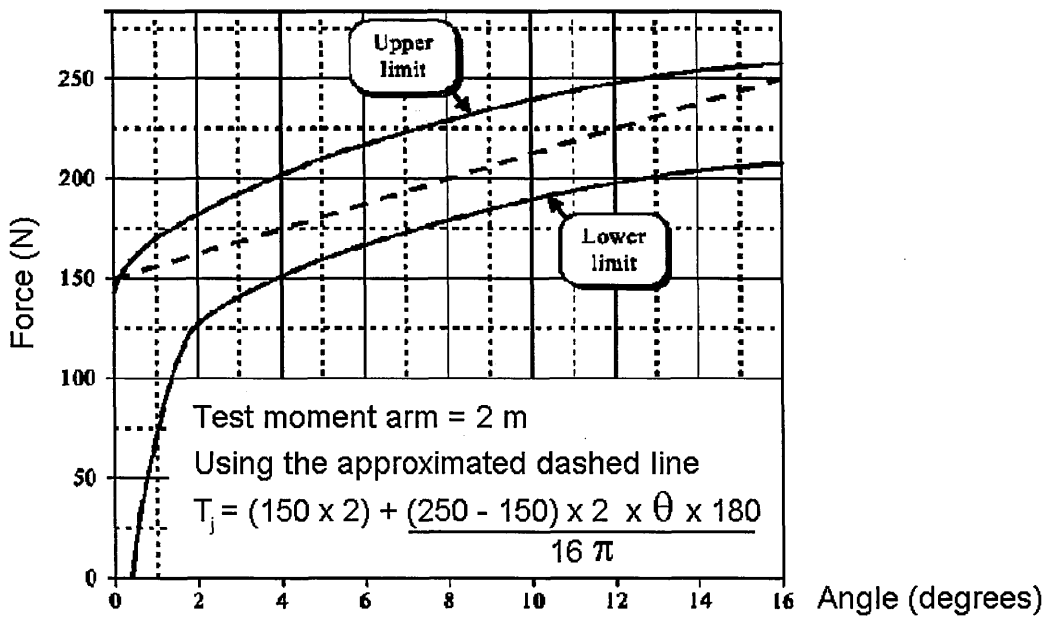

Figure 5.48 Leg impactor knee bending moment characteristics

However, due to the voluminous nature of the analytical equations and the significant assumptions related to the impactor (e.g. no shear across the connecting joint), a numerical solution, using finite element simulations, was sought instead.

5.5.4. Numerical bumper evaluation model

To assist in the development of POBSY a two stage generic parametric study was designed to evaluate simplified numerical models of the bumper system. In the reference cases the overall size and material properties of the bumpers were based on a C class vehicle bumper. Only the bumper was modelled so that the bumper characteristics could be evaluated independently of vehicle style. Although it was known that the vehicle style could influence leg injuries [EEVC 1998] it was assumed that in the first 20 ms after the impact its influence was insignificant.

The first stage involved a screening study in which several bumper designs based upon an understanding of the previous models and patents [Howard 1999-2, 2001-8] were evaluated. In the initial study certain assumptions were made concerning the bumper configurations. For example, it was assumed that the air intake could be eliminated and although this is not possible with most current vehicles it may be applicable to future vehicles (e.g. hybrid vehicles). Another assumption was that the undertray needed to be stiffer than the standard undertray and that the energy absorbing capability of the modified bumper should be greater than or equal to that of the original bumper (e.g. if the stiffness of one foam volume was reduced then the stiffness of another was increased). However, the overall bumper dimensions were restricted to those of the C class car because these dimensions were generally dependent on other requirements, such as bumper pendulum impact tests (USA part 581, ECE 42) and low speed damageability requirements (EWG 70/156).

In the second stage, the best performing bumpers were analysed in more detail using a DoE approach to understand the influence of the bumper geometry and material parameters on the measured responses and to confirm or disprove the screening stage conclusions. The models and experiments were constructed and evaluated using the same model quality guidelines as in the headlamp study.

Model construction and development

The numerical model shown in Figure 5.49 consisted of a simplified generic bumper model and a model of a sub system leg impactor [EUCAR 2000, Ford 2000-2]. The bumper system was modelled as a volume of solid elements in which the stiffness distribution could be varied for different bumper configurations. A rigid base (RIGID_GROUND) that was restrained in all freedoms (on the material card) was used to locate the elements that represented the bumper foam (BUMPER_FOAM), an air intake (no elements) and an undertray (UNDERTRAY). In all cases the bumper foam was only located in rearward and lateral directions so that the foam elements could wrap around the leg impactor. This was important because experimental tests showed that the bumper foam tends to do this [Howard 2000-2]. The undertray elements represented part of a larger panel and were therefore restrained in x, y, and z along rear face nodes.

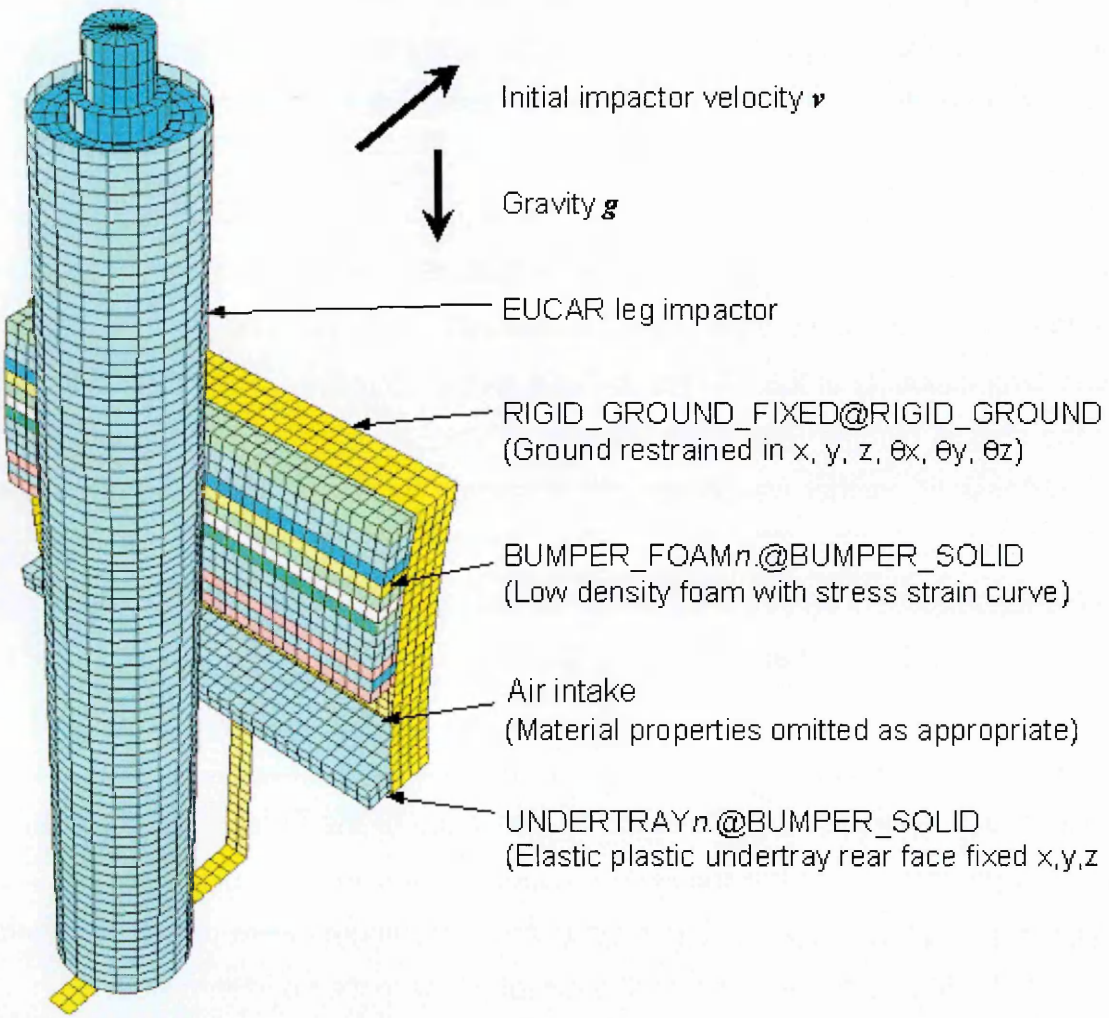

Figure 5.49 Numerical bumper evaluation model

The bumper model was constructed with a uniform element distribution of 12 mm cuboidal solids and with a depth of six elements. The naming convention and the proportions of each volume were based on the reference geometry of the C class car at Y0. Starting from the bottom, the first two rows were named UNDERTRAY_*, the second nine rows AIR_INTAKE_* and the final top rows BUMPER_FOAM_*. In this manner each element layer was constructed as a different part so that the material cards could be quickly edited or the part cards deleted for different bumper configurations. The bumper cover was not modelled because this was a generic study of the influences of changes to the bumper stiffness distribution. Including the cover would have necessitated more assumptions concerning the boundary conditions and may have reduced the influence of changes to the foam (i.e. the cover would have spread the impact load across foam regions).

Material law 57 was used for the BUMPER_FOAM parts as shown in Table 5.13 with an experimentally determined stress strain curve [fka 1999-1].

BUMPER FOAM
Material law 57

$\rho = 0.54E\text{-}10\ \text{ton/mm}^3$

$E = 3333\ \text{N/mm}^2$

Refers to stress strain curve 24

$\sigma_{\text{tension cut off}} = 50\ \text{N/mm}^2$

Hysteric unloading factor = 0.01
Decay constant to model creep in unloading = 0.0
Viscous coefficient to model damping effects = 0.1
Shape factor for unloading = 50.0
Failure option = 1.0 (tensile stress is set to zero after cutoff stress is reached)
Bulk viscosity = 0.0 (default recommended)
Young's relaxation modulus = 0.001
Decay constant = 0.01
Stiffness coefficient for contact interface stiffness = 0.0

```
*MAT_LOW_DENSITY_FOAM
        41 0.540E-10 0.333E+04 0.240E+02 0.500E+02 0.100E-01           0.100E+00
 0.500E+02 0.100E+01           0.100E-02 0.100E-01
*DEFINE_CURVE
        41         0       1.0       1.0       0.0       0.0         0
               0.0                   0.0
         0.050000001           0.21680000
          0.10000000           0.23549999
          0.15000001           0.23989999
          0.20000000           0.24850000
          0.25000000           0.26780000
          0.30000001           0.28220001
          0.34999999           0.30930001
          0.40000001           0.34009999
          0.44999999           0.38310000
          0.50000000           0.44040000
          0.55000001           0.52719998
          0.60000002           0.65509999
          0.64999998           0.88429999
          0.69999999            1.5592999
```

Table 5.13 LS-DYNA material card for reference bumper foam

Two additional stress strain graphs were also created to examine the influence of different foam stiffness as shown in Figure 5.50.

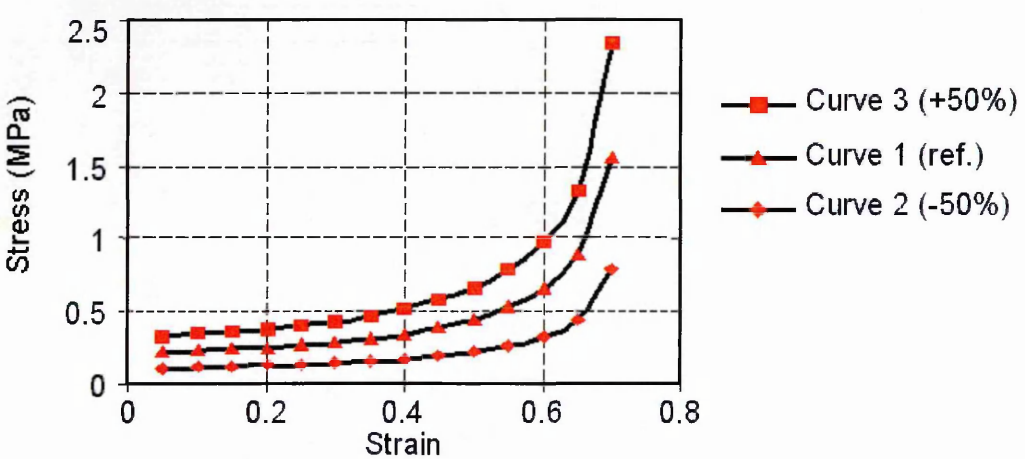

Figure 5.50 Bumper foam material properties

Material law 3 was used for the UNDERTRAY elements. These simulated a stiff polymeric component and were based on material properties determined in [Howard 2000-2] as shown in Table 5.14.

UNDERTRAY Material law 3
$\rho = 0.20\text{E-}08\,\text{ton/mm}^3$ (ABS) $E = 550\,\text{N/mm}^2$ (ABS but adjusted in draft directive simulations) $\nu = 0.25$ (ABS) $\sigma_y = 8\,\text{N/mm}^2$ (ABS) $E_T = 25\,\text{N/mm}^2$ (ABS) $\beta = 0.0$ (kinematic hardening) SRC = 0.0 (no strain rate effect) SRP = 0. 0 (no strain rate effect) FS = 0.0 (no element failure & erosion) VP = 0.0 (n.a. scale yield stress for rate)
MAT_PLASTIC_KINEMATIC $ Material 43 : UNDERTRAY 1 43 0.200E-08 0.550E+03 0.250E+00 0.800E+01 0.250E+02

Table 5.14 LS-DYNA material card for reference undertray

The Youngs Modulus was varied by +/-50% and the AIR INTAKE parts were deleted and/or material properties changed (e.g. to match the BUMPER_FOAM) according to the desired configuration. The contacts used are shown in Figure 5.51.

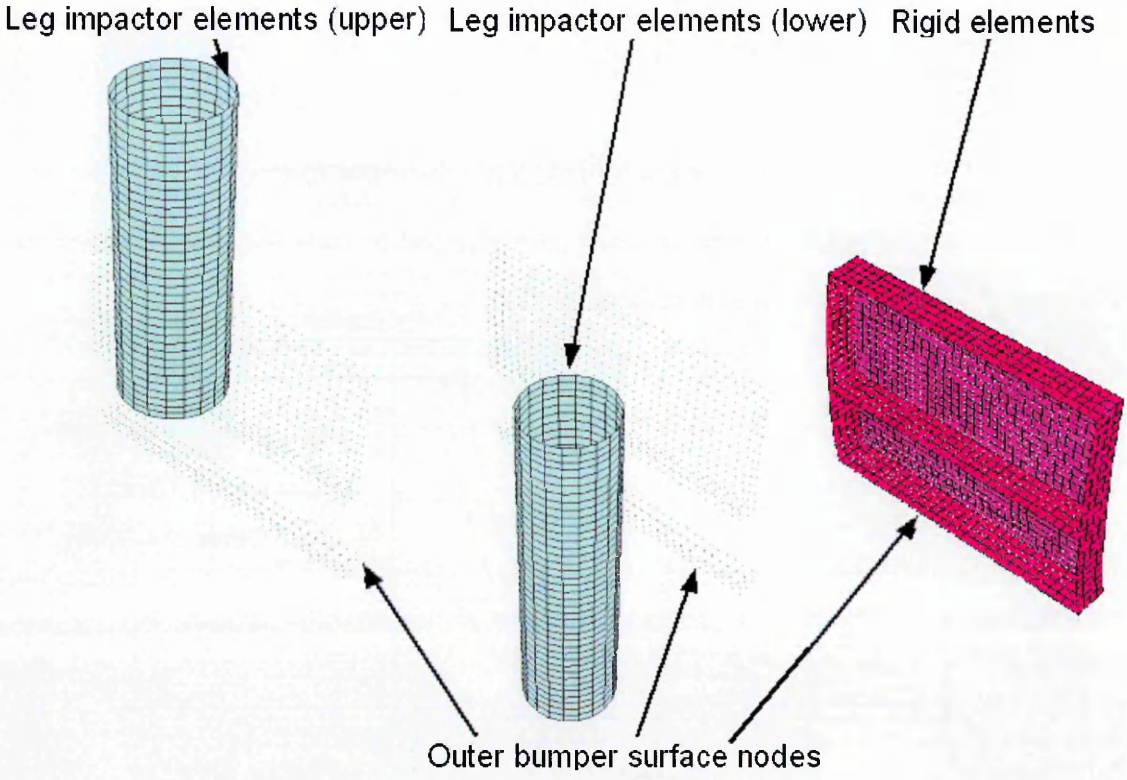

Figure 5.51 Bumper evaluation model contacts

All the contacts used an AUTOMATIC_NODES_TO_SURFACE contact (type a5). In automatic contacts the slave and master surfaces are generated internally by the code and a check is undertaken for penetrating nodes on both sides of the contact surface. A nodes to surface contact was used because the bumper model consisted of many parts that had coincident nodes and if for instance contact type AUTOMATIC_ SINGLE_SURFACE (contact type 13a) had been used then there would have been immediate contact penetrations at time zero between these parts.

The contact card for the upper leg impactor elements to the foam nodes is shown in Table 5.15. The default settings were used in this contact with part set 2 (containing the upper part of the leg impactor) and node set 2 (containing the BUMPER_FOAM nodes) used to define the contact. The contact card for the BUMPER_FOAM to RIGID_GROUND was similar to this with the default values used and a part set and node set defining the RIGID_GROUND and BUMPER_FOAM nodes respectively.

AUTOMATIC NODES TO SURFACE CONTACT CARD
Contact number 6 named Upper leg to foam Slave node set id. 2 Master part set id. 2 Node set id. definition used for the slave set id. above. Part set id. definition used for the master set id. above. No box id. specified for enclosing slave contacts or master contacts Slave side forces are output when database files requested Master side forces are output when database files requested No static coefficient of friction specified (default) No dynamic coefficient of friction specified (default) No normal tensile or shear force failure specified (default). No decay coefficient (default) No exponents for viscous friction or damping (default). Small penetration check off (default) - slave node not switched off if more than one segment thickness penetration. Birth time is zero (default) and death time is zero (default) No scale factors on slave penalty stiffness (default) or master penalty stiffness (default) No override thickness set for slave surface (default) or master surface (default) No override or scale factors on slave surface thickness (default) or master surface thickness (default No coulomb friction scale factors (default) or viscous friction scale factors (default).
*CONTACT_AUTOMATIC_NODES_TO_SURFACE_TITLE 6Upper_leg_to_foam 2 2 4 2 0 0 1 1 0.0 0.0 0.0 0.0 0.0 0 0.0 0.0 0.0 0.0 0.0 0.0 0.0 0.0 0.0 0.0

Table 5.15 Automatic nodes to surface contact upper leg to foam nodes

In the UNDERTRAY to BUMPER_FOAM contact the soft constraint formulation was specified with a recommended scale factor of 0.1 [LS-DYNA 1991-1]. This was necessary because the default contact values were based upon a contact force equation that only held true for materials with a similar Bulk Modulus and this was not true for the UNDERTRAY to impactor lower leg foam contact.

Screening study

Different bumper configurations were examined by varying the foam height, the foam density and foam location. Similar parameters were varied for the undertray. These cases represented a reduced set of bumper configurations and an overview of all the screening study bumper geometries is shown in Figure 5.52.

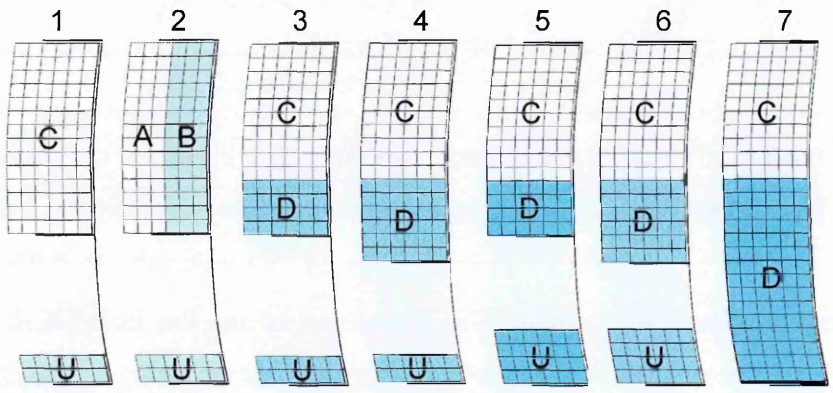

Figure 5.52 Different bumper mesh geometries used in the screening study

Cases 1 to 4 used the reference bumper geometry but the foam and undertray properties were increased or decreased to examine the influence of property changes. In cases 5 and 6 the reference bumper geometry was also used but the bumper foam was vertically divided into two regions A and B with two different foam stiffness combinations. Similarly, in cases 7 and 8 the bumper geometry was also unchanged but the foam was divided horizontally to create two volumes C and D. In cases 9 and 10, and then 11 and 12 the bumper geometry was changed so that the lower edge of the bumper foam and then the undertray were extended into the air intake volume respectively. A combination of both extensions was used in cases 13 and 14 and finally the air intake and undertray were completely replaced with the stiffer foam in cases 15 and 16.

DoE study

Using the screening study results, a number of important bumper configuration factors were identified. In the second stage a DoE was undertaken with the objective of gaining an improved understanding of how these factors influenced the lower leg impactor responses. The factors and levels are shown in Figure 5.53.

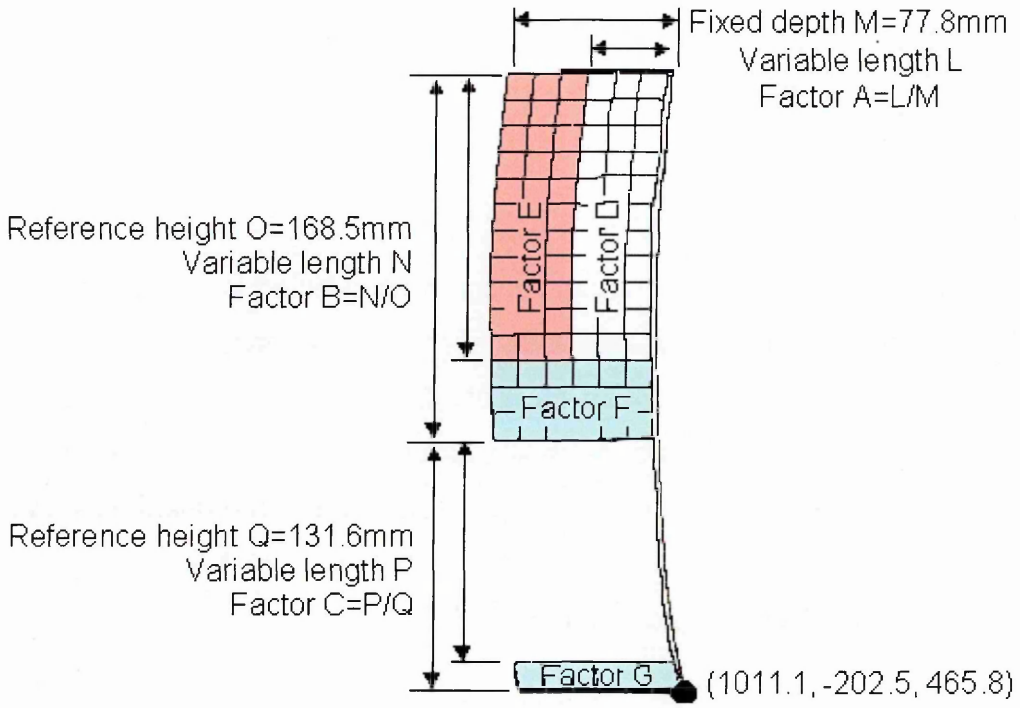

Figure 5.53 Bumper evaluation model factors and factor levels

The construction of the basic model was identical to that of the screening study model except that the total height of foam O and the air intake height Q were not varied. This simplified the DoE and ensured that any optimal configuration could be applied to the C class vehicle whilst satisfying other requirements met by the original geometry (e.g. size of air cooling intake). Unlike the screening study it was not assumed that the undertray should be stiffer or that the bumper energy absorbing capability should be greater than or equal to that of the original bumper. By varying factors B and C the bumper stiffness distribution through the bumper height could be varied. In a similar manner, factor A enabled the stiffness distribution to be varied through the bumper depth. In all cases the range of levels was set to coincide with the element mesh size and limited to less than 1 but more than zero. This meant that only the material cards needed to be changed to match the stiffness ratios and it was not possible to create any cases where the other ratios were not considered.

The three measures or responses used are shown in Table 5.16. Although [EEVC 1998] specified absolute response values, the objective was only to minimise these because the model was not correlated against experimental tests.

Response	Description	Draft directive criteria (EEVC 1998)	DoE criteria
1	Bending angle	15 degrees	Peak value minimised with C180 filter
2	Shear displacement	6 mm	Peak value minimised with C180 filter
3	Tibia acceleration	150 g	Peak value minimised with C180 filter

Table 5.16 DoE responses and objective criteria

Using Statgraphics, a response surface design was selected for the same reasons as in the headlamp DoE. Three response variables, seven factors and three levels for each were also selected. From the default arrays that were offered a face centred Draper Lin Small Composite Design array was chosen because, although it is designed to estimate the entire main effects plus the desired quadratics and two way interactions, it required the least number of experiments. A full factorial design would have required too many experiments (3^7=2187).

The Draper Lin Small Composite Design has two parts: a factorial and a star. The star portion consists of an additional set of points arranged at equal distances from the centre of the (design space) cube on radii that pass through the centrepoint in the face of the cube [Statgraphics 2000]. In this application, the array values were limited to the range of -1 to +1 because this was considered to be the maximum realistic range. The potential disadvantage of this approach was that the array was not orthogonal and therefore there was confounding. This is always a potential problem with such a compact array but in this case it was possible to cross check the results against both screening study and pedestrian accident simulation results. 15 mesh geometries were generated from the array and these are shown in Figure 5.54. The material properties were also varied to create a total of 39 bumper cases.

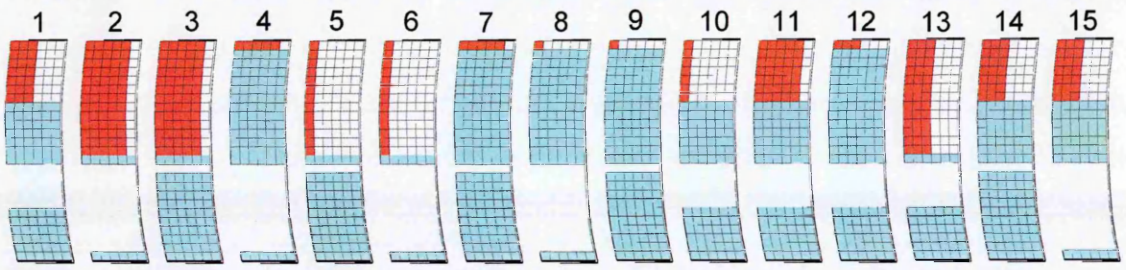

Figure 5.54 The bumper mesh geometries used in the DoE study

Screening study results

In the search for reliable data a number of principles were applied. Shear, bending

angle and acceleration were used to compare bumper designs [EEVC 1998] but less emphasis was placed on the shear because of impactor model reliability concerns [Howard 2000-2]. None of the results was compared to the absolute [EEVC 1998] requirements because no experimental validation was undertaken and as a consequence of this the response values were first ranked and subsequently analysed with DoE tools. The screening study results are shown in Table 5.17 [Howard 2001-3].

Case	FACTORS						RESPONSES		
	Bumper mesh geometry	A: Stress/ strain (% ref.)	B: Stress/ strain (% ref.)	C: Stress/ strain (% ref.)	D: Stress/ strain (% ref.)	G: E (% ref.)	Bending angle (°)	Shear displ. (mm)	Tibia accel. (g)
1	1	N/A	N/A	100	N/A	100	12.3	10.8	423.2
2	1	N/A	N/A	150	N/A	150	16.3	11.4	447.7
3	1	N/A	N/A	50	N/A	50	9.3	10.6	351.6
4	1	N/A	N/A	50	N/A	150	8.5	10.4	372.5
5	2	150	50	N/A	N/A	150	9.3	10.7	373.3
6	2	50	150	N/A	N/A	150	12.4	10.9	431.7
7	3	N/A	N/A	100	150	150	12.9	10.9	408.1
8	3	N/A	N/A	50	150	150	10.7	10.4	421.6
9	4	N/A	N/A	100	150	150	21.6	10.8	537.2
10	4	N/A	N/A	50	150	150	21.3	10.1	529.8
11	5	N/A	N/A	100	150	150	12.9	11.0	606.0
12	5	N/A	N/A	50	150	150	10.4	10.1	593.0
13	6	N/A	N/A	100	150	150	12.9	11.1	574.4
14	6	N/A	N/A	50	150	150	10.9	10.2	555.5
15	7	N/A	N/A	100	150	N/A	21.8	11.1	226.8
16	7	N/A	N/A	50	150	N/A	19.5	10.6	190.1

Table 5.17 Screening study results

The three responses are shown in Figure 5.55, Figure 5.56 and Figure 5.57 respectively. Ranking in Figure 5.58 shows the relative performance of each case.

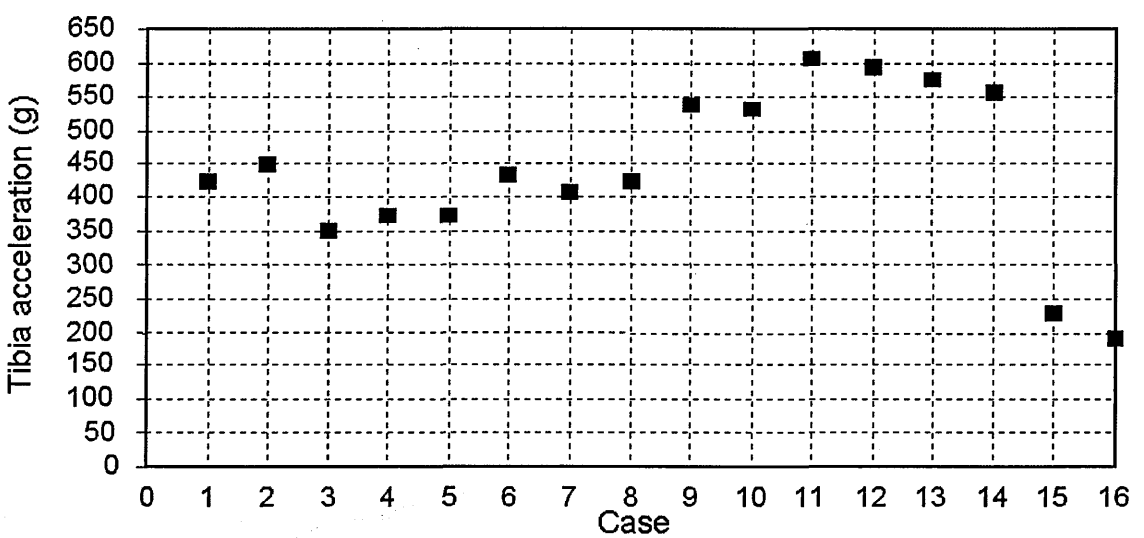

Figure 5.55 Bumper evaluation model tibia acceleration

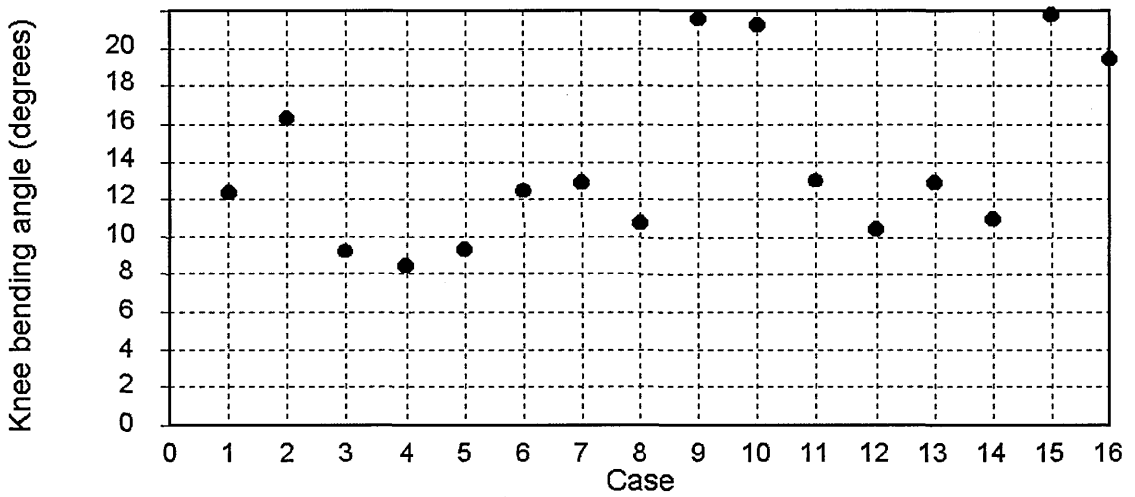

Figure 5.56 Bumper evaluation model knee bending angle

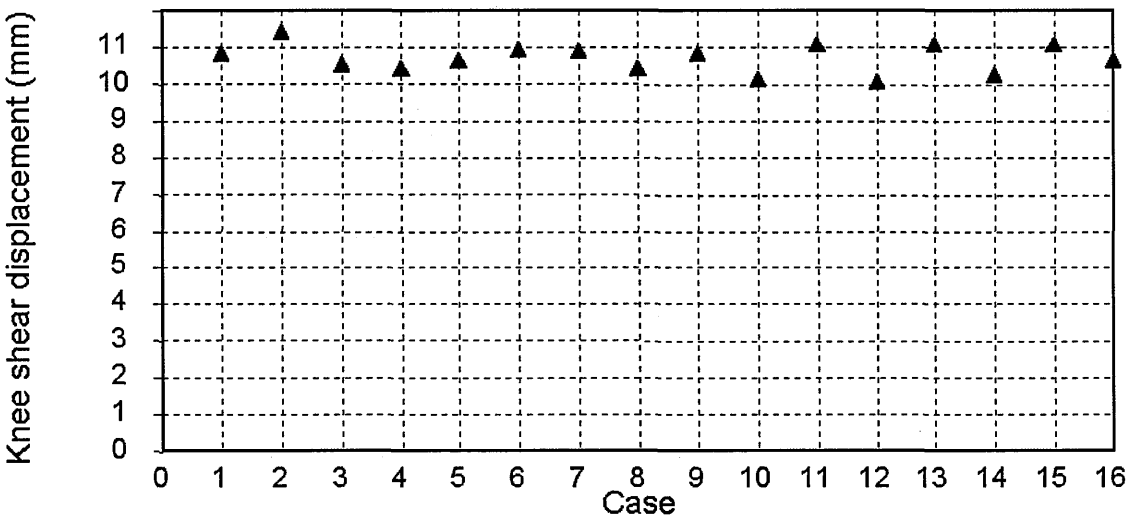

Figure 5.57 Bumper evaluation model knee shear displacement

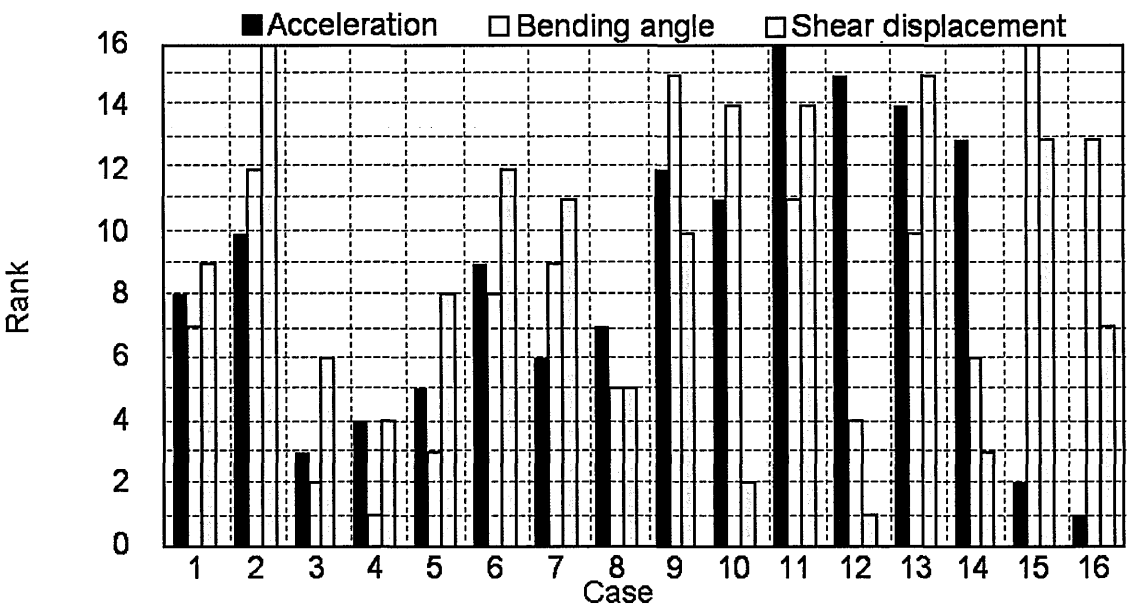

Figure 5.58 Bumper evaluation model response rankings

DoE study results

Case	Bumper mesh geom.	FACTORS							RESPONSES		
		A: Ratio L to M	B: Ratio N to O	C: Ratio P to Q	D: Stress/ strain(%)	E: Stress/ strain(%)	F: Stress/ strain(%)	G: E (%)	Bending angle (deg.)	Shear displ. (mm)	Tibia acc (g)
1	1	0.5	0.5	0.5	100	100	100	100	14.48	9.06	603.16
2	2	0.83	0.93	0.91	150	50	150	150	18.74	9.42	197.34
3	2	0.83	0.93	0.91	50	150	50	150	24.57	9.44	221.43
4	2	0.83	0.93	0.91	150	50	150	50	17.85	9.46	164.48
5	3	0.83	0.93	0.09	50	150	150	50	19.64	9.54	664.72
6	4	0.83	0.07	0.91	150	150	50	150	16.74	9.44	200.65
7	5	0.17	0.93	0.09	150	50	50	150	20.36	8.43	759.63
8	4	0.83	0.07	0.91	50	50	150	50	25.49	9.43	207.73
9	6	0.17	0.93	0.91	50	150	150	50	19.17	9.41	161.83
10	3	0.83	0.93	0.09	150	150	50	150	20.94	9.19	765.54
11	7	0.83	0.07	0.09	150	50	50	50	18.49	9.29	670.72
12	8	0.17	0.07	0.91	50	50	150	150	25.08	9.42	225.15
13	6	0.17	0.93	0.91	50	150	50	50	19.30	9.42	198.39
14	3	0.83	0.93	0.09	150	50	150	50	17.88	9.00	660.48
15	7	0.83	0.07	0.09	50	150	50	50	18.56	9.41	675.98
16	8	0.17	0.07	0.91	150	50	50	50	18.05	9.45	160.66
17	5	0.17	0.93	0.09	50	50	50	150	19.97	7.31	748.47
18	4	0.83	0.07	0.91	50	50	50	150	14.29	9.49	194.35
19	5	0.17	0.93	0.09	50	50	150	150	20.00	7.33	751.50
20	7	0.83	0.07	0.09	50	150	150	150	22.02	8.62	773.72
21	9	0.17	0.07	0.09	150	150	150	150	20.98	9.06	765.83
22	9	0.17	0.07	0.09	150	150	150	50	20.18	9.37	664.81
23	8	0.17	0.07	0.91	150	150	150	150	25.83	9.45	220.65
24	6	0.17	0.93	0.91	150	150	50	50	23.70	9.43	228.23
25	9	0.17	0.07	0.09	50	50	50	50	17.80	8.97	661.68
26	10	0.17	0.5	0.5	100	100	100	100	24.61	9.45	619.51
27	11	0.83	0.5	0.5	100	100	100	100	24.58	9.06	612.74
28	12	0.5	0.07	0.5	100	100	100	100	24.57	9.10	602.60
29	13	0.5	0.93	0.5	100	100	100	100	24.56	9.25	618.23
30	14	0.5	0.5	0.09	100	100	100	100	19.91	8.93	756.70
31	15	0.5	0.5	0.91	100	100	100	100	22.12	9.43	203.61
32	1	0.5	0.5	0.5	50	100	100	100	14.17	8.99	597.68
33	1	0.5	0.5	0.5	150	100	100	100	14.75	9.38	611.30
34	1	0.5	0.5	0.5	100	50	100	100	13.65	9.61	610.58
35	1	0.5	0.5	0.5	100	150	100	100	14.91	9.17	606.36
36	1	0.5	0.5	0.5	100	100	50	100	13.79	9.10	613.44
37	1	0.5	0.5	0.5	100	100	150	100	15.06	9.43	614.94
38	1	0.5	0.5	0.5	100	100	100	50	13.93	9.24	527.38
39	1	0.5	0.5	0.5	100	100	100	150	14.91	9.09	610.89
40	1	0.5	0.5	0.5	100	100	100	100	14.48	9.06	603.16

Table 5.18 Numerical bumper model detailed study DoE array

Figure 5.59, Figure 5.60 and Figure 5.61 show the tibia acceleration, bending angle and shear displacement values for each case.

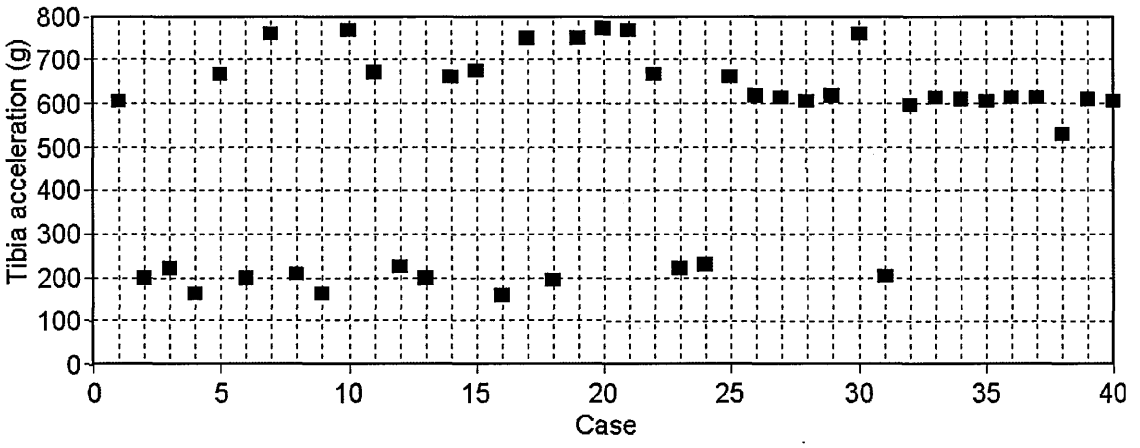

Figure 5.59 Bumper evaluation model tibia acceleration

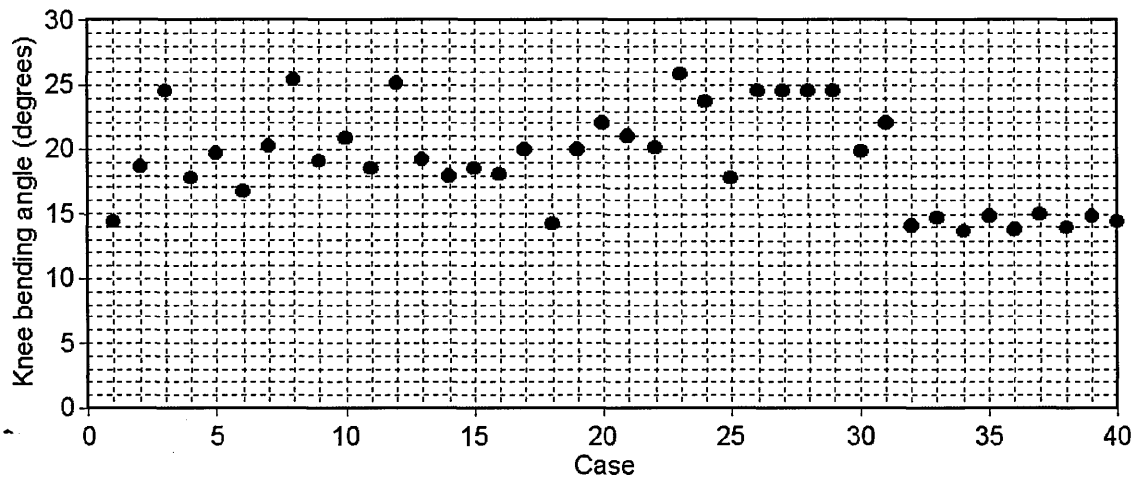

Figure 5.60 Bumper evaluation model knee bending angle

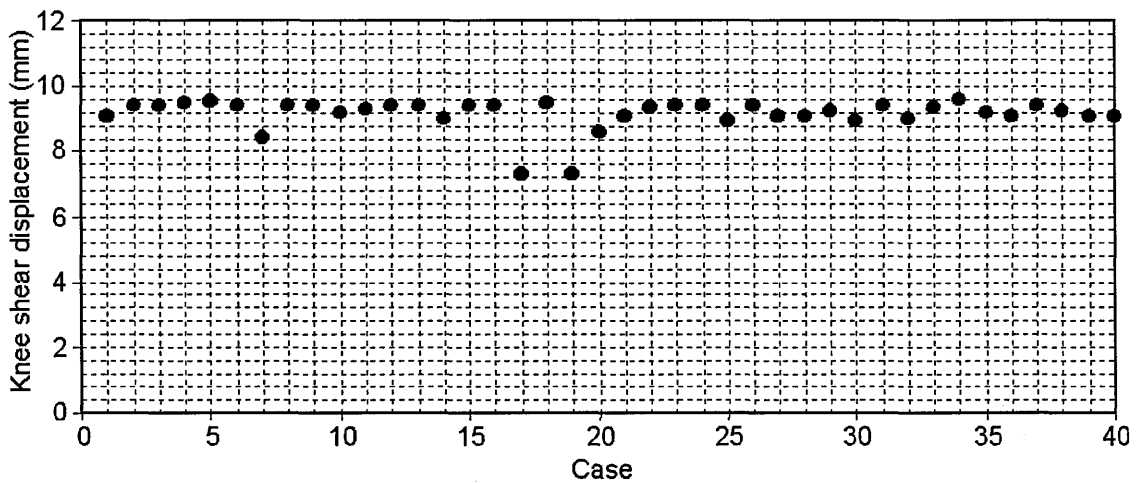

Figure 5.61 Bumper evaluation model knee shear displacement

In a similar manner to the screening stage it was possible to calculate a rank for all the cases. However with 40 cases and three response ranks this was not easily

interpreted and so a total rank was derived for each case using:

Total rank = Acceleration rank + Bending angle rank + Shear rank

A plot of the total rank for each case is shown in Figure 5.62.

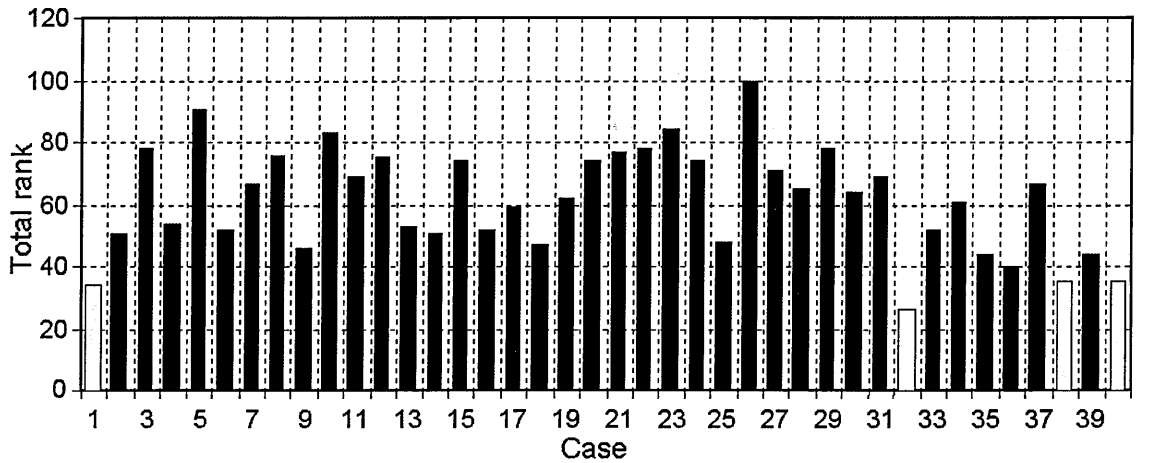

Figure 5.62 Numerical bumper model total rank responses

There were some remaining doubts with respect to the validity of the shear response and therefore the results were also analysed by a partial rank that did not include the shear response rank where:

Partial rank = Acceleration rank + Bending angle rank

A plot of the partial rank for every case is shown in Figure 5.63.

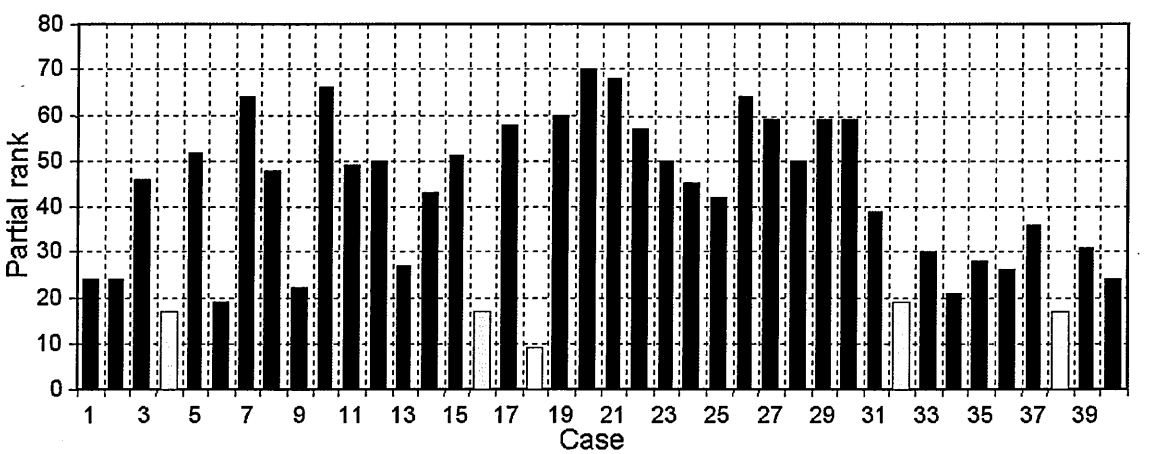

Figure 5.63 Numerical bumper model partial rank responses

Discussion of screening study results

Figure 5.55 showed the tibia acceleration for every screening case. The acceleration values were higher than those observed with production vehicle experimental tests [Howard 2000-2] using [EEVC 1998]. Two possible causes are proposed and these concern the nature of the bumper geometries and the boundary conditions.

The production vehicle test results shown in [Howard 2000-2] were achieved with a bumper that consisted of a flexible bumper cover, a bumper beam and a low stiffness foam between the bumper beam and cover. The part of the cover below the beam was unsupported and the beam was only mounted at the location of the two longitudinals. This meant that the lower part of the cover was very flexible, and in plan view, the centre part of the beam between the longitudinals, was unsupported. During the experimental tests the knee joint impacted the bumper in the central region of the foam and then the lower part of the leg impactor rotated around the knee and against the lower and more flexible part of the cover. Since the tibia acceleration was measured in this part of the leg impactor and the beam was not rigidly mounted, it was possible to achieve relatively low tibia acceleration results. In contrast to this, many of the bumper model geometries were stiffer in the region of the lower leg and immediately behind the foam, the beam was modelled as a rigid boundary. This resulted in higher loading of the lower leg and hence higher accelerations than those observed in [Howard 2000-2].

As might be anticipated (because of the even impactor loading and the removal of the stiffer undertray) the lowest acceleration results were obtained with the replacement of the complete bumper volume with foam in cases 15 and 16. The closest results to these were obtained by using single lower stiffness foam in cases 3 and 4. Marginal improvements over the reference case were achieved in cases 7 and 8 in which horizontally split dual stiffness foams were used, although lowering the upper part foam stiffness marginally increased the acceleration. This was caused by higher levels of compression in the high stiffness foam of case 8 and hence rapidly rising force levels at the measurement location, rather than distributed

between the lower and upper parts of the leg impactor.

Good results were obtained with case 5 in which vertically split dual stiffness foams were used with higher stiffness foam on the struck side. When lower stiffness foam was used on the struck side, as in case 6, the acceleration was higher than for the reference case. It is proposed that this was caused by the manner in which the foam progressively compressed. In case 6, the low stiffness foam was compressed first and absorbed relatively little energy until the high stiffness abruptly slowed down the compression. However, in case 5, there was relatively high initial energy absorption and almost immediate transfer of some of the impact energy into the lower stiffness foam. This led to more constant energy absorption with lower acceleration peaks. With the higher stiffness foam (D) extended into the air intake volume in cases 9 and 10 and even when this was combined with lower stiffness foam C, the acceleration was increased still further. The same trend was observed with cases 11 to 14 where the undertray was extended into the air intake region and then, in addition, higher stiffness foam D was used.

The results confirmed that replacing the complete bumper volume with two volumes of foam in cases 15 and 16 would reduce the tibia acceleration and this acted as a check on the expected system response at an extreme end of the design possibilities. The results also showed that the foam stiffness in the region of the tibia acceleration measure had a large influence on this measure and that the undertray in the smallest height configuration had a minor impact on this measure.

Figure 5.56 showed the bending angle results and all of these were within the range expected as compared to [Howard 2000-2]. The lowest bending angle results were achieved in case 4 that utilised lower stiffness foam and a stiffer undertray. This was closely followed by the bumper configurations used in cases 3 and 5. In case 3, single low stiffness foam was used with a weak undertray and as already described, case 5 utilised dual stiffness foam. Case 4 had similar geometry to case 3 but achieved a slightly lower bending angle because of the stiffer undertray. The bumper used in case 12, which utilised an extended and stiffer undertray, a higher

stiffness foam D and lower stiffness foam C gave the next lowest bending angle. This was closely followed by case 8 that was identical except that the undertray was not extended into the air intake region. Case 14 also provided similar bending angle results with identical material conditions to cases 8 and 12 but with extensions to both foam D and the undertray into the air intake region. All the other cases provided comparable or larger bending angles than the reference case. Of particular note were the highest bending angles with cases 9 and 10, where foam D was extended into the air intake and cases 15 and 16, where the whole bumper volume was replaced with foam. In contrast to this, cases 15 and 16 provided low tibia acceleration results. Single higher stiffness foam in case 2 led to a much larger bending angle than the reference case. In the final cases 11 and 13, higher bending angles than in the reference case were obtained when volume D was simply made stiffer and/or deeper with no changes to the stiffness of volume C but with a deeper undertray.

The bending angle results showed the benefits of a stiffer or an extended undertray and also that these benefits depended upon the stiffness distribution of the bumper foam. In certain cases, these features may increase the acceleration. The foam and undertray need to be matched to meet both acceleration and bending requirements.

Figure 5.57 showed a smaller than expected range of shear displacement values and highlighted a potential problem with this measure. Despite these concerns it was interesting to note that the lowest shear values were obtained with cases 4, 8, 10, 12 and 14. All of these used lower stiffness foam C, higher stiffness foam D (except case 4) and a stiffer undertray. The largest shear values were obtained in cases 2, 11, 13 and 15 where foam C either had an identical stiffness to the reference case or was stiffer. All other cases fell within this small range of variation.

Figure 5.58 showed that case 4 provided the largest overall performance benefit (as indicated by the shortest columns) followed by cases 3, 5 and 8. These represented bumper mesh geometry models 1, 2 and 3 as shown in Figure 5.52. The factors used in the DoE study were chosen to accommodate these mesh geometries.

Discussion of DoE results

The first observation from Figure 5.59 was that the results were concentrated into two groups. The lowest acceleration responses were obtained in cases 2, 3, 4, 6, 8, 9, 12, 13, 16, 18, 23, 24 and 31. These utilised geometries 2, 4, 6, 8 and 15 where the height of the air intake was maximised and the height of the undertray minimised (i.e. the ratio of P to Q was high). Within this group, marginal improvements in the acceleration responses were achieved in cases 4, 9 and 16 where the undertray had a lower Youngs Modulus. Both of these observations had also been made in the screening study.

The bumper configurations in cases 1, 18, and 32 to 40 all provided smaller bending angles as shown in Figure 5.60. With the exception of case 18 the geometric ratios L to M, N to O and P to Q were 0.5. In case 18 the upper bumper volume consisted of low stiffness foam with a high stiffness undertray. Similarly, small bending values were achieved in the screening study for this type of configuration. Marginally smaller values were obtained in cases 34, 36 and 38 where the values of factors E, F or G were equal to or less than the reference.

As with the screening study and shown in Figure 5.61, there was a small range of shear displacement values. However, the shear values in cases 17 and 19 where bumper geometry 5 was used, were significantly lower. The ratio of P to Q was small, such that the air intake height and the majority of the upper foam stiffness were minimised in combination with a high stiffness undertray.

On the basis of the ranking values shown in Figure 5.62 and an arbitrary cut off line of 40, cases 1 (40), 32 and 38 had the lowest totals and therefore the highest overall performance, as measured by the sum of all the ranks. However, in order to evaluate the overall ranking without the influence of the shear displacement ranking, the partial ranking values shown in Figure 5.63 indicated that cases 4, 6, 16, 18, 32 and 38 achieved the best overall ranks. The best performing cases were reduced to 2 types of design: multiple stiffness foam with an extended undertray and a single low stiffness foam design with a high stiffness undertray.

Figure 5.64 was constructed in Statgraphics to show the standardised effect of every factor and interaction on the tibia acceleration.

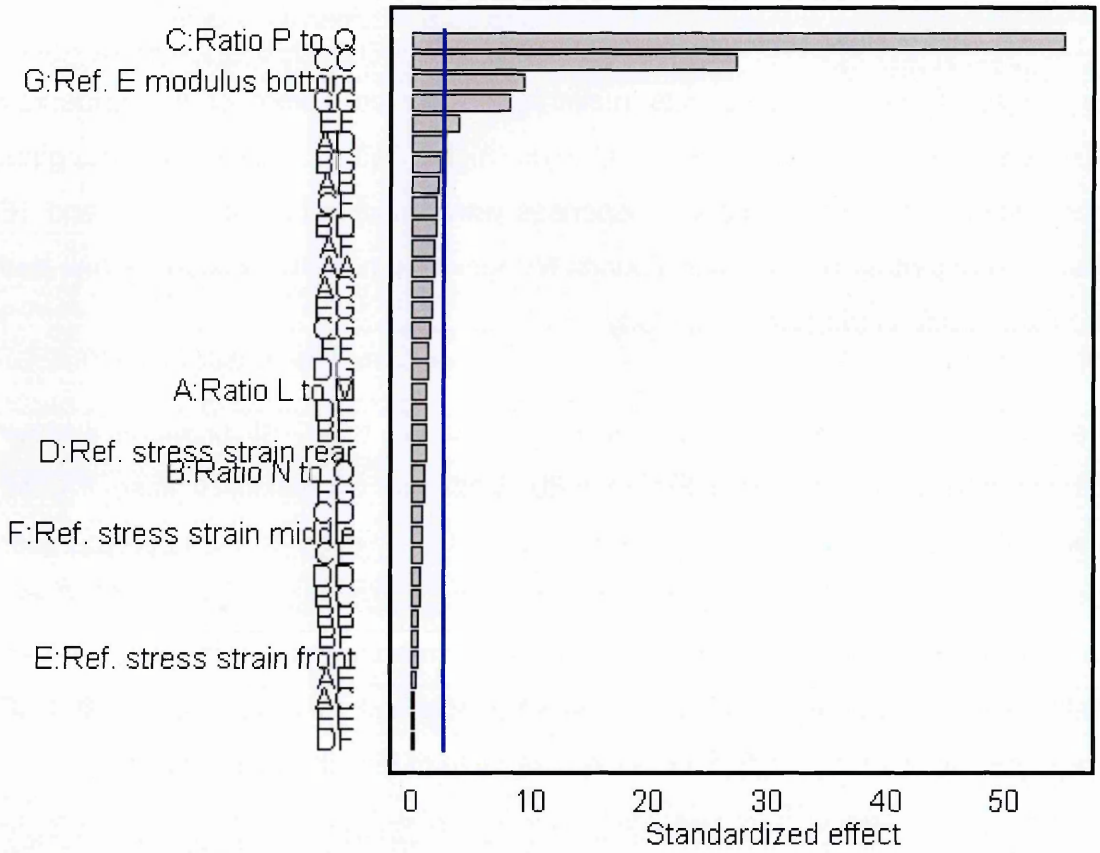

Figure 5.64 Pareto chart for tibia acceleration

The ratio of P to Q and the undertray stiffness were the most significant factors, the quadratic components of these factors CC and GG and the interactions CG, EF and AD at the 95% confidence level were also significant. This indicated that only the factors of the P to Q ratio and undertray stiffness were significant and that they were also highly non linear because of their quadratic components. Strong interaction effects existed between the ratio P to Q and the undertray stiffness, the middle and front foam stiffness, and the ratio L to M and the rear foam stiffness.

Figure 5.65 shows the influence of changes in the main effects on the tibia acceleration. Changes to the levels of the ratio P to Q and the undertray stiffness had a larger influence on tibia acceleration than the other factors. A high P to Q ratio and a low (but not the lowest) stiffness undertray led to the lowest tibia acceleration.

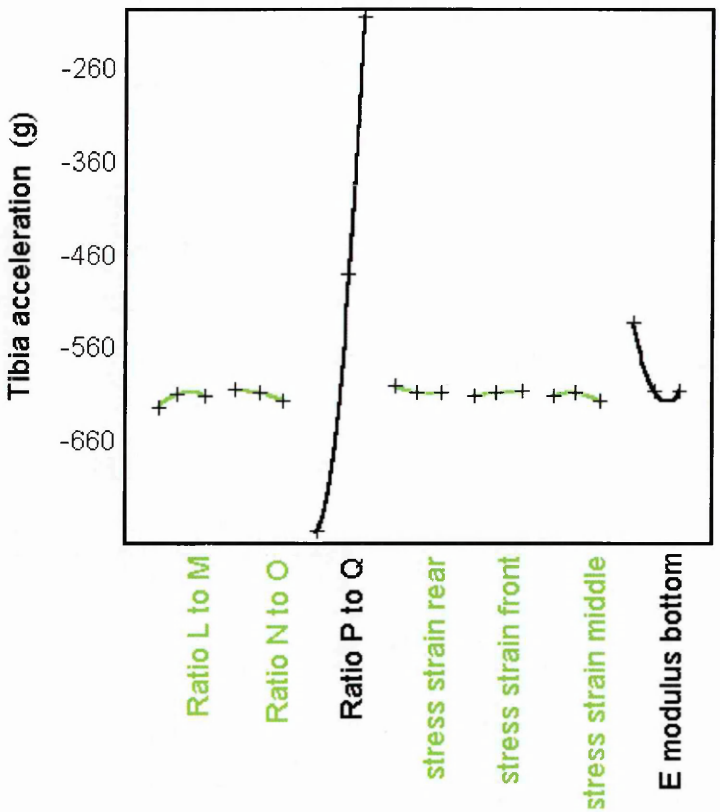

Figure 5.65 Main effects graph for tibia acceleration

Figure 5.66 shows a similar graph for the interaction effects.

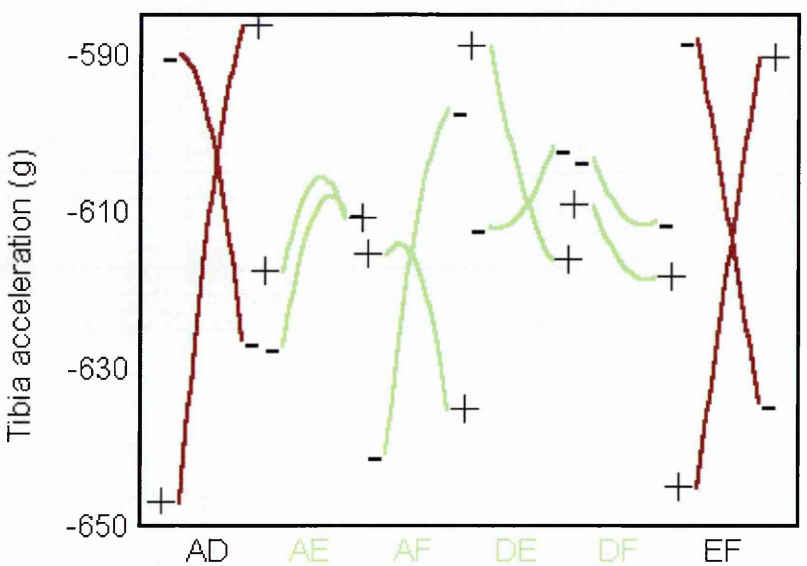

Figure 5.66 Interaction effects graph for tibia acceleration

In the AD interaction, if the rear foam was stiff, then the ratio L to M had a greater effect on the acceleration response. When the ratio L to M was increased and D had a lower stiffness, then the acceleration response was lower. Replacing the

vertically split foam with a single low density foam minimised the acceleration. This was because the combined stiffness of the split foam was higher than that of the low density foam. For the EF interaction, if the middle foam stiffness was high, then higher front foam stiffness led to lower acceleration. In this case, the impactor energy was uniformly absorbed through the bumper height with similar foam compression. This indicated that locally stiff regions on the struck side, in the region of the acceleration measure, should be avoided.

The Pareto chart for the bending angle response is shown in Figure 5.67.

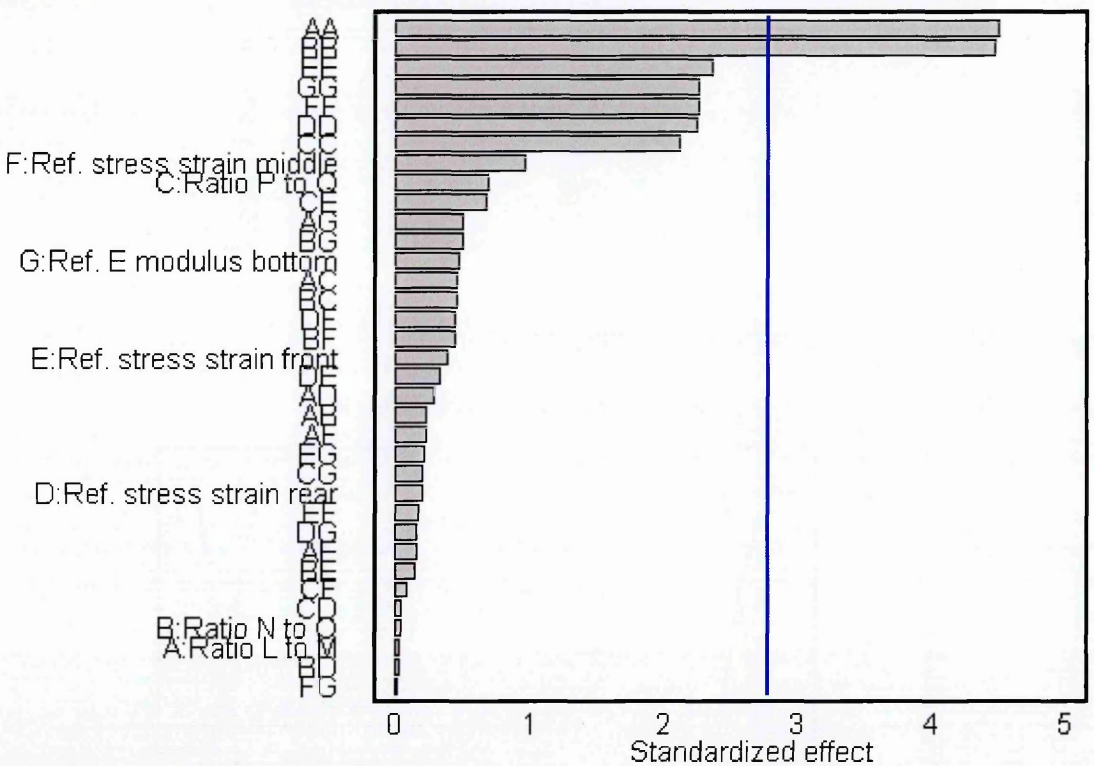

Figure 5.67 Pareto chart for bending angle

There were no significant linear factors at the 95% confidence level but the quadratic effects of AA and BB were significant. This indicated that the effects of both the ratio L to M and the ratio N to O on the angle were highly non linear. Normally, high order effects are less significant than main effects [Ford 2001-2].

The influence of changes to the main effects on the bending angle is shown in Figure 5.68. This was difficult to interpret because only the higher order components of the ratios L to M and N to O were significant. However, there

appeared to be a minimum bending angle response for central values of these ratios. There were no significant interactions and therefore they were not examined.

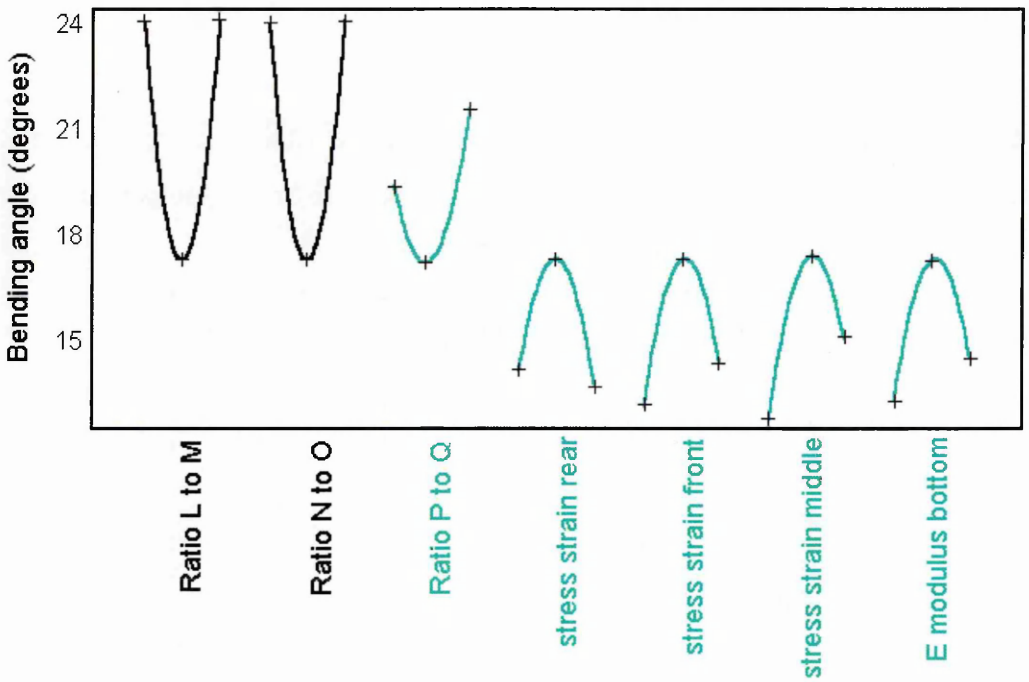

Figure 5.68 Main effects graph for bending angle

Figure 5.69 shows the Pareto chart for shear displacement.

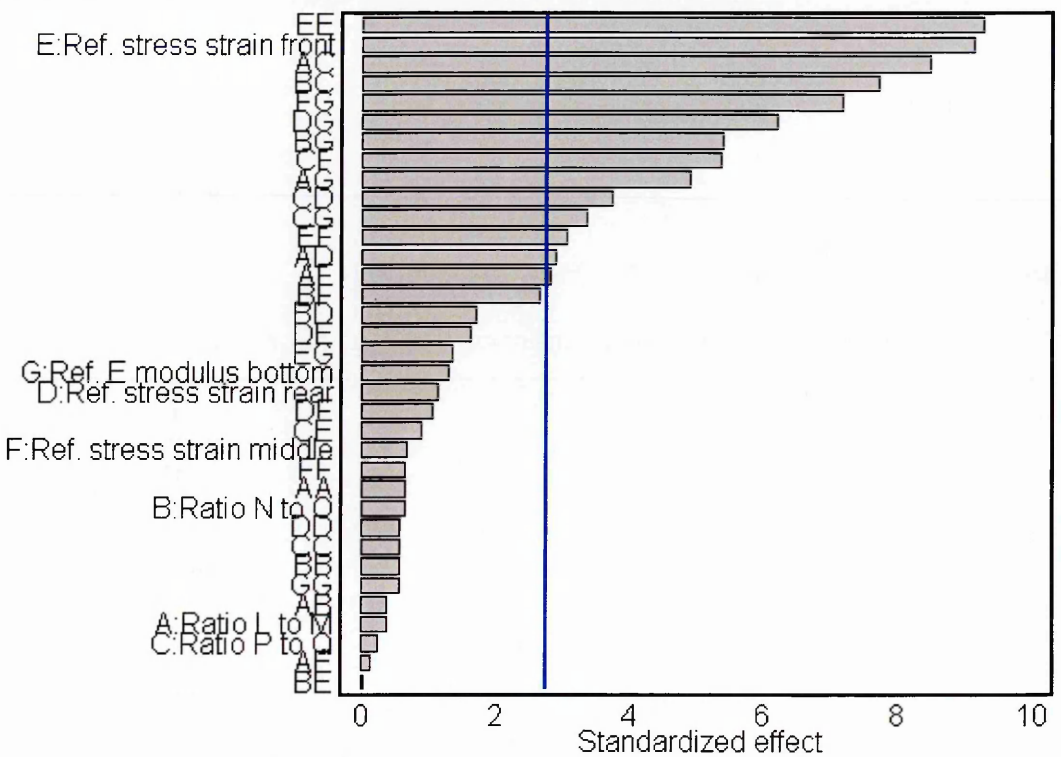

Figure 5.69 Pareto chart for shear displacement

The only significant main factors at the 95% confidence level were the front foam stiffness, the quadratic component EE of this factor and the interactions AC, BC, FG, DG, BG, CF, AG, CD, CG, EF, AD and AE.

Figure 5.70 shows the influence of changes to the main factors on the shear displacement. Lower foam stiffness on the struck side minimised shear but when the stiffness was too low the shear value increased again.

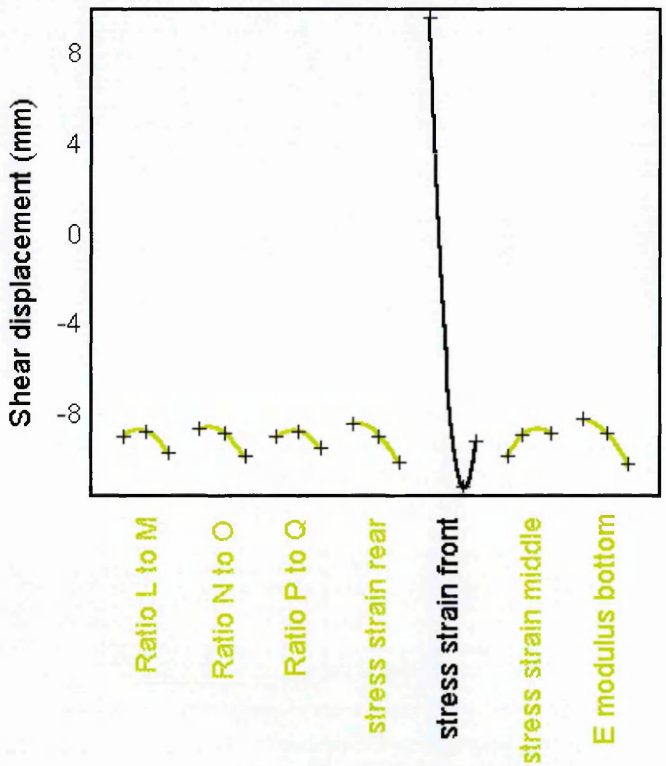

Figure 5.70 Main effects graph for shear displacement

The most significant interaction effects are shown in Figure 5.71.

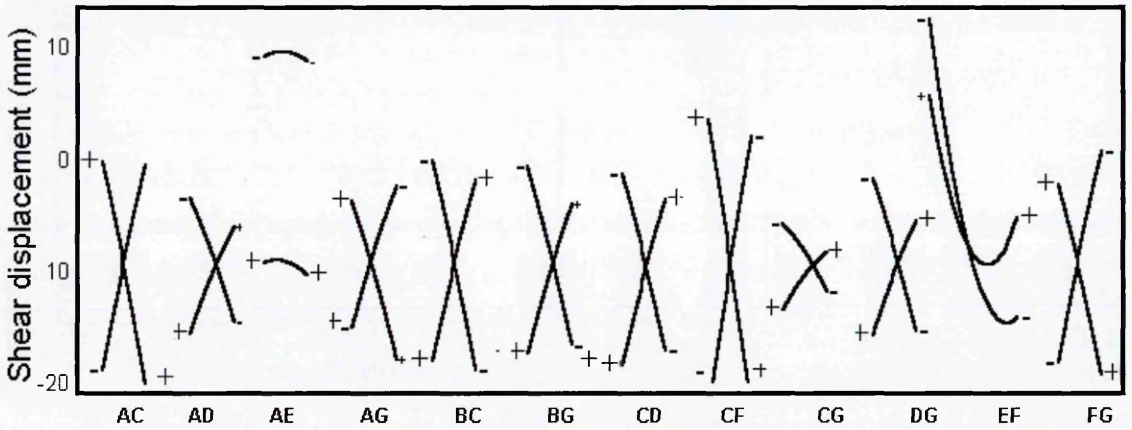

Figure 5.71 Interaction effects graph for shear displacement

The reliability of the shear displacement was uncertain and therefore it was not constructive to undertake a detailed analysis of all these interactions. However, it was clear that there were many significant interactions and no clear pattern of influence on this response.

Using the multiple response optimisation facility offered in Statgraphics and by seeking to minimise the tibia acceleration and bending angle responses the optimal solution was determined for each factor as shown in Table 5.19. The shear displacement response was not used because of the reliability concerns.

Factor	Low	High	Optimum
A: ratio L to M	-1.0	1.0	-0.461791
B: ratio N to O	-1.0	1.0	-0.901943
C: ratio P to Q	-1.0	1.0	0.999952
D: stress / strain rear foam (%)	-1.0	1.0	-0.895426
E: stress / strain front foam (%)	-1.0	1.0	-0.889301
F: stress/ strain middle foam (%)	-1.0	1.0	-0.958294
G: Youngs Modulus undertray (%)	-1.0	1.0	0.962183

Table 5.19 Bumper evaluation model optimum levels

The optimal bumper, for this loading condition and the measured responses, was a single low stiffness foam bumper with a stiff and small undertray.

Although the study provided sufficient information to determine at least two effective bumper designs, there were some limitations to the study. The DoE array generated extreme simulation cases in which only single rows of foam elements were defined with a different material property and the behaviour of such elements may not have been valid under some loading conditions (e.g. bending loads). Also the main factors and interaction effects were difficult to interpret and using such a compact array (39 instead of 2187 simulation runs) may have led to this problem.

From a modelling perspective, much of the vehicle structure that could have influenced the bumper stiffness was not modelled. However it was assumed that the same trends would be valid with or without, for instance, the bumper cover. Due to the load spreading effect of the bumper cover, it is likely that it would reduce the benefits of multiple density foam but not eliminate them. A particular weakness of the study was that it only provides general trends that are applicable to limiting the

leg impactor responses and not actual pedestrian injuries or other requirements. This means that the optimum solution of a very low density foam and stiff undertray is not necessarily a feasible solution if other performance criteria, for example, low speed damageability requirements, are considered.

Conclusions

Tibia acceleration is strongly influenced by the size of the air intake and to a lesser extent the undertray stiffness. The lowest acceleration is obtained with the largest air intake and the lowest undertray stiffness. Replacing the complete bumper volume (i.e. no air intake or undertray) with low stiffness foam significantly reduces tibia acceleration. Vertically dividing the upper foam volume into low and higher stiffness foam on the struck side is beneficial but not optimal for the one load condition considered (i.e. for the impactor requirements but not for low speed damageability, for instance). Low stiffness upper volume foam was optimal for this load condition but a multiple bumper foam construction is likely to be necessary to maintain the total energy absorbing capability.

Unlike the tibia acceleration, the bending angle is maximised when the complete bumper volume is replaced by low stiffness foam. However, the bending angle is reduced if a stiffer undertray or a vertically split foam is used. The DoE results were difficult to interpret because only the higher order components of the ratios L to M and N to O were significant. However, the model predicted that both of these should be close to 0.5 to minimise the bending angle.

There are some concerns with regard to the reliability of the shear displacement measure. However, assuming that the measure is valid for indicating general trends, shear displacement is minimised with a stiffer undertray and a horizontally split upper foam with a high stiffness foam in the lower part, and a lower stiffness in the upper part. For vertically split foam the struck side foam stiffness should be low to minimise shear displacement.

With consideration given to these observations a vertically split foam bumper with a higher density foam on the struck side and a stiff undertray (but not too stiff so that

tibia acceleration is acceptable) provides good pedestrian protection performance, whilst providing the possibility of meeting other bumper requirements.

5.6. Pedestrian protection hood kinematic system (PEHKS)

5.6.1. Biomechanical models of PEHKS

There are two main impact events between a pedestrian and vehicle hood during a pedestrian accident; first the contact with the hood leading edge and second the contact with the main hood structure. In the first impact, similar types of injuries to those received from a headlamp may be expected, because headlamps are typically positioned at the same height as the hood leading edge. Potential femur, pelvis and abdomen injuries have already been described for the headlamp technology and a similar range of injury mechanisms might be expected for the hood technologies. With regard to the second impact, a variety of pedestrian body regions may come into contact with the main hood structure. However, the most important type of impact involves the head, because they are more likely to cause serious or life threatening injuries [EEVC 1998]. Figure 5.72 shows the loading of the adult femur, child pelvis and/or abdomen and the child or adult head.

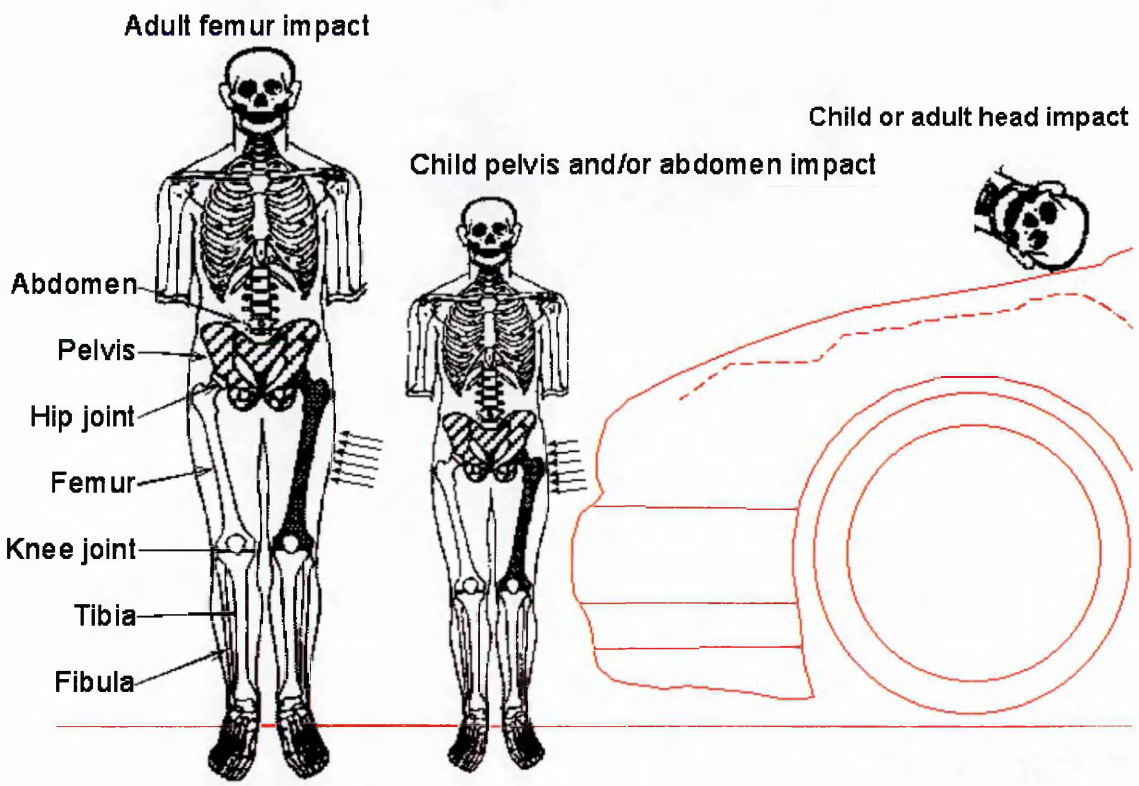

Figure 5.72 Adult and child hood impacts

The head is a division of the body that includes the skull, brain, eyes, nose, ears and mouth. Most of the research concerned with pedestrian head injuries focuses on brain injury as implied by the use of the head injury criteria (HIC) that was developed to predict such injuries. In [Bodyworks 6.0] the brain is described as ".....the primary mass of nerve tissue of the central nervous system. It is located in the cranium and its principal structures are the cerebrum, the cerebellum, the pons, the diencephalon, the midbrain, and the medulla oblongata. Nerve pathways extend from the brain to virtually every tissue and structure of the body".

A conceptual view of the direct impact between the hood and head at a point in time is shown in Figure 5.73.

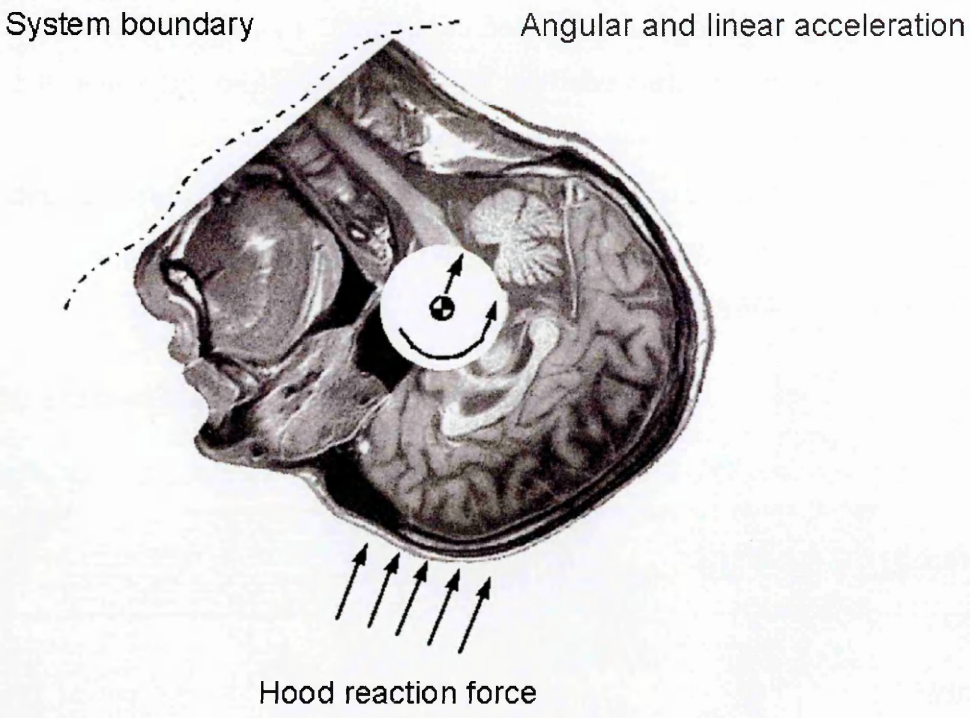

Figure 5.73 Conceptual view of the adult head loading condition

As observed in sub system impactor tests [Howard 2000-2] the hood stiffness and inertia alone may generate decelerations as the hood deforms, that are high enough to cause serious injuries (as indicated by HIC) even without later contact with engine hard points.

Thomas [Thomas 1984] provides a succinct description of potential head injuries. "Local or remote deformations of the skull cause local and remote compressive, shear and tensile strains in the underlying skull and brain while shock waves that emanate from the impact point travel through the skull and brain adding to these strains. The resultant can be the skull fractures, contusions (general damage to the brain matter) and most hematomas" (bleeding injury). "Inertial forces are generated by acceleration or deceleration of the head as it is set into motion or stopped from moving" and "The concussive injuries, prolonged coma without hematoma (diffuse axonal injury) and subdural hematoma are the injuries solely due to acceleration of the head". "Since clinical situations often include both head contact and head movement, clinical injuries are rarely pure and most often patients suffer both contact injuries and acceleration injuries".

With respect to injuries and the influence of the vehicle design, it is assumed that reducing the magnitude of the force pulse between the hood leading edge and an adult femur, child pelvis or abdomen will reduce the severity of injuries to these body regions. It is also assumed that reducing the magnitude of the force pulse between the hood and a child or adult head will reduce the severity of brain injuries.

5.6.2. Description of mechanically deployed hood systems

PEHKS is a mechanically deployed hood system [Howard 2001, 2001-6]. The objective of all such technologies is to reduce the magnitude of these hood force pulses by using the pedestrian impact energy to give a controlled rearward and upward displacement of the complete hood under predefined impact conditions. The underlying assumptions are that:

- The alternative and conventional hood leading edge structure collapses in an uncontrolled manner that leads to an unacceptably large force pulse
- There is insufficient clearance between the hood and underlying rigid structure and hence the head to hood force pulse is unacceptably large

A mechanically deployed hood should be able to control the motion of the hood leading edge in a manner that reduces both the magnitude of the force pulse and increases the contact time. It may also be possible to absorb more energy than a

conventional hood structure so that the subsequent head impact is less severe. An inherent assumption is that the inertial forces plus any structural breakaway forces (i.e. to release structural parts that allow the hood motion) are lower than the force pulse target. During the head impact it is assumed that in addition to the hood providing sufficient clearance when deployed it is also light and flexible enough not to generate unacceptable head accelerations. Figure 5.74 shows a comparison between a conventional and mechanically deployed hood.

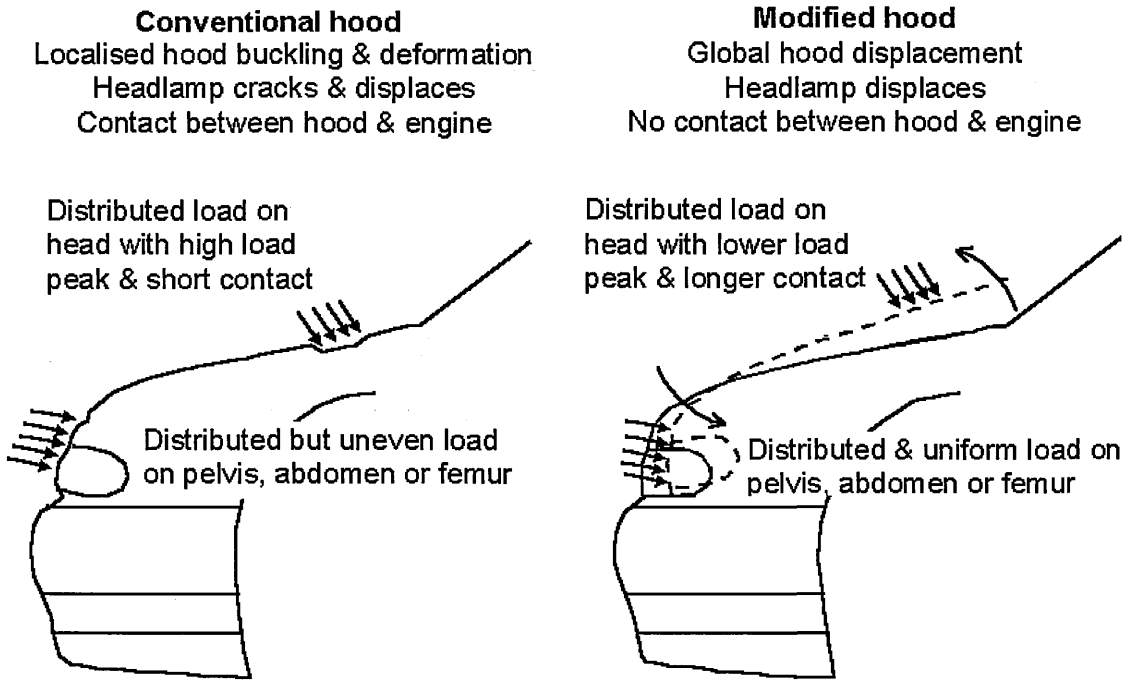

Figure 5.74 Conventional and mechanically deployed hood

The exact design of the pedestrian protection hood system is dependent on the vehicle geometry and this is a concept that needs to be translated into a specific design for a specific vehicle. Two designs are described here: the first is based on a B class car in [Howard 2001] and the second based on an interpretation of this concept as applied to a C class car [Howard 2001-6].

Figure 5.75 shows a CAD model of the mechanically deployed hood that was created in Master Series v8.0 for the B class car [Howard 2001].

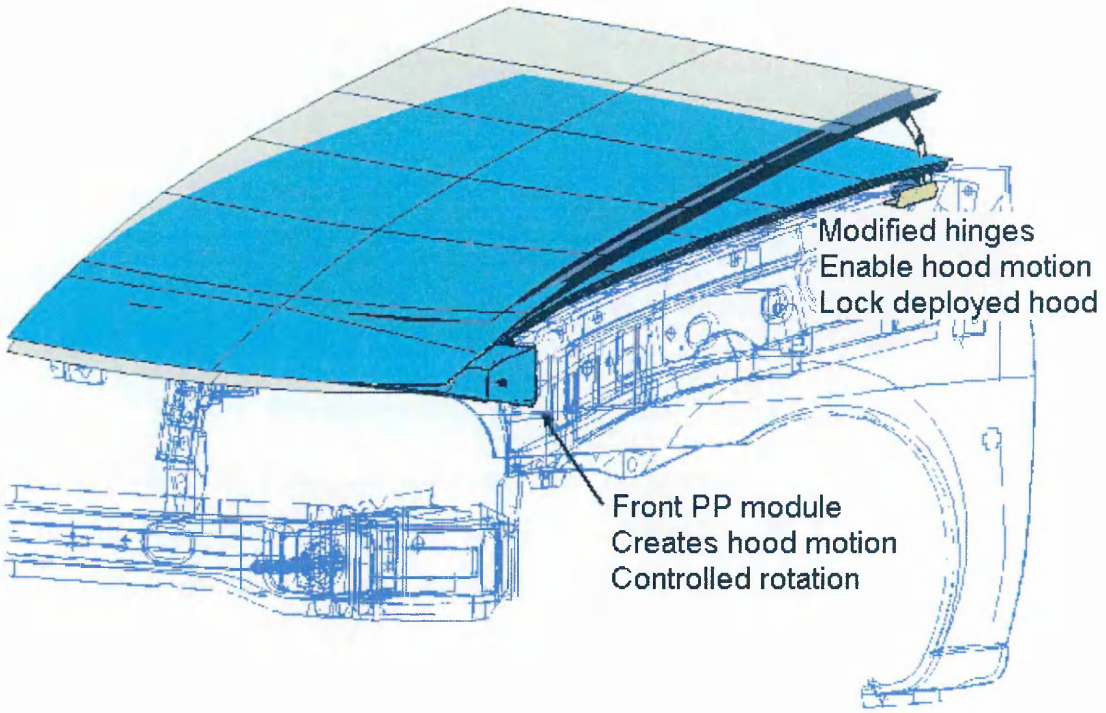

Figure 5.75 CAD model of the PP hood module device

The latch platform crossmember is used as a front end module by mounting it to rotational and eccentric joints that allow it to rotate during a predefined loading condition that would occur in a pedestrian impact. The rotation of the module is transferred into the hood lifting motion via bump stops and the rear hinges are designed to allow this motion to occur. At a certain lift height the rear hinges move into an over centre condition and lock the hood in its deployed position in preparation for the pedestrian head impact.

Upper leg impactor simulations of the sub system impactor test procedure were undertaken with a C class car [Howard 2000-2] and an analysis of the results led to the creation of a new mechanically deployed hood design. This vehicle has a large front end module (GOR or grille opening reinforcement) that carries the headlamps and cooling pack. During sub system impactor simulations it was noted that the GOR, headlamps and the hood tended to rotate together as shown in Figure 5.76 in a similar manner to the previous front end module. Furthermore this provided a small but significant amount of hood lift.

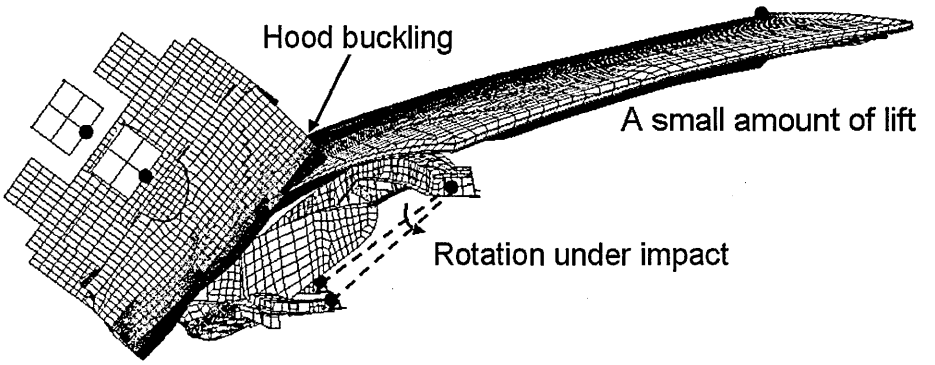

Figure 5.76 GOR motion in an upper leg impactor simulation

This observation was later developed into the hood technology [Howard 2001-6] shown in Figure 5.77 by first determining the desired hood motion, secondly identifying which components below the hood could be moved, and finally optimising the position of the component mounting conditions [Howard 2001-4].

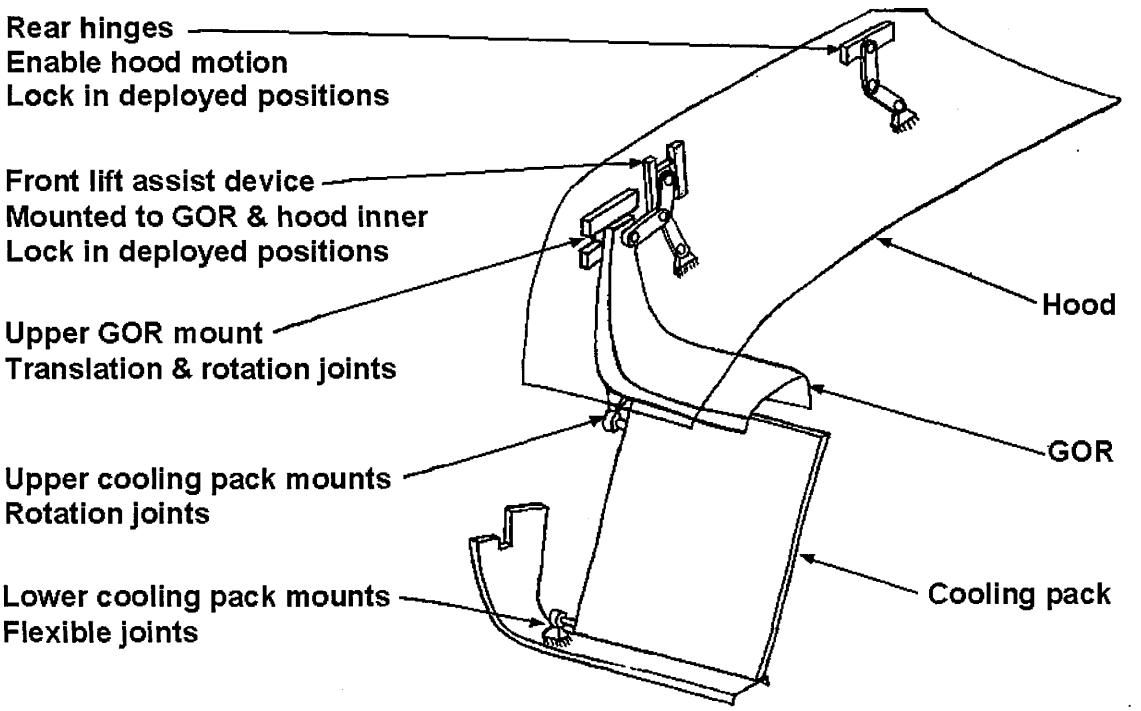

Figure 5.77 An overview of PEHKS

In this initial design and during a pedestrian impact, the GOR moves rearward and upward. This motion can occur because the lower GOR supports are released, the cooling pack is designed to rotate rearward, the upper GOR is guided in a mounting joint and the rear hinges are designed to allow this lifting motion. The lifting mechanism at the front was designed to aid the hood lift process, especially in the

child head impact region of the hood.

5.6.3. Analytical models of mechanically deployed hood systems

Two basic analytical models were created to gain a better understanding of some aspects of the mechanically deployed hood systems. Figure 5.78 shows the first pedestrian protection technology and more particularly the front module in the undeployed and deployed positions.

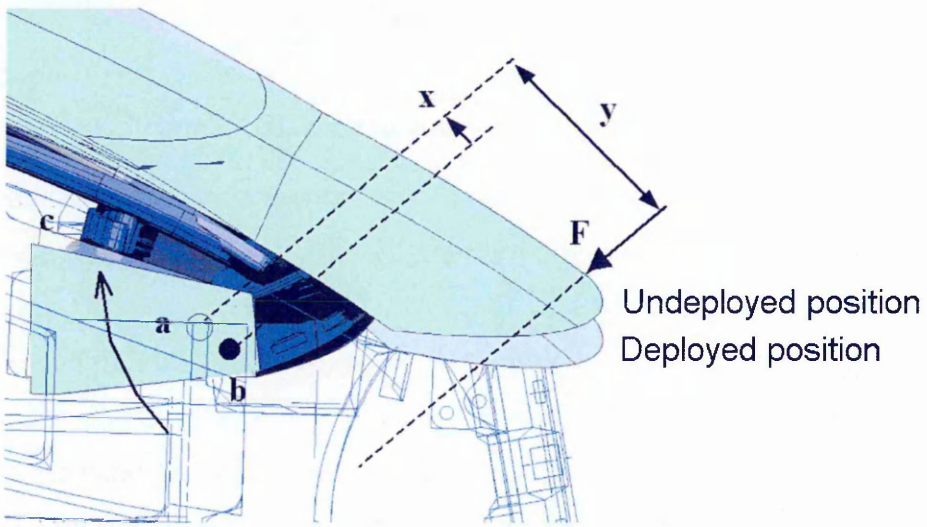

Figure 5.78 Undeployed and deployed positions of the front module

As a vehicle collides with a pedestrian, the vehicle experiences an impact force F(t) and this is a product of the effective pedestrian mass in contact with the vehicle and the deceleration at this point on the hood leading edge, at any point in time. Discounting any additional inertial effects this imposes a moment on the module about the pivot, 'a', that is resisted by the shear pin, 'b'. At a particular point in time the moment on the module is the product F.y and this is resisted by the shear pin which experiences a force F(y/x) where 'x' and 'y' are the instantaneous moment arms (i.e. the leading edge will deform). The shear pin may be designed in a variety of configurations to fail at the force F(y/x) and hence allow the module to freely rotate. The failure of the shear pin leads to a controlled collapse of the hood leading edge whilst transferring the rotation (e.g. 6°) through the bump stop 'c' into the hood inner panel. This imposes a moment into the complete hood, which is then transferred into the hinges as shown in Figure 5.79 for the undeployed and deployed conditions.

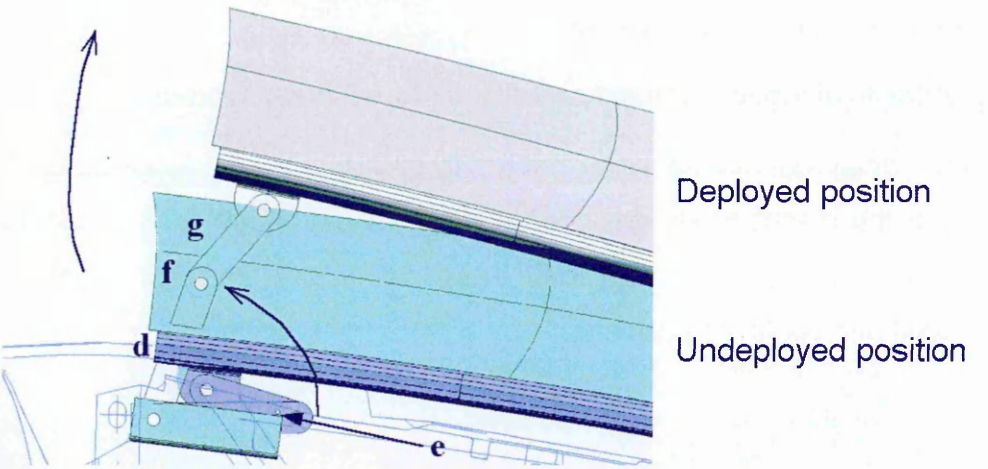

Figure 5.79 Undeployed and deployed positions of the hinge

The rear hinges are restrained to move in their normal operation by shear pin, 'e'. As a consequence of the imposed moment the shear pin fails at a predetermined moment and allows the hinges to fold out and accommodate an upward hood displacement. In this example, the target displacement was 100 mm but this can be tuned according to the chosen geometry. Hinge arm 'd' rotates anticlockwise until hinge arm g moves over centre about pivot 'f' into the locked position as shown. The hood is now locked in its deployed position by a rotational stop on pivot 'f' that may take the form of a rotational spring damper for the subsequent head impact.

The application of this concept to the C class vehicle is now described. Figure 5.80 shows the first level of analytical model construction.

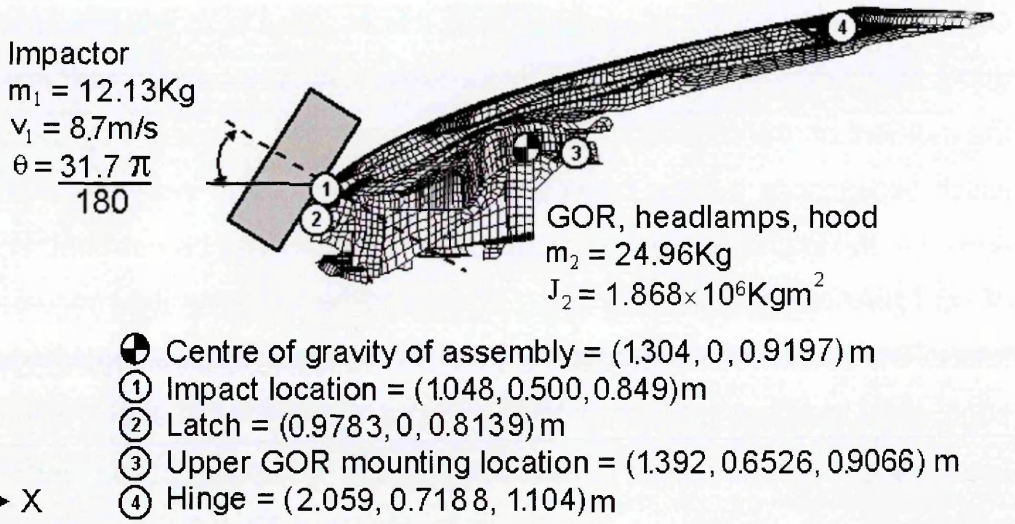

Figure 5.80 First level of model construction

The key influencing components are the hood, GOR, headlamps, latch and hinges and the hood can rotate around the hinges, GOR mounting points and latch. The system is complex and does not lend itself to an easily understood analytical solution because of the complex boundary conditions and deformation behaviour of each component that is difficult to describe analytically. In addition, although the physical property values of the key components were easily determined in the pre processor (as shown in the appendices) each of the system components has complicated deformation behaviour. However, this system can be analysed from another perspective if the hood system objective and its most effective achievement are considered.

The objective of the hood system design is to move rearward and rotate away from the impact location. This will be most effectively achieved when the hood is allowed to move in its free body motion and all attached components are modified to allow this to occur. In such an idealised system the hood system behaves as a free body unrestrained by attachments. It is assumed that this motion will be translational in the direction of the applied force and rotational about the hood assembly centre of gravity. Furthermore if the hood is considered rigid and other energy losses, for example noise, are assumed negligible, then all of the impactor kinetic energy is transferred into the hood motion rather than into internal energy of hood system deformation. Finally, gravity is not considered because its influence is small in comparison to that of the impactor and zero initial hood velocity is assumed to simplify the equations of motion. Figure 5.81 shows the second level of model construction.

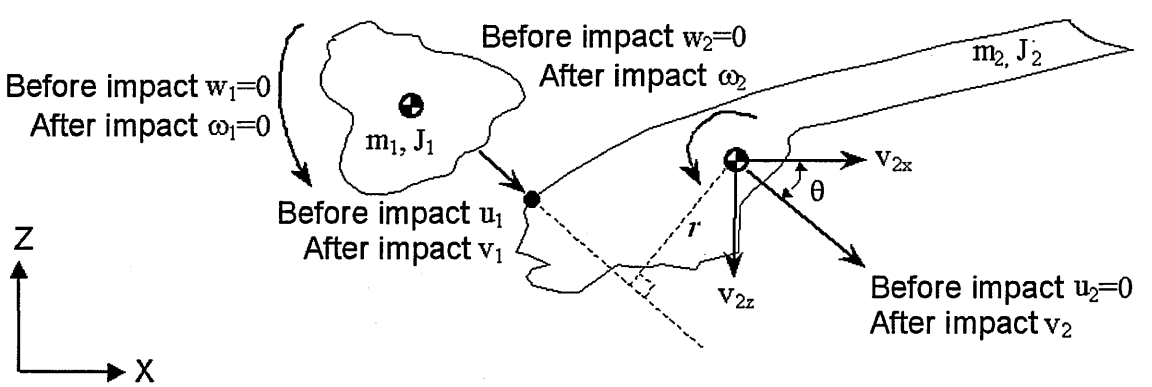

Figure 5.81 Second level of model construction

This allows the free body motion of a hood system (i.e. all the components are modelled for their inertial effect but the mechanisms that constrain their motions are not fixed to the ground) to be compared with the predicted motions of the parts when the mechanisms are fixed to the ground.

For an idealised impact, that is lossless and reversible, there is conservation of momentum and energy before and after the impact.

For linear momentum:

$$m_1u_1 + m_2u_2 = m_1v_1 + m_2v_2$$

$$m_1u_1 = m_1v_1 + m_2v_2 \quad \text{since} \quad u_2 = 0$$

$$\text{hence } v_1 = \frac{m_1u_1 - m_2v_2}{m_1} = u_1 - \frac{m_2}{m_1}v_2 \text{ and } v_2 = \frac{m_1}{m_2}(u_1 - v_1)$$

For rotational momentum about the m_2 centre of gravity:

$$J_1w_1 + J_2w_2 = J_1\omega_1 + J_2\omega_2$$

$m_1r^2w_1 + J_2w_2 = m_1r^2\omega_1 + J_2\omega_2$ assuming m_1 behaves as a point mass

$m_1r^2w_1 = m_1r^2\omega_1 + J_2\omega_2$ assuming $w_2 = 0$

$$\text{or } m_1r^2\left(\frac{u_1}{r}\right) = m_1r^2\left(\frac{v_1}{r}\right) + J_2\omega_2 \text{ assuming 'r' is the same before and after impact}$$

$$\text{hence } \omega_2 = \frac{m_1r(u_1 - v_1)}{J_2}$$

$$\text{or } \omega_2 = \frac{m_1r\left(u_1 - u_1 - \frac{m_2}{m_1}v_2\right)}{J_2} = \frac{m_2v_2r}{J_2} \text{ by substituting } v_1$$

It is assumed that the bodies are rigid and for conservation of energy there is only a transfer of kinetic energy with no other energy transformations into for instance, sound and heat, and hence:

$$\left(\frac{1}{2}m_1u_1^2 + \frac{1}{2}J_1w_1^2\right) + \left(\frac{1}{2}m_2u_2^2 + \frac{1}{2}J_2w_2^2\right) = \left(\frac{1}{2}m_1v_1^2 + \frac{1}{2}J_1\omega_1^2\right) + \left(\frac{1}{2}m_2v_2^2 + \frac{1}{2}J_2\omega_2^2\right)$$

$$\frac{1}{2}m_1u_1^2 = \frac{1}{2}m_1v_1^2 + \frac{1}{2}m_2v_2^2 + \frac{1}{2}J_2\omega_2^2 \text{ since } w_1 = w_2 = \omega_1 = u_2 = 0$$

$$m_1u_1^2 = m_1\left(\frac{m_1u_1 - m_2v_2}{m_1}\right)^2 + m_2v_2^2 + J_2\left(\frac{m_2v_2r}{J_2}\right)^2 \text{ substituting } v_1 \text{ and } \omega_2$$

$$m_1u_1^2 = m_1\left(\frac{m_1^2u_1^2 - 2m_1u_1m_2v_2 + m_2^2v_2^2}{m_1^2}\right) + m_2v_2^2 + \frac{m_2^2v_2^2r^2}{J_2}$$

$$m_1 u_1^{\,2} = m_1\left(u_1^{\,2} - \frac{2u_1 m_2 v_2}{m_1} + \left(\frac{m_2}{m_1}\right)^2 v_2^{\,2}\right) + m_2 v_2^{\,2} + \frac{m_2^{\,2} v_2^{\,2} r^2}{J_2}$$

$$2u_1 m_2 v_2 = v_2^{\,2}\left(\frac{m_2^{\,2}}{m_1} + m_2 + \frac{m_2^{\,2} r^2}{J_2}\right)$$

$$\text{hence } v_2 = \frac{2u_1 m_2}{\left(\frac{m_2^{\,2}}{m_1} + m_2 + \frac{m_2^{\,2} r^2}{J_2}\right)} = \frac{2u_1}{\left(\frac{m_2}{m_1} + 1 + \frac{m_2 r^2}{J_2}\right)}$$

There are two equations defining the free body velocities of the hood system centre of gravity after the impact in the global coordinate system:

$$v_2 = \frac{2u_1}{\left(\frac{m_2}{m_1} + 1 + \frac{m_2 r^2}{J_2}\right)} \text{ and } \omega_2 = \frac{m_2 v_2 r}{J_2}$$

The calculations determining the value of r = 0.0195 m are shown in Figure 5.82.

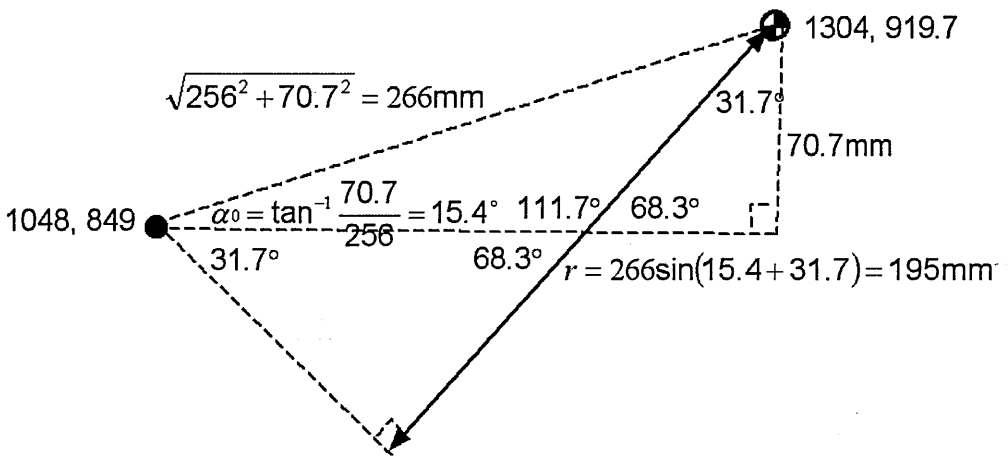

Figure 5.82 Determining the value of 'r'

From Figure 5.80 the known values are u_1=8.7 m/s, m_1=12.13 Kg, m_2=24.96 Kg and J_2=1.868×10^6 Kgm^2 and therefore:

$$v_2 = \frac{2u_1}{\left(\frac{m_2}{m_1} + 1 + \frac{m_2 r^2}{J_2}\right)} = \frac{2 \times 8.7}{\left(\frac{24.96}{12.13} + 1 + \frac{24.96 \times 0.195^2}{1.868 \times 10^6}\right)} = 4.88 \text{ m/s}$$

$$\omega_2 = \frac{m_2 v_2 r}{J_2} = \frac{24.96 \times 4.88 \times 0.195}{1.868 \times 10^6} = 12.7 \text{ radians/s}$$

Using these formulae the velocity of the hood system at any point in time after the

impact event may be determined. Figure 5.83 shows the velocity of the hood centre of gravity and impact location at time t=0 and t=t_1.

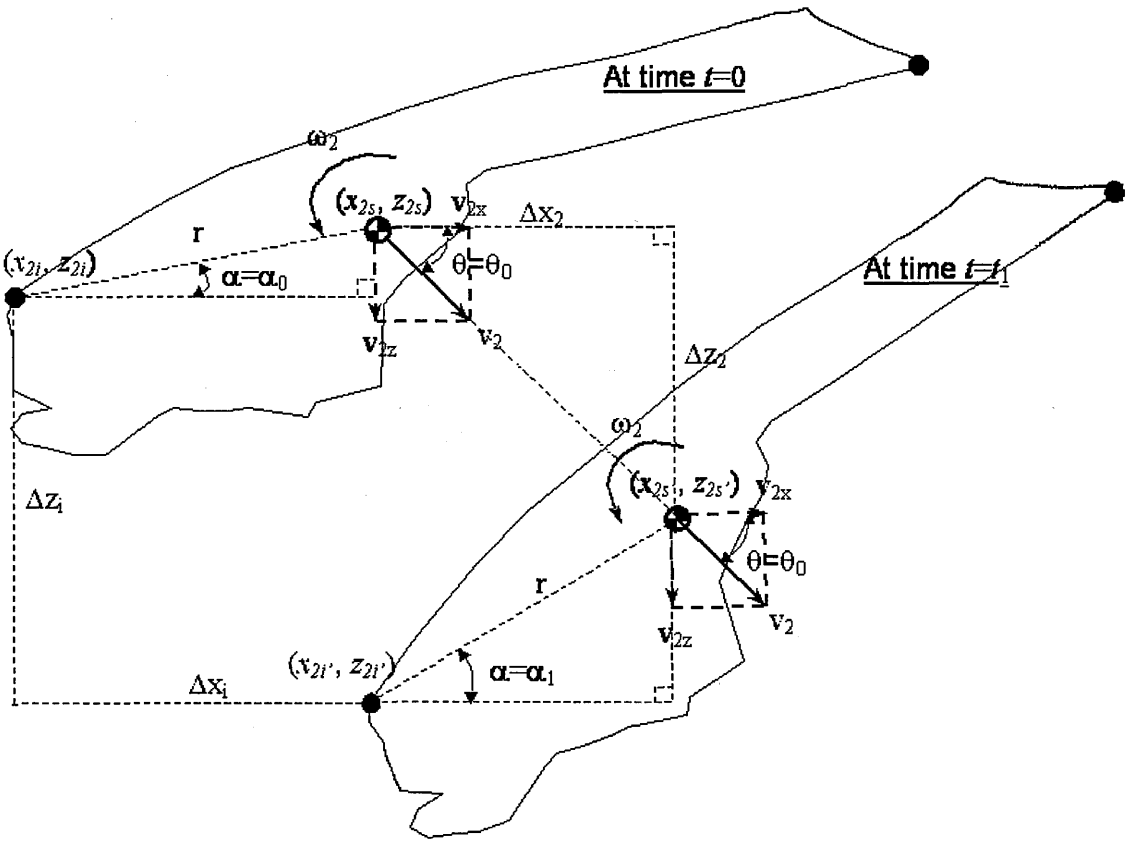

Figure 5.83 The location of the hood at time $t = 0$ and $t = t_1$

In a similar manner these relationships may be used to determine the incremental displacements of the hood system in global coordinates at any time $t = t_1$. The incremental displacement of the hood system centre of gravity is given by:

$$\Delta x_2 = v_{2x}.t_1 = (4.880 \times \cos 31.7) \times t_1 = 4.152 \times t_1$$
$$\Delta z_2 = v_{2z}.t_1 = (4.880 \times \sin 31.7) \times t_1 = 2.564 \times t_1$$

For the impact location the displacements Δx_i and Δz_i at time $t = t_1$ are given by:

$$\Delta x_i = \Delta x_2 + r \sin \frac{180\alpha}{\pi}$$
$$\Delta z_i = \Delta z_2 + r \cos \frac{180\alpha}{\pi}$$

where $\alpha = \alpha_0 + \omega.t$ and the formulae were entered into an Excel spreadsheet with a time step of 1 ms to give the motion of the three points shown in Figure 5.84.

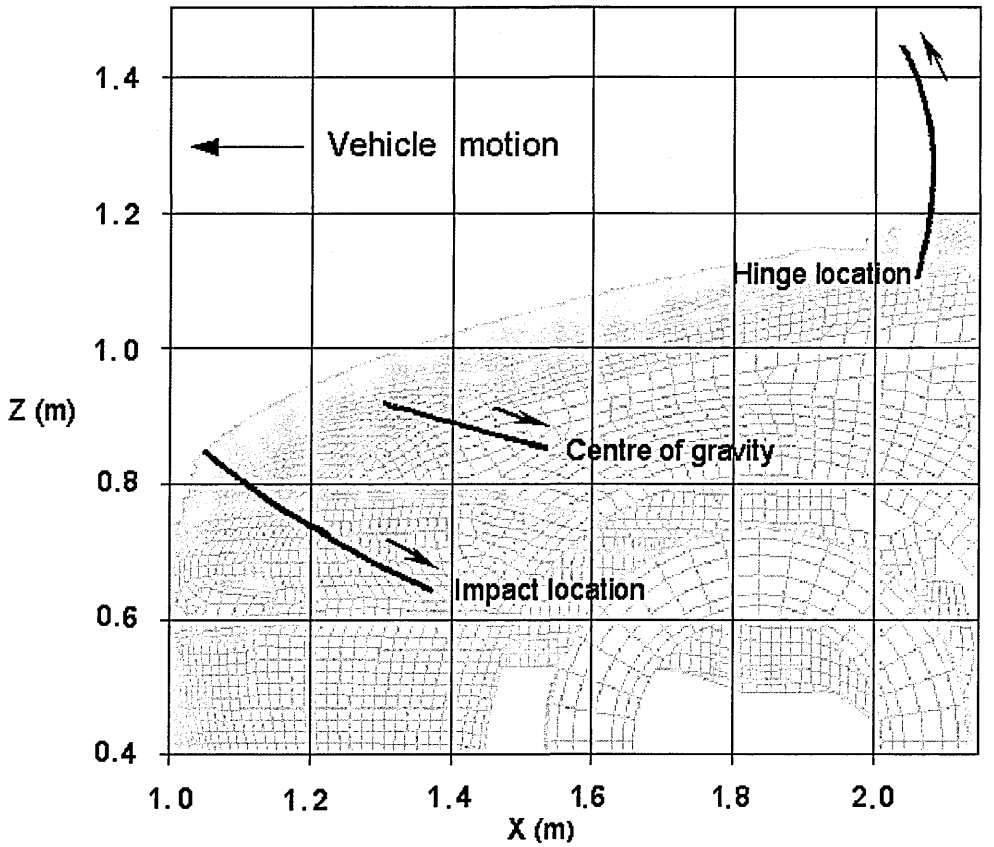

Figure 5.84 Absolute hood displacement in global coordinates

5.6.4. Numerical hood evaluation model

Simplified numerical models of different hood configurations were created in a parallel project (by Imperia) with proprietary kinematics software (i.e. not accounting for inertial effects). Although they are not described here, these models assisted in determining the number of joints and the positions of the joints shown in Figure 5.77 and to achieve the desired free body motion shown in Figure 5.84.

Conclusions

Mechanically deployed hood systems are not generic like the other technologies considered and therefore it is not possible to identify one optimal system for all vehicles. The geometry is most effectively developed and optimised for a specific vehicle by using kinematics software rather than finite element analysis. This approach allows a quicker and interactive investigation of, for instance, link lengths. Hence the solution for the C class car was developed from conceptual ideas but optimised in a separate project with the geometry used in full vehicle simulations.

6. Modified vehicle pedestrian accident simulations

6.1. Context in overall methodology

This chapter concerns the highlighted tasks shown in Figure 6.1 [Howard 2001-1]:

- The construction of modified vehicle models, with different combinations of the pedestrian protection technologies, previously evaluated in simplified component simulations.
- An analysis of pedestrian accident simulations using the modified vehicle models
- Benchmarking of the modified vehicle results against the reference vehicle results.

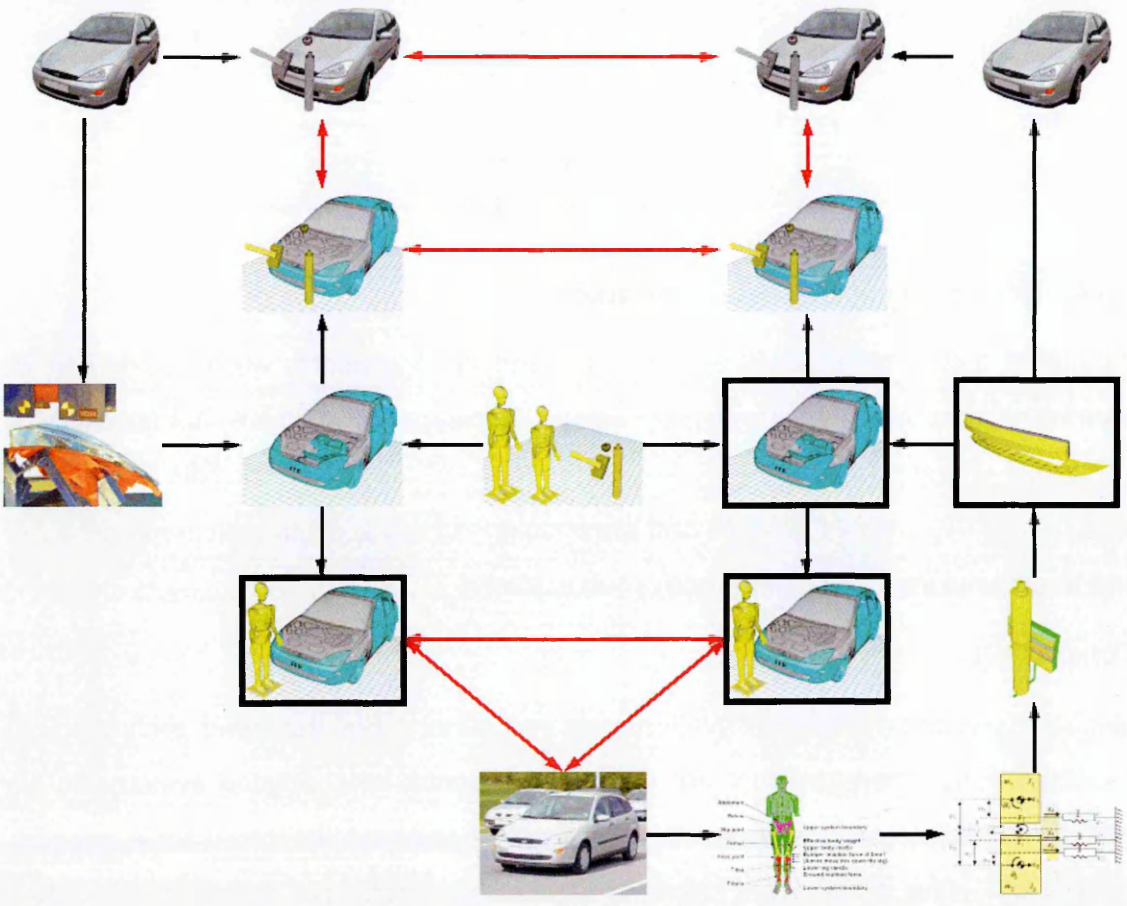

Figure 6.1 Pedestrian protection technology methodology (modified vehicle)

6.2. Vehicle models 'd1' and 'd2'

6.2.1. The construction of the vehicle models

The reference vehicle model was modified to construct two vehicle models: vehicle 'd1' and 'd2' both incorporated the bumper undertray and bumper foam but the former incorporated the headlamp technology and the latter the hood technology. There were two main reasons for choosing these vehicle configurations.

The pedestrian accident simulations with the reference vehicle revealed how the stiffness of the undertray, bumper and headlamp or hood needed to be matched. This supported the pedestrian legs in a manner that kept them as straight as possible and hence minimised bending across the leg bones and knee. This observation was also made with some of the initial pedestrian accident simulations, with a modified vehicle model, as shown in Figure 6.2.

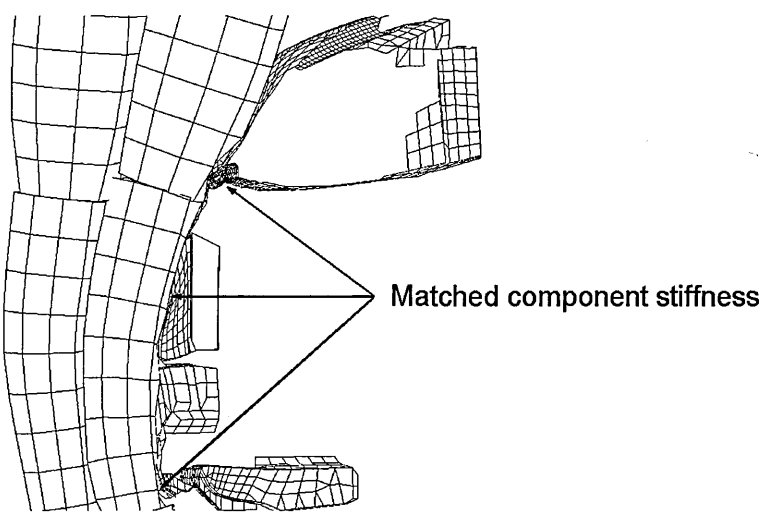

Figure 6.2 Matched component stiffness to support the pedestrian legs

Secondly, with the chosen vehicle, at least two vehicle models were required to evaluate the different technology combinations because the headlamp technology was incompatible with the hood technology. The hood technology needed sufficient energy to fully deploy and with this vehicle (due to the aerodynamic grille geometry) the available impact energy, as calculated for the upper leg impactor [EEVC 1998], was relatively small. Significant headlamp energy absorption and deformation (the main technology objectives) would have led to incomplete hood deployment.

The modified parts

The modified parts in the vehicle models 'd1' and 'd2' are shown in Figure 6.3 and Figure 6.4. All other parts were identical to the reference vehicle model 'p'.

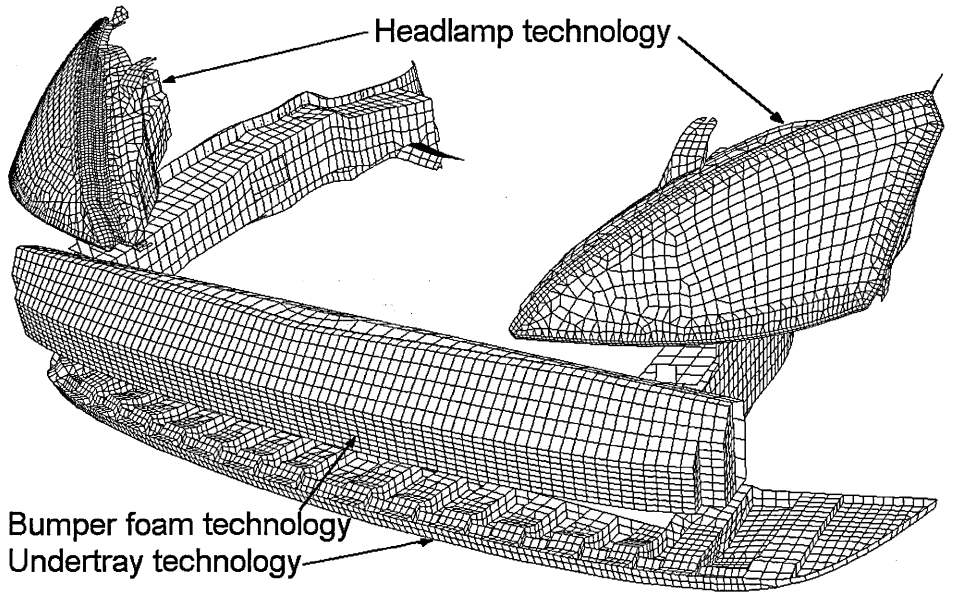

Figure 6.3 The modified parts in vehicle model 'd1'

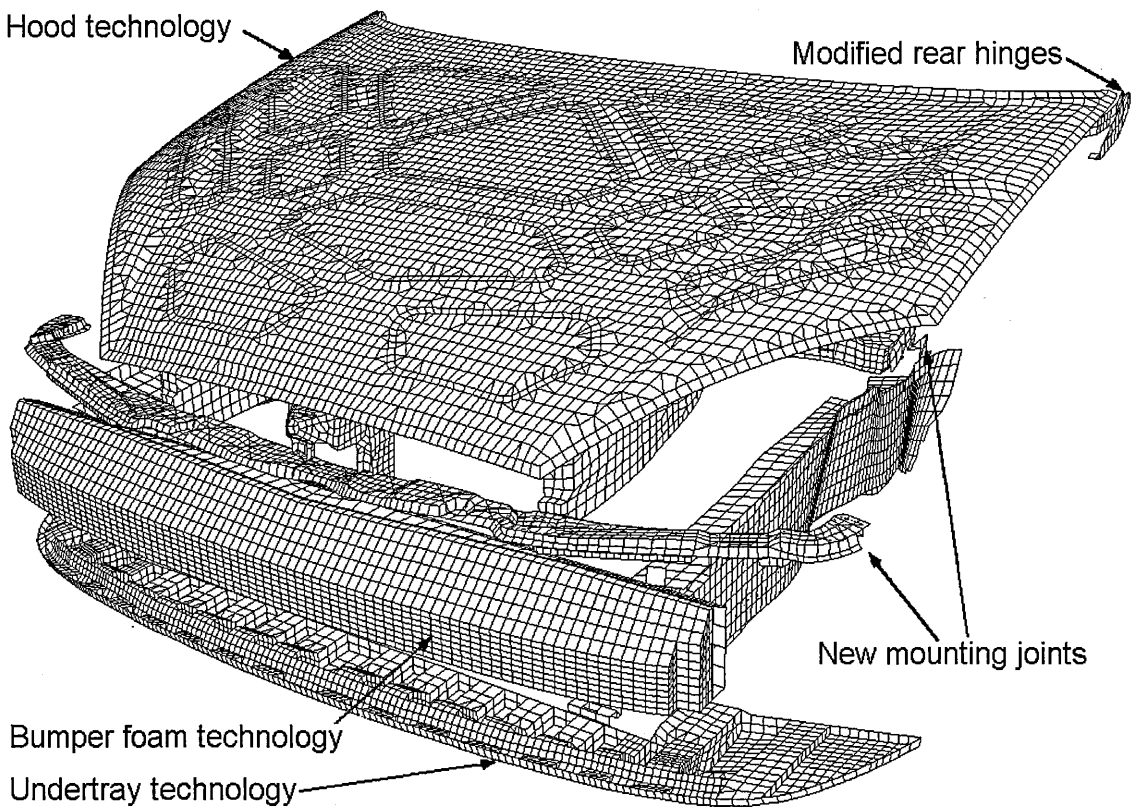

Figure 6.4 The modified parts in vehicle model 'd2'

Although optimisation of the technologies in the vehicle model was beyond the scope of this research, limited development of these parts was undertaken in some initial simulations using the 'd1' vehicle and 50th percentile pedestrian models.

Contacts for vehicle model 'd1'

An automatic single surface and automatic nodes to surface contact were defined in this model. As with the reference vehicle 'p', some parts were removed from the automatic single surface contact as shown in Figure 6.5.

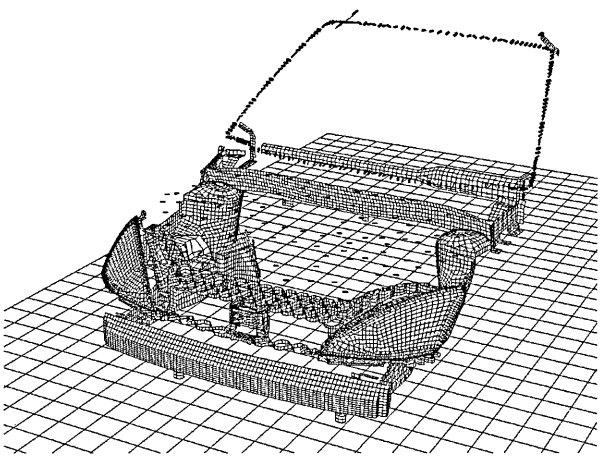

Figure 6.5 Parts removed from the automatic single surface contact

In addition to the parts that did not need to be in the contact (i.e. they did not influence the pedestrian impact) or caused contact problems (as described for the reference vehicle) some parts were defined in a new additional contact. The new automatic nodes to surface contact, as shown in Figure 6.6, included the bumpershell, the headlamp lens cover and body elements, and the nodes of the higher density foam and headlamp convolutes.

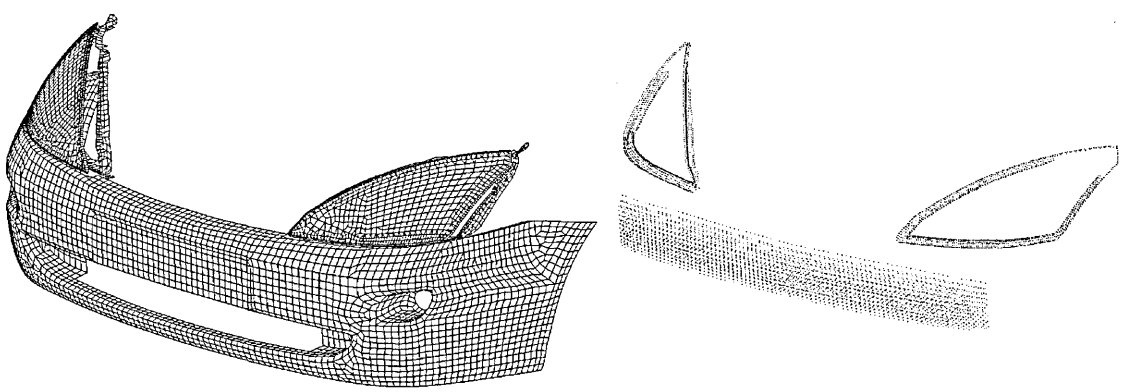

Figure 6.6 Parts and nodes in the second vehicle to vehicle contact

This second contact was necessary because the higher density and lower density foam, and the headlamp lens cover and convolutes had common nodes. A single contact would have caused initial penetrations, very high contact forces and eventually caused abortion of the simulation. Therefore, only the lower density foams, and convolutes were left in the automatic single surface. In this manner a contact existed between the lower density foam and bumper beam, and self contact of the convolute parts was appropriately modelled. The contact cards for the two contacts are shown in Table 6.1 and Table 6.2.

AUTOMATIC SINGLE SURFACE CONTACT CARD							
*CONTACT_AUTOMATIC_SINGLE_SURFACE_TITLE							
1 VEHICLE TO VEHICLE							
1	0	2	0	1	0	1	1
0.2	0.2	0.0	0.0	0.0	0	0.0	1.0E10
0.0	0.0	0.0	0.0	0.0	0.0	0.0	0.0
0	0.1	0	1.02	0.0	2	0	1
*SET_PART_LIST							
1	0.0	0.0	0.0	0.0			
1	2	3	4	5	6	8	9
10	11	12	13	14	15	16	20
21	30	31	32	33	36	37	38
39	40	41	42	43	44	45	46
47	48	50	51	52	54	55	56
57	60	61	62	63	64	65	68
69	70	71	74	76	77	78	97
105	106	107	108	109	110	111	112
113	114	115	118	123	124	125	80
83	88	91					

Table 6.1 Automatic single surface contact and part set cards

AUTOMATIC NODES TO SURFACE CONTACT CARD							
*CONTACT_AUTOMATIC_NODES_TO_SURFACE_TITLE							
2 CONTACT_NODES_2							
2	2	4	2	0	2	1	1
0.2	0.2	0.0	0.0	0.0	0	0.0	1.0E10
0.0	0.0	0.0	0.0	0.0	0.0	0.0	0.0
0	0.1	0	1.02	0.0	2	0	1
1.0E10	0	0	0	0	0		
*SET_NODE_LIST							
2	0.0	0.0	0.0	0.0			
84762	84763	84764	.	.	.	.	.
*SET_PART_LIST							
2	0.0	0.0	0.0	0.0			
74	94	95	96	81	89	79	86
87	84	92					

Table 6.2 Automatic nodes to surface contact, node and part set cards

Contacts for vehicle model 'd2'

An automatic single surface and automatic nodes to surface contact were also defined in the 'd2' vehicle. The parts removed from the automatic single surface contact are shown in Figure 6.7.

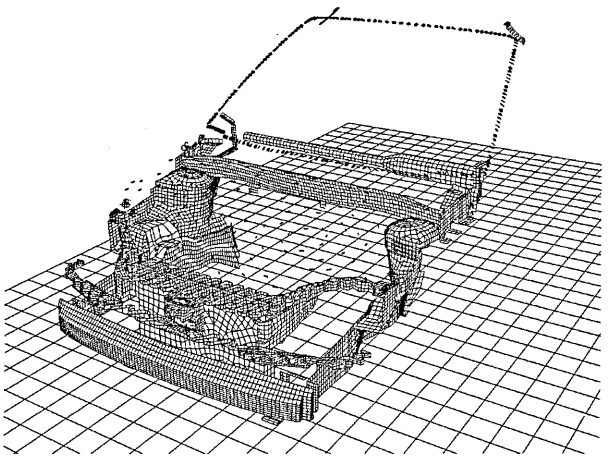

Figure 6.7 Parts removed from the automatic single surface contact

The automatic single surface contact was similar to the reference vehicle because standard headlamps were used. However, the high density bumper foam and some of the modified hood parts and the cooling pack were excluded from this contact. As with the vehicle 'd1', the low and high density foam models had common nodes. In addition, some of the parts attached to the hood system interfered with its free motion and were therefore removed. For example, the cooling pack was removed because the support bracket beneath the cooling pack generated contact forces when the cooling pack began to rotate about this bracket.

The additional automatic nodes to surface contact for the higher density to bumpershell contact is shown in Figure 6.8.

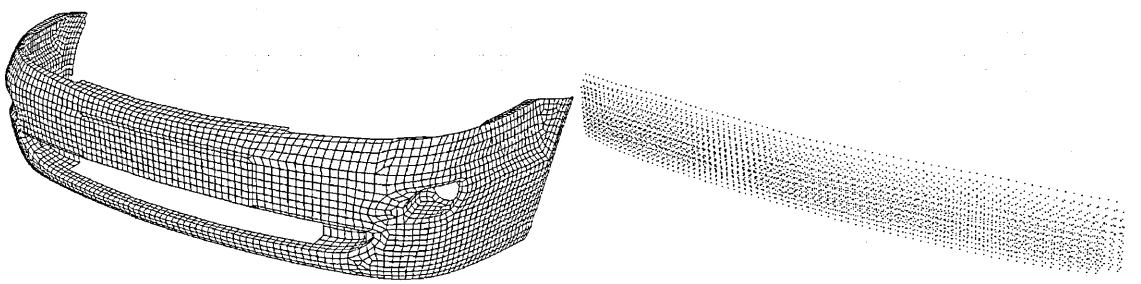

Figure 6.8 Parts included in the second vehicle to vehicle contact

The contact card variables for the contacts are shown in Table 6.3 and Table 6.4.

AUTOMATIC SINGLE SURFACE CONTACT CARD

```
*CONTACT_AUTOMATIC_SINGLE_SURFACE_TITLE
         0  VEHICLE TO VEHICLE
         1         0         2         0         1         0         1         1
 0.200E+00 0.200E+00 0.000E+00 0.000E+00 0.000E+00         0 0.000E+00 0.100E+11
 0.000E+00 0.000E+00 0.000E+00 0.000E+00 0.000E+00 0.000E+00 0.000E+00 0.000E+00
         0 0.100E+00         0 0.102E+01 0.000E+00         2         0         1
*SET_PART
         1
         1         2         3         4         5         6         8         9
        10        11        12        13        14        15        16        20
        21        30        31        32        33        36        37        38
        39        40        41        42        43        44        45        46
        47        48        50        51        52        54        55        56
        57        60        62        63        64        65        68        69
        70        71        74        76        77        78        79        80
        81        82        83        84        85        86        87        88
        89        90        91        92        93        94        95        96
        97       105       106       107       108       109       110       111
       112       113       114       115       118       123       124       125
       127       128       129
*DEFINE_BOX
         1 0.819E+03 0.508E+04-0.929E+03 0.929E+03 0.980E+02 0.172E+04
```

Table 6.3 Automatic single surface contact and part set cards

AUTOMATIC NODES TO SURFACE CONTACT CARD

```
*CONTACT_AUTOMATIC_NODES_TO_SURFACE_TITLE
         0  CONTACT_NODES_2
         2         2         4         2         0         2         1         1
 0.200E+00 0.200E+00 0.000E+00 0.000E+00 0.000E+00         0 0.000E+00 0.100E+11
 0.000E+00 0.000E+00 0.000E+00 0.000E+00 0.000E+00 0.000E+00 0.000E+00 0.000E+00
         0 0.100E+00         0 0.102E+01 0.000E+00         2         0         1
 0.100E+11         0         0         0
*SET_NODE_LIST
         2       0.0       0.0       0.0       0.0
     74645     74646     74647     74648     74649         .         .         .
*SET_PART
         2
        74
*DEFINE_BOX
         2 0.868E+03 0.157E+04-0.874E+03 0.874E+03 0.383E+03 0.835E+03
```

Table 6.4 Automatic nodes to surface contact, node and part set cards

General construction and boundary conditions

With the exception of the changes described, the construction and boundary conditions of both modified vehicles 'd1' and 'd2' were identical to those of the reference vehicle 'p'.

6.2.2. The bumper undertray model

The DoE studies indicated the benefits of a stiff undertray. In the reference vehicle the undertray was only designed to divert air on to the cooling pack and to close off the space between the bumper shell and cooling pack. As a consequence of this it lacked bending stiffness because it was relatively flat (i.e. it had a low second

moment of area) and constructed in a material with a low Young's Modulus. Therefore the mesh geometry was changed to increase its bending stiffness by adding longitudinal and lateral ribs in three development stages as shown in Figure 6.9.

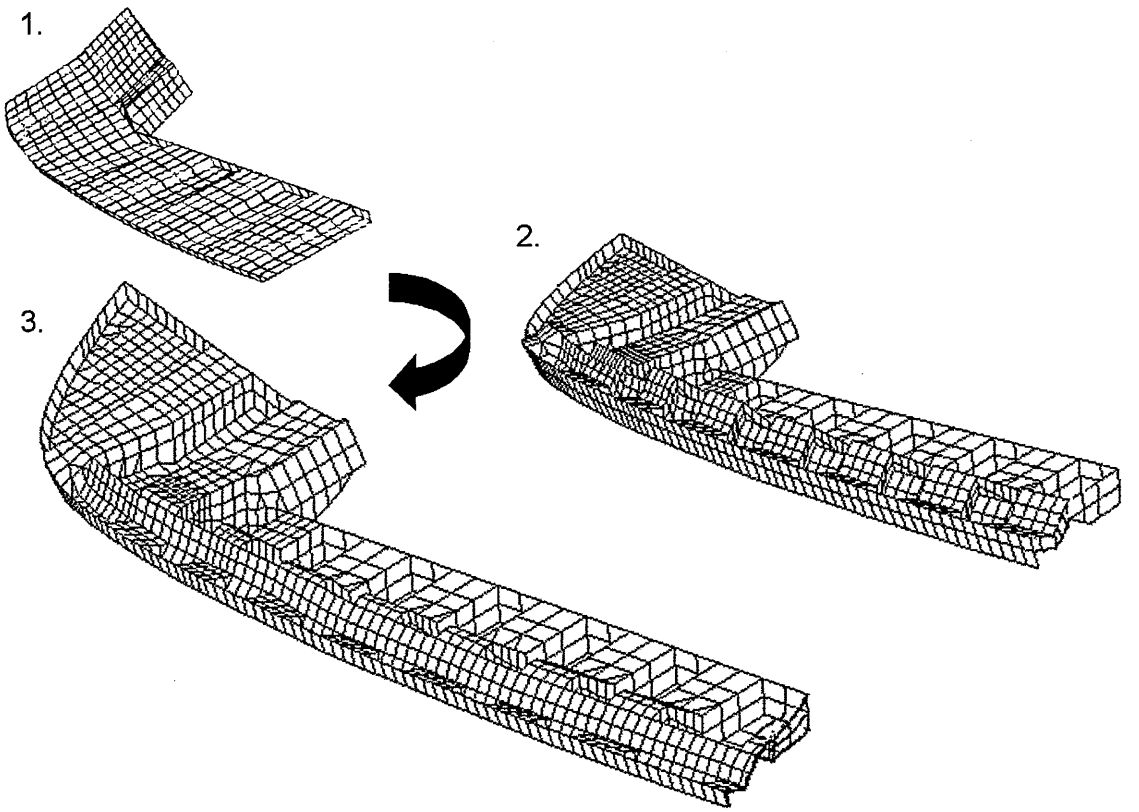

Figure 6.9 The main development stages of the undertray model

In the first stage (1.) the undertray was only reinforced with shallow longitudinal ribs, to increase the bending stiffness in the main impact direction. However, the pedestrian accident simulations showed that the deformation behaviour was similar to that of the original undertray and the changes provided no benefit in supporting the lower legs.

Deeper longitudinal ribs were added to the rear half of the undertray in the second stage (2.) with shallower ribs in the front half and a V shaped cross section. The purposes of these changes were to increase the longitudinal bending stiffness of the rear half of the undertray whilst ensuring limited deformation in the form of a plastic hinge (rather than buckling) in the V shaped cross section. This also

provided a lateral rib for increased lateral bending stiffness in the Y direction. However, as shown in Figure 6.10, up to 10 ms after the initial bumper contact the V shaped cross section deformed in the correct manner but by 20 ms, the whole undertray began to rotate upwards. This led to the legs being wrapped under the bumper in a similar manner to the reference vehicle and hence this did not improve the support condition.

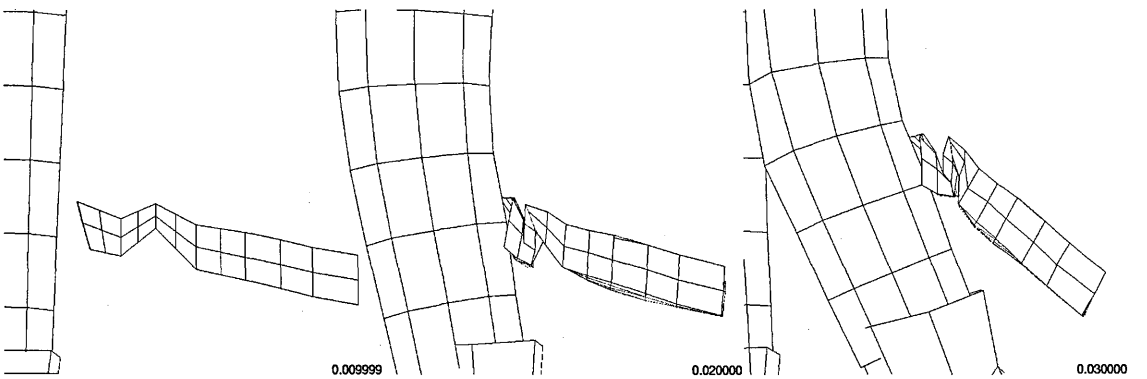

Figure 6.10 The deformation behaviour of second stage undertray model

As a result of these observations, more mounting connections were added in the final stage (3.) and further stiffening of the rear half of the undertray was undertaken with for instance, a deeper rear section. The V section apex was also narrowed to increase the likelihood of a plastic hinge forming at the front of the undertray. The new pedestrian leg and undertray deformation at Y500 is shown in Figure 6.11. In this case the lower legs were fully supported with controlled deformation of the undertray and the final design is shown in Figure 6.12 and described in [Howard 2000-7].

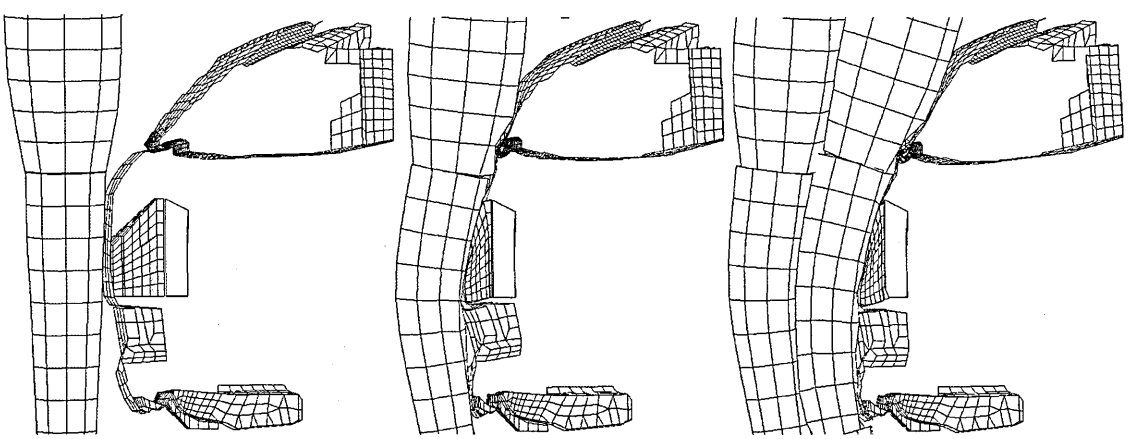

Figure 6.11 The deformation behaviour of the final undertray model

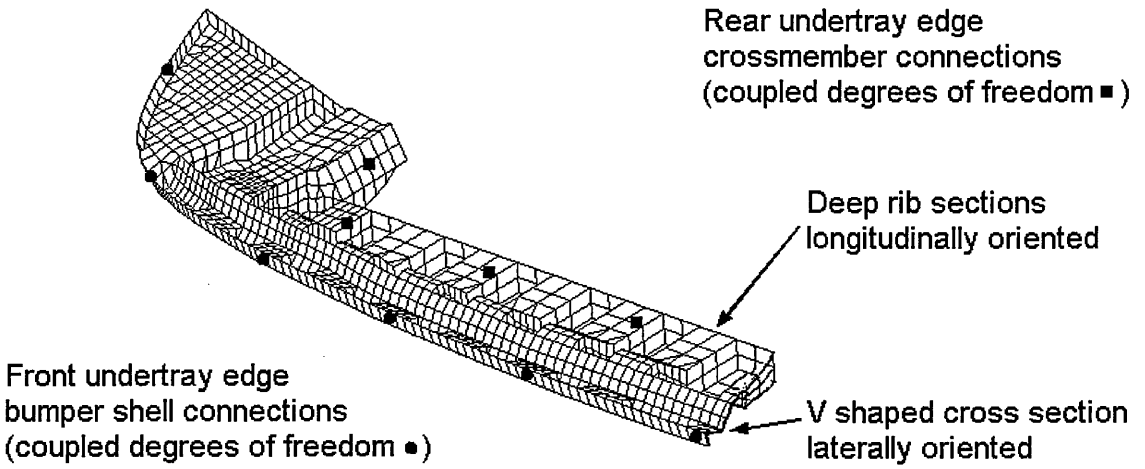

Figure 6.12 The final undertray model

Generic ABS material properties from [Ford 1997] were used as shown in Table 6.5 and the thickness was set to 3.0 mm in the section shell card 123.

UNDERTRAY						
Material law 3						
$\rho = 0.20E-08\ \text{ton/mm}^3$ $E = 3000\ \text{N/mm}^2$ $\nu = 0.25$ $\sigma_y = 62\ \text{N/mm}^2$ $E_T = 50\ \text{N/mm}^2$ $\beta = 0.0$ (kinematic hardening) SRC & SRP = 0.0 (no strain rate effect) FS = 0.0 (no element failure & erosion) VP = 0.0 (n.a. scale yield stress for rate)						
*MAT_PLASTIC_KINEMATIC $ Material 24 : UNDERTRAY 24	0.2E-8	3000.0	0.25	62.0	50.0	0.0

Table 6.5 Material card for the ABS pedestrian protection undertray

6.2.3. The bumper foam model

It was proposed in [Howard 1999-2] that the bumper face should be sloped to lower the effective bumper stiffness centre and different foam densities would allow the bumper stiffness to be tuned for multiple load cases, including pedestrian impacts. The DoE studies showed the benefits of vertically split dual density foams. Therefore dual density foam was used with a higher density on the struck side and a thin rear lower density layer. 44 g/l and 58g/l polyurethane foam were used in the bumper foam model shown in Figure 6.13. The exact foam density values were determined in an additional study that is not described.

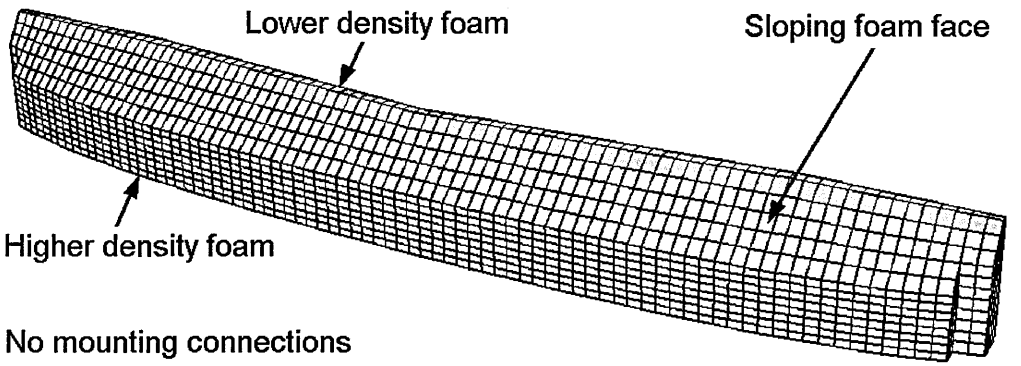

Figure 6.13 The pedestrian protection bumper foam model

There was no foam in the reference vehicle model and therefore a thinner bumper beam and shorter longitudinals were used as shown in Figure 6.14. This allowed a 78 mm foam depth as used in the component simulations, without lengthening the vehicle. The influence of these changes was investigated in the additional study.

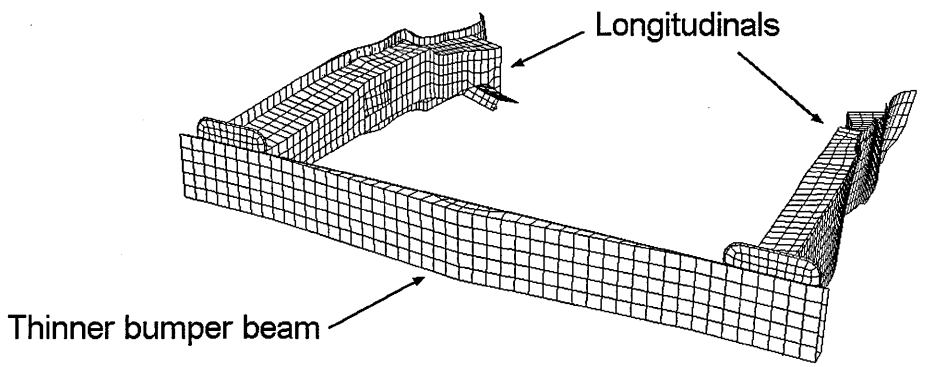

Figure 6.14 The modified beam and longitudinals parts

Material law 57 (MAT_LOW_DENSITY_FOAM) was used to model Bayer Bayfill EA bumper foams. This material law simulates the non linear behaviour of a foam under compression such that σ = f (ε) according to a series of experimentally measured data points as shown in Figure 6.15 [LS-DYNA 1999-1].

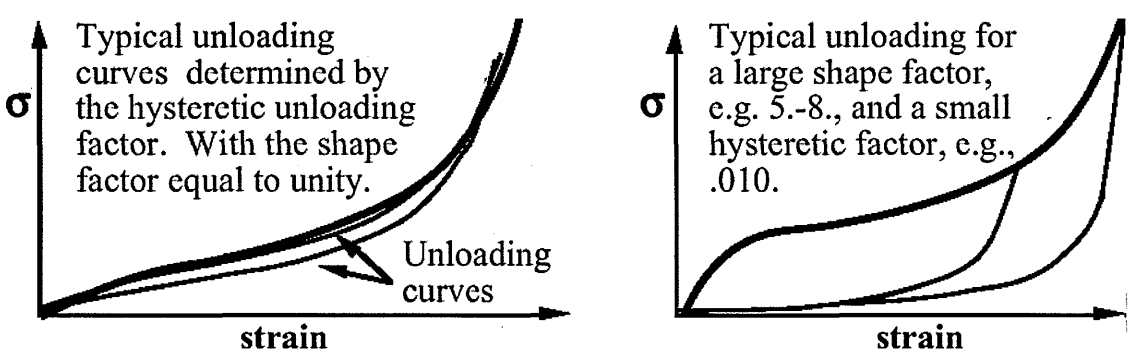

Figure 6.15 The material model used for polyurethane foam

Tension is simulated by the linear relationship of $\sigma = E.\varepsilon$ and the shape of the unloading curve is controlled by a number of additional mathematical parameters. The material law details for the two foams are shown in Table 6.6 and Table 6.7.

LOW DENSITY BUMPER FOAM
Material law 57

ρ = 0.44E-10 ton/mm^3
E = 3330 N/mm^2
Refers to stress strain curve 10 (defined with a scale factor of 1.3 for dynamic stiffness)
$\sigma_{\text{tension cut off}}$ = 50 N/mm^2
Hysteric unloading factor = 0.01
Decay constant to model creep in unloading = 0.0
Viscous coefficient to model damping effects = 0.1
Shape factor for unloading = 50.0
Failure option = 1.0 (tensile stress is set to zero after cutoff stress is reached
Bulk viscosity = 0.0 (default recommended)
Young's relaxation modulus = 0.001
Decay constant = 0.01
Stiffness coefficient for contact interface stiffness = 0.0

```
*MAT_LOW_DENSITY_FOAM
$ Material 26 : BUMPER_FOAM_LOW
        26  0.44E-10    3330.0        10      50.0    1.0E-2       0.0       0.1
      50.0       1.0       0.0    0.1E-2    1.0E-2       0.0       0.0
*DEFINE_CURVE
        10         0       1.0       1.3       0.0       0.0         0
                 0.0                 0.0
        0.0053056702        0.0089999996
         0.021885909         0.039239999
         0.044435039         0.074160002
         0.067647368         0.089460000
         0.090859711         0.093599997
          0.11407204         0.094860002
          0.13728437         0.095940001
          0.15983351         0.097020000
          0.18304583         0.098099999
          0.20625816         0.098820001
          0.22947051         0.099900000
          0.25268283          0.10098000
          0.27589515          0.10206000
          0.29910749          0.10332000
          0.32231984          0.10494000
          0.34553215          0.10674000
          0.36874449          0.10872000
          0.39195684          0.11124000
          0.41516915          0.11412000
          0.43838149          0.11736000
          0.46159384          0.12132000
          0.48480615          0.12582000
          0.50801849          0.13104001
          0.53123081          0.13716000
          0.55444318          0.14454000
          0.57765549          0.15335999
          0.60086781          0.16398001
          0.62408018          0.17730001
          0.64729249          0.19404000
          0.67050481          0.21510001
          0.69371718          0.24246000
          0.71692950          0.27810001
          0.74014181          0.32508001
          0.76335418          0.38916001
          0.78656650          0.47663999
          0.80314672          0.52829999
```

Table 6.6 Material card for lower density polyurethane foam

HIGH DENSITY BUMPER FOAM
Material law 57

ρ = 0.58E-10 ton/mm^3
E = 3330 N/mm^2
Refers to stress strain curve 10 (defined with a scale factor of 1.3 for dynamic stiffness)
$\sigma_{\text{tension cut off}}$ = 50 N/mm^2
Hysteric unloading factor = 0.01
Decay constant to model creep in unloading = 0.0
Viscous coefficient to model damping effects = 0.1
Shape factor for unloading = 50.0
Failure option = 1.0 (tensile stress is set to zero after cutoff stress is reached
Bulk viscosity = 0.0 (default recommended)
Young's relaxation modulus = 0.001
Decay constant = 0.01
Stiffness coefficient for contact interface stiffness = 0.0

```
*MAT_LOW_DENSITY_FOAM
$ Material 27 : BUMPER FOAM HIGH
        27  0.58E-10    3330.0        11      50.0    1.0E-2       0.0       0.1
      50.0       1.0       0.0    0.1E-2    1.0E-2       0.0       0.0
*DEFINE_CURVE
        11         0       1.0       1.3       0.0       0.0         0
                 0.0                 0.0
         0.0053057000          0.015000000
          0.021885900          0.065399997
          0.044434998           0.12360000
          0.067647398           0.14910001
          0.090859704           0.15600000
           0.11407200           0.15809999
           0.13728440           0.15989999
           0.15983351           0.16170000
           0.18304580           0.16350000
           0.20625819           0.16470000
           0.22947051           0.16650000
           0.25268281           0.16830000
           0.27589521           0.17010000
           0.29910749           0.17219999
           0.32231981           0.17490000
           0.34553221           0.17790000
           0.36874449           0.18120000
           0.39195681           0.18539999
           0.41516921           0.19020000
           0.43838149           0.19560000
           0.46159381           0.20220000
           0.48480621           0.20970000
           0.50801849           0.21840000
           0.53123081           0.22860000
           0.55444318           0.24089999
           0.57765549           0.25560001
           0.60086781           0.27329999
           0.62408018           0.29550001
           0.64729249           0.32339999
           0.67050481           0.35850000
           0.69371718           0.40410000
           0.71692950           0.46349999
           0.74014181           0.54180002
           0.76335418           0.64859998
           0.78656650           0.79439998
           0.80314672           0.88050002
```

Table 6.7 Material card for higher density polyurethane foam

The experimental data points needed for this model were supplied by the foam manufacturer and based upon quasistatic measurements. These were multiplied by a value of 1.3 (based upon the manufacturer's recommendation) to estimate the increased stiffness of the foam properties (due to its viscoelasticity) at impact

speeds of 40 km/h. The bumper beam material properties shown in Table 6.8 were based on Steel ST52 from [Ford 1997]. Section solid cards 75 and 125 were used for the foams and the beam thickness was 3.0 mm in the section shell card 124.

BUMPER BEAM
Material law 3
ρ = 0.78E-08 ton/mm^3 E = 203000 N/mm^2 ν = 0.30 σ_y = 345 N/mm^2 E_T = 1110 N/mm^2 β = 0.0 (kinematic hardening) SRC & SRP = 0.0 (no strain rate effect) FS = 0.0 (no element failure & erosion) VP = 0.0 (n.a. scale yield stress for rate)
*MAT_PLASTIC_KINEMATIC $ Material 25 : BUMPER_BEAM 25 0.780E-08 203000.0 0.300E+00 0.345E+03 0.111E+04

Table 6.8 Material card for the modified bumper beam

6.2.4. The headlamp model

The DoE studies showed that adding convolutes to the headlamp lens cover sides reduced the stiffness of the headlamp under a number of loading conditions and that two convolutes only provided a small benefit over a single convolute. Therefore only one convolute was incorporated into the headlamp technology model. The geometry of the convolute was based on the largest S shaped profile that could fit within the available package space. For comparison purposes the construction of the standard and modified headlamp models are shown in Figure 6.16.

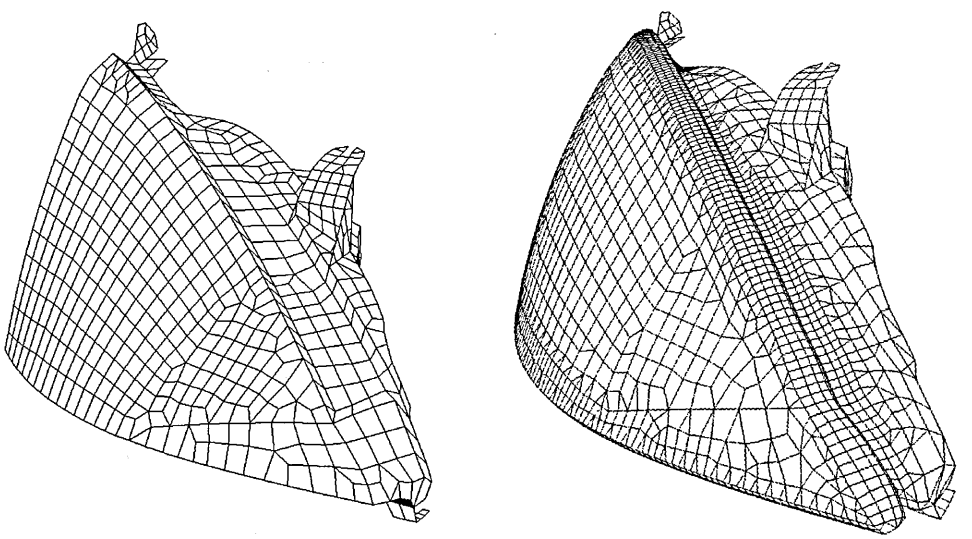

Figure 6.16 Standard and modified headlamp models

All the material models were identical to the ones previously described for the reference vehicle headlamp models. In line with the DoE results, the thickness of the headlamp convolute was set to 2 mm in section shell cards 80 and 88.

6.2.5. The hood system model

The hood technology was modelled by adding joints to the mounting locations of the hood hinges, GOR and cooling pack. To enable the hood system to move correctly the mounting connections of the GOR lower arms and headlamp to the vehicle body were also removed and the battery box reduced in size. The correct joint locations shown in Figure 6.17 were based on the results of a parameter study of the optimum locations using proprietary kinematics software [Howard 2001-4].

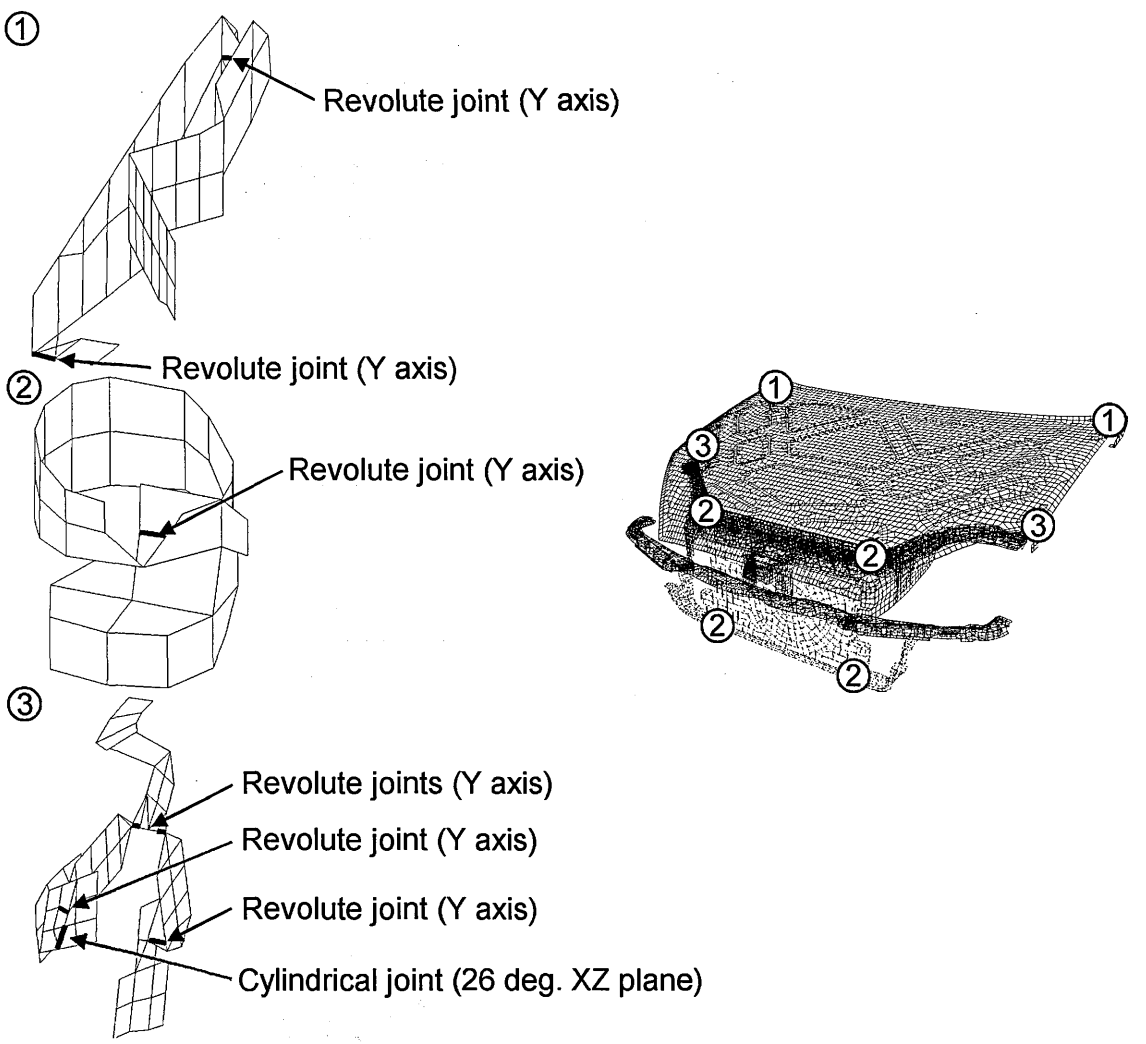

Figure 6.17 The hood technology joint models

The shell elements attached to the joints were defined with a rigid material card and

additional shell elements were added to represent the front lift supports (3). The joint card variables are shown in Table 6.9.

CONSTRAINED JOINT REVOLUTE & CYLINDRICAL CARDS

Four nodes used to define the revolute & cylindrical joints; nodes 1 & 3 are in rigid body A & nodes 2 & 4 in rigid body B
Relative penalty stiffness =1 (default)
Damping scale factor = 1 (default)

```
*CONSTRAINED_JOINT_REVOLUTE
$    NODE 1    NODE 2    NODE 3    NODE 4                    STIFFNESS
      5927      46133     46132      5921                    0.100E+01
      6006      46134     46135      6014                    0.100E+01
     72689      48588     72695     48534                    0.100E+01
     72752      48529     72746     48530                    0.100E+01
     72589      85320     72573     40192                    0.100E+01
     39934      72630     85321     72646                    0.100E+01
     85403      85284     85322     85401                    0.100E+01
     85410      85407     85408     85368                    0.100E+01
     85411      85405     85409     85316                    0.100E+01
     85518      85499     85498     85444                    0.100E+01
     85485      85503     85502     85496                    0.100E+01
     85505      85500     85504     85519                    0.100E+01
     85359      85400     85398     85396                    0.100E+01
     85476      85497     85495     85494                    0.100E+01
      5890      85535     85530     85532                    0.100E+01
      5975      85527     85528     85523                    0.100E+01
*CONSTRAINED_JOINT_CYLINDRICAL
$    NODE 1    NODE 2    NODE 3    NODE 4                    STIFFNESS
     28314      85415     28315     85416                    0.100E+01
     85434      85477     85435     85487                    0.100E+01.
```

Table 6.9 Joint cards for the hood technology

6.3. Pedestrian accident simulations with modified vehicles

6.3.1. Background

The reference vehicle study was undertaken with a total of 80 simulations and these provided a set of reference results and trends. It was not possible to undertake so many simulations in the comparative evaluation of the modified vehicles 'd1' and 'd2'. Therefore a subset of the total matrix was determined according to a number of observations from the first study.

6.3.2. Methodology for comparing pedestrian accident simulations

The results of the first study indicated that stances 'A' and 'C' provided the most useful and robust data. This was because stance 'A' maximised the impact energy transferred into the vehicle front and stance 'C' led to fewer modelling problems with the interaction of the vehicle and pedestrian kinematics. As a consequence of this only these two stances were considered. The 50th percentile pedestrian model was validated against a cadaver study [Howard 2000-3] and therefore there was a higher degree of confidence in using this model rather than the other pedestrian

models. However, it was still necessary to understand the behaviour of the technologies during child accident simulations even if the data for these pedestrian models were not fully validated. Hence the second pedestrian model chosen for this study was the 6 year old child. It was assumed that the benefits of the bumper and headlamp technologies would exist at both low and high impact velocities but the benefits would be greater (and therefore clearer) at higher velocities. Therefore, the vehicle 'd1' was only assessed with 40 km/h accident simulations. However, the vehicle 'd2' incorporated the hood technology and to fully deploy the hood required a minimum amount of energy from the pedestrian impact. Therefore the vehicle 'd2' was assessed with both 25 km/h and 40 km/h accident simulations to determine whether this amount of energy was provided at both low and high impact velocities. These considerations led to the reduced simulation matrix shown in Table 6.10.

Humanoid	FFA LSDYNA3D humanoid v7.2																											
Vehicle	Modified vehicle models (c170_d1.key, c170_d2.key)																											
Velocity (km/h)	25								30								35								40			
Location (mm)	Y0				Y500				Y0				Y500				Y0				Y500				Y0			
Stance	A	B	C	D	A	B	C	D	A	B	C	D	A	B	C	D	A	B	C	D	A	B	C	D	A	B	C	D
50th percentile	d2 1		d2 17		d2 2		d2 18																		d1 7 d2		d1 23 d2	
6 year old	d2 33		d2 41		d2 34		d2 42																		d1 35 d2		d1 43 d2	
95th percentile																												
5th percentile																												

Table 6.10 Pedestrian accident simulation matrix vehicle models 'd1', 'd2'

6.3.3. Comparison of results from pedestrian accident simulations

Figure 6.18 and Figure 6.19 show a global comparison of two types of accident simulations with three vehicle models: the reference vehicle 'p', and the modified vehicles 'd1' and 'd2'. In the first example a 50th percentile pedestrian in stance 'C' was struck by the Y500 impact location and in the second example a 6 year old pedestrian in stance 'A' was struck by the Y0 impact location. In both cases the impact velocity was 40 km/h. These two extreme examples illustrate the pedestrian motion differences between the reference vehicle and the modified vehicles.

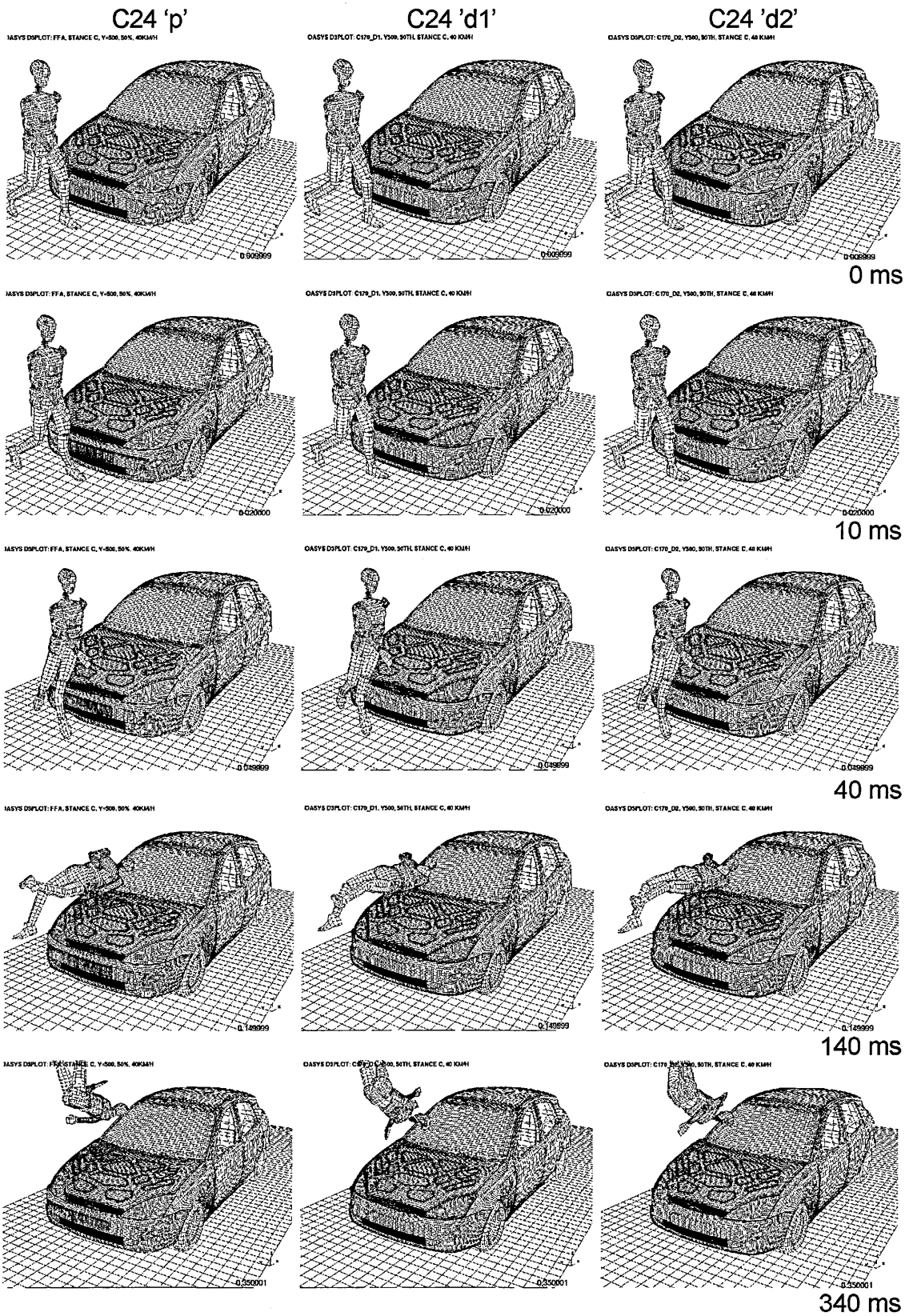

Figure 6.18 50th percentile accident simulations with vehicles 'p', 'd1', 'd2'

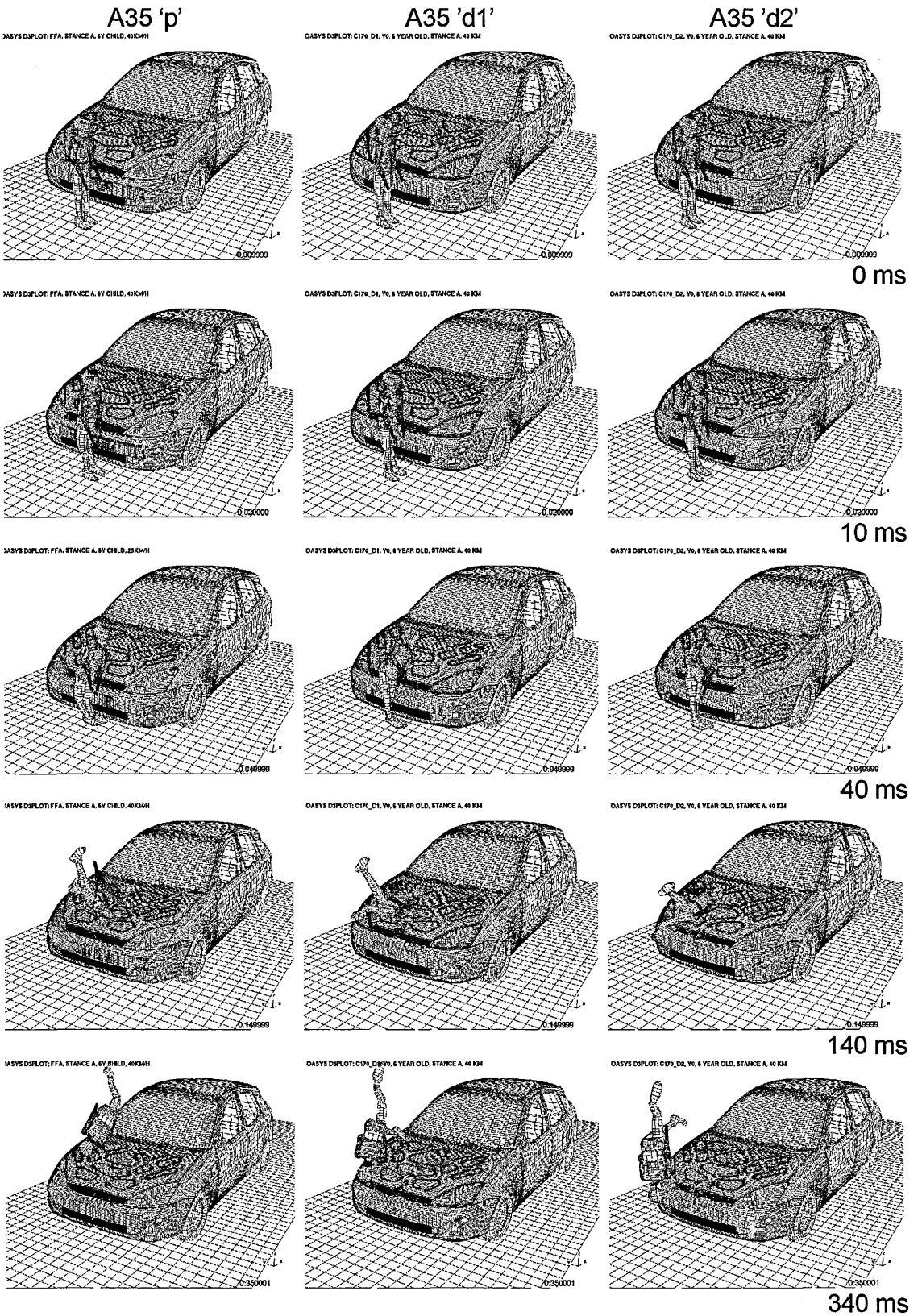

Figure 6.19 6 year old accident simulations with vehicles 'p', 'd1', 'd2'

In terms of global motion, the first example exhibited smaller differences between the pedestrian motions than the second example. Of particular note in the first example was the larger struck leg bending at 10 ms, caused by the reference vehicle, and the difference between the struck leg positions of the 50th percentile humanoid at 140 ms. It was also interesting to note that by 340 ms, the reference vehicle impact had caused the pedestrian to twist further around the X axis. It was difficult to detect any global motion differences between the modified vehicles.

For the 6 year old child there were a number of differences in motion caused by all three vehicles. At 10 ms the reference vehicle caused larger bending across the upper legs and pelvis. By 40 ms this difference was more pronounced but there were no pedestrian motion differences in the modified vehicles. In the two last sequences at 140 ms and 340 ms there were significant pedestrian motion differences between all three vehicles. As with the 50th percentile humanoid the 6 year old child legs were thrown further in Z by the reference vehicle. In the final sequence the pedestrian is thrown in front of the car by vehicle 'd2', above the bumper by vehicle 'd1' and towards the rear of the hood by the reference vehicle 'p'. Additional observations, not shown here, also revealed that the motion differences between the vehicles in cases involving stances 'B' and 'C' were smaller than those for stance 'A' cases.

It was also possible to study detailed animation sections as shown in Figure 6.20. This type of sequence assisted in identifying how different parts of the structure interacted with the pedestrian and in this case how the headlamp, foam and undertray technologies worked together to support the pedestrian legs and reduce knee shear. The two left hand animations concern the reference vehicle 'p' and the two right hand ones the modified vehicle 'd1'. In the first case there was very large bending in the struck lower leg with large horizontal relative displacement between the upper and lower legs (i.e. knee shear). There was much less bending and shear displacement in the second case because the undertray supported the lower legs, the bumper foam allowed the lower legs to be angled towards the vehicle and the headlamp supported the upper legs.

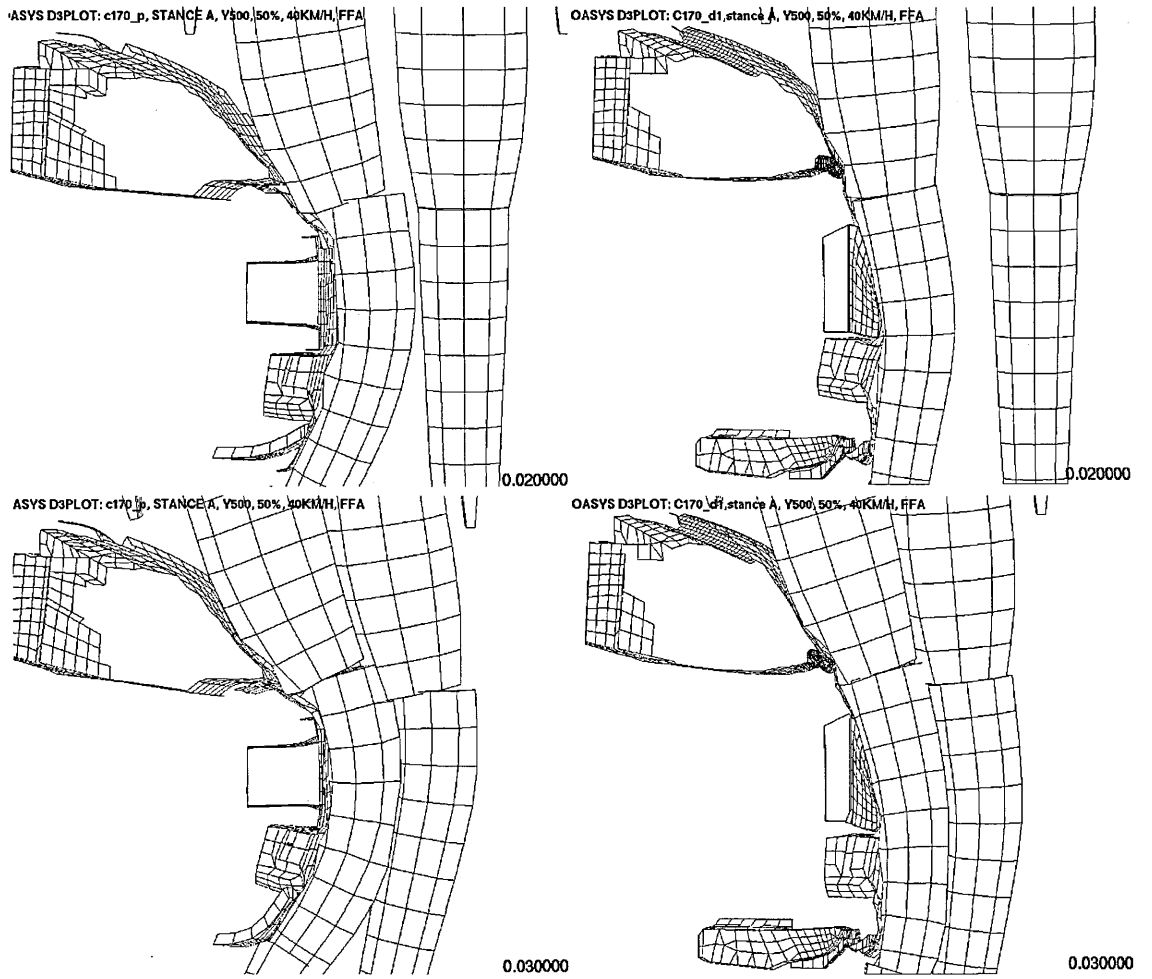

Figure 6.20 Detailed 50th percentile simulations with vehicles 'p' and 'd1'

As with the previous analysis of the reference vehicle cases, it was also possible to analyse quantitative humanoid measures with the modified vehicle cases. Due to the large quantity of results it was more efficient to construct expected ranges, based on the reference vehicle results, with the modified vehicle results. This allowed the influence of the technologies to be compared with the influence of a wide range of accident conditions and a reference vehicle. The term significant difference was used to indicate that a particular combination of technologies had a larger influence on the results than changes to the accident conditions (e.g. stance and impact location).

Table 6.11 shows the differences in impact timing between the reference and equivalent modified vehicle cases at Y0 and Y500. This set of data provided reference timing for additional technologies not described.

Impact velocity (km/h) /Vehicle	Difference in timing (ms) between vehicle 'd1' or 'd2' and standard vehicle 'p'											
	Pelvis impact				Shoulder impact				Head impact			
	6 yr		50 th		6 yr		50 th		6 yr		50 th	
	A	C	A	C	A	C	A	C	A	C	A	C
25	-2.0	0.5	0.0	-17.0	-17.0	-35.0	-16.0	-65.0	-4.0	8.0	5.5	-40.0
'd2'	-2.5	-1.0	0.0	-2.0	26.5	-27.5	-4.5	-50.0	14.0	7.5	-2.5	-43.5
40	-1.0	0.5	0.0	-4.0	1.5	5.0	-8.5	-11.5	1.5	3.5	-2.0	-3.5
'd1'	-0.5	-2.0	0.0	-1.0	4.0	0.0	1.5	2.5	5.0	2.0	-3.5	-2.0
40	-1.5	0.5	0.0	-4.0	0.0	0.5	-9.5	-9.5	1.0	3.0	2.0	-3.5
'd2'	-1.0	0.0	0.0	-1.0	0.0	15.5	6.0	0.0	2.0	3.0	-1.0	4.5

Table 6.11 Impact timing differences of reference and modified vehicles

Figure 6.21 and Figure 6.22 show the range and values of impact timing. At an impact velocity of 25 km/h, most of the 'd2' vehicle results fell within the timing ranges of the reference vehicle results. However, some results were outside these ranges for the shoulder to hood impact. More importantly, in most of the equivalent stance 'C' cases the impacts for the shoulder and head were quicker in the 'd2' vehicle than in the reference vehicle, particularly for the 50th percentile pedestrian. There were larger differences between the stance 'C' results and the stance 'A' results.

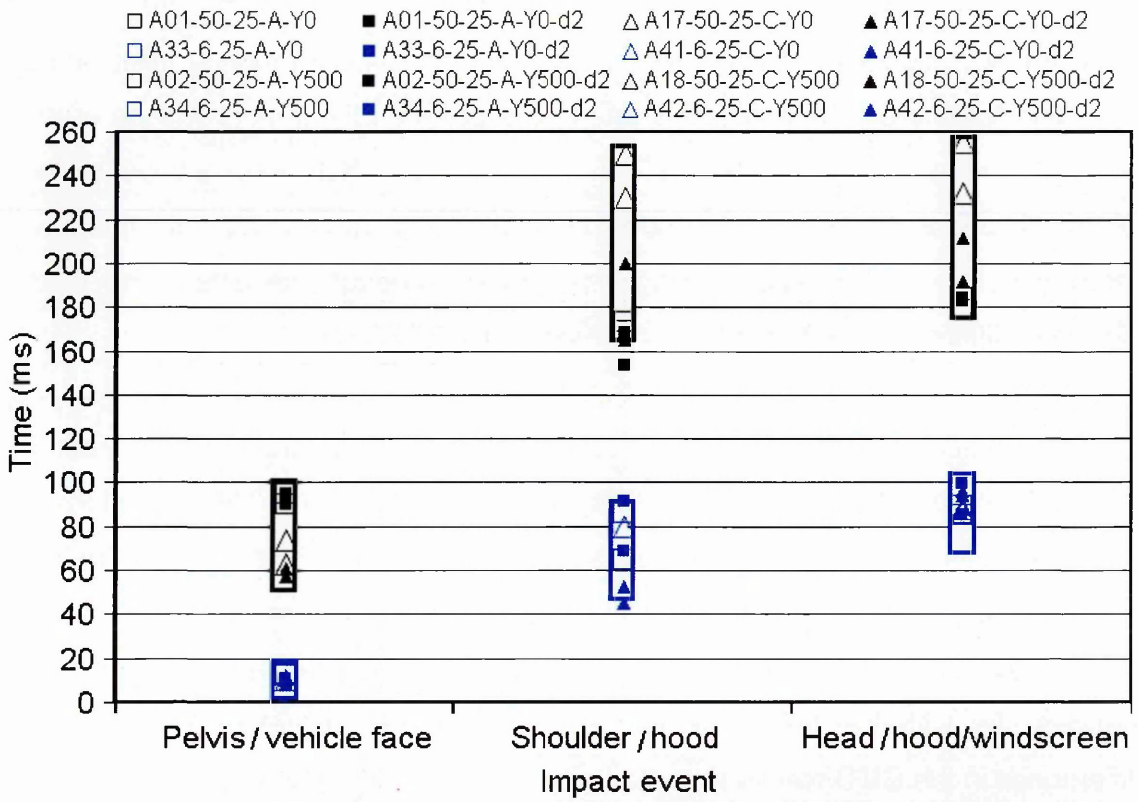

Figure 6.21 Comparison of impact timing ranges and values at 25 km/h

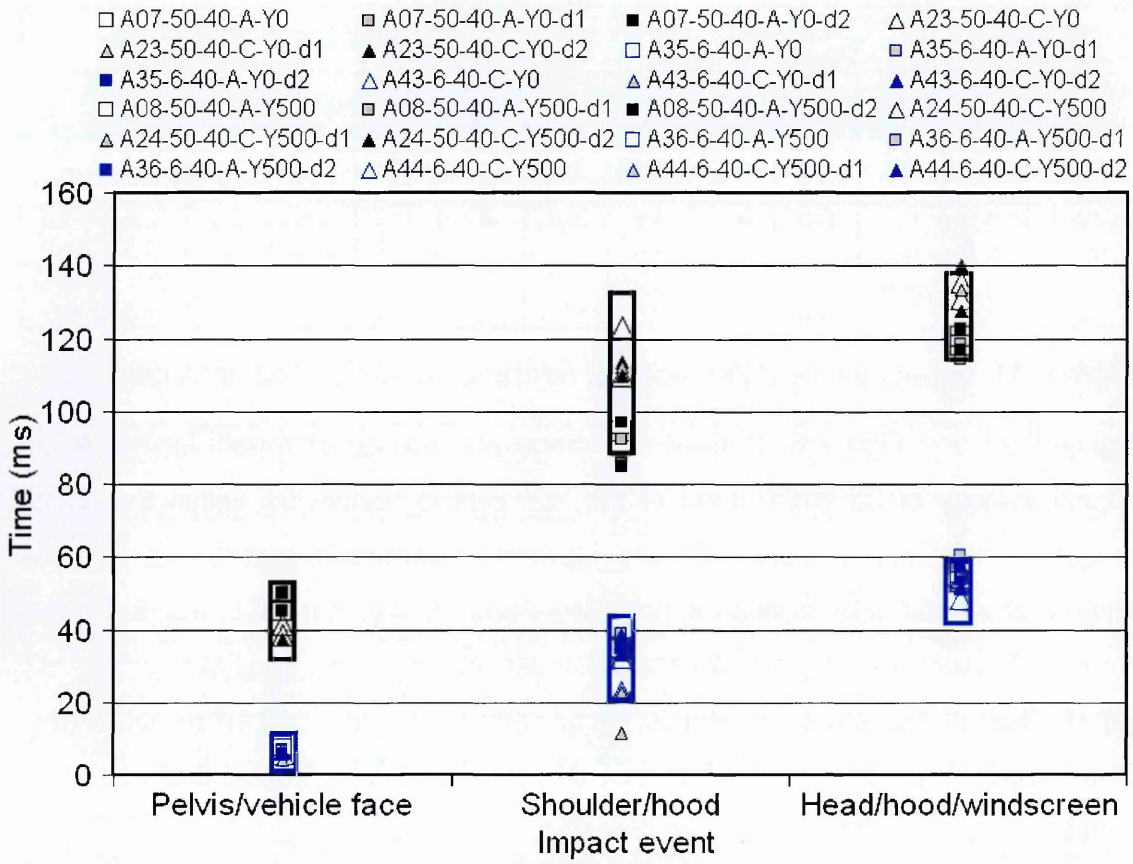

Figure 6.22 Comparison of impact timing ranges and values at 40 km/h

At an impact velocity of 40 km/h the timing differences were much smaller and it was difficult to determine consistent differences between the impact timings of the vehicles. There were both shoulder and head results that were outside of the expected ranges. In general, the shoulder impact was quicker for both modified vehicles but the head impact timing was similar, although the differences were difficult to differentiate with plot files only every 10 ms.

Figure 6.23 and Figure 6.24 show the range and absolute values of CMD. Most of the CMD results at both velocities fell within the expected ranges. The exceptions to this mainly involved the 6 year old pedestrian in stance 'C' with vehicles 'd1' and in particular 'd2'. At 25 km/h it was difficult to determine consistent differences but at 40 km/h the CMD results in X and Z were smaller and in Y larger for the modified vehicles. As with the reference vehicle results, stance 'C' often led to larger differences in the CMD results than stance 'A'.

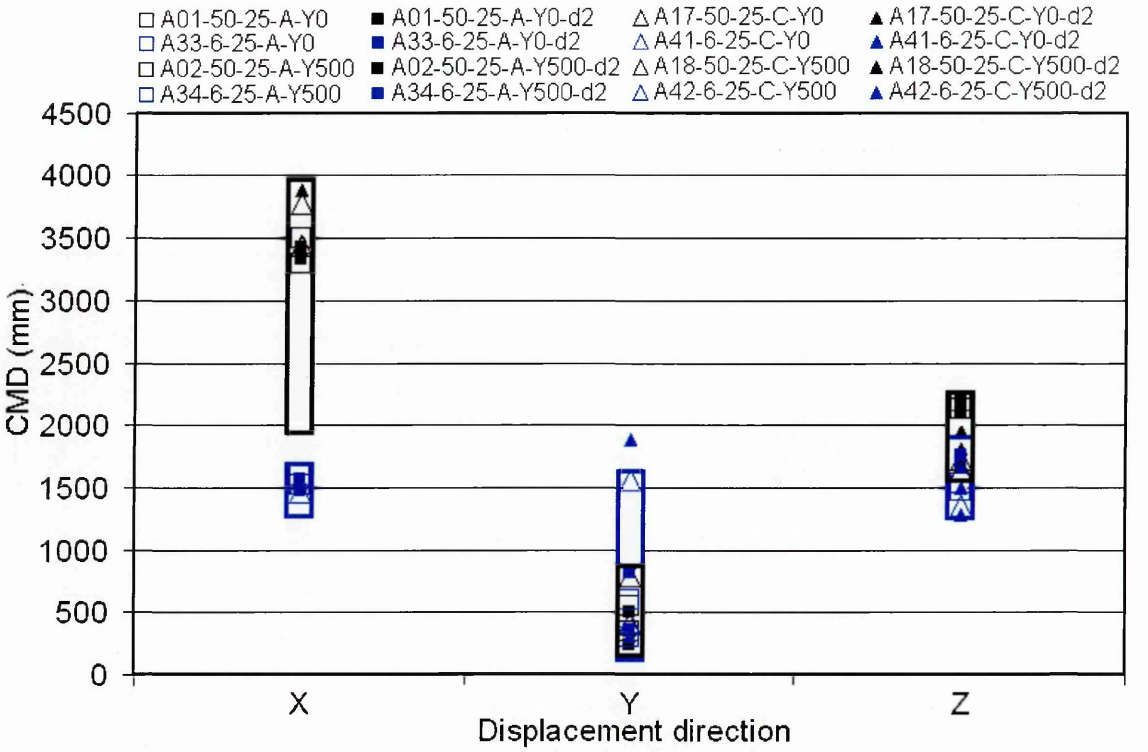

Figure 6.23 Comparison of CMD ranges and values at 25 km/h

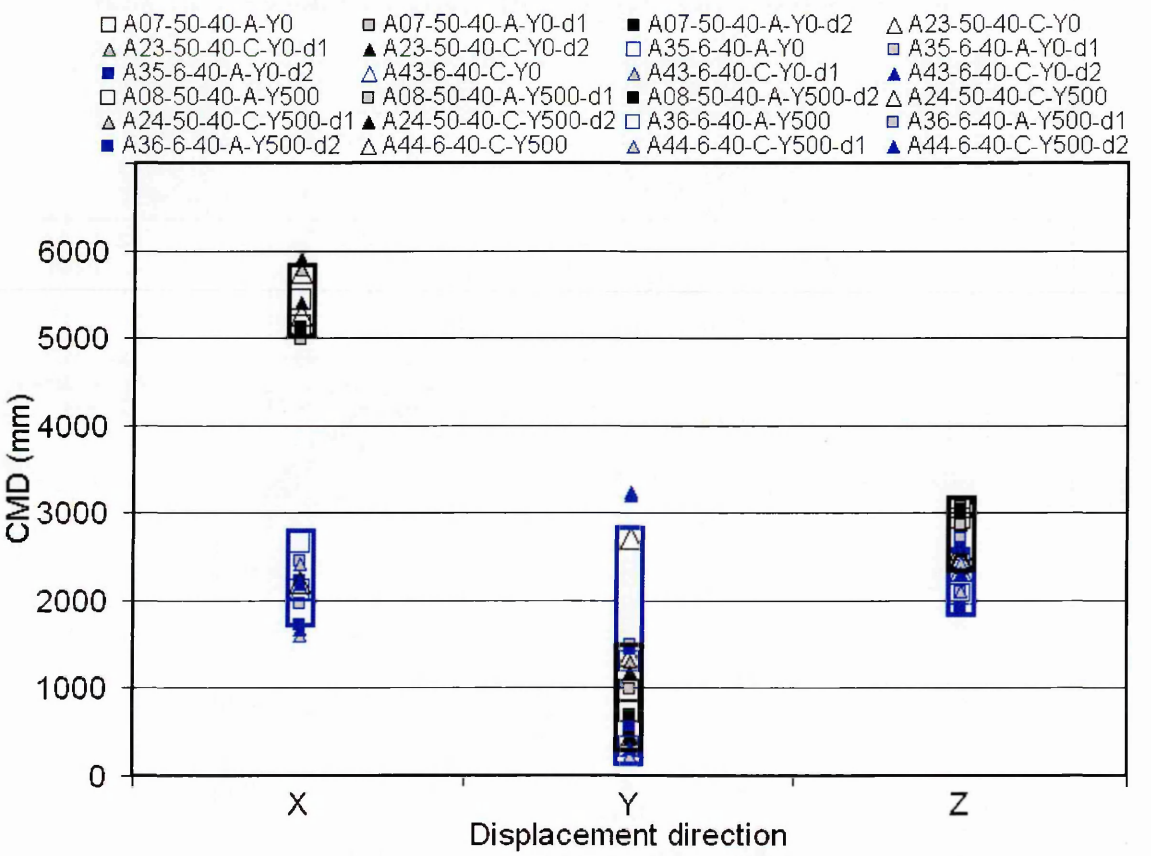

Figure 6.24 Comparison of CMD ranges and values at 40 km/h

Figure 6.25 and Figure 6.26 show the head motion results at 25 and 40 km/h.

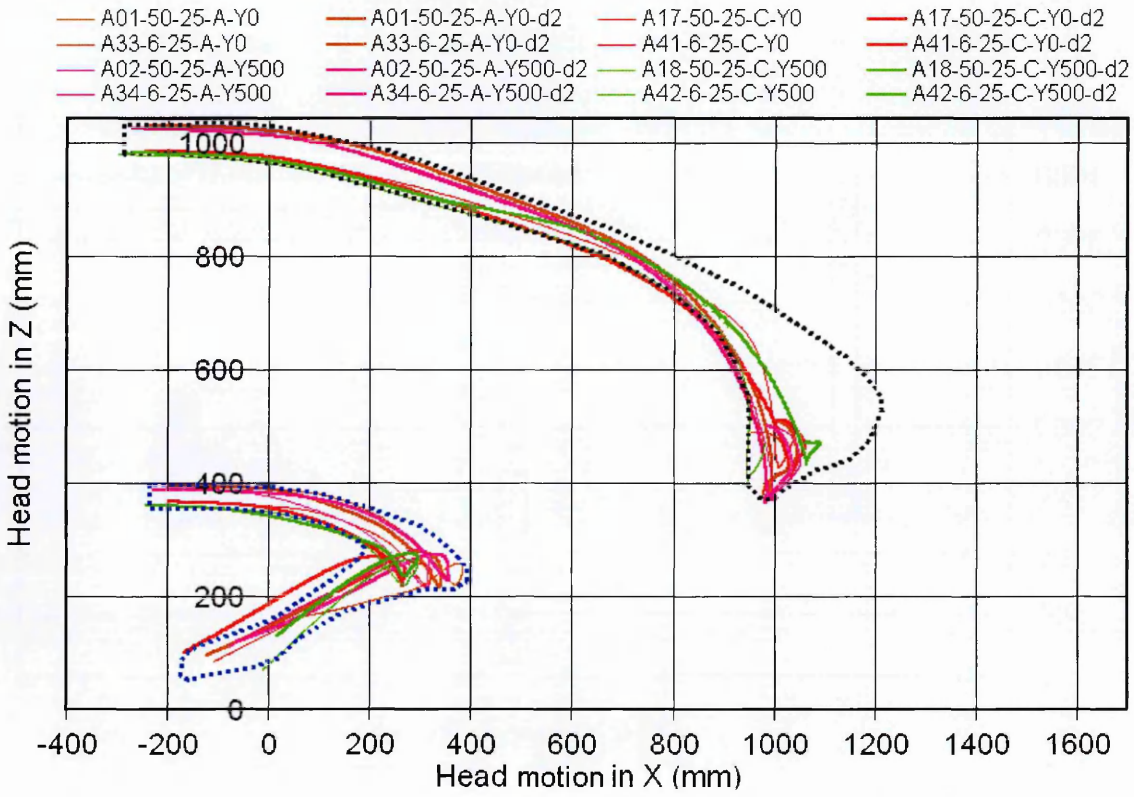

Figure 6.25 Comparison of head motion ranges and trajectories at 25 km/h

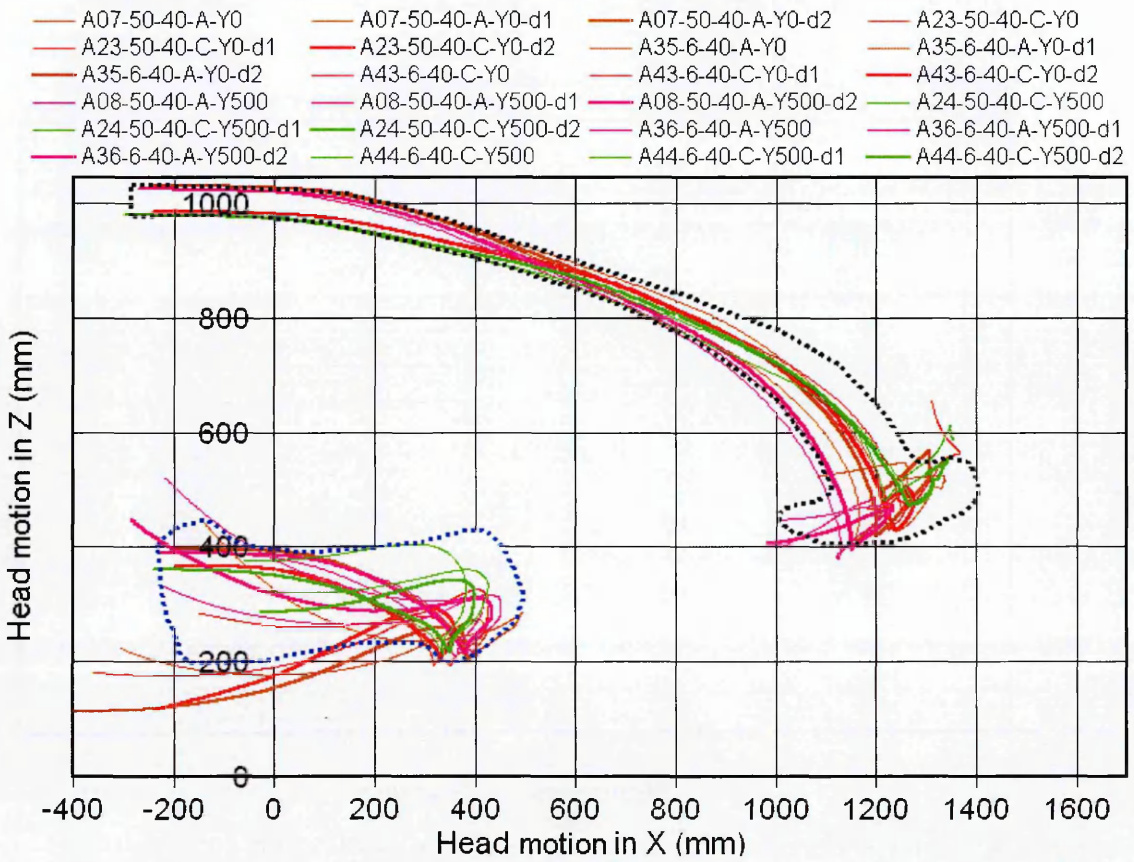

Figure 6.26 Comparison of head motion ranges and trajectories at 40 km/h

At 25 km/h it was not possible to identify consistent differences between the reference and modified vehicles. In some cases the head motion in X was increased and in some cases it was similar or it decreased. However, the differences in X were always less than 50 mm and larger than those in Z. The head trajectories at 40 km/h were even more similar but in many 'd2' vehicle cases, the post head impact motion, for both pedestrians, fell outside of the expected range.

Figure 6.27 and Figure 6.28 show a comparison of the relative head velocities. In general the modified vehicle velocity time histories fell within the expected range. At both 25 km/h and 40 km/h, vehicle 'd1' and 'd2' tended to increase the maximum head velocity for the 50th percentile pedestrian and decrease the maximum head velocity for the 6 year old. The thicker vertical lines show the timing ranges in which head impact occurred for the two pedestrians. Within these ranges there were significant differences between the velocity time histories. At the lower impact velocity, differences existed in both the shape of the velocity profile and timing and at the higher impact velocity, there were just timing differences.

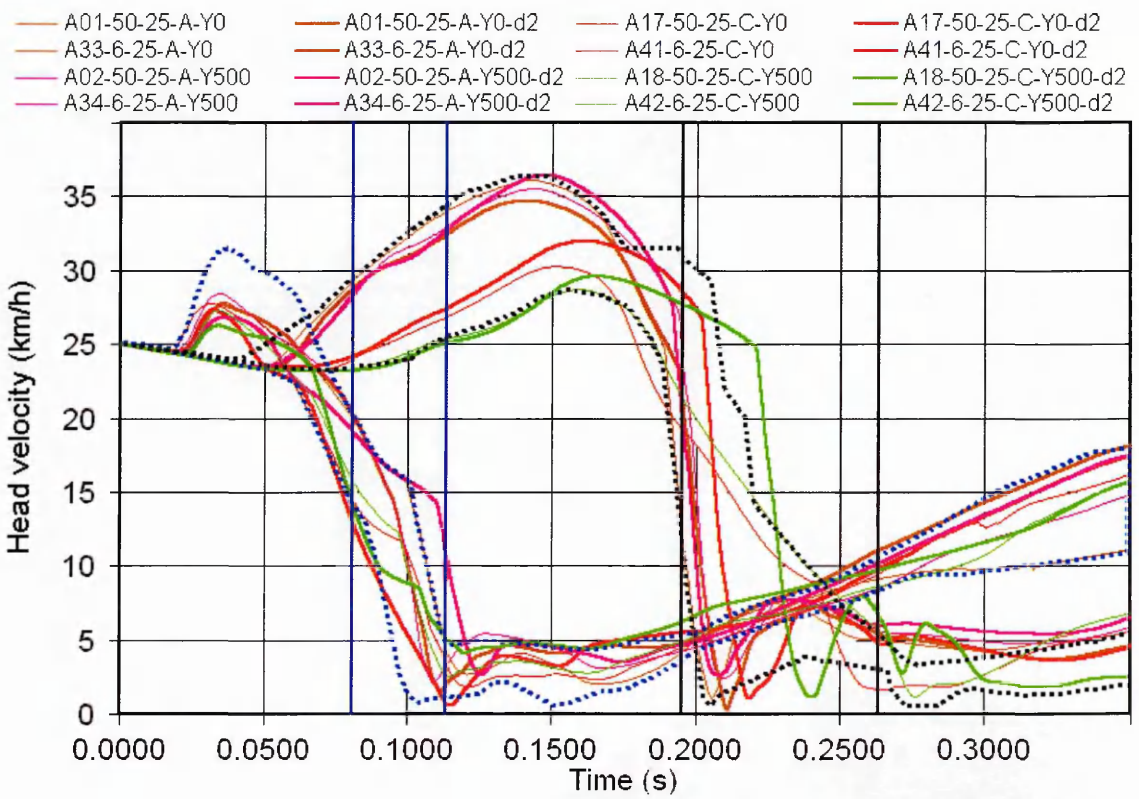

Figure 6.27 Comparison of head velocity ranges and values at 25 km/h

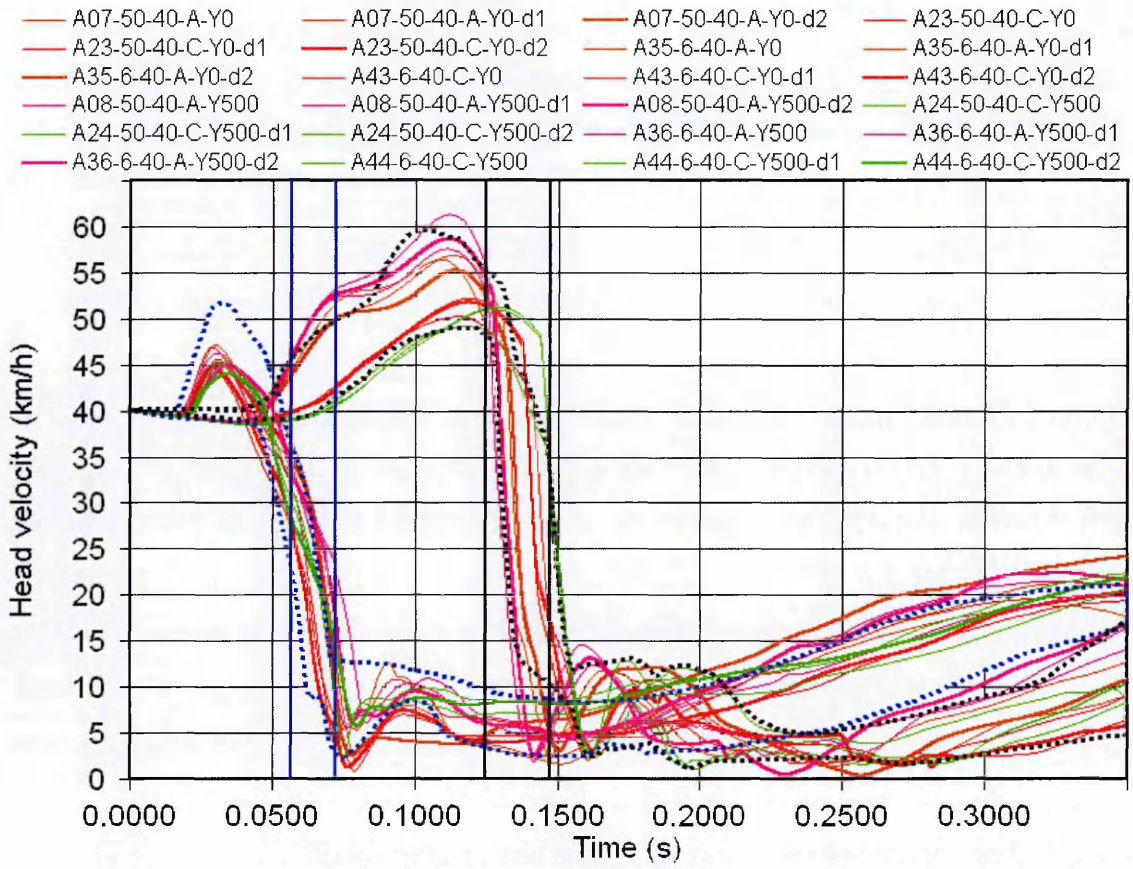

Figure 6.28 Comparison of head velocity ranges and values at 40 km/h

A comparison of HIC ranges and values are shown in Figure 6.29 and Figure 6.30.

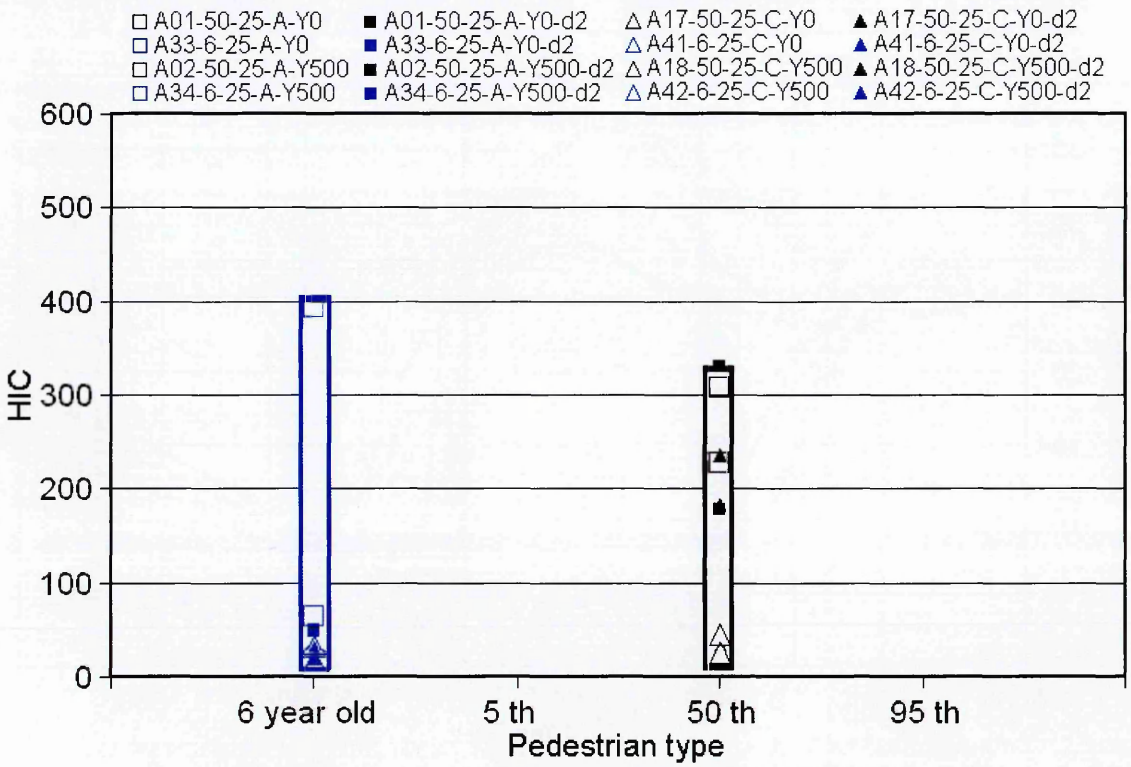

Figure 6.29 Comparison of HIC ranges and values at 25 km/h

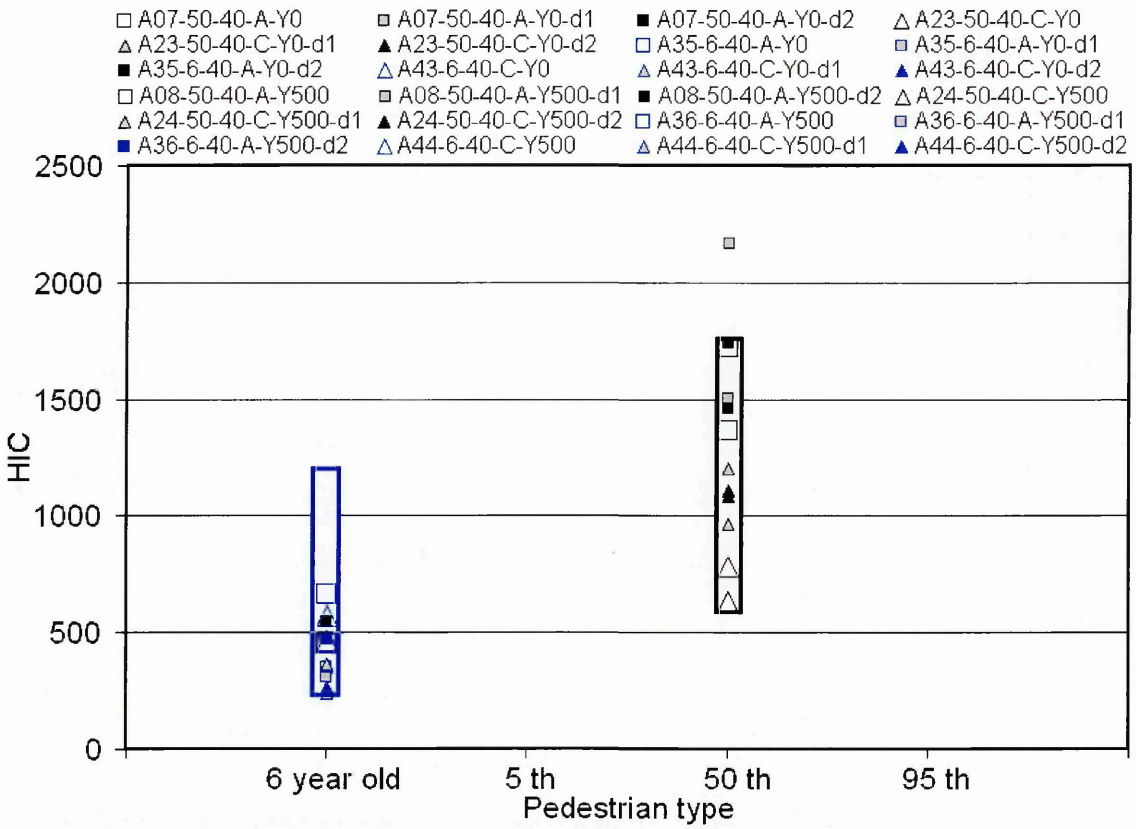

Figure 6.30 Comparison of HIC ranges and values at 40 km/h

At the lower vehicle impact velocity, all of the HIC results fell within the expected ranges as shown and were much lower than the HIC no injury criterion of 1000 [EEVC 1998]. Although all of the 6 year old pedestrian results were similar or lower, the 50th percentile pedestrian recorded much higher results for the stance 'C' cases and similar or lower results for the stance 'A' cases. At the higher vehicle impact velocity the 6 year old pedestrian HIC results were similar or lower for the modified vehicles and for the 50th percentile pedestrian similar or higher. One of the 'd1' results was significantly higher than the expected range.

The maximum pelvis acceleration results are shown in Figure 6.31 and Figure 6.32. Although there were only a few results that fell outside of the acceleration ranges some of these were relatively large. For the 6 year old pedestrian cases at the lower vehicle impact velocity, the vehicle 'd2' acceleration results were slightly lower at Y500 but much higher at Y0. The 50th percentile pedestrian measured similar results for the reference and modified vehicles with one Y0 case significantly higher and one Y500 case lower.

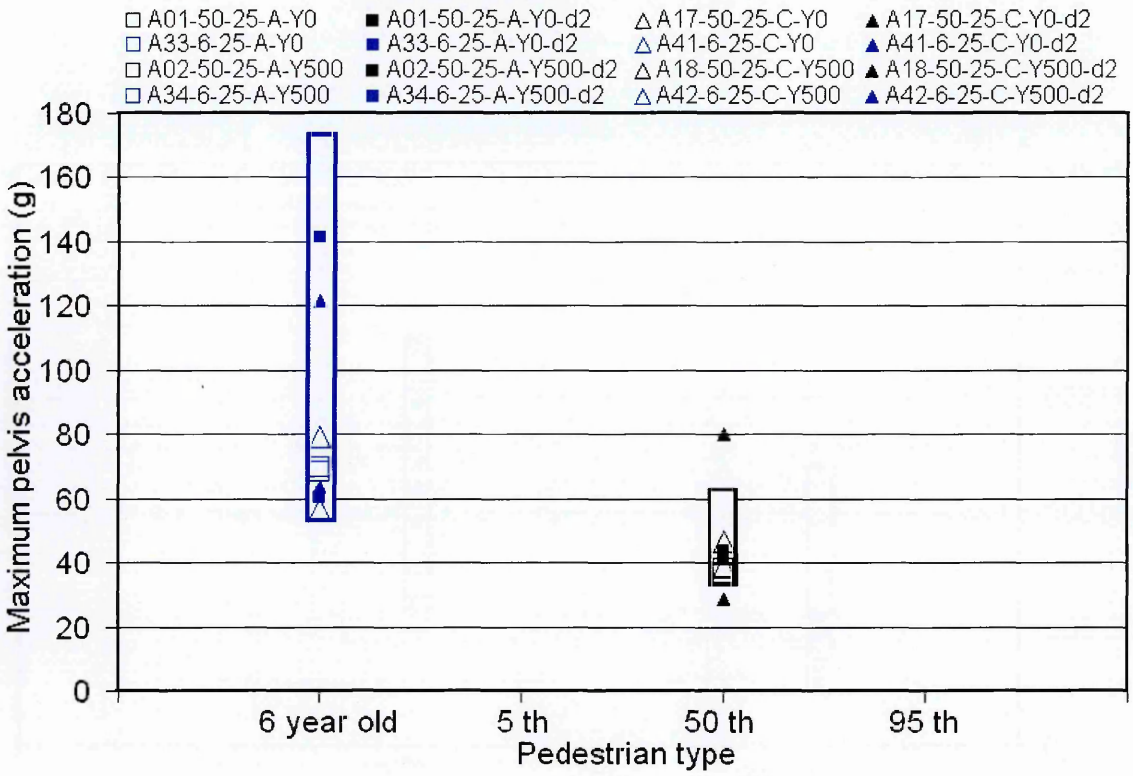

Figure 6.31 Comparison of pelvis acceleration ranges and values at 25 km/h

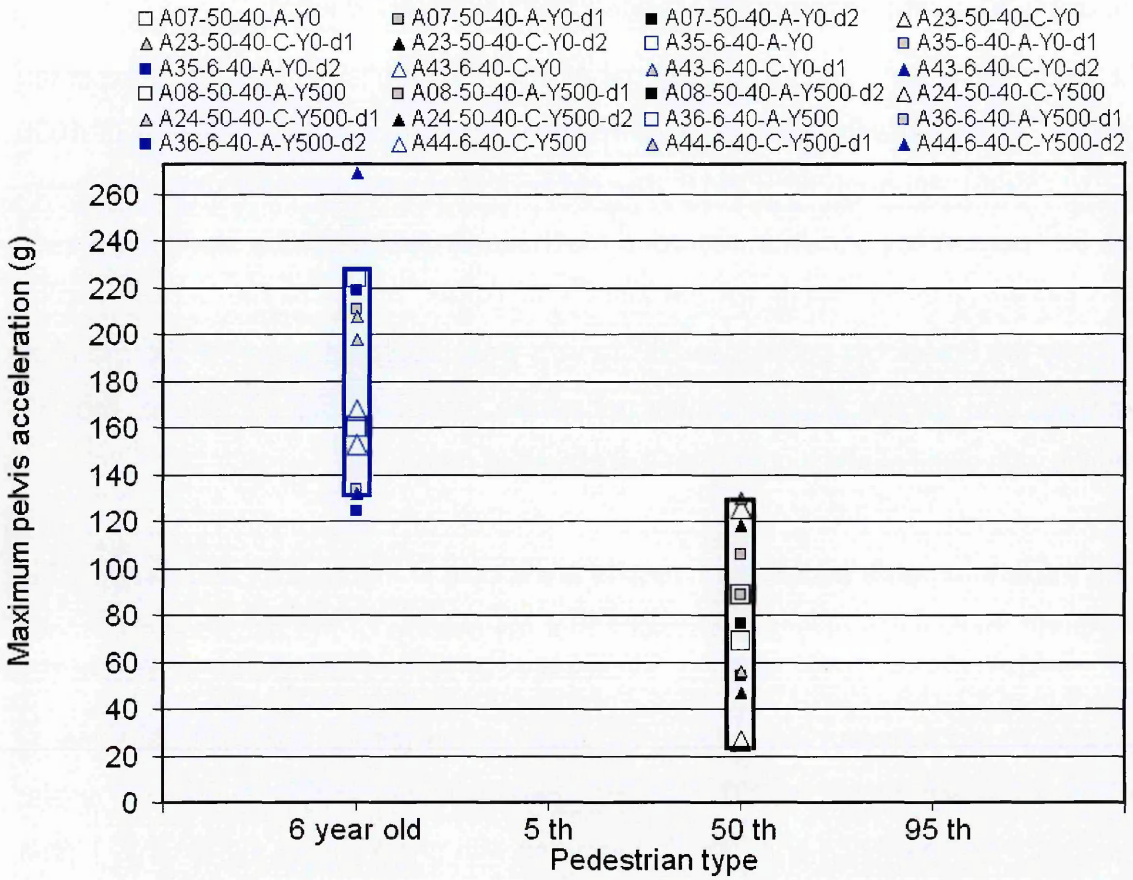

Figure 6.32 Comparison of pelvis acceleration ranges and values at 40 km/h

At 40 km/h most of the 6 year old pedestrian results for vehicle 'd2' were lower and for vehicle 'd1' higher. There were two exceptions: one for stance 'C' at Y0 and one for stance 'A' at Y0 respectively. The 50th percentile pedestrian results for vehicle 'd1' were higher and most of the vehicle 'd2' results lower than for the reference vehicle 'p'.

The maximum knee shear results are shown in Figure 6.33 and Figure 6.34. There was a very clear trend with both modified vehicles generating significantly smaller shear results than the reference vehicle in all cases. The largest improvements were achieved for the 50th percentile pedestrian at both vehicle impact velocities. Such a large difference in the results had also been clear in the detailed analysis of the animation files shown earlier in Figure 6.20. In most cases the 'd1' and 'd2' vehicle results were similar, with neither of them achieving consistently lower shear results than the other.

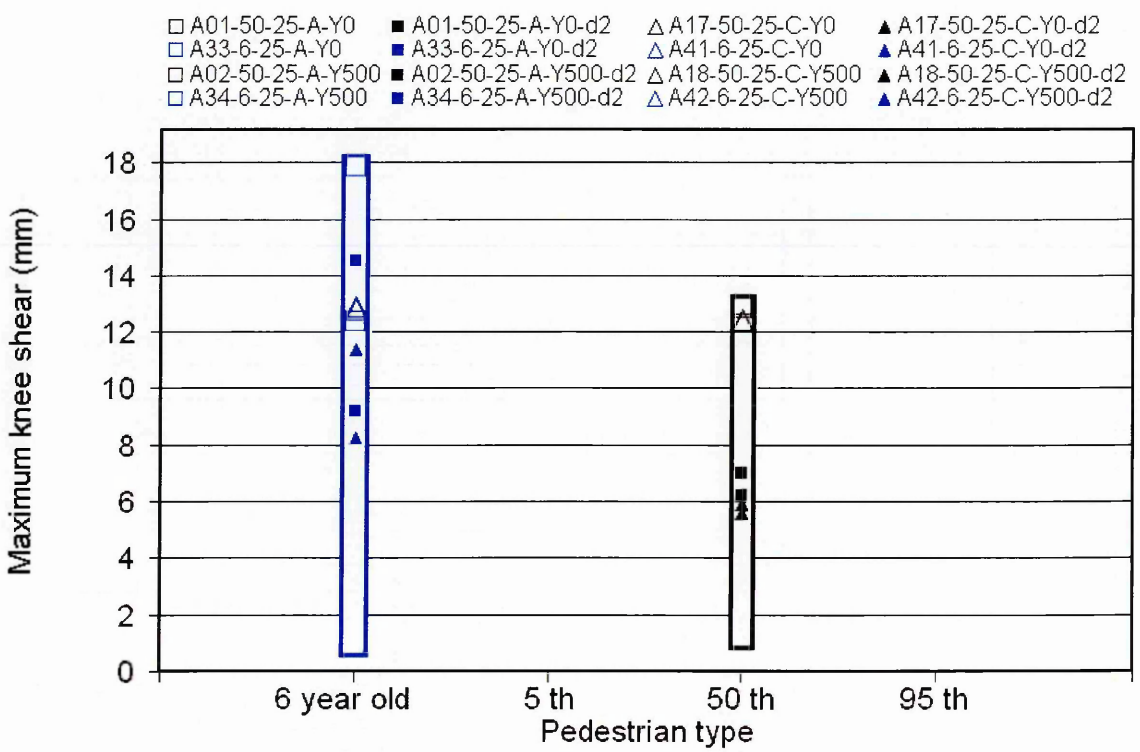

Figure 6.33 Comparison of knee shear ranges and values at 25 km/h

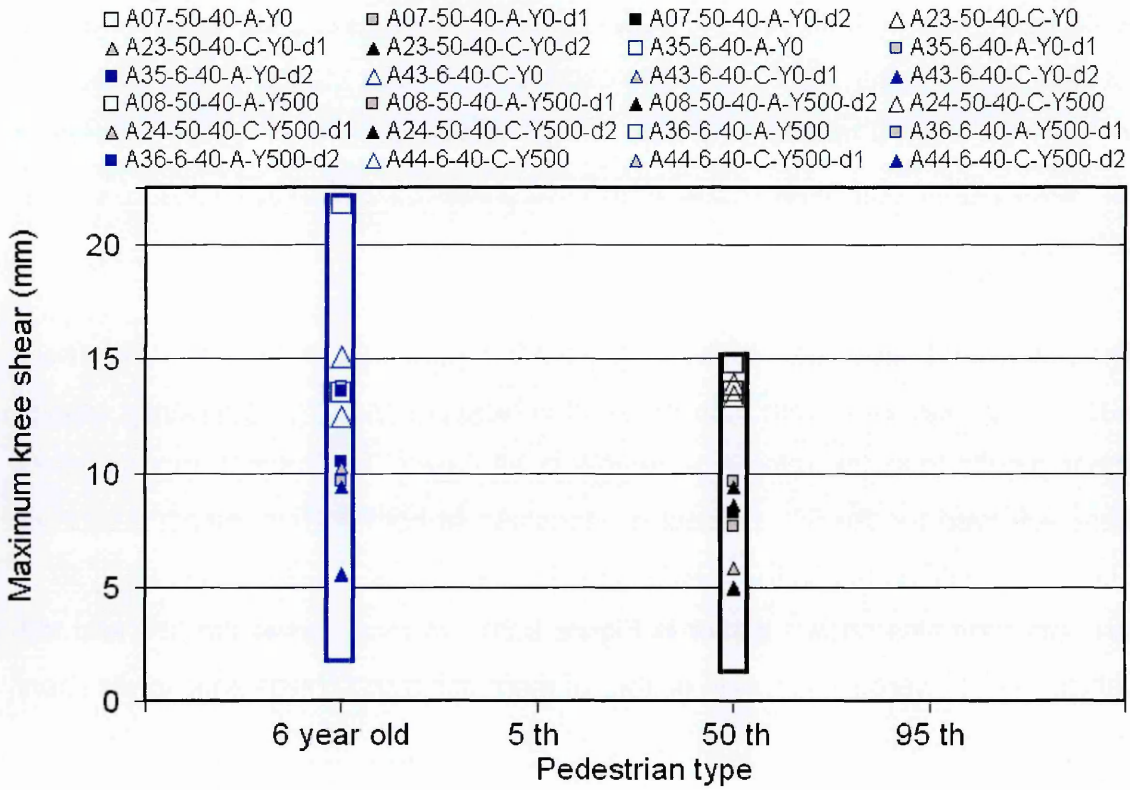

Figure 6.34 Comparison of knee shear ranges and values at 40 km/h

Figure 6.35 and Figure 6.36 show the maximum knee bending angle results.

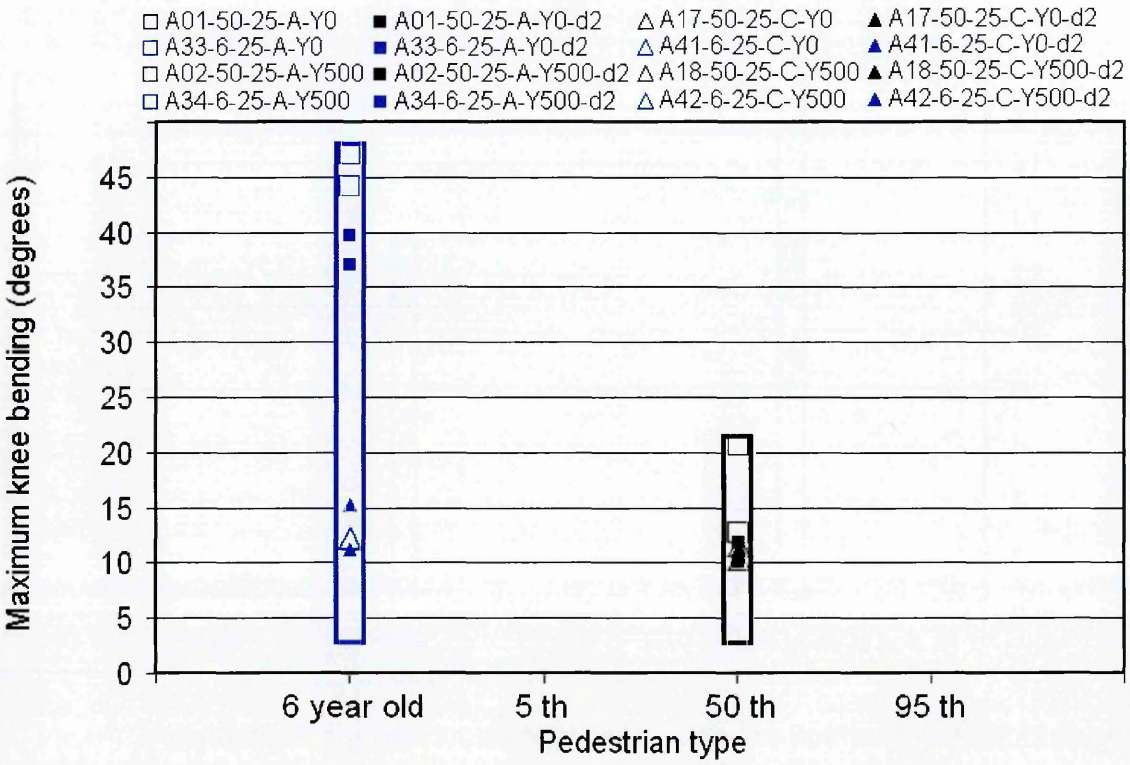

Figure 6.35 Comparison of knee bending ranges and values at 25 km/h

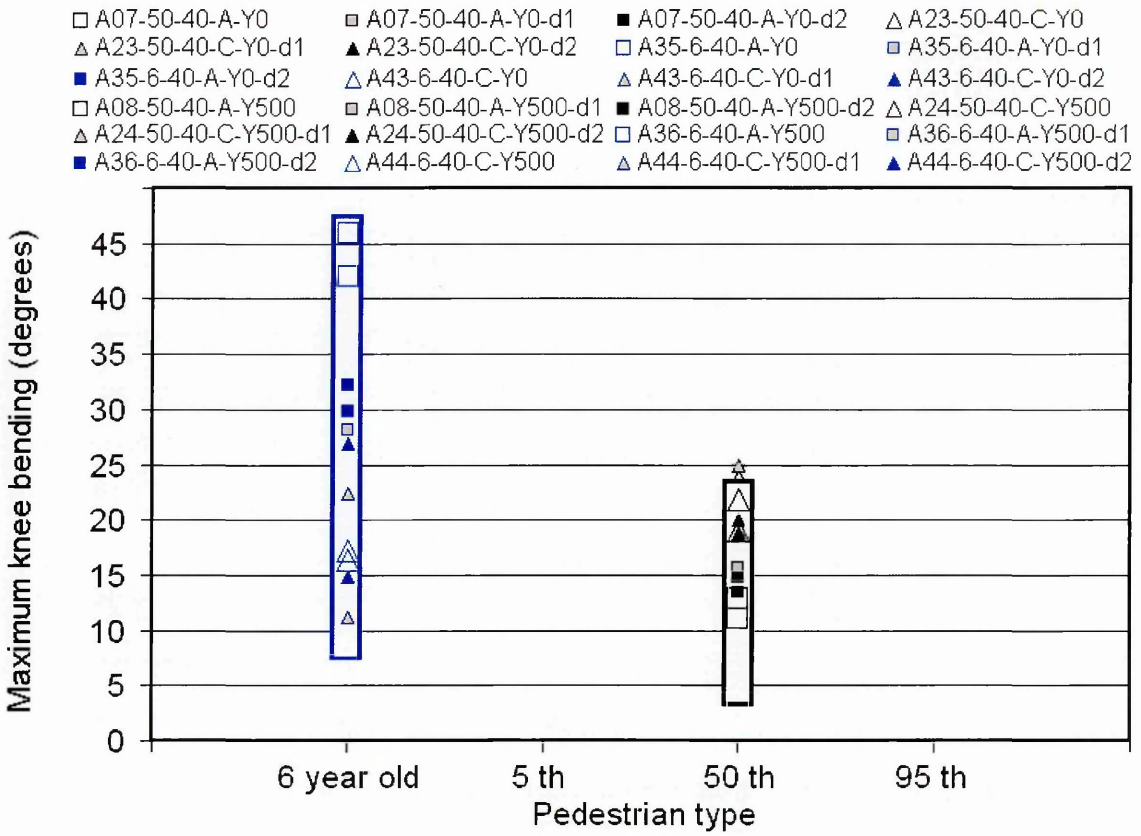

Figure 6.36 Comparison of knee bending ranges and values at 40 km/h

The majority of the bending results at the lower impact velocity for vehicle 'd2' were smaller or similar to the reference vehicle, most noticeably for stance 'A'. The 50th percentile pedestrian measured similar or marginally higher bending results for both modified vehicles at the higher impact velocity. However, the 6 year old pedestrian measured lower bending results for all stance 'A' cases. Half of the stance 'C' cases were lower for the modified vehicles.

The maximum tibia acceleration results are shown in Figure 6.37 and Figure 6.38. All of the tibia acceleration results for both modified vehicles were either significantly lower or similar to the reference vehicle. The differences were much larger for the 50th percentile pedestrian model, stance 'C' and at the higher vehicle impact velocity. As with the other leg measures it was not possible to distinguish consistent differences between the results generated by the modified vehicles.

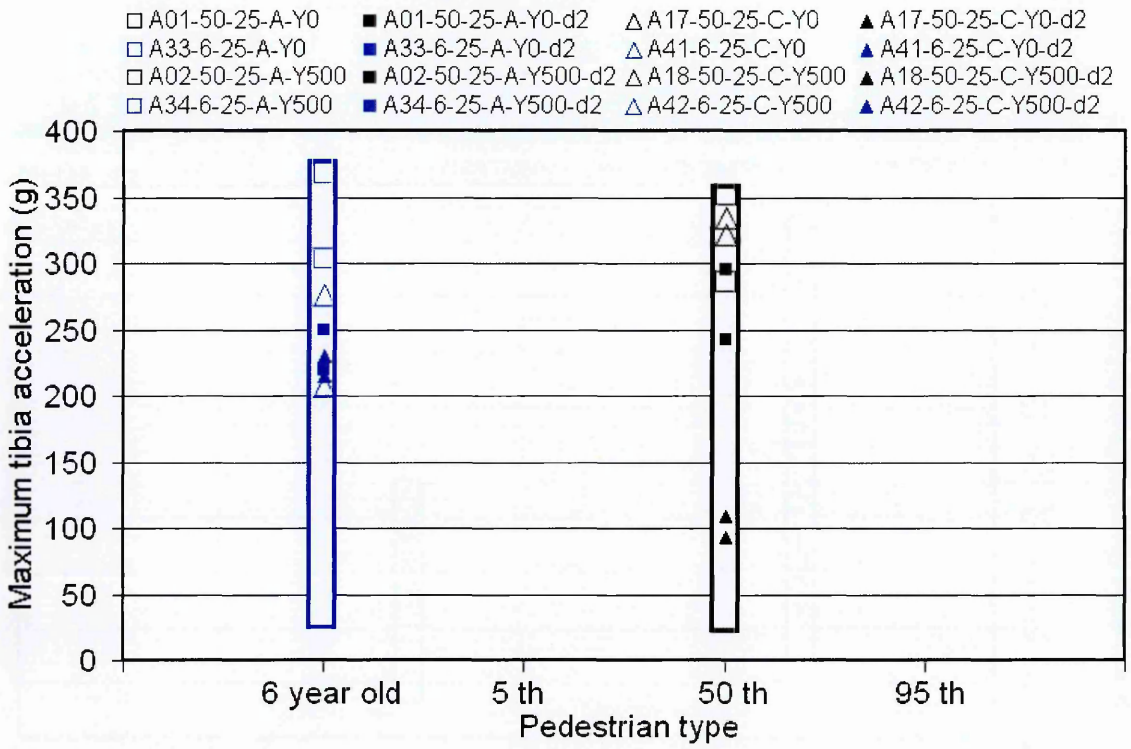

Figure 6.37 Comparison of tibia acceleration ranges and values at 25 km/h

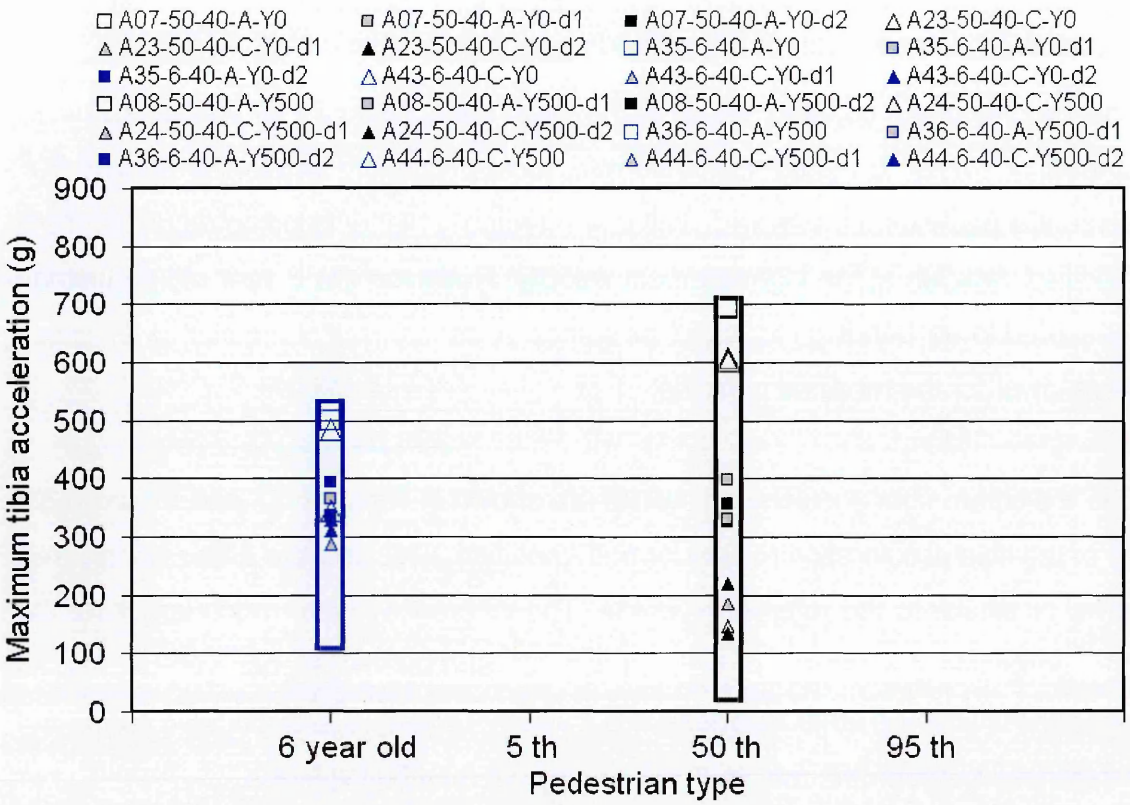

Figure 6.38 Comparison of tibia acceleration ranges and values at 40 km/h

The leg bone fracture locations were not analysed in detail because the reference

vehicle results had shown that fracture location did not exhibit any clear trends.

6.3.4. Discussion of comparative results

The influence of the technologies on global pedestrian motion was relatively small. Any differences in motion were clearer at the beginning of the simulations when the leg to bumper contact occurred and near the end of the simulations when the cumulative influence of all the technologies was sufficient to create larger differences in motion. Although it was more difficult to detect motion differences between the modified vehicle simulations, there were clear differences compared to the reference vehicle simulations.

The 6 year old pedestrian was more sensitive to changes in the vehicle structure (i.e. it had lower body inertia and hence less resistance to motion changes caused by vehicle stiffness) and therefore it was easier to identify motion differences between the three vehicles. The clearest differences were observed with the 6 year old pedestrian in stance 'A' and the highest vehicle impact velocity. Possible explanations for this were the larger interaction of the pedestrian with the vehicle structure and the greater kinetic energy available, for instance, to move the hood parts (e.g. the legs were adjacent so the effective inertia accelerated by the bumper was larger).

The technologies reduced the amount by which the pedestrian legs wrapped around the vehicle front and subsequently rebounded in the Z direction. This was because the technologies were designed to support the lower part of the pedestrian body and then absorb energy in a controlled manner with larger structure deformation. However, both the headlamp and hood technologies caused the pedestrian to be thrown further forward on the hood because they were caught by the structure and then propelled forward. In general, there was less package space beneath and towards the front of the hood, stiffer impact regions and a greater possibility of a secondary ground impact. None of these was desirable from the perspective of reducing pedestrian injuries.

Expected ranges of pedestrian injury measures provided an additional perspective

when comparing measures from the reference and modified vehicles. They demonstrated how pedestrian protection technologies could generate injury measures that are outside of the range of those for a reference vehicle under a wide range of accident conditions.

At 25 km/h and 40 km/h, the pelvis to vehicle face impact timing was very similar for the reference vehicle and modified vehicles. This was to be expected because this impact occurred very rapidly and was only influenced by the bumper technology. In contrast to this, the shoulder and head impacts often occurred much more quickly for both modified vehicles, particularly at 25 km/h and with a 50^{th} percentile pedestrian in stance 'C'. There was larger deformation of the hood and headlamp technologies and therefore the subsequent impact events occurred more quickly. At 40 km/h the relative increase in deformation was relatively small in comparison to an impact speed of 25 km/h, because, for instance, the headlamp convolutes were fully deformed. The 50^{th} percentile pedestrian was more sensitive to pelvis angle changes than the 6 year old because of the greater distance between the pelvis and head. Stance 'C' was a relatively unstable stance in comparison to stance 'A' and therefore the pedestrian motion was more sensitive to vehicle stiffness and geometry changes. Future research is required to improve the certainty of an impact event. Plots every 10 ms were not capable of capturing exactly when impacts occurred and therefore more frequent plot states need to be evaluated in future research.

Both the advantages and disadvantages of single displacement measures were observed in the CMD results. The advantage of this measure was that it took into account the displacement of many different parts of the pedestrian models and allowed a simple comparison of results. However, for precisely the same reason it was not as sensitive to vehicle model changes as, for instance, head displacement. Despite this, it showed that the modified vehicle models measurably changed the general motion of both pedestrian models, that the changes mainly occurred in the X and Y directions and that some results fell outside of the expected ranges. Of particular note was that the hood technology caused a large increase in the lateral

motion of the 6 year old, although it is not possible to predict the implications of this in an actual accident. As with impact timing, stance 'C' generated the largest CMD differences and for the same reasons. However, unlike impact timing, the 6 year old pedestrian results showed the largest differences due to the factors discussed for the overall motion.

The head trajectory results provided a means to track the motion of a specific body region against time. As with some of the other measures and for the same reasons the largest difference in results was observed for the higher vehicle impact velocity and the 6 year old pedestrian. Since the primary impact direction was in X, this explained why the largest differences were observed in X rather than Z. The out of range, post head impact motion at 40 km/h needs to be investigated further because it is undesirable (the risk of being thrown on the ground is larger) and the exact causes of this are not fully understood. Hence this warrants future research with respect to evaluating different hood mechanism geometries, for instance.

Both modified vehicles increased the maximum head velocity for the 50^{th} percentile pedestrian but decreased it for the 6 year old pedestrian. The manner in which the hood and pedestrian (in space and time) interacted was complex but the animation files revealed further information about why these trends occurred. In the case of the 6 year old, the softer vehicle structure and/or rearward motion of the hood leading edge was much closer to, and had a more direct influence on the head motion. As the 6 year old wrapped around the vehicle face, it was clear that the head was being decelerated in a more controlled manner than for the reference vehicle, because of the structure deformation and rearward motion. With the 50^{th} percentile pedestrian the vehicle face impact occurred with the legs rather than the pelvis and thorax. This meant that there was an indirect influence of the vehicle structure changes on the head motion. Less energy was absorbed in the vehicle face impact and as the velocity profiles indicated, more time was available for the head velocity to continue increasing before the vehicle structure retarded the pedestrian motion. Two additional observations can be made; the differences in maximum head velocity were relatively small (less than 10 %) and this measure

was not a good indicator of injury prediction. Pre head impact velocity would have been a better indicator but it was difficult to determine this from the results using timing ranges. Future research should examine pre head impact velocity in addition to the velocity time histories.

All of the HIC results from the lower vehicle impact velocity were less than half of the no injury criteria specified in [EEVC 1998]. Therefore it was not constructive to draw any significant conclusions from these results. At the higher vehicle impact velocity the HIC results were comparable to those previously measured using experimental head impactor tests [Howard 2000-2] and therefore, they were more reliable from the perspective of the HIC calculation. In a similar manner to the maximum head velocity results, the HIC results were higher for the 50^{th} percentile pedestrian and lower for the 6 year old child. Although many other factors influenced HIC (e.g. vehicle stiffness at the impact location) this suggested that there was a relationship between these measures. This also implied that maximum head velocity and pre impact head velocity were related in some manner because the latter is directly related to HIC. Assuming that these relationships existed (and future research should be undertaken to confirm this) then the same causes for the differences in head velocity also caused the differences in HIC.

As with some of the other results it was difficult to make general observations concerning whether the maximum pelvis acceleration results were lower or higher for either of the modified vehicles. The relative benefit (i.e. lower pelvis acceleration) of either modified vehicle depended on many factors, such as the vehicle impact location, velocity and pedestrian type. However, it was clear that, for instance, the Y0 location on vehicle 'd2' generated higher pelvis acceleration than for the reference vehicle at low impact velocities but any differences at the higher impact velocity were relatively small and without a clear trend. A known problem in the pedestrian model pelvis construction (that was described in an earlier chapter) contributed to the uncertainty. Future research should be undertaken to determine if the pedestrian models still exhibit these problems and in particular whether such large out of range results for a few cases occur, as a consequence of the

construction of the pedestrian or the vehicle model.

In comparison to the other results there was a very clear trend for the knee shear results with both modified vehicles achieving much lower shear results for all cases. This conclusion and the reasons for this had also been clear in the animation plots described in an earlier chapter. Although it was not possible to distinguish whether the 'd1' or 'd2' vehicle achieved better results, this was not surprising because the main vehicle parts that influenced this, namely the bumper and undertray, were identical in both vehicle models.

The reference vehicle knee bending results and in particular the time histories were more complex than those for the knee shear results. Unlike the maximum knee shear the maximum knee bending results did not occur in the first 10 ms. They occurred much later during, for instance, the pelvis to vehicle face impact. This impact occurred as late as 60 ms for the 50^{th} percentile pedestrian in stance 'A' (see appendices). The implication of this was that other parts of the vehicle such as the headlamp and hood influenced these results. This had not been considered in the bumper technology DoE study and may have contributed to the relatively poor performance of some of the modified vehicle cases. Future research should include a DoE study that identifies the contribution of other vehicle parts on the bending results.

Both modified vehicles generated lower bending angle results for stance 'A' cases but the benefits for stance 'C' were less consistent. Stance 'A' led to generally higher bending angle results and less complex pedestrian leg motion. However, stance 'C' was more representative of a real world pre impact stance [Isenburg 1998].

Tibia acceleration had been used to identify clear trends in the reference vehicle results and it was also possible to identify that in nearly all cases the modified vehicle acceleration results were lower. The largest improvements occurred at the higher impact velocity, where the bumper foam deformation made the greatest

contribution to reducing the acceleration by reducing the impact force.

6.3.5. Modified vehicle accident simulation conclusions

A minimum number of pedestrian accident conditions are recommended for evaluating and comparing reference and modified vehicle models. These result in sixteen simulations per vehicle with the following conditions:

- Vehicle braking deceleration of 1g with 70 mm brake dive and no pitching (these values are vehicle specific)
- Vehicle impact velocities of 25 km/h and 40 km/h at Y0 and Y500
- A 6 year old and a 50th percentile pedestrian
- Walking with the struck leg forward and legs together stances

In addition to the justification explained in a previous chapter, the results also indicate the value of these choices. For instance, the high sensitivity of the 6 year old to vehicle structure changes, stance 'A' to bumper changes, stance 'C' to hood technologies and the different benefits (and in some cases disadvantages) of pedestrian protection technologies at low and high vehicle impact velocities.

Visual examination of pedestrian accident simulation animations is essential to fully understand the three dimensional influence of the vehicle structure and pedestrian protection technologies on pedestrian motion and injuries. The influence of the vehicle structure changes on global pedestrian motion is relatively small and therefore it is necessary to examine detailed vehicle cross sections in addition to the global pedestrian and vehicle motion. There are observable differences between the pedestrian motions caused by an impact with a reference vehicle and a modified vehicle. However, it is more difficult to observe differences in motion between modified vehicles fitted with different pedestrian protection technologies. Global motion animations show how the headlamp and hood technologies cause the pedestrian to be thrown further forward on the hood. Detailed vehicle cross sections show how the bumper and undertray technologies reduce the amount by which the pedestrian legs wrap around the vehicle front and subsequently rebound in the Z direction.

The interaction between the vehicle and pedestrian is complex and therefore it is necessary to view this as a series of discrete impact events so that accident timing can be summarised. When using the humanoid models it is recommended to use the pelvis to vehicle face (e.g. headlamps, radiator grill, hood leading edge) shoulder to hood and head to hood or windscreen impact events. In general, impacts occur more quickly for smaller pedestrian and higher vehicle impact velocities. The largest differences of impact timing between reference and modified vehicles will be observed in the two latter events and for technologies such as the deployable hood and deformable headlamp, at the lower vehicle impact velocity. These two technologies led to quicker impact, particularly for the shoulder contact. In order to more accurately visualise each impact event, it is recommended to create plot states at least every 5 ms.

It is also necessary to use quantitative measures when predicting the influence of vehicle structure changes on pedestrian motion and injuries. If a wider range of accident conditions is analysed with the reference vehicle, then expected ranges could be constructed. This allows a better understanding of the influence of vehicle changes on these measures, in comparison to a wider range of accident conditions. The following quantitative measures should be used with the humanoid models:

- Composite maximum displacement (CMD)
- Head centre of gravity trajectory in the XZ plane
- Head centre of gravity resultant velocity, maximum velocity & pre impact velocity
- Head injury criterion (HIC)
- Pelvis resultant acceleration
- Knee bending and shear
- Tibia resultant acceleration

CMD is a convenient but relatively insensitive measure to compare the influence of vehicle design changes on pedestrian motion. For instance, it confirms that larger pedestrians are thrown further in the X direction and smaller pedestrians rotate in a small volume of space near the vehicle front and are more sensitive to vehicle design changes. It also shows that vehicle design changes mainly influence the X

and Y directions of motion and that the hood technology causes a large increase in the lateral motion of small pedestrians. The implications of this are not known and this is an area for more detailed future research.

Head trajectory is a more sensitive measure than CMD to different accident conditions and vehicle design changes, although a time history is more difficult to compare than a single value. In addition to confirming CMD observations it shows that stances 'A' and 'C' lead to the shortest head trajectories in direction X and 'D' the longest. This means that the head impact location will differ between different stances and hence the hood design requirements (e.g. package space below the hood) will also vary. Post head impact motion of smaller pedestrians and impacts with a vehicle that incorporates a hood technology is larger than that of larger pedestrians and a reference vehicle impact. The implications of these observations are not known and should be investigated in future research. However, larger post head impact motion can lead to a greater probability of undesirable ground contact.

Maximum head velocity increases with vehicle impact velocity and stances 'A' and 'D'. HIC shows the same trend and therefore suggests that there is a relationship between maximum head velocity and pre head impact velocity. The exact form of this is not known and should be the subject of future research because the latter is a better head injury predictor, and more difficult to determine from the results. This implies that head injury risk increases with vehicle impact velocity and certain types of stances. The technologies examined have a relatively small influence on head velocity and HIC. Maximum head velocity and HIC are increased for the 50^{th} percentile pedestrian and decreased for the 6 year old child. The implication is that the technologies cause a small increase in head injury risk for adult pedestrians and a decrease for child pedestrians. However, more research is required to determine the reasons for this and whether both velocities can be reduced with a different technology configuration.

Pelvis acceleration increases with vehicle impact velocity and is higher for a 6 year old pedestrian. This implies that pelvis fracture is more likely at higher vehicle

impact velocities and for smaller pedestrians, assuming that injury susceptibility is similar or lower. It was not possible to identify clear trends in the relative performance of the reference and modified vehicles. Future research is required to determine if this was due to a known problem in the pedestrian model pelvis construction or a realistic variation in this measure.

There is only a small increase in knee shear with vehicle impact velocity and this implies that even at 25 km/h the knee injury limit is already approached. The combination of the bumper and undertray technologies generates much lower shear results in all cases. Knee injury due to the shear mechanism is less likely with these technologies.

Knee bending is influenced by more parts of the vehicle structure than knee shear because it does not reach a maximum value until the upper legs strike other parts of the vehicle structure. This had not been considered in the DoE bumper study and future research is required to determine whether this changes the conclusions from this study with respect to minimising bending angle. Knee bending angle increases with vehicle impact velocity, smaller pedestrians and stance 'A'. Hence, knee injury risk, due to the bending mechanism, increases with these conditions. Like knee shear, the combination of the undertray and bumper technologies reduced knee bending but not for all stance 'C' cases. The knee bending injury risk benefits of such technologies are reduced in more realistic pre impact accident stances. Future research should be undertaken to establish what factors influence knee bending and how it may be more effectively reduced for all stances.

Tibia acceleration and hence tibia/fibula condyle fracture increases with vehicle impact velocity. Stance 'A' leads to the highest accelerations and the 6 year old child records the lowest accelerations. Hence, the greatest risk of such fractures occurs with relatively unrealistic stances and for adults, assuming that the relative susceptibility to this type of injury is similar. In nearly all cases the modified vehicle acceleration results were lower and therefore the undertray and bumper technologies reduced the risk of tibia/fibula condyle fracture.

7. Experimental Testing of Pedestrian Safety Vehicle (PSV)

7.1. Context in overall methodology

This final chapter briefly describes two PSV's that were constructed with the pedestrian protection technologies described and subsequently tested according to [EEVC 1998]. The tasks undertaken are highlighted in Figure 7.1 [Howard 2001-1].

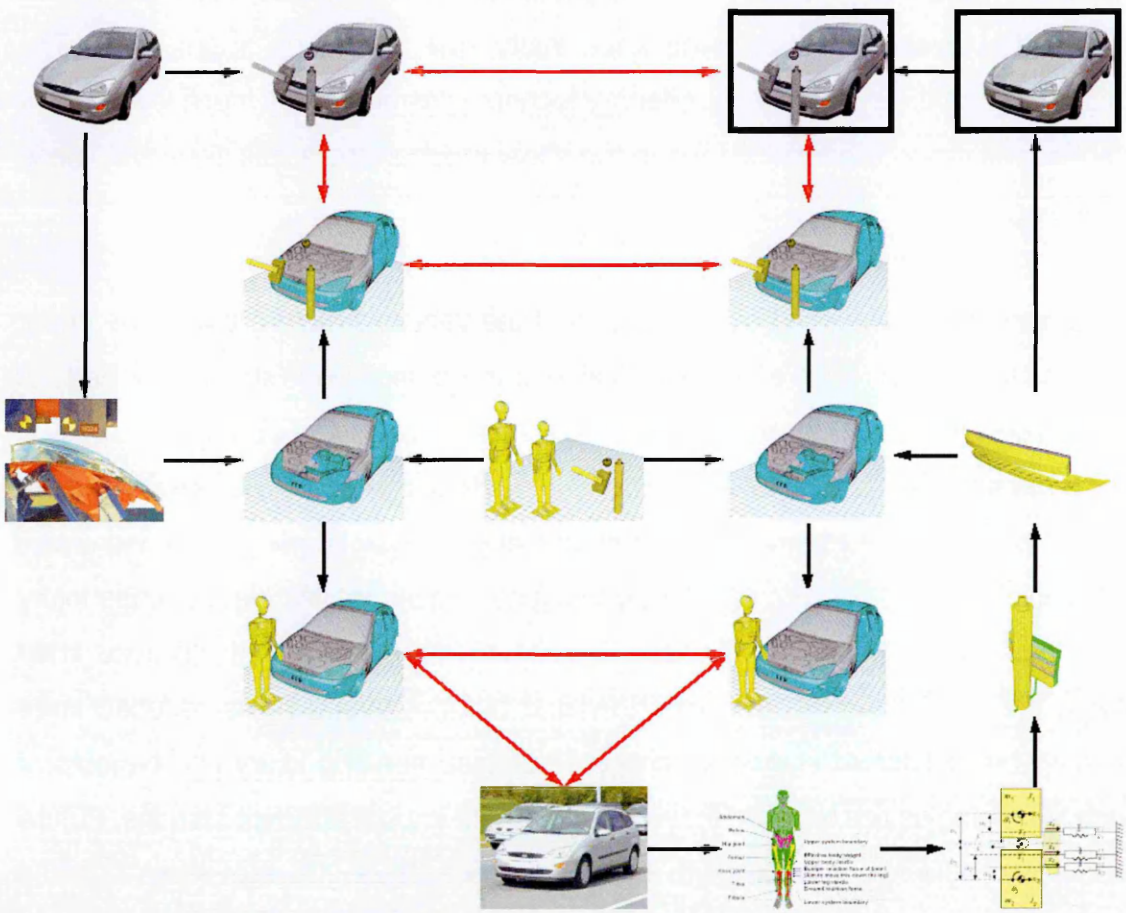

Figure 7.1 Pedestrian protection technology methodology (PSV)

7.2. The PSV's

In parallel to the development and analysis of component and vehicle simulation models, two PSV's were constructed. One of these, the test vehicle, only featured PEHKS and POBSY because it was not possible to construct mechanically representative modified headlamps within the resource constraints. The other PSV incorporated all of the pedestrian protection technologies and was used as a technology demonstration vehicle. This vehicle is shown in Figure 7.2.

Figure 7.2 The pedestrian protection technology demonstration vehicle

Inset 1 shows POBSY with the stiffness matched structural undertray and dual density energy absorbing foam. PAH is shown in inset 2 and one part of PEHKS; one of the rotational and translational joints on the end of the GOR. The frontal lift support shown in inset 3 was connected to this joint and used mechanical advantage to transfer the rearward and upward motion of the GOR into similar hood motion. In combination with the new rear hinge in inset 4, the complete vehicle front end (GOR, hood and headlamps) was designed to move rearward and upward during a pedestrian impact. Only the energy due to the pedestrian impact is used to lift the hood with no pyrotechnic or other electro-mechanical lift devices.

7.3. Experimental testing of the PSV

The experimental vehicle was tested according to the lower and upper leg impactor tests described in [EEVC 1998]. The results that are shown in Table 7.1 and Table 7.2 confirmed that according to this procedure, the pedestrian protection technologies provided improved pedestrian protection over a reference vehicle.

		Reference vehicle [EuroNCAP 2002]		PSV	
Measure	Injury limit	Worst	Best	Worst	Best
Acceleration (g)	150	542.70	483.70	153.50	131.70
Bending (deg.)	15	34.20	33.30	14.30	10.90
Shear (mm)	6	8.00	5.80	3.20	3.10

Table 7.1 The reference vehicle and PSV lower leg impactor test results

		Reference vehicle [EuroNCAP 2002]		PSV	
Measure	Injury limit	Y=0	Y=300	Y=0	Y=300
Moment (Nm)	220	315.0	224.0	228.3	169.9
Sum forces (KN)	4	4.81	3.59	2.84	2.58

Table 7.2 The reference vehicle and PSV upper leg impactor test results

The test results indicated that there were experimentally measurable benefits [EEVC 1998] of the pedestrian protection technologies for the lower and upper leg tests (it was not possible to include head impact tests within the scope of the research). However, several points were noted:

- An experimental prediction of pedestrian protection performance was only determined with a sub system testing procedure and this was not necessarily a good measure of real world benefit (but it was the only experimental procedure possible).
- Some of the results were marginal passes or failures despite a number of major design changes to the vehicle.
- Although beyond the scope of the research, there were technical compromises in the design of the vehicle structure, due to the incorporation of the pedestrian protection technologies. The degree to which these compromised other vehicle requirements, such as low speed damageability, is a subject for future research.

8. Summary and Conclusions

The research objectives were to create non-linear finite element models and methodologies to study the interaction between pedestrians and vehicles during pedestrian accidents and to apply this understanding to design, develop and evaluate some pedestrian protection technologies. In order to achieve this a number of tasks have been completed and these include the:

- Creation of a new systematic methodology to design, develop and evaluate any pedestrian protection technology
- Creation of new pedestrian protection technologies and models to underpin the methodology
- Application of the methodology to a vehicle with and without the pedestrian protection technologies to gain an improved understanding of the pedestrian and vehicle interaction during a pedestrian accident

8.1. A new systematic methodology

The new methodology is the framework that integrates all the tasks undertaken. It is designed to improve the predicted performance of a pedestrian protection technology in actual pedestrian accidents by applying four principles:

- Micro to macro transformation - whether it is a technology, vehicle or pedestrian model, it should first be understood and developed at a component or simplified level before being combined and evaluated in more complex pedestrian accident simulations
- Multiple approaches - by creating biomechanical, analytical, technology, sub system impactor and pedestrian accident simulation models, it is possible to evaluate different aspects of the technologies from different perspectives
- Benchmarking - any vehicle that incorporates pedestrian protection technologies must be benchmarked against a reference vehicle in order to predict relative performance
- Referencing - patent reviews and pedestrian accident case studies provide a way of learning from past events and obtaining feedback from what occurs in actual pedestrian accidents (confirmation and validation)

8.2. New pedestrian protection technologies and models

The new methodology has been used to create and develop a number of patent applications that concern the bumper system, headlamps and hood system. Within this methodology a review of patent applications and the associated literature has enabled a categorisation and prioritisation of pedestrian and vehicle impact regions to be undertaken. Unique biomechanical, analytical and numerical models have been created to gain an improved understanding of how the technologies should function. By incorporating biomechanical models a better understanding of how the technologies may influence actual pedestrian injuries is gained. Numerical models at both component and vehicle levels in pedestrian accident simulations provide two levels of understanding. The former provides a generic understanding of how the technology parameters may be 'optimised' using DoE. The latter provides an improved prediction of how much the technologies influence a pedestrian accident when assessed with a matrix of pedestrian accident conditions and injury measures. Some potential technical benefits of the technologies with respect to pedestrian protection have been demonstrated in both computer simulations and experimental tests. Further developments of both the technologies and models are required to address specific problems and these are described in the recommendations.

8.3. Improved understanding of pedestrian & vehicle interaction

As a consequence of attempting to construct more detailed pedestrian accident simulations than those described in the literature, the great complexity of pedestrian accidents has been revealed. Although differences in pedestrian injury and motion measures can be identified, some trends are difficult or impossible to identify, assuming that they actually exist. Pedestrian model limitations such as the pelvis construction and lack of shoulder mobility contribute to the difficulty in determining generalised trends.

Despite the problems some general trends have been identified for the reference vehicle. Larger pedestrians are thrown further rearward on the vehicle, towards the windscreen, whilst smaller pedestrians are rotated over the front of the vehicle. The throw distance increases with vehicle impact velocity and is larger for certain

stances, for example, stance 'D'. This means that the hood design requirements (e.g. package space below the hood) will also vary with both pedestrian type and stance. For the vehicle model and accident conditions evaluated, there were no adult pedestrian head contacts with the hood. Despite this, [EEVC 1998] specifies a zone of this vehicle's hood that should be tested with the adult head impactor. The motion of smaller pedestrians is more sensitive to the influence of the vehicle structure and geometry. Therefore, at least the 6 year old child model should be used to evaluate vehicle models because it is more likely to measure differences in injury levels. The severity of all injuries increases with vehicle impact velocity, although there is only a small increase for injuries such as knee shear, because even at 25 km/h very high values are already suffered. As a consequence of this, it is important to use at least a vehicle impact velocity of 40 km/h. Certain types of pedestrian models consistently measure higher values for particular injury types. For example, pelvis acceleration and knee bending are larger for smaller pedestrians but tibia acceleration is lowest. The implication is that it is not sufficient to only use the 6 year old child for evaluating vehicle models. One of the main questions that arises when comparing sub system impactor simulations with accident simulations is whether the head impact velocity is equal to or higher than the vehicle impact velocity. The accident simulations show that, in a small number of cases involving the 50^{th} and 95^{th} percentile pedestrians, it can be higher. Therefore the head impact velocity of 40 km/h specified in [EEVC 1998] does not account for all potential head injury cases.

From the perspective of comparing vehicle designs there is mixed success. Although differences between the reference and modified vehicles can be clearly identified, it is more difficult to distinguish between different impact locations on the same vehicle or between modified vehicles. Also, the conclusions from one set of accident conditions often conflict with those from another set and this has significant implications for future developments. It means that vehicle designs will need to be compromised, not only so that they can meet other vehicle requirements, but also to minimise injuries for a significant part of the pedestrian population.

A number of observations was made concerning the pedestrian protection technologies. In terms of global motion, the technologies have almost no influence on the pelvis to vehicle face impact and a variable influence on the other impact events. However, they consistently reduce the time taken, between the first leg contact and the shoulder to hood impact, at slower vehicle impact velocities. This is an important observation because some pedestrian protection technologies, rely on a bumper mounted sensor to activate and deploy, for instance, the hood, before the shoulder and head contact the vehicle. Therefore, any differences in the amount of time available for the technology, first to sense an event and then to fully deploy it, are important. The bumper and undertray technologies reduce the amount by which the pedestrian legs wrap around the vehicle front and decelerate the legs in a more controlled manner than a stiff beam. Hence they provide a measurable and consistent reduction in knee shear, knee bending and tibia/fibula condyle fractures under most accident conditions. These findings are also experimentally confirmed using the PSV and sub system test procedure [EEVC 1998]. Global motion animations show how the headlamp and hood technologies cause the pedestrian to be thrown further forward on the hood. As a possible consequence of this, there is a small increase in head injury risk for adult pedestrians and a decrease for child pedestrians. There is also larger post head impact motion that could lead to an increased risk of undesirable ground contact.

9. Recommendations

The overall methodology that has been developed provides a basis for future research. However, there are two aspects of this that require further development:

- Technology and model improvements
- Accident case study validation

9.1. Technology and model improvements

Although the potential of the *technologies* to improve pedestrian protection has largely been demonstrated, there are some results that should be investigated further. These include the:

- Increased lateral motion of small pedestrians, post head impact motion of all pedestrians and the greater risk of ground contact as a result of these increases.
- Improved child head protection but reduced adult head protection
- Lack of clear trends in some of the reference vehicle measures, such as head trajectory and pelvis acceleration
- General lack of clear and consistent differences between the modified vehicles and the reference vehicle

One method of investigating these results is to undertake a vehicle optimisation study of the technologies in a new matrix of pedestrian accident simulations. The matrix would specify a range of modified vehicle models with different technology configurations (e.g. different hood joint geometry) and the technology configurations would be optimised according to total injury rating results. This requires that each injury and injury level is prioritised in an quantitative scale so that a total injury rating can be calculated.

In addition to the conflicts concerning pedestrian protection, potential conflicts involving other vehicle requirements also exist. Each technology needs to be evaluated and developed for these additional requirements, with a component supplier. Some of the main additional requirements include those related to:

- NVH and stiffness e.g. GOR end joints rotational stiffness about X axis,

complete vehicle assessment for body stiffness and road noise

- Crash, strength and durability e.g. 8 KN horizontal and vertical tension loads on GOR, complete vehicle assessment for 30 mph frontal impact and windscreen intrusion, AZT low speed damageability, 1.5 KN vertical compression load on GOR, 2 KN latch pull out load, 0.5 KN push/pull load on GOR end joints, component durability in service such as 3000 hood slam cycles
- Functional requirements e.g. ability to reset hood after impact, service access, package space, manufacturing assembly and component alignment, cost and weight

With respect to DoE component *model* improvements, more parts of the surrounding structure (e.g. the hood leading edge) should be incorporated in future generic bumper models because the accident simulations show that knee bending is highly dependent on impacts with these other parts. The largest improvement in the vehicle model may be obtained from a validated windscreen model. This is because the pedestrian head often hits the windscreen and so it is important to achieve the correct interaction between the head and windscreen. However, the current material model used for the windscreen is taken from a frontal crash model and has not been validated for pedestrian head impact energy levels. The dynamic stiffness and failure modes of the windscreen need to be characterised with correlated head impact tests. Although this is relatively complex due to the construction of laminated glass, [Howard 2000-1] provides some examples of how other components have been validated. Finally, there are some improvements to the humanoid models that need to be progressed and these include:

- A revised pelvis construction – a suggested change in the mesh geometry is shown in an earlier chapter. The pelvis acceleration results from a modified humanoid model should be compared to the current humanoid.
- An improved shoulder and thorax construction – some background research has been initiated in a parallel project but until this is complete it is not possible to specify exactly what types of changes are required. However, the main problem to solve is a lack of flexibility in the thorax and

shoulders with respect to both the stiffness of these bodies and the limited biofidelity of the abdomen, chest and shoulder joints.

- Geometrically representative body construction – measurements such as impact timing and impact load distribution are highly dependent on the humanoid model geometry. The legs in particular should be more geometrically representative because, for the evaluation of certain types of pedestrian protection technologies (e.g. contact sensors), it is important to know exactly how the bumper is loaded. Scanned human data should be used to refine the external geometry of the legs so that they more closely match the shape of human legs.
- Further validation – this should be undertaken, in a similar manner to [Howard 2000-3] whenever improved pedestrian cadaver data and/or experimental pedestrian humanoids become available.

From the perspective of the accident simulations, the accident conditions and measures shown in Table 9.1 are recommended when comparing pedestrian protection technologies. Data output is required at least every 5 ms in order to ensure the accuracy of the impact timing predictions (as previously discussed the impact timing is critical for some pedestrian protection technologies).

Vehicle			**Pedestrian**	
Velocity	**Location**	**Braking**	**Type**	**Stance**
25 & 40 km/h	Y0 & Y500	1g, 70mm dive	6 year old & 50th adult	A & C
Benchmark animation frames, absolute values and ranges against standard vehicle				
Overall animation frames		Detailed animation frames		Pelvis/shoulder/head timing
Head trajectory in XZ plane		Relative resultant head velocity		Head velocity at impact
Head injury criteria (HIC)		Maximum pelvis acceleration *		Maximum knee shear
Maximum knee bending		Maximum tibia acceleration		Maximum chest acceleration *

* if a later version of the pedestrian humanoid is used with an improved pelvis & thorax construction

Table 9.1 The recommended accident conditions and measures

9.2. Accident case study validation

During the development of the vehicle and pedestrian models, an investigation of pedestrian accident case studies was initiated [Ford 2001-1, Koch 2001]. The

reconstruction of pedestrian accidents using case study data is the ultimate means to validate the pedestrian accident simulations and ensure the trends observed in accident simulations are similar to those observed in actual accidents. The accident simulation forms shown in the appendices list the necessary data that are required to do this. In addition, Table 9.2 lists some general questions and search criteria that can be used to analyse existing case studies for general trends.

General information	Specific and detailed information
Over what range of speeds is knee damage always observed	At least one very detailed case study requested
Over what range of speeds are leg fractures always observed	Number 1 search criteria: the vehicle type (as similar to the vehicle model as possible i.e. C class with similar styling, do not use pontoon etc. classification)
What kind of windscreen damage is observed (general impression only)	Number 2 search criteria: the vehicle speed (as near as possible to 25km/h or 40km/h)
Where do pedestrians hit the car front (e.g. the percentage split between the centre and outer two thirds)	Number 3 search criteria: the motion of the pedestrian relative to the car (ideally the car is travelling forward, not reversing and hits the pedestrian as they stand/walk at right angles to the car motion)
What is the range of vehicle impact speeds	Number 4 search criteria: 'relatively' standard sized people
What are pedestrians doing before they are hit (running, walking, freezing on the spot, facing away/towards/along the car front)	As much information as possible for the pedestrian accident simulation forms shown in the appendices
What is the weight range for some particular pedestrian group heights e.g. men that are 1.7m tall (this data may be obtained more easily through other means)	

Table 9.2 Questions and search criteria to be addressed by case studies

References

ACEA (1992), *Pedestrian accidents in Europe, developments and challenges*, Presentation to government and commission representatives, 16th September 1992

Aldman B, Kajzer J, Cesari D, Bouquet R, Zac R (1987), *A new dummy for pedestrian test, Proceedings of the 11th International Conference on Experimental Safety Vehicles*, 1987, Washington, USA.

Akiyama A, Yoshida S, Matsuhashi T, Rangarajan, Shams T, Ishikawa H., Konosu A (1999), *Development of simulation model and pedestrian dummy, Advances in Safety Technology*, SAE-1433, 1999, Michigan, USA

Appel H, Kuehnel A, Stuertz G, Gloeckner H (1978-1), *Pedestrian safety vehicle, design elements, results of in depth analyses and simulation, Proceedings of the America Association for Automotive Medicine*, 1978, Illinois, USA, vol. II, 132 - 153

Appel H (1978-2), DE 2711339, deployable hood system and deformable hood to fender interface, 1978

Ashton S J, Mackay GM (1979), *Some characteristics of the population who suffer trauma as pedestrians when hit by cars and some resulting implications, International IRCOBI Conference*, 1979, Gothenberg, Sweden

Ashton S J (1981), *Factors associated with pelvic and knee injuries in pedestrian struck by the fronts of cars, 25th Stapp Car Crash Conference*, SAE 811026, 1981, Warrendale, USA, pp. 863-902

Bodyworks v6.0 (1997), The Learning Company properties Inc.

Box G, Hunter W, Hunter J (1978), Statistics for experimenters, An introduction to design, data analysis and model building, John Wiley and Sons, ISBN 0-471-09315-7, USA

Box G, Behnken D (1960), Some new three level designs for the study of quantitative variables, Technometrics, 2: pp 455-475

Brun-Cassan F, Vallée H, Tarrière C, Fayon A, Got, C, Patel A, Hureau J (1983-1), *Reconstruction of actual car-pedestrian collisions with dummy and cadavers*, SAE 830053, 1983, Detroit, USA

Brun-Cassan F, Tarrière C, Fayon A, Mauron G (1983-2), *Comparison of behaviours for PART 572 and APROD dummies tested as pedestrians impacted by a car, under identical test conditioning*, SAE 830186, 1983, Detroit, USA

Brun-Cassan F, Tarrière C, Fayon A, Mauron G (1984), *Comparison of experimental car-pedestrian collisions performed with various modified side impact dummies and cadavers*, *Proceedings of the 28th STAPP car crash conference*, SAE 841664, 1984, Chicago, USA

Camp L (1999), *Quo Vadis – Active and passive safety in Europe and north America*, *58th Internationale Automobilausstellung (IAA)*, September 1999, Frankfurt, Germany

Cady J, Howard M.S, Fisher S, Lloyd R, Thomas A (1994), *Vehicle bonnets*, European patent 0509690B1, Jaguar, 1994

Cesari D, Alonzo F, Matyjewski M (1991), *Subsystem test for pedestrian lower leg and knee protection*, *Proceedings of the 13th International Conference on Experimental Safety Vehicles*, 1991, Paris, France

Commission of the European Communities (1984), *Frontal surfaces in the event of impact with a vulnerable road user*, Ad-hoc Working Group ERGA Passive Safety document ERGA S/60, 1984, Brussels, Belgium

Conolly W A, Hedburg E A (1969), 'Observations on fractures of the pelvis', The

Journal of Trauma, Volume 9, Number 2, pp104-111.

Cranfield Impact Centre (1997), *Pedestrian safety research – Humanoid modelling phase I*, Internal FFA pedestrian safety research program report, 1997

Cranfield Impact Centre (1998), *Pedestrian safety research – Humanoid modelling phase II*, Internal FFA pedestrian safety research program report, 1998

Cranfield Impact Centre (1999), *Pedestrian safety research – Humanoid modelling phase III*, Internal FFA pedestrian safety research program report, 1999

Cranfield Impact Centre (2000), *Pedestrian safety research – Humanoid modelling phase IV*, Internal FFA pedestrian safety research program report, 2000

Cranfield Impact Centre (2001), *Pedestrian safety research – Humanoid modelling phase V*, Internal FFA pedestrian safety research program report, 2001

Daimler Benz (1988), DE 3728752 C1, deformable element in headlamp body to lens cover interface, 1988

Daimler Benz (1990), DE 3051041 C2, bumper safety system (deployable lower bumper system), 1990

Department of the Environment (1998), Transport and the Regions, *UK official accident statistics*, Press notice: 459/transport, 11th June 1998

Du Bois P, (2001), Crashworthiness engineering with LS-DYNA, advanced user course, FFA GmbH, May 2001

Draper N.R, Lin D.K.J (1990), Small response surface designs, Technometrics, 32

EUCAR (2000), collaboration project between FFA Rover, Opel GM and Volvo,

Pedestrian safety and tools, project number E017, 2000

EuroNCAP (2002), European New Car Assessment Program web site, 20th February 2002, http://www.euroncap.com

European Experimental Vehicles Committee (1982), *Pedestrian injury accidents*, *9th Experimental Safety Vehicle Conference*, November 1982, Kyoto, Japan

European Experimental Vehicles Committee (1985), *Pedestrian injury protection by car design*, *10th Experimental Safety Vehicle Conference*, July 1985, Oxford, England

European Experimental Vehicles Committee (1989), *Study of test methods to evaluate pedestrian protection for cars*, *12th Experimental Safety Vehicle Conference*, May 1989, Gothenburg, Sweden

European Enhanced Vehicle safety Committee (1998), *Improved test methods to evaluate pedestrian protection afforded by passenger cars*, EEVC Working Group 17 report, December 1998

Fakhry G et al (1975), 'The Cruciate Ligaments of the Knee Joints', Clinical Orthopaedics and Related Research, Vol. 106, pp. 216-231

Fenton J (1996), Handbook of vehicle design analysis, Mechanical Engineering Publications, London and Bury St. Edmunds.

fka (1998-1), The dynamic characterization of the C170 GOR under pedestrian impact conditions using a systematic component analysis and testing methodology, internal report to Ford, project 6664, 1998

fka (1998-2), The dynamic characterization of the C170 headlamp under pedestrian impact conditions using a systematic component analysis and testing methodology,

internal report to Ford, project 6664, 1998

fka (1999-1), The dynamic characterization of the C170 bumper system under pedestrian impact conditions using a systematic component analysis and testing methodology, internal report to Ford, project 6664, 1999

fka (1999-2), The dynamic characterization of the C170 air filter box under pedestrian impact conditions using a systematic component analysis and testing methodology, internal report to Ford, project 6664, 1999

fka (1999-3), The dynamic characterization of the C170 intercooler ducting pipe under pedestrian impact conditions using a systematic component analysis and testing methodology, internal report to Ford, project 6664, 1999

Ford (1995), CAE guidelines, Advanced Vehicle Technology, Europe Body Engineering Durability, internal Ford report, 1995

Ford (1996), Pedestrian head impact methodology, report T240-96-028, FAO AVT CAE methods, internal Ford report, 1996

Ford (1997), Safety FEA Handbook, Advanced Vehicle Technology, Safety and Biomechanics CAE, revision 1, internal Ford report, 1997

Ford (1998), internal study with MHH database 1996 and 1997, sample size of 262 people, internal Ford report.

Ford (1999), frontal crash model CPAZTL2D00, RADIOSS input deck, 1999.

Ford (2001-1), Detaillierte Analysen von Fußgängerunfällen aus unfallrekonstruktiver und medizinischer Betrachtung im Großraum Berlin und Mecklenburg-Vorpommern, Eine retrospektive, interdisziplinäre Beobachtungsstudie im Rahmen der Verkehrsunfallforschung, Accident case study

analysis for pedestrian accident reconstruction, led by FFA with DEKRA, Unfalkrankenhaus Berlin, Ernst-Payr-Lehrstuhl für Unfallchirurgie, Ernst Moritz Arndt Universität Greifswald, 2001

Ford (2001-2), Experimental design training course, Ford Technical Education Program (FTEP), 2001

Foret-Bruno J, Raverjon G, Coz J (1998), *Injury pattern of pedestrians hit by cars of recent design*, *Proceedings of the 16th International Technical Conference of Experimental Safety Vehicles*, October 1998, Windsor, Canada

Grösch L, Heiss W (1989), *Bumper configurations for conflicting requirements: existing performance vs. pedestrian protection*, *Proceedings of the 12th International Conference on Experimental Safety Vehicles*, 1989, Gothenburg, Sweden

Guillemot H, Got C, Besnault B, Lavaste F, Robin S, Yves Le Coz J, Lassau J-P (1998), *Pelvis behaviour in side collisions: static and dynamic tests on isolated pelvic bones*, *Proceedings of the 16th International Technical Conference on the Enhanced Safety of Vehicles*, 1998, Windsor, Canada

Hardy R, Watson J, Howard M.S (2000), 'Developments in the Simulation of Real World Car to Pedestrian Accidents using a Pedestrian Humanoid Finite Element Model', International Journal of Crashworthiness, Vol. 5, no. 1

Harris J, (1985-1), *Simplified test recommendations for pedestrian protection*, *Proceedings of the 10th International Technical Conference on Experimental Safety Vehicles*, 1985, Oxford, UK

Harris J, Grew N.D (1985-2), *The influence of car design on pedestrian protection*, *Proceedings of the 10th International Technical Conference on Experimental Safety Vehicles*, 1985, Oxford, UK

Harris J. (1991), *Proposals for test methods to evaluate pedestrian protection for cars*, SAE 916038, 1991

Howard M.S (1991), *Pedestrian head XJ40 bonnet*, internal Jaguar report, project number bed/002900, 1991

Howard M.S (1995-1), *Vehicle bonnets*, European patent 0630801B1, Jaguar, 1995

Howard M.S, Nightingale B (1995-2), *The creation and calibration of the finite element pedestrian hip impactor*, internal Jaguar report, project no. JA3A7, 1995

Howard M.S, Nightingale B (1995-2), *Pedestrian safety evaluation of the X200 (clay C) and DEW98 (d9) bumper systems using a simplified leg impactor*, internal Jaguar report, 1995

Howard M.S, Thomas A.V (1998-1), *Pedestrian safety research - past, present, future*, *Euromotor: New Advances in Body Engineering*, 11th December 1998, Aachen, Germany

Howard M.S, Watson J, Hardy R (1998-2), 'The simulation of real world car to pedestrian accidents using a pedestrian humanoid finite element model', International Journal of Crashworthiness, Volume 3, Number 4

Howard M.S (1999-1), Pedestrian humanoid scaling concept, internal FFA memo, 1999

Howard M.S (1999-2), Bumper for vehicles having optimal mechanical properties to improve pedestrian protection, European patent application EP99108129.0, 24th April 1999

Howard M.S, Thomas A.V (1999-3), *An integrated approach to real world pedestrian safety research*, *Aachener Kolloquium Fahrzeug und Motorentecknik*

1999, October 1999, Germany

Howard M.S, Thomas A.V, Philipps M, Friesen F (2000-1), *A systematic modelling and testing methodology to characterise vehicle components under pedestrian impact conditions*, Report to Ministerium für Wissenschaft und Forschung des Landes Nordrhein-Westfalen, February 2000

Howard M.S, Thomas A.V, Friesen F (2000-2), *The construction, certification, validation and correlation of corporate non linear finite element impactor models and a C170 vehicle model for the simulation of the proposed European draft directive pedestrian protection test procedure*, FORD technical report, SRR-2000–0110, 2000

Howard M.S, Thomas A.V, Koch W, Hardy R, Watson J (2000-3), *Validation and application of a finite element pedestrian humanoid model for use in pedestrian accident simulations*, *2000 International IRCOBI Conference on the Biomechanics of Impact*, September 2000, Montpellier, France

Howard M.S (2000-4), *The FFA pedestrian safety research program*, Internal Ford report, 2000

Howard M.S (2001), Pedestrian safety module device, European patent EP 1078826 A1, 28th February 2001

Howard M.S (2001-1), 'FFA pedestrian safety research program', internal presentation to Volvo safety department , 25th April 2001

Howard M.S, Siebertz K (2001-2), The design and development of a pedestrian protection headlamp technology concept using a generic parametric study, FORD technical report, SRR-2001-0135, 2001

Howard M.S, Mao Y, Siebertz K (2001-3), The design & development of a

pedestrian protection bumper technology concept using a generic parametric study, FORD technical report, SRR-2001-0136, 2001

Howard M.S, Koch W, Schreiber H (2001-4), The design and development of a mechanically deployed pedestrian protection hood kinematic system (PEHKS), FORD technical report, SRR-2001– 0204, 2001

Howard M.S (2001-5), Howard M.S, Pedestrian protection headlamp, European patent EP1048895B1, 14th March 2001

Howard M.S, Schreiber H (2001-6), Vehicle hood assembly for pedestrian protection, European patent application 01124637.8, 16th October 2001

Howard M.S (2001-7), New pedestrian protection headlamp technology, European patent application 01120382.5, 25th August 2001

Howard M.S (2001-8), Bumper assembly of a motor vehicle for pedestrian protection, European patent application EP01123401.0, 28th September 2001

Huelke D.F (1986), *Anatomy of the lower extremity – and overview, Proceedings of the biomechanics and medical aspects of lower limb injuries*, SAE P-186, 861921, pp1-22, 1986

Isenberg R.A, Chidester A.B, Mavros S (1998), *Update on the pedestrian crash data study, Proceedings of the 16th International Technical Conference of Experimental Safety Vehicles*, October 1998, Windsor, USA, pp. 1212-1225

Ishikawa H, Yamazaki K, Ono K, Sasaki A (1991), *Current situation of pedestrian accidents and research into pedestrian protection in Japan, Proceedings of the 13th International Conference on Experimental Safety Vehicles*, November 1991, Paris, France, p281-293

Ishikawa H, Kajzer J, Schroeder G (1993), *Computer simulation of impact response of the human body in car pedestrian accidents*, Proceedings of 37th Stapp Car Crash Conference, San Antonio, USA, November 1993

Jager M. de, Sauren A, Thunnissen J, Wismans J (1994), *A three dimensional head neck model: validation for frontal and lateral impacts*, 38th Stapp Car Crash Conference Proceedings, SAE P-279, 1994, pp. 107-122

Jarrett K.L, Saul R.A (1998), *Pedestrian injury – analysis of the PCDS field collision data*, *Proceedings of the 16th International Technical Conference of Experimental Safety Vehicles*, October 1998, Windsor, Canada, pp. 1204-1211

Kallieris D., Schmidt G. (1988), *New aspects of pedestrian protection loading and injury pattern in simulated pedestrian accidents*, *Proceedings of the 32nd Stapp Car Crash Conference*, Chicago, USA, SAE P-215, 1988

Kajzer J, Schroeder G, Ishikawa H, Matsui Y, Bosch U (1997), *Shearing and bending effects at the knee joint at high speed lateral loading*, SAE 973326, 1997

Koch W, Sferco R, Howard M.S (2001), *Ganzhetlicher ansatz zur verbesserung der fußgängersicherheit bei fuußgänger-PKW-kollision*, *Poly-Trauma Trauma-Forschung*, 29th–30th June 2001, Ernst-Moritz-Arndt-Univesität, Germany

Konosu A, Ishikawa H, Sasaki A (1998), *A study of pedestrian impact test procedure by computer simulation – The upper legform to bonnet leading edge test*, *Proceedings of the 16th International Technical Conference of Experimental Safety Vehicles*, 98-S10-W-19, Windsor, Canada, 1998

Konosu A, Ishikawa H, Kant R (2000), *Development of computer simulation models for pedestrian subsystem impact tests*, JSAE 20004024, 2000

Kress T A et al (1995), *Fracture patterns of human cadaver long bones*,

International Research Council on the Biomechanics of Impact, 1995

Laughlin T.F, Kessler J.W. (1990), *Pedestrian head impact against the central hood of motor vehicles - test procedures and results*, NHTSA, Proceedings of the 34th Stapp Car Crash Conference, SAE 902315, 1990

Lawrence G (1989), *The influence of car shape on pedestrian impact energies and its application to sub-system tests*, 12th International Technical conference on Experimental Safety Vehicles, 1989, Gothenburg, Sweden, pp. 1253-1265

Lawrence G., Hardy B.J, Lowne R W (1993), *Costs and benefits of the EEVC pedestrian impact requirements*, project report 19, S220C/VF, Transport Research Laboratory, 1993

Lawrence G., Hardy B.J (1998), *Pedestrian safety testing using the EEVC pedestrian impactors*, *16th International Technical Conference on the Enhanced Safety of Vehicles*, 1998, Windsor, Canada

Lawson A R, Sadeghi M M (1998), *Finite element modelling of blunt or non contact head injuries*, *16th International Technical Conference on the Enhanced Safety of Vehicles*, 1998, Windsor, Canada

Levine L (1986), *A review of the long term effects of selected lower limb injuries*, Wayne State University, SAE 860501, 1986.

LS-DYNA (1999-1), LS-DYNA keyword user's manual – Non linear dynamic analysis of structures (pdf file), Version 950, Livermore Software Technology Corporation, May 1999

LS-DYNA (1999-2), LS-DYNA theoretical manual (pdf file), Version 950, Livermore Software Technology Corporation, May 1998

McInnis D, Cliff W, Ising K (1997), *A comparison of moment of inertia techniques for vehicle dynamics simulation*, International Congress and Exposition, SAE 970951, 1997, Michigan

Manoli A (1986), *Adult pedestrian injuries – medical aspects*, Biomechanics and medical aspects of lower limb injuries, P186, pp. 109-114, SAE 861928, 1986, Warrendale

Matsui Y, Ishikawa H, Sasaki A (1998), JARI, *Validation of pedestrian upper legform impact test - reconstruction of pedestrian accidents*, *Proceedings of the 16th International Conference on Experimental Safety Vehicles*, 98-S10-0-05, 1998, Windsor

Matsui Y, Ishikawa H, Sasaki A (1999), JARI, Honda, *Pedestrian injuries induced by the bonnet leading edge in current car-pedestrian accidents*, International Congress and Exposition, SAE 1999-01-0713, 1999, Michigan

MacLaughlin T.F, Hoyt T.A, Chu S (1987), *NHTSA's advanced pedestrian protection program*, 1987

Mercedes Benz (1990), DE 4401 023 C1, *Optimised hood to fender interface design*, 1990

Metzler-Poeschel (1998), *Statistisches bundesamt jahrbuch fachserie 8 reihe 7: verkehrsunfalle 1997 verlag*, 1998, Stuttgart, Germany

Mizuno K, Kajzer J (2000), Traffic Safety & Nuisance Research Institute, Nagoya university, *Head injuries in vehicle-pedestrian impact*, SAE 2000-01-0157, 2000

Montgomery D.C (1991), Design and analysis of experiments, third edition, John Wiley and Sons, New York, USA

NHTSA (1997), *Traffic safety facts*, Internet site http://www.nhtsa.dot.gov, 1997

Nissan Cars (1983), JP 58-211975, deployable hood system, 1983

Nusholtz G S, Kaiker P S, Huelke D F, Suggitt B R (1985), *Thoraco-abdominal response to steering wheel impacts*, Proceedings of the 29th STAPP car crash conference, P-162, pp 221-267, 1985

Nyquist G W (1986), *Injury tolerance characteristics of the adult human lower extremities under static and dynamic loading*, *Proceedings of symposium on biomechanics and medical aspects of lower limb injuries*, P-186, Society of Automotive Engineers, SAE 861925, pp79-90

Okamoto Y, Sugimoto T, Enomoto (2000), *Pedestrian head impact conditions depending on the vehicle front shape and its construction – full model simulation*, *2000 International IRCOBI conference on the Biomechanics of Impact*, September 2000, Montpellier, France

Organisation for Economic Co-Operation and Development (1999), International Road Traffic and Accident Database (IRTAD). Note: EU data from 1979-1983 includes the Portugal pedestrian fatality number of the year 1984 and the 1997 as well as 1996 contains 1995 data from Greece and Portugal. Fatal means 30 day period, except Italy (7 days), France (6 days), Spain before 1993 (24 hours), Greece before 1996 (3 days), Austria until 1991 (3 days), Swiss before 1992 (unlimited), Japan before 1993 (24 hours), Portugal (24 hours). For these countries and time periods correction factors are used. Note: 1995 data used except the EU figure that includes Italian and Luxembourg data from 1994

Otte D. (1991), *The influence of vehicle geometry on the injuries of pedestrians involved in accidents – an evaluation of investigations at the site of accidents in Hannover*, *International Conference on Traffic Safety*, 1991, New Delhi, India

Otte D. (1998), *Severity and mechanism of head impacts in car to pedestrian accidents*, *International Research Council on the Biomechanics of Impact*, September 1998, Gothenburg, Sweden, pp. 329-341

Otubushin A, Hughes D, Ridley N, Taylor K (1998), 'Analysis of pedestrian head impacts to the bonnets of European vehicles', International Journal of Crashworthiness

Ove Arup (2000), Oasys LS-DYNA, version 8.0 manual, volume 1, January 2000

Patent offices (2002), Europe: http://www.european-patent-office.org/, Germany: http://www.dpma.de/, USA: http://www.uspto.gov/, General sites : http://cn.net.au/, http://www.patents.cos.com/, http://www.nhtsa.dot.gov, 20th February 2002

Philipps M., Howard M.S (1999), 'FEA simulation of vehicle-pedestrian collisions', ATZ Automobiltechnische Zeitschrift, June 1999

Ryan P (1971), 'Traffic injuries of the pelvis at St. Vincent's hospital, Melbourne', Medical journal of Australia, Volume 1, pp475-479.

Sakurai M, Kobayashi K, Ono K (1994), *Evaluation of pedestrian protection test procedure in Japan - influence of upper body mass on leg impact test*, *14th International Technical Conference on Enhanced Safety of Vehicles*, Munich, Germany, Vol. 2, pp. 1114-1130

Schuster P.J, Staines B (1998), *Determination of bumper styling and engineering parameters to reduce pedestrian leg injuries*, SAE 980361

Sherwood J.A (1991), *Constitutive modelling and simulation of energy absorbing Polyurethane foam under impact loading*, Plastic and plastic composites: material properties, past performance, and process simulation, Volume 29, ASME, 1991.

Statgraphics (2000), Design of Experiments help manual (pdf file), Version 5.0, Manugistics Inc, November 2000

Thomas A, Gennarelli M (1984), *Biomechanics of head injury*, Division of Neurosurgery, University of Pennsylvania, 1984

Thunnissen J, Wismans J (1995), *Human volunteer head-neck response in frontal flexion: a new analysis*, *Proceedings of the 39th STAPP car crash conference, Society of Automotive Engineers*, SAE 952721, 1995

Toyota (1996-1), JP 08258668 A, Air bag system for protection of pedestrians, 1996

Toyota (1996-2), JP 08216826 A, Sensors for hood system, 1996

Toyota (1996-3), JP 08258668 A, Air bag system for protection of pedestrians (scuttle, vehicle face and hood with sensors), 1996

Trauma (2002), http://www.trauma.org/scores/iss.html, 10th December 2002

Volkswagen (1978), DE 28 41 315 A1, Deployable hood system via bumper sensor and bonnet lift mechanisms, 1978

Watanabe I, Furusu K, Kato C, Miki K, Hasegawa J (2001), *Development of practical and simplified human whole body FEM model*, JSAE20014065, 2001

Wijk J.V. (1983), *Experimental reconstruction and mathematical modelling of real world pedestrian accidents*, *Proceedings of the SAE congress P121*, 1983

Wollert W, Blödorn J, Appel H, Kühnel A (1983), *Realisation of pedestrian protection measures on cars*, *Proceedings of the SAE congress P121*, *Pedestrian Impact Injury and Assessment*, 1983, pp. 27-37

Yamada H (1970), *Strength of biological materials*, Baltimore, 1970

Yang J, Kajzer J. (1992), *Computer simulation of impact response of the human knee joint in car-pedestrian accidents*, *Proceedings of the 36th Stapp Car Crash Conference*, 922525, Washington, USA, 1992

Yang J (2000), *An approach to improve vehicle-front design for pedestrian protection using mathematical models*, SAE C567/023/2000

Yoshida S, Matsuhashi T, Matsuoka Y (1998), *Simulation of car pedestrian accident for evaluate car structure*, Proceedings of 16th International Technical Conference on the Enhanced Safety of Vehicles, 98-S10-W-18, Windsor 1998

Yoshida S. (1999), *Development of a vehicle structure with protective features for pedestrians*, Vehicle Aggressivity and Compatibility in Automotive Crashes, SAE-1442, 1999

Zellmer H. et al (1994), *The EEVC/WG10 head impact test procedure in practical use*, *Proceedings of the 14th International Conference on Experimental Safety Vehicles*, Munich, Germany, 1994

Appendix A - Pedestrian accident forms for accident reconstruction

ACCIDENT DETAILS	CASE NUMBER	
	VEHICLE NUMBER	
	SUBJECT NUMBER	

COMPLETE ACCIDENT SEQUENCE (include vehicle, pedestrian and road layout)

DATE OF CASE		OTHER COMMENTS
WEATHER	Dry/raining/snow	
ROAD SURFACE μ		

PEDESTRIAN IMPACT SEQUENCE DETAILS (include photographs where possible)

VEHICLE KINEMATICS		
FACTOR	DESCRIPTION	CONFIDENCE (1 high to 5)
SPEED		
DIRECTION		
BRAKING	Heavy/light/none	
PEDESTRIAN KINEMATICS		
PRE IMPACT	Walking/running/lying down	
DURING IMPACT	Bounced off/lying on vehicle/over roof	
POST IMPACT	Location and body position	

VEHICLE DETAILS	VEHICLE NUMBER	

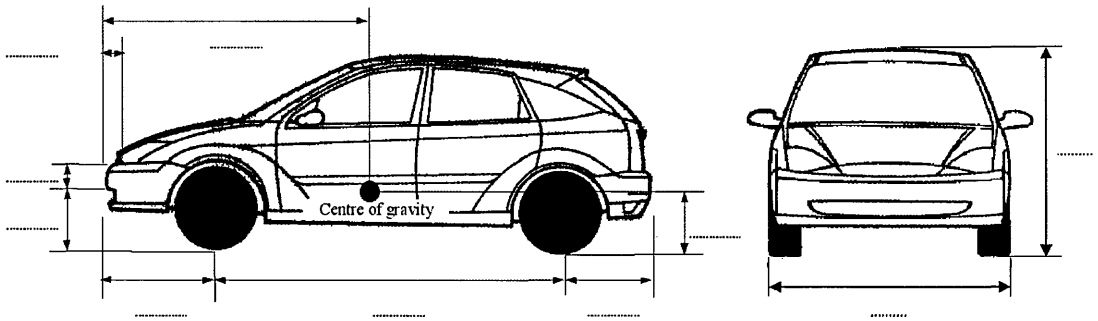

YEAR OF BUILD		WEIGHT (Kg)	
MANUFACTURER			
MODEL		COMMENTS	

OTHER DETAILS	DESCRIPTION (include photographs where possible)
BUMPER MATERIAL	
HOOD MATERIAL	
FENDER MATERIAL	
ENGINE PACKAGE	
WINDSCREEN ADH.	
NON STANDARD	

DAMAGE REGION	DESCRIPTION (digital photograph, measure)
BUMPER	
HEADLAMPS	
RADIATOR GRILL	
HOOD	
FENDERS	
SCUTTLE	
WINDSCREEN	
A PILLARS	
ROOF	
DOORS (inc. mirrors)	
OTHER PARTS	

PEDESTRIAN DETAILS	SUBJECT NUMBER	

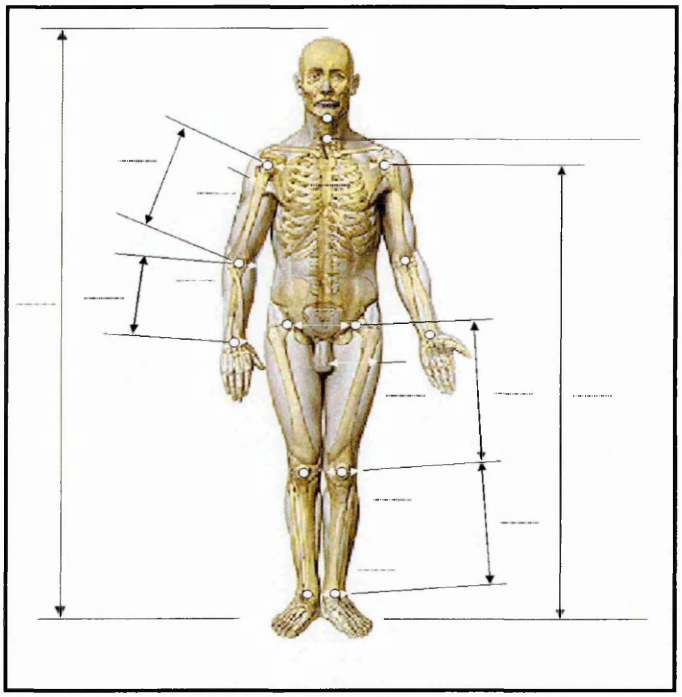

AGE (years)		BUILD (see build chart)	
SEX	male/female	CLOTHING	Light/normal/heavy
WEIGHT (Kg)		SHOE TYPE	

INJURY REGION	DESCRIPTION (include X ray photographs or diagrams etc.)
ANKLE JOINT	
LOWER LEG BONES	
KNEE JOINT	
UPPER LEG BONES	
PELVIS	
INTERNAL ORGANS	
SHOULDER JOINT	
UPPER ARM BONES	
ELBOW JOINT	
LOWER ARM BONES	
SPINE	
NECK	
HEAD	

Appendix B - The software and hardware tools used

Hardware tools

HP 700 series unix workstation (C240, 6GB hard disk and 500MB RAM).

HP multiple processor unix workstation (solving only, 4*360MHZ, 20GB hard disk).

Additional 100GB hard disk for storage.

Metaframe PC server used for PC applications on the workstations.

Software tools

Tasks	Software tools (file formats)
Planning	Microsoft Excel 97 and 2000 (*.xls) MindMan Personal v3.0 Microsoft Word 97 and 2000 (*.doc) Manugistics Inc. Statgraphics v5.0 (*.sfx)
CAD	SDRC Master Series v8.0 (*.mf1 and *.mf2)
Pre processing	SDRC Master Series v8.0 (*.mf1, *.mf2, *.unv) OASYS v8.0 Ncode (*.unv, *.key) OASYS v8.0 Primer (*.unv, *.key) Hypermesh v3.01 (*.hm)
Non linear dynamic solver	LSDYNA3D MPP 940 (*.key) LSDYNA3D 950e (*.key)
Post processing	OASYS v8.0 D3PLOT (d3plot etc) OASYS v8.0 T/HIS (*.thf etc.) Manugistics Inc. Statgraphics v5.0 (*.sfx)
Data presentation	Microsoft Word 97 and Word 2000 (*.doc) Microsoft Powerpoint 97 and Powerpoint 2000 (*.ppt) Microsoft Excel 97 (*.xls) Microsoft Access (*.mdb) Adobe Acrobat v4.0 (*.pdf) JASC Paint Shop Pro v6.0 (most graphics formats) Manugistics Inc. Statgraphics v5.0 (*.sfx)

Appendix C - Master Series to LS-DYNA translation in N/CODE

The following is extracted from page 2.23 of [Ove Arup 2000].

Element	Type
Solid brick Solid wedge Solid tetrahedron	SOLID LINEAR BRICK SOLID LINEAR WEDGE SOLID LINEAR TETRAHEDRON
Beam	BEAM LINEAR
Shell quad Shell triangular	THIN SHELL LINEAR QUAD THIN SHELL LINEAR TRIANGLE
Thick shell brick	THICK SHELL LINEAR BRICK
Translational spring Translational damper Rotational spring Grounded translational spring Grounded translational damper Grounded rotational spring Point mass	SPRING NODE-NODE TRANSLATIONAL DAMPER NODE-NODE TRANSLATIONAL SPRING NODE-NODE ROTATIONAL NODE-GROUND TRANSLATIONAL SPRING NODE-GROUND TRANSLATIONAL DAMPER NODE-GROUND ROTATIONAL SPRING MASS
Slave segment quad Slave segment triangular Master segment quad Master segment triangular	PLATE LINEAR QUAD PLATE LINEAR TRIANGLE PLATE LINEAR QUAD PLATE LINEAR TRIANGLE
Stonewall segment quad	PLATE LINEAR QUAD
Control Volume segment quad Control Volume segment tri	PLATE LINEAR QUAD PLATE LINEAR TRIANGLE
Extra node-on-rigid-body link	PIPE
Joint	CONSTRAINT
Seat belt element Retractor element Slipring element	ROD LINEAR colour GREEN ROD LINEAR colour RED ROD LINEAR colour BLUE
Nodal constraint Spotweld Rivet	COUPLED DEGREE OF FREEDOM COUPLED DEGREE OF FREEDOM colour BLUE COUPLED DEGREE OF FREEDOM colour RED

Appendix D - Pre and post processing model quality guidelines

Pre processing guidelines summarised from [Du Bois 2001] and [FORD 1997]

Mesh
Uniform mesh in energy absorbing structure with mesh parallel and orthogonal to the part edges. Sufficiently fine mesh to closely represent model surface curvatures at the neutral plane. Avoid fast transitions from small to large elements. Use the default shell type Belytschko-Tsay for robust and efficient solving times but where necessary to avoid hourglassing use fully integrated elements. Where hourglassing may occur in open or closed section walls containing Belytschko-Tsay shell elements use at least three elements when out of plane bending to avoid hourglassing. At least 6 elements should border a panel hole. Holes with a diameter of 10mm or less should be ignored. Springs representing adhesives have a consistent length and modelled normal to the panel. Avoid discontinuities in spring force-displacement curves. Maximum percentage of triangles <10% (i.e. they are stiffer than quadrilateral shells). Minimum element size of 5 mm (i.e. based on a timestep of 1×10^{-6} s). No free edges except where part boundaries are intended (i.e. no cracks). No free nodes except where these are used for other definitions such as coordinate systems. 15 degrees maximum warping with no concentration of warped elements in one region. 45 degrees < Internal angle <120 degrees for quadrilaterals and >25 degrees for triangles.
Contacts
Avoid initial penetrations at time zero and edge to edge penetrations. Contact thickness should be close to the material thickness. Sufficient mesh density and similar mesh density between master and slave to ensure correct contact function, small penetrations and correct pressure distribution on elements. If necessary set MAXPAR parameter to non default value to avoid node to edge contact problem. Avoid premature release of penetrating node by suitable value of PENMAX.
Connections
Suitable spotweld representation (i.e. do not merge nodes to represent spotwelds because this can lead to warped elements or use free edge nodes – type 9 beams with flange tied interfaces ?). Correct modelling of bolts and bushes by using concentric cylinders and contacts.
General
Set CONTROL_ACCURACY INN to on (not the default but may avoid hourglassing).

Post processing guidelines summarised from [Du Bois 2001] and [FORD 1997]

Check for normal termination message. Visual inspection of deformed shape to ensure; * no shooting nodes * smooth representation of deformed structure. * minimal contact penetrations Check for constant energy balance if no energy added to the system (e.g. by gravity). Compare contact interface energy against internal energy and kinetic energy for every part and globally. If mass scaling was used check how much mass was added and how distributed. Check plastic strain in all metallic parts reasonable (i.e. below 30%). Create analytical models of at least parts of simulation to evaluate if physically plausible. Undertake some parameter studies to identify sensitivity of model to parameter changes (e.g. mesh density and material). Correlate experimental test results against simulation model.

Appendix E - CAD & FE data sources for the reference vehicle model

FE vehicle model part	Ford CAD model	FE model geometry	FE model material
1. GENERIC_ISOTROPIC_STEEL @ HOOD_INNER	XS41-A16854-B_	Author	FORD Safety FEA handbook, v1, p42
2. GENERIC_ISOTROPIC_STEEL @ HOOD_OUTER	XS41-A16615-A_	Author	FORD Safety FEA handbook, v1, p42
3. DUMMY HIGH STRENGTH @ HOOD HINGE BRACKET RIGHT	XS41-16800-A_	Author	Author
4. DUMMY HIGH STRENGTH @ HOOD HINGE BRACKET LEFT	XS41-16800-A_	Author	Author
5. DUMMY HIGH STRENGTH @ HINGE_HOOD_RIGHT	XS41-16800-A_	Author	Author
6. DUMMY HIGH STRENGTH @ HINGE_HOOD_LEFT	XS41-16800-A_	Author	Author
8. RIGID_GENERAL @ RIGID_HINGE_HOOD_LEFT	XS41-16800-A_	Author	Author
9. RIGID_GENERAL @ RIGID_HINGE_HOOD_RIGHT	XS41-16800-A_	Author	Author
10. RIGID_GENERAL @ RIGID_HOOD_HINGE_BRACKET_RIGHT	XS41-16800-A_	Author	Author
11. RIGID_GENERAL @ RIGID_HOOD_HINGE_BRACKET_LEFT	XS41-16800-A_	Author	Author
12. DUMMY HIGH STRENGTH @ HINGE_RF_LEFT	XS41-A16A681-A_	Author	Author
13. DUMMY HIGH STRENGTH @ HINGE_RF_RIGHT	XS41-A16A681-A_	Author	Author
14. GENERIC_ISOTROPIC_STEEL @ STRIKER	XS41-16K689-A_	Author	FORD Safety FEA handbook, v1, p42
15. DUMMY HIGH STRENGTH @ LATCH_SOLID	XS41-16700-CF	Author	Author
16. RIGID_ENGINE_ASSEMBLY_&_CAR_INERTIA @" " " " " "	Partly remeshed and remodelled rear end plus engine ancillaries from RADIOSS frontal crash model CPAZTL2D00		
18. UNDERTRAY @ UNDERTRAY	Not used	Author	Author/fka
19. HIGH STRENGTH STEEL @ FRTCM	XS41-A001K43-B_	Author	FORD Safety FEA handbook, v1, p42
20. HIGH STRENGTH STEEL @ FRTCM_REINF_RIGHT	XS41-A108K34/5-B_	Author	FORD Safety FEA handbook, v1, p42
21. HIGH STRENGTH STEEL @ FRTCM_REINF_LEFT	XS41-A108K34/5-B_	Author	FORD Safety FEA handbook, v1, p42
22. HIGH STRENGTH STEEL @ FRTCM_FLR	XS41-A108461-B_	Author	FORD Safety FEA handbook, v1, p42
23. GENERIC_ISOTROPIC_STEEL @ DASHBOARD CROSS BEAM	Not used	CPAZTL2D00	FORD Safety FEA handbook, v1, p42
24. GENERIC_ISOTROPIC_STEEL @ COWL_BRKT1_RIGHT	XS41-A02015/6-AB	Author	FORD Safety FEA handbook, v1, p42
25. GENERIC_ISOTROPIC_STEEL @ COWL_BRKT2_RIGHT	XS41-02044/5-AB	Author	FORD Safety FEA handbook, v1, p42
26. GENERIC_ISOTROPIC_STEEL @ COWL_BRKT3_RIGHT	XS41-A17K26/7-AB	Author	FORD Safety FEA handbook, v1, p42
27. GENERIC_ISOTROPIC_STEEL @ COWL_BRKT1_LEFT	XS41-A02015/6-AB	Author	FORD Safety FEA handbook, v1, p42
28. GENERIC_ISOTROPIC_STEEL @ COWL_BRKT2_LEFT	XS41-02044/5-AB	Author	FORD Safety FEA handbook, v1, p42
29. GENERIC_ISOTROPIC_STEEL @ COWL_BRKT3_LEFT	XS41-A17K26/7-AB	Author	FORD Safety FEA handbook, v1, p42
30. GENERIC_ISOTROPIC_STEEL @ BODYSIDE_INNER_LEFT	XS41-A02556/7-AD	Author	FORD Safety FEA handbook, v1, p42
31. GENERIC_ISOTROPIC_STEEL @ BODYSIDE_INNER_RIGHT	XS41-A02556/7-AD	Author	FORD Safety FEA handbook, v1, p42
32. GENERIC_ISOTROPIC_STEEL @ BODYSIDE_OUTER_RIGHT	XS41-A27846/7-AD	Author	FORD Safety FEA handbook, v1, p42
33. GENERIC_ISOTROPIC_STEEL @ BODYSIDE_OUTER_LEFT	XS41-A27846/7-AD	Author	FORD Safety FEA handbook, v1, p42
34. PARTWALL_PLASTIC @ PARTWALL	Partwall.IGES	Author	CPAZTL2D00
35. GENERIC_ISOTROPIC_STEEL @ ENGINE_MOUNT_BRACKET	XS41-6B084-A_	CPAZTL2D00	FORD Safety FEA handbook, v1, p42
36. GENERIC_ISOTROPIC_STEEL @ FENDER_RIGHT	XS41-A16015/6-A_	Author	FORD Safety FEA handbook, v1, p42

37. GENERIC_ISOTROPIC_STEEL @ FENDER_LEFT	XS41-A16015/6-A_	Author	FORD Safety FEA handbook, v1, p42
38. GENERIC_ISOTROPIC_STEEL @ EXTERNAL_FENDER_RIGHT	XS41-16184/5-A_	Author	FORD Safety FEA handbook, v1, p42
39. GENERIC_ISOTROPIC_STEEL @ EXTERNAL_FENDER_LEFT	XS41-16184/5-A_	Author	FORD Safety FEA handbook, v1, p42
40. GENERIC_ISOTROPIC_STEEL @ COWLTOP_INNER	XS41-A02030-AC	Author	FORD Safety FEA handbook, v1, p42
41. GENERIC_ISOTROPIC_STEEL @ COWLGRILL	98-A02116-AR	Author	FORD Safety FEA handbook, v1, p42
42. GENERIC_ISOTROPIC_STEEL @ PLENUM_CHAMBER	XS41-A18A344-AC	Author	FORD Safety FEA handbook, v1, p42
43. ELECTRONICS BOX @ ELECTRONICS_BOX	Not used	CPAZTL2D00	CPAZTL2D00
44. INTERCOOLER @ INTERCOOLER	package1.iges 15.574.923 bytes	Author	FORD Safety FEA handbook, v1, p42
45. ABS RESERVOIR @ ABS_RESERVOIR	Not used	CPAZTL2D00	FORD Safety FEA handbook, v1, p66
46. RADIATOR_GRILLE_PLASTIC @ RADIATOR_GRILL	98AB-8200-A_	Author	FORD Safety FEA handbook, v1, p66
47. GENERIC_ISOTROPIC_STEEL @ REINF_SUSP_TOP_RIGHT	FRONT SUSPENSION	Author	FORD Safety FEA handbook, v1, p42
48. GENERIC_ISOTROPIC_STEEL @ REINF_SUSP_TOP_LEFT	FRONT SUSPENSION	Author	FORD Safety FEA handbook, v1, p42
49. WINDSCREEN_ADHESIVE @ WINDSCREEN_ADHESIVE_SPRINGS	E mail from R.Schilling - RADIOSS windscreen properties with attached Hypermesh mesh geometry		
50. GENERIC_ISOTROPIC_STEEL @ WINDSCREEN WIPER RIGHT	-	CPAZTL2D00	FORD Safety FEA handbook, v1, p42
51. GENERIC_ISOTROPIC_STEEL @ WINDSCREEN WIPER LEFT	-	CPAZTL2D00	FORD Safety FEA handbook, v1, p42
52. WINDSCREEN_GLASS @ WINDSCREEN	98AB-A03100-A_	Author	CPAZTL2D00
53. RIGID_GROUND_FIXED @ RIGID_GROUND	Not used	Author	Author
54. FOGLAMP_PLASTIC @ FOGLAMP_SOLID_RIGHT	XS41-15K201-A_	Author	fka headlamp report 6664
55. FOGLAMP_PLASTIC @ FOGLAMP_SOLID_LEFT	XS41-15K201-A_	Author	fka headlamp report 6664
56. GENERIC_ISOTROPIC_STEEL @ HEADER_RAIL	roofasy.IGES	Author	FORD Safety FEA handbook, v1, p42
57. GENERIC_ISOTROPIC_STEEL @ ROOF_PANEL	roofasy.IGES	Author	FORD Safety FEA handbook, v1, p42
58. GENERIC_ISOTROPIC_STEEL @ RAIL_ROOF_SIDE_INNER_LEFT	biw.iges, 2.072.547 bytes	Author	FORD Safety FEA handbook, v1, p42
59. GENERIC_ISOTROPIC_STEEL @ RAIL_ROOF_SIDE_INNER_RIGHT	roofasy.IGES	Author	FORD Safety FEA handbook, v1, p42
60. DUMMY HIGH STRENGTH @ COOLING_PACK_SUPPORT	COOLING PACK W/FR (diesel)	Author	Author
61. COOLING_PACK_ @ COOLING PACK	COOLING PACK W/FR (diesel)	Author	Author
62. GENERIC_ISOTROPIC_STEEL @ REINFORCEMENT_SIDE_RAIL_RIGHT	biw.iges, 2.072.547 bytes	Author	FORD Safety FEA handbook, v1, p42
63. GENERIC_ISOTROPIC_STEEL @ REINFORCEMENT_SIDE_RAIL_LEFT	biw.iges, 2.072.547 bytes	Author	FORD Safety FEA handbook, v1, p42
64. GENERIC_ISOTROPIC_STEEL @ REINF_SUSP_RIGHT	XS41-3A153-A_	Author	FORD Safety FEA handbook, v1, p42
65. GENERIC_ISOTROPIC_STEEL @ REINF_SUSP_LEFT	XS41-3A153-A_	Author	FORD Safety FEA handbook, v1, p42
66. GENERIC_ISOTROPIC_STEEL @ FRONT_SUSP_HOUSING_RIGHT	XS41-3438/9-A_	Author	FORD Safety FEA handbook, v1, p42
67. GENERIC_ISOTROPIC_STEEL @ FRONT_SUSP_HOUSING_LEFT	XS41-3438/9-A_	Author	FORD Safety FEA handbook, v1, p42
68. GENERIC_ISOTROPIC_STEEL @ SHOT_GUN_LEFT	XS41-A024A14/5-A_	Author	FORD Safety FEA handbook, v1, p42
69. GENERIC_ISOTROPIC_STEEL @ SHOT_GUN_RIGHT	XS41-A024A14/5-A_	Author	FORD Safety FEA handbook, v1, p42
70. HIGH STRENGTH STEEL @ SIDE_RAIL_FLR_LEFT	XS41-A101A88/9-C_	Author	FORD Safety FEA handbook, v1, p42
71. HIGH STRENGTH STEEL @ SIDE_RAIL_RIGHT	XS41-A10524/5-C	Author	FORD Safety FEA handbook, v1, p42
72. HIGH STRENGTH STEEL @ SIDE_RAIL_LEFT	XS41-A10524/5-C	Author	FORD Safety FEA handbook, v1, p42

73. HIGH STRENGTH STEEL @ SIDE_RAIL_FLR_RIGHT	XS41-A101A88/9-C_	Author	FORD Safety FEA handbook, v1, p42
74. BUMPERSHELL_PLASTIC @ BUMPERSHELL	fka report "The dynamic characterization of the C170 bumper system under pedestrian impact conditions using a systematic component analysis and testing procedure". CAD data file 98AB-17757-A_		
76 GENERIC_ISOTROPIC_STEEL @ BUMPER_BRKT_RIGHT	98AB-17D958-B_	Author	FORD Safety FEA handbook, v1, p42
77 GENERIC_ISOTROPIC_STEEL @ BUMPER_BRKT_LEFT	98AB-17D958-B_	Author	FORD Safety FEA handbook, v1, p42
78 BUMPER_GRILL_PLASTIC @ BUMPER_GRILL_SOLID	98AB-A018058-AA	Author	FORD Safety FEA handbook, v1, p66
79 HL_PP @ HL_PP_10_LEFT	fka model and report "The dynamic characterization of the C170 headlamp under pedestrian impact conditions using a systematic component analysis and testing procedure". The CAD data files used were; headlamp1.iges, 6.119.064 bytes. Updated to XS41-13K370-B_.		
80 HL_PC @ HL_PC_2.5_LEFT			
81 HL_PC @ HL_PC_2.6_LEFT			
82 HL_PC @ HL_PC_3.1_LEFT			
83 HL_PP @ HL_PP_2.0_LEFT			
84 HL_PC @ HL_PC_4.0_LEFT			
85 HL_PC @ HL_PC_2.7_LEFT			
86 HL_PP @ HL_PP_8_LEFT			
87. HL_PP @ HL_PP_10_RIGHT			
88. HL_PC @ HL_PC_2.5_RIGHT			
89. HL_PC @ HL_PC_2.6_RIGHT			
90. HL_PC @ HL_PC_3.1_RIGHT			
91. HL_PP @ HL_PP_2.0_RIGHT			
92. HL_PC @ HL_PC_4.0_RIGHT			
93. HL_PC @ HL_PC_2.7_RIGHT			
94. HL_PP @ HL_PP_8_RIGHT			
95. HL_PP @ HL_PP_3.0_RIGHT			
96. HL_PP @ HL_PP_3.0_LEFT			
97. GOR_ST @ GOR_ST	fka model and report "The dynamic characterization of the C170 GOR under pedestrian impact conditions using a systematic component analysis and testing procedure. The CAD data files used were; gorblech1.iges, 969.570 bytes gorblech2.iges, 38.961 bytes gorblech3.iges, 2.727.027 bytes gorksty.iges, 4.451.841 bytes gorkstz.iges, 3.017.412 bytes. Model updated to XS41-8A164-A_.		
98. GOR_PA @ GOR_PA_2			
99. GOR_PA @ GOR_PA_2.5			
100. GOR_PA @ GOR_PA_1.5			
101. GOR_PA @ GOR_PA_3			
102. GOR_PA @ GOR_PA_4			
103. GOR_PA @ GOR_PA_6			
104. GOR_PA @ GOR_PA_5			
105. AIR FILTER BOX @ AFB_PP_2.1	fka model and report "The dynamic characterization of the C170 air filter box under pedestrian impact conditions using a systematic component analysis and testing procedure". The CAD data files used were; package1.iges , 15.574.923 bytes		
106. AIR FILTER BOX @ AFB_PP_1.8			
107. AIR FILTER BOX @ AFB_PP_2.8			
108. AIR FILTER BOX @ AFB_PP_1.6			
109. AIR FILTER BOX @ AFB_PP_0.4			
110. AIR FILTER BOX @ AFB_PP_2.7			
111. AIR FILTER BOX @ AFB_PP_2.4			
112. INTERCOOLER PIPE @ IDP_ST_2.5	fka model and report "The dynamic characterization of the C170 intercooler ducting pipe under pedestrian impact conditions using a systematic component analysis and testing procedure". The CAD data files used were; package1.iges , 15.574.923 bytes		
113. INTERCOOLER PIPE @ IDP_ST_1.5			
114. INTERCOOLER PIPE @ IDP_ST_2.5_RIGHT			
115. INTERCOOLER PIPE @ IDP_ST_1.5_RIGHT			
116. GENERIC_ISOTROPIC_STEEL @ APRON_LEFT	XS41-A16044/5-A_	Author	FORD Safety FEA handbook, v1, p42
117. GENERIC_ISOTROPIC_STEEL @ APRON_RIGHT	XS41-A16044/5-A_	Author	FORD Safety FEA handbook, v1, p42
118. BUMP_STOP_RUBBER @ BUMP_STOP	91AB-16C618_AA	Author	Author (steel)
119. HOOD_ADHESIVE @ HOOD_ADHESIVE_SPRINGS	Not used	Author	FORD report T240-96-028
120. COOLING_SUSP_RUBBER @ COOLING_SUSP_RUBBER	Not used	Author	Author
121. HIGH STRENGTH STEEL @ FRCM_REINF_RIGHT	XS41-A10748-B_	Author	FORD Safety FEA handbook, v1, p42
122. HIGH STRENGTH STEEL @ FRCM_REINF_LEFT	XS41-A10748-B_	Author	FORD Safety FEA handbook, v1, p42

Appendix F - Vehicle model moment of inertia calculations

According to [McInnis 1997] the centre of gravity height and moments of inertia for front wheel drive cars may be estimated to lie within the following ranges.

h_{cog}= 535± 3%

I_{XX} = 0.1274×m×(h_{roof} + h_{cog})×t ± 6.5% (roll inertia)

I_{YY} = 0.1425×m×l×L ± 5.7% (pitch inertia)

I_{ZZ} = 0.1478×m×l×L ± 4.8% (yaw inertia)

Where

m = vehicle mass with two 75Kg occupants = 1.31 tonnes

h_{roof} = height of roof = 1481 mm

t = track width = 1508 mm

l = wheelbase = 2615 mm

L = overall vehicle length = 4178 mm

h_{cog} = height of centre of gravity = See below

I_{**} = moment of inertia about the axis ** = See below

And hence the following values are estimated for the complete vehicle 'p'

h_{cog}= 551mm (upper bound)

I_{XX}= 511406.0 tonnes mm^2 (mid point)

I_{YY}= 6082755.0 tonnes mm^2 (mid point)

I_{ZZ}= 2115367.0 tonnes mm^2 (mid point)

Appendix G – Brief element theory and its role in Hourglassing

The figure below shows a four node quadrilateral element and the local co-ordinate system in which the "... displacements, velocities and accelerations are evaluated at the nodal points. Stresses, strains and stress resultants are evaluated in the element integration points. The number of integration points and their location on the element surface depends on the element type" [DuBois 2001].

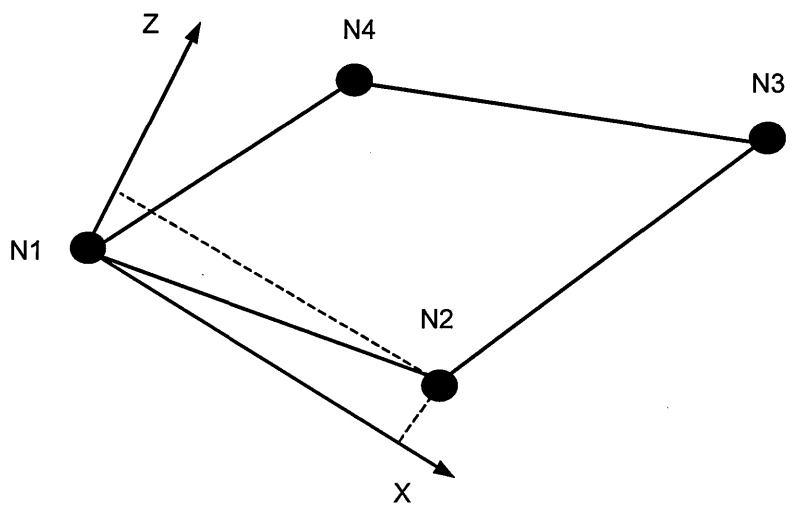

Some of the integration methods used in LS-DYNA are summarised in the table below from [DuBois 2001].

Full Integration	Selective Reduced Integration	Assumed Natural coordinate Strain element	Reduced Integration
Four Gauss points in the plane of the shell for all strain components	Four Gauss points in the plane for membrane and bending strains, one integration point in the element centre for out of plane shear strains	Four Gauss points in the plane of the shell for all strain components, a special interpretation is used for the out of plane shear strains	A single integration point in the centre of the element is used for all strain components

Du Bois continues "Full integration of bilinear elements leads to shear locking: the out of plane shear strains (and stresses) do not uniformly disappear in the case of pure bending and this results in an overstiff response of the structure. One of the ways to avoid this problem is to use reduced integration elements and restrict the strain calculation to the element centre. This also leads to computationally efficient algorithms but allows the existence of zero energy or hourglass modes".

An example hourglass mode for in plane bending is illustrated in the figure below with a 2D element that has a single degree of freedom in X for each of the nodes. Even though the element has deformed, the integration point measures a strain rate of zero and no energy change is indicated.

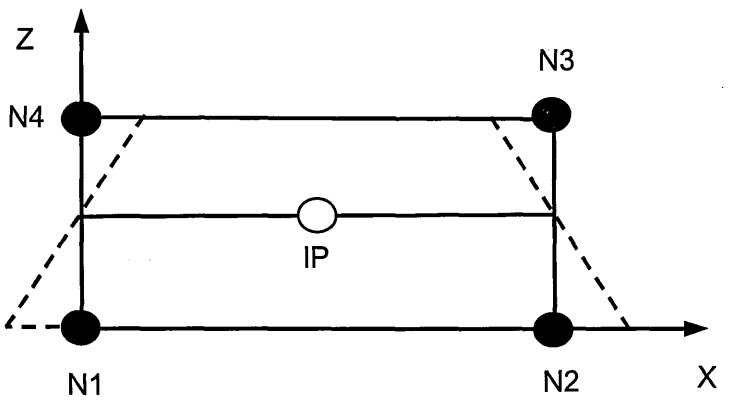

To overcome this problem a depth of at least three elements is required in typical regions where in plane bending occurs or it may be computationally more beneficial to use fully integrated elements. A similar three element rule also applies to out of plane bending and mesh refinement (finer mesh density) is the preferred method of avoiding hourglassing [DuBois 2001].

Appendix H - Pedestrian accident simulation procedure

Preprocessing in Master Series, N/CODE and Primer

c170_cp, c170_p, c170_d1 & c170_d2 vehicle models in Master Series

Ideas_ffa (starts Master Series).

Ensure model up to date with all physical properties (especially thicknesses) and naming/numbering convention only for material properties.

Note: the vehicle ground in the master series model is raised 70mm to represent vehicle brake dive.

Preprocessing of vehicle model input deck using N/CODE

Command line: oasys_80 (Ove Arup pre and post processor)

Pick N/CODE

Size of memory 3000000

Set to IDEAS

Read c170_*.unv (check screen output for relevant groups)

Ph (physical property numbering)

Control termination, 1 0.35 (350ms)

Timestep, timestep size for mass scaled solution, 5 –1e-6

Fi, Fi

Load curves, read old_c170_*.key (make sure old keyword file is updated)

Materials, read old_c170_*.key

Fi

Physical properties, default, none different (i.e. use .unv values and make sure .unv correct) or, read old_c170_*.key

Fi

Part definition (optional), INERTIA for part 16, 1 2841 (cog X in mm), 3 481 (cog Z in mm), 4 0.9 (tonnes), 5 511e3 (Ixx), 8 608e4 (Iyy), 10 212e4 (Izz), Quit, Fi

Spring, Fi (default spring physical properties read from .unv)

Loading, 3 yes (gravity loading in Z on whole model), use default of load curve 1

Rigid body, MOTION, part 16 (rear end), XT (velocity in X), 2 2 (load curve 2)

Fi

Contact surfaces, no changes required

Fi

Constraints, 1 1e20, 2 1e20 (high values to prevent problems in GOR model)

Rigid body merges, Fi

Joints, re, re, ...cyl .... (joints depend on which model used)

Modifying and checking the vehicle model input deck using PRIMER

Command line: oasys_80

Pick PRIMER

Change any nodes_to_surface etc. contacts to automatic_nodes_to_surface

Check which joints revolute or cylindrical etc. and correct as necessary

Combining vehicle & pedestrian models in PRIMER for accident simulation

Command line: oasys_80

Pick PRIMER

Read vehicle and pedestrian model keyword input files

For all pedestrian positioning move the model ONLY by selecting it by model. For stances A, B, C impacts rotate the pedestrian model by –90 degrees about the Z axis and origin but for stance D there is no need to rotate the model. Note that the Y position is correct by default provided the rotation is about the origin. THEN move the pedestrian in the Z axis by using a node on the pedestrian rigid ground to a node on the vehicle rigid ground.

The nearest distance between the pedestrian struck leg and the vehicle bumper should is set by moving the pedestrian model in X only according to the vehicle impact velocity as follows (this allows the pedestrian 10ms to settle down on the rigid ground due to gravity, before the impact). It is easier to blank all elements except LH femur solids (1050) and bumpershell (74) to do this.

Vehicle impact velocity (Km/h)	Bumper to leg distance (mm)
50	139
45	125
40	111
35	97
30	83
25	69

Choose define curve and modify CURVE 2 (this should be the velocity profile curve for 1g deceleration in X. Modify values of V1 and t in V1-9810t=0 as follows.

Vehicle impact velocity (km/h)	Time 't' to reach 0 under 1g (s)	Impact velocity 'V1' (mm/s)
50	1.42	13890
45	1.27	12500
40	1.13	11100
35	0.99	9720
30	0.85	8330
25	0.71	6940

The initial velocity for the front of the vehicle will also need to be changed so search for initial and change INITIAL_VELOCITY to a new value (V1) as appropriate.

Choose model merge option and set the pedestrian model as the master model (this will ensure that the control cards and database output cards are defined by the pedestrian model). Set the option increment slave model only on clash and merge models into model 3. Name model 3 for example, "C170_d1, Y0, 50th, stance A, 40 km/h, FFA" as appropriate (see matrix).

Create new part sets in vehicle model keyword file:

5th, 50th, 95th percentile pedestrians		
Set	Contact group description	Contains (based on c170_p)
1	VEHICLE TO VEHICLE	Defined in .unv - rename
2	SPECIAL VEHICLE TO VEHICLE (for parts that cannot be in above)	Defined in .unv – rename ? – depends on vehicle
3	HOOD/UTRAY/RGRIL/FGLAMP/BUMPE/BGRIL/HLAMP/GOR	2/18/46/54/55/74/78/80/81/88/89/97/101 (123)
4	HOOD/APOST/ FENDERS/WIPERS/SCREEN/ROOF/HLAMP	2/32/33/36/37/50/51/52/57/80/81/88/89
5		
6		
7		Defined in pedestrian model
8		Defined in pedestrian model
9		Defined in pedestrian model
10		Defined in pedestrian model

6 year old pedestrian model		
Set	Contact group description	Contains (based on c170_p)
1	VEHICLE TO VEHICLE	Defined in .unv - rename
2	SPECIAL VEHICLE TO VEHICLE	? – depends on vehicle
3	HOOD/UTRAY/APOST/RGRIL/FGLAMP/BUMPE/BGRIL/HLAMP/GOR	2/18/32/33/46/54/55/74/78/80/81/88/89/97/101
4	HOOD/APOST/FENDERS/ WIPERS/SCREEN/ ROOF/HLAMP	2/32/33/36/37/50/51/52/57/80/81/88/89
5		
6		
7		Defined in pedestrian model
8		Defined in pedestrian model
9		Defined in pedestrian model
10		Defined in pedestrian model

Modify contacts by adding appropriate part sets for vehicle side of contacts:

	5th, 50th, 95th percentile pedestrians	
	Contact type and name	Part set
1	AUTOMATIC_SINGLE_SURFACE, VEHICLE TO VEHICLE	1
2	AUTOMATIC_SURFACE_TO_SURFACE, UPPER LEG TO UPPER LEG	-
3	AUTOMATIC_SURFACE_TO_SURFACE, LOWER LEG TO LOWER LEG	-
4	RIGID_BODY_ONE_WAY_TO_RIGID_BODY, LEFT FOOT TO FLOOR	-
5	RIGID_BODY_ONE_WAY_TO_RIGID_BODY, RIGHT FOOT TO FLOOR	-
6	AUTOMATIC_SURFACE_TO_SURFACE, LEFT FOOT TO RIGHT FOOT	-
7	AUTOMATIC_SURFACE_TO_SURFACE, LEFT LOWER ARM TO LOWER TORSO (PELVIS)	-
8	AUTOMATIC_SURFACE_TO_SURFACE, LEFT LOWER ARM TO ABDOMEN	-
9	AUTOMATIC_SURFACE_TO_SURFACE, LEFT HAND TO LOWER TORSO (PELVIS)	-
10	AUTOMATIC_SURFACE_TO_SURFACE, RIGHT LOWER ARM TO LOWER TORSO	-
11	AUTOMATIC_SURFACE_TO_SURFACE, RIGHT LOWER ARM TO ABDOMEN	-
12	AUTOMATIC_SURFACE_TO_SURFACE, RIGHT HAND TO LOWER TORSO	-
13	AUTOMATIC_SURFACE_TO_SURFACE, LOWER LEFT LEG TO HOOD/UTRAY/RGRIL/FGLAMP/BUMPE/BGRIL/HLAMP/GOR	3
14	AUTOMATIC_SURFACE_TO_SURFACE, LOWER RIGHT LEG TO HOOD/UTRAY/RGRIL/FGLAMP/BUMPE/BGRIL/HLAMP/GOR	3
15	AUTOMATIC_SURFACE_TO_SURFACE, UPPER LEFT LEG TO HOOD/APOST/ FENDERS/WIPERS/SCREEN/ROOF/HLAMP	4
16	AUTOMATIC_SURFACE_TO_SURFACE, LOWER TORSO (PELVIS) TO HOOD/APOST/ FENDERS/WIPERS/SCREEN/ROOF/HLAMP	4
17	AUTOMATIC_SURFACE_TO_SURFACE, ABDOMEN TO HOOD/APOST/ FENDERS/WIPERS/SCREEN/ROOF/HLAMP	4
18	AUTOMATIC_SURFACE_TO_SURFACE, UPPER TORSO TO HOOD/APOST/ FENDERS/WIPERS/SCREEN/ROOF/HLAMP	4
19	AUTOMATIC_SURFACE_TO_SURFACE, HEAD TO HOOD/APOST/ FENDERS/WIPERS/SCREEN/ROOF/HLAMP	4
20	AUTOMATIC_SURFACE_TO_SURFACE, LEFT LOWER ARM TO HOOD/APOST/ FENDERS/WIPERS/SCREEN/ROOF/HLAMP	4
21	AUTOMATIC_SURFACE_TO_SURFACE, LEFT HAND TO HOOD/APOST/ FENDERS/WIPERS/SCREEN/ROOF/HLAMP	4
22	AUTOMATIC_SURFACE_TO_SURFACE, RIGHT UPPER ARM TO HOOD/APOST/ FENDERS/WIPERS/SCREEN/ROOF/HLAMP	4
23	AUTOMATIC_SURFACE_TO_SURFACE, RIGHT LOWER ARM TO HOOD/APOST/ FENDERS/WIPERS/SCREEN/ROOF/HLAMP	4
24	AUTOMATIC_SURFACE_TO_SURFACE, RIGHT HAND TO HOOD/APOST/ FENDERS/WIPERS/SCREEN/ROOF/HLAMP	4
25	AUTOMATIC_SURFACE_TO_SURFACE, LEFT UPPER ARM TO HOOD/APOST/ FENDERS/WIPERS/SCREEN/ROOF/HLAMP	4
26	AUTOMATIC_SURFACE_TO_SURFACE, UPPER RIGHT LEG TO HOOD/APOST/ FENDERS/WIPERS/SCREEN/ROOF/HLAMP	4
27	AUTOMATIC_SURFACE_TO_SURFACE, RIGHT FOOT TO LOWER LEG	-
28	AUTOMATIC_SURFACE_TO_SURFACE, RIGHT HAND TO UPPER LEG	-
29	SURFACE_TO_SURFACE, PELVIS TO LEFT FOOT	-
30	SURFACE_TO_SURFACE, PELVIS TO RIGHT FOOT	-
31	AUTOMATIC_SURFACE_TO_SURFACE, LEFT FOOT TO LOWER RIGHT LEG	-
32	AUTOMATIC_SURFACE_TO_SURFACE, LEFT HAND TO UPPER LEFT LEG	-
33	AUTOMATIC_SURFACE_TO_SURFACE, HEAD RIGID SHELL TO HOOD/APOST/ FENDERS/WIPERS/SCREEN/ROOF/HLAMP	4
34	AUTOMATIC_SURFACE_TO_SURFACE, LEFT HAND, LOWER ARM TO UPPER THORAX	-
35	AUTOMATIC_SURFACE_TO_SURFACE, RIGHT HAND, LOWER ARM TO UPPER THORAX	-
36	AUTOMATIC_SURFACE_TO_SURFACE, FEET TO HOOD/UTRAY/RGRIL/FGLAMP/BUMPE/BGRIL/HLAMP/GOR	3

	6 year old pedestrian	
	Contact type and name	Part set
1	AUTOMATIC_SINGLE_SURFACE, VEHICLE TO VEHICLE	-
2	AUTOMATIC_SURFACE_TO_SURFACE, UPPER LEG TO UPPER LEG	-
3	AUTOMATIC_SURFACE_TO_SURFACE, LOWER LEG TO LOWER LEG	-
4	RIGID_BODY_ONE_WAY_TO_RIGID_BODY, LEFT FOOT TO FLOOR	-
5	RIGID_BODY_ONE_WAY_TO_RIGID_BODY, RIGHT FOOT TO FLOOR	-
6	AUTOMATIC_SURFACE_TO_SURFACE, LEFT FOOT TO RIGHT FOOT	-
7	AUTOMATIC_SURFACE_TO_SURFACE, LEFT LOWER ARM TO LOWER TORSO (PELVIS)	-
8	AUTOMATIC_SURFACE_TO_SURFACE, LEFT LOWER ARM TO ABDOMEN	-
9	AUTOMATIC_SURFACE_TO_SURFACE, LEFT HAND TO LOWER TORSO (PELVIS)	-
10	AUTOMATIC_SURFACE_TO_SURFACE, RIGHT LOWER ARM TO LOWER TORSO	-
11	AUTOMATIC_SURFACE_TO_SURFACE, RIGHT LOWER ARM TO ABDOMEN	-
12	AUTOMATIC_SURFACE_TO_SURFACE, RIGHT HAND TO LOWER TORSO	-
13	AUTOMATIC_SURFACE_TO_SURFACE, LOWER LEFT LEG TO HOOD/UTRAY/APOST/RGRIL/FGLAMP/BUMPE/BGRIL/HLAMP/GOR	3
14	AUTOMATIC_SURFACE_TO_SURFACE, LOWER RIGHT LEG TO HOOD/UTRAY/APOST/RGRIL/FGLAMP/BUMPE/BGRIL/HLAMP/GOR	3
15	AUTOMATIC_SURFACE_TO_SURFACE, UPPER LEFT LEG TO HOOD/UTRAY/APOST/RGRIL/FGLAMP/BUMPE/BGRIL/HLAMP/GOR	3
16	AUTOMATIC_SURFACE_TO_SURFACE, LOWER TORSO (PELVIS) TO HOOD/UTRAY/APOST/RGRIL/FGLAMP/BUMPE/BGRIL/HLAMP/GOR	3
17	AUTOMATIC_SURFACE_TO_SURFACE, ABDOMEN TO HOOD/UTRAY/APOST/RGRIL/FGLAMP/BUMPE/BGRIL/HLAMP/GOR	3
18	AUTOMATIC_SURFACE_TO_SURFACE, UPPER TORSO TO HOOD/APOST/FENDERS/WIPERS/SCREEN/ROOF/HLAMP	4
19	AUTOMATIC_SURFACE_TO_SURFACE, HEAD TO HOOD/APOST/FENDERS/ WIPERS/SCREEN/ ROOF/HLAMP	4
20	AUTOMATIC_SURFACE_TO_SURFACE, LEFT LOWER ARM TO HOOD/UTRAY/APOST/RGRIL/FGLAMP/BUMPE/BGRIL/HLAMP/GOR	3
21	-	-
22	AUTOMATIC_SURFACE_TO_SURFACE, RIGHT UPPER ARM TO HOOD/APOST/FENDERS/ WIPERS/SCREEN/ ROOF/HLAMP	4
23	AUTOMATIC_SURFACE_TO_SURFACE, RIGHT LOWER ARM TO HOOD/UTRAY/APOST/RGRIL/FGLAMP/BUMPE/BGRIL/HLAMP/GOR	3
24	-	-
25	AUTOMATIC_SURFACE_TO_SURFACE, LEFT UPPER ARM TO HOOD/APOST/FENDERS/ WIPERS/SCREEN/ ROOF/HLAMP	4
26	AUTOMATIC_SURFACE_TO_SURFACE, UPPER RIGHT LEG TO HOOD/UTRAY/APOST/RGRIL/FGLAMP/BUMPE/BGRIL/HLAMP/GOR	3
27	AUTOMATIC_SURFACE_TO_SURFACE, RIGHT FOOT TO LOWER LEG	-
28	AUTOMATIC_SURFACE_TO_SURFACE, RIGHT HAND TO UPPER LEG	-
29	SURFACE_TO_SURFACE, PELVIS TO LEFT FOOT	-
30	SURFACE_TO_SURFACE, PELVIS TO RIGHT FOOT	-
31	AUTOMATIC_SURFACE_TO_SURFACE, LEFT FOOT TO LOWER RIGHT LEG	-
32	AUTOMATIC_SURFACE_TO_SURFACE, LEFT HAND TO UPPER LEFT LEG	-
33	AUTOMATIC_SURFACE_TO_SURFACE, HEAD RIGID SHELL TO HOOD/APOST/FENDERS/ WIPERS/SCREEN/ ROOF/HLAMP	4
34	AUTOMATIC_SURFACE_TO_SURFACE, LEFT HAND, LOWER ARM TO UPPER THORAX	-
35	AUTOMATIC_SURFACE_TO_SURFACE, RIGHT HAND, LOWER ARM TO UPPER THORAX	-
36	AUTOMATIC_SURFACE_TO_SURFACE, FEET TO HOOD/UTRAY/APOST/RGRIL/FGLAMP/BUMPE/BGRIL/HLAMP/GOR	3

Write keyword file in the appropriate directory and name again e.g. A01_*.key

ASCII editor changes to keyword file

Add * LOAD_BODY_Z back into keyword deck if PRIMER has not written this out.

Solving in LS-DYNA

Rlogin dffa049 (remote log in to solver machine to run and solve the model locally)

Cd /ford/dffa049/u/ .... etc. & copy file from home workstation into running directory

To run, dyna5e i=filename.key & (background processing mode)

Post processing in T/HIS and D3PLOT

Command line: oasys_80 , Pick T/HIS, Read d3tht output file for the following:

Measurement	6 year old	5th	50th	95th
Head				
XZ plane trajectory	N 103152	N 103152	N 103152	N 103152
Relative velocity to vehicle	N 103152	N 103152	N 103152	N 103152
Global acceleration	N 103152	N 103152	N 103152	N 103152
HIC	N 103152	N 103152	N 103152	N 103152
Max. displacement X, Y, Z	N 103152	N 103152	N 103152	N 103152
Neck				
None at present	J 8,9,10,11,12, 13,14,15,7	J 8,9,10,11,12, 13,14,15,7	J 8,9,10,11,12, 13,14,15,7	J 8,9,10,11,12, 13,14,15,7
Chest/upper torso				
Max. displacement X, Y, Z	N 218028 J 1	N 218028 J 1	N 218028 J1	N 218028 J1
Arms				
	J 17, 16, 20 18, 21, 19	J 17, 16, 20 18, 21, 19	J 17, 16, 20 18, 21, 19	J 17, 16, 20 18, 21, 19
Pelvis/lower torso				
Max. displacement X, Y, Z	N 216163	N 216163	N 216163	N 216163
Global acceleration	N 216163	N 216163	N 216163	N 216163
Femur				
First fracture location	B200095/100042 B200096/100041 B200097/100040 B200071/100044 B200072/100045 B200070/100039 B200069/100038 B200068/100037 B200067/100036 B200066/100035	B200095/100042 B200096/100041 B200097/100040 B200071/100044 B200072/100045 B200070/100039 B200069/100038 B200068/100037 B200067/100036 B200066/100035	B200095/100042 B200096/100041 B200097/100040 B200071/100044 B200072/100045 B200070/100039 B200069/100038 B200068/100037 B200067/100036 B200066/100035	B200095/100042 B200096/100041 B200097/100040 B200071/100044 B200072/100045 B200070/100039 B200069/100038 B200068/100037 B200067/100036 B200066/100035
Knee				
Bending	D100031	D100031	D100031	D100031
Shear	D100029	D100029	D100029	D100029
Max. displacement X, Y, Z	N210538/N210532	N210538/N210532	N210538/N210532	N210538/N210532
Tibia/Fibula				
Local X acceleration	N103156	N103156	N103156	N103156
First fracture location	B100016/33 B100015/34 B100014/32 B100013/31 B100012/30 B100011/29 B100010/28 B100009/27 B100008/26	B100016/33 B100015/34 B100014/32 B100013/31 B100012/30 B100011/29 B100010/28 B100009/27 B100008/26	B100016/33 B100015/34 B100014/32 B100013/31 B100012/30 B100011/29 B100010/28 B100009/27 B100008/26	B100016/33 B100015/34 B100014/32 B100013/31 B100012/30 B100011/29 B100010/28 B100009/27 B100008/26
Ankle				
	B100007/25 J4/3	B100007/25 J4/3	B100007/25 J4/3	B100007/25 J4/3
Foot				
	N216164	N216164	N216164	N216164

For each run the data may be recorded in the standard Excel sheets:

FFA_01_head_trajectories_c170_p_human_71.xls
FFA_02_head_resultant_velocity_c170_p_human_71.xls
FFA_03_head_resultant_acceleration_HIC_c170_p_human_71.xls
FFA_04_impact_timing_CMD_c170_p_human_71.xls
FFA_05_struck_knee_shear_c170_p_human_71.xls
FFA_06_struck_knee_bending_c170_p_human_71.xls
FFA_07_struck_tibia_local X_acceleration_c170_p_human_71.xls
FFA_08_pelvis_acceleration_leg_fractures_c170_p_human_71.xls

Standard setup for 3d animation file creation in D3PLOT

Colour background yellow with text colour black
Utilities, modify title, e.g. 50th Y500 40km/h no dive/deceleration if necessary
Display options, header and clock only with clock size large
Utilities, graphics, options 800 600
Car outer panels blue with pedestrian model white
Ground (53), windscreen (52), lamps (80, 81, 88, 89) yellow
Blank pedestrian model ground
Light, ambient 100%, brightness 100%
Perspective, nearer on, 10,000
Isometric view then rotate about model 20, 20, -90 degrees
File save to disk e.g. b02.ani_3d
Graphics pictures of vehicle and pedestrian models with 8000 perspective and view direction 310, 65, 34

Appendix I - Calculating physical properties for hood analytical model

Extract from the on line context help in Master Series concerning the calculation of physical properties

Calculating Mass Center of Gravity

The software calculates mass center of gravity across the sum of the elements.

$$x = \frac{\sum_i x_i M_i}{\sum_i M_i} \quad y = \frac{\sum_i y_i M_i}{\sum_i M_i} \quad z = \frac{\sum_i z_i M_i}{\sum_i M_i}$$

where

x, y, z = distance from the origin to the model center of gravity

x_i, y_i, z_i = distance from the origin to the ith element center of gravity

M_i = ith element mass

Calculating Mass Moments of Inertia

The software calculates mass moments of inertia with respect to the XYZ axes:

$$I_{xx} = \int_M R^2 \, dM = \int_V \varrho \, (y^2 + z^2) \, dV$$

where

I_{xx} = mass moment of inertia about an arbitrary X-X axis

R = distance from the X-X axis to an infinitesimal particle

y, z = orthogonal components of R

ϱ = material density

dM = differential mass

dV = differential volume

The parallel axis theorem states:

$I_{xx} = I'_{xx} + d^2 M$

where:

I'_{xx} = mass moment of inertia of an individual particle about its own local center of gravity X-X axis
d = perpendicular distance from the arbitrary X-X axis to the local center of gravity X-X axis

M = particle mass

If the particle mass is concentrated at the center of gravity of the particle, the I'_{xx} term becomes zero, and the parallel axis theorem becomes $I_{xx} = d^2 M$

The model check moment of inertia calculation considers each element to consist of small mass and volume compared to the total mass and volume of the model. Therefore, the formula shown for I_{xx} calculates the moments of inertia for all three orthogonal axes. This assumption can cause inaccuracies in checks containing a small number of elements. For example, if there is only one element, the moment of inertia lists as zero for all three axes about the center of gravity.

However, for beam elements (beams, rods, pipes), this formula can cause large errors in calculations. Therefore, the element's mass cannot be assumed to be concentrated at the center of gravity, and the software calculates I'_{xx}.

Also, for lumped mass elements, an inertia tensor can be specified on the physical property table (I_{xx}, I_{xy}, I_{zz}, I_{xy}, I_{xz}, I_{yz}) along with a mass inertia coordinate system. The tensor terms are included in the summation of mass properties following appropriate transformation from the mass inertia coordinate system to the axis of origin.

Calculating Mass Products of Inertia

The software calculates mass products of inertia with respect to two perpendicular reference planes. Typically:

$$I_{xy} = \int_M xy \, dM = \int_V \varrho \, (xy) \, dV$$

where

I_{xy} = mass product of inertia about the 2 arbitrary planes with x = constant and y = constant, respectively

x, y = coordinate distance from reference plane to the center of gravity of the particle

ϱ = material density

dM = differential mass

dV = differential volume

The parallel axis theorem states $I_{xy} = I'_{xy} + (xy) M$

where I'_{xy} = mass product of inertia of an individual particle about two reference planes based at its own local center of gravity

M = particle mass

For all non-beam elements, if the particle mass is concentrated at the particle's center of gravity, the term I'_{xy} becomes zero, and the parallel axis theorem becomes $I_{xy} = (xy) M$.

For beam elements (beams, rods, pipes), the assumption that the particle mass is concentrated at the center of gravity is invalid; therefore, I'_{xy} can't be neglected. The software calculates it.

This formula calculates the product of inertia for all three combinations of reference planes. The software calculates the mass moments and products of inertia based on the global coordinate system at both the origin and the center of gravity. The principal axes are the axes for which the product of inertia vanishes and the moments of inertia become a minimum or maximum.

Headlamps/GOR/hood

```
Volume              :  4.836D+06
Mass                :  2.496D+01
Center of gravity :  1.304D+03  -7.169D-01   9.197D+02
Moments of Inertia about c.g.
  Ixx  Iyy  Izz     :  4.436D+06   1.868D+06   5.646D+06
  Ixy  Iyz  Izx     :  2.385D+03   2.692D+03   6.414D+05
Moments of Inertia about origin
  Ixx  Iyy  Izz     :  2.555D+07   6.544D+07   4.810D+07
  Ixy  Iyz  Izx     : -2.095D+04  -1.377D+04   3.058D+07
Principal axes
  1 :  0.001  1.000  0.001
  2 : -0.918  0.001 -0.396
  3 : -0.396 -0.000  0.918
Principal Moments of Inertia
  I11  I22  I33     :  1.860D+06   4.159D+06   5.923D+06
```

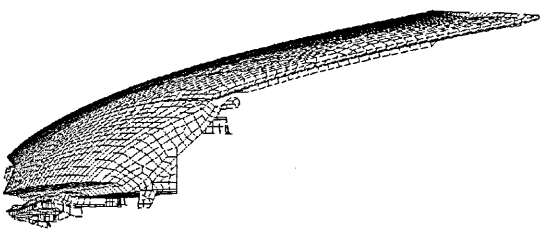

Headlamps

```
Volume              :  1.917D+06
Mass                :  2.139D+00
Center of gravity :  1.177D+03   1.902D-07   8.386D+02
Moments of Inertia about c.g.
  Ixx  Iyy  Izz     :  7.152D+05   3.499D+04   7.336D+05
  Ixy  Iyz  Izx     : -4.792D-04  -3.413D-04   8.843D+03
Moments of Inertia about origin
  Ixx  Iyy  Izz     :  2.220D+06   4.505D+06   3.699D+06
  Ixy  Iyz  Izx     : -3.884D-10  -4.448D-10   2.121D+06
Principal axes
  1 :  0.000  1.000  0.000
  2 :  0.927  0.000  0.374
  3 :  0.374  0.000 -0.927
Principal Moments of Inertia
  I11  I22  I33     :  3.499D+04   7.117D+05   7.371D+05
 2750 elements stored as processed group
```

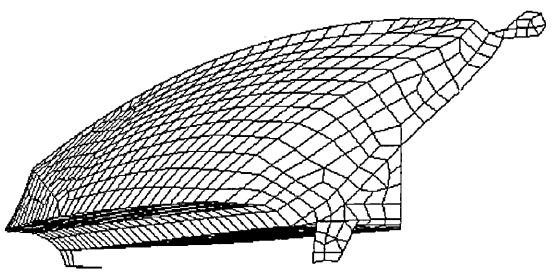

GOR

```
Volume              :  1.396D+06
Mass                :  1.091D+01
Center of gravity :  1.151D+03  -1.640D+00   8.283D+02
Moments of Inertia about c.g.
  Ixx  Iyy  Izz     :  1.421D+06   1.304D+05   1.483D+06
  Ixy  Iyz  Izx     : -3.487D+02   1.060D+03   4.653D+04
Moments of Inertia about origin
  Ixx  Iyy  Izz     :  8.909D+06   2.208D+07   1.594D+07
  Ixy  Iyz  Izx     : -2.095D+04  -1.377D+04   1.045D+07
Principal axes
  1 : -0.000  1.000  0.001
  2 : -0.882  0.000 -0.471
  3 : -0.471 -0.001  0.882
Principal Moments of Inertia
  I11  I22  I33     :  1.304D+05   1.396D+06   1.508D+06
```

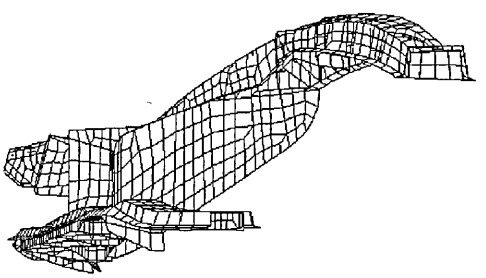

Hood

```
Volume              :  1.523D+06
Mass                :  1.191D+01
Center of gravity :  1.467D+03   3.863D-04   1.018D+03
Moments of Inertia about c.g.
  Ixx  Iyy  Izz     :  2.080D+06   8.763D+05   2.824D+06
  Ixy  Iyz  Izx     : -6.719D+00  -4.800D+00   2.206D+05
Moments of Inertia about origin
  Ixx  Iyy  Izz     :  1.442D+07   3.886D+07   2.846D+07
  Ixy  Iyz  Izx     :  3.100D-02  -1.151D-01   1.801D+07
Principal axes
  1 :  0.000  1.000  0.000
  2 :  0.964  0.000  0.264
  3 :  0.264  0.000 -0.964
Principal Moments of Inertia
  I11  I22  I33     :  8.763D+05   2.019D+06   2.884D+06
```

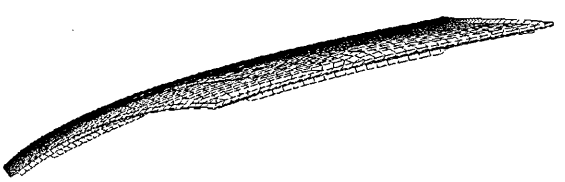

Appendix J - Original data vehicle 'p' pedestrian accident simulations

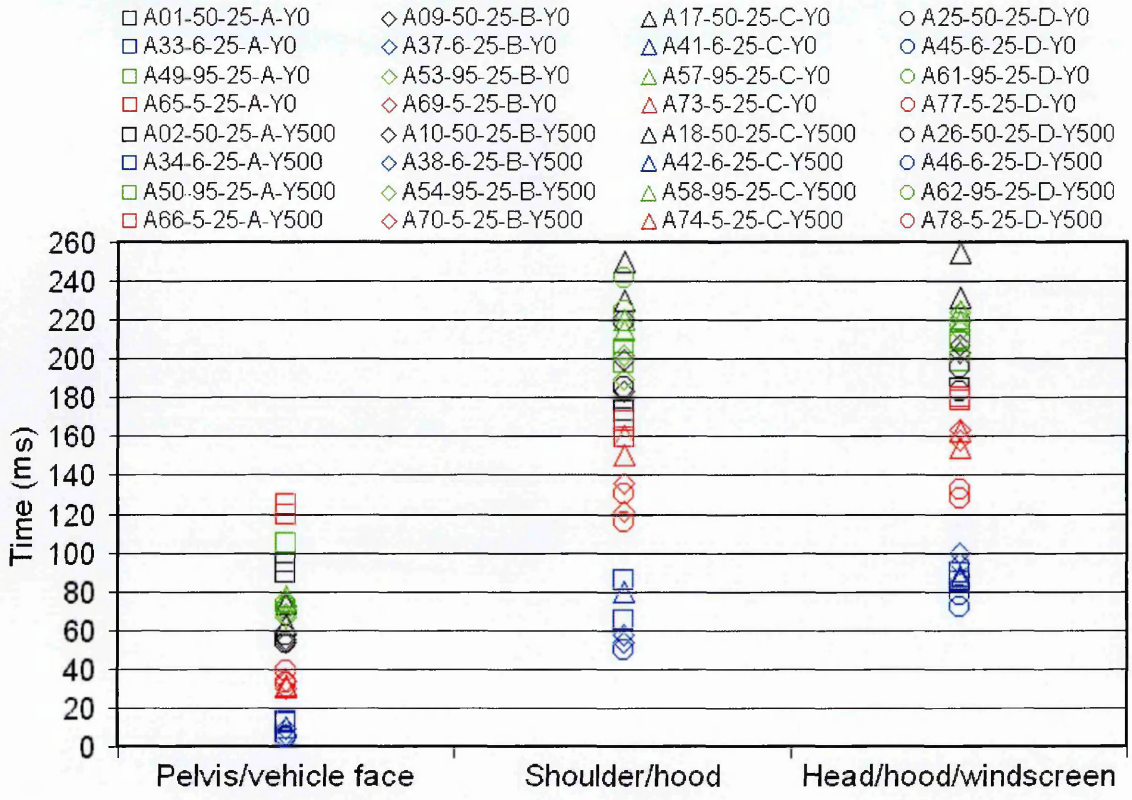

Figure A.1 All vehicle impact event timing at 25 km/h

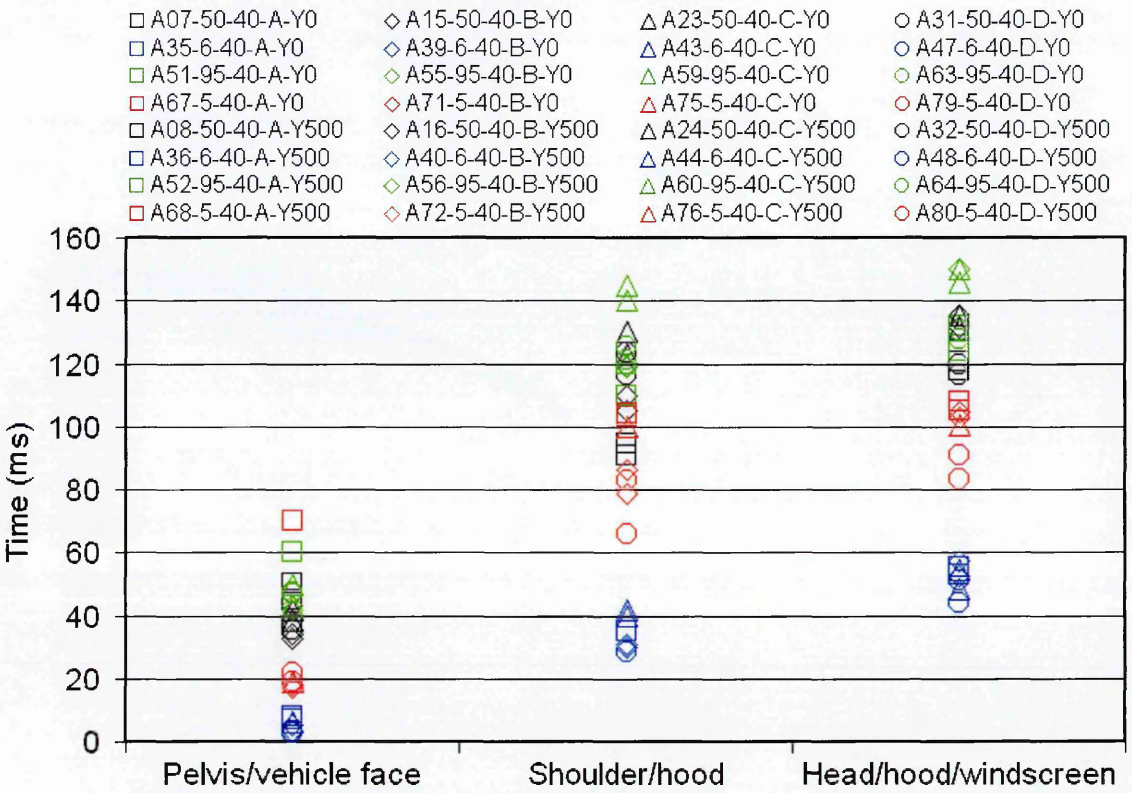

Figure A.2 All vehicle impact event timing at 40 km/h

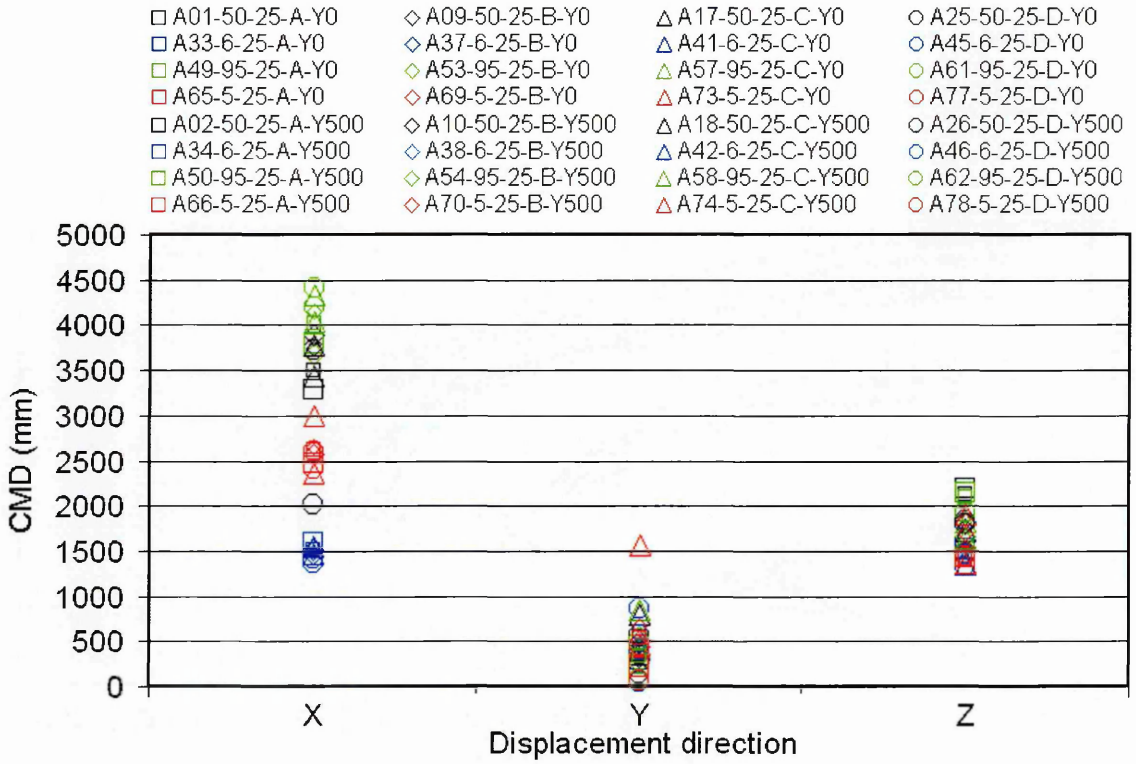

Figure A.3 All CMD values for vehicle at 25 km/h

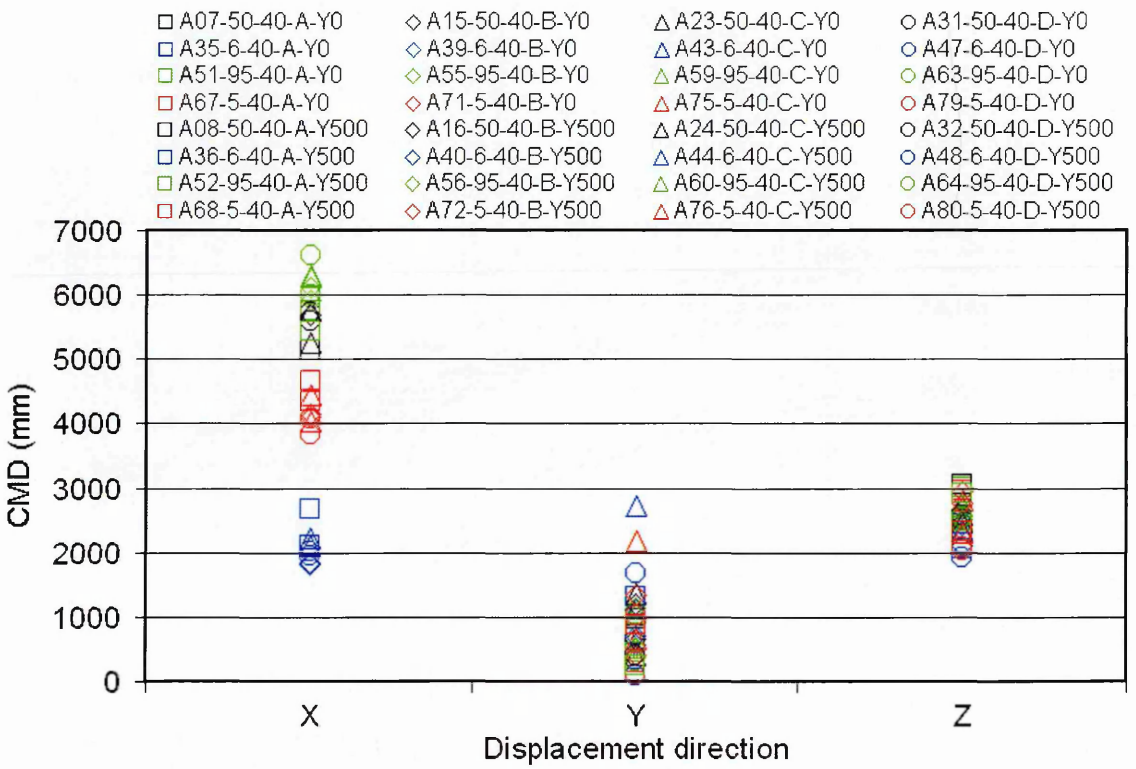

Figure A.4 All CMD values for vehicle at 40 km/h

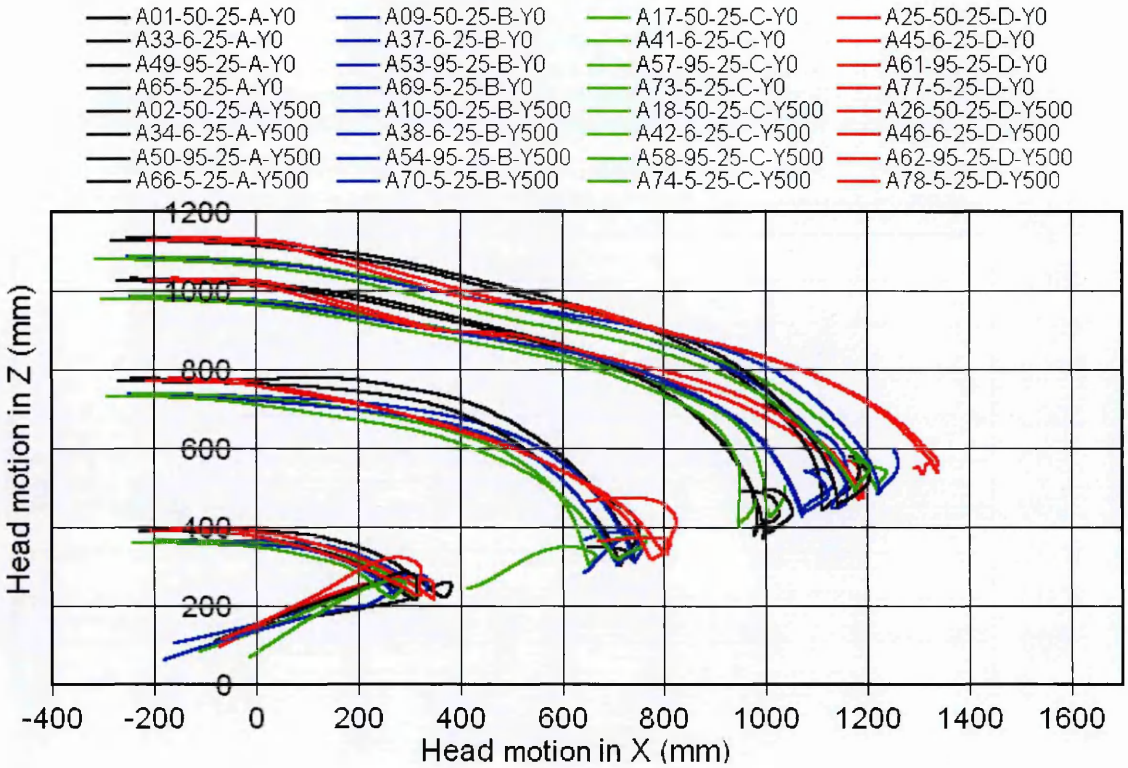

Figure A.5 All vehicle relative head trajectories at 25 km/h

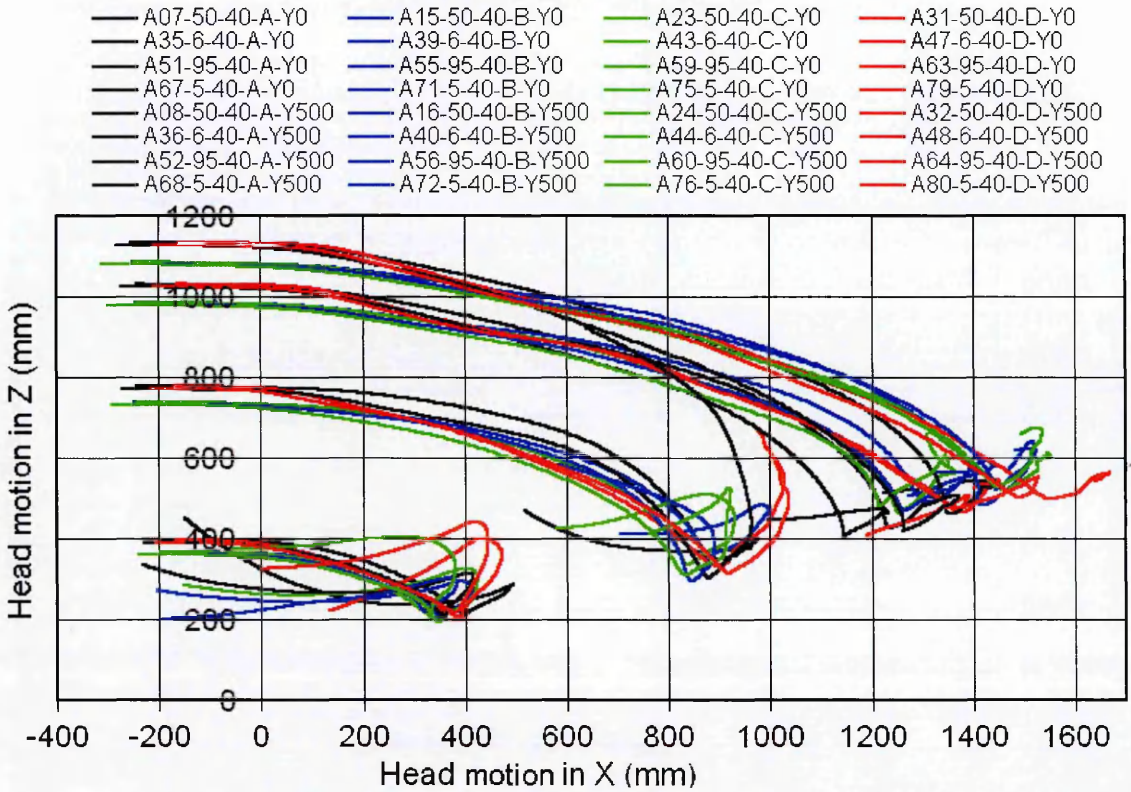

Figure A.6 All vehicle relative head trajectories at 40 km/h

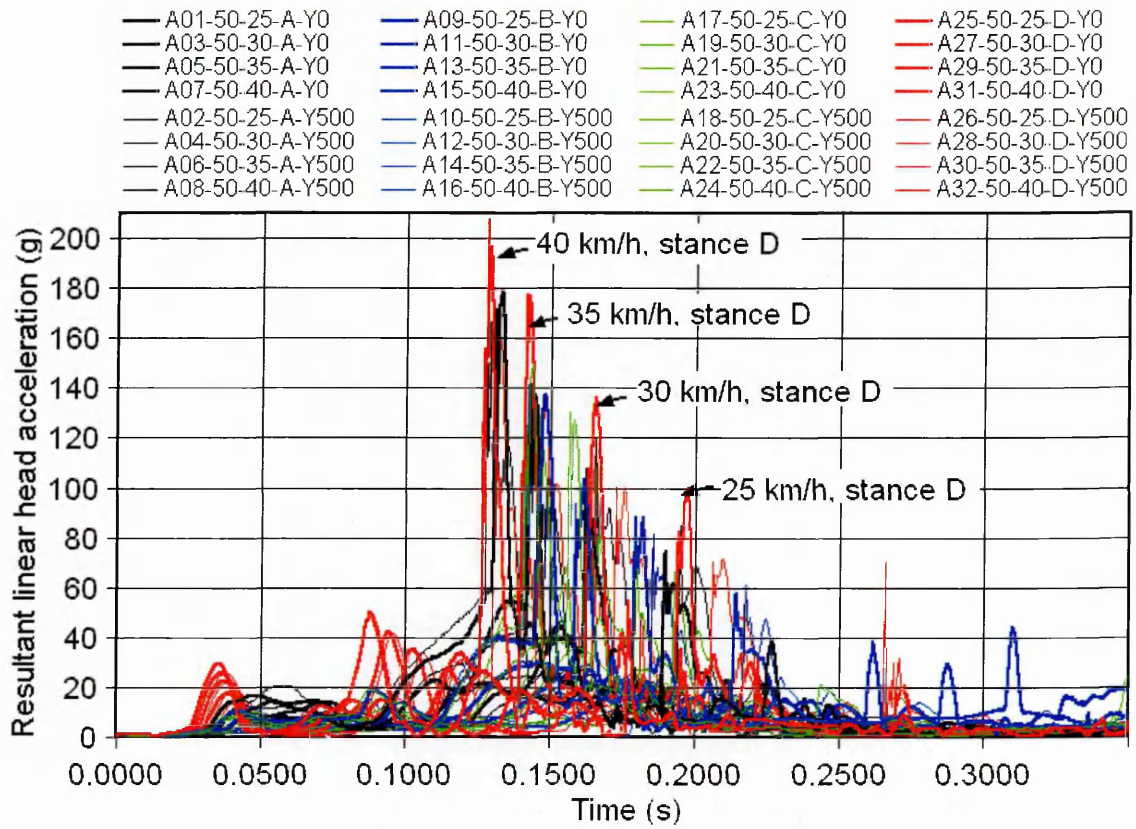

Figure A.9 50th percentile head acceleration at 25, 30, 35, 40 km/h

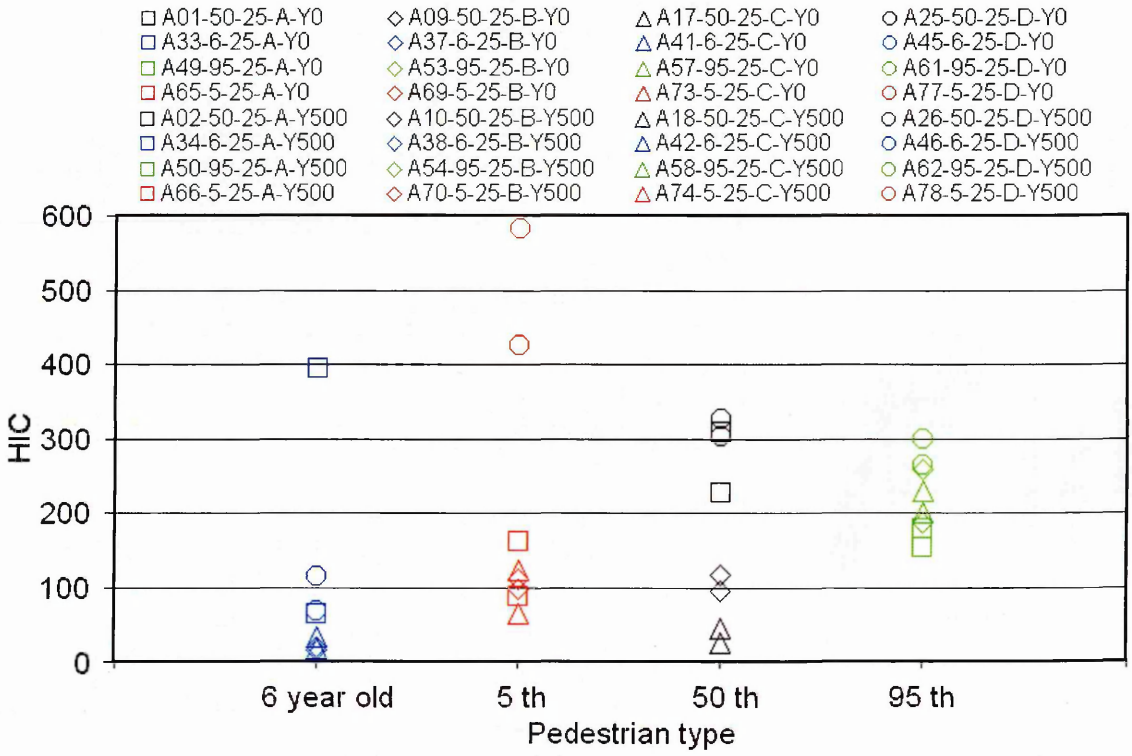

Figure A.10 All HIC values for vehicle at 25 km/h

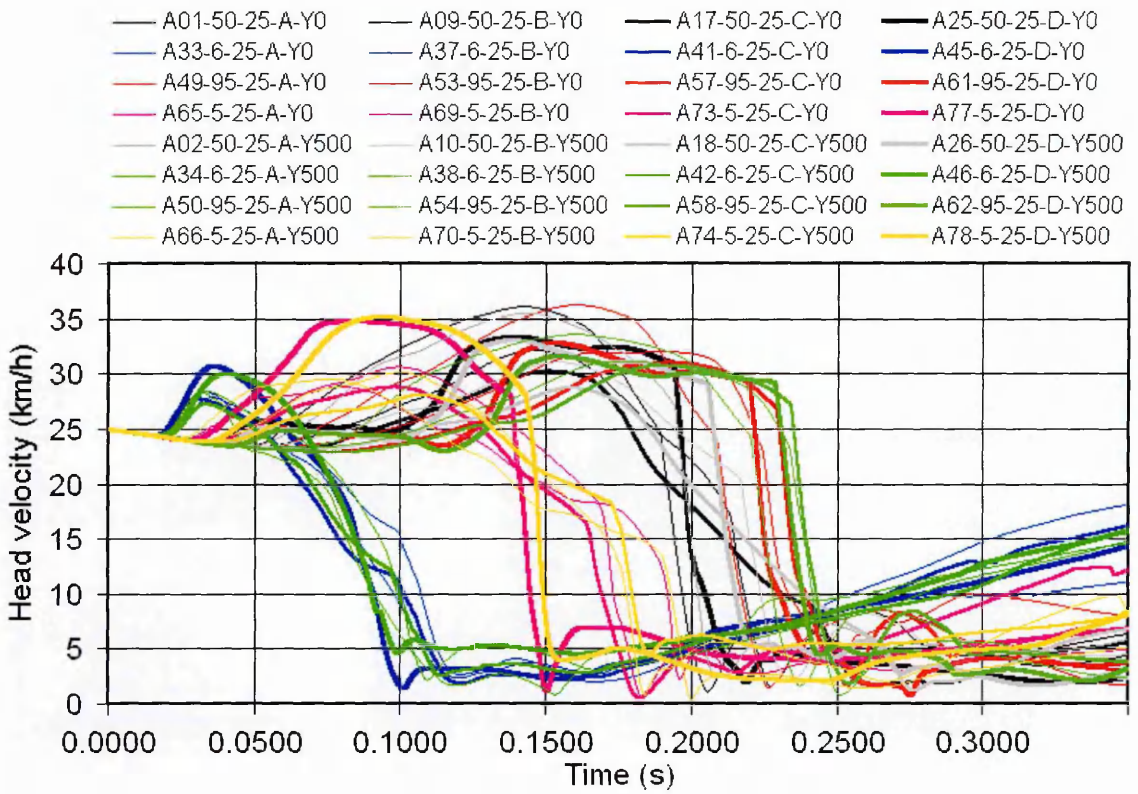

Figure A.7 All head velocities relative to hood leading edge at 25km/h

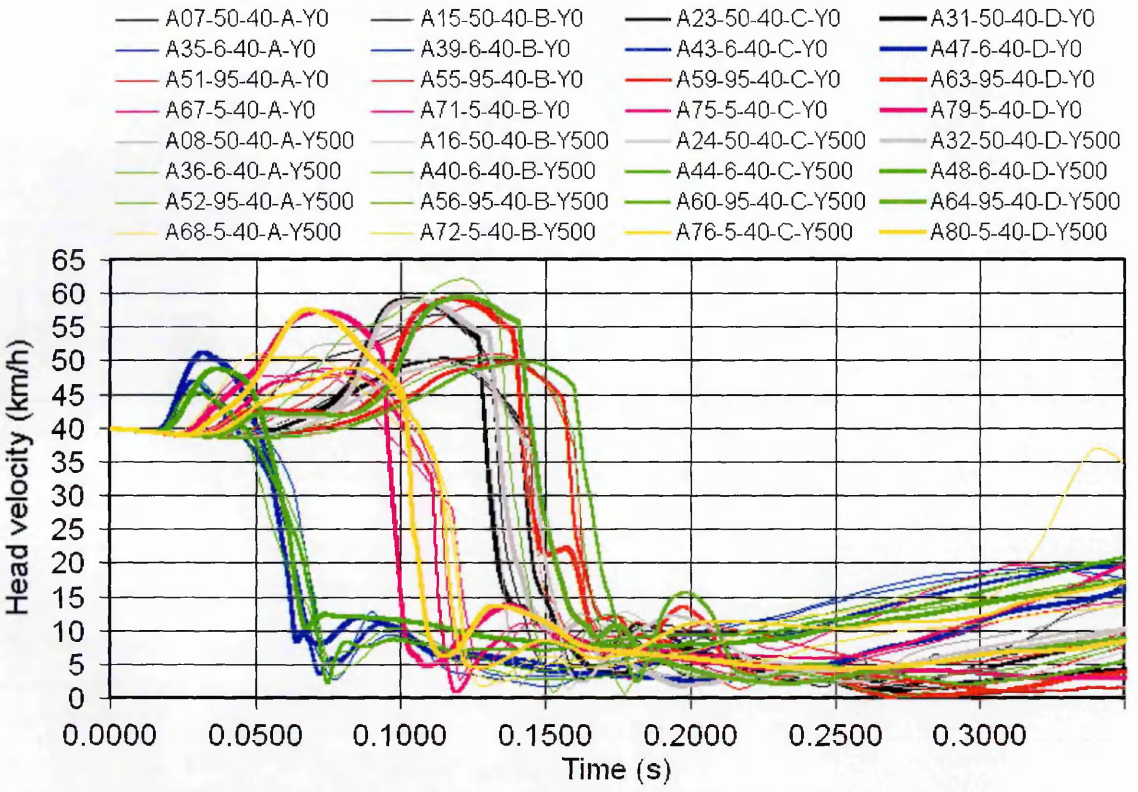

Figure A.8 All head velocities relative to hood leading edge at 40km/h

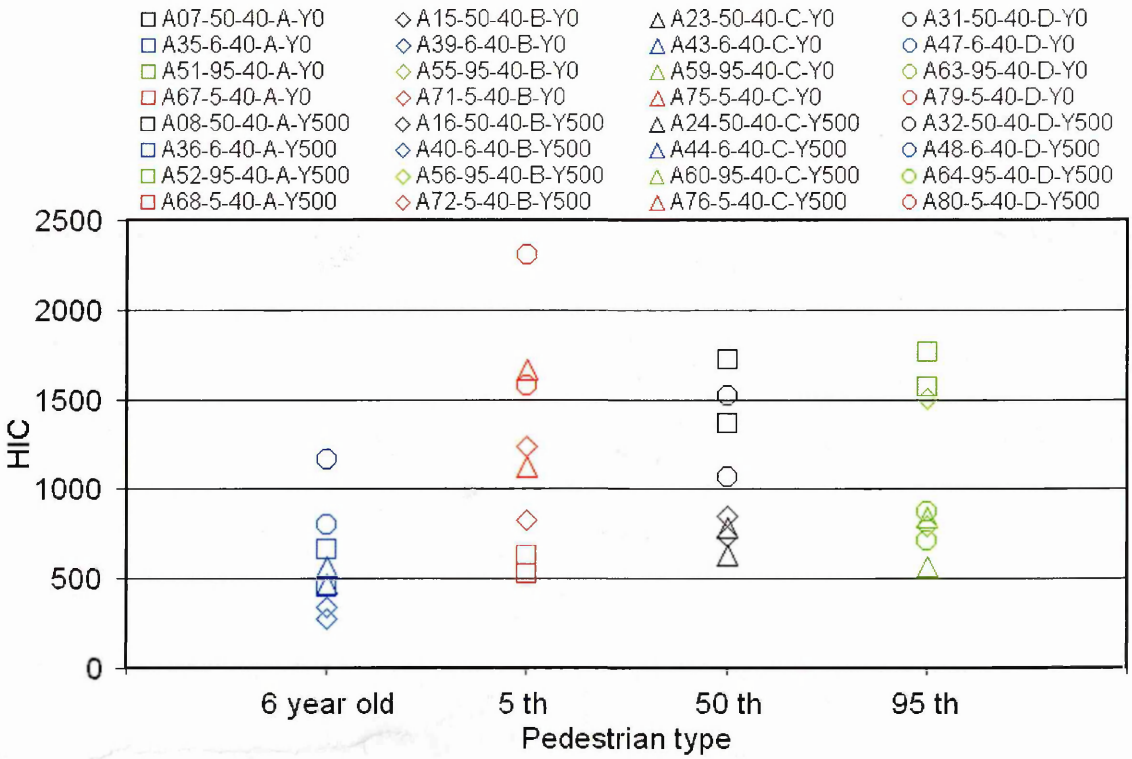

Figure A.11 All HIC values for vehicle at 40 km/h

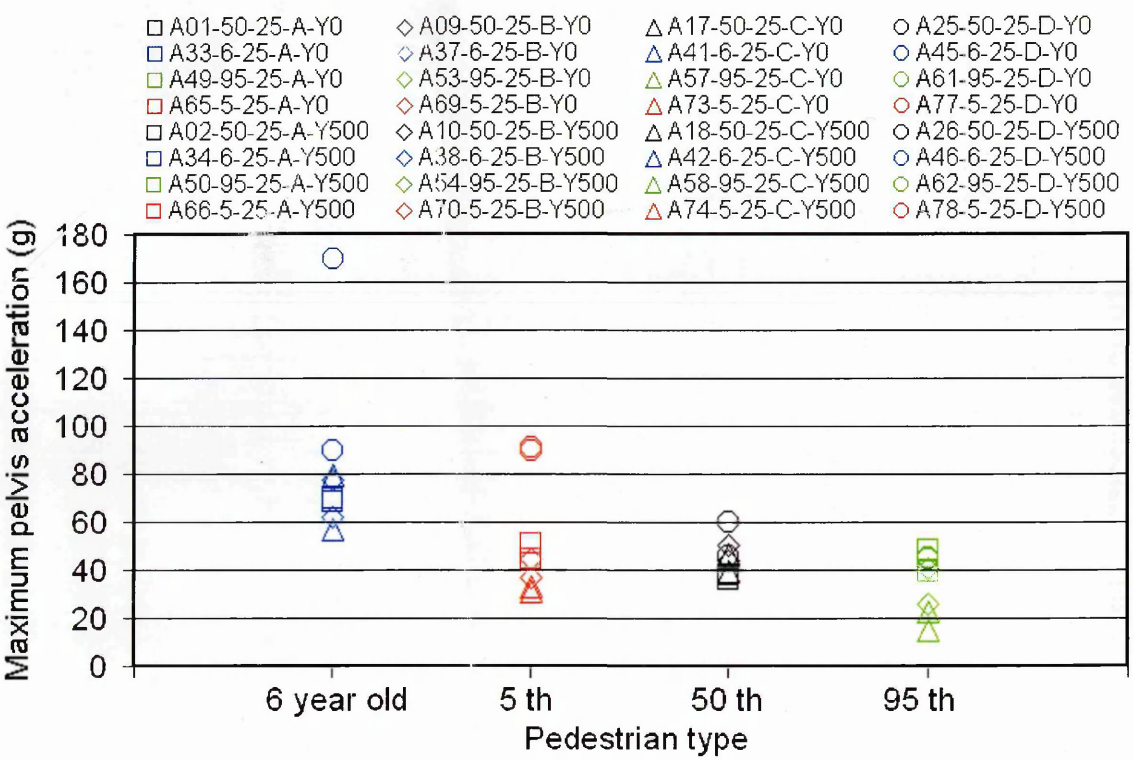

Figure A.12 All pelvis acceleration values for vehicle at 25 km/h

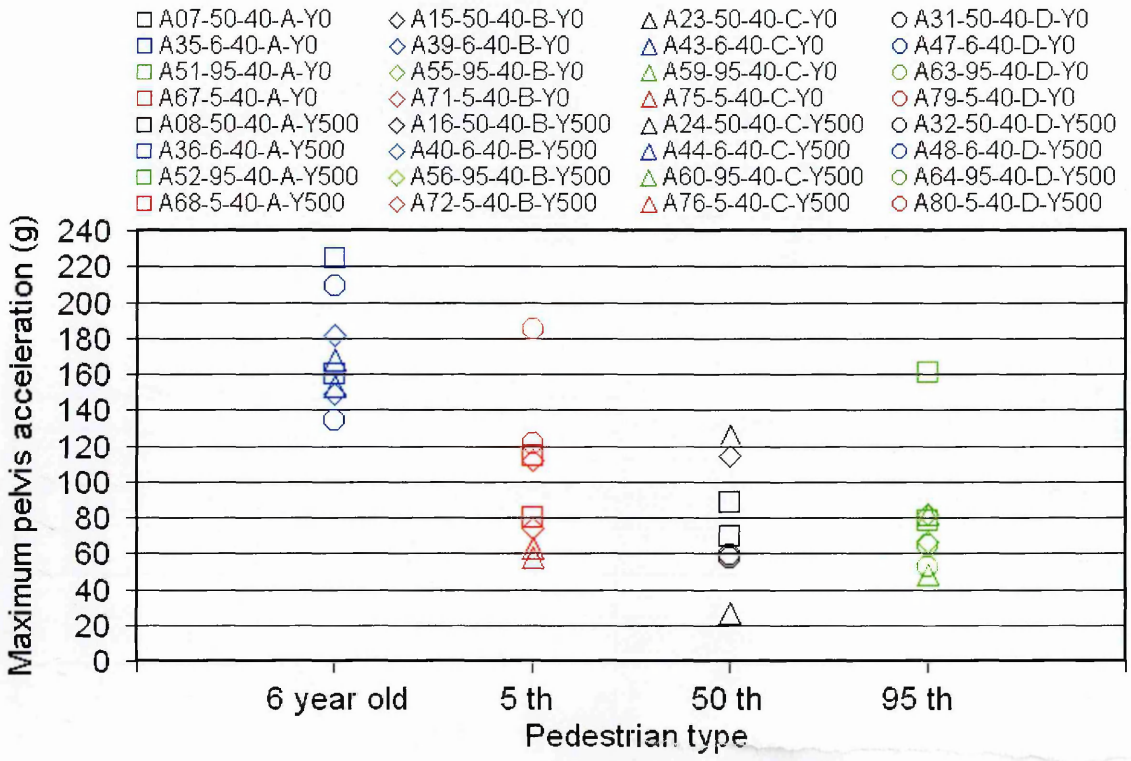

Figure A.13 All pelvis acceleration values for vehicle at 40 km/h

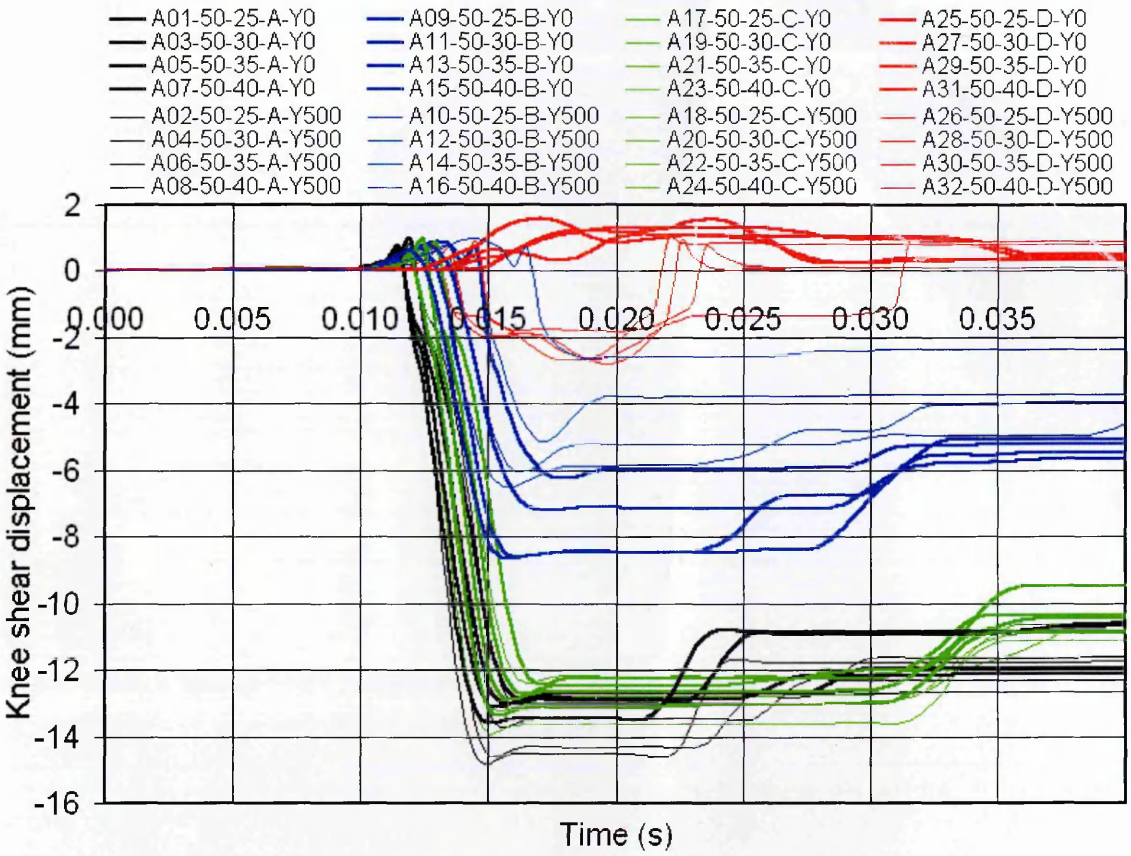

Figure A.14 50th percentile knee shear time histories

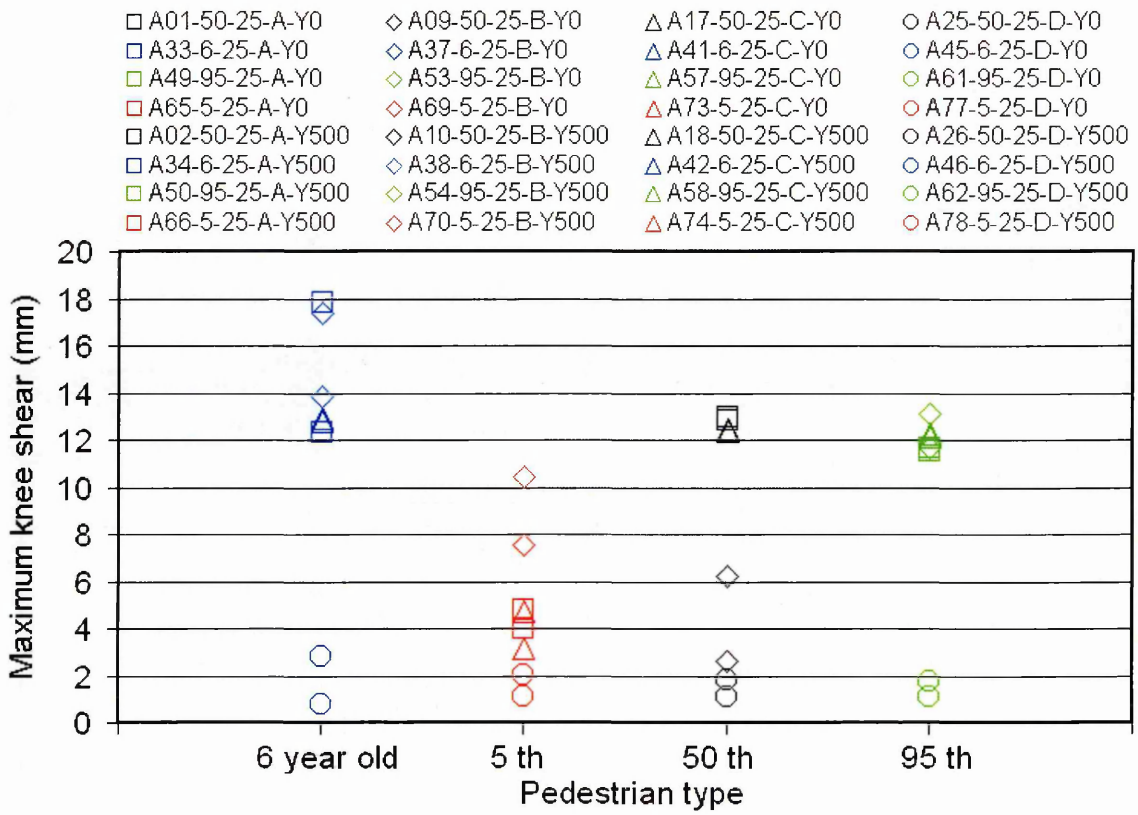

Figure A.15 All knee shear values for vehicle at 25 km/h

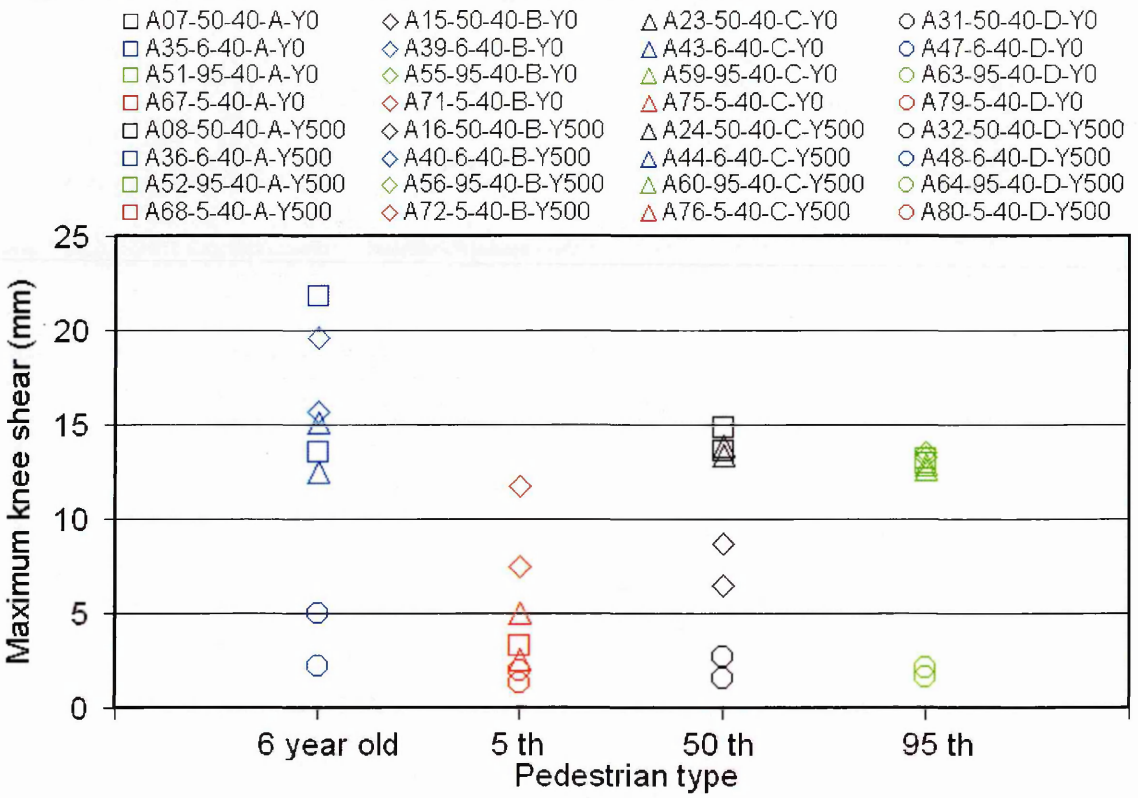

Figure A.16 All knee shear values for vehicle at 40 km/h

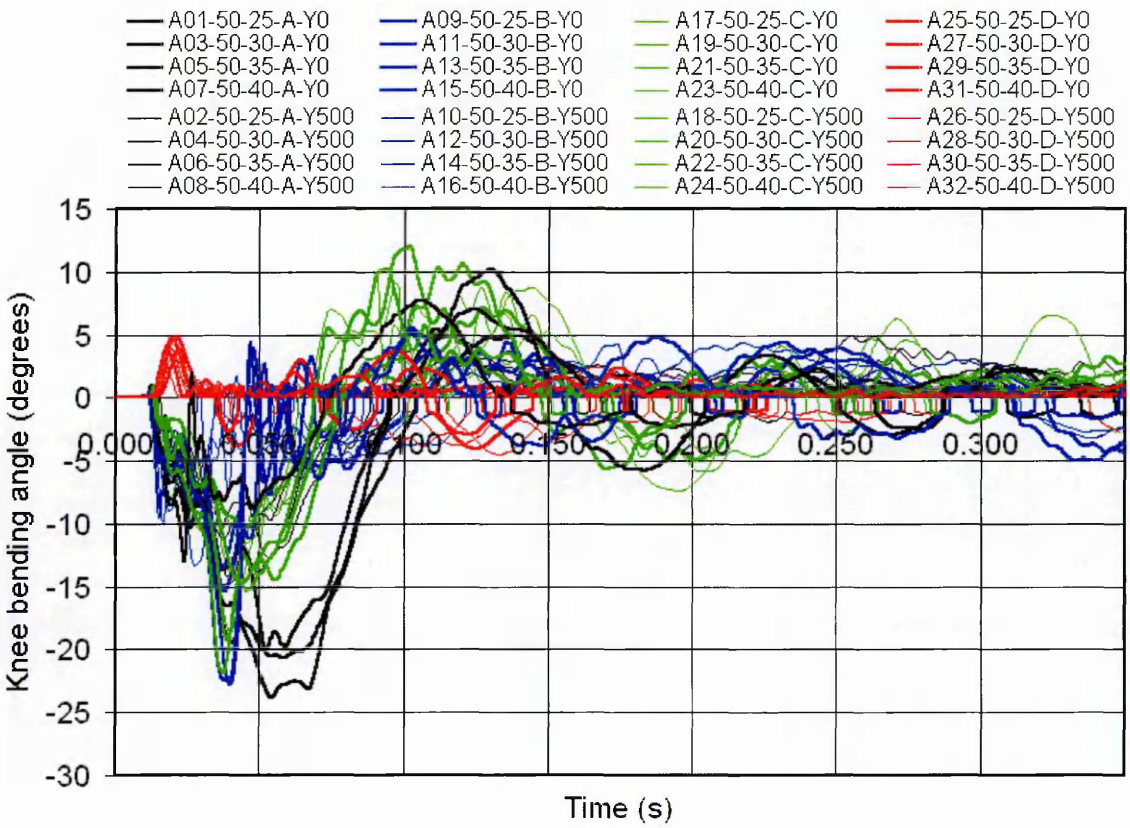

Figure A.17 50th percentile knee bending time histories

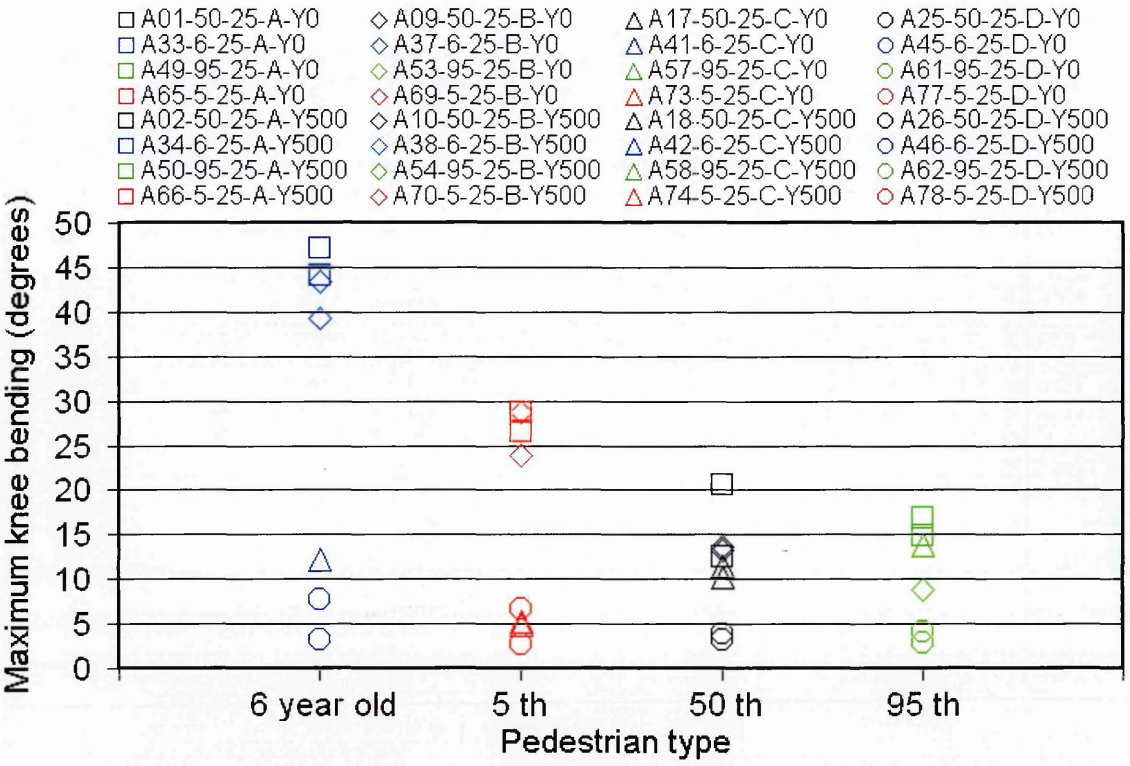

Figure A.18 All knee bending values for vehicle at 25 km/h

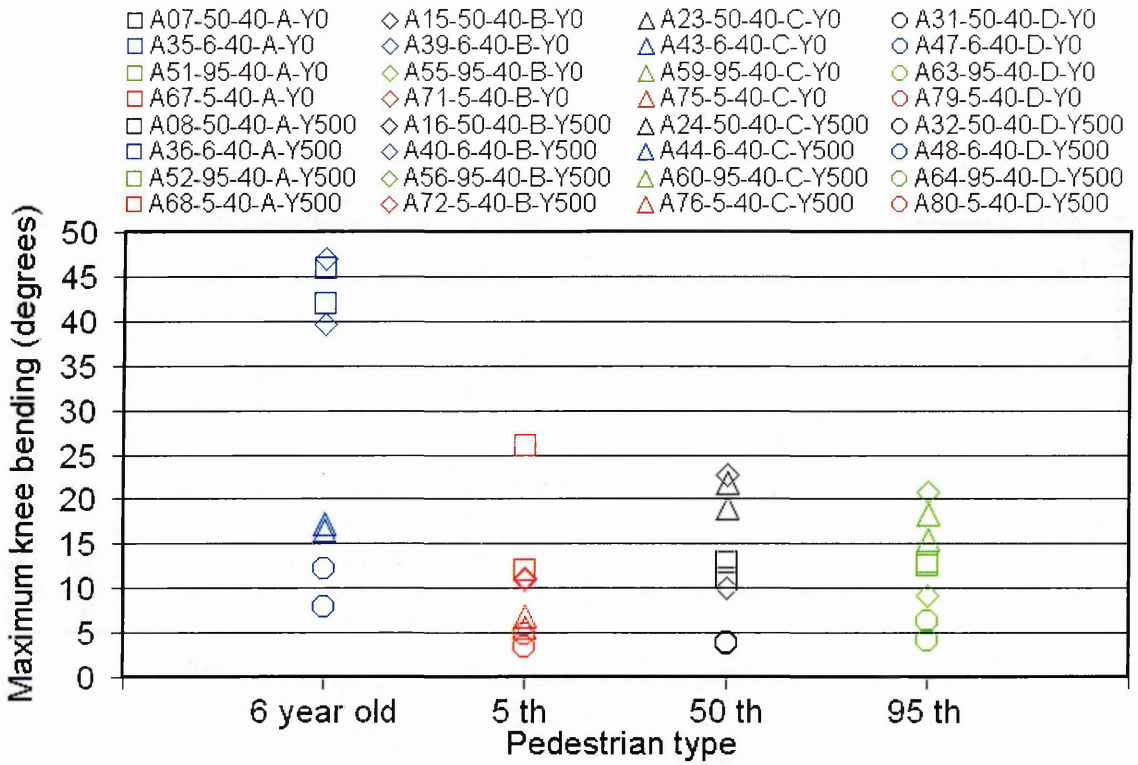

Figure A.19 All knee bending values for vehicle at 40 km/h

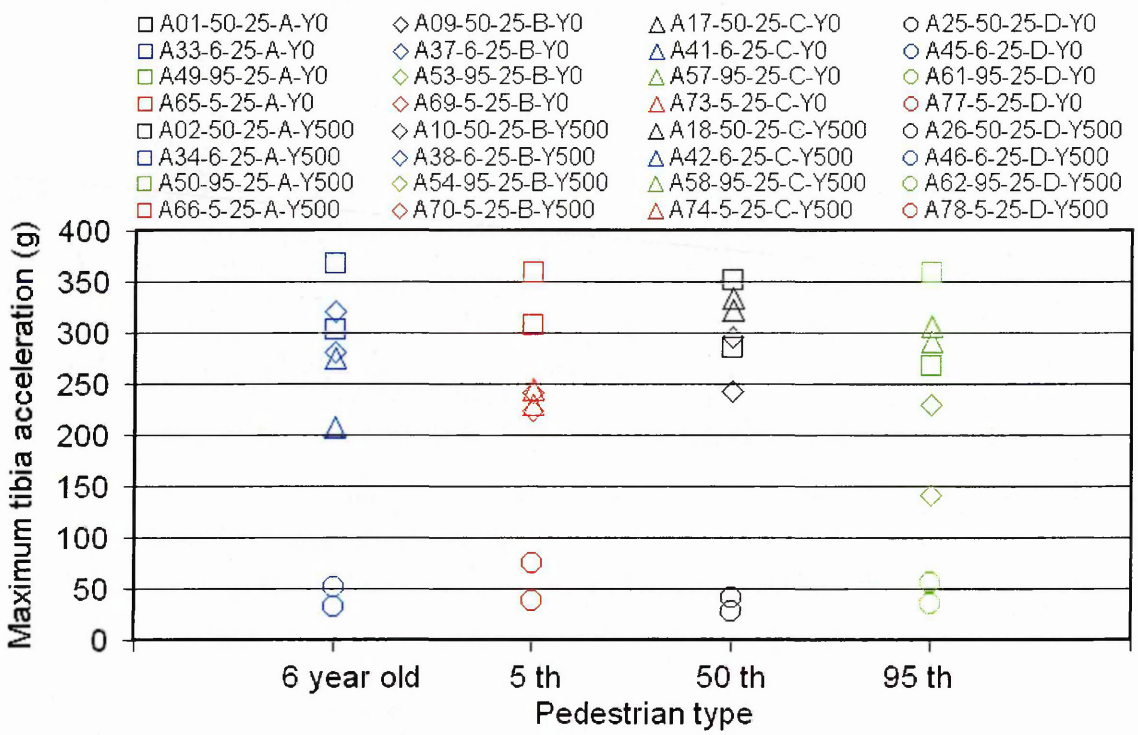

Figure A.20 All tibia acceleration values for vehicle at 25 km/h

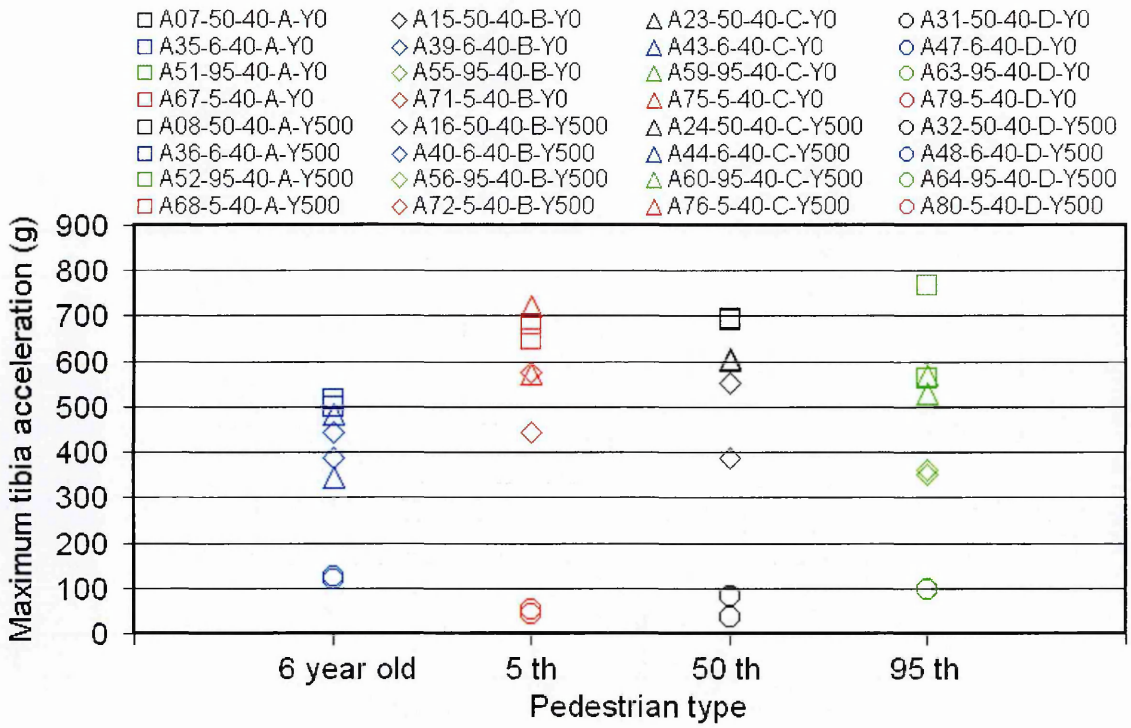

Figure A.21 All tibia acceleration values for vehicle at 40 km/h